NEW THERAPEUTIC APPROACHES AGAINST INFLAMMATION AND IMMUNE REGULATION IN METABOLIC RELATED DISEASES

EDITED BY: Yao Lu, Liang Weng, Xing Li Wang and Ning Hou
PUBLISHED IN: Frontiers in Pharmacology

frontiers Research Topics

frontiers

ISSN 1664-8714
ISBN 978-2-88974-826-6
DOI 10.3389/978-2-88974-826-6

About Frontiers

Frontiers is more than just an open-access publisher of scholarly articles: it is a pioneering approach to the world of academia, radically improving the way scholarly research is managed. The grand vision of Frontiers is a world where all people have an equal opportunity to seek, share and generate knowledge. Frontiers provides immediate and permanent online open access to all its publications, but this alone is not enough to realize our grand goals.

Frontiers Journal Series

The Frontiers Journal Series is a multi-tier and interdisciplinary set of open-access, online journals, promising a paradigm shift from the current review, selection and dissemination processes in academic publishing. All Frontiers journals are driven by researchers for researchers; therefore, they constitute a service to the scholarly community. At the same time, the Frontiers Journal Series operates on a revolutionary invention, the tiered publishing system, initially addressing specific communities of scholars, and gradually climbing up to broader public understanding, thus serving the interests of the lay society, too.

Dedication to Quality

Each Frontiers article is a landmark of the highest quality, thanks to genuinely collaborative interactions between authors and review editors, who include some of the world's best academicians. Research must be certified by peers before entering a stream of knowledge that may eventually reach the public - and shape society; therefore, Frontiers only applies the most rigorous and unbiased reviews.
Frontiers revolutionizes research publishing by freely delivering the most outstanding research, evaluated with no bias from both the academic and social point of view. By applying the most advanced information technologies, Frontiers is catapulting scholarly publishing into a new generation.

What are Frontiers Research Topics?

Frontiers Research Topics are very popular trademarks of the Frontiers Journals Series: they are collections of at least ten articles, all centered on a particular subject. With their unique mix of varied contributions from Original Research to Review Articles, Frontiers Research Topics unify the most influential researchers, the latest key findings and historical advances in a hot research area! Find out more on how to host your own Frontiers Research Topic or contribute to one as an author by contacting the Frontiers Editorial Office: frontiersin.org/about/contact

NEW THERAPEUTIC APPROACHES AGAINST INFLAMMATION AND IMMUNE REGULATION IN METABOLIC RELATED DISEASES

Topic Editors:
Yao Lu, Central South University, China
Liang Weng, Central South University, China
Xing Li Wang, Novartis (United States), United States
Ning Hou, Guangzhou Medical University, China

Citation: Lu, Y., Weng, L., Wang, X. L., Hou, N., eds. (2022). New Therapeutic Approaches Against Inflammation and Immune Regulation in Metabolic Related Diseases. Lausanne: Frontiers Media SA. doi: 10.3389/978-2-88974-826-6

Table of Contents

frontiers in Pharmacology

EDITORIAL
published: 10 March 2022
doi: 10.3389/fphar.2022.878608

Editorial: New Therapeutic Approaches Against Inflammation and Immune Regulation in Metabolic Related Diseases

Yao Lu[1]* *and Liang Weng*[2,3]*

[1]Clinical Research Center, The Third Xiangya Hospital, Central South University, Changsha, China, [2]Department of Oncology, Xiangya Cancer Center, Xiangya Hospital, Central South University, Changsha, China, [3]Key Laboratory of Molecular Radiation Oncology Hunan Province, Xiangya Hospital, Central South University, Changsha, China

Keywords: metabolic disease, inflamation, immune, cancer, diabetes, CVD (cardiovascular disease)

Editorial on the research topic

New Therapeutic Approaches Against Inflammation and Immune Regulation in Metabolic Related Diseases

Abnormal metabolism accompanied by chronic low-grade inflammation plays a vital role in the cause and progression of many metabolic-related diseases. The crosstalk of metabolism and inflammation has attracted more and more attention in maintaining tissue and organ homeostasis in recent years. In this Research Topic of Frontiers in Pharmacology, several novel findings further extend our understanding on the role of metabolism and inflammation in diseases, with emphasis on diabetes, metabolic syndrome, cardiovascular disease, cancers and kidney disease progression and treatment.

Cardiovascular disease, especially atherosclerosis is highly related to dysregulated metabolism. In addition, several immune signaling pathways and immune cells are involved in the progression of atherosclerosis. In this Research Topic, Jiang et al., reported that Caspase-11-gasdermin D-mediated pyroptosis and the subsequent proinflammatory response in macrophages are involved in the pathogenesis of atherosclerosis. Liu et al. reported that a peptide named intermedin can prevent ox-LDL–induced macrophage inflammation by inhibiting FABP4, implicating the potential application of this peptide in atherosclerosis treatment in future. Furthermore, an excellent review by Leng et al. summarized the receptor interacting protein kinases 1/3 (RIPK1/3) mediated signaling pathways in cardiovascular diseases progression and treatment.

Diabetes and metabolic syndrome are prevalent worldwide and major public health problems, which affect the health of people and impair the quality of life. This Research Topic provided new insights into the interplay between metabolism and inflammation in these diseases. Four papers (Ding et al., Hu et al., Collado et al., and Dong et al.) reported the effect of atrial natriuretic peptide (ANP), unsaturated fat, the soluble dietary fiber polydextrose (PDX) and probiotic supplementation on diabetes and metabolic syndrome treatment with inhibition of inflammatory levels. In addition, a review by Geng et al. discussed the innate immune cellular molecular events in the local microenvironment of diabetic wounds and the potential of targeting these immune pathways and cell phenotypes in diabetic wound therapy.

Kidney removes metabolic wastes and reabsorbs water, minerals and nutrients to participate in whole-body homeostasis. Abnormal metabolism and immune system function can be found in many kidney diseases. In this Research Topic, two papers described the outcomes of surgical operation in kidney diseases. Guangyu et al. analyzed the cardiovascular and cerebrovascular

OPEN ACCESS

Edited and reviewed by:
Dieter Steinhilber,
Goethe University Frankfurt, Germany

***Correspondence:**
Yao Lu
luyao0719@163.com
Liang Weng
wengliang@csu.edu.cn

Specialty section:
This article was submitted to Inflammation Pharmacology, a section of the journal Frontiers in Pharmacology

Received: *18 February 2022*
Accepted: *24 February 2022*
Published: *10 March 2022*

Citation:
Lu Y and Weng L (2022) Editorial: New Therapeutic Approaches Against Inflammation and Immune Regulation in Metabolic Related Diseases. Front. Pharmacol. 13:878608. doi: 10.3389/fphar.2022.878608

risk of postoperative acute kidney injury (AKI) in surgical patients. Single-cell transcriptomics sequencing is a powerful method to identify the composition of cell types in samples. By using this method, Zhuang et al. analyzed the immune cell subpopulations in the end-stage renal disease patients who received kidney transplantation, and revealed a novel B-cell subset ($CD19^{+}IGLC3^{low}IGKC^{high}TCL1A^{-}CD127^{+}$) in renal allograft recipients with immune accommodation. In addition, in the treatment of IgA nephropathy, Liu et al. revealed that Astragaloside IV could inhibit the secretion of galactose-deficient IgA1, which is the main cause for IgA nephropathy.

Cancer is long considered as a metabolic-related disease. As early as in 1920s, the Warburg effect, also known as aerobic glycolysis, was discovered to support cancer cell growth. In recent years, with the advances of technique in metabolomics, several other metabolic pathways were identified to be involved in tumorigenesis. Furthermore, dysregulated metabolism was also shown to modulate tumor immune surveillance. In this research topic, two papers reported a set of genes related to immune regulation and metabolism in predicting the prognosis of cancers. Liu et al. found the levels of T-cell exhaustion-associated genes and the abundance of immune cells were elevated under high HIF1A expression in glioma. Chen et al. established a prediction model with four metabolic genes as a reliable prognostic tool to accurately predict the prognosis of LUAD. Finally, a state-of-the-art review summarized the clinical efficacy and safety of anti-PD1 and anti-PD-L1 immunotherapy.

Taken together, the researches presented in this Research Topic provide the new insight into the role of metabolism and inflammation in metabolic diseases.

AUTHOR CONTRIBUTIONS

YL and LW draft this editorial together.

Conflict of Interest: The authors declare that the research was conducted in the absence of any commercial or financial relationships that could be construed as a potential conflict of interest.

frontiers in Pharmacology

REVIEW
published: 15 April 2021
doi: 10.3389/fphar.2021.655557

Targeting Liver Sinusoidal Endothelial Cells: An Attractive Therapeutic Strategy to Control Inflammation in Nonalcoholic Fatty Liver Disease

Xue-Kai Wang[1] *and Zong-Gen Peng*[1,2,3]*

[1]CAMS Key Laboratory of Antiviral Drug Research, Institute of Medicinal Biotechnology, Chinese Academy of Medical Sciences and Peking Union Medical College, Beijing, China, [2]Key Laboratory of Biotechnology of Antibiotics, National Health and Family Planning Commission, Institute of Medicinal Biotechnology, Chinese Academy of Medical Sciences and Peking Union Medical College, Beijing, China, [3]Beijing Key Laboratory of Antimicrobial Agents, Institute of Medicinal Biotechnology, Chinese Academy of Medical Sciences and Peking Union Medical College, Beijing, China

Nonalcoholic fatty liver disease (NAFLD), especially its advanced stage nonalcoholic steatohepatitis (NASH), has become a threatened public health problem worldwide. However, no specific drug has been approved for clinical use to treat patients with NASH, though there are many promising candidates against NAFLD in the drug development pipeline. Recently, accumulated evidence showed that liver sinusoidal endothelial cells (LSECs) play an essential role in the occurrence and development of liver inflammation in patients with NAFLD. LSECs, as highly specialized endothelial cells with unique structure and anatomical location, contribute to the maintenance of liver homeostasis and could be a promising therapeutic target to control liver inflammation of NAFLD. In this review, we outline the pathophysiological roles of LSECs related to inflammation of NAFLD, highlight the pro-inflammatory and anti-inflammatory effects of LSECs, and discuss the potential drug development strategies against NAFLD based on targeting to LSECs.

Keywords: nonalcoholic fatty liver disease, liver sinusoidal endothelial cell, inflammation, capillarization, endothelial dysfunction, therapeutic strategy

OPEN ACCESS

Edited by:
Xing Li Wang,
Novartis, United States

Reviewed by:
Agnieszka Barbara Najda,
University of Life Sciences of Lublin, Poland
Chi Chien Lin,
National Chung Hsing University, Taiwan

***Correspondence:**
Zong-Gen Peng
pumcpzg@126.com

Specialty section:
This article was submitted to Inflammation Pharmacology, a section of the journal Frontiers in Pharmacology

Received: *19 January 2021*
Accepted: *10 March 2021*
Published: *15 April 2021*

Citation:
Wang X-K and Peng Z-G (2021) Targeting Liver Sinusoidal Endothelial Cells: An Attractive Therapeutic Strategy to Control Inflammation in Nonalcoholic Fatty Liver Disease. Front. Pharmacol. 12:655557. doi: 10.3389/fphar.2021.655557

INTRODUCTION

Nonalcoholic fatty liver disease (NAFLD), now proposed changing to metabolic-associated fatty liver disease (MAFLD), has gradually become one of the most common liver diseases in the world (Younossi et al., 2016; Eslam et al., 2020). Technically, NAFLD is divided into nonalcoholic fatty liver (NAFL) and nonalcoholic steatohepatitis (NASH) according to pathological conditions (Stefan et al., 2019). The main feature of NAFL is at least 5% of liver steatosis without hepatocyte damage in the form of hepatocyte ballooning, whereas NASH mainly manifests more than 5% of liver steatosis with inflammation and hepatocyte damage (Stefan et al., 2019). Typically, NASH is often accompanied with liver fibrosis and may highly develop into cirrhosis and even hepatocellular carcinoma (Younossi, 2019). In recent years, NASH has gradually become a leading cause of liver transplantation among adults in European and American countries (Wong et al., 2015; Estes et al., 2018; Younossi, 2019). However, despite the high incidence and severity of NASH, no specific drug is currently approved and existing treatment methods are only aimed at symptomatic treatment rather than mechanism-based (Friedman et al., 2018).

Inflammation is one of the major engines of NASH progression (Schuster et al., 2018). Although a moderate and resolved inflammatory response contributes to homeostasis remodeling and tissue repair and thereby has hepatoprotective effects, inflammation in NASH is persistent, which leads to hepatocyte death and liver parenchymal damage (Brenner et al., 2013). Furthermore, uninterrupted low-level inflammation can cause hepatic stellate cells (HSCs) to activate and differentiate into myofibroblasts. The activated myofibroblasts release a large amount of extracellular matrix, which are rich in collagen fibers, to extracellular space and eventually result in hepatic fibrosis or cirrhosis (Schuster et al., 2018; Schwabe et al., 2020). Therefore, understanding the mechanisms of occurrence and development of inflammation in NASH is of the utmost importance for better controlling inflammation, which is essential to prevent, alleviate, and even reverse fibrosis.

Vascular endothelium is located at the junction of circulating blood and peripheral tissues. In addition to acting as a physical barrier, vascular endothelium participates in various pathophysiological processes, including inflammation, angiogenesis, vascular tone regulation, platelet function regulation, and metabolic homeostasis (Chiu and Chien, 2011; Pi et al., 2018). Hepatic sinusoidal endothelium, as a physical barrier controlling material exchanges between liver parenchyma and circulation, is constituted of liver sinusoidal endothelial cells (LSECs) which are highly specialized endothelial cells and the most abundant liver non-parenchymal cells (Brunt et al., 2014). Due to their unique anatomical location, LSECs play a critical role in the pathophysiological activities of the liver. Recently accumulated evidence showed that LSECs play an essential role in the occurrence and progression of liver inflammation in NAFLD. In this review, we briefly summarize the pathophysiological role of LSECs related to liver inflammation, highlight the occurrence and development mechanisms of inflammation of NAFLD associated with LSECs, and finally discuss the potential drug development strategies against NAFLD based on targeting to LSECs.

THE STRUCTURE AND BIOLOGICAL FUNCTION OF LIVER SINUSOIDAL ENDOTHELIAL CELLS

Due to their unique structure and anatomical location, LSECs play important physiological roles in the maintenance of liver homeostasis, including substance exchange, blood flow regulation, high endocytic capacity, and immune regulation.

Unique Structure and Biological Function of Liver Sinusoidal Endothelial Cells in Substance Exchange

LSECs are unique in structure and function distinguished from other liver vascular endothelial cells. From an evolutionary point, the hepatic sinusoids are derived from the capillary vessels of the septum transversum and have a fenestrated phenotype acquired during 10 and 20 gestation weeks, which are different from the portal vessels that are developed from the vitelline veins (Gouysse et al., 2002; Geraud et al., 2017). In terms of structure and function, the specificity of LSECs is an adaptation to local microenvironment determined by anatomical location (Potente and Makinen, 2017). LSECs are located at an interface between the liver parenchyma and the mixed blood from the hepatic artery (30%) and portal vein (70%) (Poisson et al., 2017). On the sinusoidal side, LSECs are exposed to substances circulated in the blood, such as abundant nutrients, hormones, bile acids, and oxygen. While on the abluminal side, LSECs directly communicate with HSCs and hepatocytes that are critical for glycolipid metabolism. Therefore, the distinguished location feature assigns LSECs with the possibility of excellent substance exchange capacity (Poisson et al., 2017). Under normal conditions, LSECs have hallmarks characterized as the fenestrated phenotype, lack of basement membrane, and absence of diaphragm (**Figure 1**), and the unique structure made LSECs the most permeable endothelial cells in mammals, which is of significance for achieving more substance exchanges between liver parenchyma and blood to better match the metabolic function of the liver (Poisson et al., 2017). The fenestrae of LSECs, with a diameter of 50 ~150 nm, connects the space of Disse with the sinusoidal side, allowing lipoproteins, chylomicron remnants (a small lipoprotein with a diameter of about 30~80 nm that is decomposed by chylomicrons by lipoprotein lipase on the endothelial membrane of peripheral capillaries), and other macromolecules to enter the space of Disse from the circulating blood and then to be utilized by hepatocytes (Carpenter et al., 2005; Hilmer et al., 2005; Cogger et al., 2006). Besides, LSEC's fenestrae are organized in clusters termed as sieve plates, in which the size and number of fenestrae vary in different positions and can be changed dynamically depending on physiological states such as fasting or pathological states (Wisse et al., 1985; O'Reilly et al., 2010; Xie et al., 2010; DeLeve, 2015; Monkemoller et al., 2015; Zapotoczny et al., 2019). Overall, due to their location features, structural changes, and high permeability, LSECs establish a differential and selective barrier that can be adjusted according to the changes of pathophysiological environment.

Regulation of Liver Sinusoidal Endothelial Cells in Blood Flow

As endothelial cells, LSECs also play a role in regulating blood flow. Nitric oxide (NO) and endothelin-1 (ET-1), mainly produced by LSECs under normal conditions, are the two most powerful vasoactive substances in the liver, which causes dilation and contraction of blood vessels, respectively (Rieder et al., 1991; Shah et al., 1997). Under physiological conditions, in responding to the shear stress that is a friction between the vascular endothelium and blood flow, LSECs increase NO production and down-regulate ET-1 expression, which are mediated by Kruppel-like factor 2 (KLF2), an endothelial-specific transcription factor and a crucial anti-angiogenic factor (Davies, 1995; Shah et al., 1997; Parmar et al., 2006; Zeng et al., 2015). Meanwhile, healthy LSECs maintain HSCs

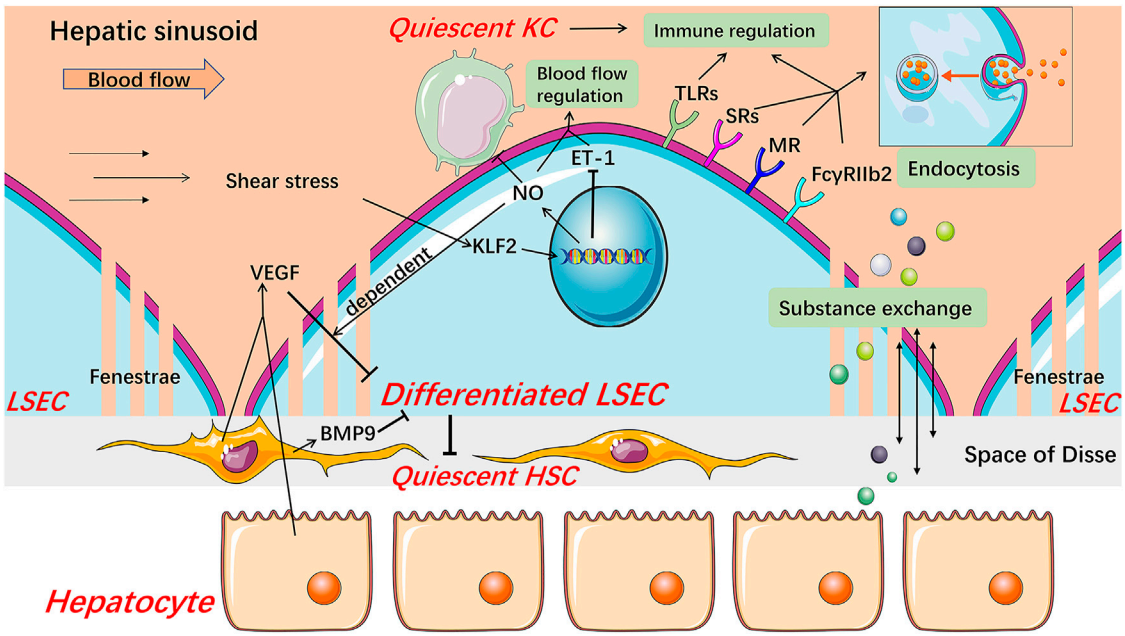

FIGURE 1 | Structure and major physiological function of LSECs. Healthy differentiated LSECs, characterized by the fenestrated phenotype and lack of basement membrane, are located at the junction of circulating blood and liver parenchyma, which state is maintained by VEGF from hepatocytes and HSCs in an LSEC-derived NO-dependent manner and BMP9 from HSCs. LSECs increase NO production and reduce ET-1 expression through KLF2 in response to the shear stress in hepatic sinusoids, thereby regulating blood flow. NO also keeps KCs and HSCs quiescent. LSECs fenestrae constitute a sieve plate that makes LSECs highly permeable to better exchange substance between liver parenchyma and blood. The expression of SRs, MR, and FcγRIIb2 endows LSECs with high endocytic capacity. These receptors, along with TLRs, are related to the immunoregulatory function of LSECs which contributes to the immune clearance and antigen presentation of LSECs. *BMP9* Bone morphogenetic protein 9, *ET-1* endothelin-1, *FcγRIIb2* Fc gamma-receptor IIb2, *HSC* hepatic stellate cell, *KC* Kupffer cell, *KLF2* Kruppel-like factor 2, *LSEC* liver sinusoidal endothelial cell, *MR* mannose receptor, *NO* nitric oxide, *SRs* scavenger receptors, *TLRs* Toll-like receptors, *VEGF* vascular endothelial growth factor.

and Kupffer cells (KCs) quiescence through NO-dependent pathways (Deleve et al., 2008; Tateya et al., 2011). These results indicate that LSECs may participate in inflammation and fibrosis under pathological conditions via NO signaling. Besides, carbon monoxide and the metabolites of the cyclooxygenase pathway, such as prostacyclin, are also associated with the regulation of blood flow in the hepatic sinusoids (Fernandez, 2015). Therefore, this regulation process involved with LSECs not only copes with the circadian change of hepatic blood flow mainly caused by digestion but also participates in maintaining the hepatic homeostasis, including inhibiting the occurrence of inflammation and fibrosis under pathophysiological condition.

High Endocytic Capacity of Liver Sinusoidal Endothelial Cells

LSECs possess the strongest potential ability of endocytosis in the human body, which is also an outstanding feature of LSECs (Smedsrod et al., 2009). Based on the dual-cell principle of waste clearance, the cells responsible for cleaning up circulating waste are divided into two types. One is professional phagocytes represented by macrophages which mainly clean up larger particles (>0.5 μm) by phagocytosis. The other is professional pinocytes represented by the scavenger endothelial cells, including LSECs, which are responsible for cleaning soluble macromolecules and smaller particles by endocytosis (Sorensen et al., 2012). Accordingly, LSECs express a variety of endocytosis receptors, including scavenger receptor (SR), mannose receptor (MR), and Fc gamma-receptor IIb2 (FcγRIIb2). SRs, including SR-A, SR-B, and SR-H (stabilin-1 and stabilin-2), are expressed on normal LSECs, and stabilin-1 and stabilin-2 are thought to play a major role (Hughes et al., 1995; McCourt et al., 1999; Zhou et al., 2000; Adachi and Tsujimoto, 2002; Malerod et al., 2002; Politz et al., 2002; Hansen et al., 2005; Sorensen et al., 2012). Stabilin-1 and stabilin-2 mediate uptake and degradation of modified proteins and lipoproteins such as advanced glycation-end products-albumin and oxidized low-density lipoproteins (ox-LDL), extracellular matrix macromolecules, protein turnover by-products including hyaluronan, heparin, and chondroitin sulfate (Sorensen et al., 2012). MR mediates the uptake of a wide range of endogenous glycoproteins and microbial glycans, the recruitment of lysosomal enzymes, and the endocytosis of other tissue turnover waste products including collagen alpha chains, tissue plasminogen activator (Stahl and Ezekowitz, 1998; Lee et al., 2002; McGreal et al., 2004; Sorensen et al., 2012). In particular, the expression and activity of MR in the liver are regulated by inflammatory stimuli and some cytokines. For example, interleukin (IL)-1 increases the expression of MR in LSECs while IL-10 reduces the activity of the receptor, therefore, MR might be involved in immunity and regulation of

glycoprotein homeostasis (Knolle et al., 1998; Arteta et al., 2010). FcγRIIb2, the only Fc gamma-receptor in LSECs, is dedicated to ingesting small soluble immune complexes and cleaning up circulating IgG immune complexes along with KCs (Hebert, 1991; Johansson et al., 1996; Mousavi et al., 2007; Sorensen et al., 2012).

Immune Regulation of Liver Sinusoidal Endothelial Cells

LSECs are continuously exposed to food and microbial antigens, which come from the gastrointestinal tract and enter hepatic sinusoids through the portal vein (Kubes and Jenne, 2018). As hepatic immune gatekeepers, LSECs maintain a hepatic immune tolerance environment and immune response to cope with other foreign pathogens and thus keep the liver from being damaged by unnecessary immune responses (Kubes and Jenne, 2018; Shetty et al., 2018). Recent studies showed that LSECs participate in both innate and adaptive immune regulation. Pattern recognition receptors including the Toll-like receptor (TLR) family, along with endocytosis receptors, assign LSECs with an ability to recognize and ingest foreign antigens (Chen and Nunez, 2010; Wu et al., 2010; Shetty et al., 2018). Furthermore, LSECs can still respond to signals mediated by these receptors even in the liver immune tolerance environment, though the activation of TLRs in LSECs is relatively limited compared to classical antigen-presenting cells (Wu et al., 2010; Shetty et al., 2018). Besides, endocytosis receptors on LSECs also play an important cell-specific role through interaction with TLRs and regulation of inflammation-related signals (Canton et al., 2013; Shetty et al., 2018). In adaptive immunity, LSECs can cross-present antigen to $CD8^+$ T cells by using SRs and induce tolerant naive $CD8^+$ T cells through enhanced interaction between programmed cell death one ligand one on LSECs and programmed cell death protein one on $CD8^+$ T cells (Limmer et al., 2000; Limmer et al., 2005; Burgdorf et al., 2007; Diehl et al., 2008; Shetty et al., 2018). Certainly, when faced with harmful pathogen stimulation, LSECs can also effectively drive T cells to respond for the rapid elimination of antigens, and this effect is regulated by inflammatory factors (Shetty et al., 2018). LSECs also express major histocompatibility complex class II molecules but are more inclined to promote the differentiation of naive $CD4^+$ T cells into regulatory T cells rather than T helper cells (Knolle et al., 1999; Carambia et al., 2014; Shetty et al., 2018).

THE PRO- AND ANTI-INFLAMMATORY DUAL EFFECTS OF LIVER SINUSOIDAL ENDOTHELIAL CELLS IN NONALCOHOLIC FATTY LIVER DISEASE

The development of liver inflammation is a key step causing liver injury, regardless of etiologies (Shetty et al., 2018). In NAFLD, infiltrated leukocytes are recruited from the circulation, mainly bone marrow-derived macrophages (BMMs) and neutrophils, into liver parenchyma, and this leads to the formation of inflammatory foci, and thus accelerates the disease progression from simple steatosis to steatohepatitis (Rinella, 2015). In general, circulating leukocytes are first captured by activated endothelial cells and then migrate through the endothelium to the site of infection or injury (Shetty et al., 2018). The recruitment of leukocytes is an outcome of multi-step adhesion cascades involving various cytokines and receptors on the surface of leukocyte and LSEC (Tanaka et al., 1993; Adams et al., 1996; Wong et al., 1997; Campbell et al., 1998; Nourshargh and Alon, 2014; McEver, 2015; Muller, 2016). In most vascular beds, selectin receptors mediate the capture of circulating leukocytes and cause them to roll on the endothelial surface, which is a general initial step for leukocyte recruitment. However, in hepatic sinusoids, the "rolling" is not an essential step for leukocyte recruitment and thus the selectin may have a minimal function due to the narrow structure and low shear stress (Adams et al., 1996; Wong et al., 1997). Further, stimulated by chemokines, the integrins on the surface of the leukocytes are activated and then mediate a firm adhesion between leukocytes and endothelium. Finally, leukocytes migrate through the endothelium into the liver parenchyma mediated by complex receptor-ligand interactions (Muller, 2016). In most organs, recruitment of leukocytes mainly occurs in post-capillary venules, while in the liver, most leukocyte recruitment occurs in sinusoidal cavities (Shetty et al., 2018). Therefore, LSECs control the key path of inflammation and thus play a pivotal role in the occurrence and progression of liver inflammation (**Figure 2**).

Pro-inflammatory Effects of Liver Sinusoidal Endothelial Cells

Capillarization of Liver Sinusoidal Endothelial Cells Promotes Inflammation in Early Nonalcoholic Fatty Liver Disease

LSECs undergo morphological changes in specific cases, such as viral infection, chronic liver diseases, and aging (Schaffner and Poper, 1963; Horn et al., 1987; Xu et al., 2003; Warren et al., 2007; Baiocchini et al., 2019; Hunt et al., 2019). Capillarization is the most common and prominent phenotypic change of LSECs, which is mainly manifested by the loss of fenestrae and the formation of a basement membrane on the abluminal surface, and thus it is also called dedifferentiation (**Figure 3**) (Maslak et al., 2015a). Capillarization of LSECs occurs in lipid-treated LSECs, animal NAFLD models, and patients with NAFLD (Akyol et al., 2005; Peng et al., 2014; Zhang et al., 2014; Miyao et al., 2015; Bravo et al., 2019; Zhang et al., 2019). Treatment with ox-LDL only or plus high glucose induced human LSEC injury and thus caused a reduction in porosity of LSECs (Zhang et al., 2014; Zhang et al., 2019). Shown with a scanning electron microscopy or marker of capillarization indicators such as CD31 and CD34, the capillarization of LSECs was observed at the early stage of NAFLD in animal models induced by diet, including high fat diet (HFD), choline-deficient L-amino acid-defined (CDAA) diet, and high fat glucose-fructose diet (HFGFD) (**Table 1**) (Peng et al., 2014; Miyao et al., 2015; Bravo et al., 2019). In patients with NAFLD, CD31 was significantly higher expressed in zone 3 (centrilobular area) (Akyol et al., 2005). Certainly, the

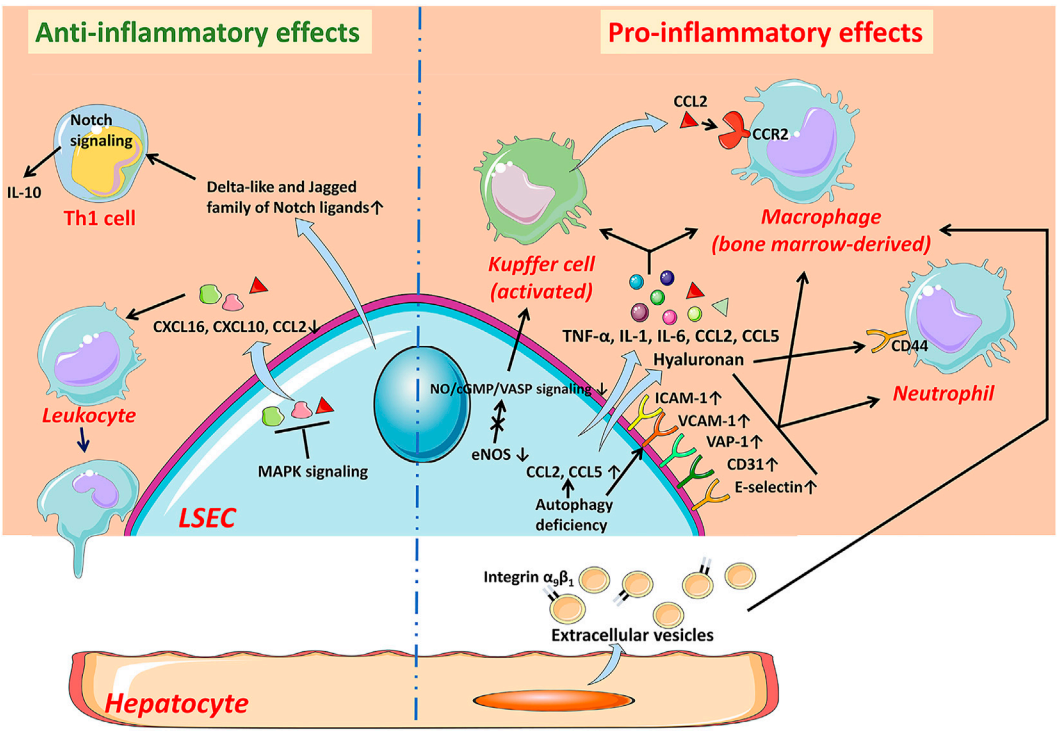

FIGURE 2 | The anti-inflammatory and pro-inflammatory effects of LSECs in NAFLD. In the early stage of NAFLD, LSECs develop an anti-inflammatory phenotype manifested by the decreased expression of chemokines CCL2, CXCL10, and CXCL16 through MAPK signaling-dependent manner. LSECs can also promote the secretion of IL-10 by Th1 cells via releasing Notch ligands to exert anti-inflammatory effects. While LSECs characterized as pro-inflammatory phenotype, increase expression of adhesion factors including VCAM-1, ICAM-1, E-selectin, CD31, and VAP-1, leading to increased recruitment of leukocytes. The deficiency of autophagy also leads to up-regulation of adhesion factors and chemokines. Pro-inflammatory mediators released by LSECs, such as TNF-α, IL-1, and IL-6, also promote the progress of inflammation. The reduction of NO bioavailability contributes to the activation of KCs and the recruitment of bone marrow-derived macrophages. The hyaluronan densely coated on the surface of LSECs facilitates the recruitment of neutrophils by interacting with CD44. In addition, hepatocyte-derived EVs contribute to the recruitment of macrophages into the hepatic sinusoids. *CCL* C-C motif chemokine ligand, *CCR* C-C motif chemokine receptor, *CXCL* C-X-C motif chemokine ligand, *eNOS* endothelial nitric oxide synthase, *ICAM-1* intercellular adhesion molecule-1, *IL* interleukin, *LSEC* liver sinusoidal endothelial cell, *NO* Nitric oxide, *TNF-α* tumor necrosis factor-α, *VAP-1* vascular adhesion protein-1, *VCAM-1* vascular cell adhesion molecule-1.

capillarization of LSECs occurs earlier than the onset of general liver inflammation. Miyao and colleagues found that the reduced porosity of LSECs was earlier than inflammation and activation of KCs and HSCs, which occurred in C57BL/6 mice after 1 week of CDAA diet (Miyao et al., 2015). Straub and colleagues found that CD45/CD68-positive inflammatory cells did not accumulate in the liver until the porosity of LSECs decreased by low-level arsenic, indicating that inflammation may be the consequence of LSECs capillarization (Straub et al., 2007). However, subjected to several variable factors, including the heterogeneity of animal models and LSECs isolated *in vitro*, the difference of detection methods, indicators, and techniques, whether the capillarization of LSECs occurs throughout NAFLD is still controversial.

Intracellular protein expression abnormality or signaling pathway disturbance contributes to capillarization of LSEC (**Figure 3**). Hedgehog signaling was activated and thus regulated phenotypic changes to form LSEC capillarization, while inhibitors of Hedgehog pathway partially reversed the capillarized LSECs to a healthy differentiated phenotype and completely prevented LSECs from becoming capillarized both *in vitro* and *in vivo* (Xie et al., 2013). Capillarization of LSEC was also inhibited by liver X receptor (LXR) α via suppressing Hedgehog signaling (Xing et al., 2016). Although LXR agonists have shown therapeutic potential in anti-inflammatory and anti-fibrotic aspects, whether these beneficial effects are mainly through alleviating the capillarization of LSECs still needs further exploration (Xing et al., 2016). Lectin-like oxidized low-density lipoprotein receptor-1 (LOX-1) mediates capillarization through reactive oxygen species/nuclear factor-κB signaling pathway in LSECs treated with ox-LDL (Zhang et al., 2014). LOX-1 was up-regulated by many pro-inflammatory cytokines, including transforming growth factor-β, IL-1α, IL-1β, IL-6, and tumor necrosis factor-α (TNF-α), indicating that capillarization and inflammatory response may be mutually reinforced in NAFLD (Navarra et al., 2010; Ozturk et al., 2015). Recently, delta-like ligand 4 (DLL4), a ligand of the Notch signaling pathway, was found to mediate the capillarization of LSECs and the vicious circle between fibrosis and pathological sinusoidal remodeling (Chen et al., 2019).

Paracrine signaling is important for maintaining the differentiated phenotype of LSEC (**Figure 3**). Bone morphogenetic protein 9 (BMP9), as a paracrine factor

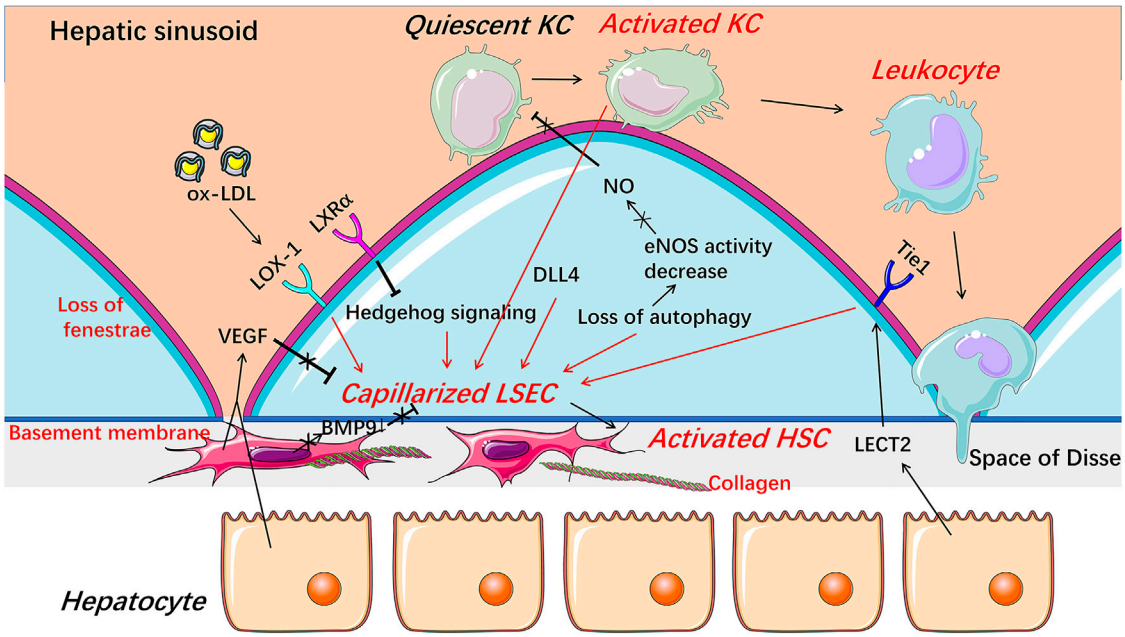

FIGURE 3 | Capillarization and endothelial dysfunction of LSECs under pathological condition. When injured, LSECs undergo capillarization represented by the loss of fenestrae and the formation of basement membrane which are involved in Hedgehog signaling, autophagy, HSCs-derived BMP9, LSECs-derived DLL4, and receptors including LOX-1, LXRα, and Tie1. The reduction of NO bioavailability is an important indicator of endothelial dysfunction and involved in the progress of the capillarization of LSECs. Capillarized and dysfunctional LSECs promote the activation of HSCs and KCs and thus promote liver fibrosis and inflammation. *BMP9* Bone morphogenetic protein 9, *DLL4* Delta-like ligand 4, *HSC* hepatic stellate cell, *KC* Kupffer cell, *LECT2* leukocyte cell-derived chemotaxin 2, *LSEC* liver sinusoidal endothelial cell, *LXRα* liver X receptor α, *LOX-1* lectin-like oxidized low-density lipoprotein receptor-1, *NO* Nitric oxide, *ox-LDL* oxidized low-density lipoproteins, *VEGF* vascular endothelial growth factor.

TABLE 1 | Summary of capillarization and endothelial dysfunction of LSECs in NAFLD animal models.

Model	Species	Capillarization	Stage	Endothelial dysfunction	Stage	Capillarization Indicator(s)	SEM	AFM	Year	Ref
HFD	C57BL/6 mice	Not mentioned	N/A	Yes	Early (4 weeks)	N/A	No	No	2011	Tateya et al. (2011)
CafD	Wistar kyoto rats	No	Early (1 month)	Yes	Early (1 month)	SE-1, CD31, CD34	No	No	2012	Pasarin et al. (2012)
HFD	SD rat	Yes	Probably early (43rd day)	Not mentioned	N/A	No	Yes	No	2014	Peng et al. (2014)
CDAA	C57BL/6 mice	Yes	Early (1 week)	Not mentioned	N/A	CD31, CD34	Yes	No	2015	Miyao et al. (2015)
HFD	C57BL/6 mice	Yes	Late (22 weeks)	Not mentioned	N/A	No	Yes	No	2015	Miyao et al. (2015)
MCD	C57BL/6 mice	Not mentioned	N/A	Yes	Early (4 weeks)	N/A	No	No	2015	Pourhoseini et al. (2015)
HFGFD	SD OFA rats	Yes	Early (10 weeks)	Yes	Early (10 weeks)	CD31	No	No	2019	Bravo et al. (2019)
HFD	C57BL/6 mice	No	Early (2 weeks) and late (20 weeks)	Not mentioned	N/A	No	Yes	Yes	2019	Kus et al. (2019)

AFM, atomic force microscopy; CafD, cafeteria diet; CDAA, choline-deficient l-amino acid-defined; HFD, high fat diet; HFGFD, high fat glucose-fructose diet; MCD, methionine and choline deficient; N/A, not applicable; SEM, scanning electron microscopy

derived from HSCs, maintains the fenestrated phenotype of LSECs, contributing to liver homeostasis (Desroches-Castan et al., 2019). In patients with NASH, hepatic mRNA expression of BMP9 was decreased (John et al., 2019). Knocking out mouse BMP9 gene induced capillarization of LSECs *in vivo*, while treatment with an addition of BMP9 maintained the fenestration of primary cultured LSECs *in vitro*, and an absence of LSEC fenestrae occurred followed by liver inflammation and fibrosis in BMP9 gene knock-out mice (Miyao et al., 2015; Desroches-Castan et al., 2019). Leukocyte

cell-derived chemotaxin 2 (LECT2), a functional ligand of Tie1 expressed by hepatocytes and endothelial cells, promotes the capillarization of LSECs in the liver fibrosis rodent model (Xu et al., 2019). Vascular endothelial growth factor (VEGF), as a paracrine signal produced by hepatocytes and HSCs, maintains the differentiated phenotype of LSECs (DeLeve et al., 2004). When co-cultured with HSCs or hepatocytes *in vitro*, the expression of CD31 on the surface of LSECs was decreased, while anti-VEGF antibody reversed the decrease (DeLeve et al., 2004). Fortuitously, NO synthase inhibitor blocked the stabilizing effect of hepatocytes or HSCs on LSECs phenotype in the co-cultured system, suggesting that NO may be also necessary for maintaining the differentiated phenotype of LSECs and that the decreased NO bioavailability may promote the capillarization of LSECs, which may be associated with endothelial dysfunction of LSECs (DeLeve et al., 2004; Flammer et al., 2012; Hammoutene and Rautou, 2019).

Capillarization of LSECs promotes the development of steatosis in NAFLD. On the one hand, the capillarization of LSECs prevents the release of very-low-density lipoprotein (VLDL) from hepatocytes into the sinusoidal cavity, resulting in the retention of lipids including cholesterol and triglycerides in the liver (Hammoutene and Rautou, 2019). On the other hand, the capillarization of LSECs prevents the entry of chylomicron remnants into hepatocytes, stimulating the *de novo* lipogenesis of liver lipids and eventually inducing steatosis in a compensatory way since the chylomicron remnants are required for the synthesis of VLDL by hepatocytes (Herrnberger et al., 2014; Tanaka and Iwakiri, 2016). However, studies showed that excessive lipid exposure, such as ox-LDL, leads to a decrease in the fenestrae diameter and porosity of LSECs (Zhang et al., 2014). Furthermore, Cogger and colleagues demonstrated that the porosity and fenestrae frequency of LSECs are negatively correlated with dietary fat intake and circulating FFA *in vivo* (Cogger et al., 2016). These data suggested that the early formation of steatosis will, in turn, promotes the capillarization of LSECs, which further facilitates the development of steatosis to inflammation in patients with NAFLD.

Dysfunction of Liver Sinusoidal Endothelial Cells Promotes Inflammation in Nonalcoholic Fatty Liver Disease

Endothelial dysfunction of LSECs is a pathological condition mainly characterized by an abnormal imbalance between vascular endothelium-derived relaxing factors and contracting factors, resulting in an inability to expand blood vessels when blood flow increase (Flammer et al., 2012). Much evidence suggest that endothelial dysfunction of LSECs promotes inflammation in NAFLD.

First, endothelial dysfunction of LSECs occurs earlier than liver inflammation in NAFLD (**Table 1**). Arterial endothelial dysfunction of LSECs was confirmed in patients with NAFLD, and the occurrence of sinusoidal endothelial dysfunction of LSECs was earlier than inflammation in various early stage NAFLD rodent models induced by diet, including cafeteria diet (CafD), HFD, and methionine-choline-deficient (MCD) diet, showing with a marked increased vascular resistance, or increased portal perfusion pressure and reduced endothelium-dependent vasodilatory response (Villanova et al., 2005; Tateya et al., 2011; Francque et al., 2012; Pasarin et al., 2012; Pourhoseini et al., 2015; Gonzalez-Paredes et al., 2016; Bravo et al., 2019). The dysfunction mechanism may be related to a decreased phosphorylation of Akt-dependent endothelial nitric oxide synthase (eNOS) and NO synthase activity, which reduces liver eNOS activity and NO content, respectively, and the consequence was occurred earlier than general liver inflammation in the rodent NAFLD model (Tateya et al., 2011; Pasarin et al., 2012; Gonzalez-Paredes et al., 2016; Bravo et al., 2019).

Second, endothelial dysfunction of LSECs promotes activation of KCs to facilitate the occurrence of inflammation in NAFLD (Lanthier, 2015). KCs are resident macrophages in liver sinusoids that are in close contact with LSECs and can be activated by various factors, including pathogen-associated molecular patterns such as lipopolysaccharide (LPS), damage-associated molecular patterns released by damaged hepatocytes, and lipids such as free fatty acids (FFAs), ceramides, and oxidized lipoproteins (Leroux et al., 2012; Sawada et al., 2014; Zannetti et al., 2016). In NASH patients, an expansion of KCs is an early phenomenon, earlier than the recruitment of other immune cells (Gadd et al., 2014). As a hepatic immune gatekeeper, LSEC maintains KCs quiescence under physiological conditions through NO-dependent pathways (Tateya et al., 2011). However, under pathological conditions, reduced endothelial NO bioavailability promotes the activation of KCs to cause liver inflammation manifested by activation of nuclear factor-κB and upregulation of pro-inflammatory factors TNF-α and IL-6 in mice (Tateya et al., 2011). The activated KCs promote the capillarization of LSECs and lead to subsequent leukocyte recruitment (Arii and Imamura, 2000; Ford et al., 2015; Shetty et al., 2018). Therefore, the dysfunction of LSECs promotes activation of KCs, which in turn contributes to the morphological changes and activation of LSECs, and this interaction leads to exacerbation of liver inflammatory response in the early stage of NAFLD. Certainly, ameliorating endothelial dysfunction of LSECs can improve liver inflammation in animal models by manipulating the NO signal pathway using sildenafil or simvastatin (Tateya et al., 2011; Wang et al., 2013; Ahsan et al., 2020).

Third, under pathological conditions, autophagy of LSECs is often abnormal. Autophagy, a major intracellular recycling system, maintains cellular homeostasis under basal conditions and acts as a survival mechanism under stress conditions (Hammoutene et al., 2020). Defect autophagy with smaller autophagic vacuoles in LSECs occurs in patients with NASH. The endothelial cell-specific loss of autophagy leads to a significant decrease in porosity and the number of fenestrae of LSECs in mice after mild acute liver injury and an increase in the expression of pro-inflammatory chemokines C-C motif chemokine ligand (CCL) 2, CCL5, and vascular cell adhesion molecule (VCAM-1), and thus promotes inflammation in mice fed with HFD (Ruart et al., 2019; Hammoutene et al., 2020). Interestingly, in different cell types, autophagy may play

differential roles in chronic liver diseases (Choi et al., 2013; Allaire et al., 2019). For example, in hepatocytes, autophagy helps to protect cells from fat accumulation and prevents liver damage by removing altered mitochondria and reducing intracellular stresses. In macrophages, it has anti-inflammatory effects and thus prevents liver inflammation and fibrosis. While in activated HSCs and LSECs, autophagy promotes liver disease progression (Berg et al., 2006; Hernandez-Gea et al., 2012; Lodder et al., 2015; Madrigal-Matute and Cuervo, 2016; Gual et al., 2017; Gracia-Sancho and Guixe-Muntet, 2018; Hammoutene et al., 2020). Therefore, the specific mechanism of autophagy abnormality in LSECs leading to capillarization and inflammation still needs more exploration.

The dysfunction of LSECs promotes steatosis by increasing intrahepatic vascular resistance, which is related to the formation of steatosis (Tateya et al., 2011; Francque et al., 2012; Gonzalez-Paredes et al., 2016; Baffy, 2018). NO plays an important role in regulating liver lipid content and fatty acid synthesis (Roediger et al., 2004; Schild et al., 2008; Tateya et al., 2011; Doulias et al., 2013). In NO-deficient eNOS knockout mice, large amounts of lipid droplets and elevated liver triglyceride levels were observed, while treatments with increasing the availability of NO improved not only liver inflammation but also liver steatosis (Schild et al., 2008; Tateya et al., 2011). However, steatosis, in turn, promotes the dysfunction of LSECs. The mechanism may be that excess lipids of steatosis decreased eNOS expression and thus reduced the bioavailability of NO (Pasarin et al., 2011; Pasarin et al., 2012; Pasarin et al., 2017). Besides, insulin resistance caused by steatosis can damage the vasodilation function of LSECs through the decrease of eNOS and the increase of inducible nitric oxide synthase (iNOS) (Chauhan et al., 2003; Pasarin et al., 2017).

Liver Sinusoidal Endothelial Cells Promote Inflammation by the Recruitment of BMMs and Neutrophils in Nonalcoholic Steatohepatitis

Recruited BMMs are an important component of chronic liver inflammation in NASH, where LSECs play a crucial role in the recruitment of BMMs (Koyama and Brenner, 2017). The dysfunction of LSECs facilitates the recruitment of macrophages in NASH through promoting KCs activation to release CCL2, which is the ligand of C-C motif chemokine receptor (CCR) two mainly expressed on monocytes and macrophages and thus is critical for the recruitment of macrophages (Tateya et al., 2011; Miura et al., 2012). Furthermore, LSECs also promote the recruitment of leukocytes, including but not limited to BMMs, directly by increasing the expression of adhesion molecules including intercellular adhesion molecule-1 (ICAM-1), VCAM-1, vascular adhesion protein-1 (VAP-1), E-selectin, and CD31, which are essential for the interaction between LSECs and leukocytes to recruit leukocytes (Edwards et al., 2005; Weston et al., 2015; Miyachi et al., 2017; Hammoutene and Rautou, 2019; Kus et al., 2019). In addition to this pro-inflammatory phenotype, LSECs produce pro-inflammatory mediators, including IL-1, IL-6, TNF-α, and CCL2, to promote activation of inflammatory cells and the recruitment, adhesion, and migration of BMMs and neutrophils in NASH (Miyachi et al., 2017; Roh and Seki, 2018; Hammoutene and Rautou, 2019).

Recent research shows that the recruitment of BMMs by LSECs is partly influenced by extracellular vesicle (EV) derived from hepatocytes. EV is a general term for membrane vesicles released by cells, it plays an important role in liver physiology and pathology, which has been reviewed well elsewhere (Hirsova et al., 2016b; Eguchi and Feldstein, 2018). In NASH, EVs released by hepatocytes under pressure stimulation contribute to the occurrence of liver inflammation by inducing pro-inflammatory cytokines expression and activating macrophage chemotaxis and thus promoting macrophages recruitment (Hirsova et al., 2016a; Garcia-Martinez et al., 2016; Ibrahim et al., 2016; Kakazu et al., 2016). Recently, Guo and colleagues found that integrin $\alpha_9\beta_1$-enriched EVs released by lysophosphatidylcholine-treated hepatocytes interact with monocytes in a topography and assist monocytes to adhere to LSECs *in vivo* and *in vitro* (Guo et al., 2019). However, the influence of other cell-derived EVs on LSECs and the effect of LSECs-derived EVs on macrophage recruitment in NASH require more researches.

Besides BMMs, neutrophil infiltration is also commonly observed in patients with NAFLD, and its severity is associated with the development of the disease (Nati et al., 2016; Cai et al., 2019). In the inflammatory state, neutrophils upregulate the expression of adhesion molecules and activate endothelial cells and KCs, which induce the further recruitment of other leukocytes including BMMs, where neutrophils are excessively activated and release proteases such as myeloperoxidase causing liver damage, and thus aggravate the ongoing inflammatory state (Arrese et al., 2016; Nati et al., 2016; Cai et al., 2019). In the inflamed hepatic sinusoids, highly coated hyaluronan on the luminal surface of LSECs interacts with CD44 on the surface of neutrophils and thus mediates the recruitment of neutrophils (McDonald et al., 2008). Unlike other vascular endothelial cells, LSEC anchoring hyaluronan does not depend on the endothelial CD44. Instead, LSECs capture the circulating hyaluronan through a variety of SRs such as stabilin-2 on the cell surface and then present it to the passing neutrophils before promoting the endocytosis of hyaluronan ultimately (McDonald and Kubes, 2015). Therefore, it is necessary to study the role of SRs on LSECs in LSECs-mediated leukocyte recruitment.

Anti-inflammatory Effects of Liver Sinusoidal Endothelial Cells in Nonalcoholic Fatty Liver Disease

Liver Sinusoidal Endothelial Cells Prevent Formation of Inflammation by Inhibiting Leukocyte Recruitment in the Early Stage of Nonalcoholic fatty liver disease

In the early stage of NAFLD models, evidence suggest that LSECs suppress leukocyte recruitment into hepatic sinusoids (McMahan et al., 2016). An anti-inflammatory phenotype of LSECs, characterized by decreased expressions of CCL2, C-X-C motif chemokine ligand (CXCL) 10, and CXCL16, was produced in both murine and human LSECs after a short time exposure to

TABLE 2 | Inflammation-targeted pharmacologic agents that have completed or are undergoing clinical trials for NASH.

Mechanism of action	Agent name	Company(s)	Trial phase	Primary endpoint(s)	Primary completion	Clinical trial ID
CCR2/5 inhibitor	Cenicriviroc	Allergan	3	1. Improvement in fibrosis without worsening steatohepatitis; 2. Long-term clinical outcomes	Oct 2021	NCT03028740
ASK1 inhibitor	Selonsertib	Gilead	3	1. Improvement in fibrosis without worsening of NASH; 2. Event-free survival	Jun 2019	NCT03053050
			3	1. Improvement in fibrosis without worsening of NASH; 2. Event-free survival	May 2019	NCT03053063
Pan-caspase inhibitor	Emricasan	Novartis/Conatus pharmaceuticals	2	Improvement in fibrosis without worsening of steatohepatitis	Jan 2019	NCT02686762
			2	Improvement in event-free survival based on a composite clinical endpoint	Aug 2019	NCT03205345
TLR-4 antagonist	JKB-121	TaiwanJ	2	Change from baseline in hepatic fat	Sept 2017	NCT02442687
	JKB-122	TaiwanJ	2	1. Reduction in NAS without worsening of fibrosis; 2. Improvement in fibrosis without worsening of NAS	Jun 2023	NCT04255069
Mineralocorticoid receptor antagonist	MT-3995	Mitsubishi tanabe pharma	2	Percent change from baseline in ALT	Mar 2018	NCT02923154
VAP-1 inhibitor	BI-1467335	Boehringer ingelheim	2	Target enzyme activity relative to baseline in percent	Jun 2019	NCT03166735
	TERN-201	Terns pharmaceuticals	1	Safety and tolerability		

ALT, alanine aminotransferase; ASK1, apoptosis signal-regulating kinase 1; CCR2/5, C-C motif chemokine receptor 2/5; NAS, non-alcoholic fatty liver disease activity score; NASH, non-alcoholic steatohepatitis; TLR-4, toll-like receptor-4; VAP-1, vascular adhesion protein-1.

FFA, and thus reduced the recruitment of pro-inflammatory monocytes. Primary LSECs isolated from obese mice also showed the consequence (McMahan et al., 2016). Further study demonstrated the anti-inflammatory ability produced by LSECs under FFA induction depends on the MAPK signaling pathway, which is important for the survival of LSECs in the case of lipid induction, and it also may be involved with signal transducer and activator of transcription 3 (STAT3) for its expression in LSECs alleviated mice liver inflammation induced by alcohol (Miller et al., 2010; Hang et al., 2012; McMahan et al., 2016).

Liver Sinusoidal Endothelial Cells Regulate Lymphocytes to Exert Anti-inflammatory Effects

LSECs regulate a behavior of lymphocytes under both physiological and pathological conditions (Poisson et al., 2017). Under physiological conditions, LSECs maintain the intrahepatic tolerance environment through inducing tolerant $CD8^+$ T cell and immunosuppressed regulatory T cells (Limmer et al., 2000; Carambia et al., 2014). While under inflammatory conditions, LSECs express high levels of Delta-like and Jagged family of Notch ligands and induce the expression of Notch target genes in Th1 cells, by which increases the expression of inflammatory cytokine IL-10 in Th1 cells to exert an anti-inflammatory effect (Neumann et al., 2015).

THERAPEUTIC PERSPECTIVES

Currently, no specific drug has been approved for clinical use to treat patients with NASH. There are many promising candidates in the drug development pipeline, and some have shown very useful for improving NASH by controlling inflammation in clinical trials (**Table 2**), such as dual CCR2/5 inhibitor, apoptosis signal-regulating kinase 1 (ASK1) inhibitor, and caspase inhibitor (Romero et al., 2020). Unfortunately, the latest clinic outcomes of selonsertib (an ASK1 inhibitor) and emricasan (a pan-caspase inhibitor) are not satisfied (Loomba et al., 2018; Harrison et al., 2020; Ratziu et al., 2020; Romero et al., 2020). Thus, it is still urgent and important to find new anti-inflammatory targets in NASH. Most encouragingly, the essential role of LSECs in liver inflammation provides new insights into the development of treatment strategies for NAFLD/NASH.

Targeting Adhesion-Related Molecules to Alleviate Inflammation in Nonalcoholic Steatohepatitis

Adhesion molecules are abnormally expressed on LSECs in response to liver injury and regulate inflammation via corresponding ligands. Therefore, adhesion molecules and their ligands related to LSECs are provided with multiple potential targets to control inflammation in NASH. The pro-inflammatory phenotype of LSECs showed increased expression of adhesion molecules including VAP-1, VCAM-1, CD31, ICAM-1, and E-selectin (Hammoutene and Rautou, 2019; Kus et al., 2019). Blocking these molecules or their ligands is efficacious to control inflammation in various NASH models (Edwards et al., 2005; Weston et al., 2015; Miyachi et al., 2017; Hammoutene and Rautou, 2019). In particular, VAP-1 inhibitors have entered clinical trials. However, unfortunately, a VAP-1 inhibitor BI 1467335 was recently discontinued for NASH indications due to its interaction with other drugs, although the results of the latest clinical studies (phase IIa, NCT03166735) did not indicate a direct failure of BI 1467335 in terms of efficacy and tolerance (Boehringer ingelheim, 2019). Another potent VAP-1 inhibitor, TERN-201, is still undergoing clinical trials in China for the treatment of NASH (Terns

Pharmaceuticals., 2019). Blocking the interaction between the adhesion molecule CD44 and its ligand hyaluronan using an anti-CD44 antibody also exhibits a potential inflammation-controlling effect both in LPS-induced or diet-induced mouse models, but further research is still needed in NASH (McDonald et al., 2008; Kodama et al., 2015; McDonald and Kubes, 2015).

Chemokines are chemo-attractants for leukocyte trafficking, growth, and activation in injured and inflammatory tissues (Roh and Seki, 2018). They are also abnormally expressed and secreted by LSECs under pathological conditions. The anti-inflammatory phenotype of LSECs showed decreased expression of chemokines including CXCL10, CXCL16, and CCL2 (McMahan et al., 2016). Hopefully, the dual CCR2/5 inhibitor cenicriviroc was well tolerated in NASH patients and is currently undergoing a phase III clinical trial (NCT03028740) (Ratziu et al., 2020).

Targeting Nitric Oxide Signaling to Improve Nonalcoholic fatty liver disease

LSECs are the major producers of NO in the liver (Shah et al., 1997). The balance of NO is critical in maintaining the morphology and endothelial function of LSECs to keep the quiescence of HSCs and KCs, it also fundamentally participates in the regulation of liver lipid and glucose homeostasis (Maslak et al., 2015a). Therefore, targeting NO-related signaling is an attractive therapeutic strategy to improve liver inflammation and alleviate liver damage. Some efforts to improve the bioavailability of NO in NAFLD have been made. V-PYRRO/NO, a stable hepato-selective NO-releasing prodrug, improved liver steatosis and postprandial glucose tolerance in NAFLD mice fed HFD (Maslak et al., 2015b). Praliciguat, a soluble guanylate cyclase stimulator, effectively reduced inflammation, fibrosis, and steatosis by enhancing NO signaling in preclinical NASH models (Hall et al., 2019). Besides, improvement of the NO/cGMP signaling pathway by using phosphodiesterase-5 inhibitor sildenafil or simvastatin prevented liver inflammation in NAFLD rodents fed HFD (Tateya et al., 2011; Wang et al., 2013; Ahsan et al., 2020).

Targeting Angiogenesis to Improve Nonalcoholic fatty liver disease

Hepatic angiogenesis, including the capillarization of LSECs, is an important event in the progression of NAFLD, especially in the formation of hepatic fibrosis (Coulon et al., 2011; Coulon et al., 2012; Coulon et al., 2013; Iwakiri et al., 2014). New blood vessels are produced in the liver of NASH patients, but not in individuals with simple steatosis or healthy liver (Kitade et al., 2008; Kitade et al., 2009; Lefere et al., 2019). In the serum of patients with NASH, the level of VEGF, a major pro-angiogenesis regulator, was increased significantly (Yoshiji et al., 2006; Coulon et al., 2011; Tamaki et al., 2013; Lefere et al., 2019). Evidence of abnormal angiogenesis was also found in animal models of NASH (Coulon et al., 2013).

A variety of anti-angiogenic therapies have shown anti-inflammatory effects in NASH animal models. Coulon and colleagues used specific antibodies to block vascular endothelial growth factor receptor 2 (VEGFR2) and found that liver inflammation and liver vasculature were significantly improved in the MCD-induced mouse NASH model, both in a preventive and therapeutic setting (Coulon et al., 2013). Studies have shown that serum level of angiopoietin-2, a key factor involved in regulating angiogenesis, is elevated in patients with NASH (Lefere et al., 2019). Inhibiting the interaction between angiopoietin-2 and its receptor Tie2 by using peptibody L1-10 effectively improved liver inflammation and damage in the NASH model induced by MCD (Lefere et al., 2019). It is worth noting that the therapeutic effect of L1-10, at least in part, is mediated by LSECs as evidenced by the downregulation of VCAM-1, ICAM-1, and CCL2 expression in liver endothelial cells isolated from the liver of NASH mouse (Lefere et al., 2019). Besides, LECT2, a functional ligand of endothelial cell-specific receptor Tie1, was recently found to promote liver fibrosis by inhibiting portal angiogenesis and promoting capillarization of liver sinusoids in various liver fibrosis models, providing a novel possible target for LSECs-mediated liver fibrosis (Xu et al., 2019). Therefore, studies on angiogenesis in the liver including capillarization of LSECs may provide new targets for NASH treatment.

Targeting Pro-inflammatory EVs Specifically to Improve Inflammation

Hepatocyte-derived EVs exert a regulatory ability in the recruitment of leukocytes to hepatic sinusoids. Therefore, blocking the production pathway of pro-inflammatory EVs or targeting pro-inflammatory cargos carried by EVs may improve liver inflammation in NASH, though the research in this area has only just begun (Hirsova et al., 2016a; Garcia-Martinez et al., 2016; Ibrahim et al., 2016; Kakazu et al., 2016; Guo et al., 2019). Using fasudil, an inhibitor of Rho-associated coiled coil-containing protein kinase one that is required for membrane blebbing, to reduce the serum levels of hepatocytes-derived EVs, or using anti-integrin $\alpha_9\beta_1$ antibody alleviated liver damage, inflammation, and fibrosis in diet-induced NASH model (Hirsova et al., 2016a; Guo et al., 2019). However, EVs are widely involved in human physiology, and their cargos play different roles in different environments. Therefore, how to achieve cell- or tissue-specific targeting of EVs will be the focus of future research.

Promoting Anti-inflammatory Behavior of Liver Sinusoidal Endothelial Cells to Improve Inflammation

As the recruiter of BMMs and neutrophils, LSECs also have compensatory anti-inflammatory behaviors. On the one hand, LSECs can resist the recruitment of leukocytes through the production of anti-inflammatory phenotype, which is mainly manifested as a decrease in the expression of chemokines (McMahan et al., 2016). Therefore, increasing the ratio of the anti-inflammatory phenotype to the pro-inflammatory phenotype of LSECs may be an effective strategy to improve inflammation. However, the mechanism still needs to be further

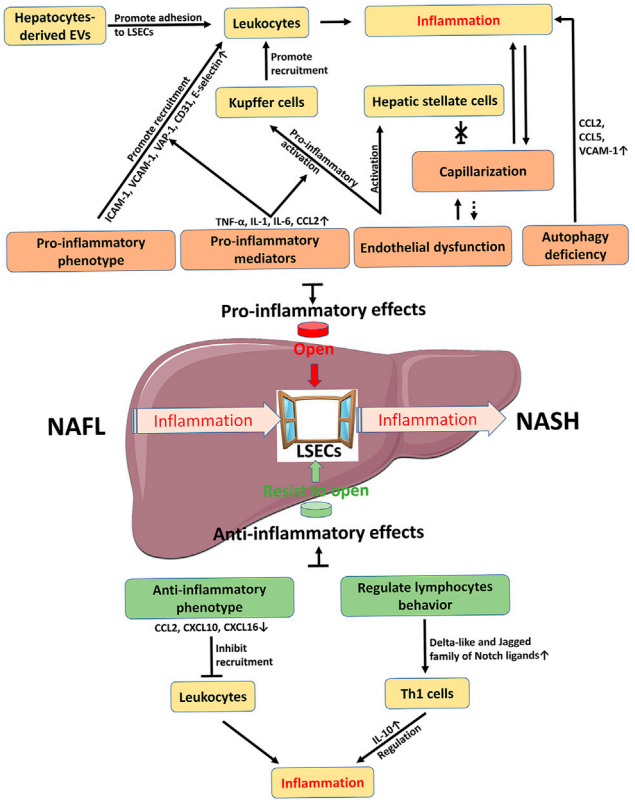

FIGURE 4 | Schematic summary on the role of LSECs in NAFLD inflammation. Inflammation is a key factor in the development of NAFL to NASH. LSEC as a window controls the occurrence and progression of inflammation. The pro-inflammatory effect of LSECs promotes the opening of the window, while the anti-inflammatory effect of LSECs acts as an opponent to prevent the passage of inflammation. Therefore, how to control the window provides new strategies for the R&D of novelty drugs against NAFLD/NASH. The dotted line is a possible relationship. *CCL* C-C motif chemokine ligand, *CXCL* C-X-C motif chemokine ligand, *EVs* extracellular vesicles, *ICAM-1* intercellular adhesion molecule-1, *IL* interleukin, *LSECs* liver sinusoidal endothelial cells, *NAFL,* nonalcoholic fatty liver, *NASH* nonalcoholic steatohepatitis, *TNF-α* tumor necrosis factor-α, *VAP-1* vascular adhesion protein-1, *VCAM-1* vascular cell adhesion molecule-1.

demonstrated that how LSECs switch their phenotype into anti-inflammatory phenotype during the occurrence and development of NAFLD inflammation. On the other hand, LSECs can drive lymphocytes to down-regulate inflammation. Under inflammatory conditions, LSECs release Notch ligands and thereby facilitate Th1 cells to secrete IL-10, an anti-inflammatory cytokine (Neumann et al., 2015). The clue indicates that effectively controlling the behavior of LSECs to indirectly regulate inflammation may be a potential research direction.

CONCLUSION

Under physiological conditions, LSECs have multiple functions due to their unique structure and anatomical position, including substance exchange and clearance, blood flow regulation, and immune regulation, and therefore LSECs contribute to the maintenance of liver homeostasis. In NAFLD, LSECs have dual roles in inflammation (**Figures 2**, **4**). On one hand, LSECs block the occurrence of inflammation by generating anti-inflammatory phenotype and regulating lymphocyte behavior. On the other hand, LSECs show pro-inflammatory effects including promoting the activation of KCs and the recruitment of leukocytes. The detailed mechanisms are involved with multiple alterations of LSECs, including morphology and endothelial function, paracrine and autocrine signals, hepatocyte-derived EVs, and autophagy abnormalities. Accordingly, changing these abnormalities of LSECs with new drug candidates is an attractive therapeutic strategy to control inflammation in NAFLD/NASH by regulating LSECs via several variable factors, including adhesion molecules and chemokines expressed by LSECs, capillarization and endothelial dysfunction of LSECs, and other regulatory factors such as EVs. However, the current challenge in this research area is still to clarify the mechanism of LSEC alteration in NAFLD and to further validate the clinical efficacy with those drug candidates specifically targeted to LSEC-related molecules.

AUTHOR CONTRIBUTIONS

Both authors listed wrote the manuscript, edited the document, and approved it for publication.

FUNDING

This work was supported by CAMS Innovation Fund for Medical Sciences (grant number 2017-I2M-3-012); National Mega-Project for "R&D for Innovative drugs", Ministry of Science and Technology, China (grant number 2018ZX09711001-003-010).

REFERENCES

Adachi, H., and Tsujimoto, M. (2002). FEEL-1, a novel scavenger receptor with *in vitro* bacteria-binding and angiogenesis-modulating activities. *J. Biol. Chem.* 277 (37), 34264–34270. doi:10.1074/jbc.M204277200

Adams, D. H., Hubscher, S. G., Fisher, N. C., Williams, A., and Robinson, M. (1996). Expression of E-selectin and E-selectin ligands in human liver inflammation. *Hepatol.* 24 (3), 533–538. doi:10.1002/hep.510240311

Ahsan, F., Oliveri, F., Goud, H. K., Mehkari, Z., Mohammed, L., Javed, M., et al. (2020). Pleiotropic effects of statins in the light of non-alcoholic fatty liver disease and non-alcoholic steatohepatitis. *Cureus* 12 (9), e10446. doi:10.7759/cureus.10446

Akyol, G., Erdem, O., and Yilmaz, G. (2005). Nonalcoholic fatty liver disease. Correlation with histology and viral hepatitis. *Saudi Med. J.* 26 (12), 1904–1910.

Allaire, M., Rautou, P.-E., Codogno, P., and Lotersztajn, S. (2019). Autophagy in liver diseases: time for translation?. *J. Hepatol.* 70 (5), 985–998. doi:10.1016/j.jhep.2019.01.026

Arii, S., and Imamura, M. (2000). Physiological role of sinusoidal endothelial cells and Kupffer cells and their implication in the pathogenesis of liver injury. *J. Hepato-Biliary-Pancreatic Surg.* 7 (1), 40–48. doi:10.1007/s005340050152

Arrese, M., Cabrera, D., Kalergis, A. M., and Feldstein, A. E. (2016). Innate immunity and inflammation in NAFLD/NASH. *Dig. Dis. Sci.* 61 (5), 1294–1303. doi:10.1007/s10620-016-4049-x

Arteta, B., Lasuen, N., Lopategi, A., Sveinbjörnsson, B., Smedsrød, B., and Vidal-Vanaclocha, F. (2010). Colon carcinoma cell interaction with liver sinusoidal endothelium inhibits organ-specific antitumor immunity through interleukin-1-induced mannose receptor in mice. *Hepatol.* 51 (6), 2172–2182. doi:10.1002/hep.23590

Baffy, G. (2018). Origins of portal hypertension in nonalcoholic fatty liver disease. *Dig. Dis. Sci.* 63 (3), 563–576. doi:10.1007/s10620-017-4903-5

Baiocchini, A., Del Nonno, F., Taibi, C., Visco-Comandini, U., D'Offizi, G., Piacentini, M., et al. (2019). Liver sinusoidal endothelial cells (LSECs) modifications in patients with chronic hepatitis C. *Sci. Rep.* 9 (1), 8760. doi:10.1038/s41598-019-45114-1

Berg, M., Wingender, G., Djandji, D., Hegenbarth, S., Momburg, F., Hämmerling, G., et al. (2006). Cross-presentation of antigens from apoptotic tumor cells by liver sinusoidal endothelial cells leads to tumor-specific CD8+ T cell tolerance. *Eur. J. Immunol.* 36 (11), 2960–2970. doi:10.1002/eji.200636033

Bravo, M., Raurell, I., Hide, D., Fernández-Iglesias, A., Gil, M., Barberá, A., et al. (2019). Restoration of liver sinusoidal cell phenotypes by statins improves portal hypertension and histology in rats with NASH. *Sci. Rep.* 9 (1), 20183. doi:10.1038/s41598-019-56366-2

Brenner, C., Galluzzi, L., Kepp, O., and Kroemer, G. (2013). Decoding cell death signals in liver inflammation. *J. Hepatol.* 59 (3), 583–594. doi:10.1016/j.jhep.2013.03.033

Brunt, E. M., Gouw, A. S. H., Hubscher, S. G., Tiniakos, D. G., Bedossa, P., Burt, A. D., et al. (2014). Pathology of the liver sinusoids. *Histopathology* 64 (7), 907–920. doi:10.1111/his.12364

Boehringer ingelheim (2019). *Boehringer Ingelheim discontinues development of BI 1467335 for NASH* Available at: http://www.pharmaxis.com.au/investor-centre/news/view/boehringer-ingelheim-discontinues-development-of-bi-1467335-for-nash (Accessed Dec 18, 2019).

Burgdorf, S., Kautz, A., Bohnert, V., Knolle, P. A., and Kurts, C. (2007). Distinct pathways of antigen uptake and intracellular routing in CD4 and CD8 T cell activation. *Science* 316 (5824), 612–616. doi:10.1126/science.1137971

Cai, J., Zhang, X. J., and Li, H. (2019). The role of innate immune cells in nonalcoholic steatohepatitis. *Hepatol.* 70 (3), 1026–1037. doi:10.1002/hep.30506

Campbell, J. J., Hedrick, J., Zlotnik, A., Siani, M. A., Thompson, D. A., and Butcher, E. C. (1998). Chemokines and the arrest of lymphocytes rolling under flow conditions. *Science* 279 (5349), 381–384. doi:10.1126/science.279.5349.381

Canton, J., Neculai, D., and Grinstein, S. (2013). Scavenger receptors in homeostasis and immunity. *Nat. Rev. Immunol.* 13 (9), 621–634. doi:10.1038/nri3515

Carambia, A., Freund, B., Schwinge, D., Heine, M., Laschtowitz, A., Huber, S., et al. (2014). TGF-β-dependent induction of CD4+CD25+Foxp3+ Tregs by liver sinusoidal endothelial cells. *J. Hepatol.* 61 (3), 594–599. doi:10.1016/j.jhep.2014.04.027

Carpenter, B., Lin, Y., Stoll, S., Raffai, R. L., McCuskey, R., and Wang, R. (2005). VEGF is crucial for the hepatic vascular development required for lipoprotein uptake. *Development* 132 (14), 3293–3303. doi:10.1242/dev.01902

Chauhan, S. D., Seggara, G., Vo, P. A., Macallister, R. J., Hobbs, A. J., and Ahluwalia, A. (2003). Protection against lipopolysaccharide-induced endothelial dysfunction in resistance and conduit vasculature of iNOS knockout mice. *FASEB j.* 17 (6), 773–775. doi:10.1096/fj.02-0668fje

Chen, G. Y., and Nuñez, G. (2010). Sterile inflammation: sensing and reacting to damage. *Nat. Rev. Immunol.* 10 (12), 826–837. doi:10.1038/nri2873

Chen, L., Gu, T., Li, B., Li, F., Ma, Z., Zhang, Q., et al. (2019). Delta-like ligand 4/DLL4 regulates the capillarization of liver sinusoidal endothelial cell and liver fibrogenesis. *Biochim. Biophys. Acta (Bba) - Mol. Cel Res.* 1866 (10), 1663–1675. doi:10.1016/j.bbamcr.2019.06.011

Chiu, J.-J., and Chien, S. (2011). Effects of disturbed flow on vascular endothelium: pathophysiological basis and clinical perspectives. *Physiol. Rev.* 91 (1), 327–387. doi:10.1152/physrev.00047.2009

Choi, A. M., Ryter, S. W., and Levine, B. (2013). Autophagy in human health and disease. *N. Engl. J. Med.* 368 (19), 1845–1846. doi:10.1056/nejmc1303158

Cogger, V. C., Hilmer, S. N., Sullivan, D., Muller, M., Fraser, R., and Le Couteur, D. G. (2006). Hyperlipidemia and surfactants: the liver sieve is a link. *Atherosclerosis* 189 (2), 273–281. doi:10.1016/j.atherosclerosis.2005.12.025

Cogger, V. C., Mohamad, M., Solon-Biet, S. M., Senior, A. M., Warren, A., O'Reilly, J. N., et al. (2016). Dietary macronutrients and the aging liver sinusoidal endothelial cell. *Am. J. Physiology-Heart Circulatory Physiol.* 310 (9), H1064–H1070. doi:10.1152/ajpheart.00949.2015

Coulon, S., Francque, S., Colle, I., Verrijken, A., Blomme, B., Heindryckx, F., et al. (2012). Evaluation of inflammatory and angiogenic factors in patients with non-alcoholic fatty liver disease. *Cytokine* 59 (2), 442–449. doi:10.1016/j.cyto.2012.05.001

Coulon, S., Heindryckx, F., Geerts, A., Van Steenkiste, C., Colle, I., and Van Vlierberghe, H. (2011). Angiogenesis in chronic liver disease and its complications. *Liver Int.* 31 (2), 146–162. doi:10.1111/j.1478-3231.2010.02369.x

Coulon, S., Legry, V., Heindryckx, F., Van Steenkiste, C., Casteleyn, C., Olievier, K., et al. (2013). Role of vascular endothelial growth factor in the pathophysiology of nonalcoholic steatohepatitis in two rodent models. *Hepatol.* 57 (5), 1793–1805. doi:10.1002/hep.26219

Davies, P. F. (1995). Flow-mediated endothelial mechanotransduction. *Physiol. Rev.* 75 (3), 519–560. doi:10.1152/physrev.1995.75.3.519

DeLeve, L. D. (2015). Liver sinusoidal endothelial cells in hepatic fibrosis. *Hepatol.* 61 (5), 1740–1746. doi:10.1002/hep.27376

Deleve, L. D., Wang, X., and Guo, Y. (2008). Sinusoidal endothelial cells prevent rat stellate cell activation and promote reversion to quiescence. *Hepatol.* 48 (3), 920–930. doi:10.1002/hep.22351

DeLeve, L. D., Wang, X., Hu, L., McCuskey, M. K., and McCuskey, R. S. (2004). Rat liver sinusoidal endothelial cell phenotype is maintained by paracrine and autocrine regulation. *Am. J. Physiology-Gastrointestinal Liver Physiol.* 287 (4), G757–G763. doi:10.1152/ajpgi.00017.2004

Desroches-Castan, A., Tillet, E., Ricard, N., Ouarné, M., Mallet, C., Belmudes, L., et al. (2019). Bone morphogenetic protein 9 is a paracrine factor controlling liver sinusoidal endothelial cell fenestration and protecting against hepatic fibrosis. *Hepatol.* 70 (4), 1392–1408. doi:10.1002/hep.30655

Diehl, L., Schurich, A., Grochtmann, R., Hegenbarth, S., Chen, L., and Knolle, P. A. (2008). Tolerogenic maturation of liver sinusoidal endothelial cells promotes B7-homolog 1-dependent CD8+ T cell tolerance. *Hepatol.* 47 (1), 296–305. doi:10.1002/hep.21965

Doulias, P.-T., Tenopoulou, M., Greene, J. L., Raju, K., and Ischiropoulos, H. (2013). Nitric oxide regulates mitochondrial fatty acid metabolism through reversible protein S-nitrosylation. *Sci. Signaling* 6 (256), rs1. doi:10.1126/scisignal.2003252

Edwards, S., Lalor, P. F., Nash, G. B., Rainger, G. E., and Adams, D. H. (2005). Lymphocyte traffic through sinusoidal endothelial cells is regulated by hepatocytes. *Hepatol.* 41 (3), 451–459. doi:10.1002/hep.20585

Eguchi, A., and Feldstein, A. E. (2018). Extracellular vesicles in non-alcoholic and alcoholic fatty liver diseases. *Liver Res.* 2 (1), 30–34. doi:10.1016/j.livres.2018.01.001

Eslam, M., Sanyal, A. J., George, J., Sanyal, A., Neuschwander-Tetri, B., Tiribelli, C., et al. (2020). MAFLD: a consensus-driven proposed nomenclature for metabolic associated fatty liver disease. *Gastroenterol.* 158 (7), 1999–2014. doi:10.1053/j.gastro.2019.11.312

Estes, C., Razavi, H., Loomba, R., Younossi, Z., and Sanyal, A. J. (2018). Modeling the epidemic of nonalcoholic fatty liver disease demonstrates an exponential increase in burden of disease. *Hepatol.* 67 (1), 123–133. doi:10.1002/hep.29466

Fernandez, M. (2015). Molecular pathophysiology of portal hypertension. *Hepatol.* 61 (4), 1406–1415. doi:10.1002/hep.27343

Flammer, A. J., Anderson, T., Celermajer, D. S., Creager, M. A., Deanfield, J., Ganz, P., et al. (2012). The assessment of endothelial function. *Circulation* 126 (6), 753–767. doi:10.1161/circulationaha.112.093245

Ford, A. J., Jain, G., and Rajagopalan, P. (2015). Designing a fibrotic microenvironment to investigate changes in human liver sinusoidal endothelial cell function. *Acta Biomater.* 24, 220–227. doi:10.1016/j.actbio.2015.06.028

Francque, S., Laleman, W., Verbeke, L., Van Steenkiste, C., Casteleyn, C., Kwanten, W., et al. (2012). Increased intrahepatic resistance in severe steatosis: endothelial dysfunction, vasoconstrictor overproduction and altered microvascular architecture. *Lab. Invest.* 92 (10), 1428–1439. doi:10.1038/labinvest.2012.103

Friedman, S. L., Neuschwander-Tetri, B. A., Rinella, M., and Sanyal, A. J. (2018). Mechanisms of NAFLD development and therapeutic strategies. *Nat. Med.* 24 (7), 908–922. doi:10.1038/s41591-018-0104-9

Gadd, V. L., Skoien, R., Powell, E. E., Fagan, K. J., Winterford, C., Horsfall, L., et al. (2014). The portal inflammatory infiltrate and ductular reaction in human nonalcoholic fatty liver disease. *Hepatol.* 59 (4), 1393–1405. doi:10.1002/hep.26937

Garcia-Martinez, I., Santoro, N., Chen, Y., Hoque, R., Ouyang, X., Caprio, S., et al. (2016). Hepatocyte mitochondrial DNA drives nonalcoholic steatohepatitis by activation of TLR9. *J. Clin. Invest.* 126 (3), 859–864. doi:10.1172/JCI83885

Géraud, C., Koch, P.-S., Zierow, J., Klapproth, K., Busch, K., Olsavszky, V., et al. (2017). GATA4-dependent organ-specific endothelial differentiation controls liver development and embryonic hematopoiesis. *J. Clin. Invest.* 127 (3), 1099–1114. doi:10.1172/JCI90086

Gonzalez-Paredes, F. J., Hernández Mesa, G., Morales Arraez, D., Marcelino Reyes, R., Abrante, B., Diaz-Flores, F., et al. (2016). Contribution of cyclooxygenase end products and oxidative stress to intrahepatic endothelial dysfunction in early non-alcoholic fatty liver disease. *PLoS One* 11 (5), e0156650, doi:10.1371/journal.pone.0156650

Gouysse, G., Couvelard, A., Frachon, S., Bouvier, R., Nejjari, M., Dauge, M.-C., et al. (2002). Relationship between vascular development and vascular differentiation during liver organogenesis in humans. *J. Hepatol.* 37 (6), 730–740. doi:10.1016/s0168-8278(02)00282-9

Gracia-Sancho, J., and Guixé-Muntet, S. (2018). The many-faced role of autophagy in liver diseases. *J. Hepatol.* 68 (3), 593–594. doi:10.1016/j.jhep.2017.09.015

Gual, P., Gilgenkrantz, H., and Lotersztajn, S. (2017). Autophagy in chronic liver diseases: the two faces of Janus. *Am. J. Physiology-Cell Physiol.* 312 (3), C263–C273. doi:10.1152/ajpcell.00295.2016

Guo, Q., Furuta, K., Lucien, F., Gutierrez Sanchez, L. H., Hirsova, P., Krishnan, A., et al. (2019). Integrin β1-enriched extracellular vesicles mediate monocyte adhesion and promote liver inflammation in murine NASH. *J. Hepatol.* 71 (6), 1193–1205. doi:10.1016/j.jhep.2019.07.019

Hall, K. C., Bernier, S. G., Jacobson, S., Liu, G., Zhang, P. Y., Sarno, R., et al. (2019). sGC stimulator praliciguat suppresses stellate cell fibrotic transformation and inhibits fibrosis and inflammation in models of NASH. *Proc. Natl. Acad. Sci. USA* 116 (22), 11057–11062. doi:10.1073/pnas.1821045116

Hammoutene, A., Biquard, L., Lasselin, J., Kheloufi, M., Tanguy, M., Vion, A.-C., et al. (2020). A defect in endothelial autophagy occurs in patients with non-alcoholic steatohepatitis and promotes inflammation and fibrosis. *J. Hepatol.* 72 (3), 528–538. doi:10.1016/j.jhep.2019.10.028

Hammoutene, A., and Rautou, P.-E. (2019). Role of liver sinusoidal endothelial cells in non-alcoholic fatty liver disease. *J. Hepatol.* 70 (6), 1278–1291. doi:10.1016/j.jhep.2019.02.012

Hang, T.-C., Lauffenburger, D. A., Griffith, L. G., and Stolz, D. B. (2012). Lipids promote survival, proliferation, and maintenance of differentiation of rat liver sinusoidal endothelial cells *in vitro*. *Am. J. Physiology-Gastrointestinal Liver Physiol.* 302 (3), G375–G388. doi:10.1152/ajpgi.00288.2011

Hansen, B., Longati, P., Elvevold, K., Nedredal, G., Schledzewski, K., Olsen, R., et al. (2005). Stabilin-1 and stabilin-2 are both directed into the early endocytic pathway in hepatic sinusoidal endothelium via interactions with clathrin/AP-2, independent of ligand binding. *Exp. Cel Res.* 303 (1), 160–173. doi:10.1016/j.yexcr.2004.09.017

Harrison, S. A., Goodman, Z., Jabbar, A., Vemulapalli, R., Younes, Z. H., Freilich, B., et al. (2020). A randomized, placebo-controlled trial of emricasan in patients with NASH and F1-F3 fibrosis. *J. Hepatol.* 72 (5), 816–827. doi:10.1016/j.jhep.2019.11.024

Hebert, L. A. (1991). The clearance of immune complexes from the circulation of man and other primates. *Am. J. Kidney Dis.* 17 (3), 352–361. doi:10.1016/s0272-6386(12)80488-4

Hernández-Gea, V., Ghiassi-Nejad, Z., Rozenfeld, R., Gordon, R., Fiel, M. I., Yue, Z., et al. (2012). Autophagy releases lipid that promotes fibrogenesis by activated hepatic stellate cells in mice and in human tissues. *Gastroenterol.* 142 (4), 938–946. doi:10.1053/j.gastro.2011.12.044

Herrnberger, L., Hennig, R., Kremer, W., Hellerbrand, C., Goepferich, A., Kalbitzer, H. R., et al. (2014). Formation of fenestrae in murine liver sinusoids depends on plasmalemma vesicle-associated protein and is required for lipoprotein passage. *PLoS One* 9 (12), e115005, doi:10.1371/journal.pone.0115005

Hilmer, S. N., Cogger, V. C., Fraser, R., McLean, A. J., Sullivan, D., and Le Couteur, D. G. (2005). Age-related changes in the hepatic sinusoidal endothelium impede lipoprotein transfer in the rat. *Hepatol.* 42 (6), 1349–1354. doi:10.1002/hep.20937

Hirsova, P., Ibrahim, S. H., Krishnan, A., Verma, V. K., Bronk, S. F., Werneburg, N. W., et al. (2016a). Lipid-induced signaling causes release of inflammatory extracellular vesicles from hepatocytes. *Gastroenterol.* 150 (4), 956–967. doi:10.1053/j.gastro.2015.12.037

Hirsova, P., Ibrahim, S. H., Verma, V. K., Morton, L. A., Shah, V. H., LaRusso, N. F., et al. (2016b). Extracellular vesicles in liver pathobiology: small particles with big impact. *Hepatol.* 64 (6), 2219–2233. doi:10.1002/hep.28814

Horn, T., Christoffersen, P., and Henriksen, J. H. (1987). Alcoholic liver injury: defenestration in noncirrhotic livers-a scanning electron microscopic study. *Hepatol.* 7 (1), 77–82. doi:10.1002/hep.1840070117

Hughes, D. A., Fraser, I. P., and Gordon, S. (1995). Murine macrophage scavenger receptor:*in vivo* expression and function as receptor for macrophage adhesion in lymphoid and non-lymphoid organs. *Eur. J. Immunol.* 25 (2), 466–473. doi:10.1002/eji.1830250224

Hunt, N. J., Kang, S. W., Lockwood, G. P., Le Couteur, D. G., and Cogger, V. C. (2019). Hallmarks of aging in the liver. *Comput. Struct. Biotechnol. J.* 17, 1151–1161. doi:10.1016/j.csbj.2019.07.021

Ibrahim, S. H., Hirsova, P., Tomita, K., Bronk, S. F., Werneburg, N. W., Harrison, S. A., et al. (2016). Mixed lineage kinase 3 mediates release of C-X-C motif ligand 10-bearing chemotactic extracellular vesicles from lipotoxic hepatocytes. *Hepatol.* 63 (3), 731–744. doi:10.1002/hep.28252

Iwakiri, Y., Shah, V., and Rockey, D. C. (2014). Vascular pathobiology in chronic liver disease and cirrhosis - current status and future directions. *J. Hepatol.* 61 (4), 912–924. doi:10.1016/j.jhep.2014.05.047

Johansson, A. G., Lövdal, T., Magnusson, K., Berg, T., and Skogh, T. (1996). Liver cell uptake and degradation of soluble immunoglobulin G immune complexesin vivoandin vitroin rats. *Hepatol.* 24 (1), 169–175. doi:10.1002/hep.510240128

John, M., Kim, K.-J., Bae, S. D. W., Qiao, L., and George, J. (2019). Role of BMP-9 in human liver disease. *Gut* 68 (11), 2097–2100. doi:10.1136/gutjnl-2018-317543

Kakazu, E., Mauer, A. S., Yin, M., and Malhi, H. (2016). Hepatocytes release ceramide-enriched pro-inflammatory extracellular vesicles in an IRE1α-dependent manner. *J. Lipid Res.* 57 (2), 233–245. doi:10.1194/jlr.M063412

Kitade, M., Yoshiji, H., Kojima, H., Ikenaka, Y., Noguchi, R., Kaji, K., et al. (2008). Neovascularization and oxidative stress in the progression of non-alcoholic steatohepatitis. *Mol. Med. Rep.* 1 (4), 543–548. doi:10.3892/mmr.1.4.543

Kitade, M., Yoshiji, H., Noguchi, R., Ikenaka, Y., Kaji, K., Shirai, Y., et al. (2009). Crosstalk between angiogenesis, cytokeratin-18, and insulinresistance in the progression of non-alcoholic steatohepatitis. *Wjg* 15 (41), 5193–5199. doi:10.3748/wjg.15.5193

Knolle, P. A., Uhrig, A., Hegenbarth, S., LÖser, E., Schmitt, E., Gerken, G., et al. (1998). IL-10 down-regulates T cell activation by antigen-presenting liver sinusoidal endothelial cells through decreased antigen uptake via the mannose receptor and lowered surface expression of accessory molecules. *Clin. Exp. Immunol.* 114 (3), 427–433. doi:10.1046/j.1365-2249.1998.00713.x

Knolle, P., Schmitt, E., Jin, S., Germann, T., Duchmann, R., Hegenbarth, S., et al. (1999). Induction of cytokine production in naive CD4+ T cells by antigen-presenting murine liver sinusoidal endothelial cells but failure to induce differentiation toward Th1 cells. *Gastroenterol.* 116 (6), 1428–1440. doi:10.1016/s0016-5085(99)70508-1

Kodama, K., Toda, K., Morinaga, S., Yamada, S., and Butte, A. J. (2015). Anti-CD44 antibody treatment lowers hyperglycemia and improves insulin resistance, adipose inflammation, and hepatic steatosis in diet-induced obese mice. *Diabetes* 64 (3), 867–875. doi:10.2337/db14-0149

Koyama, Y., and Brenner, D. A. (2017). Liver inflammation and fibrosis. *J. Clin. Invest.* 127 (1), 55–64. doi:10.1172/JCI88881

Kubes, P., and Jenne, C. (2018). Immune responses in the liver. *Annu. Rev. Immunol.* 36, 247–277. doi:10.1146/annurev-immunol-051116-052415

Kus, E., Kaczara, P., Czyzynska-Cichon, I., Szafranska, K., Zapotoczny, B., Kij, A., et al. (2019). LSEC fenestrae are preserved despite pro-inflammatory phenotype of liver sinusoidal endothelial cells in mice on high fat diet. *Front. Physiol.* 10, 6. doi:10.3389/fphys.2019.00006

Lanthier, N. (2015). Targeting Kupffer cells in non-alcoholic fatty liver disease/non-alcoholic steatohepatitis: why and how?. *Wjh* 7 (19), 2184–2188. doi:10.4254/wjh.v7.i19.2184

Lee, S. J., Evers, S., Roeder, D., Parlow, A. F., Risteli, J., Risteli, L., et al. (2002). Mannose receptor-mediated regulation of serum glycoprotein homeostasis. *Science* 295 (5561), 1898–1901. doi:10.1126/science.1069540

Lefere, S., Van de Velde, F., Hoorens, A., Raevens, S., Van Campenhout, S., Vandierendonck, A., et al. (2019). Angiopoietin-2 promotes pathological angiogenesis and is a therapeutic target in murine nonalcoholic fatty liver disease. *Hepatol.* 69 (3), 1087–1104. doi:10.1002/hep.30294

Leroux, A., Ferrere, G., Godie, V., Cailleux, F., Renoud, M.-L., Gaudin, F., et al. (2012). Toxic lipids stored by Kupffer cells correlates with their pro-inflammatory phenotype at an early stage of steatohepatitis. *J. Hepatol.* 57 (1), 141–149. doi:10.1016/j.jhep.2012.02.028

Limmer, A., Ohl, J., Kurts, C., Ljunggren, H.-G., Reiss, Y., Groettrup, M., et al. (2000). Efficient presentation of exogenous antigen by liver endothelial cells to CD8+ T cells results in antigen-specific T-cell tolerance. *Nat. Med.* 6 (12), 1348–1354. doi:10.1038/82161

Limmer, A., Ohl, J., Wingender, G., Berg, M., Jüngerkes, F., Schumak, B., et al. (2005). Cross-presentation of oral antigens by liver sinusoidal endothelial cells leads to CD8 T cell tolerance. *Eur. J. Immunol.* 35 (10), 2970–2981. doi:10.1002/eji.200526034

Lodder, J., Denaës, T., Chobert, M.-N., Wan, J., El-Benna, J., Pawlotsky, J.-M., et al. (2015). Macrophage autophagy protects against liver fibrosis in mice. *Autophagy* 11 (8), 1280–1292. doi:10.1080/15548627.2015.1058473

Loomba, R., Lawitz, E., Mantry, P. S., Jayakumar, S., Caldwell, S. H., Arnold, H., et al. (2018). The ASK1 inhibitor selonsertib in patients with nonalcoholic steatohepatitis: a randomized, phase 2 trial. *Hepatol.* 67 (2), 549–559. doi:10.1002/hep.29514

Madrigal-Matute, J., and Cuervo, A. M. (2016). Regulation of liver metabolism by autophagy. *Gastroenterol.* 150 (2), 328–339. doi:10.1053/j.gastro.2015.09.042

Malerød, L., Juvet, L., Gjøen, T., and Berg, T. (2002). The expression of scavenger receptor class B, type I (SR-BI) and caveolin-1 in parenchymal and nonparenchymal liver cells. *Cell Tissue Res.* 307 (2), 173–180. doi:10.1007/s00441-001-0476-9

Maslak, E., Gregorius, A., and Chlopicki, S. (2015a). Liver sinusoidal endothelial cells (LSECs) function and NAFLD; NO-based therapy targeted to the liver. *Pharmacol. Rep.* 67 (4), 689–694. doi:10.1016/j.pharep.2015.04.010

Maslak, E., Zabielski, P., Kochan, K., Kus, K., Jasztal, A., Sitek, B., et al. (2015b). The liver-selective NO donor, V-PYRRO/NO, protects against liver steatosis and improves postprandial glucose tolerance in mice fed high fat diet. *Biochem. Pharmacol.* 93 (3), 389–400. doi:10.1016/j.bcp.2014.12.004

McCourt, P. A. G., Smedsrød, B. H., Melkko, J., and Johansson, S. (1999). Characterization of a hyaluronan receptor on rat sinusoidal liver endothelial cells and its functional relationship to scavenger receptors. *Hepatol.* 30 (5), 1276–1286. doi:10.1002/hep.510300521

McDonald, B., and Kubes, P. (2015). Interactions between CD44 and hyaluronan in leukocyte trafficking. *Front. Immunol.* 6, 68. doi:10.3389/fimmu.2015.00068

McDonald, B., McAvoy, E. F., Lam, F., Gill, V., de la Motte, C., Savani, R. C., et al. (2008). Interaction of CD44 and hyaluronan is the dominant mechanism for neutrophil sequestration in inflamed liver sinusoids. *J. Exp. Med.* 205 (4), 915–927. doi:10.1084/jem.20071765

McEver, R. P. (2015). Selectins: initiators of leucocyte adhesion and signalling at the vascular wall. *Cardiovasc. Res.* 107 (3), 331–339. doi:10.1093/cvr/cvv154

McGreal, E., Martinezpomares, L., and Gordon, S. (2004). Divergent roles for C-type lectins expressed by cells of the innate immune system. *Mol. Immunol.* 41 (11), 1109–1121. doi:10.1016/j.molimm.2004.06.013

McMahan, R. H., Porsche, C. E., Edwards, M. G., and Rosen, H. R. (2016). Free fatty acids differentially downregulate chemokines in liver sinusoidal endothelial cells: insights into non-alcoholic fatty liver disease. *PLoS One* 11 (7), e0159217, doi:10.1371/journal.pone.0159217

Miller, A. M., Wang, H., Park, O., Horiguchi, N., Lafdil, F., Mukhopadhyay, P., et al. (2010). Anti-inflammatory and anti-apoptotic roles of endothelial cell STAT3 in alcoholic liver injury. *Alcohol. Clin. Exp. Res.* 34 (4), 719–725. doi:10.1111/j.1530-0277.2009.01141.x

Miura, K., Yang, L., van Rooijen, N., Ohnishi, H., and Seki, E. (2012). Hepatic recruitment of macrophages promotes nonalcoholic steatohepatitis through CCR2. *Am. J. Physiology-Gastrointestinal Liver Physiol.* 302 (11), G1310–G1321. doi:10.1152/ajpgi.00365.2011

Miyachi, Y., Tsuchiya, K., Komiya, C., Shiba, K., Shimazu, N., Yamaguchi, S., et al. (2017). Roles for cell-cell adhesion and contact in obesity-induced hepatic myeloid cell accumulation and glucose intolerance. *Cel Rep.* 18 (11), 2766–2779. doi:10.1016/j.celrep.2017.02.039

Miyao, M., Kotani, H., Ishida, T., Kawai, C., Manabe, S., Abiru, H., et al. (2015). Pivotal role of liver sinusoidal endothelial cells in NAFLD/NASH progression. *Lab. Invest.* 95 (10), 1130–1144. doi:10.1038/labinvest.2015.95

Mönkemöller, V., Øie, C., Hübner, W., Huser, T., and McCourt, P. (2015). Multimodal super-resolution optical microscopy visualizes the close connection between membrane and the cytoskeleton in liver sinusoidal endothelial cell fenestrations. *Sci. Rep.* 5, 16279. doi:10.1038/srep16279

Mousavi, S. A., Sporstøl, M., Fladeby, C., Kjeken, R., Barois, N., and Berg, T. (2007). Receptor-mediated endocytosis of immune complexes in rat liver sinusoidal endothelial cells is mediated by FcγRIIb2. *Hepatol.* 46 (3), 871–884. doi:10.1002/hep.21748

Muller, W. A. (2016). Transendothelial migration: unifying principles from the endothelial perspective. *Immunol. Rev.* 273 (1), 61–75. doi:10.1111/imr.12443

Nati, M., Haddad, D., Birkenfeld, A. L., Koch, C. A., Chavakis, T., and Chatzigeorgiou, A. (2016). The role of immune cells in metabolism-related liver inflammation and development of non-alcoholic steatohepatitis (NASH). *Rev. Endocr. Metab. Disord.* 17 (1), 29–39. doi:10.1007/s11154-016-9339-2

Navarra, T., Del Turco, S., Berti, S., and Basta, G. (2010). The lectin-like oxidized low-density lipoprotein receptor-1 and its soluble form: cardiovascular implications. *Jat* 17 (4), 317–331. doi:10.5551/jat.3228

Neumann, K., Rudolph, C., Neumann, C., Janke, M., Amsen, D., and Scheffold, A. (2015). Liver sinusoidal endothelial cells induce immunosuppressive IL-10-producing Th1 cells via the Notch pathway. *Eur. J. Immunol.* 45 (7), 2008–2016. doi:10.1002/eji.201445346

Nourshargh, S., and Alon, R. (2014). Leukocyte migration into inflamed tissues. *Immunity* 41 (5), 694–707. doi:10.1016/j.immuni.2014.10.008

O'Reilly, J. N., Cogger, V. C., Fraser, R., and Le Couteur, D. G. (2010). The effect of feeding and fasting on fenestrations in the liver sinusoidal endothelial cell. *Pathol.* 42 (3), 255–258. doi:10.3109/00313021003636469

Ozturk, O., Colak, Y., Senates, E., Yilmaz, Y., Ulasoglu, C., Doganay, L., et al. (2015). Increased serum soluble lectin-like oxidized low-density lipoprotein receptor-1 levels in patients with biopsy-proven nonalcoholic fatty liver disease. *Wjg* 21 (26), 8096–8102. doi:10.3748/wjg.v21.i26.8096

Parmar, K. M., Larman, H. B., Dai, G., Zhang, Y., Wang, E. T., Moorthy, S. N., et al. (2006). Integration of flow-dependent endothelial phenotypes by Kruppel-like factor 2. *J. Clin. Invest.* 116 (1), 49–58. doi:10.1172/JCI24787

Pasarín, M., Abraldes, J. G., Liguori, E., Kok, B., and Mura, V. L. (2017). Intrahepatic vascular changes in non-alcoholic fatty liver disease: potential role of insulin-resistance and endothelial dysfunction. *Wjg* 23 (37), 6777–6787. doi:10.3748/wjg.v23.i37.6777

Pasarín, M., Abraldes, J. G., Rodríguez-Vilarrupla, A., La Mura, V., García-Pagán, J. C., and Bosch, J. (2011). Insulin resistance and liver microcirculation in a rat model of early NAFLD. *J. Hepatol.* 55 (5), 1095–1102. doi:10.1016/j.jhep.2011.01.053

Pasarín, M., La Mura, V., Gracia-Sancho, J., García-Calderó, H., Rodríguez-Vilarrupla, A., García-Pagán, J. C., et al. (2012). Sinusoidal endothelial dysfunction precedes inflammation and fibrosis in a model of NAFLD. *PLoS One* 7 (4), e32785, doi:10.1371/journal.pone.0032785

Peng, Q., Zhang, Q., Xiao, W., Shao, M., Fan, Q., Zhang, H., et al. (2014). Protective effects of Sapindus mukorossi Gaertn against fatty liver disease induced by high fat diet in rats. *Biochem. Biophysical Res. Commun.* 450 (1), 685–691. doi:10.1016/j.bbrc.2014.06.035

Pi, X., Xie, L., and Patterson, C. (2018). Emerging roles of vascular endothelium in metabolic homeostasis. *Circ. Res.* 123 (4), 477–494. doi:10.1161/CIRCRESAHA.118.313237

Poisson, J., Lemoinne, S., Boulanger, C., Durand, F., Moreau, R., Valla, D., et al. (2017). Liver sinusoidal endothelial cells: physiology and role in liver diseases. *J. Hepatol.* 66 (1), 212–227. doi:10.1016/j.jhep.2016.07.009

Politz, O., Gratchev, A., McCourt, P. A. G., Schledzewski, K., Guillot, P., Johansson, S., et al. (2002). Stabilin-1 and -2 constitute a novel family of fasciclin-like hyaluronan receptor homologues. *Biochem. J.* 362 (Pt 1), 155–164. doi:10.1042/0264-6021:3620155

Potente, M., and Mäkinen, T. (2017). Vascular heterogeneity and specialization in development and disease. *Nat. Rev. Mol. Cel Biol.* 18 (8), 477–494. doi:10.1038/nrm.2017.36

Pourhoseini, S., Seth, R. K., Das, S., Dattaroy, D., Kadiiska, M. B., Xie, G., et al. (2015). Upregulation of miR21 and repression of Grhl3 by leptin mediates sinusoidal endothelial injury in experimental nonalcoholic steatohepatitis. *PLoS One* 10 (2), e0116780. doi:10.1371/journal.pone.0116780

Ratziu, V., Sanyal, A., Harrison, S. A., Wong, V. W. S., Francque, S., Goodman, Z., et al. (2020). Cenicriviroc treatment for adults with nonalcoholic steatohepatitis and fibrosis: final analysis of the phase 2b centaur study. *Hepatol.* 72 (3), 892–905. doi:10.1002/hep.31108

Rieder, H., Ramadori, G., and Meyer zum Büschenfelde, K. H. (1991). Sinusoidal endothelial liver cells *in vitro* release endothelin - augmentation by transforming growth factorβ and Kupffer cell-conditioned media. *Klin Wochenschr* 69 (9), 387–391. doi:10.1007/bf01647411

Rinella, M. E. (2015). Nonalcoholic fatty liver disease. *JAMA* 313 (22), 2263–2273. doi:10.1001/jama.2015.5370

Roediger, W., Hems, R., Wiggins, D., and Gibbons, G. (2004). Inhibition of hepatocyte lipogenesis by nitric oxide donor: could nitric oxide regulate lipid synthesis?. *IUBMB Life (International Union Biochem. Mol. Biol. Life)* 56 (1), 35–40. doi:10.1080/15216540310001649822

Roh, Y.-S., and Seki, E. (2018). Chemokines and chemokine receptors in the development of NAFLD. *Adv. Exp. Med. Biol.* 1061, 45–53. doi:10.1007/978-981-10-8684-7_4

Romero, F. A., Jones, C. T., Xu, Y., Fenaux, M., and Halcomb, R. L. (2020). The race to bash NASH: emerging targets and drug development in a complex liver disease. *J. Med. Chem.* 63 (10), 5031–5073. doi:10.1021/acs.jmedchem.9b01701

Ruart, M., Chavarria, L., Campreciós, G., Suárez-Herrera, N., Montironi, C., Guixé-Muntet, S., et al. (2019). Impaired endothelial autophagy promotes liver fibrosis by aggravating the oxidative stress response during acute liver injury. *J. Hepatol.* 70 (3), 458–469. doi:10.1016/j.jhep.2018.10.015

Sawada, K., Ohtake, T., Hasebe, T., Abe, M., Tanaka, H., Ikuta, K., et al. (2014). Augmented hepatic Toll-like receptors by fatty acids trigger the pro-inflammatory state of non-alcoholic fatty liver disease in mice. *Hepatol. Res.* 44 (8), 920–934. doi:10.1111/hepr.12199

Schaffner, F., and Popper, H. (1963). Capillarization of hepatic sinusoids in man. *Gastroenterol.* 44, 239–242. doi:10.1016/s0016-5085(63)80130-4

Schild, L., Dombrowski, F., Lendeckel, U., Schulz, C., Gardemann, A., and Keilhoff, G. (2008). Impairment of endothelial nitric oxide synthase causes abnormal fat and glycogen deposition in liver. *Biochim. Biophys. Acta (Bba) - Mol. Basis Dis.* 1782 (3), 180–187. doi:10.1016/j.bbadis.2007.12.007

Schuster, S., Cabrera, D., Arrese, M., and Feldstein, A. E. (2018). Triggering and resolution of inflammation in NASH. *Nat. Rev. Gastroenterol. Hepatol.* 15 (6), 349–364. doi:10.1038/s41575-018-0009-6

Schwabe, R. F., Tabas, I., and Pajvani, U. B. (2020). Mechanisms of fibrosis development in nonalcoholic steatohepatitis. *Gastroenterol.* 158 (7), 1913–1928. doi:10.1053/j.gastro.2019.11.311

Shah, V., Haddad, F. G., Garcia-Cardena, G., Frangos, J. A., Mennone, A., Groszmann, R. J., et al. (1997). Liver sinusoidal endothelial cells are responsible for nitric oxide modulation of resistance in the hepatic sinusoids. *J. Clin. Invest.* 100 (11), 2923–2930. doi:10.1172/JCI119842

Shetty, S., Lalor, P. F., and Adams, D. H. (2018). Liver sinusoidal endothelial cells - gatekeepers of hepatic immunity. *Nat. Rev. Gastroenterol. Hepatol.* 15 (9), 555–567. doi:10.1038/s41575-018-0020-y

Smedsrød, B., Le Couteur, D., Ikejima, K., Jaeschke, H., Kawada, N., Naito, M., et al. (2009). Hepatic sinusoidal cells in health and disease: update from the 14th International Symposium. *Liver Int.* 29 (4), 490–501. doi:10.1111/j.1478-3231.2009.01979.x

Sørensen, K. K., McCourt, P., Berg, T., Crossley, C., Couteur, D. L., Wake, K., et al. (2012). The scavenger endothelial cell: a new player in homeostasis and immunity. *Am. J. Physiology-Regulatory, Integr. Comp. Physiol.* 303 (12), R1217–R1230. doi:10.1152/ajpregu.00686.2011

Stahl, P. D., and Ezekowitz, R. A. B. (1998). The mannose receptor is a pattern recognition receptor involved in host defense. *Curr. Opin. Immunol.* 10 (1), 50–55. doi:10.1016/s0952-7915(98)80031-9

Stefan, N., Häring, H.-U., and Cusi, K. (2019). Non-alcoholic fatty liver disease: causes, diagnosis, cardiometabolic consequences, and treatment strategies. *Lancet Diabetes Endocrinol.* 7 (4), 313–324. doi:10.1016/S2213-8587(18)30154-2

Straub, A. C., Stolz, D. B., Vin, H., Ross, M. A., Soucy, N. V., Klei, L. R., et al. (2007). Low level arsenic promotes progressive inflammatory angiogenesis and liver blood vessel remodeling in mice. *Toxicol. Appl. Pharmacol.* 222 (3), 327–336. doi:10.1016/j.taap.2006.10.011

Tamaki, Y., Nakade, Y., Yamauchi, T., Makino, Y., Yokohama, S., Okada, M., et al. (2013). Angiotensin II type 1 receptor antagonist prevents hepatic carcinoma in rats with nonalcoholic steatohepatitis. *J. Gastroenterol.* 48 (4), 491–503. doi:10.1007/s00535-012-0651-7

Tanaka, M., and Iwakiri, Y. (2016). The hepatic lymphatic vascular system: structure, function, markers, and lymphangiogenesis. *Cell Mol. Gastroenterol. Hepatol.* 2 (6), 733–749. doi:10.1016/j.jcmgh.2016.09.002

Tanaka, Y., Adams, D. H., Hubscher, S., Hirano, H., Siebenlist, U., and Shaw, S. (1993). T-cell adhesion induced by proteoglycan-immobilized cytokine MIP-lβ. *Nature* 361 (6407), 79–82. doi:10.1038/361079a0

Tateya, S., Rizzo, N. O., Handa, P., Cheng, A. M., Morgan-Stevenson, V., Daum, G., et al. (2011). Endothelial NO/cGMP/VASP signaling attenuates Kupffer cell activation and hepatic insulin resistance induced by high-fat feeding. *Diabetes* 60 (11), 2792–2801. doi:10.2337/db11-0255

Terns Pharmaceuticals (2019). *TERNS pharmaceuticals announces positive interim results from ongoing phase 1 clinical trial of TERB-201, a SSAO inhibitor in development for NASH* Available at: https://www.ternspharma.com/8-13-19-terns-announces-positive-interim-results-from-ongoing-phase-1-clinical-trial-of-tern-201 (Accessed August 13, 2019).

Villanova, N., Moscatiello, S., Ramilli, S., Bugianesi, E., Magalotti, D., Vanni, E., et al. (2005). Endothelial dysfunction and cardiovascular risk profile in nonalcoholic fatty liver disease. *Hepatol.* 42 (2), 473–480. doi:10.1002/hep.20781

Wang, W., Zhao, C., Zhou, J., Zhen, Z., Wang, Y., and Shen, C. (2013). Simvastatin ameliorates liver fibrosis via mediating nitric oxide synthase in rats with non-alcoholic steatohepatitis-related liver fibrosis. *PLoS One* 8 (10), e76538, doi:10.1371/journal.pone.0076538

Warren, A., Bertolino, P., Benseler, V., Fraser, R., McCaughan, G. W., and Le Couteur, D. G. (2007). Marked changes of the hepatic sinusoid in a transgenic mouse model of acute immune-mediated hepatitis. *J. Hepatol.* 46 (2), 239–246. doi:10.1016/j.jhep.2006.08.022

Weston, C. J., Shepherd, E. L., Claridge, L. C., Rantakari, P., Curbishley, S. M., Tomlinson, J. W., et al. (2015). Vascular adhesion protein-1 promotes liver inflammation and drives hepatic fibrosis. *J. Clin. Invest.* 125 (2), 501–520. doi:10.1172/JCI73722

Wisse, E., De Zanger, R. B., Charels, K., Van Der Smissen, P., and McCuskey, R. S. (1985). The liver sieve: considerations concerning the structure and function of endothelial fenestrae, the sinusoidal wall and the space of Disse. *Hepatol.* 5 (4), 683–692. doi:10.1002/hep.1840050427

Wong, J., Johnston, B., Lee, S. S., Bullard, D. C., Smith, C. W., Beaudet, A. L., et al. (1997). A minimal role for selectins in the recruitment of leukocytes into the inflamed liver microvasculature. *J. Clin. Invest.* 99 (11), 2782–2790. doi:10.1172/JCI119468

Wong, R. J., Aguilar, M., Cheung, R., Perumpail, R. B., Harrison, S. A., Younossi, Z. M., et al. (2015). Nonalcoholic steatohepatitis is the second leading etiology of liver disease among adults awaiting liver transplantation in the United States. *Gastroenterol.* 148 (3), 547–555. doi:10.1053/j.gastro.2014.11.039

Wu, J., Meng, Z., Jiang, M., Zhang, E., Trippler, M., Broering, R., et al. (2010). Toll-like receptor-induced innate immune responses in non-parenchymal liver cells are cell type-specific. *Immunol.* 129 (3), 363–374. doi:10.1111/j.1365-2567.2009.03179.x

Xie, G., Choi, S. S., Syn, W.-K., Michelotti, G. A., Swiderska, M., Karaca, G., et al. (2013). Hedgehog signalling regulates liver sinusoidal endothelial cell capillarisation. *Gut* 62 (2), 299–309. doi:10.1136/gutjnl-2011-301494

Xie, G., Wang, L., Wang, X., Wang, L., and DeLeve, L. D. (2010). Isolation of periportal, midlobular, and centrilobular rat liver sinusoidal endothelial cells enables study of zonated drug toxicity. *Am. J. Physiology-Gastrointestinal Liver Physiol.* 299 (5), G1204–G1210. doi:10.1152/ajpgi.00302.2010

Xing, Y., Zhao, T., Gao, X., and Wu, Y. (2016). Liver X receptor α is essential for the capillarization of liver sinusoidal endothelial cells in liver injury. *Sci. Rep.* 6, 21309. doi:10.1038/srep21309

Xu, B., Broome, U., Uzunel, M., Nava, S., Ge, X., Kumagai-Braesch, M., et al. (2003). Capillarization of hepatic sinusoid by liver endothelial cell-reactive autoantibodies in patients with cirrhosis and chronic hepatitis. *Am. J. Pathol.* 163 (4), 1275–1289. doi:10.1016/S0002-9440(10)63487-6

Xu, M., Xu, H.-H., Lin, Y., Sun, X., Wang, L.-J., Fang, Z.-P., et al. (2019). LECT2, a ligand for Tie1, plays a crucial role in liver fibrogenesis. *Cell* 178 (6), 1478–1492. doi:10.1016/j.cell.2019.07.021

Yoshiji, H., Kuriyama, S., Noguchi, R., Ikenaka, Y., Kitade, M., Kaji, K., et al. (2006). Angiotensin-II and vascular endothelial growth factor interaction plays an important role in rat liver fibrosis development. *Hepatol. Res.* 36 (2), 124–129. doi:10.1016/j.hepres.2006.07.003

Younossi, Z. M., Koenig, A. B., Abdelatif, D., Fazel, Y., Henry, L., and Wymer, M. (2016). Global epidemiology of nonalcoholic fatty liver disease-Meta-analytic assessment of prevalence, incidence, and outcomes. *Hepatol.* 64 (1), 73–84. doi:10.1002/hep.28431

Younossi, Z. M. (2019). Non-alcoholic fatty liver disease - a global public health perspective. *J. Hepatol.* 70 (3), 531–544. doi:10.1016/j.jhep.2018.10.033

Zannetti, C., Roblot, G., Charrier, E., Ainouze, M., Tout, I., Briat, F., et al. (2016). Characterization of the inflammasome in human kupffer cells in response to synthetic agonists and pathogens. *J.I.* 197 (1), 356–367. doi:10.4049/jimmunol.1502301

Zapotoczny, B., Szafranska, K., Kus, E., Braet, F., Wisse, E., Chlopicki, S., et al. (2019). Tracking fenestrae dynamics in live murine liver sinusoidal endothelial cells. *Hepatol.* 69 (2), 876–888. doi:10.1002/hep.30232

Zeng, X.-Q., Li, N., Pan, D.-Y., Miao, Q., Ma, G.-F., Liu, Y.-M., et al. (2015). Kruppel-like factor 2 inhibit the angiogenesis of cultured human liver sinusoidal endothelial cells through the ERK1/2 signaling pathway. *Biochem. Biophysical Res. Commun.* 464 (4), 1241–1247. doi:10.1016/j.bbrc.2015.07.113

Zhang, Q., Liu, J., Liu, J., Huang, W., Tian, L., Quan, J., et al. (2014). oxLDL induces injury and defenestration of human liver sinusoidal endothelial cells via LOX1. *J. Mol. Endocrinol.* 53 (2), 281–293. doi:10.1530/JME-14-0049

Zhang, Q., Yu, J., Guo, T., Tian, L., Quan, J., Lin, W., et al. (2019). High glucose/ox-LDL induced hepatic sinusoidal capillarization via αvβ5/FAK/ERK signaling pathway. *Biochem. Biophysical Res. Commun.* 513 (4), 1055–1062. doi:10.1016/j.bbrc.2019.04.082

Zhou, B., Weigel, J. A., Fauss, L., and Weigel, P. H. (2000). Identification of the hyaluronan receptor for endocytosis (HARE). *J. Biol. Chem.* 275 (48), 37733–37741. doi:10.1074/jbc.M003030200

Conflict of Interest: The authors declare that the research was conducted in the absence of any commercial or financial relationships that could be construed as a potential conflict of interest.

frontiers in Pharmacology

ORIGINAL RESEARCH
published: 16 April 2021
doi: 10.3389/fphar.2021.658236

Astragaloside IV Inhibits Galactose-Deficient IgA1 Secretion *via* miR-98-5p in Pediatric IgA Nephropathy

Caiqiong Liu[1,2], *Xiaoyan Li*[1,2], *Lanjun Shuai*[1,2], *Xiqiang Dang*[1,2], *Fangrong Peng*[1,2], *Mingyi Zhao*[3], *Shiqiu Xiong*[1,2], *Ying Liu*[3] *and Qingnan He*[3]*

[1]*Department of Pediatrics, The Second Xiangya Hospital, Central South University, Changsha, China,* [2]*Department of Pediatrics Nephrology, Children's Medical Center, The Second Xiangya Hospital, Central South University, Changsha, China,* [3]*Department of Pediatrics, The Third Xiangya Hospital, Central South University, Changsha, China*

Purpose: The factor associated with IgA nephropathy (IgAN) is an abnormality of IgA known as galactose-deficient IgA1 (Gd-IgA1). The purpose of this study was to determine the molecular role played by miRNAs in the formation of Gd-IgA1 in IgAN and investigate the regulatory role of Astragaloside IV (AS-IV) in miRNAs.

Patients and methods: Bioinformatics analysis, along with functional and mechanistic experiments, were used to investigate the relationship and function of miRNA, β-1, 3-galactosyltransferase (C1GALT1), Gd-IgA1, and AS-IV. Analyses involved a series of tools, including quantitative real-time polymerase chain reaction (qRT-qPCR), Western blot, enzyme-linked immunosorbent assay (ELISA), Vicia Villosa lectin-binding assay (VVA), Cell counting kit-8 assay (CCK-8), and the dual-luciferase reporter assay.

Results: miRNA screening and validation showed that miR-98-5p was significantly upregulated in the peripheral blood mononuclear cells (PBMCs) of pediatric patients with IgAN compared with patients diagnosed with mesangial proliferative glomerulonephritis (MsPGN) and immunoglobulin A vasculitis nephritis (IgAV-N), and healthy controls ($p < 0.05$). Experiments with the dual-luciferase reporter confirmed that miR-98-5p might target C1GALT1. The overexpression of miR-98-5p in DAKIKI cells decreased both the mRNA and protein levels of C1GALT1 and increased the levels of Gd-IgA1 levels; these effects were reversed by co-transfection with the C1GALT1 plasmid, and *vice versa*. In addition, AS-IV downregulated the levels of Gd-IgA1 level in DAKIKI cells by inhibiting miR-98-5p.

Conclusions: Our results revealed that AS-IV could inhibit Gd-IgA1 secretion *via* miR-98-5p. Increased levels of miR-98-5p in pediatric IgAN patients might affect the glycosylation of IgA1 by targeting C1GALT1. In addition, our analyses suggest that the pathogenesis of IgAN may differ from that of IgAV-N. Collectively, these results provide significant insight into the pathogenesis of IgAN and identify a potential therapeutic target.

Keywords: immunity, galactose-deficient IgA1, astragaloside IV, miR-98-5p, IgA nephropathy, β-1, 3-galactosyltransferase

OPEN ACCESS

Edited by:
Ning Hou,
Guangzhou Medical University, China

Reviewed by:
Zhi Qiang Huang,
University of Alabama at Birmingham, United States
Satish Ramalingam,
SRM Institute of Science and Technology, India

***Correspondence:**
Qingnan He
heqn2629@csu.edu.cn

Specialty section:
This article was submitted to Inflammation Pharmacology, a section of the journal Frontiers in Pharmacology

Received: *25 January 2021*
Accepted: *29 March 2021*
Published: *16 April 2021*

Citation:
Liu C, Li X, Shuai L, Dang X, Peng F, Zhao M, Xiong S, Liu Y and He Q (2021) Astragaloside IV Inhibits Galactose-Deficient IgA1 Secretion via miR-98-5p in Pediatric IgA Nephropathy. Front. Pharmacol. 12:658236. doi: 10.3389/fphar.2021.658236

INTRODUCTION

IgA nephropathy (IgAN) is the most prevalent form of primary glomerulonephritis and predominantly affects children and young adults. The most striking feature of IgAN is the mesangial deposition of IgA or IgA-containing immune complexes (Cambier et al., 2020; Coppo and Robert, 2020). IgAN may represent a systemic immune dysregulation rather than an intrinsic abnormality of resident renal cells (Moroni et al., 2019). The mainstream pathogenesis of IgAN is described by the multi-hit hypothesis which involves four major steps: the overproduction of galactose-deficient IgA1 (Gd-IgA1) and autoantibodies against Gd-IgA1, the formation of circulating immune complexes (CICs) which are subsequently deposited in the glomeruli, and the activation of mesangial cells, thus resulting in renal injury (Suzuki et al., 2011). These data indicate that Gd-IgA1 plays a crucial role in the pathogenesis of IgAN. However, we know very little about the molecular mechanisms underlying these processes.

Human IgA has two subclasses: IgA1 and IgA2 (Placzek et al., 2018). The IgA1 molecule differs from the IgA2 subclass in that it features a unique hinge region. This region has many serine threonine and proline residues, and nine potential O-glycosylation sites (usually, 3–6 sites of each hinge region are O-glycosylated); these residues can be affected by various disorders (Novak et al., 2018). IgA1 O-glycosylation needs N-acetyl-galactosamine (GalNAc) to be added to the serine or threonine residues, followed by galactose (Gal). β-1,3-galactosyltransferase (C1GALT1) catalyzes the addition of Gal residue. Finally, O-glycosylation is completed by the addition of sialic acid residues (Lai et al., 2019). Gd-IgA1 can then be formed as the result of the reduced activity or expression of C1GALT1, and the elevation of α2,6-sialyltransferase (ST6GALNAcII) (Lai et al., 2019). Genome-wide association analyses have revealed the crucial role of the C1GALT1 in the secretion of Gd-IgA1 (Kiryluk et al., 2017). However, the C1GALT1 genotype explains only 3% of the variance in Gd-IgA1 levels, thus suggesting that transcriptional or post-transcriptional regulation also plays a key role (Kiryluk et al., 2017).

MicroRNAs (miRNAs) are endogenous small non-coding RNAs that can down regulate targeted mRNAs by pairing to specific sites within the 3'-untranslated regions (3'UTRs) (Wang J. et al., 2019). Previous research suggests that miRNAs target up to 60% of human mRNAs (Hennino et al., 2016). Recent insights have also revealed that miRNAs regulate a variety of cellular processes, including immune reactions and the pathogenesis of kidney disease (Zhao et al., 2019). miRNAs are also closely related to immune responses. For instance, the upregulation of miR-210 has been shown to inhibit B cell activity and autoantibody synthesis, while the upregulation of miR-148a and miR-19-92 disrupted the central tolerance of B cells and accelerated autoimmunity (Mok et al., 2013; Gonzalez-Martin et al., 2016; Xiao et al., 2020). This suggests that miRNAs play an important role in renal diseases.

Astragalus membranaceus is a traditional Chinese herb that is often used in the clinical treatment of kidney diseases (Wang E. et al., 2020). Astragaloside IV(AS-IV) is a saponin molecule isolated from *A. membranaceus*. AS-IV exhibits a range of beneficial biological and pharmacological activities, including anti-inflammatory effects, immunomodulatory effects, cardioprotection, and renoprotection (Wang E. et al., 2020; Wang Z. et al., 2020). Recent studies have reported that AS-IV can suppress kidney fibrosis and exert beneficial effects on diabetes and its related complications *via* multiple mechanisms (Wang E. et al., 2020). AS-IV is also known to function as a regulator of miRNAs levels (Gong et al., 2018; Cui et al., 2020). We therefore hypothesized that miR-98-5p might participate in the pathological process of Gd-IgA1 production and could be regulated by AS-IV in IgAN.

METHODS

Bioinformatics Analysis of miRNAs

First, we used specific keywords ("IgA nephropathy, IgA nephritis, or Berger's disease" and "peripheral blood mononuclear cells (PBMCs)" and "microRNA") to search the Gene Expression Omnibus (GEO) (http://www.ncbi.nlm.nih.gov/geo/); this allowed us to acquire the GSE25590 miRNA microarray dataset (Serino et al., 2012). Next, we downloaded the raw data and used the normalizeBetweenArrays function in the Limma package of R to normalize the expression values within the quartile and then obtained standard expressions by Log_2 transformation. Differentially expressed miRNAs (DEmiRNAs) were screened using the Limma package of R using $|\log_2$fold change (FC)$| > 1$ and p-value < 0.05 as thresholds. Next, we used TargetScan (http://www.targetscan.org/vert_72/) and miRDB (http://mirdb.org/) to predict the upstream regulated miRNAs for C1GALT1. miRNAs that were common to both databases were defined as predicted miRNAs. The intersection between the DEmiRNAs and the predicted miRNAs were then used for further analysis.

The Collection of Samples From Patients and Controls

A total of 24 pediatric cases were enrolled in our study; these cases were divided into four groups with six cases in each group: a group of patients with IgAN, a group of patients with mesangial proliferative glomerulonephritis (MsPGN), a group of patients with immunoglobulin A vasculitis nephritis (IgAV-N), and a group of healthy controls. All patients had normal renal function. None of the patients underwent treatment with steroids, immunosuppressive agents, antibiotics, or non-steroidal anti-inflammatory agents. All healthy controls had a normal urine test. We collated clinical data from each patient and collected venous blood on the day of kidney biopsy (for patients) or recruitment (for healthy controls). Blood samples were treated with an anticoagulant and centrifuged at 1000 g at room temperature for 10 min; we then collected the supernatant (plasma) for analysis. The remaining blood was diluted with an equal volume of Phosphate Buffer Saline (PBS). Next, we used a Ficoll-Hypaque (Ficoll-Paque Plus, Solarbio, Beijing) gradient (800 g for 30 min at room temperature) to isolate PBMCs *via*

density separation. The layer of PBMCs was collected and washed three times with PBS. Both PBMCs suspension and plasma were stored at −80°C for subsequent experiments. This study was approved by the Medical Ethical Committee of the Second Xiangya Hospital of Central South University (No. 2019–190S (161), Changsha, China). Written informed consent was signed by every case's legal guardian or next of kin.

Cell Culture, Transfection, and Treatment

The DAKIKI cell line was a gift from Professor Liu Youxia of Tianjin Medical University General Hospital. This cell line was authenticated by short tandem repeat profiling (Genetic Testing Biotechnology, Suzhou, China). DAKIKI cells were cultured in RPMI 1640 medium containing 10% heat-inactivated fetal bovine serum (FBS), 1% penicillin-streptomycin (Shanghai, China); this was carried out in a humidified environment of 95% atmospheric air and 5% CO_2. miR-98-5p mimics and inhibitors (anti-miR-98-5p oligonucleotides) (Krützfeldt et al., 2005), silent C1GALT1 (si-C1GALT1) and silent scramble (si-scramble), pc-DNA-C1GALT1 and pc-DNA-vector plasmids, were purchased from Jikai Genechem Co., Ltd. (Shanghai China). The sequences of the si-C1GALT1 and si-scramble were as follow: si-C1GALT1, 5'-TATACGTTCAGGTAAGGTAGG-3' and si-scramble, 5'-TTC TCCGAACGTGTCACGT-3'. Transfection was performed using Mirus TransIT-TKO transfection reagent (Mirus Inc., Madison, WI, United States) in accordance with the manufacturer's guidelines. Mock transfection was carried out with a mock reagent. DAKIKI cells were treated with AS-IV (Yuanye biomart, Shanghai, China) at different concentrations (0, 5, 10, 20, 40, and 80 μM) for 24 h. Then, the DAKIKI cells were treated with either vehicle or AS-IV (20 μM) and transfected with miRNA mimics.

Quantitative Real-Time Polymerase Chain Reaction

Total RNA was extracted from isolated PBMCs and DAKIKI cells with TRIzol Reagent (Invitrogen, CA, United States). Reverse Transcription Systems (for miRNA: CW2141, for mRNA: CW2569, CoWin Biosciences, Beijing, China) were used to reverse transcribe 1 μg of total RNA into cDNA. Levels of miR-98-5p, miR-152-3p, and C1GALT1, were then determined by qRT-PCR using the UltraSYBR Mixture (CW2601, CoWin Biosciences, Beijing, China) on a qRT-PCR detection system (Thermo Fisher, Pikoreal96, United States). Primers are shown in **Supplementary Table S1**. U6 snRNA and β-actin were used for normalization. Gene expression levels were calculated by the $2^{-\Delta\Delta CT}$ method. All experiments were replicated three times.

Western Blotting

Total protein was extracted from isolated PBMCs and cultured cells using a protein extraction kit (Beyotime, Shanghai, China). Protein concentrations were determined using the BCA Protein Assay Kit (CW 2011, CoWin Biosciences, Beijing, China). The proteins were then separated by 10% sodium dodecyl sulfate polyacrylamide gel electrophoresis (SDS-PAGE) and transferred to nitrocellulose membranes (Pall Corporation, United States). Next, the membranes were blocked in 5% skimmed milk at room temperature for 2 h and probed at 4°C overnight with anti-C1GALT1 (1: 450; rabbit-anti-human; Santa Cruz Biotechnology, TX, United States), followed by incubation with a HRP-conjugated goat-anti-rabbit IgG antibody (1:7,000, goat-anti-rabbit, Proteinte, Chicago, United States) at room temperature for 2 h. Bands were then detected by an electrochemiluminescence detection kit (Advansta, California, United States) to produce a chemiluminescence signal that was captured on X-ray film. The same membranes were stripped and then re-probed with an anti-β-actin antibody (1:5,000 mouse-anti-human, Proteintech, Chicago, United States). This was then followed by incubation with a HRP-conjugated goat anti-mouse IgG antibody (1:5,000, goat-anti-mouse; Proteintech, Chicago, United States). Bands were then detected and captured, as described previously.

IgA1 and Galactose-Deficient IgA1 Measurement

Levels of total IgA1 levels in plasma or the supernatant of DAKIKI cell were determined in duplicate by ELISA, in accordance with the manufacturer's recommendations. In brief, 96-well immunoplates were coated with mouse anti-human IgA1 antibody (SouthernBiotech, United States) at 4°C overnight. After blocking with BSA, samples or standard human IgA1 (Santa Cruz Biotechnology, United States) were incubated (in duplicate) at 37°C for 2 h. Mouse biotin-labeled anti-human IgA1 specific antibodies (Southern Biotech Associates) were added and incubated for 1 h, then incubated with HRP-labeled Streptavidin (Beyotime, Shanghai, China) for 1 h. Positive staining was developed with tetramethyl benzidine dilution (TMB) and detected at 450 nm. The concentration of IgA1 was then determined by the use of a standard curve.

Gd-IgA1 levels were measured by the Vicia Villosa lectin-binding assay (VV, Vector Laboratories Associates, Peterborough, United Kingdom) (VVA). Immunoplates were coated with anti-IgA1 antibody and blocked with BSA, as described earlier. Next, 100 μl per well with 100 ng IgA1 of each sample (according to the concentration of IgA1) were added in duplicate. The plates were incubated at 4°C overnight, then incubated with biotinylated VV lectin (Vector Laboratories, Peterborough, United Kingdom) at 37°C for 2 h. Plates were then incubated with HRP-labeled Streptavidin (Beyotime, Shanghai, China) for a further 1 h. Positive staining was then developed and detected as described above; optical density (OD) units for each sample were expressed relative to IgA1(%VV).

Cell Counting Kit-8 Assay

The CCK-8 toxicity assay was used to analyze the potentially toxic effects of AS-IV on the viability of DAKIKI cells. In brief, 4×10^5 cells per well were seeded into 96-well plates and treated with different concentrations of AS-IV (0, 5, 10, 20, 40, and 80 μm) for 24 h. Then, 20 μl of Cell Counting Kit-8 solution (CCK-8, Dojindo Molecular Technologies, Kyushu, Japan) was added into each well. After incubation at 37°C for 4 h, the OD of

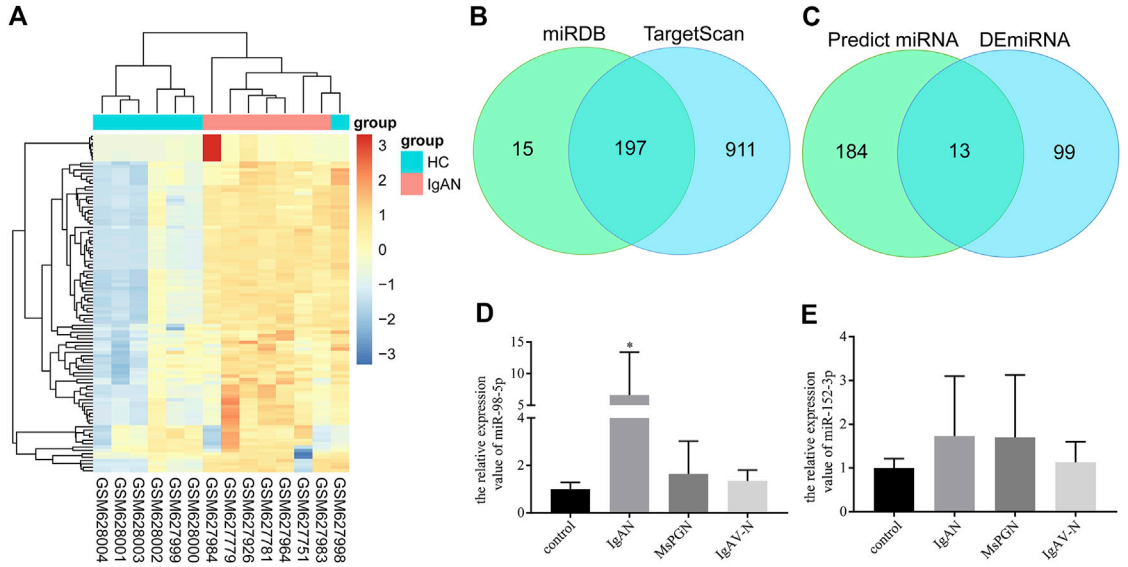

FIGURE 1 | miRNA screening and validation. **(A)** Heatmap of DEmiRNAs in GSE25590. Red and blue: upregulated and downregulated. Columns represent different samples, rows indicates different genes. Significantly differential miRNA were defined by $|\log_2(FC)|>1$ and p-value < 0.05. **(B)** Venn diagram showing the intersection miRNAs predicted by TargetScan and miRDB. **(C)** Venn diagram showing the intersection of DEmiRNAs and predicted miRNAs. **(D)** Validation of the differential expression of miR-98-5p in PBMCs among patients with IgAN, healthy controls, patients with MsPGN, and patients with IgAV-N (the fold change of IgAN vs. healthy control, MsPGN and IgAV-N were 6.60 ± 6.20 vs. 1.00 ± 0.26, 6.60 ± 6.20 vs. 1.64 ± 1.26 and 6.60 ± 6.20 vs. 1.35 ± 0.42, respectively, all $p < 0.05$). **(E)** Validation of the differential expression of miR-152-3p among different groups. Each bar represents the mean ± SD of six cases in each group. Compared with the other groups, $^*p < 0.05$. Note: DEmiRNA, differentially expressed miRNAs; FC, fold change; PBMCs, peripheral blood mononuclear cells; IgAN, IgA nephropathy; MsPGN, mesangial proliferative glomerulonephritis; IgAV-N, immunoglobulin A vasculitis nephritis; SD, standard deviation.

each well was analyzed using a Microplate Reader (MB-530, HEALES, Shenzhen, China) at 450 nm.

Dual-Luciferase Reporter Assay

The dual-luciferase reporter assay is a reporting system for detecting firefly luciferase activity using luciferin as a substrate. Luciferase can catalyze the oxidation of Luciferin to oxyluciferin. Bioluminescence is emitted during the oxidation of Luciferin; this bioluminescence can be measured with a fluorescence analyzer. The dual luciferase assay involves firefly luciferase and ranilla luciferase. One of these enzymes is used as an internal reference while the other is attached to the target gene 3'-UTR; this can be inhibited by miRNA and can therefore be used for target gene validation.

The potential complementary binding sequence between C1GALT1 and miR-98-5p was predicted by TargetScan and miRDB. Reporter constructs containing the wild-type (WT) or mutant-type (MUT) human C1GALT1 3'-UTRs synthesized by HonorGene (Changsha, China), were cloned into the pHG-MirTarget-C1GALT1 luciferase reporter vector (HonorGene, Changsha, China). Then, 293 A cells were seeded in 24-well plates and co-transfected with 2 μg pHG-MirTarget-C1GALT1-3U-WT or pHG-MirTarget-C1GALT1-3U-MUT, and 50 nm miR-98-5p mimic, or mimic NC by Lipofectamine 2000 reagent (Invitrogen; Thermo Fisher Scientific, Inc.). Firefly and Renilla luciferase activities were then determined by dual-luciferase reporter assays (Promega, GloMax 20/20 United States) at 48 h post-transfection in accordance with the manufacturer's instruction. Values were normalized with Renilla luciferase.

Statistical Analysis

Statistical analyses were performed with IBM-SPSS version 22.0 (Chicago, United States) statistical software and graphs were plotted with GraphPad Prism 7.0 (San Diego, CA). For continuous variables, normally distributed data were expressed as mean ± SD and were compared by an independent-sample t-test or one-way analysis of variance (ANOVA); Pearson's correlation was also used if necessary. Other forms of data were expressed as the median (first quartile and third quartile) and analyzed by the Mann-Whitney U test. A two-tailed $p < 0.05$ was considered to be statistically significant.

RESULTS

miRNA Screening and Validation

First, 112 mature differentially expressed miRNAs were identified from the GSE25590 dataset, including 91 upregulated and 21 downregulated miRNAs (**Supplementary Table S2**), the DEmiRNAs heatmap were shown in **Figure 1A**. TargetScan and miRDB were then used to predict potential upstream regulated miRNAs of C1GALT1, and got 197 predicted miRNAs (**Figure 1B**, **Supplementary Table S3**). A total of 13 target miRNAs were then identified based on the intersection of DEmiRNAs and predicted miRNAs (**Figure 1C**, **Supplementary**

TABLE 1 | Demographic and clinical features of the healthy control group, and patients with IgAN, MsPGN, and IgAV-N.

variables[a]	Healthy control (n = 6)	IgAN (n = 6)	MsPGN (n = 6)	IgAV-N (n = 6)	*p*
Age (years)	9.43 ± 2.85	10.60 ± 3.80	6.12 ± 5.43	9.72 ± 1.11	0.191
Male (%)	3 (50.0)	3 (50.0)	3 (50.0)	5 (83.3)	0.621[b]
Systolic BP (mmHg)	101.17 ± 7.78	102.50 ± 9.23	96.33 ± 7.99	103.17 ± 6.37	0.452
Diastolic BP (mmHg)	68.00 ± 2.45	63.33 ± 10.86	57.33 ± 8.94	66.83 ± 6.18	0.111
Serum albumin (g/L)	40.9 (40.2–42.38)	34.9 (26.7–38.7)	42.2 (31.5–43.9)	41.9 (35.5–43.6)	0.288
eGFR (ml/min/1.73 m^2)	149.7 ± 19.1	164.2 ± 26.7	156.9 ± 31.8	179.6 ± 14.6	0.201
24 h urinary protein (mg)	—	905.7 (94.5–1,618.0)	429.2 (99.9–2,166.6)	145.7 (78.8–453.9)	0.002[c]

[a]*Normally distributed continuous variables (values were expressed as mean ± SD). Non-normally distributed continuous variables were expressed as the median (first quartile and third quartile). For qualitative variables, values are expressed as n (%).*

[b]*Fisher's exact chi-square test, $\chi^2 = 2.161$.*

[c]*The pairwise comparison of IgAN, MsPGN and IgAV-N group showed no statistical significance.*

Abbreviations: HC, Healthy Control; IgAN, IgA nephropathy; MsPGN, mesangial proliferative glomerulonephritis; IgAV-N, immunoglobulin A vasculitis nephritis (IgAV-N); SD, standard deviation; BP, blood presure.

Table S4). Then we selected miR-98-5p and miR-152-3p for further validation.

A total of 24 pediatric cases were enrolled in our study. The demographic and clinical features of these cases are shown in **Table 1**. The levels of miR-98-5p were significantly higher in patients with IgAN than those in healthy controls (IgAN vs. control: 6.60 ± 6.20 vs. 1.00 ± 0.26, $p < 0.05$). Then, we investigated whether miR-98-5p was upregulated only in IgAN. We compared the same miR-98-5p levels of patients with IgAN with patients diagnosed with MsPGN and IgAV-N and found that miR-98-5p levels were also upregulated in patients with IgAN (IgAN vs. MsPGN and IgAV-N: 6.60 ± 6.20 vs. 1.64 ± 1.26 and 1.35 ± 0.42 respectively, $p < 0.05$) (**Figure 1D**). These results confirmed that the upregulation of miR-98-5p expression was specific for IgAN. There were no significant differences in the levels of miR-152-3p when compared between groups (**Figure 1E**).

The Expression Levels of miR-98-5p, C1Galactosyltransferase1, and Galactose-Deficient IgA1, in IgA Nephropathy, and the Relationships Between These Different Factors

C1GALT1 is a necessary enzyme for the addition of galactose in the process of O-glycosylation and is directly associated with the onset of IgAN. We tested the mRNA expression levels of C1GALT1 in PBMCs by qRT-PCR and found a significant reduction in patients with IgAN when compared to healthy controls and patients with MsPGN (IgAN vs. healthy control and MsPGN: 1.47 ± 0.43 vs. 4.50 ± 1.30 and 4.17 ± 3.01, $p < 0.05$). There was no significant difference between patients with IgAV-N and IgAN (**Figure 2A**). We also measured the protein levels of C1GALT1 in PBMCs and found that the results were consistent with mRNA levels (**Figures 2D,E**). We then measured the plasma IgA1 concentration in the four groups and found no significant difference when compared between the different groups (**Figure 2B**). Next, we evaluated the levels of Gd-IgA1 in plasma samples from the same cases by VVA. Analysis showed that the levels of Gd-IgA1 were significantly higher in patients with IgAN than healthy controls (IgAN vs. control: 1.50 ± 0.15 vs. 1.04 ± 0.05, $p < 0.001$), patients with MsPGN (IgAN vs. MsPGN: 1.50 ± 0.15 vs. 1.08 ± 0.10, $p < 0.001$), and patients with IgAV-N (IgAN vs. IgAV-N: 1.50 ± 0.15 vs. 1.22 ± 0.07, $p < 0.01$). Furthermore, we found that the levels of Gd-IgA1 were significantly higher in patients with IgAV-N than in healthy controls (IgAV-N vs. control: 1.22 ± 0.07 vs. 1.04 ± 0.05, $p < 0.05$) (**Figure 2C**). These results suggest that C1GALT1 was significantly downregulated in IgAN and IgAV-N, but more significantly in IgAN; Gd-IgA1 was significantly upregulated in IgAN and IgAV-N, but more significantly in IgAN. Both C1GALT1 and Gd-IgA1 abnormal involved in IgAN pathogenesis.

Pearson correlation analysis showed that the expression levels of miR-98-5p and C1GALT1 mRNA were negatively correlated ($R^2 = 0.787$, $p = 0.018$; **Figure 2F**); the C1GALT1 mRNA expression and Gd-IgA1 levels were negatively correlated ($R^2 = 0.793$, $p = 0.040$; **Figure 2G**); and the expression of miR-98-5p and the levels of Gd-IgA1 were not significantly correlated ($R^2 = 0.599$, $p = 0.079$; **Figure 2H**). These results suggest that C1GALT1 might be a target gene of miR-98-5p.

miR-98-5p Regulates C1Galactosyltransferase1 Expression and Galactose-Deficient IgA1 Levels in DAKIKI Cells

PBMCs include lymphocytes (including both T and B lymphocytes) and monocytes. B lymphocytes can secrete antibodies in response to antigen stimulation. IgA is the most secreted antibody (Mestecky et al., 1986), and only IgA and IgD contain O-glycosylation in immunoglobulins (Smith et al., 2006). O-glycosylation requires C1GALT1. The O-glycosylation of IgD is normal in IgAN (Smith et al., 2006), this demonstrates the fact that the most affected cells are those that are IgA1-positive.

Next, we carried out *in vitro* experiments using human B lymphoma DAKIKI cells which are known to produce IgA1. The expression of C1GALT1 was almost completely lost, at both the mRNA and protein levels, when cells were treated with si-C1GALT1 when compared with cells treated with si-Scramble

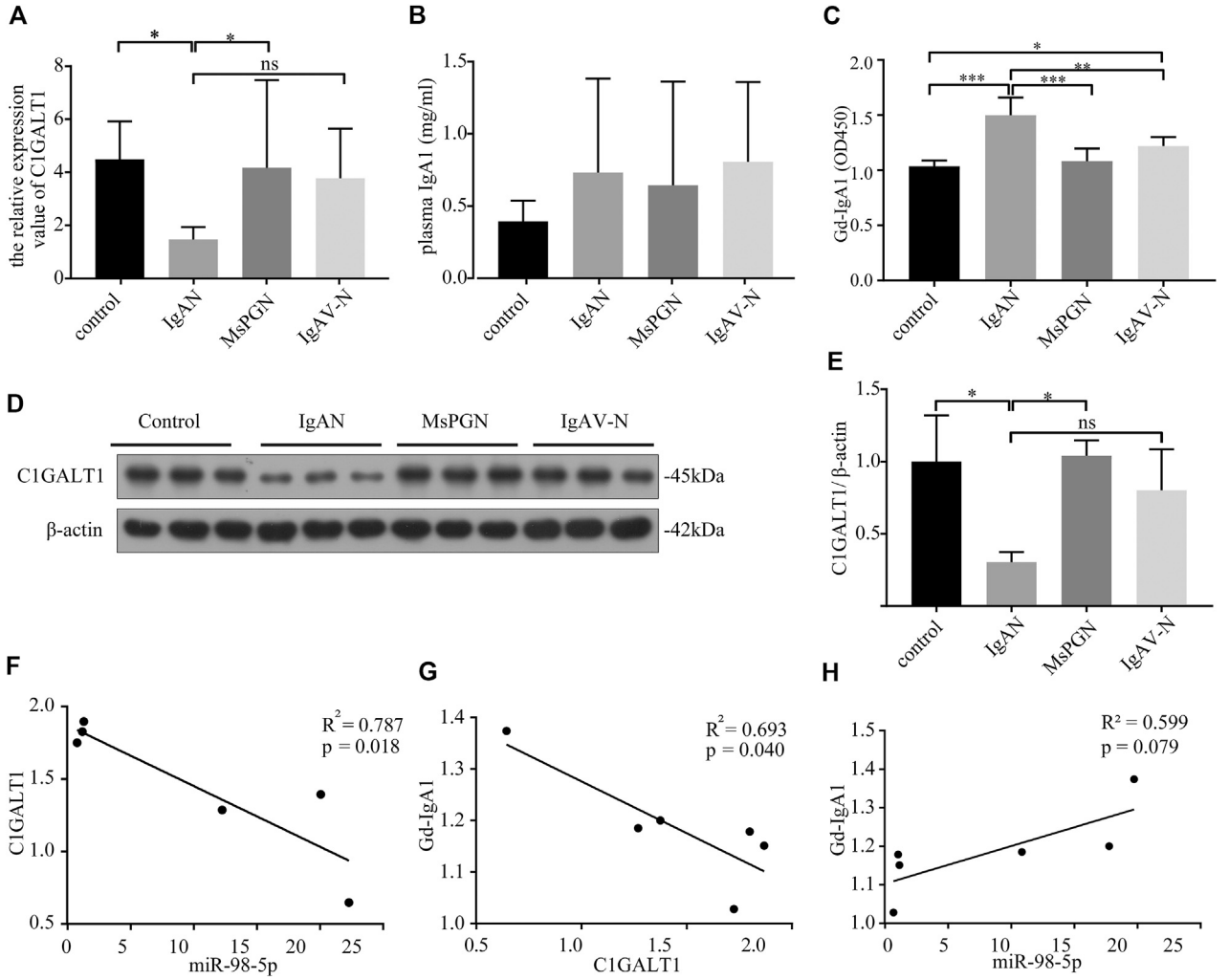

FIGURE 2 | The expression levels and relationships among miR-98-5p, C1GALT1, and Gd-IgA1 in IgAN. **(A)** The expression levels of C1GALT1 mRNA were analyzed by qRT-PCR. The expression levels in control, IgAN, MsPGN and IgAV-N groups were 4.50 ± 1.30, 1.47 ± 0.43, 4.17 ± 3.01 and 3.76 ± 1.71 respectively. **(B)** The plasma IgA1 level was analyzed by ELISA, There were no significance between IgAN and other groups. **(C)** The relative level of Gd-IgA1 in the plasma was analyzed by VVA. The relative level of Gd-IgA1 in control, IgAN, MsPGN and IgAV-N groups were 1.04 ± 0.05, 1.50 ± 0.15, 1.08 ± 0.10 and 1.22 ± 0.07 respectively. **(D)** The expression of C1GALT1 protein was analyzed by Western blotting. **(E)** Fold changes were calculated by determining the ratios of the C1GALT1/β-actin band intensities. The semiquantitative relative level of C1GALT1 protein in control, IgAN, MsPGN and IgAV-N groups were 1.00 ± 0.26, 0.30 ± 0.06, 1.04 ± 0.09 and 0.80 ± 0.23. **(F)** The relationship between C1GALT1 and miR-98-5p. **(G)** The relationship between Gd-IgA1 and the mRNA of C1GALT1 **(H)** The relationship between Gd-IgA1 and miR-98-5p. Each bar represents the mean ± SD of six cases in each group. ns, no significance; *$p < 0.05$, **$p < 0.01$, ***$p < 0.001$. Note: C1GALT1, β-1, 3-galactosyltransferase; Gd-IgA1, galactose-deficient IgA1; IgAN, IgA nephropathy; qRT-PCR, quantitative real-time polymerase chain reaction; ELISA, enzyme-linked immunosorbent assay; VVA, Vicia Villosa lectin-binding assay; SD, standard deviation.

(si-C1GALT1 vs. si-Scramble: mRNA: 0.24 ± 0.02 vs. 0.92 ± 0.06, $p < 0.001$; protein: 0.29 ± 0.12 vs. 1.02 ± 0.15, $p < 0.05$) (**Supplementary Figure S1A–C**). The levels of Gd-IgA1 in the supernatant of DAKIKI cells was significantly elevated in the si-C1GALT1-treated group (si-C1GALT1 vs .si-Scramble: 0.47 ± 0.01 vs. 0.32 ± 0.00, $p < 0.001$) (**Supplementary Figure S1D**). The expression of C1GALT1 was significantly increased, both at the mRNA and protein levels, in cells that had been treated with pcDNA-C1GALT1 when compared with those treated with the pcDNA-vector (pcDNA-C1GALT1 vs. pcDNA-vector: mRNA: 4.47 ± 0.13 vs. 0.96 ± 0.12, $p < 0.001$, protein: 1.95 ± 0.39 vs. 0.99 ± 0.24, $p < 0.001$) (**Supplementary Figure S1E–G**). The levels of Gd-IgA1 in the supernatant of DAKIKI cells was significantly reduced in the pcDNA-C1GALT1-treated group (pcDNA-C1GALT1 vs. pcDNA-vector: 0.21 ± 0.00 vs. 0.31 ± 0.01, $p < 0.001$) (**Supplementary Figure S1H**). These results indicated that C1GALT1 negatively regulated the production of Gd-IgA1.

Next, we confirmed the causal relationship between miR-98-5p expression and Gd-IgA1 secretion by carrying out *in vitro* experiments. We transfected DAKIKI cells with blank, mimic NC, miR-98-5p mimic, miR-98-5p mimic + inhibitor NC, and miR-98-5p mimic + miR-98-5p inhibitor. First, we proved that the transfection had been successful by detecting the expression of miR-98-5p (miR-98-5p mimic vs. blank and mimic NC: 5.39 ±

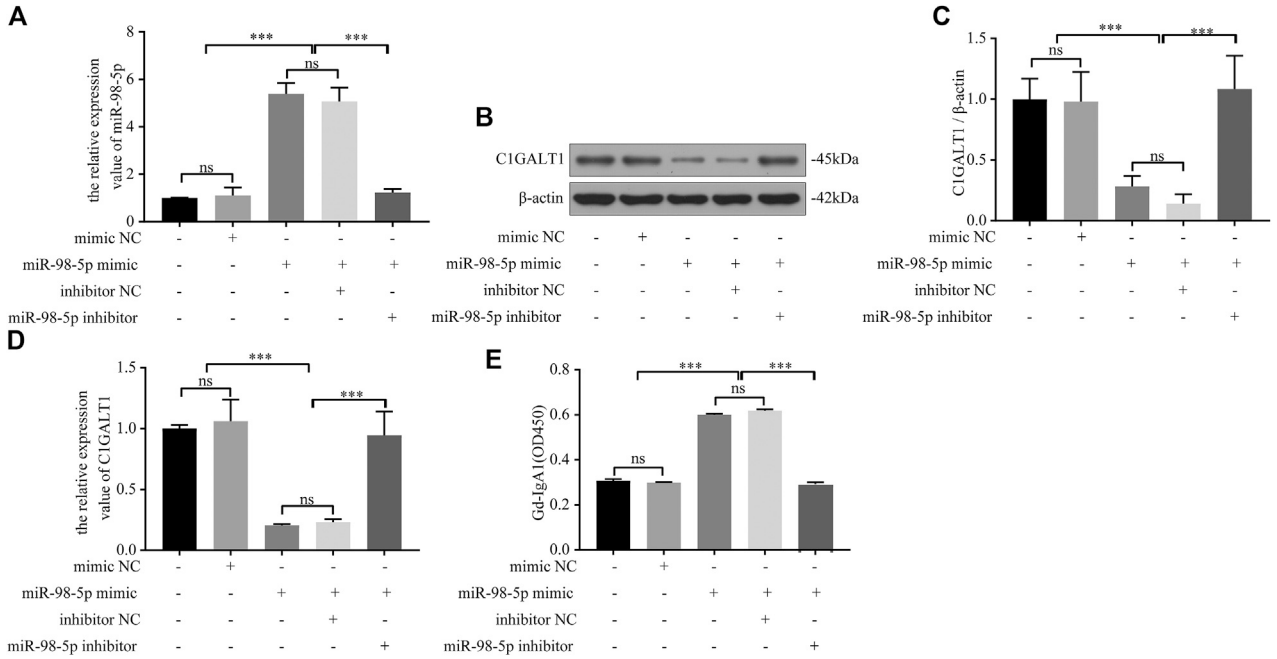

FIGURE 3 | miR-98-5p regulated the expression of C1GALT1 and Gd-IgA1 levels in DAKIKI cells. **(A)** The expression level of miR-98-5p was analyzed by qRT-PCR in DAKIKI cells. The relative expression level of miR-98-5p in the blank, mimic NC, miR-98-5p mimic, miR-98-5p mimic + inhibitor NC, and miR-98-5p mimic + miR-98-5p inhibitor groups were 1.00 ± 0.01, 1.11 ± 0.27, 5.39 ± 0.38, 5.07 ± 0.50 and 1.22 ± 0.13. **(B)** The expression of C1GALT1 protein was analyzed by western blotting in DAKIKI cells. **(C)** Fold changes were calculated by determining the ratios of C1GALT1/β-actin band intensities in DAKIKI cells. The semiquantitative relative level of C1GALT1 protein in the blank, mimic NC, miR-98-5p mimic, miR-98-5p mimic + inhibitor NC, and miR-98-5p mimic + miR-98-5p inhibitor groups were 1.00 ± 0.14, 0.98 ± 0.20, 0.28 ± 0.07, 014 ± 0.06 and 1.08 ± 0.22. **(D)** The expression levels of C1GALT1 mRNA were analyzed by qRT-PCR in DAKIKI cells. The relative expression levels of C1GALT1 mRNA in the blank, mimic NC, miR-98-5p mimic, miR-98-5p mimic + inhibitor NC, and miR-98-5p mimic + miR-98-5p inhibitor groups were 1.00 ± 0.02, 1.06 ± 0.15, 0.21 ± 0.01, 0.23 ± 0.02 and 0.95 ± 0.16. **(E)** The relative levels of Gd-IgA1 level were analyzed by VVA in the supernatant of DAKIKI cells. The relative levels of Gd-IgA1 level in the blank, mimic NC, miR-98-5p mimic, miR-98-5p mimic + inhibitor NC, and miR-98-5p mimic + miR-98-5p inhibitor groups were 0.31 ± 0.00, 0.30 ± 0.00, 0.60 ± 0.00, 0.62 ± 0.01 and 0.29 ± 0.01. ns, no significance; ***$p < 0.001$. Note: C1GALT1, β-1, 3-galactosyltransferase; Gd-IgA1, galactose-deficient IgA1; qRT-PCR, quantitative real-time polymerase chain reaction; VVA, Vicia Villosa lectin-binding assay.

0.38 vs. 1.00 ± 0.01and 1.11 ± 0.27, miR-98-5p mimic vs. miR-98-5p mimic + miR-98-5p inhibitor: 5.39 ± 0.38 vs. 1.22 ± 0.13, all $p < 0.001$) (**Figure 3A**). C1GALT1 protein and mRNA expression were significantly downregulated in the miR-98-5p mimic and miR-98-5p mimic + inhibitor NC groups (miR-98-5p mimic and miR-98-5p mimic + inhibitor NC vs. blank: 0.28 ± 0.07 and 0.14 ± 0.06 vs. 1.00 ± 0.14, $p < 0.001$). Co-transfection with the miR-98-5p inhibitor reversed this effect (**Figures 3B–D**). The levels of Gd-IgA1 in the supernatant were increased significantly in the miR-98-5p mimic and miR-98-5p mimic + inhibitor NC groups (miR-98-5p mimic and miR-98-5p mimic + inhibitor NC vs. blank and mimic NC: 0.60 ± 0.00 and 0.62 ± 0.01 vs. 0.31 ± 0.00 and 0.30 ± 0.00, $p < 0.001$); this effect was reversed by the miR-98-5p inhibitor (**Figure 3E**). These results indicated that miR-98-5p downregulated the expression of C1GALT1 and upregulated the expression of Gd-IgA1.

Identification of miR-98-5p Targeting C1Galactosyltransferase1

Next, we used TargetScan and miRDB to predict the upstream miRNAs that regulated C1GALT1 and found that miR-98-5p could target C1GALT1 with good levels of interspecies conservation (**Figure 4A**). Next, we confirmed this hypothesis by using a standard dual-luciferase reporter assay. We constructed and cloned wild-type and mutant-type C1GALT1-3'-UTR sequences (C1GALT1-WT and C1GALT1-MUT) into the pHG-MirTarget-C1GALT1 luciferase reporter vector (**Figure 4B**). Co-transfection with the C1GALT1-WT and miR-98-5p mimic significantly reduced the relative luciferase activity when compared to that in the NC mimic group (mimic NC vs. miR-98-5p mimic: 1.00 ± 0.16 vs. 0.57 ± 0.01, $p < 0.001$); co-transfection with the C1GALT1-MUT and miR-98-5p mimic or the NC mimic did not affect fluorescence intensity (**Figure 4C**). These results proved that miR-98-5p might specifically target C1GALT1.

miR-98-5p Upregulated Galactose-Deficient IgA1 Levels by Targeting C1Galactosyltransferase1 in DAKIKI Cells

We transfected DAKIKI cells with miR-98-5p inhibitor, mimics, or co-transfected with si-C1GALT1 or pcDNA-C1GALT1 to

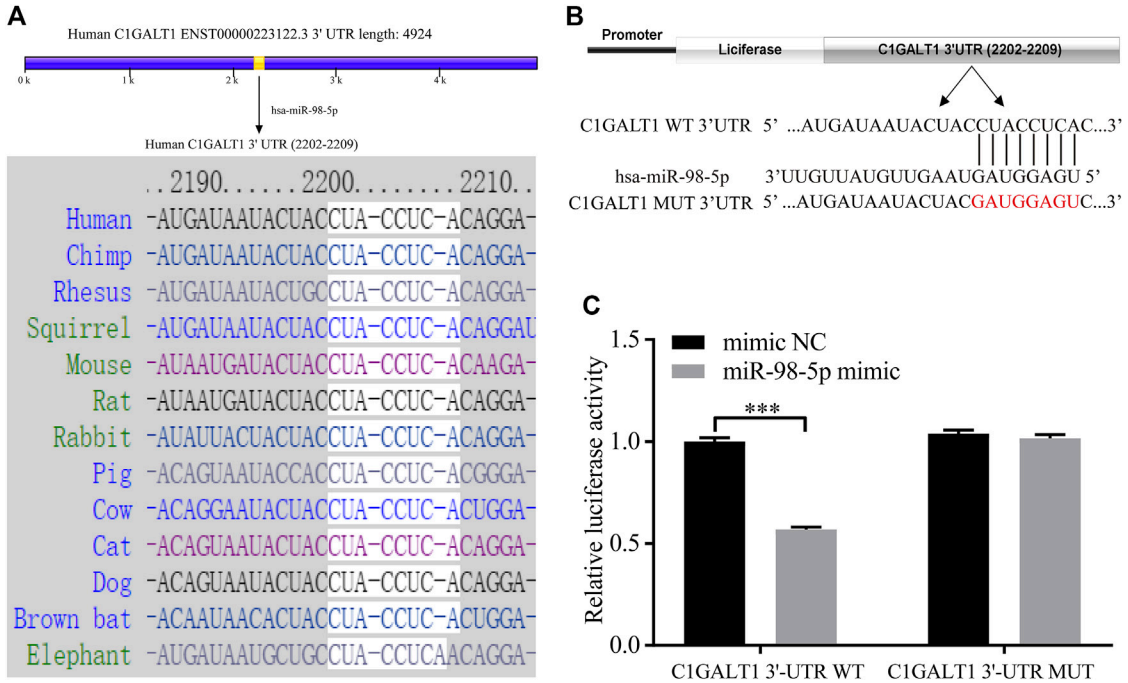

FIGURE 4 | C1GALT1 represents a potential target gene of miR-98-5p. **(A)** Schematic diagram depicting the prediction of C1GALT1 as a potential target gene of miR-98-5p, as determined by TargetScan. **(B)** Schematic view of the luciferase reporter vector. **(C)** Relative luciferase activity of the C1GALT1-3′UTR WT or C1GALT1-3′UTR MUT reporter co-transfected with miR-98-5p mimic or mimic NC. The relative luciferase activity of C1GALT1-3′UTR WT reporter in mimic NC and miR-98-5p were 1.00 ± 0.16 and 0.57 ± 0.01; the relative luciferase activity of C1GALT1-3′UTR MUT reporter in mimic NC and miR-98-5p were 1.04 ± 0.15 and 1.02 ± 0.02. NC, negative control. ***$p < 0.001$. Note: C1GALT1, β-1, 3-galactosyltransferase; WT, wild type; MUT, mutant type.

confirm whether C1GALT1 was a functional target gene of miR-98-5p. Non-transfected cells served as a control group (blank group). The miR-98-5p inhibitor upregulated the mRNA and protein levels of C1GALT1 when compared with the blank group; this effect was significantly reversed by si-C1GALT1 (miR-98-5p inhibitor vs. blank and miR-98-5p inhibitor + si-C1GALT1: mRNA: 6.97 ± 0.29 vs. 1.00 ± 0.05 and 1.66 ± 0.29, both $p < 0.001$; protein: 1.54 ± 0.20 vs. 1.07 ± 0.13 and 0.80 ± 0.09, $p < 0.05$ and $p < 0.01$) (**Figures 5A–C**). When compared with the blank group, the downregulation of miR-98-5p significantly inhibited Gd-IgA secretion; this effect was significantly rescued by si-C1GALT1 (miR-98-5p inhibitor vs. blank and miR-98–5p inhibitor + si-C1GALT1: 0.19 ± 0.01 vs. 0.33 ± 0.00 and 0.19 ± 0.01, both $p < 0.001$) (**Figure 5D**). When compared with the blank group, the miR-98-5p mimic notably significantly downregulated the mRNA and protein levels of C1GALT1; this effect was reversed by pcDNA-C1GALT1 (miR-98-5p mimic vs. blank and miR-98-5p mimic + pcDNA-C1GALT1: mRNA: 0.22 ± 0.03 vs. 1.04 ± 0.15 and 0.84 ± 0.04, both $p < 0.01$; protein: 0.24 ± 0.08 vs. 1.00 ± 0.13 and 0.65 ± 0.09, $p < 0.001$ and $p < 0.05$) (**Figures 5E–G**). When compared with the blank group, the overexpression of miR-98-5p significantly promoted Gd-IgA secretion; this effect was significantly reversed by pcDNA-C1GALT1 (miR-98-5p mimic vs. blank and miR-98-5p mimic + pcDNA-C1GALT1: 0.51 ± 0.01 vs. 0.31 ± 0.01 and 0.41 ± 0.01, both $p < 0.001$) (**Figure 5H**).

Astragaloside IV Downregulated Galactose-Deficient IgA1 Levels *via* miR-98-5p in DAKIKI Cells

AS-IV has multiple pharmacological effects, including antioxidant and anti-inflammatory effects and cardiovascular and renal protection. Combined with our previous findings that miR-98-5p promoted the secretion of Gd-IgA1, we hypothesized that AS-IV might interact with miR-98-5p to function as a renal protector.

First, DAKIKI cells were treated with different concentrations of AS-IV for 24 h. The toxicity of AS-IV was then tested by CCK-8 assay. The cell viability began to decline when the concentration of AS-IV exceeded 20 μm/ml (**Figure 6A**). As the concentration of AS-IV increased, the levels of miR-98-5p decreased (**Figure 6B**). These results indicated that AS-IV inhibited the expression of miR-98-5p in DAKIKI cells. Based on the toxicity of AS-IV, and the levels of miR-98-5p, we chose 20 μm/ml of AS-IV to perform further experiments. The mRNA and protein levels of C1GALT1 were significantly downregulated in the miR-98-5p mimic group when compared to the vehicle and mimic NC group, but was reversed by AS-IV treatment (miR-98-5p mimic + vehicle

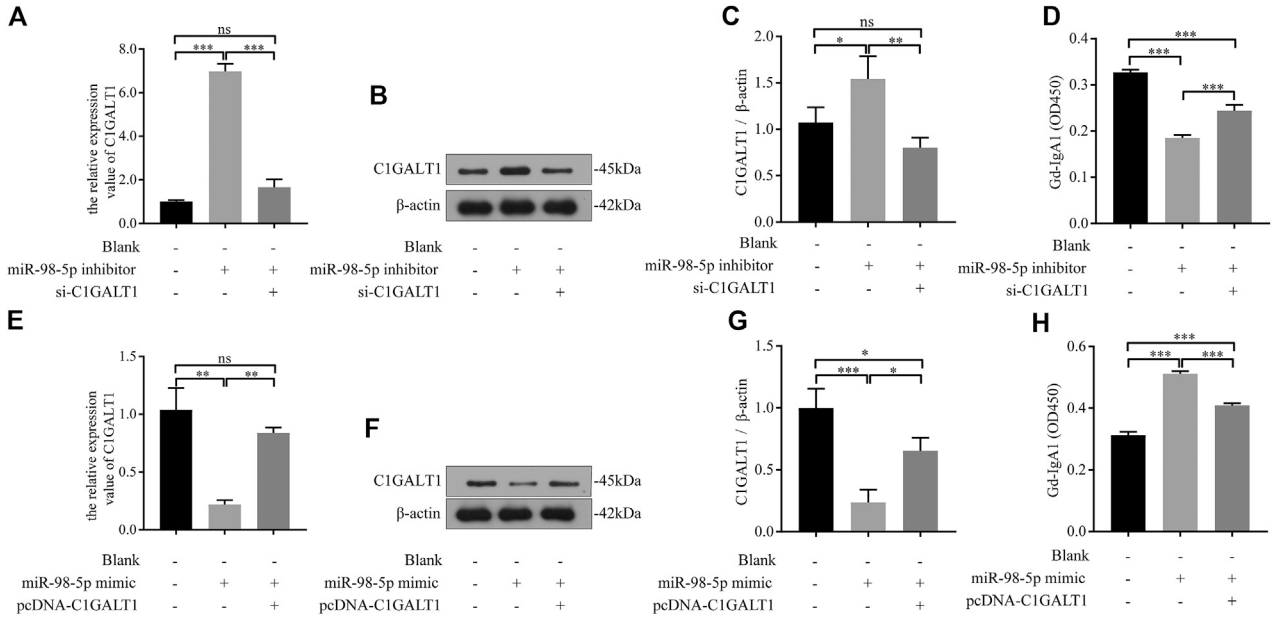

FIGURE 5 | miR-98–5p upregulated the levels of Gd-IgA1 by targeting C1GALT1 in DAKIKI cells. **(A,E)** The expression levels of C1GALT1 mRNA were analyzed by qRT-PCR in DAKIKI cells. The relative expression level of C1GALT1 mRNA in the blank, miR-98-5p inhibitor and miR-98-5p inhibitor + si-C1GALT1 groups were 1.00 ± 0.05, 6.97 ± 0.29 and 1.66 ± 0.29. The relative expression level of C1GALT1 mRNA in the blank, miR-98-5p mimic and miR-98-5p mimic + pcDNA-C1GALT1 groups were 1.04 ± 0.15, 0.22 ± 0.03 and 0.84 ± 0.04. **(B,F)** The expression of C1GALT1 protein were analyzed by Western blotting in DAKIKI cells. **(C,G)** Fold changes were calculated by determining the ratios of the C1GALT1/β-actin band intensities in DAKIKI cells. The semiquantitative relative level of C1GALT1 protein in the blank, miR-98-5p inhibitor and miR-98-5p inhibitor + si-C1GALT1 groups were 1.07 ± 0.13, 1.54 ± 0.20 and 0.80 ± 0.09. The semiquantitative relative level of C1GALT1 protein in the blank, miR-98-5p mimic and miR-98-5p mimic + pcDNA-C1GALT1 groups were 1.00 ± 0.13, 0.24 ± 0.08 and 0.65 ± 0.09. **(D,H)** The relative levels of Gd-IgA1 were analyzed by VVA in the supernatant of DAKIKI cells. The relative levels of Gd-IgA1 in the blank, miR-98-5p inhibitor and miR-98-5p inhibitor + si-C1GALT1 groups were 0.33 ± 0.00, 0.19 ± 0.01 and 0.24 ± 0.01. The relative levels of Gd-IgA1 in the blank, miR-98-5p mimic and miR-98-5p mimic + pcDNA-C1GALT1 groups were 0.31 ± 0.01, 0.51 ± 0.01 and 0.41 ± 0.01. ns, no significance; *$p < 0.05$, **$p < 0.01$, ***$p < 0.001$. Note: Gd-IgA1, galactose-deficient IgA1; C1GALT1, β-1, 3-galactosyltransferase; qRT-PCR, quantitative real-time polymerase chain reaction; VVA, Vicia Villosa lectin-binding assay.

vs.: miR-98-5p mimic + AS-IV: mRNA: 0.24 ± 0.02 vs. 1.33 ± 0.10, $p < 0.001$; protein: 0.20 ± 0.20 vs. 0.37 ± 0.03, $p < 0.01$) (**Figures 6C–E**). In contrast to C1GALT1, the levels of Gd-IgA1 were significantly higher in the miR-98–5p mimic group than the vehicle and the mimic NC group (miR-98–5p mimic + vehicle vs. vehicle and vehicle + mimic NC: 4.57 ± 0.20 vs. 1.01 ± 0.13 and 1.06 ± 0.04, both $p < 0.001$), but could also be reversed by AS-IV treatment (miR-98-5p mimic + vehicle vs.: miR-98-5p mimic + AS-IV: 0.60 ± 0.01 vs. 0.30 ± 0.01, $p < 0.001$) (**Figure 6F**). Collectively, these data showed that AS-IV downregulated the levels of Gd-IgA1 by downregulating miR-98-5p levels in DAKIKI cells.

DISCUSSION

The first and most important factor underlying IgAN is abnormalities in IgA itself. The diagnosis of IgAN is based on certain pathological features: IgA-containing CIC deposition, usually with IgG and C3 co-deposition (Irabu et al., 2020). The form of IgA that is deposited in renal tissues is mainly Gd-IgA1 with deficient Gal residues on the O-glycans in the hinge region of the heavy chains. At present, IgAN is regarded as an autoimmune disease; the pathogenesis of this condition is described by the "multi-hit hypothesis" (Moroni et al., 2019). Based on the multi-hit hypothesis, Gd-IgA1 is the origin and driving factor of IgAN.

IgA1 is specific for humans and hominoid primates. IgA1 contains a core of one O-glycans composed of GalNAc with β1,3-linked Gal (Lai et al., 2019). C1GALT1 catalyzes the transfer of Gal from UDP-Gal to GalNAc-alpha-1-Ser/Thr to generate the common core one O-glycan structure. A reduction in the activity or expression levels of C1GALT1 can lead to the abnormal addition of Gal residues, thus resulting in the formation of Gd-IgA1. Numerous studies have confirmed that Gd-IgA1 is contained within the CIC and that deposition in the mesangial tissues of patients with IgAN was mainly Gd-IgA1 (Maixnerova et al., 2019). We found that the levels of Gd-IgA1 increased in the plasma, and that the mRNA and protein levels of C1GALT1 decreased in the PBMCs of patients with IgAN. The levels of C1GALT1 were negatively correlated with the levels of Gd-IgA1 in DAKIKI cells. This is consistent with previous literature reports (Liu et al., 2020).

Previous studies have used Genome-Wide Association Studies (GWAS) to investigate whether C1GALT1 is genetically altered in the IgAN population. One study found that the variance in serum Gd-IgA1 levels in 7% of Europeans and 2% of East Asians could be explained by the C1GALT1 and C1GALTC1 loci (Kiryluk

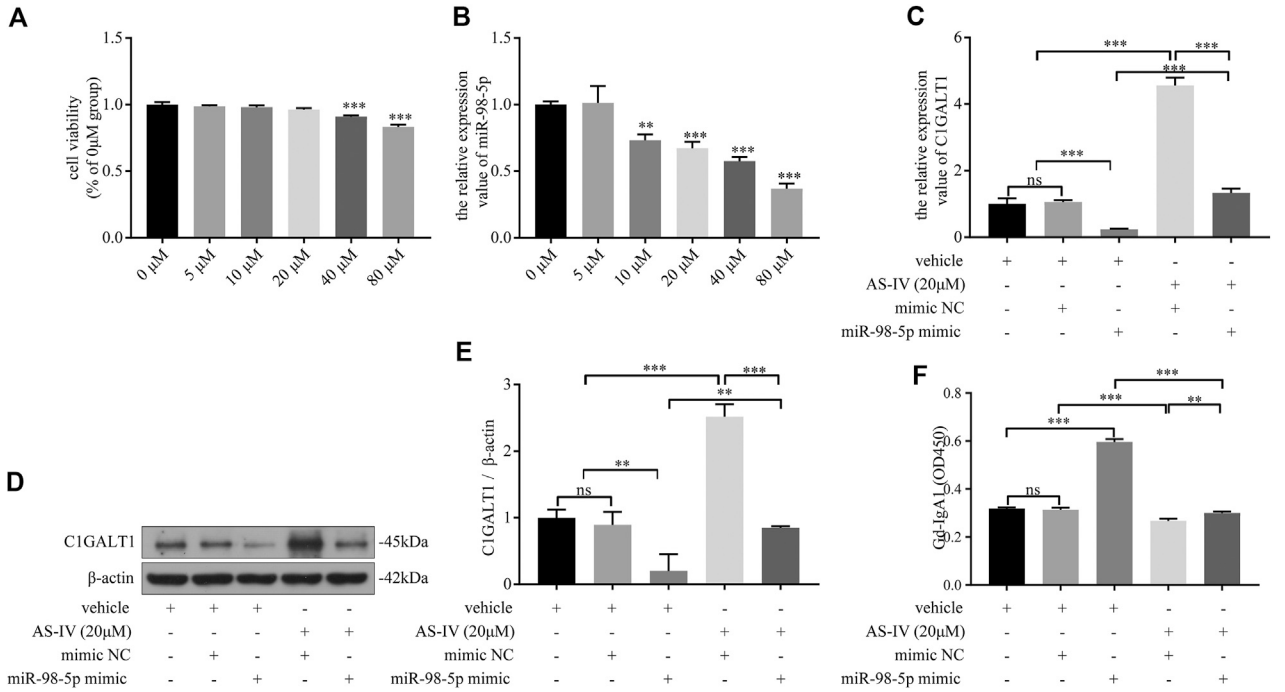

FIGURE 6 | AS-IV downregulated Gd-IgA1 levels *via* miR-98-5p in DAKIKI cells. **(A)** Different concentrations of AS-IV toxicity were determined by CCK-8 assay. The cell viability (of the percentage of 0 μM in) in 5, 10, 20, 40 and 80 μM groups were 0.99 ± 0.01, 0.98 ± 0.01, 0.96 ± 0.01, 0.91 ± 0.01, 0.83 ± 0.1. **(B)** The expression levels of miR-98-5p were analyzed by qRT-PCR in DAKIKI cells treated with different concentrations of AS-IV. The relative expression level of miR-98-5p in the 0, 5, 10, 20, 40 and 80 μM groups were 1.00 ± 0.02, 1.01 ± 0.10, 0.73 ± 0.04, 0.67 ± 0.04, 0.58 ± 0.03 and 0.37 ± 0.03. **(C)** The expression levels of C1GALT1 mRNA were analyzed by qRT-PCR in DAKIKI cells. The relative expression levels of C1GALT1 mRNA in the vehicle, vehicle + mimic NC, vehicle + miR-98-5p, AS-IV + mimic NC and AS-IV + miR-98-5p groups were 1.01 ± 0.13, 1.06 ± 0.04, 0.24 ± 0.02, 4.56 ± 0.20 and 1.33 ± 0.10. **(D)** The expression of C1GALT1 protein were analyzed by western blotting in DAKIKI cells. **(E)** Fold changes were calculated by determining the ratios of the C1GALT1/β-actin band intensities in DAKIKI cells. The semiquantitative relative level of C1GALT1 protein in the vehicle, vehicle + mimic NC, vehicle + miR-98-5p, AS-IV + mimic NC and AS-IV + miR-98-5p groups were 1.00 ± 0.10, 0.89 ± 0.16, 0.20 ± 0.20, 2.52 ± 0.15, 0.85 ± 0.02, and 0.37 ± 0.03. **(F)** The relative levels of Gd-IgA1 were analyzed by VVA in the supernatant of DAKIKI cells. The relative levels of Gd-IgA1 in the vehicle, vehicle + mimic NC, vehicle + miR-98-5p, AS-IV + mimic NC and AS-IV + miR-98-5p groups were 0.32 ± 0.00, 0.31 ± 0.01, 0.60 ± 0.01, 0.27 ± 0.01, and 0.30 ± 0.01. ns, no significance; $^{**}p < 0.01$, $^{***}p < 0.001$. Note: AS-IV, Astragaloside IV; Gd-IgA1, galactose-deficient IgA1; CCK-8, cell counting kit-8 assay; qRT-PCR, quantitative real-time polymerase chain reaction; C1GALT1, β-1, 3-galactosyltransferase; VVA, Vicia Villosa lectin-binding assay.

et al., 2017). This indicated that the C1GALT1 gene itself could only explain a small part of the observed variance of serum Gd-IgA1 in patients with IgAN. This indicates that further research is needed with regards to the regulatory network in IgAN. Studies have demonstrated that C1GALT1 can be regulated by cytokines, Golgi matrix protein 130 (GM130), as well as by miRNA (Xiao et al., 2017; Selvaskandan et al., 2018; Wang C. et al., 2019).

miRNAs regulate target mRNAs at the post-transcriptional level by inducing mRNA degradation or by inhibiting translation (Zhao et al., 2019). Therefore, the biological role of miRNA can be reflected by its regulated target gene. Numerous studies have found that miRNAs play a vital role in the occurrence and development of IgAN and can be used as non-invasive biomarkers for diagnosis and or the evaluation of renal damage (Selvaskandan et al., 2018). Recent insights have also revealed that miRNAs such as miR-148b, let-7b, and miR-155, play crucial roles in IgAN (Wang et al., 2011; Serino et al., 2012; Serino et al., 2015).

By analyzing the GSE25590 miRNA microarray, we identified 112 mature DEmiRNAs, including 91 upregulated and 21 downregulated miRNAs. Next, we set C1GALT1 as the target gene and used Targetscan and miRDB to predict 197 target miRNAs. Next, we identified the intersection of the DEmiRNAs and predicted miRNAs and identified a total of 13 target miRNAs for further study. The expression trend for the miRNAs was opposite to that for the target gene; consequently, we excluded the down-regulated hsa-miR-590-3p and hsa-miR-488-3p. We set the filter conditions of the Pct value in TargetScan at > 0.75, and the TargetScore in miRDB >60, to compare conservation between species and the possibility of miRNA targeting target genes; this practice led to the exclusion of hsa-miR-488-3p and hsa-miR-543. Previous studies have demonstrated that the increased expression of miR-148 and let-7b promotes Gd-IgA1 secretion by targeting C1GALT1 and UDP-N-acetyl-α-D-galactosamine:polypeptide N-acetylgalactosaminyltransferase 2 (GALNT2), respectively (Serino et al., 2012; Serino et al., 2015). Therefore, we also excluded miR-148b-3p. Since let-7s exhibit a similar structure and function, we also excluded hsa-let-7a-5p, hsa-let-7b-5p hsa-let-7c-5p, hsa-let-7d-5p, hsa-let-7f-5p, hsa-let-7g-5p, and hsa-let-7i-5p. Previous reports have revealed that miR-98 (now referred to as miR-98-5p) is associated with systemic lupus erythematosus, diabetic nephropathy, and B cell-related immune inflammations

(Gonzalez-Martin et al., 2016). However, whether this plays a role in IgAN remains unknown. Therefore, we selected miR-98-5p and miR-152-3p for further validation. PCR results showed that only miR-98-5p was upregulated in pediatric patients of IgAN and was therefore selected for further analysis. miR-98-5p is highly conserved in terms of sequence and spatiotemporal expression across different species and exhibits a range of physiological functions, including the inhibition of cytokine synthesis, the regulation of lipid metabolism, and regulation of the immune system (Chen et al., 2017; Sun et al., 2018). Since Gd-IgA1 is synthesized by B cells, any form of B cell dysfunction may promote its secretion.

We found that the levels of miR-98-5p were negatively correlated with C1GALT1 in PBMCs from pediatric patients with IgAN and in DAKIKI cells. miR-98-5p significantly inhibited the activity of the wild-type C1GALT1 gene; the mutant-type was not affected, as confirmed by dual-luciferase reporter gene experiments. We then conducted a rescue experiment to verify the relationship between miR-98-5p and C1GALT1. Our experiments found that the increased levels of Gd-IgA1 induced by the miR-98-5p mimic could be significantly reversed by the overexpression of C1GAL1. Furthermore, the reduction of Gd-IgA1 secretion caused by the miR-98-5p inhibitor could be impaired by the silencing of C1GALT1. These results demonstrated that the stimulatory effect of miR-98-5p on Gd-IgA1 secretion was mediated by the downregulation of C1GALT1.

We measured the mRNA and protein levels of C1GALT1 in healthy controls and pediatric patients with MsPGN, IgAV-N, and IgAN, and found the levels of C1GALT1 were significantly reduced in patients with IgAN and IgAV-N. We therefore hypothesize that the occurrence and development of IgAN and IgAV-N may both be related to Gd-IgA1. However, miR-98-5p was only significantly increased in patients with IgAN, thus suggesting that the regulatory mechanism of C1GALT1 in IgAN and IgAV-N was different. However, our sample size was small; larger sample sizes are now needed to verify our current findings.

Astragalus membranaceus (Huangqi in Chinese) is a traditional Chinese herbal medicine that is commonly used for clinical treatments. AS-IV is an active ingredient of *Astragalus membranaceus* and has been shown to exert cardioprotective, neuroprotective, and renoprotective activities (Wang E. et al., 2020; Wang Z. et al., 2020; Xia et al., 2020). Thus, we hypothesized that AS-IV might also have a protective effect on IgAN. In our investigations, we treated DAKIKI cells with AS-IV and found that an elevated concentration of AS-IV could down-regulate miR-98-5p. Next, we further investigated the relationship between AS-IV and miR-98-5p in DAKIKI cells. Data revealed that 20 μM/mL of AS-IV could abolish the regulatory effect caused by the overexpression of miR-98-5p on both C1GALT1 and Gd-IgA1, thus confirming that miR-98-5p might be a downstream molecule of AS-IV that regulates the levels of C1GALT1 and Gd-IgA1.

Our study has several limitations that need to be considered. First of all, the sample size was small; larger sample sizes are now needed to verify our findings. Secondly, the experiments were performed only with PBMCs and the DAKIKI cell line; we did not carry out any experiments in animal models because we do not have the experimental conditions to create humanized mice. Thirdly, this study only observed the effect of AS-IV on the DAKIKI cell line, not PBMCs from patients with IgAN. Although *Astragalus membranaceus* has been widely used for clinical treatment in China, AS-IV has not.

In conclusion, our results reveal that AS-IV could inhibit Gd-IgA1 secretion *via* miR-98-5p. Increased levels of miR-98-5p in pediatric IgAN patients might affect the glycosylation of IgA1 by targeting C1GALT1, thus leading to the excessive synthesis of Gd-IgA1. In addition, our analyses suggest that the pathogenesis of IgAN may differ from that of IgAV-N. Collectively, these results provide significant insight into the pathogenesis of IgAN and identify a potential therapeutic target.

DATA AVAILABILITY STATEMENT

The raw data supporting the conclusions of this article will be made available by the authors, without undue reservation.

ETHICS STATEMENT

The study was approved by the Medical Ethical Committee of the Second Xiangya Hospital of Central South University. Written informed consent to participate in this study was provided by the participants' legal guardian/next of kin.

AUTHOR CONTRIBUTIONS

CL design, data curation, investigation, methodology, writing-original draft. XL, LS, XD, and FP investigation, resources, methodology. MZ project administration and writing-review and editing. SX and YL methodology, validation and writing-review and editing. QH conceptualization, resources, supervision, funding acquisition. All authors have read and approved the final version of the manuscript.

FUNDING

This work was supported by Hunan innovative province construction project (Grant No. 2019SK2211) and Changsha Science and Technology Planning Project (Grant No. kq2001044).

ACKNOWLEDGMENTS

The authors thanks professor Liu Youxia of Tianjin University General Hospital for giving DAKIKI cell line. The authors thanks Huang Yanxia for professional experimental guidance.

SUPPLEMENTARY MATERIAL

The Supplementary Material for this article can be found online at: https://www.frontiersin.org/articles/10.3389/fphar.2021.658236/full#supplementary-material.

REFERENCES

Cambier, A., Rabant, M., El Karoui, K., Peuchmaur, M., Servais, A., Hertig, A., et al. (2020). Clinical and histological differences between adults and children in new onset IgA nephropathy. *Pediatr. Nephrol.* 35 (10), 1897–1905. doi:10.1007/s00467-020-04614-3

Chen, S., Wen, X., Zhang, W., Wang, C., Liu, J., and Liu, C. (2017). Hypolipidemic effect of oleanolic acid is mediated by the miR-98-5p/PGC-1β axis in high-fat diet-induced hyperlipidemic mice. *FASEB J.* 31 (3), 1085–1096. doi:10.1096/fj.201601022R

Coppo, R., and Robert, T. (2020). IgA nephropathy in children and in adults: two separate entities or the same disease?. *J. Nephrol.* 33 (6), 1219–1229. doi:10.1007/s40620-020-00725-0

Cui, X., Jiang, X., Wei, C., Xing, Y., and Tong, G. (2020). Astragaloside IV suppresses development of hepatocellular carcinoma by regulating miR-150-5p/β-catenin axis. *Environ. Toxicol. Pharmacol.* 78, 103397. doi:10.1016/j.etap.2020.103397

Gong, L., Chang, H., Zhang, J., Guo, G., Shi, J., and Xu, H. (2018). Astragaloside IV protects rat cardiomyocytes from hypoxia-induced injury by down-regulation of miR-23a and miR-92a. *Cell Physiol. Biochem.* 49 (6), 2240–2253. doi:10.1159/000493827

Gonzalez-Martin, A., Adams, B. D., Lai, M., Shepherd, J., Salvador-Bernaldez, M., Salvador, J. M., et al. (2016). The microRNA miR-148a functions as a critical regulator of B cell tolerance and autoimmunity. *Nat. Immunol.* 17 (4), 433–440. doi:10.1038/ni.3385

Hennino, M.-F., Buob, D., van der Hauwaert, C., Gnemmi, V., Jomaa, Z., Pottier, N., et al. (2016). miR-21-5p renal expression is associated with fibrosis and renal survival in patients with IgA nephropathy. *Sci. Rep.* 6, 27209. doi:10.1038/srep27209

Irabu, H., Shimizu, M., Kaneko, S., Inoue, N., Mizuta, M., Ohta, K., et al. (2020). Clinical significance of serum galactose-deficient IgA1 level in children with IgA nephropathy. *J. Immunol. Res.* 2020, 1–10. doi:10.1155/2020/4284379

Kiryluk, K., Li, Y., Moldoveanu, Z., Suzuki, H., Reily, C., Hou, P., et al. (2017). GWAS for serum galactose-deficient IgA1 implicates critical genes of the O-glycosylation pathway. *PLoS Genet.* 13, e1006609. doi:10.1371/journal.pgen.1006609

Krützfeldt, J., Rajewsky, N., Braich, R., Rajeev, K. G., Tuschl, T., Manoharan, M., et al. (2005). Silencing of microRNAs *in vivo* with 'antagomirs'. *Nature* 438 (7068), 685–689. doi:10.1038/nature04303

Lai, L., Liu, T., Yan, M., Shang, D., Qian, J., Hao, C., et al. (2019). Abnormal glucose metabolism and galactose-deficient immunoglobulin A1 (IgA1) synthesis: a possible mechanism of IgA nephropathy. *Discov. Med.* 28 (151), 39–45.

Liu, D., Xia, M., Liu, Y., Tan, X., He, L., Liu, Y., et al. (2020). The upregulation of miR-98-5p affects the glycosylation of IgA1 through cytokines in IgA nephropathy. *Int. Immunopharmacol.* 82, 106362. doi:10.1016/j.intimp.2020.106362

Maixnerova, D., Ling, C., Hall, S., Reily, C., Brown, R., Neprasova, M., et al. (2019). Galactose-deficient IgA1 and the corresponding IgG autoantibodies predict IgA nephropathy progression. *PLoS One* 14 (2), e0212254. doi:10.1371/journal.pone.0212254

Mestecky, J., Russell, M. W., Jackson, S., and Brown, T. A. (1986). The human IgA system: a reassessment. *Clin. Immunol. Immunopathol.* 40 (1), 105–114. doi:10.1016/0090-1229(86)90073-5

Mok, Y., Schwierzeck, V., Thomas, D. C., Vigorito, E., Rayner, T. F., Jarvis, L. B., et al. (2013). MiR-210 is induced by Oct-2, regulates B cells, and inhibits autoantibody production. *J. Immunol.* 191 (6), 3037–3048. doi:10.4049/jimmunol.1301289

Moroni, G., Belingheri, M., Frontini, G., Tamborini, F., and Messa, P. (2019). Immunoglobulin A nephropathy. Recurrence after renal transplantation. *Front. Immunol.* 10, 1332. doi:10.3389/fimmu.2019.01332

Novak, J., Barratt, J., Julian, B. A., and Renfrow, M. B. (2018). Aberrant glycosylation of the IgA1 molecule in IgA nephropathy. *Semin. Nephrol.* 38 (5), 461–476. doi:10.1016/j.semnephrol.2018.05.016

Placzek, W. J., Yanagawa, H., Makita, Y., Renfrow, M. B., Julian, B. A., Rizk, D. V., et al. (2018). Serum galactose-deficient-IgA1 and IgG autoantibodies correlate in patients with IgA nephropathy. *PLoS One* 13, e0190967. doi:10.1371/journal.pone.0190967

Selvaskandan, H., Pawluczyk, I., and Barratt, J. (2018). MicroRNAs: a new avenue to understand, investigate and treat immunoglobulin A nephropathy?. *Clin. Kidney J.* 11 (1), 29–37. doi:10.1093/ckj/sfx096

Serino, G., Sallustio, F., Cox, S. N., Pesce, F., and Schena, F. P. (2012). Abnormal miR-148b expression promotes aberrant glycosylation of IgA1 in IgA nephropathy. *Jasn* 23 (5), 814–824. doi:10.1681/ASN.2011060567

Serino, G., Sallustio, F., Curci, C., Cox, S. N., Pesce, F., De Palma, G., et al. (2015). Role of let-7b in the regulation ofN-acetylgalactosaminyltransferase 2 in IgA nephropathy. *Nephrol. Dial. Transpl.* 30 (7), 1132–1139. doi:10.1093/ndt/gfv032

Smith, A. C., de Wolff, J. F., Molyneux, K., Feehally, J., and Barratt, J. (2006). O-glycosylation of serum IgD in IgA nephropathy. *J. Am. Soc. Nephrol.* 17, 1192–1199. doi:10.1681/ASN.2005101115

Sun, X., Li, X., Ma, S., Guo, Y., and Li, Y. (2018). MicroRNA-98-5p ameliorates oxygen-glucose deprivation/reoxygenation (OGD/R)-induced neuronal injury by inhibiting Bach1 and promoting Nrf2/ARE signaling. *Biochem. Biophysical Res. Commun.* 507 (1–4), 114–121. doi:10.1016/j.bbrc.2018.10.182

Suzuki, H., Kiryluk, K., Novak, J., Moldoveanu, Z., Herr, A. B., Renfrow, M. B., et al. (2011). The pathophysiology of IgA nephropathy. *J. Am. Soc. Nephrol.* 22, 1795–1803. doi:10.1681/ASN.2011050464

Wang, G., Kwan, B. C.-H., Lai, F. M.-M., Chow, K.-M., Li, P. K.-T., and Szeto, C.-C. (2011). Elevated levels of miR-146a and miR-155 in kidney biopsy and urine from patients with IgA nephropathy. *Dis. Markers* 30 (4), 171–179. doi:10.3233/DMA-2011-076610.1155/2011/304852

Wang, C., Ye, M., Zhao, Q., Xia, M., Liu, D., He, L., et al. (2019). Loss of the Golgi matrix protein 130 cause aberrant IgA1 glycosylation in IgA nephropathy. *Am. J. Nephrol.* 49 (4), 307–316. doi:10.1159/000499110

Wang, J., Li, X., Wu, X., Wang, Z., Zhang, C., Cao, G., et al. (2019). Expression profiling of exosomal miRNAs derived from the peripheral blood of kidney recipients with DGF using high-throughput sequencing. *Biomed. Res. Int.* 2019, 1759697. doi:10.1155/2019/1759697

Wang, E., Wang, L., Ding, R., Zhai, M., Ge, R., Zhou, P., et al. (2020). Astragaloside IV acts through multi-scale mechanisms to effectively reduce diabetic nephropathy. *Pharmacol. Res.* 157, 104831. doi:10.1016/j.phrs.2020.104831

Wang, Z., Zhu, Y., Zhang, Y., Zhang, J., Ji, T., Li, W., et al. (2020). Protective effects of AS-IV on diabetic cardiomyopathy by improving myocardial lipid metabolism in rat models of T2DM. *Biomed. Pharmacother.* 127, 110081. doi:10.1016/j.biopha.2020.110081

Xia, M.-L., Xie, X.-H., Ding, J.-H., Du, R.-H., and Hu, G. (2020). Astragaloside IV inhibits astrocyte senescence: implication in Parkinson's disease. *J. Neuroinflammation* 17 (1), 105. doi:10.1186/s12974-020-01791-8

Xiao, C., Nemazee, D., and Gonzalez-Martin, A. (2020). MicroRNA control of B cell tolerance, autoimmunity and cancer. *Semin. Cancer Biol.* 64, 102–107. doi:10.1016/j.semcancer.2019.04.004

Xiao, J., Wang, M., Xiong, D., Wang, Y., Li, Q., Zhou, J., et al. (2017). TGF-β1 mimics the effect of IL-4 on the glycosylation of IgA1 by downregulating core 1 β1, 3-galactosyltransferase and Cosmc. *Mol. Med. Rep.* 15 (2), 969–974. doi:10.3892/mmr.2016.6084

Zhao, H., Ma, S.-X., Shang, Y.-Q., Zhang, H.-Q., and Su, W. (2019). microRNAs in chronic kidney disease. *Clinica Chim. Acta.* 491, 59–65. doi:10.1016/j.cca.2019.01.008

Conflict of Interest: The authors declare that the research was conducted in the absence of any commercial or financial relationships that could be construed as a potential conflict of interest.

frontiers in Pharmacology

ORIGINAL RESEARCH
published: 20 April 2021
doi: 10.3389/fphar.2021.656244

Oral Unsaturated Fat Load Impairs Postprandial Systemic Inflammation in Primary Hypercholesterolemia Patients

Aida Collado[1,2†], *Elena Domingo*[1†], *Patrice Marques*[1,2†], *Eva Perello*[2,3], *Sergio Martínez-Hervás*[2,3,4], *Laura Piqueras*[1,2,3], *Juan F. Ascaso*[2,3,4], *José T. Real*[2,3,4*‡] and *Maria-Jesus Sanz*[1,2,3*‡]

[1]Department of Pharmacology, Faculty of Medicine and Odontology, University of Valencia, Valencia, Spain, [2]Institute of Health Research INCLIVA, University Clinic Hospital of Valencia, Valencia, Spain, [3]CIBERDEM-Spanish Biomedical Research Center in Diabetes and Associated Metabolic Disorders, Carlos III Health Institute, Madrid, Spain, [4]Department of Medicine, Faculty of Medicine and Odontology, University of Valencia, Valencia, Spain

OPEN ACCESS

Edited by:
Yao Lu,
Central South University, China

Reviewed by:
Zhou Jiang,
University of Texas MD Anderson Cancer Center, United States
Belal Chami,
The University of Sydney, Australia

***Correspondence:**
José T. Real
Jose.T.Real@uv.es
Maria-Jesus Sanz
Maria.J.Sanz@uv.es

†These authors have contributed equally to this work and share first authorship
‡These authors have contributed equally to this work and share last authorship

Specialty section:
This article was submitted to Inflammation Pharmacology, a section of the journal Frontiers in Pharmacology

Received: 20 January 2021
Accepted: 18 March 2021
Published: 20 April 2021

Citation:
Collado A, Domingo E, Marques P, Perello E, Martínez-Hervás S, Piqueras L, Ascaso JF, Real JT and Sanz M-J (2021) Oral Unsaturated Fat Load Impairs Postprandial Systemic Inflammation in Primary Hypercholesterolemia Patients. Front. Pharmacol. 12:656244. doi: 10.3389/fphar.2021.656244

Context: Primary hypercholesterolemia (PH) is a lipid disorder characterized by elevated levels of cholesterol and low-density lipoprotein (LDL). Low-grade systemic inflammation is associated with PH, which might explain the higher incidence of cardiovascular diseases in this setting.

Objective: To evaluate the effect of an oral unsaturated fat load (OUFL) on different immune parameters and functional consequences in patients with PH in postprandial state.

Design: A commercial liquid preparation of long-chain triglycerides (Supracal®; ω6/ω3 ratio >20/1, OUFL) was administered to 20 patients and 10 age-matched controls. Whole blood was collected before (fasting state) and 4 h after administration (postprandial state). Flow cytometry was employed to determine platelet and leukocyte activation, and the levels of circulating platelet-leukocyte aggregates. Soluble markers were determined by ELISA, and the parallel-plate flow chamber was employed to study leukocyte adhesion to the dysfunctional arterial endothelium.

Results: The PH group had a lower percentage of activated platelets and circulating type 1 monocytes, and blunted neutrophil activation after the OUFL, accompanied by a significant increase in the percentage of regulatory T lymphocytes. In this group, the OUFL led to a significant impairment of leukocyte adhesion to the dysfunctional [tumor necrosis factor α (TNFα)-stimulated] endothelium and reduced the plasma levels of soluble P-selectin, platelet factor-4 (PF-4)/CXCL4, CXCL8, CCL2, CCL5, and TNFα.

Conclusion: The OUFL has a beneficial impact on the pro-thrombotic and pro-inflammatory state of PH patients and might be a promising macronutrient approach to dampen the systemic inflammation associated with PH and the development of further cardiovascular events.

Keywords: primary hypercholesterolemia, oral unsaturated fat load, systemic inflammation, platelet activation, leukocytes, inflammatory mediators, endothelial dysfunction

INTRODUCTION

Cardiovascular disease (CVD) remains one of the leading causes of death in Western societies (Benjamin et al., 2017; Wilkins et al., 2017). The main risk factors for CVD include age, hypertension, obesity, diabetes *mellitus* and high circulating levels of low-density lipoprotein (LDL) (Wong et al., 2016). Despite improvements in primary prevention and the identification of new pharmacological agents to reduce blood cholesterol levels, the adoption of unhealthy lifestyle habits has led to an increased incidence of hypercholesterolemia, diabetes *mellitus* and obesity, which in turn has increased the incidence and prevalence of atherosclerosis–the predominant cause of CVD (Hedrick 2015; Zimmer et al., 2015).

Primary hypercholesterolemia (PH) is a metabolic disorder characterized by elevated plasma levels of cholesterol, in particular, LDL and apolipoprotein B (apoB). PH is genetically heterogeneous and includes both familial hypercholesterolemia (FH, prevalence of 1:200–1:500) and non-familial polygenic hypercholesterolemia, which is far more frequent (Langslet et al., 2015). The marked increase of LDL in the bloodstream in PH can trigger the development of atherosclerotic plaques in arteries, increasing the risk of premature coronary artery disease (Defesche et al., 2017), which for untreated hypercholesterolemia can be 20% higher than in control subjects (Sniderman et al., 2014). Yet, it has become more evident that systemic inflammation seems to be the main driver of premature atherosclerosis and its complications, together with elevated LDL plasma levels (Catapano et al., 2017). Indeed, several studies have demonstrated that low-grade systemic inflammation is associated with PH, which might explain the higher incidence of CVD in these patients beyond elevated LDL cholesterol plasma values (Langslet et al., 2015; Barale et al., 2018; Collado et al., 2018a).

The oral unsaturated fat load (OUFL) test is a standardized method to study postprandial lipemia that allows the evaluation of the relationship between fatty acids and different parameters in a non-fasting situation (Garcia-Garcia et al., 2019). In this regard, an OUFL challenge in patients with FH was found to modulate oxidative/antioxidative status, reducing overall oxidative stress (Pedro et al., 2013; Cortes et al., 2014) and the levels of some atherosclerosis-related chemokines (Cortes et al., 2016). The postprandial effect of unsaturated fats on the immune state in patients with PH has, by comparison, received much less attention.

We previously reported the existence of low-grade systemic inflammation in patients with PH, which is accompanied by a pro-thrombotic state driven by exacerbated platelet activation and endothelial dysfunction, likely explaining the higher incidence of further CVD (Collado et al., 2018a). In the present study, we tested whether a 4 h OUFL challenge in patients with PH favorably impacts different immune and functional outcomes. A secondary aim was to examine whether the inflammatory state and tumor necrosis factor α (TNFα)-induced endothelial leukocyte adhesion, a key feature of endothelial dysfunction, was improved after this time. To do this, we enrolled age-matched controls and untreated, primarily diagnosed patients with PH.

MATERIALS AND METHODS

The present study was performed following The Code of Ethics of the World Medical Association outlined in the Declaration of Helsinki of 1975 and revised in 1983 for experiments that involve human subjects. The Clinical Research Ethics Committee of the University Clinic Hospital of Valencia, Spain approved the protocol for this study. All subjects signed the appropriate written informed consent to participate in the study, and the privacy rights of subjects were always observed.

This manuscript is in line with the Recommendations for the Conduct, Reporting, Editing, and Publication of Scholarly Work in Medical Journals and aims for the inclusion of representative human populations (gender, age, and ethnicity) as per those recommendations.

Cell Culture

Human umbilical artery endothelial cells (HUAEC) were isolated from human umbilical cords by collagenase treatment as previously described (Jaffe et al., 1973). Cells were maintained in human endothelial cell basal medium-2 supplemented with endothelial growth medium-2 (both from Lonza Group, Basel, Switzerland) with 10% fetal bovine serum (Biowest, Nuaillé, France). Cells were grown to confluence up to passage 1 to preserve endothelial features. Before every experiment, cells were incubated for 24 h in medium containing 2% fetal bovine serum.

Human Study Populations

Twenty patients with PH and 10 age-matched controls were included in the study, and all were recruited by the Endocrinology and Nutrition Service at the University Clinic Hospital of Valencia, Spain.

Subjects fulfilled the diagnosis, inclusion and exclusion criteria to be considered for the study (Collado et al., 2018a), as described in **Table 1**.

Oral Unsaturated Fat Load Administration

The study started at 8:30 a.m. and blood was drawn by venipuncture after a fasting period of at least 12 h. Anthropometric parameters and blood pressure were measured using standardized procedures: body mass index (BMI; kg/m^2), waist circumference (midpoint between the edge lower rib and iliac crest; cm) and blood pressure (mmHg). Blood samples from PH patients and age-matched controls were taken and collected in Vacutainer® blood collection tubes containing sodium citrate (3.2%), or in Vacutainer® PST™ II tubes with lithium/heparin (17 IU/ml) as anticoagulant agents (BD Biosciences, San Jose, CA, United States) and subsequently subjected to different analytical determinations including complete biochemistry with glycemic and lipid profile, and quantification of creatinine as a measure of renal function.

After the first blood sampling (time 0; T0), both patients and controls ingested a commercial OUFL of 25 g of a high-fat meal per m^2 of body surface area, prepared with a commercial long-chain triglycerides (TG) liquid preparation (Supracal®; SHS International, Liverpool, United Kingdom). Each 100 ml of the formula contained 50 g of fat (450 kcal), of which 9.6 g was saturated, 28.2 g

TABLE 1 | Diagnosis, inclusion and exclusion criteria for patients and age-matched controls to participate in the study (Collado et al., 2018a)[1].

Diagnosis criteria (PH patients)	Inclusion criteria (age-matched controls)	Exclusion criteria (both groups)
TC > 260 mg/dl and/or LDL >160 mg/dl	TC < 200 mg/dl and apoB <120 mg/dl	CVD, hypertension, diabetes, chronic diseases or cancer
TG < 150 mg/dl	TG < 150 mg/dl Fasting plasma glucose <100 mg/dl The absence of dyslipidemia, CVD or diabetes	Smoking Alcohol consumption >30 g/day Renal or hepatic insufficiency and hypothyroidism Pregnancy or lactation Infection, inflammatory disease (including asthma, allergy, and autoimmune deficiency) or drugs able to alter inflammation six weeks before the study

[1]*apoB, apolipoprotein B; CVD, cardiovascular disease; LDL, low-density lipoprotein; PH, primary hypercholesterolemia; TC, total cholesterol; TG, triglycerides.*

monounsaturated and 10 g polyunsaturated, with a $\omega 6/\omega 3$ ratio >20/1. Fatty acid content and the complete composition are detailed in **Supplementary Table S1**, as explained previously (Pedro et al., 2013). Subjects were only allowed to drink mineral water during the test. Blood samples were taken before and 4 h after the OUFL challenge for the various measurements.

Flow Cytometry

Whole blood was stained with saturated amounts of antibodies as indicated by the manufacturers. A Fc blocker was not used since flow cytometry studies have been performed in whole blood. Under these circumstances it is widely accepted that whole blood contains enough amounts of IgGs to block Fc receptor. All samples were analyzed in a FACSVerse™ flow cytometer (BD Biosciences) and data analyzed with FlowJo® v10.0.7 software (FlowJo LLC, Ashland, OR).

Measurement of Platelet Activation

To assess platelet activation, PAC-1$^+$ platelets and P-selectin expression were assessed by flow cytometry. Samples of citrated blood were diluted in glucose buffer [1:10; 1 mg/ml glucose in phosphate-buffered saline (PBS) containing 0.35% bovine serum albumin (BSA); Sigma-Aldrich, St. Louis, MO, United States] (Murugappa and Kunapuli, 2006), and then incubated for 30 min with a 5-carboxyfluorescein (CF)-Blue™-conjugated monoclonal antibody (mAb) against human CD41 (clone HIP8, IgG_1; Immunostep, Salamanca, Spain), a fluorescein isothiocyanate (FITC)-conjugated mouse mAb against human PAC-1 (clone PAC-1, IgM; BD Biosciences) or with an allophycocyanin (APC)-conjugated mAb against human P-selectin (CD62P, clone HI62P, IgG_1; Immunostep).

The identification of the platelet population was achieved based on their morphology according to size and complexity [side scatter (SSC) *vs.* forward scatter (FSC)]. They were subsequently selected as the CD41$^+$ population and expressed as the percentage of positive platelets, as illustrated in the gating strategy in **Supplementary Figure S1**.

Leukocyte Subpopulation Studies

Neutrophils

To assess the polymorphonuclear population present in blood samples, a high SSC and staining with a Pacific Blue (PB)™-conjugated mouse mAb against human CD45 (clone HI30, IgG_1; BioLegend, San Diego, CA, United States) were combined to select the neutrophil population. Analysis with a FITC-conjugated mouse mAb against human CD16 (clone 3G8, IgG_1; BD Biosciences) was first performed to distinguish them, and the possible presence of platelets was studied using two different experimental approaches. First, heparinized whole blood was analyzed to detect neutrophils attached to platelets. Second, and in parallel, blood samples were incubated with 10 mM ethylenediaminetetraacetic acid (EDTA; PanReac AppliChem GmbH, Darmstadt, Germany), for 15 min at 37°C to promote platelet dissociation, as described (Postea et al., 2012). In both cases, a phycoerythrin (PE)/Cy™7-conjugated mouse mAb against human CD41 (clone HIP8, IgG_1; BioLegend) was used to determine the neutrophil-platelet aggregates (**Supplementary Figure S2**). The activation state in this cell population was determined with an APC-conjugated mouse mAb against human integrin CD11b (clone ICRF44, IgG_1; BioLegend) and a PE-conjugated mAb against human CD69 (clone FN50, IgG_1; Immunostep).

Monocytes

An APC-conjugated mouse mAb against human CD14 (clone 47-3D6, IgG_{2A}; Immunostep) was used to distinguish monocytes from other leukocyte types and positive cells were selected. To identify the different types of monocytes, the CD14 population was confronted with a FITC-conjugated mouse mAb against human CD16 (clone 3G8, IgG_1; BD Biosciences) and a brilliant violet BV421™-conjugated mouse mAb against human CD192 (CCR2, clone K036C2, IgG_{2A}; BioLegend) (**Supplementary Figure S3**) (Collado et al., 2018a). Consequently, three subpopulations of monocytes were distinguished as described in **Supplementary Table S2**. Monocyte-platelet aggregates were determined following the same strategy as explained above.

A PE-conjugated mouse mAb against human integrin CD11b (clone CBRM1/5, IgG_1; BioLegend) was used to determine the activation state of these cell populations. Similarly, fractalkine/CX_3CL1 receptor (CX_3CR1) expression was also determined in these three monocyte subpopulations using a PE-conjugated rat mAb against human CX_3CR1 (clone 2A9-1, IgG_{2B}; BioLegend).

T Lymphocytes

The markers CD3 (T lymphocytes), CD4 (T helper lymphocytes; Th), and CD8 (cytotoxic T lymphocytes) were used to identify T lymphocyte populations within the leukocytes present in peripheral blood. The gating strategy consisted in a selection through an APC-conjugated mouse mAb against human CD3 (clone 33-2A3, IgG_{2A}; Immunostep), a V450-conjugated mouse mAb against human CD4 (clone RPA-T4, IgG_1; BD Biosciences), and a FITC-conjugated mouse

TABLE 2 | Clinical and fasting biochemical characteristics of the study groups[1].

Parameter	Control volunteers (n = 10)	PH patients (n = 20)	p-value
Gender M/F (%)	3/7 (30.0/70.0)	4/16 (20.0/80.0)	0.95
Age (years)	46.8 ± 4.2	50.1 ± 3.0	0.54
BMI (kg/m^2)	25.9 ± 1.1	25.8 ± 0.8	0.92
Waist circumference (cm)	85.6 ± 2.9	86.1 ± 1.8	0.90
SBP (mmHg)	115.4 ± 2.6	124.8 ± 3.6	0.11
DBP (mmHg)	73.5 ± 3.1	78.5 ± 2.7	0.28
Glucose (mg/dl)	83.8 ± 1.7	88.1 ± 1.8	0.16
TC (mg/dl)	215.6 ± 12.9	266.6 ± 9.1**	**0.004**
LDL (mg/dl)	137.0 ± 10.2	184.0 ± 6.3**	**0.0004**
TG (mg/dl)	93.5 ± 13.7	112.7 ± 8.5	0.24
HDL (mg/dl)	66.8 ± 3.6	63.6 ± 3.1	0.53
apoB (mg/dl)	94.7 ± 7.0	128.4 ± 5.2**	**0.001**
GOT (U/L)	23.0 ± 1.0	22.8 ± 1.1	0.91
GPT (U/L)	20.0 ± 3.4	18.6 ± 1.1	0.72
Creatinine (mg/dl)	0.7 ± 0.0	0.7 ± 0.0	0.83
IgG (mg/dl)	959.6 ± 61.5	954.6 ± 31.2	0.94
IgM (mg/dl)	103.6 ± 10.6	123.5 ± 14.6	0.40
IgE total (IU/L)	36.8 ± 12.2	49.0 ± 17.2	0.66

apoB, apolipoprotein B; BMI, body mass index; DBP, diastolic blood pressure; GOT, glutamic-oxalacetic transaminase; GPT, glutamate-pyruvate transaminase; HDL, high-density lipoprotein; Ig, immunoglobulin; LDL, low-density lipoprotein; PH, primary hypercholesterolemia; TC, total cholesterol; TG, triglycerides; SBP, systolic blood pressure.
[1]Data are presented as mean ± SEM.
***p < 0.01 relative to values in the control group.*

mAb against human CD8 (clone SK1, IgG_1; BD Biosciences) (**Supplementary Figure S4**). After the identification of the different subpopulations, the possible contribution of platelets and T lymphocyte activation was studied as described above.

T Helper Lymphocytes

To select the different Th lymphocyte subpopulations, we first used a PerCP/Cy™5.5-conjugated mouse mAb against human CD4 (clone RPA-T4, IgG_1; BD Biosciences). Once detected, Th subpopulations were identified (as shown in **Supplementary Table S3**) with an Alexa Fluor® 488-conjugated mouse mAb against human CD183 (CXCR3, clone 1C6/CXCR3, IgG_1; BD Biosciences) and a BV421™-conjugated mouse mAb against human CD196 (CCR6, clone 11A9, IgG_1; BD Biosciences) (**Supplementary Figure S5**).

Heparinized whole blood incubated or not with EDTA was employed to determine the Th lymphocyte-platelet complexes or platelet-free Th lymphocytes using a PE/Cy™7-conjugated mouse mAb against human CD41 (clone HIP8, IgG_1; BioLegend). The activation state was determined using an APC-conjugated mouse mAb against human CD69 (clone FN50, IgG_1; BD Biosciences).

Regulatory T Lymphocytes (Treg)

To identify the Treg population, we used a human regulatory T cell cocktail (BD Pharmingen™ Human Regulatory T Cell Cocktail; BD Biosciences). Th lymphocytes were first identified with the marker CD4 (FITC-conjugated mouse mAb, clone SK3, IgG_1; BD Biosciences). Then, an Alexa Fluor® 647-conjugated mouse mAb against human CD127 (clone HIL-7R-M21, IgG_1; BD Biosciences) and a PE/Cy™7-conjugated mouse mAb against human CD25 (clone 2A3, IgG_1; BD Biosciences) were used to determine natural Treg cells (**Supplementary Figure S6**). As previously indicated, two experimental approaches were carried out in parallel: one with heparinized whole blood and the other with EDTA-treated blood, to determine the percentage of Treg lymphocyte-platelet aggregates. For this purpose, a CF-Blue™-conjugated mAb against human CD41 (clone HIP8, IgG_1; Immunostep) was employed.

Quantification of Soluble Metabolic and Inflammatory Markers

Human soluble adiponectin, leptin and ghrelin, as well as cytokines and chemokines including interleukin (IL)-6, IL-8/CXCL8, IL-10, IL-12, growth-regulated oncogene α (GROα)/CXCL1, fractalkine/CX_3CL1, TNFα, interferon γ (IFNγ), monocyte chemoattractant protein-1 (MCP-1)/CCL2, regulated upon activation, normal T cell expressed and secreted (RANTES)/CCL5, platelet factor-4 (PF-4)/CXCL4 and soluble P-selectin (sP-selectin) were measured in plasma samples using commercial ELISA (Human DuoSet® ELISA; R&D Systems, Inc., Minneapolis, MN, United States). Results are expressed as pg/mL or ng/mL of mediator in plasma.

Leukocyte-Endothelial Cell Interactions Under Flow Conditions

To measure leukocyte adhesion, HUAEC were seeded on 35-mm-diameter pre-treated culture plates. Once confluence was reached, plates were placed in a parallel flow chamber (GlycoTech, Gaithersburg, MD, United States). Whole blood from subjects was diluted 1:10 in Hanks balanced salt solution (Lonza Group) and perfused across HUAEC monolayers previously stimulated or not with TNFα (20 ng/ml; Sigma-Aldrich) for 24 h.

Leukocyte adhesion was determined after 7 min at 0.5 dyn/cm^2. Experiments were carried out in heparinized whole blood, incubated or not with EDTA (10 mM, for 15 min, 37°C; PanReac AppliChem GmbH) to evaluate the contribution of platelets to

TABLE 3 | Effect of an oral unsaturated fat load test on different biochemical characteristics and immunoglobulins in controls and in patients with primary hypercholesterolemia[1].

Parameter	Study group	Fasting	4 h	*p*-value
Glucose (mg/dl)	Control volunteers	83.8 ± 1.7	83.7 ± 1.4	0.96
	PH patients	88.1 ± 1.8	88.3 ± 1.6	0.94
TG (mg/dl)	Control volunteers	93.5 ± 13.7	133.0 ± 21.0	0.13
	PH patients	112.7 ± 8.5	177.5 ± 17.9**	**0.0034**
IgG (mg/dl)	Control volunteers	959.6 ± 61.5	1002.1 ± 67.1	0.64
	PH patients	954.6 ± 31.2	958.6 ± 32.8	0.93
IgM (mg/dl)	Control volunteers	103.6 ± 10.6	105.9 ± 11.0	0.88
	PH patients	123.5 ± 14.6	123.3 ± 14.3	0.99
IgE total (IU/L)	Control volunteers	36.8 ± 12.2	37.3 ± 11.9	0.97
	PH patients	49.0 ± 17.2	50.0 ± 18.0	0.97

Ig, immunoglobulin; PH, primary hypercholesterolemia; TG, triglycerides.
***p < 0.01 relative to values in patients in fasting conditions.*
[1]Data are presented as mean ± SEM.

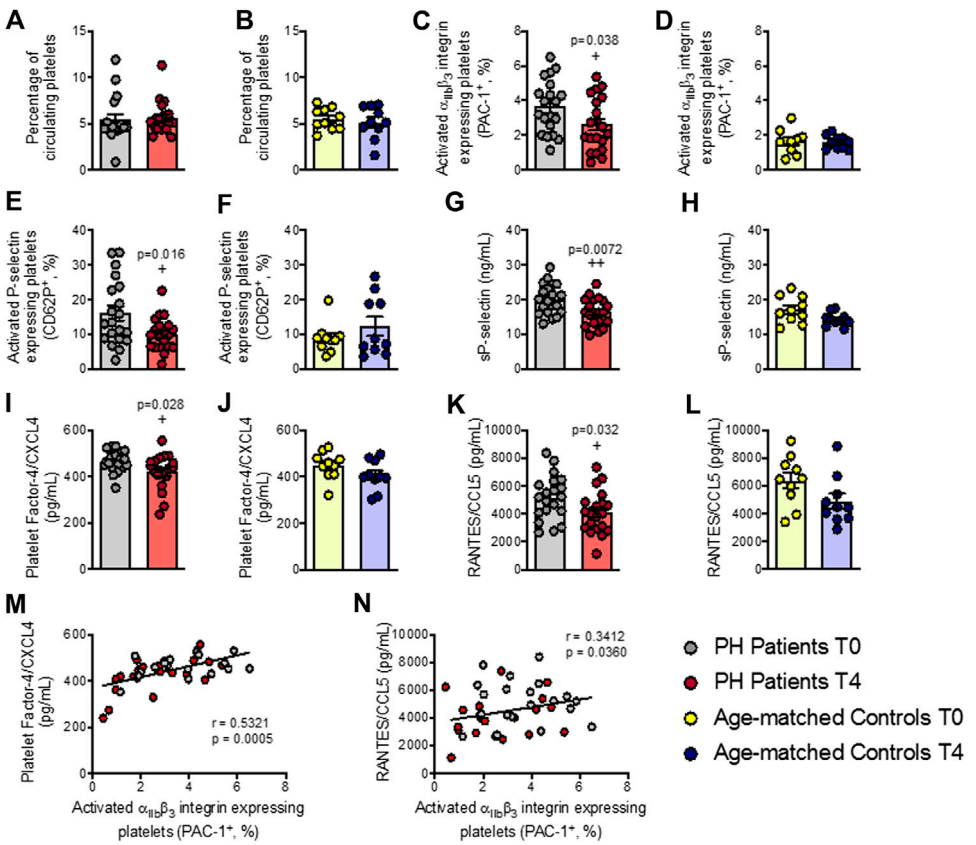

FIGURE 1 | Platelet activation and related soluble markers are reduced in patients with primary hypercholesterolemia four hours after an oral unsaturated fat load but not in age-matched controls**.** Flow cytometry analysis of platelets stained with conjugated antibodies against CD41 **(A,B)**, CD41 and PAC-1 **(C,D)**, and CD41 and P-selectin **(E,F)**. Results are presented as the percentage of positive cells. sP-selectin **(G,H)**, PF-4/CXCL4 **(I**,**J)**, and RANTES/CCL5 **(K**,**L)** plasma levels (ng/mL or pg/mL) were measured by ELISA (*n* = 20 PH patients) and 10 age-matched controls. Values are expressed as mean ± SEM. +*p* < 0.05 or ++*p* < 0.01 relative to values in the PH group at time 0 (T0). Positive correlations between the percentage of platelets expressing PAC-1 and plasma levels of PF-4/CXCL4 **(M)** and RANTES/CCL5 **(N)** in PH patients. Data sets B, C, D, E, G H, J, K, and L were compared using two-tailed Student's t-test; data sets (A,F), and I were compared using Mann-Whitney U-test; correlations M and N were calculated by the Spearman correlation method. PF-4, platelet factor-4; PH, primary hypercholesterolemia; RANTES, regulated upon activation, normal T cell expressed and secreted; sP-selectin, soluble P-selectin; T0, time 0; T4, time 4.

leukocyte adhesion (Postea et al., 2012). Cells interacting with the surface of the endothelium were visualized and recorded (×20 objective, ×10 eyepiece) with an inverted microscope (Axio Observer A1; ZEISS International, Oberkochen, Germany). At least five fields were recorded for 10 s each. Finally, recorded images were saved on a computer for further analyses.

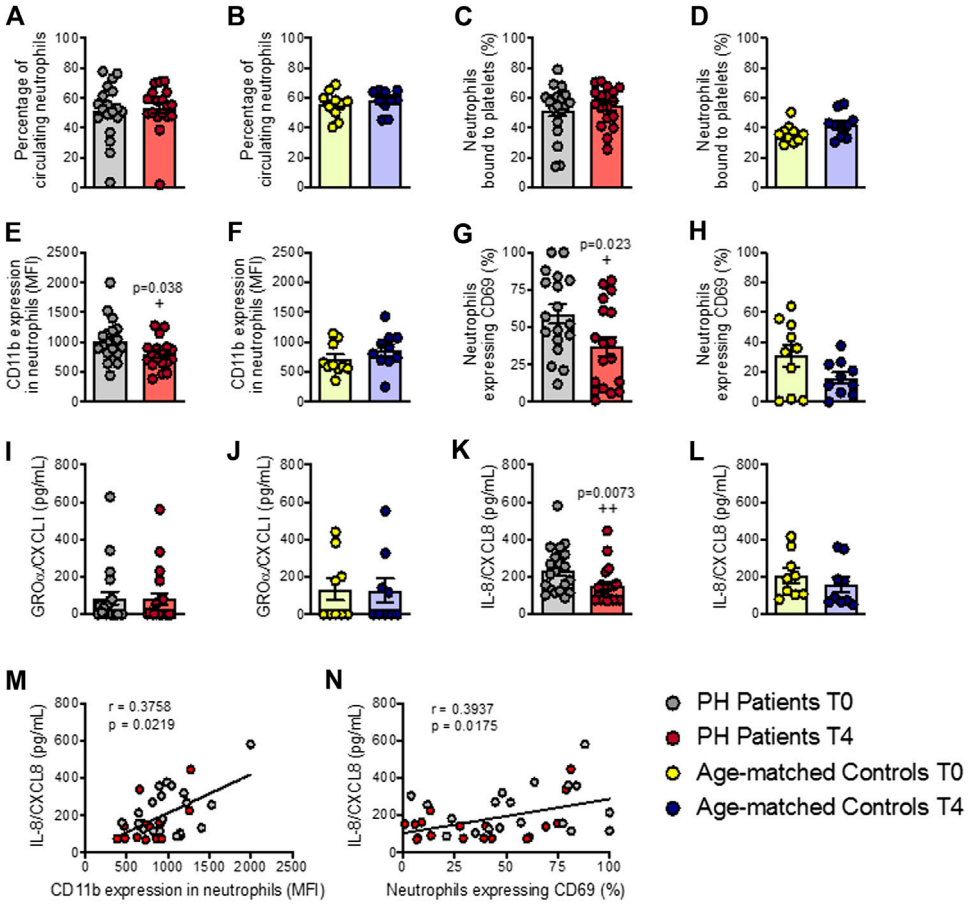

FIGURE 2 | Neutrophil activation and circulating levels of IL-8/CXCL8 are reduced in patients with primary hypercholesterolemia after an oral unsaturated fat load but not in age-matched controls. Flow cytometry analysis of heparinized whole blood co-stained with specific markers for platelets and neutrophils **(A–D)**. Neutrophils were also stained for CD11b integrin **(E,F)** and CD69 **(G,H)**. Results are presented as the percentage of positive cells or median fluorescence intensity (MFI). GROα/CXCL1 **(I,J)** and IL-8/CXCL8 **(K,L)** plasma levels (pg/ml) were measured by ELISA (n = 20 PH patients) and 10 age-matched controls. Values are expressed as mean ± SEM. $+p < 0.05$ or $++p < 0.01$ relative to values in the PH group at time 0 (T0). Positive correlations between IL-8/CXCL8 plasma levels and CD11b expression in neutrophils **(M)** and in neutrophils expressing CD69 **(N)** in PH patients. Data sets B, D, E, G, H, and L were compared using two-tailed Student's t-test; data sets A, C, F, I, J, and K were compared using Mann-Whitney U-test; correlations M and N were calculated by the Spearman correlation method. GROα, growth-regulated oncogene α; PH, primary hypercholesterolemia; T0, time 0; T4, time 4.

Statistical Analysis

All results were analyzed using GraphPad Prism software version 8.0 (GraphPad Software, Inc., La Jolla, CA, United States). Values are expressed as individual data points, percentages or mean ± SEM when appropriate. For two-group comparisons, paired or unpaired two-tailed Student´s t test was used in data that passed both normality (Kolmogorov-Smirnov) and equal variance (Levene) tests, as appropriate; otherwise, the non-parametric Mann-Whitney U test was performed. For comparisons among multiple groups, one-way ANOVA followed by *post hoc* Bonferroni analysis was used in data that passed both normality and equal variance tests; otherwise, the non-parametric Kruskal-Wallis test followed by Dunn´s *post hoc* analysis was used. Data were considered statistically significant at $p < 0.05$. Additionally, some correlations between experimental findings were calculated using the Spearman correlation method.

RESULTS

In total, 20 patients (4 males and 16 females, aged 50.1 ± 3.0 years) and 10 age-matched controls (3 males and 7 females, aged 46.8 ± 4.2 years) were studied. Demographic, clinical and biochemical characteristics of subjects in fasting conditions are shown in **Table 2**. No statistically significant differences were found for age, gender, BMI, or waist circumference between the two groups (**Table 2**). By contrast, baseline levels of total cholesterol (TC), LDL, and apoB were significantly higher in patients than in controls (**Table 2**). After the OUFL challenge to both groups, only the circulating levels of TG were significantly increased in patients **Table 3** and not the levels of the three clinical features of PH, apoB, LDL and TC, as described previously for other studies (Langsted et al., 2008).

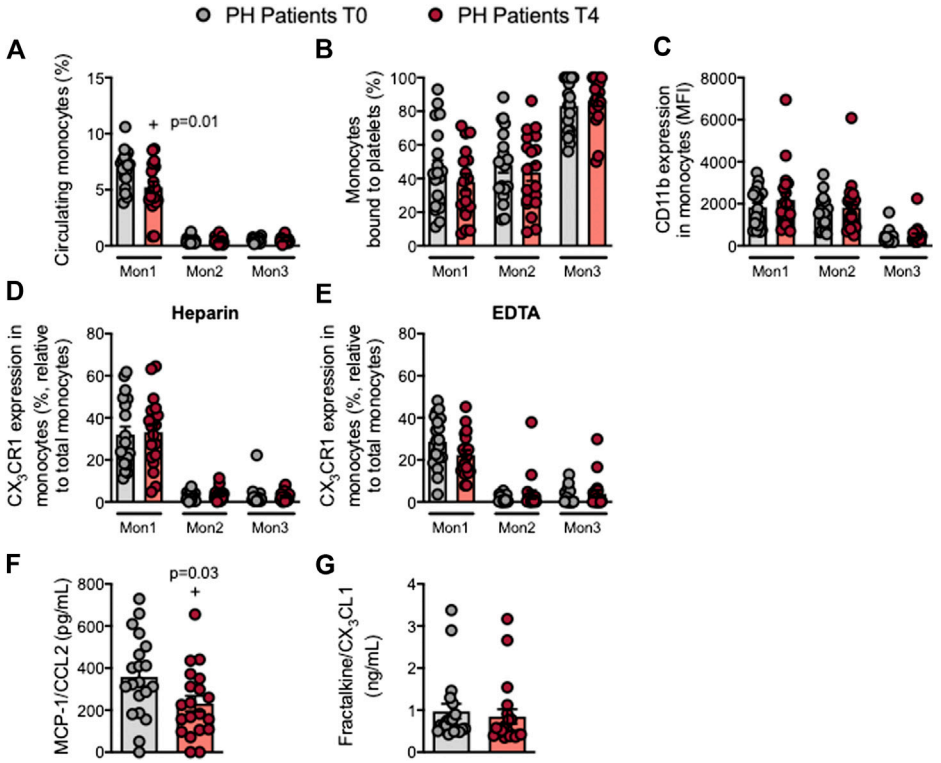

FIGURE 3 | Circulating Mon1 monocytes and MCP-1/CCL2 plasma levels are reduced in patients with primary hypercholesterolemia after an oral unsaturated fat load. Flow cytometry analysis of heparinized or EDTA-treated whole blood co-stained with specific markers for platelets and Mon1, 2, and 3 monocytes **(A,B)**, CD11b integrin **(C)**, and CX_3CR1 in heparinized **(D)** and EDTA-treated whole blood **(E)**. Results are presented as the percentage of positive cells or median fluorescence intensity (MFI). MCP-1/CCL2 **(F)** and fractalkine/CX_3CL1 **(G)** plasma levels (ng/mL or pg/mL) were measured by ELISA (n = 20 PH patients). Values are expressed as mean ± SEM. +$p < 0.05$ relative to values in the PH group at time 0 (T0). Data sets A, B, C and F were compared using two-tailed Student's t-test; data sets D, E, and G were compared using Mann-Whitney U-test. MCP-1, monocyte chemoattractant protein-1; Mon1/2/3, type 1/2/3 monocytes; PH, primary hypercholesterolemia; T0, time 0; T4, time 4.

Platelet Activation and Related Soluble Markers are Reduced in Patients with Primary Hypercholesterolemia After an Oral Unsaturated Fat load

No changes were observed in the percentage of circulating platelets in either group after the OUFL (**Figures 1A,B**). By contrast, the percentage of activated platelets (PAC-1^+ and P-selectin/$CD62P^+$) was significantly lower after the OUFL in patients with PH (**Figures 1C,E**), but not in age-matched controls (**Figures 1D,F**). Since P-selectin expression on the platelet surface can be cleaved and released into circulation as soluble P-selectin (sP-selectin), we determined its circulating levels in plasma, finding that levels were significantly lower after OUFL challenge in the PH group but not in the control group (**Figures 1G,H**). Likewise, circulating plasma levels of PF-4/CXCL4 and RANTES/CCL5 – chemokines that are released upon platelet activation–were significantly lower after the OUFL in patients, but no differences were detected in controls (**Figures 1I–L**). Of note, we found positive correlations between circulating levels of PF-4/CXCL4 and RANTES/CCL5 and the percentage of platelets expressing PAC-1 in PH patients (**Figures 1M,N**, respectively).

Neutrophil Activation and Circulating Levels of IL-8/CXCL8 Are Reduced in Patients With Primary Hypercholesterolemia After an Oral Unsaturated fat Load

We next evaluated several parameters related to the activation of different leukocyte subsets after the OUFL. No changes were observed in the percentage of circulating neutrophils or in platelet-neutrophil aggregates in either group before or after the OUFL (**Figures 2A–D**). By contrast, a significant reduction in the activation state of neutrophils (CD11b expression and $CD69^+$) was evident after the OUFL in patients (**Figures 2E,G**), but not in controls (**Figures 2F,H**). As some chemokines can promote neutrophil activation and chemotaxis, including GROα/CXCL1 and IL-8/CXCL8, we quantified their plasma levels before and after the OUFL. No differences were found for GROα/CXCL1 in either group after the OUFL (**Figures 2I,J**). Plasma levels of IL-8/CXCL8 were, however, significantly lower in the PH group after the OUFL (**Figures 2K,L**). Also, the circulating concentration of IL-8/CXCL8 positively correlated with CD11b expression on neutrophils (**Figure 2M**) and with the percentage of activated neutrophils in PH patients ($CD69^+$, **Figure 2N**).

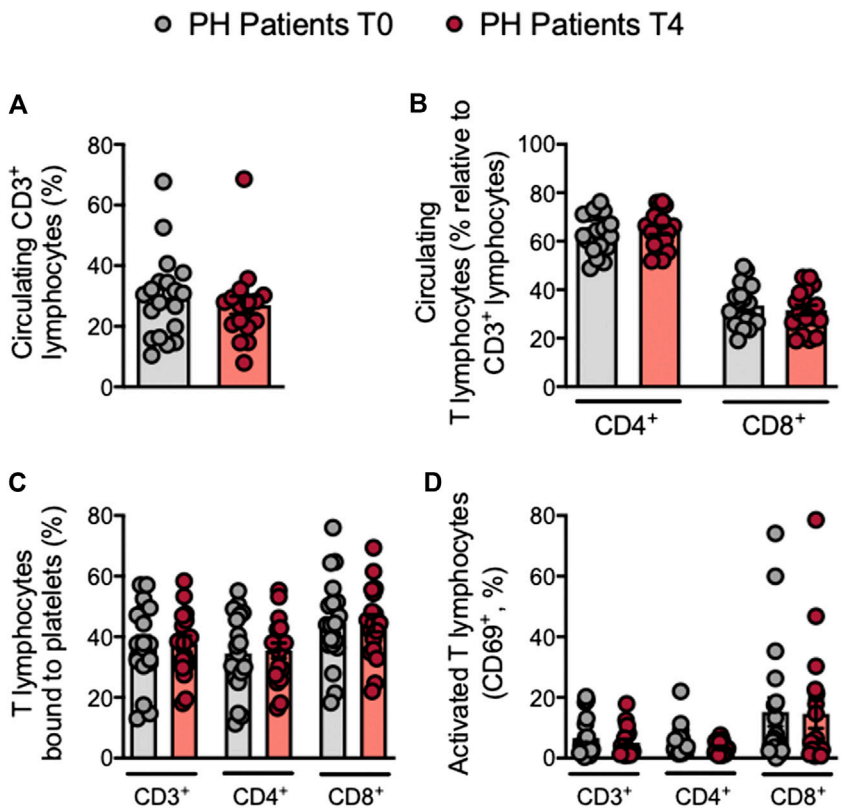

FIGURE 4 | No changes in circulating T lymphocytes, platelet T lymphocyte aggregates and T lymphocyte activation in patients with primary hypercholesterolemia after an oral unsaturated fat load. Heparinized whole blood was co-stained with specific markers for platelets, $CD3^+$, $CD4^+$ and $CD8^+$ lymphocytes **(A–C)**, and activated lymphocytes ($CD69^+$) **(D)**. Results are presented as the percentage of positive cells (n = 20 PH patients). Values are expressed as mean ± SEM. Data sets B and C were compared using two-tailed Student's t-test; data sets A and D were compared using Mann-Whitney U-test. PH, primary hypercholesterolemia; T0, time 0; T4, time 4.

Circulating Mon1 Monocytes and MCP-1/CCL2 Plasma Levels Are Reduced in Patients With Primary Hypercholesterolemia After an Oral Unsaturated Fat Load

Three monocyte subpopulations have been described in peripheral blood based on their differential expression of the cell surface markers CD14, CD16 and CCR2 (as described in **Supplementary Table S2**). Following the OUFL, a significant decrease in the percentage of circulating type 1 monocytes (Mon1) was observed in patients but not in controls (**Figure 3A**; **Supplementary Figure S7A**), whereas the percentage of Mon2 and 3 monocytes did not differ between groups before or after the OUFL (**Figure 3A**; **Supplementary Figure S7A**). Likewise, platelet-monocyte aggregates, CD11b integrin and CX_3CR1 expression and plasma concentrations of fractalkine/CX_3CL1 were unchanged by the OUFL in either group (**Figures 3B–E,G**; **Supplementary Figures S7B–E,G**). Notably, the levels of MCP-1/CCL2 were significantly reduced by the OUFL in patients but not in controls (**Figure 3F**; **Supplementary Figure S7F**).

The Percentage of Circulating Treg Cells is Increased in Patients With Primary Hypercholesterolemia After an Oral Unsaturated Fat Load

Mature T cells express the general marker CD3 and either CD4 or CD8 depending on the T cell type. Following the OUFL no significant differences were found in the percentage of circulating $CD3^+$, $CD3^+CD4^+$ or $CD3^+CD8^+$ cells, the percentage of platelet T lymphocyte aggregates, or the activation state of these cells in patients and controls (**Figures 4A–D**; **Supplementry Figures S8A–D**). Similarly, no differences in these parameters were detected in the different Th lymphocyte subpopulations before or after the OUFL administration in either group (**Figures 5A–C**; **Supplementary Figures S9A–C**). Interestingly, the percentage of circulating Treg lymphocytes after the OUFL was significantly higher in patients but not in controls (**Figure 5D**; **Supplementary Figure S9D**). No differences were observed in the percentage of Treg lymphocyte-platelet aggregates, the Treg/Th17 ratio or the plasma levels of different soluble markers associated with T lymphocytes (IL-12, IFNγ, or IL-10) before or after the OUFL in either group (**Figures 5E–I**; **Supplementary Figures S9E–I**).

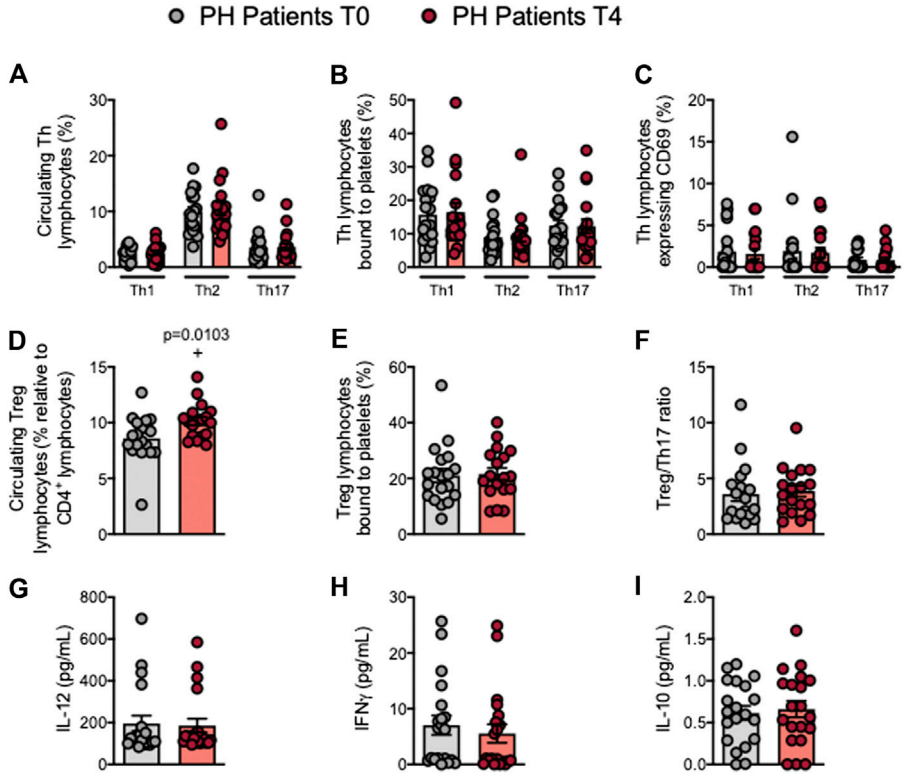

FIGURE 5 | The percentage of circulating Treg cells is increased in patients with primary hypercholesterolemia after an oral unsaturated fat load. Heparinized whole blood was co-stained with specific markers for platelets and Th1, Th2, Th17, and Treg lymphocytes **(A–E)** and for activated lymphocytes ($CD69^+$) **(C)**. The Treg/Th17 ratio was also determined **(F)**. Results are presented as the percentage of positive cells. IL-12 **(G)**, IFNγ **(H)**, and IL-10 **(I)** plasma levels (pg/ml) were measured by ELISA (n = 20 PH patients). Values are expressed as mean ± SEM. $+p < 0.05$ relative to values in the PH group at time 0 (T0). Data sets E, F, and I were compared using two-tailed Student's t-test; data sets A, B, C, D, G, and H were compared using Mann-Whitney U-test. IFNγ, interferon γ; PH, primary hypercholesterolemia; T0, time 0; T4, time 4; Th, T helper; Treg, regulatory T cells.

Circulating Levels of TNFα Are Reduced in Patients With Primary Hypercholesterolemia After an Oral Unsaturated Fat Load

Increased plasma levels of TNFα and IL-6 have been reported in patients with PH (Sampietro et al., 1997; Real et al., 2010; Holven et al., 2014; Collado et al., 2018a). We found that circulating plasma TNFα levels were significantly lower after the OUFL in patients and similar to those found in controls, which did not change 4 h after the administration (**Figure 6A**; **Supplementary Figure S10A**). Conversely, plasma concentrations of IL-6, adiponectin, leptin or ghrelin were unchanged after the OUFL in both groups (**Figures 6B–E**; **Supplementary Figures S10B–E**).

Circulating Platelet-Leukocyte Aggregates and Leukocytes From Patients With Primary Hypercholesterolemia Show Reduced Adhesiveness to TNFα-Stimulated Endothelial Cells After an Oral Unsaturated Fat Load

Endothelial dysfunction is the earliest stage of atherogenesis and is characterized by an increase in the adhesiveness of leukocytes to the endothelium, and their subsequent migration to the arterial subendothelial space (Landmesser et al., 2004). We previously demonstrated that the plasma levels of TNFα are elevated in patients with PH and that the adhesion of platelet-leukocyte aggregates and leukocytes from these patients to dysfunctional arterial endothelium (TNFα-stimulated) is enhanced when compared with age-matched controls (Collado et al., 2018a). We performed the flow chamber adhesion analysis before and following the OUFL, finding that the number of platelet-leukocyte aggregates (heparin) or platelet-free leukocytes (EDTA) adhered to the unstimulated or TNFα-stimulated arterial endothelium was reduced after the OUFL in patients (**Figures 7A,B**) but not in controls (**Supplementary Figures S11A,B**). Of note, we found positive correlations between patient leukocyte adhesion and PF-4/CXCL4 (**Figure 7C**), RANTES/CCL5 (**Figure 7D**), and MCP-1/CCL2 (**Figure 7E**) plasma levels.

DISCUSSION

PH is characterized by elevated plasma levels of cholesterol–specifically, LDL and apoB–which contribute to the development of atherosclerosis and associated ischemic events (Sampietro et al., 1997; Chironi et al., 2006; Real et al., 2010; Holven et al., 2014; Cortes et al., 2016; Collado et al., 2018a; Hansen et al., 2019). In addition, there is increasing evidence that

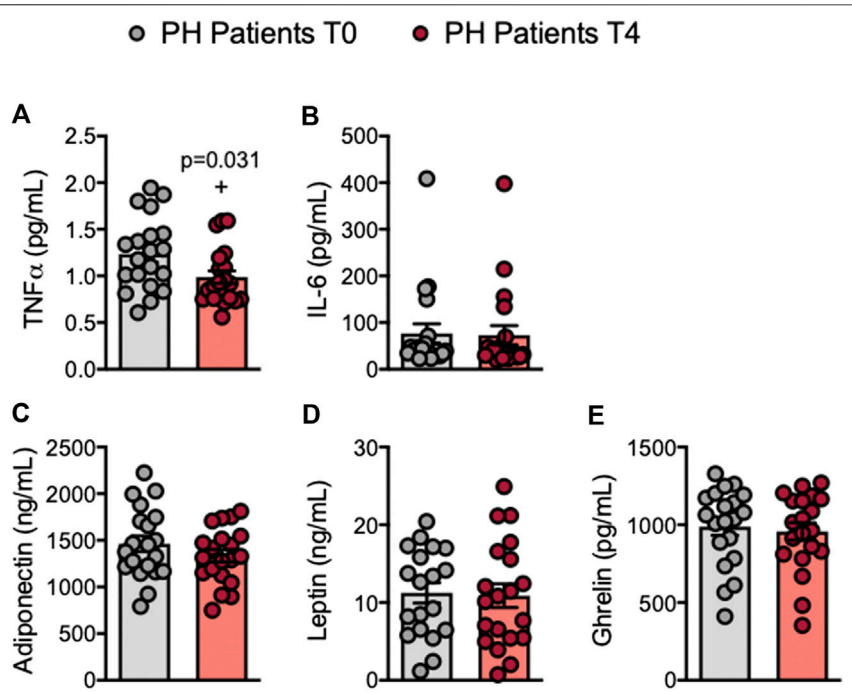

FIGURE 6 | Circulating levels of TNFα are reduced in patients with primary hypercholesterolemia after an oral unsaturated fat load**.** TNFα **(A)**, IL-6 **(B)**, adiponectin **(C)**, leptin **(D)**, and ghrelin **(E)** plasma levels (ng/mL or pg/mL) were measured by ELISA (n = 20 PH patients). Values are expressed as mean ± SEM. $+p < 0.05$ relative to values in the PH group at time 0 (T0). Data sets A, C, D, and E were compared using two-tailed Student's t-test; data set B was compared using Mann-Whitney U-test. PH, primary hypercholesterolemia; T0, time 0; T4, time 4.

systemic inflammation is the main driver of premature atherosclerosis (Catapano et al., 2017) and is a component of PH (Langslet et al., 2015; Barale et al., 2018; Collado et al., 2018a). In the present study, we have extensively analyzed the acute impact (4 h) of an OUFL containing 58% oleic acid and 20% linoleic acid (**Supplementary Table S1**) on the systemic inflammatory response associated with PH. We show that an OUFL challenge beneficially modulates different immune players, reduces the levels of inflammatory cytokines and chemokines and impairs a prominent feature of the atherogenesis–the adhesiveness of leukocytes to the dysfunctional arterial endothelium. In agreement with our findings, oleic acid has been shown to protect against CVD and insulin resistance, and to improve endothelial dysfunction in response to pro-inflammatory signals (Perdomo et al., 2015). And in the same line, dietary intake of linoleic acid is inversely associated with the risk of coronary heart disease (Farvid et al., 2014).

Inflammation triggers platelet activation, which in turn plays an important role in several processes such as homeostasis (Manne, 2017; Periayah et al., 2017) and thrombosis (Mancuso and Santagostino, 2017). Activated platelets are now also recognized as essential immune-modulators (Lam et al., 2015) by their expression of specific cell adhesion molecules such as P-selectin, which plays a crucial role in the recruitment of leukocytes to the inflammatory site. Additionally, they can release various inflammatory chemokines, including PF-4/CXCL4 or RANTES/CCL5 which can be deposited in the endothelium to stimulate monocyte and lymphocyte recruitment (von Hundelshausen and Schmitt, 2014). Patients with PH show a pro-thrombotic state characterized by increased platelet activation, which is reflected by the presence of P-selectin$^+$ and PAC-1$^+$ platelets (Collado et al., 2018a). We found that a lipid OUFL challenge significantly reduced platelet activation in patients, pointing to the potential anti-thrombotic effects of the intervention. Additionally, OUFL reduced the circulating levels of several inflammatory mediators linked to platelet activation including sP-selectin, PF-4/CXCL4 and RANTES/CCL5, again suggesting that in postprandial state this treatment may impair the pro-thrombotic state associated with PH and the progression of atherogenesis (von Hundelshausen and Schmitt, 2014).

To understand the immune state of the PH environment, we surveyed different leukocyte subtypes following OUFL challenge. Neutrophils are known to be one of the major players in acute inflammation (Kolaczkowska and Kubes, 2013), as they express integrin CD11b/CD18 that is up-regulated upon activation and promotes leukocyte adhesion and transmigration across the vascular endothelium through its interaction with its cognate ligands intercellular adhesion molecule (ICAM)-1 and ICAM-2 (Diacovo et al., 1996). Our analysis showed that while there no differences were evident in the percentage of circulating neutrophils and neutrophil-platelet aggregates after the OUFL in patients, there was a significant reduction in their activation state (CD11b expression and CD69$^+$). This was accompanied by a clear reduction in the circulating levels of IL-8/CXCL8, which induces neutrophil activation and chemotaxis (Kolaczkowska and Kubes, 2013). Both outcomes were positively correlated, thus indicating an improvement in the immune state of patients with PH and ameliorating the proatherogenic status.

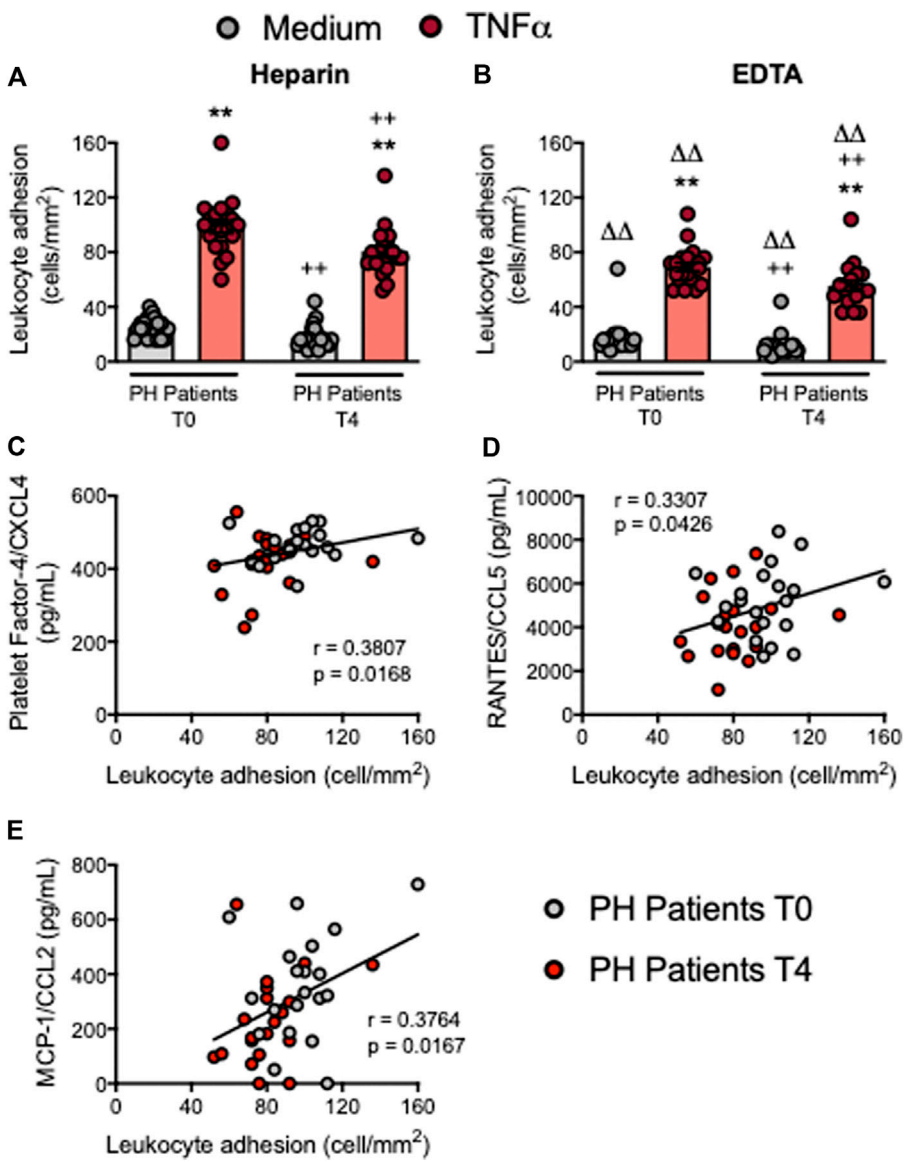

FIGURE 7 | Circulating platelet-leukocyte aggregates and leukocytes from patients with primary hypercholesterolemia display lower adhesiveness to TNFα-stimulated HUAEC after an oral unsaturated fat load. HUAEC were stimulated or not with TNFα (20 ng/ml) for 24 h. Subsequently, whole blood from all patients, incubated without **(A)** or with EDTA **(B)**, was perfused across the endothelial monolayers for 7 min at 0.5 dyn/cm^2 and leukocyte adhesion quantified (cells/mm^2). Values are expressed as mean ± SEM ($n = 20$ PH patients). $^{**}p < 0.01$ relative to values in the medium-only group; $^{++}p < 0.01$ relative to the respective values at time 0 (T0); $^{\Delta\Delta}p < 0.01$ relative to the respective values in the heparin group. Positive correlations between leukocyte adhesion and plasma levels of PF-4/CXCL4 **(C)**, RANTES/CCL5 **(D)**, and MCP-1/CCL2 **(E)**. Data sets A and B were compared using Kruskal-Wallis (Dunn's *post hoc*) test; correlations C, D and E were calculated by the Spearman correlation method. HUAEC, human umbilical artery endothelial cells; MCP-1, monocyte chemoattractant protein-1; PF-4, platelet factor-4; PH, primary hypercholesterolemia; RANTES, regulated upon activation, normal T cell expressed and secreted; T0, time 0; T4, time 4.

Human circulating monocytes comprise a heterogeneous cell population that is commonly classified into three subtypes: classical CD14^{++}CD16^{-}CCR2^{+} (Mon1), intermediate CD14^{++}CD16^{+}CCR2^{+} (Mon2), and non-classical CD14^{+}CD16^{++}CCR2^{-} (Mon3) (Weber et al., 2016), with the Mon1 subtype more commonly known as classical or inflammatory monocytes. We found that an OUFL led to a significant reduction in the percentage of circulating Mon1 monocytes. Interestingly, there is evidence to support that adults with FH have a pro-inflammatory imbalance in circulating monocyte subpopulations (Mon1) (Fadini et al., 2014). Although different studies in humans have noted increases in circulating CD16^{+} monocytes in CVD (Kratofil et al., 2017), we observed no changes in Mon2 and Mon3 populations, monocyte activation state (CD11b expression) or CX_3CR1 expression after the OUFL. By contrast, MCP-1/CCL2 circulating levels were significantly reduced in patients with PH after the OUFL, confirming a previous report in patients with FH (Cortes et al., 2016). MCP-1/CCL2 mainly recruits Mon1 and Mon2 monocytes to inflammatory sites through

interaction with its CCR2 receptor (Weber et al., 1999; Deshmane et al., 2009), and this inflammatory axis has been widely associated with CVD development (Franca et al., 2017).

T lymphocyte analysis revealed no changes in total T or Th lymphocytes after the OUFL in patients with PH but a significant increase in the percentage of Treg lymphocytes, which might contribute to the anti-inflammatory environment created by this intervention. However, neither the Treg/Th17 ratio nor the circulating levels of IL-10 were improved by the OUFL, although it is tempting to speculate that changes in these parameters might be evident at later time points. Of note, plasma levels of TNFα were significantly reduced in patients after the OUFL being normalized to control subjects' levels. In this regard, a prior study in FH found that a similar intervention decreased the circulating levels of several inflammatory chemokines including macrophage inflammatory protein (MIP)-1α, MIP-1β, and interferon γ-induced protein-10 (IP-10)/CXCL10, among others, with values close to those found in control subjects (Cortes et al., 2016).

Finally, we used the dynamic flow chamber to explore the functional consequences of platelet-leukocyte-endothelium (heparin) or leukocyte-endothelium (EDTA) interactions. We previously showed that adhesion of platelet-leukocyte aggregates to HUAEC stimulated or not with TNFα is significantly higher in patients with PH than in controls (Collado et al., 2018a). When these parameters were evaluated after the OUFL challenge, we found lowered adhesion of both platelet-leukocyte aggregates (heparin) and platelet-free leukocytes (EDTA) to dysfunctional arterial endothelium. The reduction in leukocyte adhesion is likely the consequence of several of the aforementioned experimental observations. First, the reduced activation state of neutrophils (CD11b/CD18 integrin down-regulation) can lead to decreased interactions with the constitutively or inducible (TNFα-stimulated) expressed endothelial ICAM-1. Second, since activated platelets can mediate the endothelial adhesion of circulating leukocytes–a characteristic feature of the dysfunctional endothelium (Rius et al., 2013; Landmesser et al., 2004; Marques et al., 2017; Collado et al., 2018a; Collado et al., 2018b; Furio et al., 2018) – their decreased activation may alter leukocyte arrest. Third, a reduction in the percentage of circulating inflammatory (classical) monocytes (Mon1) results in diminished monocyte adhesion. Finally, the decreased levels of circulating chemokines may also affect the adhesion of leukocytes to endothelium in patients with PH. Supporting this concept, neutralization of CCL2 activity was found to decrease the endothelial arrest of Mon1 monocytes (Marques et al., 2019). Likewise, platelet deposition of RANTES/CCL5 in the endothelium can trigger monocyte arrest (von Hundelshausen et al., 2001) and PF-4/CXCL4 has multiple atherogenic activities and synergizes with CCL5 (von Hundelshausen and Schmitt, 2014). Leukocyte adhesion in this setting positively correlates with the plasma levels of these chemokines.

Our study has limitations. First, to date the acute intervention of the OUFL do not allow us to extrapolate these results to those with a long-term intervention and second, Supracal® cannot be considered a physiological ingestion of fat. Nevertheless, preclinical studies in animal models of hypercholesterolemia will be designed to evaluate the long-term effects of the OUFL.

In summary, administration of an OUFL has beneficial acute effects on the postprandial pro-thrombotic and pro-inflammatory state of PH patients. Further long-term studies are, however, warranted. Our findings indicate that the modulation of the cellular and soluble inflammatory components in PH might be crucial to prevent further cardiovascular complications.

DATA AVAILABILITY STATEMENT

The original contributions presented in the study are included in the article/**Supplementary Material**, further inquiries can be directed to the corresponding authors.

ETHICS STATEMENT

The studies involving human participants were reviewed and approved by the University Clinic Hospital of Valencia. The patients/participants provided their written informed consent to participate in this study.

AUTHOR CONTRIBUTIONS

JR, JA, and M-JS designed research; AC, ED, PM, EP, SM-H, and LP performed research; AC, ED, PM, EP, SM-H, LP, JA, JR, and M-JS analyzed and interpreted the data; AC, ED, PM, JR, and M-JS drafted the manuscript and SM-H, LP, and JA revised it critically for important intellectual content. M-JS had primary responsibility for final content. All the authors have read and approved the final version of the manuscript.

FUNDING

This work was supported by the Spanish Ministry of Science and Innovation (grant number SAF 2017-89714-R); Carlos III Health Institute (grant numbers PI18/00,209); Generalitat Valenciana (grant number PROMETEO/2019/032, Gent T CDEI-04/20-A, and AICO/2019/2500, and the European Regional Development Fund. AC and ED acknowledge pre-doctoral funding from the Generalitat Valenciana and PM to the Spanish Ministry of Science and Innovation (FPI). SM-H is an investigator in the 'Juan Rodes' program (JR18/00,051) financed by the Instituto de Salud Carlos III and the European Regional Development Fund (FEDER).

ACKNOWLEDGMENTS

We would like to acknowledge Dr. Guadalupe Herrera for providing technical assistance.

SUPPLEMENTARY MATERIAL

The Supplementary Material for this article can be found online at: https://www.frontiersin.org/articles/10.3389/fphar.2021.656244/full#supplementary-material.

REFERENCES

Barale, C., Frascaroli, C., Senkeev, R., Cavalot, F., and Russo, I. (2018). Simvastatin effects on inflammation and platelet activation markers in hypercholesterolemia. *Biomed. Res. Int.* 2018, 6508709. doi:10.1155/2018/6508709

Benjamin, E. J., Blaha, M. J., Chiuve, S. E., Cushman, M., Das, S. R., Deo, R., et al. (2017). Heart disease and stroke statistics-2017 update: a report from the American heart association. *Circulation* 135 (10), e146–603. doi:10.1161/cir.0000000000000485

Catapano, A. L., Pirillo, A., and Norata, G. D. (2017). Vascular inflammation and low-density lipoproteins: is cholesterol the link? A lesson from the clinical trials. *Br. J. Pharmacol.* 174 (22), 3973–3985. doi:10.1111/bph.13805

Chironi, G., Dosquet, C., Delpino, M., Denarie, N., Megnien, J., Drouet, L., et al. (2006). Relationship of circulating biomarkers of inflammation and hemostasis with preclinical atherosclerotic burden in nonsmoking hypercholesterolemic men. *Am. J. Hypertens.* 19 (10), 1025–1031. doi:10.1016/j.amjhyper.2006.03.016

Collado, A., Marques, P., Domingo, E., Perello, E., González-Navarro, H., Martinez-Hervás, S., et al. (2018a). Novel immune features of the systemic inflammation associated with primary hypercholesterolemia: changes in cytokine/chemokine profile, increased platelet and leukocyte activation. *J Clin Med.* 8 (1), 18. doi:10.3390/jcm8010018

Collado, A., Marques, P., Escudero, P., Rius, C., Domingo, E., Martinez-Hervás, S., et al. (2018b). Functional role of endothelial CXCL16/CXCR6-platelet-leucocyte axis in angiotensin II-associated metabolic disorders. *Cardiovasc. Res.* 114 (13), 1764–1775. doi:10.1093/cvr/cvy135

Cortes, R., Ivorra, C., Martínez-Hervás, S., Pedro, T., González-Albert, V., Artero, A., et al. (2016). Postprandial changes in chemokines related to early atherosclerotic processes in familial hypercholesterolemic subjects: a preliminary study. *Arch. Med. Res.* 47 (1), 33–39. doi:10.1016/j.arcmed.2016.01.002

Cortes, R., Martinez-Hervas, S., Ivorra, C., De Marco, G., Gonzalez-Albert, V., Rojo-Martínez, G., et al. (2014). Enhanced reduction in oxidative stress and altered glutathione and thioredoxin system response to unsaturated fatty acid load in familial hypercholesterolemia. *Clin. Biochem.* 47 (18), 291–297. doi:10.1016/j.clinbiochem.2014.09.006

Defesche, J. C., Gidding, S. S., Harada-Shiba, M., Hegele, R. A., Santos, R. D., and Wierzbicki, A. S. (2017). Familial hypercholesterolaemia. *Nat. Rev. Dis. Primers* 3, 17093. doi:10.1038/nrdp.2017.93

Deshmane, S. L., Kremlev, S., Amini, S., and Sawaya, B. E. (2009). Monocyte chemoattractant protein-1 (MCP-1): an overview. *J. Interferon Cytokine Res.* 29 (6), 313–326. doi:10.1089/jir.2008.0027

Diacovo, T., Roth, S., Buccola, J., Bainton, D., and Springer, T. (1996). Neutrophil rolling, arrest, and transmigration across activated, surface-adherent platelets via sequential action of P-selectin and the beta 2-integrin CD11b/CD18. *Blood* 88 (1), 146–157. doi:10.1182/blood.v88.1.146.bloodjournal881146

Fadini, G. P., Simoni, F., Cappellari, R., Vitturi, N., Galasso, S., Vigili de Kreutzenberg, S., et al. (2014). Pro-inflammatory monocyte-macrophage polarization imbalance in human hypercholesterolemia and atherosclerosis. *Atherosclerosis* 237 (2), 805–808. doi:10.1016/j.atherosclerosis.2014.10.106

Farvid, M. S., Ding, M., Pan, A., Sun, Q., Chiuve, S. E., Steffen, L. M., et al. (2014). Dietary linoleic acid and risk of coronary heart disease: a systematic review and meta-analysis of prospective cohort studies. *Circulation* 130 (18), 1568–1578. doi:10.1161/circulationaha.114.010236

França, C. N., Izar, M. C. O., Hortêncio, M. N. S., do Amaral, J. B., Ferreira, C. E. S., Tuleta, I. D., et al. (2017). Monocyte subtypes and the CCR2 chemokine receptor in cardiovascular disease. *Clin. Sci. (Lond)* 131 (12), 1215–1224. doi:10.1042/cs20170009

Furio, E., García-Fuster, M., Redon, J., Marques, P., Ortega, R., Sanz, M., et al. (2018). CX3CR1/CX3CL1 *Axis* mediates platelet-leukocyte adhesion to arterial endothelium in younger patients with a history of idiopathic deep vein thrombosis. *Thromb. Haemost.* 118 (3), 562–571. doi:10.1055/s-0038-1629897

Garcia-Garcia, A. B., Martinez-Hervas, S., Real, J. T., Marin-Garcia, P., de Marco, G., Priego, A., et al. (2019). Gene expression profile following an oral unsaturated fat load in abdominal obese subjects. *Eur. J. Nutr.* 58 (3), 1331–1337. doi:10.1007/s00394-018-1659-4

Hansen, M., Kuhlman, A. C. B., Sahl, R. E., Kelly, B., Morville, T., Dohlmann, T. L., et al. (2019). Inflammatory biomarkers in patients in Simvastatin treatment: No effect of co-enzyme Q10 supplementation. *Cytokine* 113, 393–399. doi:10.1016/j.cyto.2018.10.011

Hedrick, C. C. (2015). Lymphocytes in atherosclerosis. *Arterioscler Thromb. Vasc. Biol.* 35 (2), 253–257. doi:10.1161/atvbaha.114.305144

Holven, K. B., Narverud, I., Lindvig, H. W., Halvorsen, B., Langslet, G., Nenseter, M. S., et al. (2014). Subjects with familial hypercholesterolemia are characterized by an inflammatory phenotype despite long-term intensive cholesterol lowering treatment. *Atherosclerosis* 233 (2), 561–567. doi:10.1016/j.atherosclerosis.2014.01.022

Jaffe, E. A., Nachman, R. L., Becker, C. G., and Minick, C. R. (1973). Culture of human endothelial cells derived from umbilical veins. Identification by morphologic and immunologic criteria. *J. Clin. Invest.* 52 (11), 2745–2756. doi:10.1172/jci107470

Kolaczkowska, E., and Kubes, P. (2013). Neutrophil recruitment and function in health and inflammation. *Nat. Rev. Immunol.* 13 (3), 159–175. doi:10.1038/nri3399

Kratofil, R. M., Kubes, P., and Deniset, J. F. (2017). Monocyte conversion during inflammation and injury. *Arterioscler Thromb. Vasc. Biol.* 37 (1), 35–42. doi:10.1161/atvbaha.116.308198

Lam, F. W., Vijayan, K. V., and Rumbaut, R. E. (2015). Platelets and their interactions with other immune cells. *Compr. Physiol.* 5 (3), 1265–1280. doi:10.1002/cphy.c140074

Landmesser, U., Hornig, B., and Drexler, H. (2004). Endothelial function: a critical determinant in atherosclerosis? *Circulation* 109 (21 Suppl. 1), II27-33. doi:10.1161/01.cir.0000129501.88485.1f

Langslet, G., Emery, M., and Wasserman, S. M. (2015). Evolocumab (AMG 145) for primary hypercholesterolemia. *Expert Rev. Cardiovasc. Ther.* 13 (5), 477–488. doi:10.1586/14779072.2015.1030395

Langsted, A., Freiberg, J. J., and Nordestgaard, B. G. (2008). Fasting and nonfasting lipid levels. *Circulation* 118 (20), 2047–2056. doi:10.1161/circulationaha.108.804146

Mancuso, M. E., and Santagostino, E. (2017). Platelets: much more than bricks in a breached wall. *Br. J. Haematol.* 178 (2), 209–219. doi:10.1111/bjh.14653

Manne, B. K. (2017). Platelet secretion in inflammatory and infectious diseases. *Platelets*. 28 (2), 155–164. doi:10.1080/09537104.2016.1240766

Marques, P., Collado, A., Escudero, P., Rius, C., González, C., Servera, E., et al. (2017). Cigarette smoke increases endothelial CXCL16-leukocyte CXCR6 adhesion in vitro and in vivo. Potential consequences in chronic obstructive pulmonary disease. *Front. Immunol.* 8, 1766. doi:10.3389/fimmu.2017.01766

Marques, P., Collado, A., Martinez-Hervás, S., Domingo, E., Benito, E., Piqueras, L., et al. (2019). Systemic inflammation in metabolic syndrome: increased platelet and leukocyte activation, and key role of cx3cl1/cx3cr1 and CCL2/CCR2 axes in arterial platelet-proinflammatory monocyte adhesion. *J Clin Med.* 8 (5), 708. doi:10.3390/jcm8050708

Murugappa, S., and Kunapuli, S. P. (2006). The role of ADP receptors in platelet function. *Front. Biosci.* 11, 1977–1986. doi:10.2741/1939

Pedro, T., Martinez-Hervas, S., Tormo, C., García-García, A. B., Saez-Tormo, G., Ascaso, J. F., et al. (2013). Oxidative stress and antioxidant enzyme values in lymphomonocytes after an oral unsaturated fat load test in familial hypercholesterolemic subjects. *Translational Res.* 161 (1), 50–56. doi:10.1016/j.trsl.2012.09.002

Perdomo, L., Beneit, N., Otero, Y. F., Escribano, O., Diaz-Castroverde, S., Gomez-Hernandez, A., et al. (2015). Protective role of oleic acid against cardiovascular insulin resistance and in the early and late cellular atherosclerotic process. *Cardiovasc. Diabetol.* 14, 75. doi:10.1186/s12933-015-0237-9

Periayah, M. H., Halim, A. S., and Mat Saad, A. Z. (2017). Mechanism action of platelets and crucial blood coagulation pathways in hemostasis. *Int. J. Hematol. Oncol. Stem Cel Res* 11 (4), 319–327.

Postea, O., Vasina, E. M., Cauwenberghs, S., Projahn, D., Liehn, E. A., Lievens, D., et al. (2012). Contribution of platelet CX3CR1 to platelet-monocyte complex formation and vascular recruitment during hyperlipidemia. *Arterioscler Thromb. Vasc. Biol.* 32 (5), 1186–1193. doi:10.1161/atvbaha.111.243485

Real, J. T., Martinez-Hervas, S., Garcia-Garcia, A. B., Civera, M., Pallardo, F. V., Ascaso, J. F., et al. (2010). Circulating mononuclear cells nuclear factor-kappa B activity, plasma xanthine oxidase, and low grade inflammatory markers in adult

patients with familial hypercholesterolaemia. *Eur. J. Clin. Invest.* 40 (2), 89–94. doi:10.1111/j.1365-2362.2009.02218.x

Rius, C., Company, C., Piqueras, L., Cerdá-Nicolás, J. M., González, C., Servera, E., et al. (2013). Critical role of fractalkine (CX3CL1) in cigarette smoke-induced mononuclear cell adhesion to the arterial endothelium. *Thorax* 68 (2), 177–186. doi:10.1136/thoraxjnl-2012-202212

Sampietro, T., Tuoni, M., Ferdeghini, M., Ciardi, A., Marraccini, P., Prontera, C., et al. (1997). Plasma cholesterol regulates soluble cell adhesion molecule expression in familial hypercholesterolemia. *Circulation* 96 (5), 1381–1385. doi:10.1161/01.cir.96.5.1381

Sniderman, A. D., Tsimikas, S., and Fazio, S. (2014). The severe hypercholesterolemia phenotype. *J. Am. Coll. Cardiol.* 63 (19), 1935–1947. doi:10.1016/j.jacc.2014.01.060

von Hundelshausen, P., and Schmitt, M. M. (2014). Platelets and their chemokines in atherosclerosis-clinical applications. *Front. Physiol.* 5, 294. doi:10.3389/fphys.2014.00294

von Hundelshausen, P., Weber, K. S. C., Huo, Y., Proudfoot, A. E. I., Nelson, P. J., Ley, K., et al. (2001). RANTES deposition by platelets triggers monocyte arrest on inflamed and atherosclerotic endothelium. *Circulation* 103 (13), 1772–1777. doi:10.1161/01.cir.103.13.1772

Weber, C., Shantsila, E., Hristov, M., Caligiuri, G., Guzik, T., Heine, G. H., et al. (2016). Role and analysis of monocyte subsets in cardiovascular disease. Joint consensus document of the European society of cardiology (ESC) working groups "atherosclerosis & vascular biology" and "thrombosis". *Thromb. Haemost.* 116 (4), 626–637. doi:10.1160/TH16-02-0091

Weber, K. S. C., Nelson, P. J., Gröne, H.-J., and Weber, C. (1999). Expression of CCR2 by endothelial cells. *Arterioscler Thromb. Vasc. Biol.* 19 (9), 2085–2093. doi:10.1161/01.atv.19.9.2085

Wilkins, E., Wilson, L., Wickramasinghe, K., Bhatnagar, P., Leal, J., Luengo-Fernandez, R., et al. (2017). *European cardiovascular disease statistics 2017*. Brussels, Belgium: European Heart Network.

Wong, N. D., Zhao, Y., Patel, R., Patao, C., Malik, S., Bertoni, A. G., et al. (2016). Cardiovascular risk factor targets and cardiovascular disease event risk in diabetes: a pooling project of the atherosclerosis risk in communities study, multi-ethnic study of atherosclerosis, and jackson heart study. *Dia Care* 39 (5), 668–676. doi:10.2337/dc15-2439

Zimmer, S., Grebe, A., and Latz, E. (2015). Danger signaling in atherosclerosis. *Circ. Res.* 116 (2), 323–340. doi:10.1161/circresaha.116.301135

Conflict of Interest: The authors declare that the research was conducted in the absence of any commercial or financial relationships that could be construed as a potential conflict of interest.

frontiers in Pharmacology

REVIEW
published: 21 April 2021
doi: 10.3389/fphar.2021.653940

Innate Immunity in Diabetic Wound Healing: Focus on the Mastermind Hidden in Chronic Inflammatory

Kang Geng[1,2,3,4,5,6†], *Xiumei Ma*[1,2,3,4†], *Zongzhe Jiang*[3,4], *Wei Huang*[7,3,4], *Chenlin Gao*[7,3,4], *Yueli Pu*[3,4], *Lifang Luo*[3,4], *Youhua Xu*[1,2*] *and Yong Xu*[1,2,3,4,7*]

[1]Faculty of Chinese Medicine, Macau University of Science and Technology, Avenida Wai Long, Taipa, China, [2]State Key Laboratory of Quality Research in Chinese Medicine (Macau University of Science and Technology), Avenida Wai Long, Taipa, China, [3]Cardiovascular and Metabolic Diseases Key Laboratory of Luzhou, Luzhou, China, [4]Sichuan Clinical Research Center for Nephropathy, Luzhou, China, [5]Department of Plastic and Burn Surgery, The Affiliated Hospital of Southwest Medical University, Luzhou, China, [6]National Key Clinical Construction Specialty, Luzhou, China, [7]Department of Endocrinology and Metabolism, The Affiliated Hospital of Southwest Medical University, Luzhou, China

OPEN ACCESS

Edited by:
Xing Li Wang,
Novartis (United States), United States

Reviewed by:
Ying Hu Shen,
Baylor College of Medicine,
United States
Ming-Hui Zou,
Georgia State University, United States

***Correspondence:**
Youhua Xu
yhxu@must.edu.mo
Yong Xu
xywyll@swmu.edu.cn

[†]These authors have contributed equally to this work

Specialty section:
This article was submitted to Inflammation Pharmacology, a section of the journal Frontiers in Pharmacology

Received: 15 January 2021
Accepted: 24 February 2021
Published: 21 April 2021

Citation:
Geng K, Ma X, Jiang Z, Huang W, Gao C, Pu Y, Luo L, Xu Y and Xu Y (2021) Innate Immunity in Diabetic Wound Healing: Focus on the Mastermind Hidden in Chronic Inflammatory. Front. Pharmacol. 12:653940. doi: 10.3389/fphar.2021.653940

A growing body of evidence suggests that the interaction between immune and metabolic responses is essential for maintaining tissue and organ homeostasis. These interacting disorders contribute to the development of chronic diseases associated with immune-aging such as diabetes, obesity, atherosclerosis, and nonalcoholic fatty liver disease. In Diabetic wound (DW), innate immune cells respond to the Pathogen-associated molecular patterns (PAMAs) and/or Damage-associated molecular patterns (DAMPs), changes from resting to an active phenotype, and play an important role in the triggering and maintenance of inflammation. Furthermore, the abnormal activation of innate immune pathways secondary to immune-aging also plays a key role in DW healing. Here, we review studies of innate immune cellular molecular events that identify metabolic disorders in the local microenvironment of DW and provide a historical perspective. At the same time, we describe some of the recent progress, such as TLR receptor-mediated intracellular signaling pathways that lead to the activation of NF-κB and the production of various pro-inflammatory mediators, NLRP3 inflammatory via pyroptosis, induction of IL-1β and IL-18, cGAS-STING responds to mitochondrial injury and endoplasmic reticulum stress, links sensing of metabolic stress to activation of pro-inflammatory cascades. Besides, JAK-STAT is also involved in DW healing by mediating the action of various innate immune effectors. Finally, we discuss the great potential of targeting these innate immune pathways and reprogramming innate immune cell phenotypes in DW therapy.

Keywords: innate immunity, diabetic wound, wound healing, inflammation, senescence

INTRODUCTION

Diabetes mellitus (DM) is a chronic metabolic, endocrine disease characterized by persistent hyperglycemia. Chronic complications are its main hazards, often involving microvessels, large vessels, and the nervous system, resulting in heart, brain, kidney, and other essential organ lesions (Brennan et al., 2019; Tellechea et al., 2020). Besides, peripheral vascular and neuropathy lesions are often combined with pathogenic microbial infections to cause diabetic foot disease. According to the IDF global report in 2019, foot complications have been one of the most severe and expensive

treatment complications of DM (https://diabetesatlas.org/en/sections/individual-social-and-economic-impact.html).and affect 40 to 60 million people. As the most common manifestation of foot complications, DFUs have a lifetime risk of up to 25% in DM patients (Rahelic, 2016; Ogurtsova et al., 2017; Cho et al., 2018). Continuous inflammation activation is not only the primary cause of chronic refractory DW, but also an essential factor leading to DFUs, gangrene, and amputation (toe), and even the root cause of the increased length of hospitalization and cost of wound management.

The pathogenesis of DW is complex and involves many different pathways. Although it is traditionally believed to be related to the local hyperglycemic environment, accumulation of advanced glycation end products (AGEs), oxidative stress injury, chronic inflammation, etc., more and more evidence points to the key roles of Cellular Senescence and immune aging in DW healing (Tomic-Canic and DiPietro, 2019; Berlanga-Acosta et al., 2020). Cellular Senescence is a normal physiological process in which cells lose their ability to proliferate, the essence of DW is chronic low-grade inflammation and an increased burden of senescent cells (Prattichizzo et al., 2018). In Non-DW, transient induction of a senescent phenotype such as senescent fibroblasts and endothelial cells appear very early in response to a cutaneous wound, where they accelerate wound closure by inducing myofibroblast differentiation through the secretion of platelet-derived growth factor AA (PDGF-AA) (Demaria et al., 2014), but in DW, senescent cells rapidly accumulate, these greater numbers of senescent cells and senescence-associated secretory phenotype (SASP).paly a negative role in DW healing (Wilkinson et al., 2019). Firstly, senescence is a known consequence of hyperglycemia, the direct association between hyperglycemia and SASP in endothelial cells and macrophages also suggests that SASP may exacerbate low-grade inflammation in diabetes (Prattichizzo et al., 2018). Secondly, AGEs and increased oxidative stress which lead to endoplasmic reticulum stress also promote cell senescence (Liu et al., 2014). Besides, bone marrow (BM).and mesenchymal stem cells (BMSCs).become prematurely senescent under the pressure of diabetes metabolic stress, continued release of inflammatory cytokines resulted in the loss of BMSCs number and function, which prevented DW healing (Lu et al., 2016). All of this suggests that in DW, hyperglycemia, AGEs, oxidative stress, DNA damage, inflammatory cytokines act as major drivers sculpturing the senescent phenotype (Longo et al., 2019; Palmer et al., 2019). This is reflected not only in the reduced number of cytokines and growth factors secreted and the number of receptors but also in the decline of non-functional intracellular signals (Telgenhoff and Shroot, 2005), It further affects the function of T cells and B cells, increasing susceptibility, and SASP continuously releases "inflammatory" signals to activate the innate immune system, aggravating the level of inflammatory cytokines and the secretion of cytotoxic mediators. For example, the decrease of Naive T-cell phenotype and the increase of memory and effector T-cell phenotype (Moura et al., 2017), the level of B-cell activating factor (BAFF) which implicit in B-cell dysfunction increased gradually with the progression of DFU, and the circulating BAFF was positively correlated with C-reactive protein (CRP) and TNF-α (Dhamodharan et al., 2019) (**Table 1**). This review focuses on the changes in innate immune cells from dormant to active phenotype in DW, to further clarify its effect on DW sustained activation of inflammation, and then discusses several kinds of immune pathways that the pattern recognition receptors or cell surface receptor trigger inflammation-related: Toll-like receptor (TLR) signal, nucleotide-binding oligomerization domain (NOD) receptor (NLR) signals, cGAS - STING signals, JAK-STAT signals, Focusing on the progress of the immune mechanisms behind chronic inflammation in DW, we finally comment on the potential of targeting these innate immune-inflammatory pathways in DW therapy. Focusing on the progress of the immune mechanisms behind chronic inflammation in DW, we finally comment on the potential of targeting these innate immune-inflammatory pathways in DW therapy.

CONTINUOUS ACTIVATION OF INNATE IMMUNITY HIDDEN UNDER IMMUNE-AGING AND INFLAMM-AGING HINDERS DIABETIC WOUND HEALING

Innate immune can resist the invasion of pathogens, clear out the endogenous signals released by damaged cells, and start the repair process, which helps maintain the steady-state of the body. However, excessive inflammation caused by immune hyperfunction can also lead to tissue damage. DW healing seems to be affected by the balance between "good" and "bad" inflammation. However, the essence is closely related to the balance of "immune response-inflammation resolution-normal healing" and "immune-aging-chronic inflammation-abnormal healing".

In the state of normal circumstances, the immune response, coagulation cascade, and inflammatory reaction are activated after wound formation, immune cells (neutrophils, monocytes/macrophages, dendritic cells, mast cells, etc.) and repair cells (keratinocytes, epithelial cells, fibroblasts, endothelial cells, etc.) and extracellular matrix have significant changes, which in turn affect the subsequent proliferation, differentiation, migration, and remodeling (Criscitelli, 2018). The coagulation cascade forms a fibrin matrix rich in cytokines and growth factors through platelet aggregation and blood coagulation provides scaffolds for subsequent infiltrating cells (leukocytes, keratinocytes, fibroblasts, endothelial cells, etc.) (Gurtner et al., 2008; Minutti et al., 2017; Bando et al., 2018; Criscitelli, 2018). Then, immune cells migrate to the wound under the influence of chemokines and release a large number of cytokines to initiate the inflammatory response (Bando et al., 2018; Akita, 2019), neutrophils are first recruited to the wound and reach a peak within 24 h (Kim et al., 2008), by changing the phenotype and expression of macrophages to generate the innate immune response (Park and Barbul, 2004; Acosta et al., 2008; Suga et al., 2014). Subsequently, monocytes are recruited in the wound within 48–96 h after injury and differentiate into macrophages, carry out the function of engulfing pathogens and cellular debris, promote the secretion of cytokines, growth

TABLE 1 | Markers of immune cells that can be used for diagnosis and/or treatment in DW.

Immune cells	Differentiation markers	Diagnosis and/or treatment
T Cells	Effector T-cells↑ Memory T-cells↑ Naive T-cells↓	The accumulation of effector T-cells is the core of DFU, diminish T-cells activation and tissue accumulation may accelerate DW healing Moura et al. (2017)
B Cells	BAFF↑	The BAFF levels were superior to that of CRP levels in diagnosing DFUDhamodharan et al. (2019)
Neutrophils (PMNs).	NETs↑ PAD4, H3Cit↑	PAD4 inhibition and cleavage of NETs by dnaseImay improve DW healing Wong et al. (2015)
	NET-specific markers H3Cit↑	NET-specific markers H3Cit negatively correlated with wound healing in DFU patients Yang et al. (2020)
	C5a↑ C3-fragment deposition↑	Inhibitor of complement C1 (PIC1). may reduce the infiltration of PMNS and improve DW healing Cunnion et al. (2017)
Monocytes/Macrophages (Mo/Mp).	Proportions of bone MyP↑circulating Ly6C^{Hi} Mo↑ Spleen Ly6C^{Hi} Mo↑ HSPC response↑ MPP2, MMP-3↓	Myeloid lineage commitment in BM may contribute to increased mp numbers observed in DW strategies to regulate monopoiesis during homeostasis or post wounding may improve DW healing Barman et al. (2019)
	The influx of Ly6C^{Hi} Mo↑ Maturation to Ly6C^{Lo} Mo↓	Time-dependent control of Mo/Mp influx after an injury such as anti-mcp-1 antibody may represent a novel therapeutic target for impaired DW healing Kimball et al. (2018)
	IL-1β, MMP-9, TNF-α↑ CD206, IGF-1↓ TGF-β, il-10↓	Inhibiting IL-1β downregulate proinflammatory mp and upregulate prohealing mp in DW which may improve DW healing Mirza et al. (2013)
	CD68, iNOS, TNF-α, IFN-γ↑ CD206, PDGF↓	Blocking the AGE-RAGE interaction may improve the function of Mp Wang Q. et al. (2017)
	Jmjd3, IL-12↑ H3K27me3↓	Histone demethylase inhibitor such as GSK-J4 may improve chronic inflammation and DW healing Gallagher et al. (2015)
	UA, XO↑ Setdb2, H3K9me3↓ IFNβ↓	IFNβ may be an attractive therapeutic target and XO inhibitors such as allopurinol may reduce the production of IL-1β and improve DW healing Kimball et al. (2019)
	Mp senescence↑ CXCR2↑ SASP↑	CXCR2 antagonist treatment such as SB265610 reduces inflammation Immune-aging and improve DW healing Wilkinson et al. (2019)

Partial Abbreviations: BAFF: B-cell activating factor, PAD4: Peptidylarginine deiminase 4 (encoded by Padi4 in mice)., H3Cit: Citrullinated histone H3, NETs: Neutrophil extracellular traps, BM: Bone marrow, HSPC: Hematopoietic stem and progenitor cell, MyP: Marrow myeloid progenitors, MPP: Multipotent progenitor, Ly6C^{Hi}: CX3CR1^{low}CCR2^{+}Ly6C^{+}, Ly6C^{Lo}: CX3CR1^{high}CCR2^{-}Ly6C^{-}, IL-1β: Interleukin-1β, TNF-α: Tumor necrosis factor-α, MMP-9: Matrix metalloprotein-9, IL-10: Interleukin-10, TGF-β: Transforming growth factor-β, IGF-1: Insulin-like growth factor-1, AGEs: Advanced glycation end products, PDGF: Platelet derived growth factor, Jmjd3: JumanjiC (JmjC) domain-containing protein, UA: Uric acid, XO: Xanthine oxidase, SASP: Senescence-associated secretory phenotype.

factors, and chemokines, stimulate collagen synthesis and angiogenesis, promote the conversion of fibroblasts to myofibroblasts to fill and contract the wound, and provide supports for subsequent cell proliferation, migration, and re-epithelialization (Snyder et al., 2016; Kim and Nair, 2019). When the granulation tissue formed by fibroblasts, endothelial cells, and macrophages replaces the fibrin matrix, keratinocytes and epithelial cells migrate on the new scaffolds until the skin barrier function is restored (Gurtner et al., 2008; Bainbridge, 2013).

Immune senescence in DW is further evidenced by reduced recruitment of immune cells and poor control of inflammatory response due to dysregulation of transcriptional networks. The study found that: Transcription factors FOXM1 and STAT3, which activate and promote the survival of immune cells, are inhibited in DFU (Sawaya et al., 2020), In the state of DM, the insufficient inflammatory response in the early stage of the wound and the large number of immune cells infiltrating in local subsequently (Moura et al., 2017), releasing proinflammatory cytokines make the healing stagnate in the inflammatory period and difficult to enter the proliferation and remodeling period (Liu et al., 2019) are the pathological basis of chronic refractory DW (Zhao et al., 2016). Moreover, innate immune cells such as neutrophils and macrophages continuously infiltrate during the inflammatory phase and interact with the high expression of chemokines, Macrophage inflammatory protein-2 (MIP-2) and Monocyte chemotactic protein-1 (MCP-1), up-regulate inflammatory mediators IL-1β, TNF-α, etc. result in continual amplification of signals of inflammatory until 13 days or more after injury (Wetzler et al., 2000; Tousoulis et al., 2013; Mo et al., 2019). Meanwhile, the continual differentiation and formation of proinflammatory macrophages can also stimulate the synthesis of Matrix metalloproteinases (MMPs) jointly with TNF-α, cause excessive destruction of extracellular Matrix and damaged granulation tissue formation (Acosta et al., 2008), inhibit proliferation and migration of fibroblasts and angiogenesis (Xu et al., 2013), activate innate immunity through ROS generated by oxidative stress (Warnatsch et al., 2015), activate NLRP3 inflammasome and lead to exacerbating wound inflammation (Lee et al., 2013; Mirza et al., 2014; Dai et al., 2017). It can be seen that the intensified innate immune response and the continuous infiltration of innate immune cells will destroy the balance between anti-inflammatory and proinflammatory during DW healing, interfere with the homeostasis of DW, and form a chronic refractory wound characterized by DFUs (Chen et al., 2012). (**Table 1**).

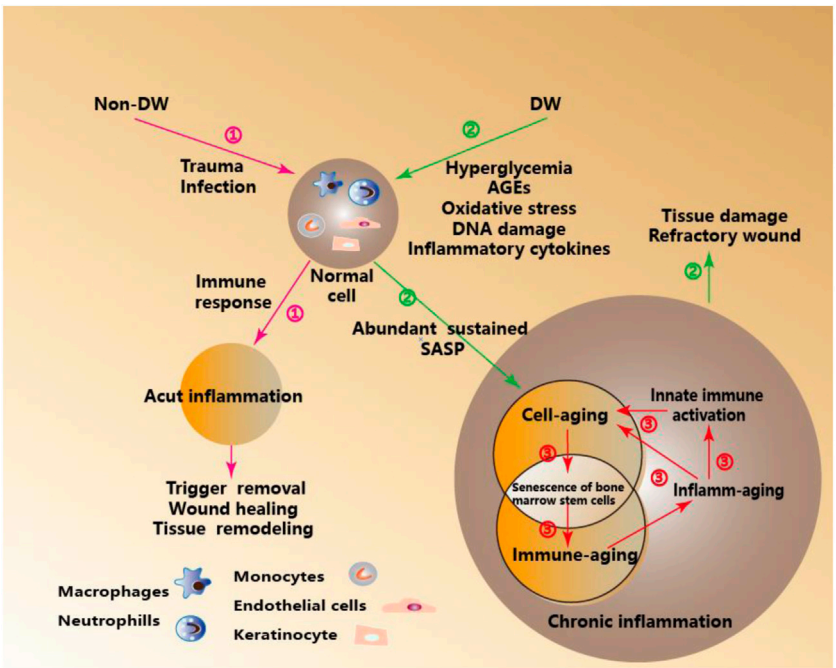

FIGURE 1 | Immune- Aging and Inflamm-Aging under Metabolic Stress in DW. ①Acute inflammation-mediated wound healing, tissue remodeling, and other orderly outcomes under the immune response in Non-DW. ②Inflamm-aging induced by metabolic pressure mediated tissue damage and hinders wound healing in DW. ③In the process cell senescence in DW, adaptive immunity significantly decreased, which is called immune-aging, while innate immunity is activated, thus inducing a unique pro-inflammatory response, which is called inflamm-aging.

In a word, Inflamm-aging and Immune-aging seem to run in parallel and form a vicious cycle. Increased inflammatory cytokines characteristic of inflamm-aging contributes to the decrease of the adaptive immune response and eventually to immune-aging. In contrast, the decrease of the adaptive immune response reinforces the stimulation of the innate immune response (as the means to protect an organism from infections in the circumstances when adaptive immunity fails)., leading to chronic inflammation (Salminen et al., 2008; Fulop et al., 2017). (**Figure 1**).

INNATE IMMUNE CELLS AFFECTED BY IMMUNE-AGING IN DIABETIC WOUND

The Ongoing Recruitment and Activation of Neutrophils (Polymorphonuclear leukocytes, PMNs). and the Feedback Loop of Oxidative Stress Aggravate the Damage in Diabetic wound

PMNs phagocytize, neutralize, and remove microorganisms, cell debris, and other substances through phagocytosis, degranulation, generation of high concentrations of ROS, and Neutrophil extracellular traps (NETs) (Fox et al., 2010; Mikhalchik et al., 2018; Papayannopoulos, 2018). It can also regulate the phenotype of macrophages and the expression of cytokines to mediate the innate immune response, secrete a variety of inflammatory mediators, and an enzyme to regulate the activity of inflammatory cells and the inflammatory response (Daley et al., 2005). In the state of DM, the chemotaxis, phagocytosis, oxidative burst, and apoptosis of PMNs in DW induced by high glucose are deficient (Nguyen et al., 2013). PMNs infiltrate local tissues, combine with AGEs and release a large number of proinflammatory factors to cause inflammation. Meanwhile, PMNs promote excessive production of ROS and upregulate the expression of EGFR, ERK, and IL-8, further aggravate the degree of local infiltration (Lan et al., 2013). This continuous inflammation feedback loop driven by PMNs is an important reason for the aggravation of DW injury. Besides, the orderly resolution of PMNs is also the key to wound healing as scheduled. In the state of normal circumstances, PMNs are specially recognized and cleared by macrophages through apoptosis, to avoid entering a state of chronic inflammation and further tissue damage (Nepal et al., 2019; Perez et al., 2019). Surviving PMNs can also be "reverse-migrated" into the circulation and leave the site of inflammation by Specialized pro-resolving mediators (SPMs) (Robertson et al., 2014). However, in the state of DW, PMNs are more likely to die in the form of NETosis, forming NETs to induce innate immune cells to infiltrate the wound and mediate abnormal inflammation. Recent studies have shown that NETs can activate NLRP3 inflammasome, thus inducing the expression and release of inflammatory factors such as IL-1β and leading to inflammatory storms. After giving PAD4 inhibitor (Cl-amidine) (Fadini et al., 2016), dnasel, N-acetylcysteine (NAC) (Liu et al., 2019), targeted inhibition of the formation of NETs can

inhibit the activation of NLRP3 inflammasome and the release of inflammatory mediators, reduce local infiltration of PMNs, promote macrophages appearance in advance and accelerate the resolving of PMNs, thereby promoting wound healing (Wong et al., 2015; Liu et al., 2019; Yang et al., 2020). Besides, the activation of the complement system (CS) in the early stage of DW also promotes leukocytes (the vast majority of the leukocytes were PMNS) infiltration, It was found that increased anaphylatoxin C5A and C3-fragment deposition in DW fluid associated with a 76% increase in PMNS, use the novel classical CS inhibitor, Peptide Inhibitor of Complement C1(PIC1) reduced inflammation as reflected by reduced CS components and PMNs infiltration (Kimball et al., 2018). Thus, inducing the apoptosis of PMNs, promoting the degradation of NETs, negative regulation of the complement system, and promoting the "reverse-migrated" of PMNs through SPMs will change the chaotic state of "Activation in the early period and resolving in the late period delayed" PMNs, thereby promoting DW healing.

Spatial and Temporal Expression Difference of Monocytes Is a Double-Edged Sword for Diabetic wound Healing

Mo in peripheral blood of mice is divided into two subgroups: $CX3CR1^{low}$ $CCR2^{+}$ $Ly6C^{+}$ ($Ly6C^{+}$) and $CX3CR1^{high}$ $CCR2^{-}Ly6C^{-}$ ($Ly6C^{-}$). After the wound is formed, $Ly6C^{+}$ first migrates to the wound and differentiate into macrophages and secrete pro-inflammatory factors such as TNF-α, IL-1β to participate in the early inflammatory response (Daley et al., 2010; Brancato and Albina, 2011). Subsequently, $Ly6C^{-}$ appears on the wound through vascular patrol and is involved in anti-inflammatory and tissue repair (Carlin et al., 2013; Italiani and Boraschi, 2014). Besides, $Ly6C^{+}$ can also induce apoptosis of PMNs, while $Ly6C^{-}$ has the effect of removing PMNs fragments after apoptosis (Peng et al., 2009). The chemotactic activity of $Ly6C^{+}$ is mainly dependent on CCL2/CCR2. Current studies have shown that delayed response and impaired activity of macrophages, which differentiated from $Ly6C^{+}$ at the early stage of DW are related to decreased expression of CCL2 chemokines (Wood et al., 2014). Animal experiments have shown that the use of CCL2 on the wound of db/db mice can not only solve the delayed early inflammatory response and macrophage dysfunction, promote re-epithelialization, but also restore the amount of Mo and promote the chemotaxis of Mo (Weinheimer-Haus et al., 2014; Wood et al., 2014). Besides, knocking out the CCR2 gene can cause a decreased amount of $Ly6C^{+}$ recruited to the wound tissue, leading to tissue repair disorders (Weinheimer-Haus et al., 2014). However, excessive expression of Ly6C + on the wound can also affect wound healing, which requires strict control of the timing of the use of CCR2. The chronic refractory DW is related to increased secretion of Ly6C+ and decreased secretion of $Ly6C^{-}$ in circulating blood (Galstyan et al., 2019). Studies have shown that the influx of secondary mononuclear/macrophage will increase in wounds around 96 h after injury. Therefore, selective inhibition of CCL2/CCR2 at 72 h after dBinjury can improve the persistent state of DW inflammation and promote healing by blocking the second influx of $Ly6C^{+}$ (Kimball et al., 2018). In summary, using chemokines as the target to regulate the timing of Mo appears on the wound will be expected to become an effective means to promote DW healing.

The Persistent Proinflammatory Phenotype of Macrophages in the Metabolic Immune Microenvironment Aggravates the Difficulty in Diabetic wound Healing

Mp involved in wound healing includes Tissue-resident macrophages (TRMs). (Ganesh and Ramkumar, 2020) and Wound-associated macrophages (WAMs). (Wang et al., 2014). Skin TRMs include Langerhans cell (LC) in the *epidermis* and macrophage population ($CD11b^{+}$/ $F4/80^{+}$) in the dermis, through self-amplification (Chorro et al., 2009; Hoeffel et al., 2012; Sieweke and Allen, 2013) and the differentiation of circulating blood Mo in the inflammatory state (Sieweke and Allen, 2013) to supplement, play the role as a sentinel for tissue homeostasis, initiate an inflammatory response and form a locally pro-inflammatory environment by way of PRRs identifying PAMPs or DAMPs in the immediate or early stages of trauma (Smyth and Bertram, 2019). Under steady-state conditions, TRMs maintain homeostasis. Once damaged, WAMs are recruited to wound in large quantities and promote the progress of wound healing together with TRMs. With the assistance of some new techniques such as cell tracking and single-cell RNA-seq, the heterogeneity of TRMs and WAMs appears more in the study of wound healing. TRMs are considered to be involved in the induction of inflammation (Stojadinovic et al., 2013). At the same time, WAMs are not only crucial in the initial inflammation stage of wound healing but also play a vital role in the subsequent stage of wound healing by coordinating the inflammatory response (Willenborg et al., 2012). (**Table 2**).

Under the influence of different microenvironments, Mp is polarized into pro-inflammatory M1 (Classically activated macrophages type 1) and anti-inflammatory M2 (Alternatively activated macrophages), which respectively play roles in different stages of wound healing (Das et al., 2015; Krzyszczyk and et al., 2018). In the stage of an inflammatory response, the wound is dominated by M1, which play an antibacterial and clearance of necrotic tissue role through phagocytosis, producing ROS, secreting various proteases and pro-inflammatory mediators (such as IL-1β, TNF-α, NO and IL-6). Thereafter, M1 gradually polarize to M2 which promote cell proliferation, Extracellular matrix (ECM) synthesis, angiogenesis, and tissue remodeling through secreting anti-inflammatory factors (such as IL-10, IL-8, etc.), various ECM proteins and growth factors (such as TGF-β1, bFGF, PDGF and VEGF, etc.) (Murray et al., 2014; Wang et al., 2014; Boniakowski et al., 2017). The orderly transformation of M1 to M2 is the key to wound healing (Ganesh and Ramkumar, 2020), If Mp cannot acquire the M2 phenotype, sustained pro-inflammatory signals will amplify the pro-inflammatory effect of M1 in the form of positive feedback by continuously activating NLRP3 inflammasome and promoting IL-1β release (Warnatsch et al., 2015). Besides, the persistent state of inflammation caused by such phenotypic imbalance of Mp also hinders the proliferation and migration of endothelial cells and

TABLE 2 | Function and relationship of Mo/Mp subpopulations in wound homeostasis and repair.

Mo/Mp	Function		
	Feature the steady-state		Wound healing
$Ly6C^+$ (Sieweke and Allen, 2013)	CCL2 can regulate its chemotactic activity Willenborg et al. (2012), Gupta et al. (2013), Dal-Secco et al. (2015)	1.A precursor of the TRMs Italiani and Boraschi, (2014)	1.Upregulate TNF-α, IL-1β 2.Activate a function similar to M1 Daley et al. (2010), Brancato and Albina, (2011)
		2.A precursor of $Ly6C^-$ in blood and bone marrow Varol et al. (2007), Yona et al. (2013)	3.Die in the wound during the inflammatory, repair, proliferation period Albina et al. (1990) 4.Enter the non-lymphoid organs and circulated to the lymph nodes Jakubzick et al. (2013)
$Ly6C^-$ (Sieweke and Allen, 2013)	Fractalkine (CX3CL1) can regulate its chemotactic activity Ishida et al. (2008), Lauvau et al. (2015)	1.Patrol the signs of endothelial inflammation or injury Auffray et al. (2007), Carlin et al. (2013)	1.Upregulate TGF-β, VEGF
		2.Produce inflammatory mediators and coordinate the repair of damaged vascular endothelium Carlin et al. (2013), Italiani and Boraschi, (2014)	2.Activate a function similar to M2 Daley et al. (2010), Brancato and Albina, (2011)
TRMs $F4/80^+$ (Ganesh and Ramkumar, 2020; Sieweke and Allen, 2013)	Bone marrow/Circulation Sieweke and Allen, (2013) and embryonic progenitor cells (yolk sac, fetal liver) derived Mp Chorro et al. (2009), Hoeffel et al. (2012), Sieweke and Allen, (2013)	Local proliferation and self-renewal of mature differentiated cells without changing their differentiation phenotype Chorro et al. (2009), Hashimoto et al. (2013), Sieweke and Allen, (2013)	1.Involve in the induction of inflammation Stojadinovic et al. (2013) 2. Compensatory regulation through early recruitment and late self-proliferation Davies et al. (2011), Sieweke and Allen, (2013) 3. Activate a function similar to M2 Brancato and Albina, (2011)
WAMs $F4/80^-$ (Wang et al., 2014; Sieweke and Allen, 2013)	M1 Koh et al. (2013)	GM-CSF, IFN-γ, TNF-α, LPS induce Koh et al. (2013)	1.M1 has the function of promoting inflammation
	M2 Koh et al. (2013)	M2a: IL-4, IL-13 induce Lech et al. (2012)	2.M2 has the function of anti-inflammatory, repairing tissue, promoting angiogenesis
		M2b: Immune complexes, TLR receptor agonists, IL-1 receptor agonists induce Mantovani et al. (2004)	3.M2a promote matrix reconstruction and tissue repair
		M2c: IL-10, TGF-β, glucocorticoid induce Lech et al. (2012)	4.M2b and M2c mainly play the function of immune regulation Brancato and Albina, (2011)

Partial Abbreviations: CCL2: Chemokine C-C-motif ligand 2, TRMs: Tissue-resident macrophages, TNF-α: Tumor necrosis factor-α, IL: Interleukin, CX3CL1: Chemokine C-X3-C-motif Ligand 1, TLR: Toll-like receptor, TGF-β: Transforming growth factor-β, VEGF: Vascular endothelial growth factor, WAMs: Wound-associated macrophages, GM-CSF: Granulocyte-macrophage colony-stimulating factor, LPS: Lipopolysaccharide.

keratinocytes, prevents fibroblasts from secreting extracellular matrix, and secretes a large number of proteases to degrade the extracellular matrix (Pierce, 2001), these degraded extracellular matrix fragments further aggravate the pro-inflammatory state of the wound through the action of immune stimulation (Sorokin, 2010). Clinical studies have shown that Mp isolated from DW express high levels of pro-inflammatory molecules IL-1β, MMP-9 and TNF-α and low levels of healing-related molecules IGF-1, TGF-β, and IL-10. A similar phenomenon is also observed in animal experiments. Mp in Non-DM mice shows M2 phenotype 5–10°days after injury while DM mice maintain the M1 phenotype. Also, the IL-1β and TNF-α released by DM mice Mp on the fifth and 10th°day after injury are always maintained at high levels, and IGF-1, TGF-β are maintained at low levels. IL-1β neutralizing antibody or knocking out IL-1R1 gene can block IL-1β signal, thereby down-regulating M1, up-regulating M2, and promoting DW healing (Mirza et al., 2013).

The act of PMNs clearance by Mp can induce the phenotypic switch of M1 macrophages to M2, hyperglycemia, and AGEs impede the phagocytic capacity of Mp to clear apoptotic PMNs thereby promoting a sustained pro-inflammatory state (Hesketh et al., 2017). Further, differential iron regulation by Mp is another factor that affects Mp phenotype (Cairo et al., 2011; Wang H. et al., 2017), iron overloading in Mp maintaining M1 phenotype, enhanced TNF-α and hydroxyl radical release and induce nearby fibroblasts senescence. In addition to the cellular and molecular mechanisms of the effect of microenvironment on the Mp phenotype, the effect of epigenetics has also become a new focus of recent research, Skin wounding increased HSPC numbers and promoted Mo expansion in the BM of mice (Barman et al., 2019), even hyperglycemia preprogrammed HSPCs toward myeloid lineage commitment (Nagareddy et al., 2013), diabetic mice exhibited increased proportions of bone MyP and circulating inflammatory Mo before skin wounding and enhanced myeloid output maintained following injury, contributing to a greater number of M1 phenotype (Barman et al., 2019). Further, Histone methylation can also alter the Mp phenotype to affect DW healing (Boniakowski et al., 2017). For example, MLL1-mediated epigenetic alterations activated H3K4me3-TLR4-MyD88, use TLR4 inhibitor TAK-242 as well as genetic depletion of either $TLR4^{-/-}$ or myeloid-specific $TLR4^{f/f}Lyz2^{Cre+}$ resulted in a reduction in Mp-mediated inflammation and improved DW healing (Davis et al., 2020). In another study, the decreased expression of H3K27me3 corresponds

to the increased Jmjd3 and IL12 expression promoting the exaggerated pro-inflammatory response seen in diabetic Mp (Gallagher et al., 2015). This suggested that both target systemic changes in the BM stem cells thus influence Mp peripheral phenotypes and blocking the M1 phenotype in DW may contribute to the development of new therapeutic strategies for DW and is a promising research direction.

The Homeostasis of Mast cell Degranulation Regulates Ordered Healing in Diabetic wound

After wound formation, MCs participate in and regulate the inflammatory response by releasing multiple mediators (Moon et al., 2010). On the one hand, MCs induce the secretion of cytokines and chemokines by degranulation (Sun et al., 2012; Mukai et al., 2018; Zelechowska et al., 2018), On the other hand, MCs recruit immune cells to the wound by promoting the secretion of vascular permeability factors and proteases (Liu et al., 2009). Subsequently, MCs can stimulate the proliferation of fibroblasts by secreting IL-4, VEGF, and bFGF (Qu et al., 1998), promote granulation formation, cell migration, angiogenesis, collagen maturation, and angiogenesis in wound tissues (Sismanopoulos et al., 2012; González-de-Olano and Álvarez-Twose, 2018), and also participate in wound healing with Mp, endothelial cells and fibroblasts (Egozi et al., 2003; Nishida et al., 2019). Current clinical studies have shown that the total MCs before lower limb skin trauma in DM patients are regular, but the number of degranulation is increasing, and MCs degranulation is positively correlated with the number of dermal inflammatory cells and inflammatory markers IL-6 and TNF-α (Tellechea et al., 2016). Animal experiments have shown that intraperitoneal injection of DSCG (MCs degranulation inhibitor) before trauma can reduce the number of MCs degranulation in DM mice to the same level as non-DM mice, and effectively improve wound healing. Besides, DSCG can restore the ratio of M1/M2 to the level of non-DW through the interaction between MCs and Mp, and promote wound healing (Tellechea et al., 2016). In addition to the difference in pre-trauma degranulation, the current studies also have found that: in the state of diabetes, although MCs degranulation increased significantly before the trauma, it cannot increase after trauma, and the blocked MCs degranulation also reduces the ability of acute inflammatory response after trauma and delays the process of wound healing. In the early stage of wound formation, the local application of MCs stabilizer MCS-01 to treat DM mice can play the same role as the intraperitoneal injection of DSCG to promote wound healing (Tellechea et al., 2020). It can be seen that maintaining the steady-state of degranulation of MCs before trauma and degranulation in time after trauma will effectively promote DW healing.

INNATE IMMUNE SIGNALING AND DIABETIC WOUND

In the state of DW, the "abnormal epithelial barrier" caused by changes of microbiome located in the skin and their metabolites, environmental damage or the genetic tendency of the host, as well as the cellular contents released after necrosis and cell membrane destruction caused by stress, injury and metabolic pressure, recruit and activate innate immune cells and initiate innate immunity not only through intracellular DAMPs but also through extracellular DAMPs and PAMPs released by extracellular matrix recruitment (Matzinger, 2002; Huebener and Schwabe, 2013). When the activated innate immunity plays a role in removing pathogens and necrotic tissues, the high concentration of ROS produced also cause lipid peroxidation damage to the cell membrane, increase membrane permeability, destroy the critical balance of ion concentration inside and outside the cell, and further aggravate the release of DAMPs (Mayer et al., 2018). This subtle relationship as initiating factors regulate the balance between innate immunity and pro-inflammatory microenvironment and participate in the process of DW healing. It is necessary to understand further these PRRs that recognize PAMPs or DAMPs, including transmembrane receptors on the cell membrane surface, such as Toll-like receptor(TLR), C-type lectin receptor(CLR), etc. and intracytoplasmic receptor, such as RIG-1-like receptor(RLR), Nucleotide-binding oligomerization domain-like receptor (NLR).etc. And Cytosolic DNA Sensor (CDS) , such as cGAS, STING, etc. (**Figure 2**)

Increased Toll-Like Receptor Expression and Activation Prolonged Inflammatory Condition in Diabetic wound

TLR can respond to various pathogens (such as bacterial LPS, viral double-stranded RNA, etc.) or endogenous signals released after cellular stress and injury (such as HSP, HMGB1, Hyaluronic acid, Fibrinogen, etc.), and play a key role in inflammation, immune cell regulation and proliferation (Huebener and Schwabe, 2013). TLR signaling can be divided into MyD88-dependent pathway and TRIF-dependent pathway, the former mainly activates NF-κB and MAPKs, while the latter mainly activates NF-κB and IRF3(Kawai and Akira, 2007). The activation time of TLR binding with ligands and its relationship with the local microenvironment determine the effect of TLR in DW (Dasu and Rivkah Isseroff, 2012; Portou et al., 2015). In Non-DW, the expressions of TLR2 and TLR4 were up-regulated in the inflammatory stage (Suga et al., 2014), gradually decreased after the repair stage and recovered to the baseline level in 10°days later (Chen et al., 2013), regulates the release of IL-1β and IL-6, and participates in the orderly wound healing via TLR4-p38/JNK-MAPK signaling. But in DW, TLR2, 4, and 6 were consistently highly expressed from the injury to the 10th°day, continuously activated the NF-κB signal axis, and continuously amplified the pro-inflammatory signals such as IL-1β, IL-6, and TNF-α, which hindered the healing of DW (Dasu et al., 2010; Singh et al., 2015). More studies have also pointed to the negative regulatory role of abnormal inflammation caused by continued activation of TLR3, 7, and 9 in DW healing (Singh et al., 2016; Wu et al., 2016). Clinical studies of DW have also found that the levels of TLR1, 2, 4, and 6 and corresponding expression of downstream adapter proteins such as MyD88, IRAK-1 and NF-κB in DW were significantly higher than those in Non-DW (Dasu and Martin, 2014). This shows activated TLR-MyD88-NF-κB signaling and increased oxidative stress contributes to the increased

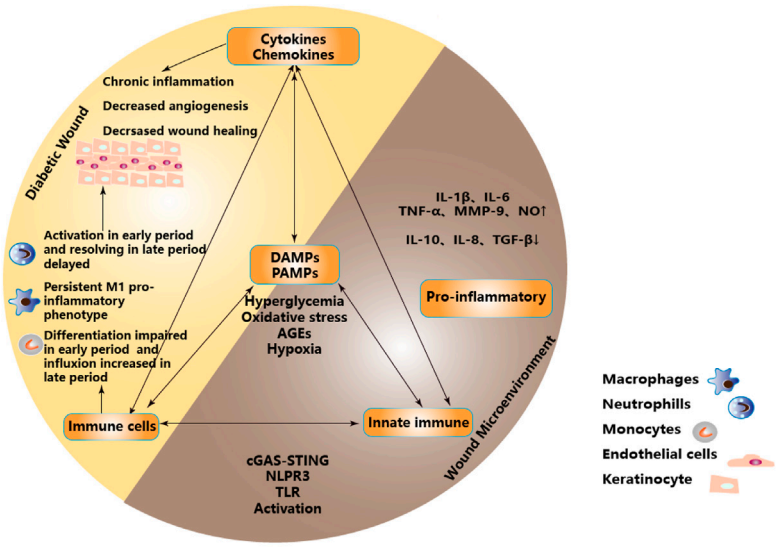

FIGURE 2 | Proinflammatory microenvironment in DW due to dysregulation of immune and metabolic responses. Metabolic stress such as hyperglycemia, oxidative stress, AGEs, and hypoxia acted as the initiators of PAMPs and DAMPs to activate PRRs. Inducing infiltration of innate immune cells and activation of innate immune pathways, regulating the balance between innate immunity and inflammatory microenvironment, forming a pro-inflammatory microenvironment, and participating in DW healing. Partial abbreviation: IL-1β: Interleukin-1β, IL-6: Interleukin-6, TNF-α: Tumor necrosis factor-α, MMP-9: Matrix metalloprotein-9, NO: Nitric oxide, IL-10: Interleukin-10, IL-8: Interleukin-8, TGF-β: Transforming growth factor-β, DAMPs: Damage-associated molecular patterns, PAMPs: Pathogen-associated molecular patterns, TLR: Toll-like receptor.

local pro-inflammatory cytokines and unhealed DW. Besides, high glucose up-regulated transcription and translation of TLR2 and TLR4 in a time-dependent and dose-dependent manner, inducing heterodimerization of TLR2/TLR6, leading to recruitment of MyD88 and activation of downstream inflammatory pathways, and the secretion of IL-1β and TNF-α(Dasu et al., 2008)keeping DW in an inflammatory state (Dasu and Martin, 2014; Kishibe et al., 2018), while inhibiting TLR2 and TLR4 can block the excessive inflammation caused by the positive feedback effect of IL-1β, thereby promoting DW healing (Dasu et al., 2010). (**Figure 3A**).

Therapeutic Targeting of Toll-Like Receptor Signaling in Diabetic wound

In keratinocytes, hyperglycemia dose-dependently up-regulates the expression of TNF-α to reduce the expression of Thrombomodulin (TM) and TLR4, exogenous supplementation of Recombinant sTM can increase the expression of TLR4 and promote DW healing (Cheng et al., 2015). Besides, hyperglycemia can also inhibit the expression of IL-33, which is induced by IL-17 in keratinocytes through glycosylation, down-regulate Regenerating islet-derived protein 3A (REG3A), and up-regulate the expression of TLR3, supplementing REG3A can induce SHP-1 negatively regulating the TLR3-JNK2 signal axis to down-regulate TNF-α and IL-6, thereby improving chronic inflammation of DW (Wu et al., 2016). However, the study of Mo has found that using NADPH and PKC inhibitors to down-regulate the expression of TLR2 and TLR4 can improve the continuous inflammation induced by hyperglycemia (Dasu et al., 2008). It is suggested that targeting TLR2 and 4 can reduce the release of inflammatory signals IL-1β and TNF-α, improve the sustained inflammatory state of the wound surface, and also show the effective role of targeting TLR signaling in different effector cells of DW. Besides, PPARγ agonists can also down-regulate the expression of TLR4 (Ji et al., 2009). Using Pioglitazone-loaded fibrous mats which are prepared from pioglitazone hydrochloride (PHR) on the wound of DM rats, it is found that both burst-release and sustained-release kinetics can down-regulate the expression of TNF-α and promote DW healing, but the sustained-release form is more effective in reducing PMNs infiltration and inflammation, promoting epidermal regeneration and fibroblast proliferation (Cam et al., 2020), Similarly, topically using GQ-11 (a partial/dual PPAR α/γ agonist) and Pioglitazone on the wound of DM mice can also down-regulate IL-1β and TNF-α, promote DW healing (Silva et al., 2019). An in-depth understanding of the relationship between TLR signaling pathways and drug regulation targets, as well as the impact of different types of drugs on drug delivery and efficacy, can provide a feasible direction for the treatment of DW. (**Table 3**).

Overactivation of NLR Signaling Under Pathological Conditions Promotes Cascading Amplification of the Inflammatory Response in Diabetic wound

NLR is a critical member of the cytoplasmic PRRs family and plays a unique role in the innate immune response. The NLR protein usually exists in an inactivated state in the cytoplasm, which is in an auto-repressed form. When directly or indirectly combine with DAMPs or PAMPs, a conformational change

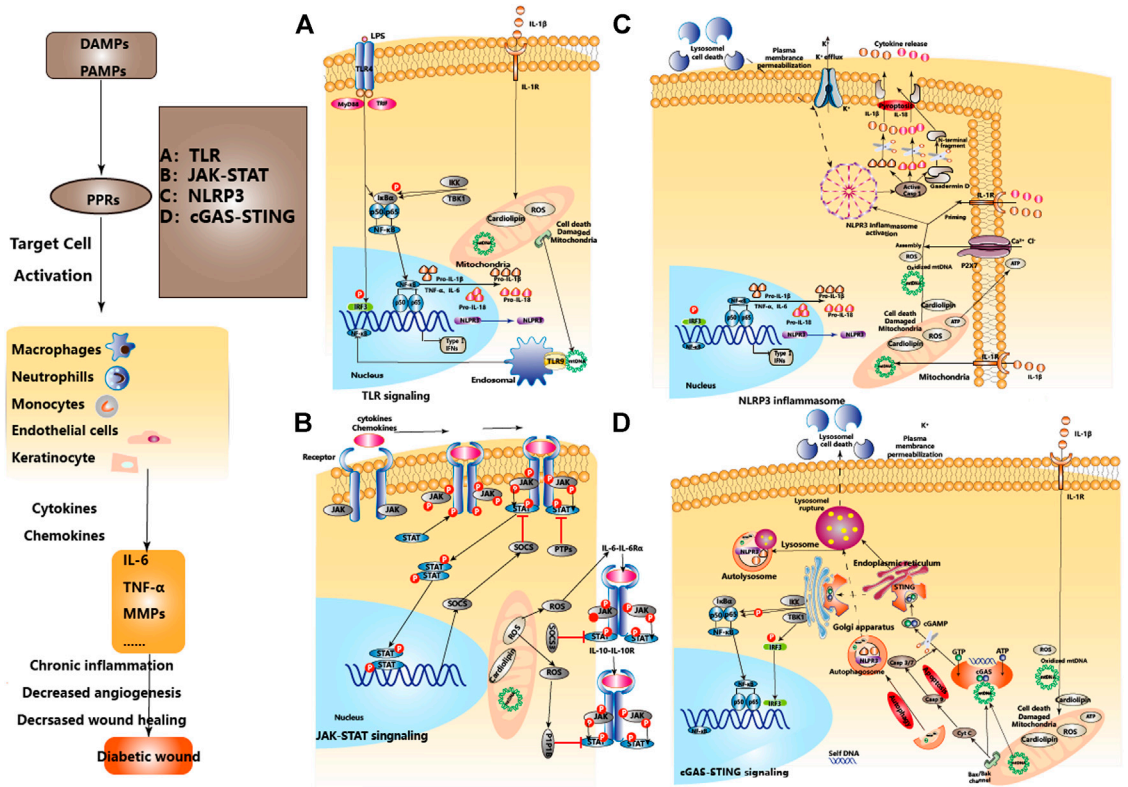

FIGURE 3 | The regulatory relationship between different innate immune pathways in DW and homeostasis. The effects of the regulatory relationship between TLR, JAK-STAT, NLPR3, cGAS-STING signal pathways, and homeostasis in DW. After the formation of DW, PAMPs and DAMPs activate PRRs as initiating factors, inducing the activation of TLR, NLPR3, and cGAS-STING signal pathways, activate the expression of type I interferon and other immunoregulatory molecules. JAK-STAT mediates extracellular-nuclear regulation of various cytokines/chemokines. Mitochondrial damage, endoplasmic reticulum stress, and lysosomal membrane permeabilization are involved in the activation and regulation of signal pathways. Mitochondrial autophagy and apoptosis play an immune silencing role in maintaining immune homeostasis. A, B, C, and D represent four signaling pathways respectively.

occurs and the NACHT domain is exposed, thereby triggering oligomerization and participating in the activation of multiple signal transduction pathways (Sharif et al., 2019). For example, NOD1 and NOD2 activate NF-κB and MAPK signaling pathways by interacting with RIPK2, while NLRP1, NLRP3, and NLRC4 activate inflammasome through multimerization to produce activated caspase-1 (Platnich and Muruve, 2019). After activation of caspase-1, the inactive pro-IL-1β and pro-IL-18 are cleaved into mature IL-1β and IL-18, thus exerting an immune response and pro-inflammatory effects (Wen et al., 2011). Among them, the NLRP3 inflammasome is a multi-protein complex composed of NLRP3, adaptor protein ASC and pro-caspase-1 (Lamkanfi and Dixit, 2012), which participates in the induction of aseptic inflammation (Vandanmagsar et al., 2011; Wen et al., 2011). Under the pathological conditions of stress and inflammatory, caspase-1 released after the activation of NLRP3 inflammasome can also mediate a rapid programmed cell death pattern characterized by accompanying inflammatory response, called "Pyroptosis" (Wu et al., 2018). Pyroptosis induces the release of a large number of pro-inflammatory factors, eventually forming a cascade of amplified inflammatory responses (Jorgensen and Miao, 2015; Wang S. et al., 2019). In the state of DW, ROS and IL-1β can activate the NLRP3 inflammasome in Mp, promote the maturation and secretion of IL-1β, aggravate local inflammation through positive feedback, and hinder wound healing (Lee et al., 2013; Mirza et al., 2014; Dai et al., 2017). Meanwhile, NETs formed from PMNs which are recruited on the wound can also activate NLRP3 inflammasome through TLR-4/TLR-9/NF-κB and ROS/TXNIP signaling pathways (Liu et al., 2019). Therefore, inhibiting the activities of NLRP3 and caspase-1 and reducing the production of inflammatory factors such as IL-1β, IL-18 may play a role in alleviating inflammation and accelerating DW healing (Bitto et al., 2014). (**Figure 3C**).

Therapeutic Targeting of NLR Signaling in Diabetic wound

Currently, researches on NLR mainly focus on NLRP3 inflammasomes and related signaling pathways. Activation of NLRP3 inflammasome requires two steps: Priming and Assembly. Priming mainly targets NF-κB-dependent transcription of NLRP3 and pro-IL-1β(Qiao et al., 2012). Assembly is associated with NLRP3 in mitochondrial relocalization, mitochondrial stress, and cytokines

TABLE 3 | Effects of modulating innate immunity pathways in experimental DW.

Innate immune pathway	Knockout mice models	Intervention (agent)	Mechanism
TLR signaling	$TLR2^{-/-}$	—	TLR2/6-MyD88-NF-κb↓ IL- 1β, TNF-α↓ DW Healing ↑ Dasu et al. (2010)
	$TLR4^{-/-}$	—	TLR4-NF-κb↓ IL-6, TNF-α↓ DW Healing ↑ Dasu and Jialal, (2013)
	$Lepr^{db/db}$	nAChR agonists (nicotine).	TLR2-NF-κb↓ AMP, IL-6↓ DW Healing ↑ Kishibe et al. (2018)
	$TLR3^{-/-}$	REG3A	IL-33, REG3A/ RegIIIγ ↑ TLR3–JNK2 ↓ IL-6, TNF-α↓
	$JNK2^{-/-}$	SHP-1 inhibitor (SSG).	DW Healing ↑ Wu et al. (2016)
	$Mll1^{f/f}Lyz2^{Cre+}$	TLR4 inhibition	MLL1-mediated H3K4me3 ↑ TLR4-MyD88↓
	$TLR4^{-/-}$	(TAK-242).	DW Healing↑Davis et al. (2020)
NLRP3 inflammasome	$Lepr^{db/db}$ Bitto et al. (2014)	HSWang et al. (2018) I-κb kinase-β inhibitor (BAY 11–7,082). Purinergic P2X7 receptor inhibitor (brilliant blue G).	NLRP3 inflammasome-caspase-1-il-1β/il-18 axis↓ IL-1β, IL-18↓ DW Healing ↑ Bitto et al. (2014)
	—	PPARα agonists (Fenofibrate).	ROS/TXNIP-NLRP3 inflammasome-caspase-1-il-1β/il-18 axis↓ DW Healing ↑ Deng et al. (2017)
	—	NLRP3 inhibitor (MCC950). TLR-4 inhibitor (CLI-095). TLR-9 inhibitor (ODN 2088). ROS inhibitor (NAC, dnase I).	TLR-4/TLR-9-NF-κb↓ ROS/TXNIP-NLRP3 inflammasome-caspase-1-il-1β/il-18 axis↓ IL-1β, IL-18↓ DW Healing ↑ Liu et al. (2019)
	$Lepr^{db/db}$	ROS inhibitor (NAC, dnase I). IL-1β blocking antibody (IL-1R1). Glyburide caspase-1 inhibitor (YVAD).	NLRP3 inflammasome-caspase-1-il-1β/il-18 axis↓ IL-1β, IL-18↓ DW Healing ↑ Mirza et al. (2014)
cGAS-STING signaling	$STING^{-/-}$	—	Mitochondrial damage-cGAS-STING-IRF3 ↓ ICAM-1↓ Improve IR, Glucose intolerance Mao et al. (2017)
JAK-STAT signaling	$Lepr^{db/db}$	—	IL-12-Stat4↑ CCL2-CCR2↑ DW Healing ↓ Cunnion et al. (2017)
	—	—	IL-6 -il-6rα-jak-stat3↑ SCOS3, DW Healing ↓ Lee et al. (2019)

Partial abbreviation: TLR: Toll-like receptor, STZ: Streptozotocin, NF-κB: Nuclear factor-κB, IL: Interleukin, TNF-α: Tumor necrosis factor-α, nAChRs: Nicotinic acetylcholine receptors, AMP: Adenosine monophosphate, REG3A: Regenerating islet-derived protein 3A, SHP-1: domain-containing protein-tyrosine phosphatase-1, HS: Heparan sulfate, PPARα: Peroxisome proliferator-activated receptors α, EPC: Endothelial progenitor cells, IGF-1: Insulin-like growth factor-1, TGF-β: Transforming growth factor-β, IR: Insulin resistance.

released into the cytoplasm after injury (mtROS, mtDNA, or cardiolipin), ion channel potassium outflow, sodium/calcium influx, and cathepsin release after lysosomal injury (Lamkanfi and Dixit, 2012; Guo et al., 2015). PPARα agonists (such as Fenofibrate) can reduce the expression of TXNIP, NLRP3, and caspase-1 in endothelial precursor cells (EPC) of DM mice and accelerate wound healing of DM mice (Deng et al., 2017). External use of sulfonylureas (such as Glibenclamide) can inhibit the activation of NLRP3, up-regulate IL-10, IGF-1 and TGF-β, down-regulate IL-1β, IL-18, and TNF-α, and as a result down-regulate the pro-inflammatory M1 phenotype, up-regulate the pro-healing M2 phenotype and promote wound healing in DM mice (Mirza et al., 2014). After blocking the P2X7 receptors of the sodium/calcium influx channel, the activities of NLRP3 and caspase-1 are down-regulated, the production of IL-1β and IL-18 is reduced, and the rate of DW angiogenesis and healing is accelerated (Bitto et al., 2014). Blocking the potassium efflux channel (TWIK2) can also down-regulate NLRP3 activation in Mp (Di et al., 2018). Besides, Metformin inhibits NLRP3 activation through the AMPK/mTOR signaling pathway and promotes M2-type polarization of Mp, and is beneficial to Non-DW healing (Qing et al., 2019). Recent studies have found that phosphorylation of NLRP3 inflammasome at the S194 site is an important initiation event for its activation, and blocking NLRP3 phosphorylation by S194A mutation or JNK1 inhibitor can inhibit NLRP3 inflammasome activation (Song et al., 2017). This suggests that preventive regulation of the aggregation of inflammatory cells from upstream may have a beneficial effect on the prevention and treatment of DW. (**Table 3**).

Targeting Abnormal Activation of cGAS-STING Signaling Under Metabolic Stress Shows the Potential to Promote Diabetic wound Healing

cGAS-STING signaling was initially thought to activate innate immunity by identifying DNA derived from microorganisms such

as viruses or bacteria. However, existing studies have shown that under certain pathological conditions, this signaling pathway can also sense cytoplasmic DNA as a cellular danger signal. Cytoplasmic DNA triggers a STING-dependent inflammatory response and is associated with a variety of severe auto-inflammatory and immune diseases in humans (Ahn et al., 2012), such as Aicardi-Goutières Syndrome (AGS) (Pokatayev et al., 2016), Associated Vasculopathy With Onset in Infancy (SAVI) (Liu et al., 2014), and Systemic Lupus Erythematosus (SLE) (Kato et al., 2018). Besides, abnormal activation of cGAS-STING under mitochondrial dysfunction or metabolic stress can also induce more common diseases, such as obesity (Luo et al., 2018; Bai et al., 2020) and obesity-induced inflammation (Bai et al., 2017), insulin resistance, and glucose intolerance (Mao et al., 2017), Non-Alcoholic Steatohepatitis (NASH) (Yu et al., 2019), Chronic Obstructive Pulmonary disease (COPD) (Qin et al., 2019), Age-related macular degeneration (AMD) (Wu et al., 2019), and Parkinson's disease (PD) (Sliter et al., 2018), etc. These diseases are often characterized by the excessive signal of interferons and/or cytokines associated with cGAS-STING activation (Li et al., 2013).

Acute pancreatitis (AP).is an acute inflammatory disease characterized by extensive necrosis of pancreatic cells. The DNA released after the death of pancreatic acinar cells activates the STING signal in Mp, promotes the expression of downstream TNF-α and IFN-β lead to aggravating the inflammation and pancreatic injury. DMXAA-induced STING activation can further aggravate the symptoms of AP. At the same time, inhibiting the activity of STING through degrading the released DNA from dead acinar cells by dnaselor inactivate the pathway can both down-regulate the expression of TNF-α and IFN-β, improve the progression of acute inflammation (Zhao et al., 2018). Hidradenitis Suppurativa (HS).is a stubborn and relapsed chronic skin inflammatory disease. Affected by the imbalance of intracellular homeostasis and spontaneous DNA damage caused by replication stress, IFI16 relocates from the nucleus to the cytoplasm. It forms a complex with cGAS, prompting keratinocytes to recognize cytoplasmic DNA to activate STING, and prompting replication stress through cGAS/IFI16-STING positive feedback from chronic and persistent inflammation (Orvain and et al., 2020). It suggests that targeting the cGAS-STING pathway can produce beneficial effects on acute and chronic inflammatory diseases. Adipose tissue-specific knockout of Oxidoreductase-like protein (DsbA-L) can lead to impaired mitochondrial function, promote mtDNA release, and activate the cGAS-STING pathway to cause inflammation and insulin resistance (Bai et al., 2017). Inhibiting STING can down-regulate IL-6, IL-1β, MCP-1, TNF-α, IFNα, and IFNβ, reduce cardiac inflammation and fibrosis in mice with myocardial hypertrophy. Compared with Endoplasmic reticulum stress (ES) inhibitor (4-PBA), ES activator (Tg) pretreatment significantly increases the expression of STING and up-regulates TBK1, IRF3, and NF-κB (Zhang P. et al., 2020). It suggests that ES and mitochondrial damage caused by metabolic stress can also activate the cGAS-STING pathway, and targeting the cGAS-STING pathway has therapeutic potential for the treatment of metabolic diseases (Chung et al., 2019). Finally, knockout STING can improve the systemic insulin resistance and glucose intolerance in high-fat fed mice (Mao et al., 2017), and the analysis of Mp found that STING defect also decreased Mp proinflammatory M1 phenotype (Luo et al., 2018). Finally, Palmitic acid (PA) induces the release of mtDNA into the cytoplasm in a lipotoxic manner, activates the cGAS-STING-IRF3 pathway (Mao et al., 2017), On the one hand, up-regulates the expression of ICAM-1and induces endothelial cell inflammation (Mao et al., 2017), on the other hand, mediates the inactivation of Hippo-YAP pathway of endothelial cells and inhibits angiogenesis (Yuan et al., 2017). This suggests the therapeutic prospect of targeting the cGAS-STING signaling pathway in diabetes and related complications such as DW. (**Figure 3D** and **Table 3**).

Targeted Negative Regulation of JAK-STAT Signaling in Diabetic wound Specific Phases May Promote Healing

JAK-STAT signaling includes four JAKs (JAK1, JAK2, JAK3, and Tyk2).and seven STATs (STAT1, STAT2, STAT3, STAT4, STAT5A, STAT5B, AND STAT6). (Wan et al., 2021), and is essential for the maintenance of homeostasis. Elevated IFN-γ and JAK-STAT1 in obese patients induce adipocyte dysfunction and insulin resistance (McGillicuddy et al., 2009). Knockout STAT4 effectively improved adipose tissue inflammation and insulin resistance in high-fat fed mice (Dobrian et al., 2013), and knockdown of Stat3 activity prevent diabetic glomerulopathy inflammation and abnormal matrix synthesis at an early stage (Lu et al., 2009). A significant increase in expression of STAT4 and the downstream Mp chemokine CCL2 and its receptor CCR2 were also found in early DW, which may be related to the release of IL-12 by pro-inflammatory Mp and the continuous activation of IL-12-STAT4 (Cunnion et al., 2017). It is suggested that STAT4 inhibition can improve the inflammatory response in DW and promote healing.

Cytokines (pro-inflammatory and anti-inflammatory)., growth factors, and chemokines in DW can activate the JAK-STAT pathway, however, they trigger different transcriptional programs. Posttranslational modifications of STAT proteins, such as tyrosine phosphorylation, are essential to ensure differential expression of STAT target genes (Dodington et al., 2018). JAK-STAT signaling is inhibited by SH2-containing phosphatase, protein inhibitors against STATs, and suppressor of cytokine signaling suppressor of cytokine signaling (SOCS). (Wormald and Hilton, 2004; Galic et al., 2014), protein tyrosine phosphatases (PTPs).are also important negative regulators of this signaling pathway (Gurzov et al., 2015). A recent study found that there is nearly 2-fold decreased SOCS3 expression in DW, and greater up to 6-fold IL-6 and IL-6Rα protein expression throughout the majority of the wound healing period, leading to a subsequent increase in phosphorylation of STAT3, this suggests that the apparent upregulation of IL-6 and its receptor in the diabetic skin, as well as inhibition of SOCS3, may lead to increased STAT3 activation and ultimately result in dysregulated inflammation in DW (Lee et al., 2019). Furthermore, STAT3 activation by IL-6 was partly attenuated by Mito-Q, a mitochondrial-targeted antioxidant, suggesting that mtROS potentiates STAT3 signaling in response to IL-6 exposure (Abid et al., 2020), and also suggested that targeted oxidative stress and mitochondrial damage could inhibit the activation of

JAK-STAT signals and promote DW healing. IL-6R-mediated gp130 /JAK-STAT3 signal loops are also negatively modulated by SOCS3, SOCS3 is expressed in the epithelium at the edge of the injured wound (Goren et al., 2006; Linke et al., 2010), and SOCS3 overexpressed specifically strongly disturbs DW healing by interfering with keratinocyte proliferation and migration (Linke et al., 2010), However, specific deletion of SOCS3 in keratinocytes delayed healing as well, resulting in the hyperproliferative *epidermis* and prolonged inflammation (Zhu et al., 2008). The research on JAK-STAT regulation immune cells in DW indicated that deregulated immune response in which impaired activation, recruitment and survival of immune cells mediated by downregulation of FOXM1 and STAT3 contribute to the delayed wound healing in DFU (Sawaya et al., 2020). This suggests that we need to further understand the effects of SOCS3 on the positive and/or negative regulation of different effector cells in DW. Furthermore, hyperglycemia up-regulated the expression of PTP1B and inhibited VEGF-induced vascular formation, proliferation, and migration (Zhang et al., 2015), PTP1B activity was significantly elevated in DW, topically applied PTP1B inhibitor may help counterbalance ER stress (Thiebaut et al., 2018) and accelerate DW healing (Zhang et al., 2017; Figueiredo et al., 2020). This may be due to the distinct tissue environments or the competing effects of cytokines that signal through JAK-STAT. IL-6R activates the JAK1/JAK2-STAT3 cascade, IL-10R activates the JAK1/TYK2-STAT3 cascade, also both JAK2 and TYK2 are targets of PTP1B, but PTP1B was not required for inhibition of the proinflammatory receptor IL-6R, PTP1B may be particularly important in regulating IL-10R given that this receptor does not contain a SOCS3-binding site (Pike et al., 2014). In a word, the manipulation of JAK-STAT signaling is a promising therapeutic angle for the treatment of DW. Nonetheless, the pleiotropic biological activities of JAK-STAT signaling imply that targeting therapy to isolated cytokines and/or chemokines at specific stages of the disease might be most beneficial. (**Figure 3B** and **Table 3**).

The Contact Between the Innate Immune Signaling

Just as the factors affecting wound healing are not only single factors, TLR, NLRP3 inflammasome, and cGAS-STING are also associated with DW. First, LPS cannot induce the production of NLRP3 or pro-IL-1β in TLR4 defects or MyD88 and TRIF double-defects cells, and the induced expression of NLRP3 is positively correlated with NF-κB (Bauernfeind et al., 2009). It suggests that the TLR4 pathway and downstream activated NF-κB can regulate the activation of NLRP3, which can regulate the pathologic inflammation associated with NLRP3 inflammasome by targeting TLR. Second, the detection of DNA in the cytoplasm by cGAS-STING triggers lysosomal membrane permeabilization leading to lysosomal cell death (LCD), induces the efflux of potassium, and drives the activation of NLRP3 inflammasome. It suggests that targeting the cGAS-STING-LCD-NLRP3 pathway can improve pathologic inflammation associated with cytoplasmic DNA (Gaidt et al., 2017). Besides, during the activation of typical or atypical inflammasome triggered by inflammatory cell activation, all inflammatory caspases (caspase-1, 4, 5, 11) can cleave cGAS to regulate the cGAS-STING pathway negatively (Wang Y. et al., 2017), and apoptotic caspases (caspase-3, 7) released at the time of apoptosis can also cleave cGAS to prevent unnecessary or excessive immune activation (Ning et al., 2019). It suggests that it is vital to clarify the mechanisms of precise regulation between different innate immune pathways to maintain homeostasis.

Mitochondrial damage or loss of membrane integrity leading to the release or exposure of Mitochondrial components (mtDNA, ROS, cardiolipin) to the cytoplasm, which plays a key regulatory role in the activation of the NLRP3 inflammasome, TLR, cGAS-STING pathway and the formation of NETs. For example, any pathological state that causes mtDNA to leak into the cytoplasm can promote the activation of the cGAS-STING pathway. The appearance of cardiolipin (Iyer et al., 2013; Toksoy et al., 2017), mtDNA, and ROS (Lamkanfi and Dixit, 2012; Guo et al., 2015) in the cytoplasm lead to the activation of the NLRP3 inflammasome. MtDNA activates TLR9 and STING pathways to promote the formation of NETs. These suggest that the pivotal role of mitochondrial homeostasis in innate immune signals, and treatments that promote mitochondrial homeostasis will also accelerate DW healing. (**Figure 3**).

CONCLUSION

Innate immunity is like a double-edged sword. While protecting the body against metabolic stress or injury pressure, there is also a risk of "hurt both enemies and selves". Therefore, regulating it to maintain a balanced state will play a promoting role in the treatment of DW. Just as the spatial and temporal synchronization in the expression of innate immune cells during the healing process of DW, these different innate immune pathways also have complex connections. Multiple different innate immune pathways may regulate the process of DW, or the transduction of different innate immune pathways may vary at different stages of DW healing. At present, there are few studies based on the crosstalk between multiple signal pathways of the same disease, or the roles of different signal pathways in different periods of the same disease. Therefore, further in-depth study of the differences in the temporal and spatial expression of these innate immune signals will also help us to clarify the pathogenic mechanisms of DW and provide evidence for further prevention and treatment. Besides, activating or inhibiting innate immune signal pathways may improve the disease. However, it may also lead to the proliferation and deterioration of tumor cells or immune deficiency and increased susceptibility. Therefore, whether the activation or inhibition of innate immune pathways has more advantages than disadvantages for DW healing is also worth further discussion.

In this review, the relationship between chronic inflammation and continuously innate immune activation in DW was discussed from the perspective of immune-aging. Firstly, the phenotype changes of innate immune cells under the cell senescent

phenotype in DW were identified, such as the feedback loop from delayed activation early and fade delay late of PMNs and oxidative stress aggravate tissue damage, the persistent proinflammatory phenotype of Mp in the metabolic immune microenvironment maintains the release of pro-inflammatory factors. In addition, we discussed several immune-related pathways that trigger inflammation from the perspective of mitochondrial injury and endoplasmic reticulum stress under metabolic stress. Then, make a point that continuous activation of TLR, NLR, and cGAS-STING signals may negatively regulate DW healing. Cytokine and/or chemokine targeting therapy in response to the pleiotropic bioactivity of the JAK-STAT signal. In summary, we provide a series of new potential therapeutic targets for future research on DW.

Positive Effect of Specialized Pro-Resolving Mediators in Promoting the Timely Resolution of Inflammation and Reconstructing the Self-Limiting Mechanism of Inflammation

As a new therapeutic method in many acute and chronic inflammatory diseases, Specialized pro-resolving mediators (SPMs).has become a research hotspot (Fullerton and Gilroy, 2016). Low levels of circulating SPMs in DM patients give this population the potential to be treated with SPMs (Spite et al., 2014; Brennan et al., 2019). SPMs promote PMNs clearance, inflammation regression, and epithelial tissue repair (Quiros and Nusrat, 2019), local injection of Resolvin D1 (RvD1).in DW can correct the phagocytosis functional defects of Mp, clearance of apoptotic PMNs, and promote wound healing (Tang et al., 2013). Further research has found that RvD1 can also alleviate oxidative stress damage, reduce PMNs infiltration, up-regulate M2 phenotype of Mp by reducing the expression of IL-1β and TNF-α, to promote corneal epithelial wound healing in DM mice (Zhang et al., 2018). Subsequent research also pointed to the role of RvD1 in inhibiting the activation of NLRP3 inflammasome. By inhibiting the activation of NLRP3, ASC, caspase-1, and NF-κB to reduce the production of IL-1β and IL-18, propelling RvD1 to be expected an effective means to alleviate the progression of diabetic retinopathy (Yin et al., 2017). Studies on the other members of the SPMs family such as Resolvin D2 (RvD2). also found similar mechanisms (Lopategi et al., 2019). Maresin-1 (MaR1).promotes the differentiation of Mp to M2 phenotype and accelerates the regeneration of damaged tissue (Abdulnour et al., 2014), besides, MaR1 helps maintain normal mitochondrial function, alleviates the damage to mitochondria from oxidative stress by reducing the production of ROS, and avoids the release of mtDNA (Gu et al., 2018). Recently, the discovery of MAR1-specific binding receptors RORα(Han et al., 2019)and LGR6 (Chiang et al., 2019)also opened a new direction for the research of MAR1 (Im, 2020). A clinical correlation study also found that decreased plasma Mar1 concentration is associated with DFU (Miao et al., 2020), which further suggests that MAR1 may have a therapeutic effect in DW, but the deeper mechanism and the regulation of innate immune pathways need further study.

Regulating Oxidative Stress and Protecting Mitochondrial Homeostasis

Resveratrol and synthetic sirtuin activators (Maiese, 2015) have a well-established diminished oxidative stress action, may contribute to the conferring effect of reducing chronic low-grade inflammation and promote DW healing, and further studies will develop new therapeutic strategies for DW (Zhang Y. et al., 2020).

Improve Autophagy Pathway Defects

Endoplasmic reticulum stress-induced autophagy deficiency is associated with chronic inflammation observed in patients with diabetes (Wang et al., 2013), AURKA via Targeting FOXO3a enhanced autophagy of Adipose-Derived Stem Cells (ADSC).promote DW healing (Yin et al., 2020). Exosomes from ADSC can also induce miR-128-3p/SIRT1-mediated autophagy to promote DW healing (Shi et al., 2020). Given the protective role of autophagy in the inhibition of apoptosis and the overactivation of NLPR3 and cGAS-STING, targeted autophagy will also become an effective means in DW healing.

Suppression of Ferroptosis

Targeting Ferroptosis in immune cells and immunotherapy has shown significant effects (Wang W. et al., 2019). Recent studies have shown that iron overload can induce Ferroptosis in Mp (Wang Q. et al., 2017), GPX4 is a key protein in inhibiting Ferroptosis, and RSL3, as an inhibitor of GPX4, can induce Ferroptosis in M2 Mp (Kapralov et al., 2020). Some Ferroptosis-related metal transporters such as ZIP14 (SLC39A14).may also play a regulatory role in the immune system (Yu et al., 2020). Therefore, elucidating the molecular mechanism of Ferroptosis in immune cells will contribute to the development of new therapeutic strategies for DW, which is a promising research direction.

In a word, it is foreseeable that with the strategy of "promoting the timely regression of inflammation and reconstructing the self-limiting mechanism of inflammation", by reprogramming immune cells rather than inhibiting the inflammatory response, finding the spatial and temporal synchronization in innate immune response and inflammatory response during the process of DW healing, will be a promising area of research with the potential to identify novel therapeutic strategies.

AUTHOR CONTRIBUTIONS

YX provided the scope of the research, conceived the manuscript structure. KG and XM oversaw the writing of the manuscript and drafted the final version of the manuscript; YX conducted the literature review and wrote the first draft of the manuscript; ZJ, HW, CG, YP and LL revised the manuscript for important intellectual content.

FUNDING

The work was supported by grants from the National Natural Science Foundation of China (NO. 81970676), Science and

Technology Development Fund of Macau (File No. 0055/2019/AMJ), Sichuan Science and Technology Program (NOs. 2019YFS0537, 2020YFS0456) and Luzhou-Southwest Medical University cooperation project (2018LZXNYD-ZK11).

REFERENCES

Abdulnour, R.-E. E., Dalli, J., Colby, J. K., Krishnamoorthy, N., Timmons, J. Y., Tan, S. H., et al. (2014). Maresin 1 biosynthesis during platelet-neutrophil interactions is organ-protective. *Proc. Natl. Acad. Sci. USA* 111 (46), 16526–16531. doi:10.1073/pnas.1407123111

Abid, H., Ryan, Z. C., Delmotte, P., Sieck, G. C., and Lanza, I. R. (2020). Extramyocellular interleukin-6 influences skeletal muscle mitochondrial physiology through canonical JAK/STAT signaling pathways. *FASEB j.* 34 (11), 14458–14472. doi:10.1096/fj.202000965rr

Acosta, J. B., Garcia del Barco, D., Cibrian Vera, D., Savigne, W., Lopez-Saura, P., Guillen Nieto, G., et al. (2008). The pro-inflammatory environment in recalcitrant diabetic foot wounds. *Int. Wound J.* 5 (4), 530–539. doi:10.1111/j.1742-481x.2008.00457.x

Ahn, J., Gutman, D., Saijo, S., and Barber, G. N. (2012). STING manifests self DNA-dependent inflammatory disease. *Proc. Natl. Acad. Sci.* 109 (47), 19386–19391. doi:10.1073/pnas.1215006109

Akita, S. (2019). Wound repair and regeneration: mechanisms, signaling. *Int. J. Mol. Sci.* 20 (24). doi:10.3390/ijms20246328

Albina, J. E., Mills, C. D., Henry, W. L., and Caldwell, M. D. (1990). Temporal expression of different pathways of 1-arginine metabolism in healing wounds. *J. Immunol.* 144 (10), 3877–3880.

Auffray, C., Fogg, D., Garfa, M., Elain, G., Join-Lambert, O., Kayal, S., et al. (2007). Monitoring of blood vessels and tissues by a population of monocytes with patrolling behavior. *Science* 317 (5838), 666–670. doi:10.1126/science.1142883

Bai, J., Cervantes, C., He, S., He, J., Plasko, G. R., Wen, J., et al. (2020). Mitochondrial stress-activated cGAS-STING pathway inhibits thermogenic program and contributes to overnutrition-induced obesity in mice. *Commun. Biol.* 3 (1), 257. doi:10.1038/s42003-020-0986-1

Bai, J., Cervantes, C., Liu, J., He, S., Zhou, H., Zhang, B., et al. (2017). DsbA-L prevents obesity-induced inflammation and insulin resistance by suppressing the mtDNA release-activated cGAS-cGAMP-STING pathway. *Proc. Natl. Acad. Sci. USA* 114 (46), 12196–12201. doi:10.1073/pnas.1708744114

Bainbridge, P. (2013). Wound healing and the role of fibroblasts. *J. Wound Care* 22 (8), 407–412. doi:10.12968/jowc.2013.22.8.407

Bando, T., Yokoyama, H., and Nakamura, H. (2018). Wound repair, remodeling, and regeneration. *Develop. Growth Differ.* 60 (6), 303–305. doi:10.1111/dgd.12566

Barman, P. K., Urao, N., and Koh, T. J. (2019). Diabetes induces myeloid bias in bone marrow progenitors associated with enhanced wound macrophage accumulation and impaired healing. *J. Pathol.* 249 (4), 435–446. doi:10.1002/path.5330

Bauernfeind, F. G., Horvath, G., Stutz, A., Alnemri, E. S., MacDonald, K., Speert, D., et al. (2009). Cutting edge: NF-κB activating pattern recognition and cytokine receptors license NLRP3 inflammasome activation by regulating NLRP3 expression. *J. Immunol.* 183 (2), 787–791. doi:10.4049/jimmunol.0901363

Berlanga-Acosta, J. A., Guillén-Nieto, G. E., Rodríguez-Rodríguez, N., Mendoza-Mari, Y., Bringas-Vega, M. L., Berlanga-Saez, J. O., et al. (2020). Cellular senescence as the pathogenic hub of diabetes-related wound chronicity. *Front. Endocrinol. (Lausanne)*11, 573032. doi:10.3389/fendo.2020.573032

Bitto, A., Altavilla, D., Pizzino, G., Irrera, N., Pallio, G., Colonna, M. R., et al. (2014). Inhibition of inflammasome activation improves the impaired pattern of healing in genetically diabetic mice. *Br. J. Pharmacol.* 171 (9), 2300–2307. doi:10.1111/bph.12557

Boniakowski, A. E., Kimball, A. S., Jacobs, B. N., Kunkel, S. L., and Gallagher, K. A. (2017). Macrophage-mediated inflammation in normal and diabetic wound healing. *J.I.* 199 (1), 17–24. doi:10.4049/jimmunol.1700223

Brancato, S. K., and Albina, J. E. (2011). Wound macrophages as key regulators of repair. *Am. J. Pathol.* 178 (1), 19–25. doi:10.1016/j.ajpath.2010.08.003

Brennan, E. P., Mohan, M., Andrews, D., Bose, M., and Kantharidis, P. (2019). Specialized pro-resolving mediators in diabetes: novel therapeutic strategies. *Clin. Sci. (Lond)*133 (21), 2121–2141. doi:10.1042/cs20190067

Cairo, G., Recalcati, S., Mantovani, A., and Locati, M. (2011). Iron trafficking and metabolism in macrophages: contribution to the polarized phenotype. *Trends Immunol.* 32 (6), 241–247. doi:10.1016/j.it.2011.03.007

Cam, M. E., Yildiz, S., Alenezi, H., Cesur, S., Ozcan, G. S., Erdemir, G., et al. (2020). Evaluation of burst release and sustained release of pioglitazone-loaded fibrous mats on diabetic wound healing: an *in vitro* and *in vivo* comparison study. *J. R. Soc. Interf.* 17 (162), 20190712. doi:10.1098/rsif.2019.0712

Carlin, L. M., Stamatiades, E. G., Auffray, C., Hanna, R. N., Glover, L., Vizcay-Barrena, G., et al. (2013). Nr4a1-Dependent Ly6Clow monocytes monitor endothelial cells and orchestrate their disposal. *Cell* 153 (2), 362–375. doi:10.1016/j.cell.2013.03.010

Chen, L., Guo, S., Ranzer, M. J., and DiPietro, L. A. (2013). Toll-like receptor 4 has an essential role in early skin wound healing. *J. Invest. Dermatol.* 133 (1), 258–267. doi:10.1038/jid.2012.267

Chen, X., Liu, Y., and Zhang, X. (2012). Topical insulin application improves healing by regulating the wound inflammatory response. *Wound Repair Regen.* 20 (3), 425–434. doi:10.1111/j.1524-475x.2012.00792.x

Cheng, T.-L., Lai, C.-H., Chen, P.-K., Cho, C.-F., Hsu, Y.-Y., Wang, K.-C., et al. (2015). Thrombomodulin promotes diabetic wound healing by regulating toll-like receptor 4 expression. *J. Invest. Dermatol.* 135 (6), 1668–1675. doi:10.1038/jid.2015.32

Chiang, N., Libreros, S., Norris, P. C., de la Rosa, X., and Serhan, C. N. (2019). Maresin 1 activates LGR6 receptor promoting phagocyte immunoresolvent functions. *J. Clin. Invest.* 129 (12), 5294–5311. doi:10.1172/jci129448

Cho, N. H., Shaw, J. E., Karuranga, S., Huang, Y., da Rocha Fernandes, J. D., Ohlrogge, A. W., et al. (2018). IDF Diabetes Atlas: global estimates of diabetes prevalence for 2017 and projections for 2045. *Diabetes Res. Clin. Pract.* 138, 271–281. doi:10.1016/j.diabres.2018.02.023

Chorro, L., Sarde, A., Li, M., Woollard, K. J., Chambon, P., Malissen, B., et al. (2009). Langerhans cell (LC) proliferation mediates neonatal development, homeostasis, and inflammation-associated expansion of the epidermal LC network. *J. Exp. Med.* 206 (13), 3089–3100. doi:10.1084/jem.20091586

Chung, K. W., Dhillon, P., Huang, S., Sheng, X., Shrestha, R., Qiu, C., et al. (2019). Mitochondrial damage and activation of the STING pathway lead to renal inflammation and fibrosis. *Cel Metab.* 30 (4), 784–799. doi:10.1016/j.cmet.2019.08.003

Criscitelli, T. (2018). The future of wound care. *AORN J.* 107 (4), 427–429. doi:10.1002/aorn.12118

Cunnion, K. M., Krishna, N. K., Pallera, H. K., Pineros-Fernandez, A., Rivera, M. G., Hair, P. S., et al. (2017). Complement activation and STAT4 expression are associated with early inflammation in diabetic wounds. *PLoS One* 12 (1), e0170500. doi:10.1371/journal.pone.0170500

Dai, J., Zhang, X., Li, L., Chen, H., and Chai, Y. (2017). Autophagy inhibition contributes to ROS-producing NLRP3-dependent inflammasome activation and cytokine secretion in high glucose-induced macrophages. *Cell Physiol Biochem* 43 (1), 247–256. doi:10.1159/000480367

Dal-Secco, D., Wang, J., Zeng, Z., Kolaczkowska, E., Wong, C. H. Y., Petri, B., et al. (2015). A dynamic spectrum of monocytes arising from the *in situ* reprogramming of CCR2+ monocytes at a site of sterile injury. *J. Exp. Med.* 212 (4), 447–456. doi:10.1084/jem.20141539

Daley, J. M., Brancato, S. K., Thomay, A. A., Reichner, J. S., and Albina, J. E. (2010). The phenotype of murine wound macrophages. *J. Leukoc. Biol.* 87 (1), 59–67. doi:10.1189/jlb.0409236

Daley, J. M., Reichner, J. S., Mahoney, E. J., Manfield, L., Henry, W. L., Mastrofrancesco, B., et al. (2005). Modulation of macrophage phenotype by soluble product(s) released from neutrophils. *J. Immunol.* 174 (4), 2265–2272. doi:10.4049/jimmunol.174.4.2265

Das, A., Sinha, M., Datta, S., Abas, M., Chaffee, S., Sen, C. K., et al. (2015). Monocyte and macrophage plasticity in tissue repair and regeneration. *Am. J. Pathol.* 185 (10), 2596–2606. doi:10.1016/j.ajpath.2015.06.001

Dasu, M. R., Devaraj, S., Zhao, L., Hwang, D. H., and Jialal, I. (2008). High glucose induces toll-like receptor expression in human monocytes: mechanism of activation. *Diabetes* 57 (11), 3090–3098. doi:10.2337/db08-0564

Dasu, M. R., and Jialal, I. (2013). Amelioration in wound healing in diabetic toll-like receptor-4 knockout mice. *J. Diabetes its Complications* 27 (5), 417–421. doi:10.1016/j.jdiacomp.2013.05.002

Dasu, M. R., and Martin, S. J. (2014). Toll-like receptor expression and signaling in human diabetic wounds. *Wjd* 5 (2), 219–223. doi:10.4239/wjd.v5.i2.219

Dasu, M. R., and Rivkah Isseroff, R. (2012). Toll-like receptors in wound healing: location, accessibility, and timing. *J. Invest. Dermatol.* 132 (8), 1955–1958. doi:10.1038/jid.2012.208

Dasu, M. R., Thangappan, R. K., Bourgette, A., DiPietro, L. A., Isseroff, R., and Jialal, I. (2010). TLR2 expression and signaling-dependent inflammation impair wound healing in diabetic mice. *Lab. Invest.* 90 (11), 1628–1636. doi:10.1038/labinvest.2010.158

Davies, L. C., Rosas, M., Smith, P. J., Fraser, D. J., Jones, S. A., and Taylor, P. R. (2011). A quantifiable proliferative burst of tissue macrophages restores homeostatic macrophage populations after acute inflammation. *Eur. J. Immunol.* 41 (8), 2155–2164. doi:10.1002/eji.201141817

Davis, F. M., denDekker, A., Kimball, A., Joshi, A. D., El Azzouny, M., Wolf, S. J., et al. (2020). Epigenetic regulation of TLR4 in diabetic macrophages modulates immunometabolism and wound repair. *J.I.* 204 (9), 2503–2513. doi:10.4049/jimmunol.1901263

Demaria, M., Ohtani, N., Youssef, S. A., Rodier, F., Toussaint, W., Mitchell, J. R., et al. (2014). An essential role for senescent cells in optimal wound healing through secretion of PDGF-AA. *Dev. Cel* 31 (6), 722–733. doi:10.1016/j.devcel.2014.11.012

Deng, Y., Han, X., Yao, Z., Sun, Y., Yu, J., Cai, J., et al. (2017). PPARα agonist stimulated angiogenesis by improving endothelial precursor cell function via a NLRP3 inflammasome pathway. *Cel Physiol Biochem* 42 (6), 2255–2266. doi:10.1159/000479999

Dhamodharan, U., Teena, R., Vimal Kumar, R., Changam, S. S., Ramkumar, K. M., and Rajesh, K. (2019). Circulatory levels of B-cell activating factor of the TNF family in patients with diabetic foot ulcer: association with disease progression. *Wound Rep. Reg.* 27 (5), 442–449. doi:10.1111/wrr.12720

Di, A., Xiong, S., Ye, Z., Malireddi, R. K. S., Kometani, S., Zhong, M., et al. (2018). The TWIK2 potassium efflux c hannel in macrophages mediates NLRP3 inflammasome-induced inflammation. *Immunity* 49 (1), 56–65. doi:10.1016/j.immuni.2018.04.032

Dobrian, A. D., Galkina, E. V., Ma, Q., Hatcher, M., Aye, S. M., Butcher, M. J., et al. (2013). STAT4 deficiency reduces obesity-induced insulin resistance and adipose tissue inflammation. *Diabetes* 62 (12), 4109–4121. doi:10.2337/db12-1275

Dodington, D. W., Desai, H. R., and Woo, M. (2018). JAK/STAT - emerging players in metabolism. *Trends Endocrinol. Metab.* 29 (1), 55–65. doi:10.1016/j.tem.2017.11.001

Egozi, E. I., Ferreira, A. M., Burns, A. L., Gamelli, R. L., and Dipietro, L. A. (2003). Mast cells modulate the inflammatory but not the proliferative response in healing wounds. *Wound Repair Regen.* 11 (1), 46–54. doi:10.1046/j.1524-475x.2003.11108.x

Fadini, G. P., Menegazzo, L., Rigato, M., Scattolini, V., Poncina, N., Bruttocao, A., et al. (2016). NETosis delays diabetic wound healing in mice and humans. *Diabetes* 65 (4), 1061–1071. doi:10.2337/db15-0863

Figueiredo, A., Leal, E. C., and Carvalho, E. (2020). Protein tyrosine phosphatase 1B inhibition as a potential therapeutic target for chronic wounds in diabetes. *Pharmacol. Res.* 159, 104977. doi:10.1016/j.phrs.2020.104977

Fox, S., Leitch, A. E., Duffin, R., Haslett, C., and Rossi, A. G. (2010). Neutrophil apoptosis: relevance to the innate immune response and inflammatory disease. *J. Innate Immun.* 2 (3), 216–227. doi:10.1159/000284367

Fullerton, J. N., and Gilroy, D. W. (2016). Resolution of inflammation: a new therapeutic Frontier. *Nat. Rev. Drug Discov.* 15 (8), 551–567. doi:10.1038/nrd.2016.39

Fulop, T., Larbi, A., Dupuis, G., Le Page, A., Frost, E. H., Cohen, A. A., et al. (2017). Immunosenescence and inflamm-aging as two sides of the same coin: friends or foes? *Front. Immunol.* 8, 1960. doi:10.3389/fimmu.2017.01960

Gaidt, M. M., Ebert, T. S., Chauhan, D., Ramshorn, K., Pinci, F., Zuber, S., et al. (2017). The DNA inflammasome in human myeloid cells is initiated by a STING-cell death program upstream of NLRP3. *Cell* 171 (5), 1110–1124. doi:10.1016/j.cell.2017.09.039

Galic, S., Sachithanandan, N., Kay, T. W., and Steinberg, G. R. (2014). Suppressor of cytokine signalling (SOCS) proteins as guardians of inflammatory responses critical for regulating insulin sensitivity. *Biochem. J.* 461 (2), 177–188. doi:10.1042/bj20140143

Gallagher, K. A., Joshi, A., Carson, W. F., Schaller, M., Allen, R., Mukerjee, S., et al. (2015). Epigenetic changes in bone marrow progenitor cells influence the inflammatory phenotype and alter wound healing in type 2 diabetes. *Diabetes* 64 (4), 1420–1430. doi:10.2337/db14-0872

Galstyan, K. O., Nedosugova, L. V., Martirosian, N. S., Nikiforov, N. G., Elizova, N. V., Kolmychkova, K. I., et al. (2019). Modification of tumor necrosis factor-alpha and C-C motif chemokine ligand 18 secretion by monocytes derived from patients with diabetic foot syndrome. *Biology (Basel)*9 (1). doi:10.3390/biology9010003

Ganesh, G. V., and Ramkumar, K. M. (2020). Macrophage mediation in normal and diabetic wound healing responses. *Inflamm. Res.* 69 (4), 347–363. doi:10.1007/s00011-020-01328-y

González-de-Olano, D., and Álvarez-Twose, I. (2018). Mast cells as key players in allergy and inflammation. *J. Investig. Allergol. Clin. Immunol.* 28 (6), 365–378. doi:10.18176/jiaci.0327

Goren, I., Linke, A., Müller, E., Pfeilschifter, J., and Frank, S. (2006). The suppressor of cytokine signaling-3 is upregulated in impaired skin repair: implications for keratinocyte proliferation. *J. Invest. Dermatol.* 126 (2), 477–485. doi:10.1038/sj.jid.5700063

Gu, J., Luo, L., Wang, Q., Yan, S., Lin, J., Li, D., et al. (2018). Maresin 1 attenuates mitochondrial dysfunction through the ALX/cAMP/ROS pathway in the cecal ligation and puncture mouse model and sepsis patients. *Lab. Invest.* 98 (6), 715–733. doi:10.1038/s41374-018-0031-x

Guo, H., Callaway, J. B., and Ting, J. P.-Y. (2015). Inflammasomes: mechanism of action, role in disease, and therapeutics. *Nat. Med.* 21 (7), 677–687. doi:10.1038/nm.3893

Gupta, M., Chaturvedi, R., and Jain, A. (2013). Role of monocyte chemoattractant protein-1 (MCP-1) as an immune-diagnostic biomarker in the pathogenesis of chronic periodontal disease. *Cytokine* 61 (3), 892–897. doi:10.1016/j.cyto.2012.12.012

Gurtner, G. C., Werner, S., Barrandon, Y., and Longaker, M. T. (2008). Wound repair and regeneration. *Nature* 453 (7193), 314–321. doi:10.1038/nature07039

Gurzov, E. N., Stanley, W. J., Brodnicki, T. C., and Thomas, H. E. (2015). Protein tyrosine phosphatases: molecular switches in metabolism and diabetes. *Trends Endocrinol. Metab.* 26 (1), 30–39. doi:10.1016/j.tem.2014.10.004

Han, Y.-H., Shin, K.-O., Kim, J.-Y., Khadka, D. B., Kim, H.-J., Lee, Y.-M., et al. (2019). A maresin 1/RORα/12-lipoxygenase autoregulatory circuit prevents inflammation and progression of nonalcoholic steatohepatitis. *J. Clin. Invest.* 129, 1684–1698. doi:10.1172/jci124219

Hashimoto, D., Chow, A., Noizat, C., Teo, P., Beasley, M. B., Leboeuf, M., et al. (2013). Tissue-resident macrophages self-maintain locally throughout adult life with minimal contribution from circulating monocytes. *Immunity* 38 (4), 792–804. doi:10.1016/j.immuni.2013.04.004

Hesketh, M., Sahin, K. B., West, Z. E., and Murray, R. Z. (2017). Macrophage phenotypes regulate scar formation and chronic wound healing. *Int. J. Mol. Sci.* 18 (7). doi:10.3390/ijms18071545

Hoeffel, G., Wang, Y., Greter, M., See, P., Teo, P., Malleret, B., et al. (2012). Adult Langerhans cells derive predominantly from embryonic fetal liver monocytes with a minor contribution of yolk sac-derived macrophages. *J. Exp. Med.* 209 (6), 1167–1181. doi:10.1084/jem.20120340

Huebener, P., and Schwabe, R. F. (2013). Regulation of wound healing and organ fibrosis by toll-like receptors. *Biochim. Biophys. Acta (Bba) - Mol. Basis Dis.* 1832 (7), 1005–1017. doi:10.1016/j.bbadis.2012.11.017

Im, D.-S. (2020). Maresin-1 resolution with RORα and LGR6. *Prog. Lipid Res.* 78, 101034. doi:10.1016/j.plipres.2020.101034

Ishida, Y., Gao, J.-L., and Murphy, P. M. (2008). Chemokine receptor CX3CR1 mediates skin wound healing by promoting macrophage and fibroblast accumulation and function. *J. Immunol.* 180 (1), 569–579. doi:10.4049/jimmunol.180.1.569

Italiani, P., and Boraschi, D. (2014). From monocytes to M1/M2 macrophages: phenotypical vs. Functional differentiation. *Front. Immunol.* 5, 514. doi:10.3389/fimmu.2014.00514

Iyer, S. S., He, Q., Janczy, J. R., Elliott, E. I., Zhong, Z., Olivier, A. K., et al. (2013). Mitochondrial cardiolipin is required for Nlrp3 inflammasome activation. *Immunity* 39 (2), 311–323. doi:10.1016/j.immuni.2013.08.001

Jakubzick, C., Gautier, E. L., Gibbings, S. L., Sojka, D. K., Schlitzer, A., Johnson, T. E., et al. (2013). Minimal differentiation of classical monocytes as they survey steady-state tissues and transport antigen to lymph nodes. *Immunity* 39 (3), 599–610. doi:10.1016/j.immuni.2013.08.007

Ji, Y., Liu, J., Wang, Z., Liu, N., and Gou, W. (2009). PPARγ agonist, rosiglitazone, regulates angiotensin II-induced vascular inflammation through the TLR4-dependent signaling pathway. *Lab. Invest.* 89 (8), 887–902. doi:10.1038/labinvest.2009.45

Jorgensen, I., and Miao, E. A. (2015). Pyroptotic cell death defends against intracellular pathogens. *Immunol. Rev.* 265 (1), 130–142. doi:10.1111/imr.12287

Kapralov, A. A., Yang, Q., Dar, H. H., Tyurina, Y. Y., Anthonymuthu, T. S., Kim, R., et al. (2020). Redox lipid reprogramming commands susceptibility of macrophages and microglia to ferroptotic death. *Nat. Chem. Biol.* 16 (3), 278–290. doi:10.1038/s41589-019-0462-8

Kato, Y., Park, J., Takamatsu, H., Konaka, H., Aoki, W., Aburaya, S., et al. (2018). Apoptosis-derived membrane vesicles drive the cGAS-STING pathway and enhance type I IFN production in systemic lupus erythematosus. *Ann. Rheum. Dis.* 77 (10), 1507–1515. doi:10.1136/annrheumdis-2018-212988

Kawai, T., and Akira, S. (2007). TLR signaling. *Semin. Immunol.* 19 (1), 24–32. doi:10.1016/j.smim.2006.12.004

Kim, M.-H., Liu, W., Borjesson, D. L., Curry, F.-R. E., Miller, L. S., Cheung, A. L., et al. (2008). Dynamics of neutrophil infiltration during cutaneous wound healing and infection using fluorescence imaging. *J. Invest. Dermatol.* 128 (7), 1812–1820. doi:10.1038/sj.jid.5701223

Kim, S. Y., and Nair, M. G. (2019). Macrophages in wound healing: activation and plasticity. *Immunol. Cel Biol* 97 (3), 258–267. doi:10.1111/imcb.12236

Kimball, A., Schaller, M., Joshi, A., Davis, F. M., denDekker, A., Boniakowski, A., et al. (2018). Ly6CHiBlood monocyte/macrophage drive chronic inflammation and impair wound healing in diabetes mellitus. *Arterioscler Thromb. Vasc. Biol.* 38 (5), 1102–1114. doi:10.1161/atvbaha.118.310703

Kimball, A. S., Davis, F. M., denDekker, A., Joshi, A. D., Schaller, M. A., Bermick, J., et al. (2019). The histone methyltransferase Setdb2 modulates macrophage phenotype and uric acid production in diabetic wound repair. *Immunity* 51 (2), 258–271. doi:10.1016/j.immuni.2019.06.015

Kishibe, M., Griffin, T. M., Goslawski, M., Sinacore, J., Kristian, S. A., and Radek, K. A. (2018). Topical nicotinic receptor activation improves wound bacterial infection outcomes and TLR2-mediated inflammation in diabetic mouse wounds. *Wound Rep. Reg.* 26 (6), 403–412. doi:10.1111/wrr.12674

Koh, T. J., Novak, M. L., and Mirza, R. E. (2013). Assessing macrophage phenotype during tissue repair. *Methods Mol. Biol.* 1037, 507–518. doi:10.1007/978-1-62703-505-7_30

Krzyszczyk, P., Schloss, R., Palmer, A., and Berthiaume, F. (2018). The role of macrophages in acute and chronic wound healing and interventions to promote pro-wound healing phenotypes. *Front. Physiol.* 9, 419. doi:10.3389/fphys.2018.00419

Lamkanfi, M., and Dixit, V. M. (2012). Inflammasomes and their roles in health and disease. *Annu. Rev. Cel Dev. Biol.* 28, 137–161. doi:10.1146/annurev-cellbio-101011-155745

Lan, C.-C. E., Wu, C.-S., Huang, S.-M., Wu, I.-H., and Chen, G.-S. (2013). High-glucose environment enhanced oxidative stress and increased interleukin-8 secretion from keratinocytes: new insights into impaired diabetic wound healing. *Diabetes* 62 (7), 2530–2538. doi:10.2337/db12-1714

Lauvau, G., Loke, P. n., and Hohl, T. M. (2015). Monocyte-mediated defense against bacteria, fungi, and parasites. *Semin. Immunol.* 27 (6), 397–409. doi:10.1016/j.smim.2016.03.014

Lech, M., Gröbmayr, R., Weidenbusch, M., and Anders, H. J. (2012). Tissues use resident dendritic cells and macrophages to maintain homeostasis and to regain homeostasis upon tissue injury: the immunoregulatory role of changing tissue environments. *Mediators Inflamm.* 2012, 951390. doi:10.1155/2012/951390

Lee, E. G., Luckett-Chastain, L. R., Calhoun, K. N., Frempah, B., Bastian, A., and Gallucci, R. M. (2019). Interleukin 6 function in the skin and isolated keratinocytes is modulated by hyperglycemia. *J. Immunol. Res.* 2019, 5087847. doi:10.1155/2019/5087847

Lee, H.-M., Kim, J.-J., Kim, H. J., Shong, M., Ku, B. J., and Jo, E.-K. (2013). Upregulated NLRP3 inflammasome activation in patients with type 2 diabetes. *Diabetes* 62 (1), 194–204. doi:10.2337/db12-0420

Li, X., Shu, C., Yi, G., Chaton, C. T., Shelton, C. L., Diao, J., et al. (2013). Cyclic GMP-AMP synthase is activated by double-stranded DNA-induced oligomerization. *Immunity* 39 (6), 1019–1031. doi:10.1016/j.immuni.2013.10.019

Linke, A., Goren, I., Bösl, M. R., Pfeilschifter, J., and Frank, S. (2010). The suppressor of cytokine signaling (SOCS)-3 determines keratinocyte proliferative and migratory potential during skin repair. *J. Invest. Dermatol.* 130 (3), 876–885. doi:10.1038/jid.2009.344

Liu, D., Yang, P., Gao, M., Yu, T., Shi, Y., Zhang, M., et al. (2019). NLRP3 activation induced by neutrophil extracellular traps sustains inflammatory response in the diabetic wound. *Clin. Sci. (Lond)*133 (4), 565–582. doi:10.1042/cs20180600

Liu, J., Divoux, A., Sun, J., Zhang, J., Clément, K., Glickman, J. N., et al. (2009). Genetic deficiency and pharmacological stabilization of mast cells reduce diet-induced obesity and diabetes in mice. *Nat. Med.* 15 (8), 940–945. doi:10.1038/nm.1994

Liu, J., Huang, K., Cai, G.-Y., Chen, X.-M., Yang, J.-R., Lin, L.-R., et al. (2014). Receptor for advanced glycation end-products promotes premature senescence of proximal tubular epithelial cells via activation of endoplasmic reticulum stress-dependent p21 signaling. *Cell Signal.* 26 (1), 110–121. doi:10.1016/j.cellsig.2013.10.002

Liu, Y., Jesus, A. A., Marrero, B., Yang, D., Ramsey, S. E., Montealegre Sanchez, G. A., et al. (2014). Activated STING in a vascular and pulmonary syndrome. *N. Engl. J. Med.* 371 (6), 507–518. doi:10.1056/nejmoa1312625

Longo, M., Bellastella, G., Maiorino, M. I., Meier, J. J., Esposito, K., and Giugliano, D. (2019). Diabetes and aging: from treatment goals to pharmacologic therapy. *Front. Endocrinol. (Lausanne)*10, 45. doi:10.3389/fendo.2019.00045

Lopategi, A., Flores-Costa, R., Rius, B., López-Vicario, C., Alcaraz-Quiles, J., Titos, E., et al. (2019). Frontline Science: specialized proresolving lipid mediators inhibit the priming and activation of the macrophage NLRP3 inflammasome. *J. Leukoc. Biol.* 105 (1), 25–36. doi:10.1002/jlb.3hi0517-206rr

Lu, H., Wu, X., Wang, Z., Li, L., Chen, W., Yang, M., et al. (2016). Erythropoietin-activated mesenchymal stem cells promote healing ulcers by improving microenvironment. *J. Surg. Res.* 205 (2), 464–473. doi:10.1016/j.jss.2016.06.086

Lu, T.-C., Wang, Z.-H., Feng, X., Chuang, P. Y., Fang, W., Shen, Y., et al. (2009). Knockdown of Stat3 activity *in vivo* prevents diabetic glomerulopathy. *Kidney Int.* 76 (1), 63–71. doi:10.1038/ki.2009.98

Luo, X., Li, H., Ma, L., Zhou, J., Guo, X., Woo, S.-L., et al. (2018). Expression of STING is increased in liver tissues from patients with NAFLD and promotes macrophage-mediated hepatic inflammation and fibrosis in mice. *Gastroenterol.* 155 (6), 1971–1984. doi:10.1053/j.gastro.2018.09.010

Maiese, K. (2015). New insights for oxidative stress and diabetes mellitus. *Oxid Med. Cel Longev* 2015, 875961. doi:10.1155/2015/875961

Mantovani, A., Sica, A., Sozzani, S., Allavena, P., Vecchi, A., and Locati, M. (2004). The chemokine system in diverse forms of macrophage activation and polarization. *Trends Immunol.* 25 (12), 677–686. doi:10.1016/j.it.2004.09.015

Mao, Y., Luo, W., Zhang, L., Wu, W., Yuan, L., Xu, H., et al. (2017). STING-IRF3 triggers endothelial inflammation in response to free fatty acid-induced mitochondrial damage in diet-induced obesity. *Atvb* 37 (5), 920–929. doi:10.1161/atvbaha.117.309017

Matzinger, P. (2002). The danger model: a renewed sense of self. *Science* 296 (5566), 301–305. doi:10.1126/science.1071059

Mayer, D., Armstrong, D., Schultz, G., Percival, S., Malone, M., Romanelli, M., et al. (2018). Cell salvage in acute and chronic wounds: a potential treatment strategy. Experimental data and early clinical results. *J. Wound Care* 27 (9), 594–605. doi:10.12968/jowc.2018.27.9.594

McGillicuddy, F. C., Chiquoine, E. H., Hinkle, C. C., Kim, R. J., Shah, R., Roche, H. M., et al. (2009). Interferon γ attenuates insulin signaling, lipid storage, and differentiation in human adipocytes via activation of the JAK/STAT pathway. *J. Biol. Chem.* 284 (46), 31936–31944. doi:10.1074/jbc.m109.061655

Miao, T., Huang, B., He, N., Sun, L., Du, G., Gong, X., et al. (2020). Decreased plasma maresin 1 concentration is associated with diabetic foot ulcer. *Mediators Inflamm.* 2020, 4539035. doi:10.1155/2020/4539035

Mikhalchik, E. V., Maximov, D. I., Ostrovsky, E. M., Yaskevich, A. V., Vlasova, I. I., Vakhrusheva, T. V., et al. (2018). Neutrophils as a source of factors that increase the length of the inflammatory phase of wound healing in patients with type 2 diabetes mellitus. *Biomed. Khim* 64 (5), 433–438. doi:10.18097/pbmc20186405433

Minutti, C. M., Knipper, J. A., Allen, J. E., and Zaiss, D. M. W. (2017). Tissue-specific contribution of macrophages to wound healing. *Semin. Cel Dev. Biol.* 61, 3–11. doi:10.1016/j.semcdb.2016.08.006

Mirza, R. E., Fang, M. M., Ennis, W. J., and Koh, T. J. (2013). Blocking interleukin-1 induces a healing-associated wound macrophage phenotype and improves healing in type 2 diabetes. *Diabetes* 62 (7), 2579–2587. doi:10.2337/db12-1450

Mirza, R. E., Fang, M. M., Weinheimer-Haus, E. M., Ennis, W. J., and Koh, T. J. (2014). Sustained inflammasome activity in macrophages impairs wound healing in type 2 diabetic humans and mice. *Diabetes* 63 (3), 1103–1114. doi:10.2337/db13-0927

Mo, Y., Sarojini, H., Wan, R., Zhang, Q., Wang, J., Eichenberger, S., et al. (2019). Intracellular ATP delivery causes rapid tissue regeneration via upregulation of cytokines, chemokines, and stem cells. *Front. Pharmacol.* 10, 1502. doi:10.3389/fphar.2019.01502

Moon, T. C., St Laurent, C. D., Morris, K. E., Marcet, C., Yoshimura, T., Sekar, Y., et al. (2010). Advances in mast cell biology: new understanding of heterogeneity and function. *Mucosal Immunol.* 3 (2), 111–128. doi:10.1038/mi.2009.136

Moura, J., Rodrigues, J., Gonçalves, M., Amaral, C., Lima, M., and Carvalho, E. (2017). Impaired T-cell differentiation in diabetic foot ulceration. *Cell Mol Immunol* 14 (9), 758–769. doi:10.1038/cmi.2015.116

Mukai, K., Tsai, M., Saito, H., and Galli, S. J. (2018). Mast cells as sources of cytokines, chemokines, and growth factors. *Immunol. Rev.* 282 (1), 121–150. doi:10.1111/imr.12634

Murray, P. J., Allen, J. E., Biswas, S. K., Fisher, E. A., Gilroy, D. W., Goerdt, S., et al. (2014). Macrophage activation and polarization: nomenclature and experimental guidelines. *Immunity* 41 (1), 14–20. doi:10.1016/j.immuni.2014.06.008

Nagareddy, P. R., Murphy, A. J., Stirzaker, R. A., Hu, Y., Yu, S., Miller, R. G., et al. (2013). Hyperglycemia promotes myelopoiesis and impairs the resolution of atherosclerosis. *Cel Metab.* 17 (5), 695–708. doi:10.1016/j.cmet.2013.04.001

Nepal, S., Tiruppathi, C., Tsukasaki, Y., Farahany, J., Mittal, M., Rehman, J., et al. (2019). STAT6 induces expression of Gas6 in macrophages to clear apoptotic neutrophils and resolve inflammation. *Proc. Natl. Acad. Sci. USA* 116 (33), 16513–16518. doi:10.1073/pnas.1821601116

Nguyen, K. T., Seth, A. K., Hong, S. J., Geringer, M. R., Xie, P., Leung, K. P., et al. (2013). Deficient cytokine expression and neutrophil oxidative burst contribute to impaired cutaneous wound healing in diabetic, biofilm-containing chronic wounds. *Wound Repair Regen.* 21 (6), 833–841. doi:10.1111/wrr.12109

Ning, X., Wang, Y., Jing, M., Sha, M., Lv, M., Gao, P., et al. (2019). Apoptotic caspases suppress type I interferon production via the cleavage of cGAS, MAVS, and IRF3. *Mol. Cel* 74 (1), 19–31. doi:10.1016/j.molcel.2019.02.013

Nishida, K., Hasegawa, A., Yamasaki, S., Uchida, R., Ohashi, W., Kurashima, Y., et al. (2019). Mast cells play role in wound healing through the ZnT2/GPR39/IL-6 axis. *Sci. Rep.* 9 (1), 10842. doi:10.1038/s41598-019-47132-5

Ogurtsova, K., da Rocha Fernandes, J. D., Huang, Y., Linnenkamp, U., Guariguata, L., Cho, N. H., et al. (2017). IDF Diabetes Atlas: global estimates for the prevalence of diabetes for 2015 and 2040. *Diabetes Res. Clin. Pract.* 128, 40–50. doi:10.1016/j.diabres.2017.03.024

Orvain, C., Lin, Y. L., Jean-Louis, F., Hocini, H., Hersant, B., Bennasser, Y., et al. (2020). Hair follicle stem cell replication stress drives IFI16/STING-dependent inflammation in hidradenitis suppurativa. *J. Clin. Invest.* 130 (7), 3777–3790. doi:10.1172/JCI131180

Palmer, A. K., Gustafson, B., Kirkland, J. L., and Smith, U. (2019). Cellular senescence: at the nexus between ageing and diabetes. *Diabetologia* 62 (10), 1835–1841. doi:10.1007/s00125-019-4934-x

Papayannopoulos, V. (2018). Neutrophil extracellular traps in immunity and disease. *Nat. Rev. Immunol.* 18 (2), 134–147. doi:10.1038/nri.2017.105

Park, J. E., and Barbul, A. (2004). Understanding the role of immune regulation in wound healing. *Am. J. Surg.* 187 (5A), 11S–16S. doi:10.1016/s0002-9610(03)00296-4

Peng, Y., Latchman, Y., and Elkon, K. B. (2009). Ly6ClowMonocytes differentiate into dendritic cells and cross-tolerize T cells through PDL-1. *J. Immunol.* 182 (5), 2777–2785. doi:10.4049/jimmunol.0803172

Perez, D. A., Galvão, I., Athayde, R. M., Rezende, B. M., Vago, J. P., Silva, J. D., et al. (2019). Inhibition of the sphingosine-1-phosphate pathway promotes the resolution of neutrophilic inflammation. *Eur. J. Immunol.* 49 (7), 1038–1051. doi:10.1002/eji.201848049

Pierce, G. F. (2001). Inflammation in nonhealing diabetic wounds. *Am. J. Pathol.* 159 (2), 399–403. doi:10.1016/s0002-9440(10)61709-9

Pike, K. A., Hutchins, A. P., Vinette, V., Theberge, J.-F., Sabbagh, L., Tremblay, M. L., et al. (2014). Protein tyrosine phosphatase 1B is a regulator of the interleukin-10-induced transcriptional program in macrophages. *Sci. Signaling* 7 (324), ra43. doi:10.1126/scisignal.2005020

Platnich, J. M., and Muruve, D. A. (2019). NOD-like receptors and inflammasomes: a review of their canonical and non-canonical signaling pathways. *Arch. Biochem. Biophys.* 670, 4–14. doi:10.1016/j.abb.2019.02.008

Pokatayev, V., Hasin, N., Chon, H., Cerritelli, S. M., Sakhuja, K., Ward, J. M., et al. (2016). RNase H2 catalytic core Aicardi-Goutières syndrome-related mutant invokes cGAS-STING innate immune-sensing pathway in mice. *J. Exp. Med.* 213 (3), 329–336. doi:10.1084/jem.20151464

Portou, M. J., Baker, D., Abraham, D., and Tsui, J. (2015). The innate immune system, toll-like receptors and dermal wound healing: a review. *Vasc. Pharmacol.* 71, 31–36. doi:10.1016/j.vph.2015.02.007

Prattichizzo, F., De Nigris, V., Mancuso, E., Spiga, R., Giuliani, A., Matacchione, G., et al. (2018). Short-term sustained hyperglycaemia fosters an archetypal senescence-associated secretory phenotype in endothelial cells and macrophages. *Redox Biol.* 15, 170–181. doi:10.1016/j.redox.2017.12.001

Qiao, Y., Wang, P., Qi, J., Zhang, L., and Gao, C. (2012). TLR-induced NF-κB activation regulates NLRP3 expression in murine macrophages. *FEBS Lett.* 586 (7), 1022–1026. doi:10.1016/j.febslet.2012.02.045

Qin, H., Huang, G., Gao, F., Huang, B., Wang, D., Hu, X., et al. (2019). Diminished stimulator of interferon genes production with cigarette smoke-exposure contributes to weakened anti-adenovirus vectors response and destruction of lung in chronic obstructive pulmonary disease model. *Exp. Cel Res.* 384 (1), 111545. doi:10.1016/j.yexcr.2019.111545

Qing, L., Fu, J., Wu, P., Zhou, Z., Yu, F., and Tang, J. (2019). Metformin induces the M2 macrophage polarization to accelerate the wound healing via regulating AMPK/mTOR/NLRP3 inflammasome singling pathway. *Am. J. Transl Res.* 11 (2), 655–668.

Qu, Z., Huang, X., Ahmadi, P., Stenberg, P., Liebler, J. M., Le, A.-C., et al. (1998). Synthesis of basic fibroblast growth factor by murine mast CellsRegulation by transforming growth factor beta, tumor necrosis factor Alpha, and stem cell factor. *Int. Arch. Allergy Immunol.* 115 (1), 47–54. doi:10.1159/000023829

Quiros, M., and Nusrat, A. (2019). Saving problematic mucosae: SPMs in intestinal mucosal inflammation and repair. *Trends Mol. Med.* 25 (2), 124–135. doi:10.1016/j.molmed.2018.12.004

Rahelic, D. (2016). [7th edition of idf diabetes atlas--call for immediate action]. *Lijec Vjesn* 138 (1-2), 57–58.

Robertson, A. L., Holmes, G. R., Bojarczuk, A. N., Burgon, J., Loynes, C. A., Chimen, M., et al. (2014). A zebrafish compound screen reveals modulation of neutrophil reverse migration as an anti-inflammatory mechanism. *Sci. Translational Med.* 6 (225), 225ra29. doi:10.1126/scitranslmed.3007672

Salminen, A., Huuskonen, J., Ojala, J., Kauppinen, A., Kaarniranta, K., and Suuronen, T. (2008). Activation of innate immunity system during aging: NF-kB signaling is the molecular culprit of inflamm-aging. *Ageing Res. Rev.* 7 (2), 83–105. doi:10.1016/j.arr.2007.09.002

Sawaya, A. P., Stone, R. C., Brooks, S. R., Pastar, I., Jozic, I., Hasneen, K., et al. (2020). Deregulated immune cell recruitment orchestrated by FOXM1 impairs human diabetic wound healing. *Nat. Commun.* 11 (1), 4678. doi:10.1038/s41467-020-18276-0

Sharif, H., Wang, L., Wang, W. L., Magupalli, V. G., Andreeva, L., Qiao, Q., et al. (2019). Structural mechanism for NEK7-licensed activation of NLRP3 inflammasome. *Nature* 570 (7761), 338–343. doi:10.1038/s41586-019-1295-z

Shi, R., Jin, Y., Hu, W., Lian, W., Cao, C., Han, S., et al. (2020). Exosomes derived from mmu_circ_0000250-modified adipose-derived mesenchymal stem cells promote wound healing in diabetic mice by inducing miR-128-3p/SIRT1-mediated autophagy. *Am. J. Physiology-Cell Physiol.* 318 (5), C848–C856. doi:10.1152/ajpcell.00041.2020

Sieweke, M. H., and Allen, J. E. (2013). Beyond stem cells: self-renewal of differentiated macrophages. *Science* 342 (6161), 1242974. doi:10.1126/science.1242974

Silva, J. C., Pitta, M. G. R., Pitta, I. R., Koh, T. J., and Abdalla, D. S. P. (2019). New peroxisome proliferator-activated receptor agonist (GQ-11) improves wound healing in diabetic mice. *Adv. Wound Care* 8 (9), 417–428. doi:10.1089/wound.2018.0911

Singh, K., Agrawal, N. K., Gupta, S. K., Mohan, G., Chaturvedi, S., and Singh, K. (2015). Genetic and epigenetic alterations in Toll like receptor 2 and wound healing impairment in type 2 diabetes patients. *J. Diabetes its Complications* 29 (2), 222–229. doi:10.1016/j.jdiacomp.2014.11.015

Singh, K., Agrawal, N. K., Gupta, S. K., Mohan, G., Chaturvedi, S., and Singh, K. (2016). Increased expression of endosomal members of toll-like receptor family abrogates wound healing in patients with type 2 diabetes mellitus. *Int. Wound J.* 13 (5), 927–935. doi:10.1111/iwj.12411

Sismanopoulos, N., Delivanis, D.-A., Alysandratos, K.-D., Angelidou, A., Therianou, A., Kalogeromitros, D., et al. (2012). Mast cells in allergic and inflammatory diseases. *Cpd* 18 (16), 2261–2277. doi:10.2174/138161212800165997

Sliter, D. A., Martinez, J., Hao, L., Chen, X., Sun, N., Fischer, T. D., et al. (2018). Parkin and PINK1 mitigate STING-induced inflammation. *Nature* 561 (7722), 258–262. doi:10.1038/s41586-018-0448-9

Smyth, I. M., and Bertram, J. F. (2019). Seminars in cell and developmental biology. *Semin. Cel Dev. Biol.* 91, 84–85. doi:10.1016/j.semcdb.2018.11.003

Snyder, R. J., Lantis, J., Kirsner, R. S., Shah, V., Molyneaux, M., and Carter, M. J. (2016). Macrophages: a review of their role in wound healing and their therapeutic use. *Wound Rep. Reg.* 24 (4), 613–629. doi:10.1111/wrr.12444

Song, N., Liu, Z.-S., Xue, W., Bai, Z.-F., Wang, Q.-Y., Dai, J., et al. (2017). NLRP3 phosphorylation is an essential priming event for inflammasome activation. *Mol. Cel* 68 (1), 185–197. doi:10.1016/j.molcel.2017.08.017

Sorokin, L. (2010). The impact of the extracellular matrix on inflammation. *Nat. Rev. Immunol.* 10 (10), 712–723. doi:10.1038/nri2852

Spite, M., Clària, J., and Serhan, C. N. (2014). Resolvins, specialized proresolving lipid mediators, and their potential roles in metabolic diseases. *Cel Metab.* 19 (1), 21–36. doi:10.1016/j.cmet.2013.10.006

Stojadinovic, O., Yin, N., Lehmann, J., Pastar, I., Kirsner, R. S., and Tomic-Canic, M. (2013). Increased number of Langerhans cells in the *epidermis* of diabetic foot ulcers correlates with healing outcome. *Immunol. Res.* 57 (1-3), 222–228. doi:10.1007/s12026-013-8474-z

Suga, H., Sugaya, M., Fujita, H., Asano, Y., Tada, Y., Kadono, T., et al. (2014). TLR4, rather than TLR2, regulates wound healing through TGF-β and CCL5 expression. *J. Dermatol. Sci.* 73 (2), 117–124. doi:10.1016/j.jdermsci.2013.10.009

Sun, S., Ji, Y., Kersten, S., and Qi, L. (2012). Mechanisms of inflammatory responses in obese adipose tissue. *Annu. Rev. Nutr.* 32, 261–286. doi:10.1146/annurev-nutr-071811-150623

Tang, Y., Zhang, M. J., Hellmann, J., Kosuri, M., Bhatnagar, A., and Spite, M. (2013). Proresolution therapy for the treatment of delayed healing of diabetic wounds. *Diabetes* 62 (2), 618–627. doi:10.2337/db12-0684

Telgenhoff, D., and Shroot, B. (2005). Cellular senescence mechanisms in chronic wound healing. *Cell Death Differ* 12 (7), 695–698. doi:10.1038/sj.cdd.4401632

Tellechea, A., Bai, S., Dangwal, S., Theocharidis, G., Nagai, M., Koerner, S., et al. (2020). Topical application of a mast cell stabilizer improves impaired diabetic wound healing. *J. Invest. Dermatol.* 140 (4), 901–911. doi:10.1016/j.jid.2019.08.449

Tellechea, A., Leal, E. C., Kafanas, A., Auster, M. E., Kuchibhotla, S., Ostrovsky, Y., et al. (2016). Mast cells regulate wound healing in diabetes. *Diabetes* 65 (7), 2006–2019. doi:10.2337/db15-0340

Thiebaut, P.-A., Delile, E., Coquerel, D., Brunel, J.-M., Renet, S., Tamion, F., et al. (2018). Protein tyrosine phosphatase 1B regulates endothelial endoplasmic reticulum stress; role in endothelial dysfunction. *Vasc. Pharmacol.* 109, 36–44. doi:10.1016/j.vph.2018.05.011

Toksoy, A., Sennefelder, H., Adam, C., Hofmann, S., Trautmann, A., Goebeler, M., et al. (2017). Potent NLRP3 inflammasome activation by the HIV reverse transcriptase inhibitor abacavir. *J. Biol. Chem.* 292 (7), 2805–2814. doi:10.1074/jbc.m116.749473

Tomic-Canic, M., and DiPietro, L. A. (2019). Cellular senescence in diabetic wounds: when too many retirees stress the system. *J. Invest. Dermatol.* 139 (5), 997–999. doi:10.1016/j.jid.2019.02.019

Tousoulis, D., Papageorgiou, N., Androulakis, E., Siasos, G., Latsios, G., Tentolouris, K., et al. (2013). Diabetes mellitus-associated vascular impairment. *J. Am. Coll. Cardiol.* 62 (8), 667–676. doi:10.1016/j.jacc.2013.03.089

Vandanmagsar, B., Youm, Y.-H., Ravussin, A., Galgani, J. E., Stadler, K., Mynatt, R. L., et al. (2011). The NLRP3 inflammasome instigates obesity-induced inflammation and insulin resistance. *Nat. Med.* 17 (2), 179–188. doi:10.1038/nm.2279

Varol, C., Landsman, L., Fogg, D. K., Greenshtein, L., Gildor, B., Margalit, R., et al. (2007). Monocytes give rise to mucosal, but not splenic, conventional dendritic cells. *J. Exp. Med.* 204 (1), 171–180. doi:10.1084/jem.20061011

Wan, S., Wan, S., Jiao, X., Cao, H., Gu, Y., Yan, L., et al. (2021). Advances in understanding the innate immune-associated diabetic kidney disease. *FASEB J.* 35 (2), e21367. doi:10.1096/fj.202002334r

Wang, H.An, P., Xie, E., Wu, Q., Fang, X., Gao, H., et al. (2017). Characterization of ferroptosis in murine models of hemochromatosis. *Hepatology* 66 (2), 449–465. doi:10.1002/hep.29117

Wang, N., Liang, H., and Zen, K. (2014). Molecular mechanisms that influence the macrophage m1-m2 polarization balance. *Front. Immunol.* 5, 614. doi:10.3389/fimmu.2014.00614

Wang, Q.Zhu, G., Cao, X., Dong, J., Song, F., and Niu, Y. (2017). Blocking AGE-RAGE signaling improved functional disorders of macrophages in diabetic wound. *J. Diabetes Res.* 2017, 1428537. doi:10.1155/2017/1428537

Wang, S.Yuan, Y.-H., Chen, N.-H., and Wang, H.-B. (2019). The mechanisms of NLRP3 inflammasome/pyroptosis activation and their role in Parkinson's disease. *Int. Immunopharmacology* 67, 458–464. doi:10.1016/j.intimp.2018.12.019

Wang, T., Zhao, J., Zhang, J., Mei, J., Shao, M., Pan, Y., et al. (2018). Heparan sulfate inhibits inflammation and improves wound healing by downregulating the NLR family pyrin domain containing 3 (NLRP3) inflammasome in diabetic rats. *J. Diabetes* 10 (7), 556–563. doi:10.1111/1753-0407.12630

Wang, W.Green, M., Choi, J. E., Gijón, M., Kennedy, P. D., Johnson, J. K., et al. (2019). CD8+ T cells regulate tumour ferroptosis during cancer immunotherapy. *Nature* 569 (7755), 270–274. doi:10.1038/s41586-019-1170-y

Wang, Y., Li, Y.-b., Yin, J.-j., Wang, Y., Zhu, L.-b., Xie, G.-y., et al. (2013). Autophagy regulates inflammation following oxidative injury in diabetes. *Autophagy* 9 (3), 272–277. doi:10.4161/auto.23628

Wang, Y.Ning, X., Gao, P., Wu, S., Sha, M., Lv, M., et al. (2017). Inflammasome activation triggers caspase-1-mediated cleavage of cGAS to regulate responses to DNA virus infection. *Immunity* 46 (3), 393–404. doi:10.1016/j.immuni.2017.02.011

Warnatsch, A., Ioannou, M., Wang, Q., and Papayannopoulos, V. (2015). Neutrophil extracellular traps license macrophages for cytokine production in atherosclerosis. *Science* 349 (6245), 316–320. doi:10.1126/science.aaa8064

Weinheimer-Haus, E. M., Judex, S., Ennis, W. J., and Koh, T. J. (2014). Low-intensity vibration improves angiogenesis and wound healing in diabetic mice. *PLoS One* 9 (3), e91355. doi:10.1371/journal.pone.0091355

Wen, H., Gris, D., Lei, Y., Jha, S., Zhang, L., Huang, M. T.-H., et al. (2011). Fatty acid-induced NLRP3-ASC inflammasome activation interferes with insulin signaling. *Nat. Immunol.* 12 (5), 408–415. doi:10.1038/ni.2022

Wetzler, C., Kämpfer, H., Stallmeyer, B., Pfeilschifter, J., and Frank, S. (2000). Large and sustained induction of chemokines during impaired wound healing in the genetically diabetic mouse: prolonged persistence of neutrophils and macrophages during the late phase of repair. *J. Invest. Dermatol.* 115 (2), 245–253. doi:10.1046/j.1523-1747.2000.00029.x

Wilkinson, H. N., Clowes, C., Banyard, K. L., Matteuci, P., Mace, K. A., and Hardman, M. J. (2019). Elevated local senescence in diabetic wound healing is linked to pathological repair via CXCR2. *J. Invest. Dermatol.* 139 (5), 1171–1181. doi:10.1016/j.jid.2019.01.005

Willenborg, S., Lucas, T., van Loo, G., Knipper, J. A., Krieg, T., Haase, I., et al. (2012). CCR2 recruits an inflammatory macrophage subpopulation critical for angiogenesis in tissue repair. *Blood* 120 (3), 613–625. doi:10.1182/blood-2012-01-403386

Wong, S. L., Demers, M., Martinod, K., Gallant, M., Wang, Y., Goldfine, A. B., et al. (2015). Diabetes primes neutrophils to undergo NETosis, which impairs wound healing. *Nat. Med.* 21 (7), 815–819. doi:10.1038/nm.3887

Wood, S., Jayaraman, V., Huelsmann, E. J., Bonish, B., Burgad, D., Sivaramakrishnan, G., et al. (2014). Pro-inflammatory chemokine CCL2 (MCP-1) promotes healing in diabetic wounds by restoring the macrophage response. *PLoS One* 9 (3), e91574. doi:10.1371/journal.pone.0091574

Wormald, S., and Hilton, D. J. (2004). Inhibitors of cytokine signal transduction. *J. Biol. Chem.* 279 (2), 821–824. doi:10.1074/jbc.r300030200

Wu, X., Zhang, H., Qi, W., Zhang, Y., Li, J., Li, Z., et al. (2018). Nicotine promotes atherosclerosis via ROS-NLRP3-mediated endothelial cell pyroptosis. *Cell Death Dis* 9 (2), 171. doi:10.1038/s41419-017-0257-3

Wu, Y., Quan, Y., Liu, Y., Liu, K., Li, H., Jiang, Z., et al. (2016). Hyperglycaemia inhibits REG3A expression to exacerbate TLR3-mediated skin inflammation in diabetes. *Nat. Commun.* 7, 13393. doi:10.1038/ncomms13393

Wu, Y., Wei, Q., and Yu, J. (2019). The cGAS/STING pathway: a sensor of senescence-associated DNA damage and trigger of inflammation in early age-related macular degeneration. *Cia* 14, 1277–1283. doi:10.2147/cia.s200637

Xu, F., Zhang, C., and Graves, D. T. (2013). Abnormal cell responses and role of TNF-alpha in impaired diabetic wound healing. *Biomed. Res. Int.* 2013, 754802. doi:10.1155/2013/754802

Yang, S., Gu, Z., Lu, C., Zhang, T., Guo, X., Xue, G., et al. (2020). Neutrophil extracellular traps are markers of wound healing impairment in patients with diabetic foot ulcers treated in a multidisciplinary setting. *Adv. Wound Care* 9 (1), 16–27. doi:10.1089/wound.2019.0943

Yin, Y., Chen, F., Wang, W., Wang, H., and Zhang, X. (2017). Resolvin D1 inhibits inflammatory response in STZ-induced diabetic retinopathy rats: possible involvement of NLRP3 inflammasome and NF-κB signaling pathway. *Mol. Vis.* 23, 242–250.

Yin, Y., Chen, F., Li, J., Yang, J., Li, Q., and Jin, P. (2020). AURKA enhances autophagy of adipose derived stem cells to promote diabetic wound repair via targeting FOXO3a. *J. Invest. Dermatol.* 140 (8), 1639–1649. doi:10.1016/j.jid.2019.12.032

Yona, S., Kim, K.-W., Wolf, Y., Mildner, A., Varol, D., Breker, M., et al. (2013). Fate mapping reveals origins and dynamics of monocytes and tissue macrophages under homeostasis. *Immunity* 38 (1), 79–91. doi:10.1016/j.immuni.2012.12.001

Yu, Y., Liu, Y., An, W., Song, J., Zhang, Y., and Zhao, X. (2019). STING-mediated inflammation in Kupffer cells contributes to progression of nonalcoholic steatohepatitis. *J. Clin. Invest.* 129 (2), 546–555. doi:10.1172/JCI121842

Yu, Y., Jiang, L., Wang, H., Shen, Z., Cheng, Q., Zhang, P., et al. (2020). Hepatic transferrin plays a role in systemic iron homeostasis and liver ferroptosis. *Blood* 136 (6), 726–739. doi:10.1182/blood.2019002907

Yuan, L., Mao, Y., Luo, W., Wu, W., Xu, H., Wang, X. L., et al. (2017). Palmitic acid dysregulates the Hippo-YAP pathway and inhibits angiogenesis by inducing mitochondrial damage and activating the cytosolic DNA sensor cGAS-STING-IRF3 signaling mechanism. *J. Biol. Chem.* 292 (36), 15002–15015. doi:10.1074/jbc.m117.804005

Zelechowska, P., Agier, J., Kozłowska, E., and Brzezińska-Błaszczyk, E. (2018). Mast cells participate in chronic low-grade inflammation within adipose tissue. *Obes. Rev.* 19 (5), 686–697.

Zhang, J., Li, L., Li, J., Liu, Y., Zhang, C.-Y., Zhang, Y., et al. (2015). Protein tyrosine phosphatase 1B impairs diabetic wound healing through vascular endothelial growth factor receptor 2 dephosphorylation. *Arterioscler Thromb. Vasc. Biol.* 35 (1), 163–174. doi:10.1161/atvbaha.114.304705

Zhang, P.Li, T., Wu, X., Nice, E. C., Huang, C., and Zhang, Y. (2020). Oxidative stress and diabetes: antioxidative strategies. *Front. Med.* 14 (5), 583–600. doi:10.1007/s11684-019-0729-1

Zhang, Y.Chen, W., and Wang, Y. (2020). STING is an essential regulator of heart inflammation and fibrosis in mice with pathological cardiac hypertrophy via endoplasmic reticulum (ER) stress. *Biomed. Pharmacother.* 125, 110022. doi:10.1016/j.biopha.2020.110022

Zhang, Y., Li, Q., Youn, J. Y., and Cai, H. (2017). Protein phosphotyrosine phosphatase 1B (PTP1B) in calpain-dependent feedback regulation of vascular endothelial growth factor receptor (VEGFR2) in endothelial cells. *J. Biol. Chem.* 292 (2), 407–416. doi:10.1074/jbc.m116.766832

Zhang, Z., Hu, X., Qi, X., Di, G., Zhang, Y., Wang, Q., et al. (2018). Resolvin D1 promotes corneal epithelial wound healing and restoration of mechanical sensation in diabetic mice. *Mol. Vis.* 24, 274–285.

Zhao, Q., Wei, Y., Pandol, S. J., Li, L., and Habtezion, A. (2018). STING signaling promotes inflammation in experimental acute pancreatitis.*Gastroenterol.* 154 (6), 1822–1835. doi:10.1053/j.gastro.2018.01.065

Zhao, R., Liang, H., Clarke, E., Jackson, C., and Xue, M. (2016). Inflammation in chronic wounds. *Int. J. Mol. Sci.* 17 (12). doi:10.3390/ijms17122085

Zhu, B. M., Ishida, Y., Robinson, G. W., Pacher-Zavisin, M., Yoshimura, A., Murphy, P. M., et al. (2008). SOCS3 negatively regulates the gp130-STAT3 pathway in mouse skin wound healing. *J. Invest. Dermatol.* 128 (7), 1821–1829. doi:10.1038/sj.jid.5701224

Conflict of Interest: The authors declare that the research was conducted in the absence of any commercial or financial relationships that could be construed as a potential conflict of interest.

frontiers in Pharmacology

ORIGINAL RESEARCH
published: 26 April 2021
doi: 10.3389/fphar.2021.657486

Caspase-11-Gasdermin D-Mediated Pyroptosis Is Involved in the Pathogenesis of Atherosclerosis

Mengqing Jiang[1†], Xuejing Sun[1†], Suzhen Liu[1], Yan Tang[1], Yunming Shi[1], Yuanyuan Bai[1], Yujie Wang[1], Qiong Yang[1], Qize Yang[2], Weihong Jiang[1], Hong Yuan[3], Qixia Jiang[4‡] and Jingjing Cai[1,3*‡]*

[1]Department of Cardiology, The Third Xiangya Hospital, Central South University, Changsha, China, [2]Suzhou Science and Technology Town Foreign Language School, Jiangsu, China, [3]The Center of Clinical Pharmacology, The Third Xiangya Hospital, Central South University, Changsha, China, [4]Department of Cardiology, Tongren Hospital, Shanghai Jiao Tong University School of Medicine, Shanghai, China

OPEN ACCESS

Edited by:
Ning Hou,
Guangzhou Medical University, China

Reviewed by:
Chi Chien Lin,
National Chung Hsing University, Taiwan
Yun Zhang,
Shandong University, China

***Correspondence:**
Qixia Jiang
vivian830505@aliyun.com
Jingjing Cai
caijingjing83@hotmail.com

[†]These authors have contributed equally to this work and share first authorship
[‡]These authors have contributed equally to this work and share last authorship

Specialty section:
This article was submitted to Inflammation Pharmacology, a section of the journal Frontiers in Pharmacology

Received: 23 January 2021
Accepted: 06 April 2021
Published: 26 April 2021

Citation:
Jiang M, Sun X, Liu S, Tang Y, Shi Y, Bai Y, Wang Y, Yang Q, Yang Q, Jiang W, Yuan H, Jiang Q and Cai J (2021) Caspase-11-Gasdermin D-Mediated Pyroptosis Is Involved in the Pathogenesis of Atherosclerosis. Front. Pharmacol. 12:657486. doi: 10.3389/fphar.2021.657486

Background: Pyroptosis is a form of cell death triggered by proinflammatory signals. Recent studies have reported that oxidized phospholipids function as caspase-11 agonists to induce noncanonical inflammasome activation in immune cells. As the levels of oxidized phospholipids derived from ox-LDL are largely elevated in atherosclerotic lesions, this study sought to determine whether oxidized lipids trigger pyroptosis and subsequent inflammation in the pathogenesis of atherosclerosis.

Methods and Results: In our current study, after integrating transcriptomic data available from the Gene Expression Omnibus with data from hyperlipidemic mice and ox-LDL-treated peritoneal macrophages, we discovered that caspase-4/11-gasdermin D-associated inflammatory signaling was significantly activated. Consistently, the mRNA expression of caspase-4 and gasdermin D was upregulated in peripheral blood mononuclear cells from patients with coronary heart disease. In particular, the expression of caspase-4 was closely associated with the severity of lesions in the coronary arteries. An *in vivo* study showed that caspase-11-gasdermin D activation occurred in response to a high-fat/high-cholesterol (HFHC) diet in ApoE$^{-/-}$ mice, while caspase-11 deletion largely attenuated the volume and macrophage infiltration of atherosclerotic lesions. An *in vitro* mechanistic study showed that caspase-11-mediated inflammation occurred partly via gasdermin D-mediated pyroptosis in macrophages. Suppressing gasdermin D in HFHC-fed ApoE$^{-/-}$ mice via delivery of an adeno-associated virus markedly decreased lesion volume and infiltrating macrophage numbers.

Conclusion: Caspase-11-gasdermin D-mediated pyroptosis and the subsequent proinflammatory response in macrophages are involved in the pathogenesis of atherosclerosis. Therefore, targeting the caspase 11-gasdermin D may serve as an alternative strategy for the treatment of atherosclerosis.

Keywords: atherosclerosis, inflammation, pyroptosis, macrophage, caspase-11, gasdermin D, cardiovascular diseases, immunity

INTRODUCTION

Pyroptosis is a highly regulated cell death process and plays a pivotal role in the pathogenesis of various cardiovascular diseases (CVDs), which can be facilitated by many factors, including lipid stimulation (Libby et al., 2019; Zhaolin et al., 2019). Atherosclerosis is a CVD with low-grade chronic inflammation. Anti-lipoprotein therapies, anti-inflammatory therapies, and immunomodulatory therapies for atherosclerosis have previously been tested or are currently being tested in clinical trials (Zhao and Mallat, 2019). However, a significant number of patients continue to suffer from atherosclerosis (Bruikman et al., 2017). Therefore, the development and rigorous testing of novel targets and therapeutics that address unmet needs are urgently needed. The discovery of pyroptosis has broadened our understanding of CVDs, and targeting this process may provide new avenues for the treatment and management of atherosclerosis.

Caspase-11, a cytosolic endotoxin [lipopolysaccharide (LPS)] receptor, mediates pyroptosis under conditions of LPS stimulation in endotoxemia and bacterial sepsis (Deng et al., 2018). Human caspase-4/5 is homologous to mouse caspase-11, which has been confirmed to directly senses intracellular LPS derived from Gram-negative bacteria during macrophage inflammatory responses (Shi et al., 2014). Recognition of intracellular LPS facilitates the rapid oligomerization of caspase-11/4/5, which results in the cleavage of the pore-forming protein gasdermin D (GSDMD), cell pyroptosis, and the release of proinflammatory cytokines, e.g., IL-1β and IL-18 (Eren et al., 2020; Karmakar et al., 2020).

The accumulation of plasma cholesterol, low-density lipoprotein (LDL) cholesterol, and apolipoproteins is regarded as the main cause of the initiation and progression of clinical atherosclerosis (Back et al., 2019). Oxidized phospholipid-stimulated macrophages and dendritic cells can induce the activation of various inflammasomes (Westerterp et al., 2017). Moreover, studies have reported that oxidized phospholipids also induce noncanonical inflammasome activation via caspase-11 in immune cells (Shi et al., 2014). Additionally, the structures of lipids or fatty acids (i.e., ox-PAPC10 and stearoyl lysophosphatidylcholine 11) are similar to that of lipid A, which can bind to caspase-11 and subsequently induce caspase-11-dependent interleukin (IL)-1 release (Zanoni et al., 2016). These findings inspired us to explore whether oxidized lipids trigger pyroptosis and subsequent inflammation in the pathogenesis of atherosclerosis. Understanding the mechanism of pyroptosis in atherosclerosis could facilitate the discovery of potential therapeutic targets that may be beneficial for atherosclerosis treatment.

METHODS

Microarray Data Retrieval and Analysis

To identify differences in gene expression between models fed a normal chow diet or a high-fat high-cholesterol (HFHC) diet, we retrieved four mouse microarray datasets (GSE2372, GSE39264, GSE40156, and GSE60086) from the National Center for Biotechnology Information Gene Expression Omnibus (GEO) website (https://www.ncbi.nlm.nih.gov/geo/) (Houde and Van Eck, 2018). We downloaded robust multiarray-averaging normalized microarray expression profiles and the corresponding annotation files. Gene probe identification was matched to the corresponding gene symbol after the files were downloaded. For situations in which multiple probes were used for one gene, we retained the probe that showed a significant gene expression value (adjusted *p*-value) after deleting the non-mRNA probes. The identification of significant differentially expressed genes (DEGs) was performed according to the matched matrix file. The GSE2372 dataset, tested on the GPL1261 platform based on the Affymetrix Mouse Genome 430 2.0 Array (*Mus musculus*), and the GSE39264 dataset, tested on the GPL8759 platform based on the Affymetrix HT Mouse Genome 430A Array, contained gene expression data that was used determine gene expression changes in the aorta during atherosclerotic lesion progression. The GSE40156 dataset, tested on the GPL1261 platform based on the Affymetrix Mouse Genome 430 2.0 Array, and the GSE60086 dataset, tested on the GPL213730 platform based on the Affymetrix Mouse Gene 1.0 ST Array, contained gene expression data used to examine the hyperlipidemia-induced modulation of vascular cell gene expression during early atherosclerosis. The limma package (version 3.30.3) was used to identify DEGs between the aorta of HFHC-treated mice and that of control mice. The q-value between gene expression levels was determined using the T-test and adjusted using the Benjamin-Hochberg (BH) method. Genes that met the cutoff criteria of a q-value < 0.05 and |log2 (fold change (FC)| > 1.5 were considered DEGs. Gene Ontology (GO) term (Lopategi et al., 2019) and Kyoto Encyclopedia of Genes and Genomes (KEGG) (Schroder et al., 2010) pathway enrichment analyses of DEGs were performed using the DAVID bioinformatic database (https://david.ncifcrf.gov/, version 6.8) (Grebe et al., 2018) with thresholds of count ≥2 and *p*-value < 0.05.

RNA Sequencing

Total RNA was isolated from ox-LDL-treated peritoneal macrophages using TRIzol. Then, RNA degradation and contamination were examined with 1% agarose gels. We checked RNA purity by using a NanoPhotometer spectrophotometer (IMPLEN, Munich, Germany), and RNA concentration was measured using the Qubit RNA Assay Kit with a Qubit 2.0 fluorometer (Life Technologies, Carlsbad, CA, United States). RNA sequencing was performed with a standard protocol using a BGISEQ-500 platform (BGI, Guangdong, China). Data quality was assessed with FastQC, and reads were aligned to a mouse genome (mm9) with HiSat2 2.0.5, sorted with SamTools 1.4 and assembled with StringTie (1.3.3.13 R package); scater was used for quality control. After log-normalizing the data, the principal component analysis was performed for dimension reduction. Heatmaps and volcano plots of the RNA-seq data were plotted with the R package ggplot2 (version 3.1.0). GO, KEGG, and genome pathway analyses were performed with DAVID, as previously described. Gene set

enrichment analysis (GSEA) was performed with GSEA (version 3.0) software.

Human Samples

Human peripheral blood samples were collected from patients with coronary arterial disease ($n = 28$) upon hospital admission at the Third Xiangya Hospital of Central South University. Only nonacute coronary arteriopathy patients diagnosed by coronary arteriography were enrolled in our study. Patients meeting any of the following criteria were excluded from the study: 1) acute myocardial infarction; 2) acute infection; 3) diabetes; 4) malignant tumor; or 5) liver and kidney dysfunction. The severity of coronary arterial disease was defined by the SYNTAX score. The control group included coronary angiography patients with no stenosis in the coronary arteries. Clinical characteristics of the included patients are shown in **Supplementary Table S1**. All procedures that involved human sample collection were approved by the ethics committee of the Third Xiangya Hospital of Central South University and adhered to the principles of the Declaration of Helsinki.

Animals

ApoE$^{-/-}$ mice were purchased from the Model Animal Research Center of Nanjing University (Nanjing, China). Caspase-11$^{-/-}$ mice were from Professor Lu Ben, Third Xiangya Hospital of Central South University. All mice were on the C57BL/6 background, and ApoE$^{-/-}$Caspase-11$^{-/-}$ mice were obtained by backcrossing ApoE$^{-/-}$ mice to caspase-11$^{-/-}$ mice for more than 10 generations. The genotypic identification of various strains is shown in **Supplementary Figure S1** and **Supplementary Table S2**. All animals were maintained under a 12-h light/dark cycle in a pathogen-free facility at the animal facility of Central South University (Changsha, Hunan, China) and Hunan Normal University (Changsha, Hunan, China) at 22 ± 2°C, and the humidity was maintained at 50–60%. All animal protocols were approved by the Animal Care and Use Committee of the Third Xiangya Hospital of Central South University and Hunan Normal University.

Establishment of an Atherosclerotic Mouse Model

An atherosclerotic model was established (shown in **Supplementary Figure S2**) with 8- to 10-week-old male ApoE$^{-/-}$ mice fed a HFHC diet (protein, 20%; fat, 40%; carbohydrates, 40%; cholesterol, 1.25%) (D12108C, Research Diets, New Brunswick, NJ, United States) for twelve continuous weeks. ApoE$^{-/-}$ mice fed normal chow served as controls.

Adeno-Associated Virus-5 Construction and Injection

An AAV-5 delivery system was used to suppress gasdermin D expression in ApoE$^{-/-}$ mice. The AAV-5 delivery system carried a gasdermin D-specific construct to suppress gasdermin D expression in ApoE$^{-/-}$ mice and was developed by Hanbi (Shanghai, China) (Jain and Ridker, 2005). The titers of the vector genome were measured with qPCR performed with vector-specific primers (shown in **Supplementary Table S3**). APOE$^{-/-}$ mice were injected via the tail vein with 100 µl of virus containing 2×10^8 µg of AAV-5 vector genome at 8 weeks of age.

Flow Cytometry Analysis of Macrophages Within the Mouse Aorta

Mouse aorta macrophages were isolated as previously described (Sabatine et al., 2017). Briefly, aortic arteries were dissected from the aortic arch to femoral bifurcations and digested in an enzyme solution containing papain (2 mg/ml) (P4762, Sigma-Aldrich, Santa Clara, CA, United States) in phosphate-buffered saline (PBS) at 37°C for 1 h. A single-cell suspension was prepared by passing the aortic pieces through a strainer and subsequently stained for flow cytometry. Cell suspensions were stained with (APC)-Cy7-conjugated anti-Zombie (423101, BioLegend, San Diego, CA, United States), V500-conjugated anti-CD45 (103138, BioLegend, San Diego, CA, United States), PE-Cy7-conjugated anti-CD11b (123109, BioLegend, San Diego, CA, United States), and PE-conjugated anti-F4/80 (123109, BioLegend, San Diego, CA, United States) antibodies for 15 min at 4°C. Absolute cell counts were detected by flow cytometry (BD FACSCalibur, United States) and analyzed using FlowJo software version X (Tree Star Inc., United States).

Isolation of Human Peripheral Blood Monocytes

Whole blood samples from patients with coronary arterial disease or control patients with a coronary angiography SYNTAX score of zero were processed within 2 h of sample collection. The whole EDTA k+-anticoagulated blood sample was diluted 1:1 with PBS (SH30256.01, HyClone, UT, United States). Then, 4 ml of diluted blood was added to 3 ml of Ficoll-Paque Plus (17144003, GE Healthcare Life Sciences, Pittsburgh, PA, United States) and centrifuged for 40 min at 400 g and 18–22°C. After centrifugation, the peripheral blood mononuclear cell (PBMC) layer was collected and washed twice in PBS at 4°C, and total monocytes were isolated from the human PBMCs using the MojoSort™ Human Pan Monocyte Isolation Kit (480060, BioLegend, San Diego, CA, United States) according to the instructions.

Isolation of Mouse Peritoneal Macrophages

Mouse peritoneal macrophages were isolated and cultured as previously described (Lehrer-Graiwer et al., 2015). Briefly, 8- to 10-week-old mice were intraperitoneally injected with 3 ml of sterile 3% thioglycollate (70157, Sigma-Aldrich, Santa Clara, CA, United States) broth to elicit peritoneal macrophages. Peritoneal macrophages were collected by three rounds of peritoneal cavity lavage using 5 ml of RPMI 1640 medium (SH30809.01, Gibco, Carlsbad, CA, United States) on the third day after thioglycollate infusion. Peritoneal macrophages collected from the peritoneal cavity were resuspended in RPMI 1640 medium supplemented

with 10% fetal bovine serum (10099141, Gibco, Carlsbad, CA, United States) and 1% antibiotics-antimycotic containing 10,000 units/ml penicillin, 10,000 μg/ml streptomycin, and 25 μg/ml Fungizone™ (15240-062, Gibco, Carlsbad, CA, United States). Peritoneal macrophages (10^6 cells per well) were plated in 12-well plates for further treatment.

Supernatant Cytokine Parameter Analysis

The concentration of the cytokine IL-1β (VAL601, Novus, San Diego, CA, United States) and IL-18 (DY7625-05, Novus, San Diego, CA, United States) in the supernatant was measured by ELISA according to the manufacturer's instructions. Briefly, peritoneal macrophage supernatant was gathered and centrifuging at 400g for 5 min, following add 100 μl of diluted sample to each well in a 96-well plate according to the manufacturer's instructions, then the optical density (OD value) of each well were detected by microplate reader (Perkin Elmer, Waltham, Mass, United States) at 450 nm wavelength and the level of IL-1β and IL-18 were determined using Microsoft's excel software (Tree Star Inc., United States) based on the standard curve according to the manufacturer's instructions. LDH release was detected using an LDH assay kit (C0017, Beyotime Biotechnology, Shanghai, China) according to the manufacturer's instructions. LDH release (%) = (absorbance of samples − absorbance of the blank hole)/(absorbance of Maximum enzyme activity − absorbance of the blank hole) × 100.

Hematoxylin and Eosin, Oil Red O and Immunofluorescence Staining

To visualize lipid accumulation in the aorta, we performed H&E (GHS216, 48900, Sigma-Aldrich, Santa Clara, CA, United States) and ORO staining (O0625, Sigma-Aldrich, Santa Clara, CA, United States) on frozen sections of 4% paraformaldehyde-fixed aortic roots. To identify macrophage infiltration in atherosclerotic lesions, immunofluorescence staining for macrophages was performed using an anti-F4/80 antibody (ab6640, Abcam, Cambridge, MA, United States). The local expression of caspase-11 and gasdermin D was determined by immunofluorescence staining using anti-caspase-11 (919916, R&D Systems, MN, United States) and anti-gasdermin D (SC-393581, Santa Cruz, Dallas, TX, United States) antibodies.

Fluorescence images were captured by fluorescence microscopy (Perkin Elmer, Waltham, Mass, United States), and lesion size was quantified using ImageJ software (National Institutes of Health, United States). Immunofluorescence images were captured and recorded by a fluorescence microscope (ZEISS) with Vert.A.1 software, and the signal intensity of target proteins was calculated by ImageJ software (National Institutes of Health, United States).

OCT-embedded tissues were sectioned (10 μm) and subjected to H&E and ORO staining as previously reported. Histological staining images were observed and recorded using a light microscope (PerkinElmer). Signal intensity was determined by ImageJ software (National Institutes of Health, United States). The infiltration of inflammatory cells into aorta sections was tested by immunofluorescence staining with primary antibodies against F4/80 (ab6640, Abcam, Cambridge, MA, United States), caspase-11 (919916, R&D, MN, United States), IL-1β (AF5103, Affinity, Cincinnati, OH, United States), IL-18 (DF6252, Affinity, Cincinnati, OH, United States), and gasdermin D (393581, Santa Cruz, Dallas, TX, United States). After incubation with a primary antibody overnight at 4°C, aorta sections were incubated with a secondary antibody, washed and then mounted with DAPI (236276, Roche, Switzerland). Immunofluorescence images were captured and recorded by a fluorescence microscope (ZEISS) with Vert.A.1 software.

Quantitative Real-Time PCR and Western Blot Analyses

RT-PCR and western blot analyses were conducted as previously described with minor modifications (O'Donoghue et al., 2014). For the RT-PCR assay, total mRNA was extracted using TRIzol reagent (15596-026, Invitrogen, Carlsbad, CA, United States) and then reverse transcribed into cDNA. PCR amplification was performed with SYBR Green PCR Master Mix (1725214, Bio-Rad, Hercules, CA, United States). The mRNA expression of genes of interest was normalized to that of Gapdh. The primer pairs used in this study are listed in **Supplementary Table S4**.

For western blot analysis, total protein samples were extracted from murine aortic tissue and peritoneal macrophages using RIPA lysis buffer (P0013BB, Beyotime, China). Protein concentrations were examined using the Pierce® BCA Protein Assay Kit (P0012, Beyotime, China). The obtained protein (40 μg) was separated on a 10% SDS-PAGE gel, transferred to a polyvinylidene fluoride (PVDF) membrane (IPVH0010, Merck Millipore, Darmstadt, Germany), blocked with 5% milk which is dissolved in TBST (50 mM Tris-HCl, pH 7.5, 150 mM NaCl, 0.1% Tween 20) for 1 h, and incubated with a primary antibody at 4°C for 12 h and a secondary antibody at room temperature for 1 h, and the relevant signal intensity was determined using ImageJ software (National Institutes of Health, United States). β-Actin served as a loading control.

Correlation Coefficient Analysis

In this study, the Pearson correlation coefficient analysis was applied to describe the proportion of the variance in the dependent variable that is predictable from the independent variables. Specifically, the association of the mRNA levels of caspase-4 in PBMCs with the SYNTAX score, which indicated the severity of coronary atherosclerosis was analyzed. The correlation coefficient R^2 measures the strength and direction of a linear relationship between two analyzed variables on a scatterplot. p-value less than 0.05 defined as statistically significant.

Statistical Analysis

All data are expressed as the mean ± standard deviation (SD). Data were first analyzed for normality test (by Shapiro-Wilk test or D'Agostino and Pearson test where indicated). Data passed the normality test were then assessed by unpaired two-tailed t test (two groups) or one-way ANOVA with Tukey's test (three groups or more), where indicated. Non-normally distributed data (two

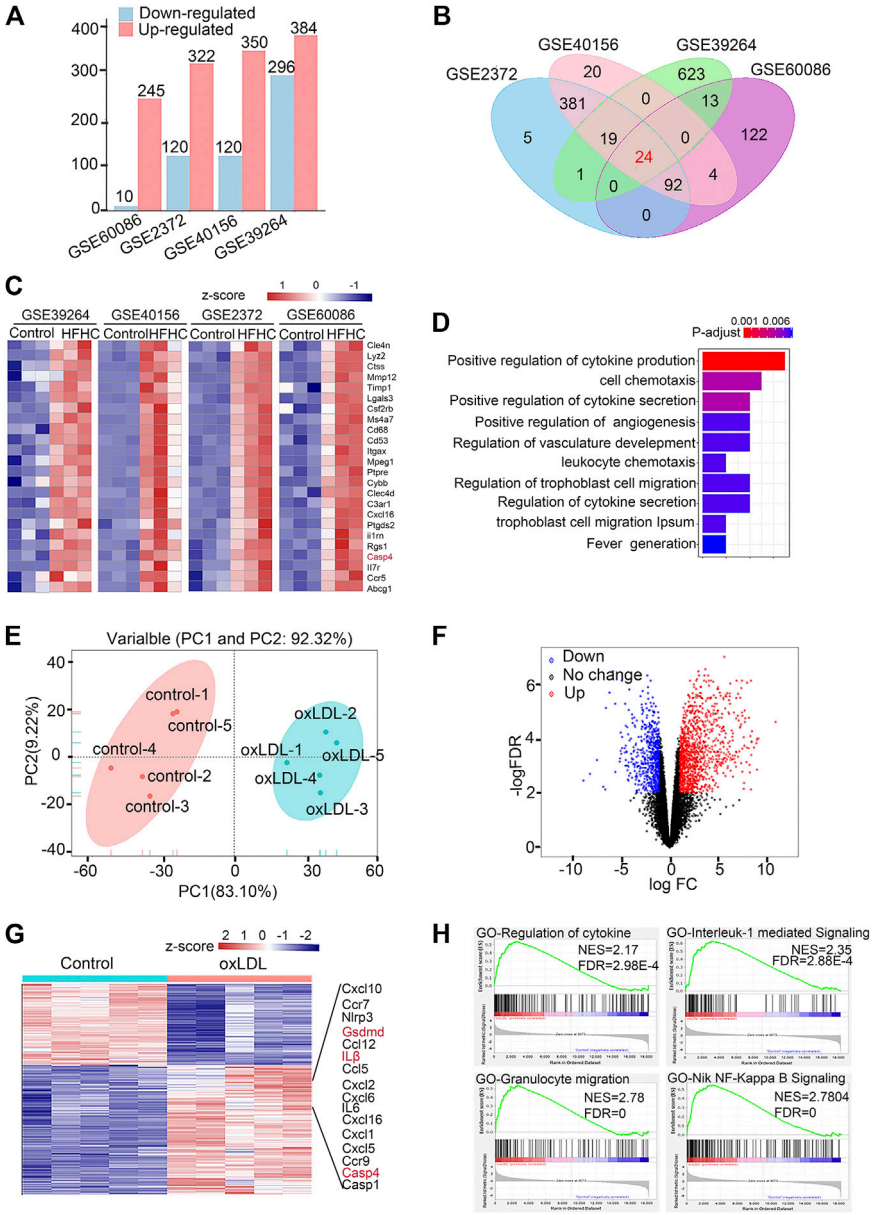

FIGURE 1 | Caspase-11-gasdermin D medicated pyroptosis signaling is involved in the pathogenesis of atherosclerosis. **(A)** Histogram showing numbers of different expression genes (DEGs) of included datasets in GEO database. DEGs with the cut-off criteria of –log10 False Discovery Rate (–logFDR) > 2 and |log2 fold change (FC)| > 2 were colored in red for up-regulated gens while in blue for down-regulated genes. **(B)** Venn diagrams depict 24 genes with consistent pattern of expression across four available transcriptomic datasets from aortic arterial tissue from C57BL/6J or ApoE$^{-/-}$ mice fed with normal chow diet or HFHC in the GEO database. **(C)** Heatmap of 24 DEGs in four datasets of mouse aortas from normal chow diet or HFHC diet. The abscisa represents different GEO datasets and samples, and the ordinate represents different genes. The red boxes indicate up-regulated genes, and the blue boxes indicate down-regulated genes. **(D)** GO term enrichment analysis illustrating number of significantly up-regulated in the most affected up-regulated genes common in HFHC diet mice aortas compared to the controls. **(E)** Principal component analysis of bulk RNA-seq data in peritoneal macrophages primed with LPS followed by 16 h of ox-LDL stimulation of control and LDL-treated macrophages. **(F)** Volcano plot indicating transcriptomic changes in control and LDL-treated macrophages. The red dots indicate up-regulated genes, and the blue dots indicate down-regulated genes. **(G)** Heatmap with differentially expressed genes in control and LDL-treated macrophages. DEGs with the cut-off criteria of –log10 False Discovery Rate (–logFDR) > 2 and |log2 fold change (FC)| > 2 were colored in red for up-regulated gens while in blue for down-regulated genes. The abscisa represents samples, and the ordinate represents different genes. The red boxes indicate up-regulated genes, and the blue boxes indicate down-regulated genes. **(H)** Gene Set Enrichment Analysis in control and LDL-treated macrophages. GEO, Gene Expression Omnibus; HFHC, high fat high cholesterol; GO term, Gene Ontology term; PCA, Principal component analysis.

groups) were analyzed by Mann-Whitney test. $p < 0.05$ was considered to be statistically significant. For linear regression analysis, data were also first tested and passed the normality test (D'Agostino and Pearson test). No experiment-wide multiple test correction was applied in our study. Representative images were chosen for similarity to the quantification data (close to the

average expression) and the image quality. Statistical calculations in the animal experiments were performed on at least three independent experiments. A *p*-value less than 0.05 was considered to indicate statistical significance. Statistical analysis was performed using the statistical software GraphPad Prism 7 (www.graphpad.com/scientific-software/prism/).

RESULTS

Caspase-11-Gasdermin D-Mediated Pyroptosis Signaling Was Involved in the Pathogenesis of Atherosclerosis

Since previous studies demonstrated that oxidized phospholipids function as caspase-11 agonists to induce noncanonical inflammasome activation in immune cells and the levels of oxidized phospholipids derived from ox-LDL are largely elevated in atherosclerotic lesions, we integrated the transcriptomic data available from the GEO database with data from hyperlipidemic mice and ox-LDL-treated peritoneal macrophages (details are shown in **Supplementary Table S5**). The upregulated and downregulated genes in the control and overnutrition diet-challenged groups were identified by analyzing DEGs (**Figure 1A**). The Venn diagram shows 24 genes with consistent expression patterns across the four DEG datasets (**Figure 1B**). Notably, 24 genes at the intersection exhibited upregulated expression in aortic tissue from mice fed the overnutrition diet (**Figure 1C**), and caspase-4/11 was among the top upregulated genes across the datasets. According to GO analysis, the top three gene-enriched biological processes were related to cytokine production and cell chemotaxis (**Figure 1D**). These results indicate that the proinflammatory response plays a dominant role in the pathogenesis of atherosclerosis. Since lesion macrophages are essential in mediating the proinflammatory response, we further verified whether the caspase-4/11-associated inflammatory response is triggered in ox-LDL-treated macrophages. Bulk RNA-seq was performed to assess peritoneal macrophages primed with LPS and then stimulated with ox-LDL for 16 h. The principal component analysis gene expression profiles of the control and ox-LDL-treated groups were clearly distinct (**Figure 1E**). Principal component loading plots 1 (PC1) and 2 (PC2) described 92.32% of the total variation in the control and ox-LDL treated groups. Among the DEGs that met the cutoff criteria of a −log10 (false discovery rate (FDR)) > 2 and |log2 (fold change (FC)| > 2, the upregulated genes are shown in red, and the downregulated genes are shown in blue. A total of 1,388 downregulated and 855 upregulated genes were identified (**Figures 1F,G**). GSEA showed that the dominant upregulated pathways in ox-LDL-treated macrophages were associated with the IL-1-mediated signaling pathway, response to cytokine stimulus, and granulocyte migration (**Figure 1H**). Genes involved in the caspase-11-gasdermin D pathway and the downstream signaling pathway were among the top 16 upregulated genes in macrophages treated with ox-LDL (**Figure 1G**). The evidence from public databases and ox-LDL-treated macrophages indicate that caspase-4/11-gasdermin D-associated inflammation may be involved in the progression of atherosclerosis.

Caspase-4/11 Was Activated in Atherosclerotic Arteries and Ox-LDL-Treated Macrophage Pyroptosis

We further tested whether caspase-11 expression is upregulated in an atherosclerotic animal model. Western blot analysis showed that caspase-11 was activated in ApoE$^{-/-}$ mice after twelve weeks of HFHC diet feeding. The level of cleaved caspase-11 at 30kD was significantly upregulated in ApoE$^{-/-}$ mice fed a HFHC diet compared to ApoE$^{-/-}$ mice fed a chow diet. Interestingly, the levels of pro-caspase-11 at 38kD and 43kD were upregulated in ApoE$^{-/-}$ mice fed a chow diet and wild-type (WT) mice fed a HFHC diet (**Figure 2A**). Immunofluorescence staining revealed that the expression of caspase-11 was upregulated in macrophages resided in the atherosclerotic plaques in ApoE$^{-/-}$ mice after 12-week of HFHC diet. Consistently, the expression of inflammatory cytokines (e.g., IL-1β and IL-18) associated with cell pyroptosis were increased in the section of atherosclerotic plaques in HFHC treated ApoE$^{-/-}$ mice. The induction of cytokines was suppressed in caspase-11$^{-/-}$ApoE$^{-/-}$ mice with 12-week of HFHC diet. The image also showed that HFHC treatment fails to induce a significant increase in the expression of caspase 11 and inflammatory cytokines at 4-week time point in ApoE$^{-/-}$ strain (**Supplementary Figure S3**). The ratio of apoptotic cell and the release of proinflammatory cytokines (e.g., IL-1β, IL-18) were increased after ox-LDL exposure in ApoE$^{-/-}$ mice derived peritoneal macrophage (**Figures 2C,D**), while ox-LDL induced cell apoptosis and cytokine release were significantly decreased in ApoE$^{-/-}$Caspase-11$^{-/-}$ mice isolated peritoneal macrophage (**Supplementary Figure S4**). As circulating monocytes have been shown to be involved in the development of atherosclerotic lesions by invading the intima and undergoing transformation into foam cells, we further tested whether the expression of caspase-4, the gene in humans homologous to mouse caspase-11, is altered in circulating monocytes in patients with coronary angiogram (CAG)- confirmed coronary heart disease (CHD). We found that the mRNA expression of caspase-4 in PBMCs was higher in patients with CHD than in normal controls (**Figure 2E**). The level of caspase-4 mRNA expression in PBMCs was positively correlated with the severity of coronary atherosclerosis, which was indicated by the SYNTAX score (**Figure 2F**). These data suggest that caspase-4/11 and its role in macrophages may be pivotal in the pathogenesis of atherosclerosis.

Genetic Deletion of Caspase-11 Attenuated Atherosclerotic Plaque Progression and Macrophage Infiltration in ApoE$^{-/-}$ Mice

To further verify whether caspase-11 depletion can slow the development of atherosclerosis and the subsequent inflammatory response, we generated ApoE$^{-/-}$Caspase-11$^{-/-}$ mice that were fed a HFHC diet or normal chow for 4 or

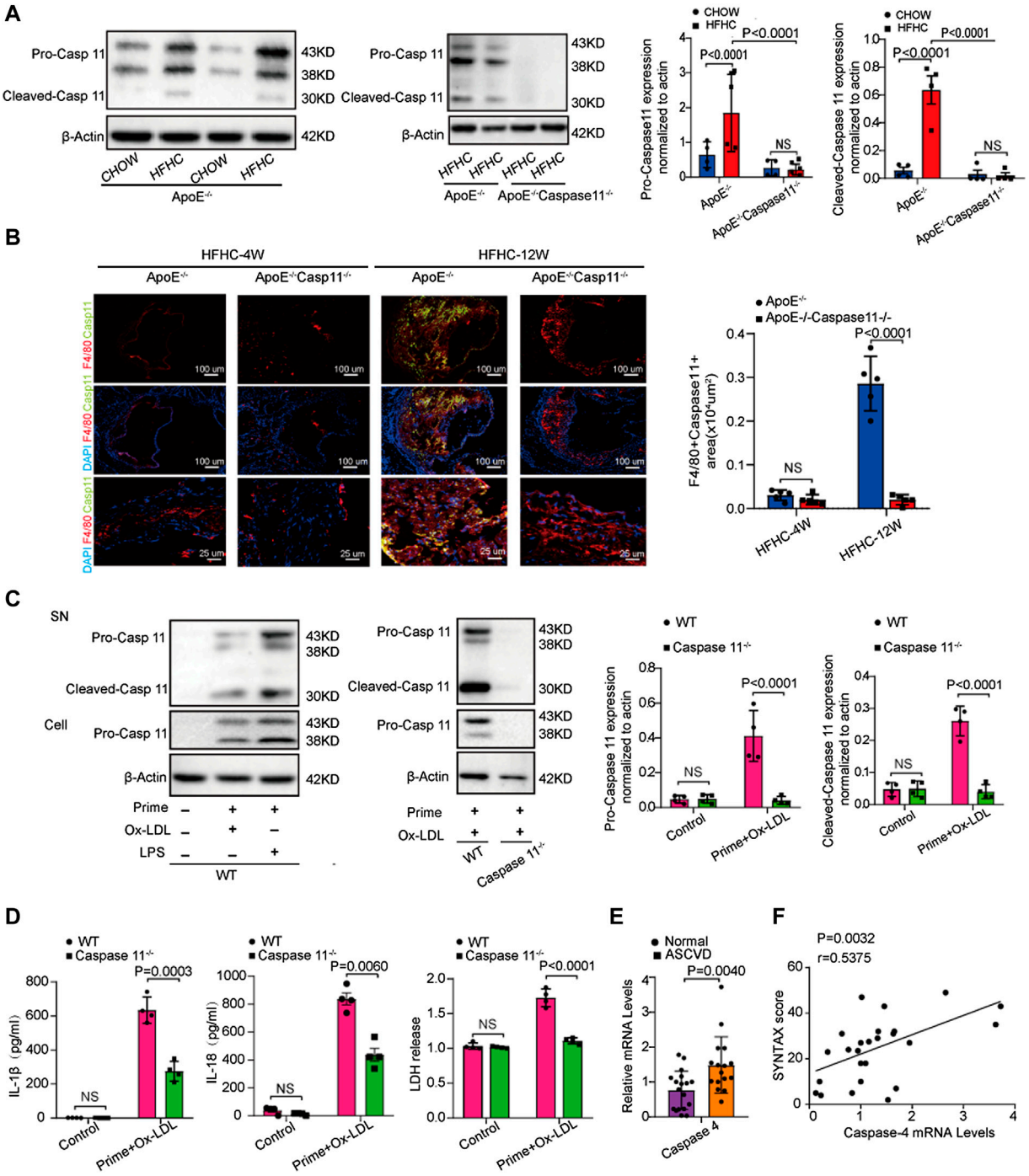

FIGURE 2 | Caspase-4/11 accelerates lipid-promoted atherosclerosis and ox-LDL-treated macrophage pyroptosis. **(A)** Left, western blot analysis and quantification of caspase-11 and its cleaved fragment expression in aortic arteries from WT, ApoE$^{-/-}$, and ApoE$^{-/-}$Caspase-11$^{-/-}$ mice fed with chow diet and HFHC diet for twelve weeks (n = 4 per group). Middle, quantification results of the level of cleaved caspase-11 in indicated groups. Right, quantification results of the level of pro-caspase-11 in indicated groups. **(B)** Left, representative images of caspase-11 (green), F4/80 (red) and DAPI (blue) in immunofluorescent staining of aortic root sections of indicated group, and quantification of the F4/80 and caspase-11 positive area of aortic root sections (n = 4 per group). Right, quantification results of the level of F4/80 and caspase-11 positive area of aortic root sections in the indicated groups. **(C)** Left, representative immunoblots of cleaved caspase-11 in peritoneal macrophage primed with 16-h ox-LDL stimulation in the indicated groups (n = 4 per group). Right, quantification results of the level of cleaved caspase-11 in indicated groups. **(D)** IL-1β (Left), IL-18 (Middle) and LDH release (Right) level secreted in peritoneal macrophage primed with LPS for 5 h and then treated with ox-LDL for 16 h after LPS administration was measured via enzyme-linked immunosorbent assay (ELISA) kits (n = 4 in each group). **(E)** Quantification results of the mRNA levels of caspase-4 genes in peripheral blood monocytes in patients with coronary heart diseases and the control group (n = 10 in each group). **(F)** Pearson comparison analyses of the correlations between caspase-4 mRNA levels in PBMC and SYNTAX score of patients with coronary heart diseases (n = 25). $p < 0.05$ for all of these correlations,

(*Continued*)

FIGURE 2 | by Pearson's rank correlation coefficient analysis. Data shown are mean ± SD **(A–F)**. Data were first analyzed and passed normality test [Shapiro-Wilk test in **(A–E)**, D'Agostino and Pearson test in **(F)**]. *p* values were shown and assessed by one-way ANOVA with Tukey's test **(A, B)**, by Mann-Whitney test **(C)** and by unpaired two-tailed *t* test **(D, E)**. All of the *p* values were labeled on the pictures and $p < 0.05$ was considered to indicate statistical significance. Ox-LDL, Oxidized low-density lipoprotein; PBMC, peripheral blood monocuclear cell; SYNTAX, Synergy Between Percutaneous Coronary Intervention with Taxus and Cardiac Surgery.

12 weeks. The baseline characteristics of the aorta were comparable among the various groups of mice. ORO staining revealed that the numbers of atherosclerotic lesions were markedly reduced in ApoE$^{-/-}$Caspase-11$^{-/-}$ mice compared with ApoE$^{-/-}$ mice fed a HFHC diet for 4 or 12 weeks (**Figure 3A**). Consistently, the incidence of atherosclerotic lesions at the aortic root was also significantly reduced in ApoE$^{-/-}$Caspase-11$^{-/-}$ mice after 4 or 12 weeks of HFHC diet feeding, which was shown by H&E and ORO staining (**Figure 3B**). To further determine whether caspase-11 depletion protects against atherosclerosis via modulation of macrophage-mediated vascular inflammation and immune infiltration, we performed flow cytometry to analyze macrophages in aortic arteries. The numbers of CD11b+F4/80+ macrophages in aortic arteries were increased after 12 weeks of HFHC diet feeding, whereas caspase-11 deletion attenuated macrophage infiltration into aortic arteries (**Figure 3C**). Similar results were obtained by immunofluorescence staining of the aortic root, and the macrophage infiltration area (marked by F4/80) in the aortic root was reduced in ApoE$^{-/-}$Caspase-11$^{-/-}$ mice fed a HFHC diet (**Figure 3D**). Furthermore, immunofluorescence staining also revealed that the increased numbers of macrophages in the aortic root were mainly confined to proliferative atherosclerotic plaques and progressively increased with the extension of the HFHC diet feeding time (**Figure 3D**). These data suggested that the genetic deletion of caspase-11 attenuated atherosclerotic plaque progression by reducing macrophage infiltration.

Caspase 11 Deficiency Attenuated Atherosclerosis by Blocking the Activation of Gasdermin D in Macrophages

Cytoplasmic gasdermin D is the key substrate for caspase-11 and can be cleaved by caspase-11 to create an N-terminal fragment that functions as a key determinant for proinflammatory cell death (Kayagaki et al., 2015). We tested whether caspase-11 deficiency attenuates atherosclerosis by blocking the activation of gasdermin D. The levels of both full-length gasdermin D (GSDMD-FL) and the pyroptosis-inducing fragment GSDMD-N were upregulated in the aorta of ApoE$^{-/-}$ and WT mice fed a HFHC diet for 12 weeks compared with those fed a chow diet (**Figure 4A**). Immunofluorescence staining revealed that the upregulated gasdermin D expression was mainly confined to plaque F4/80 positive macrophages in the aortic root and that the gasdermin D staining area increased with the extension of the HFHC diet feeding time (**Figure 4B**). The levels of the pyroptosis-inducing fragment GSDMD-N in ApoE$^{-/-}$ aortic tissue were reversed by depleting caspase-11 (**Figure 4A**). Consistently, as shown by immunofluorescence staining, gasdermin D-stained macrophage numbers were decreased in caspase-11-depleted ApoE$^{-/-}$ mice (**Figure 4B**). Western blot analysis showed that gasdermin D was activated in ox-LDL-treated macrophages from WT mice, while its activation was markedly attenuated in ox-LDL-treated macrophages from caspase 11$^{-/-}$ mice (**Figure 4C**). Further, we found that the mRNA expression of gasdermin D and inflammatory cytokines (represented by IL-1β and CCL5) was upregulated in PBMCs from patients with CAG-proven CHDs (**Figure 4D**). These results suggest that caspase-11 promotes vascular inflammation and that the development of atherosclerotic lesions is mediated by gasdermin D activation in plaque macrophages.

Suppression of Gasdermin D Attenuated Atherosclerotic Plaque Progression and Macrophage Infiltration in ApoE$^{-/-}$ Mice

To further confirm the effects of gasdermin D suppression on atherosclerosis, AAV-5- gasdermin D (AAV-D) was administered to suppress gasdermin D expression in the arteries of ApoE$^{-/-}$ mice who were fed a HFHC diet for 12 weeks. ORO staining revealed that the area of atherosclerotic lesions in the whole aortic artery was smaller in ApoE$^{-/-}$ mice treated with AAV-D than in those in the AAV-control group (**Figure 5A**). Similarly, H&E and ORO staining showed that atherosclerotic lesions were less severe at the aortic root in the ApoE$^{-/-}$ mice treated with AAV-D than in the mice in the AAV-control group (**Figure 5B**). Flow cytometry and immunofluorescence staining revealed that the fractions of F4/80+ macrophages in the whole aortic artery and aortic root were smaller in ApoE$^{-/-}$ mice treated with AAV-D than in ApoE$^{-/-}$ mice treated with AAV-control (**Figures 5C,D**). These preliminary data indicate that the suppression of gasdermin D attenuated atherosclerotic plaque progression and macrophage infiltration in ApoE$^{-/-}$ mice.

DISCUSSION

This study revealed that caspase-11-gasdermin D-mediated pyroptosis and the subsequent proinflammatory response in macrophages participate in the pathogenesis of atherosclerosis. First, we found this potential mechanism by exploring transcriptomic data from hyperlipidemic mice available in the GEO database. Second, an *in vivo* study showed that caspase-11-gasdermin D activation occurred in response to HFHC diet consumption in ApoE$^{-/-}$ mice, while the genetic deletion of caspase-11 or AAV-mediated suppression of gasdermin D largely attenuated the volume and macrophage infiltration of atherosclerotic lesions. Finally, an *in vitro* mechanistic study also supported the conclusion that lipid-associated inflammation

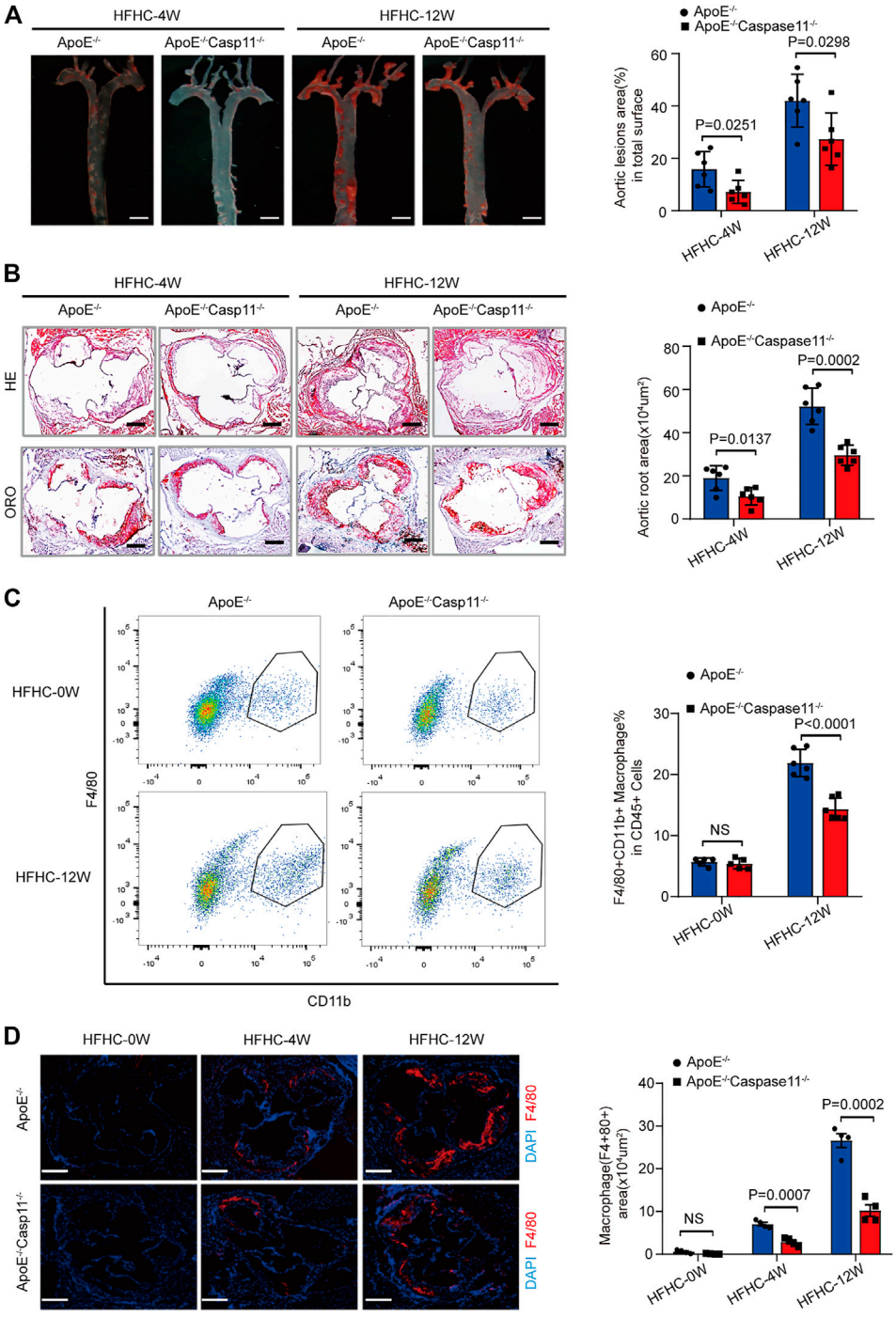

FIGURE 3 | Genetic deletion of caspase-11 attenuated atherosclerosis plaque progression and macrophage infiltration in ApoE$^{-/-}$ mice. **(A)** Left, overall comparison of representative whole-aortas stained with Oil-Red-O staining (n = 5 mice per group; scale bar, 1 mm). Right, quantitative results of the stained area in the entire aortas in ApoE$^{-/-}$ and ApoE$^{-/-}$Caspase-11$^{-/-}$ mice with 4 or 12-week HFHC diet. **(B)** Left, histological analysis of aortic root sections stained with H&E and ORO staining in the aortic root sections in ApoE$^{-/-}$ and ApoE$^{-/-}$Caspase-11$^{-/-}$ mice after 4 or 12-week HFHC diet (n = 5 mice per group; scale bar, 100 μm). Right, quantitative results for the lesion formation in the aortic root sections in the indicated groups ($n \geq 20$ fields per group). **(C)** Left, flow cytometric analysis of aortic macrophage content, determined as F4/80+CD11b+ cells per aorta and statistical results for aortic macrophage content in ApoE$^{-/-}$ and ApoE$^{-/-}$Caspase-11$^{-/-}$ mice after 0 and 12-week HFHC diet treatment (n = 5 mice per group). Right, quantitative results of flow cytometric analysis. **(D)** Left, representative images of F4/80 (red) and DAPI (blue) in aortic root sections in ApoE$^{-/-}$, ApoE$^{-/-}$Caspase-11$^{-/-}$ mice after 0, 4 and 12-week of HFHC treatment (n = 5 mice per group; scale bar, 100 μm). Right, quantification analysis of the F4/80 positive area of aortic root sections in the indicated groups ($n \geq 20$ fields per group). Data shown are mean ± SD **(A–D)**. Data were first analyzed and passed normality test (Shapiro-Wilk test). p values were shown and assessed by Mann-Whitney test **(A–D)**. All of the p values were labeled on the pictures and $p < 0.05$ was considered to indicate statistical significance. ORO, Oil-Red-O; H&E, hematoxylin and eosin; HFHC, High fat and high cholesterol.

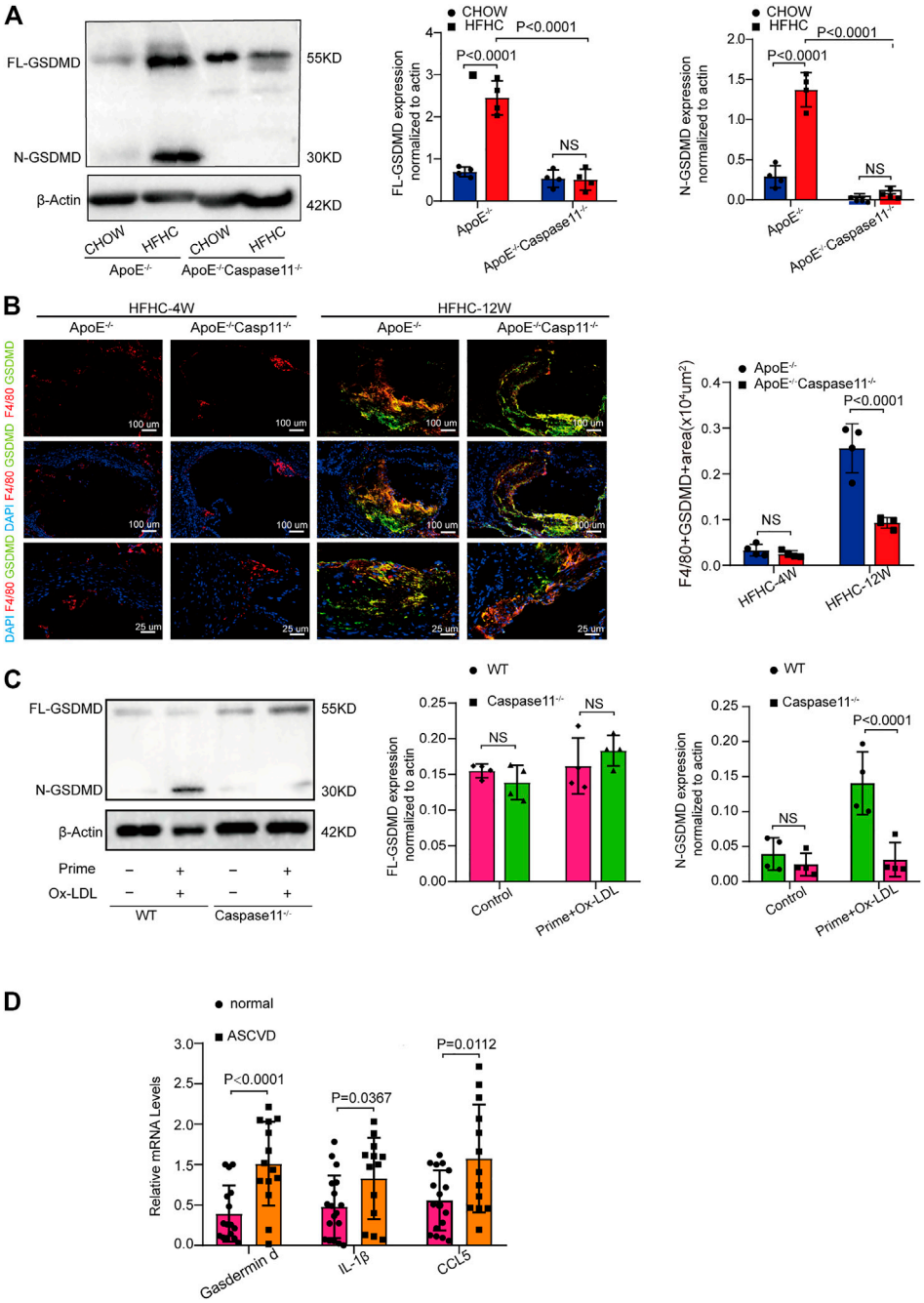

FIGURE 4 | Caspase-11 deficiency attenuates atherosclerosis via blocking the activation of gasdermin D in macrophage. **(A)** Left, representative western blot of the cleaved and total protein levels of gasdermin D in the aortas of WT, ApoE$^{-/-}$ and ApoE$^{-/-}$Caspase-11$^{-/-}$ mice after twelve weeks of chow diet or HFHC diet (n = 4 mice per group). Middle, quantitative analysis of the levels of N-GSDMD. Right, quantitative results of the protein levels of FL-GSDMD. **(B)** Left, representative images of gasdermin D (green), F4/80 (red) and DAPI (blue) of the F4/80 and gasdermin D positive area of aortic root sections in ApoE$^{-/-}$ and ApoE$^{-/-}$Caspase11$^{-/-}$ mice after 4 and 12 weeks of HFHC diet (n = 4 per group). Right, quantification analysis of the F4/80 and gasdermin D positive area of aortic root sections in the indicated groups ($n \geq 20$ fields per group). **(C)** Left, the protein expression of the cleaved and total protein levels of gasdermin D in peritoneal macrophage from WT and caspase-11$^{-/-}$ mice primed with LPS for 5 h and then treated with ox-LDL for 16 h after LPS administration was determined by western blotting. Middle, quantitative analysis of the levels of N-GSDMD. Right, quantitative results of the protein levels of FL-GSDMD (n = 4 samples per group). **(D)** The quantification of gasdermin D, IL-1β, CCL5 mRNA levels in peripheral blood monocytes in patients with coronary heart diseases and the control group (n = 10 per group). Data shown are mean ± SD **(A–D)**. Data were first analyzed and passed normality test (Shapiro-Wilk test). p values were shown and assessed by one-way ANOVA with Tukey's test **(A)**, by Mann-Whitney test **(B, C)** and by unpaired two-tailed t test (D). All of the p values were labelled on the pictures and $p < 0.05$ was considered to indicate statistical significance. GSDMD, gasdermin D.

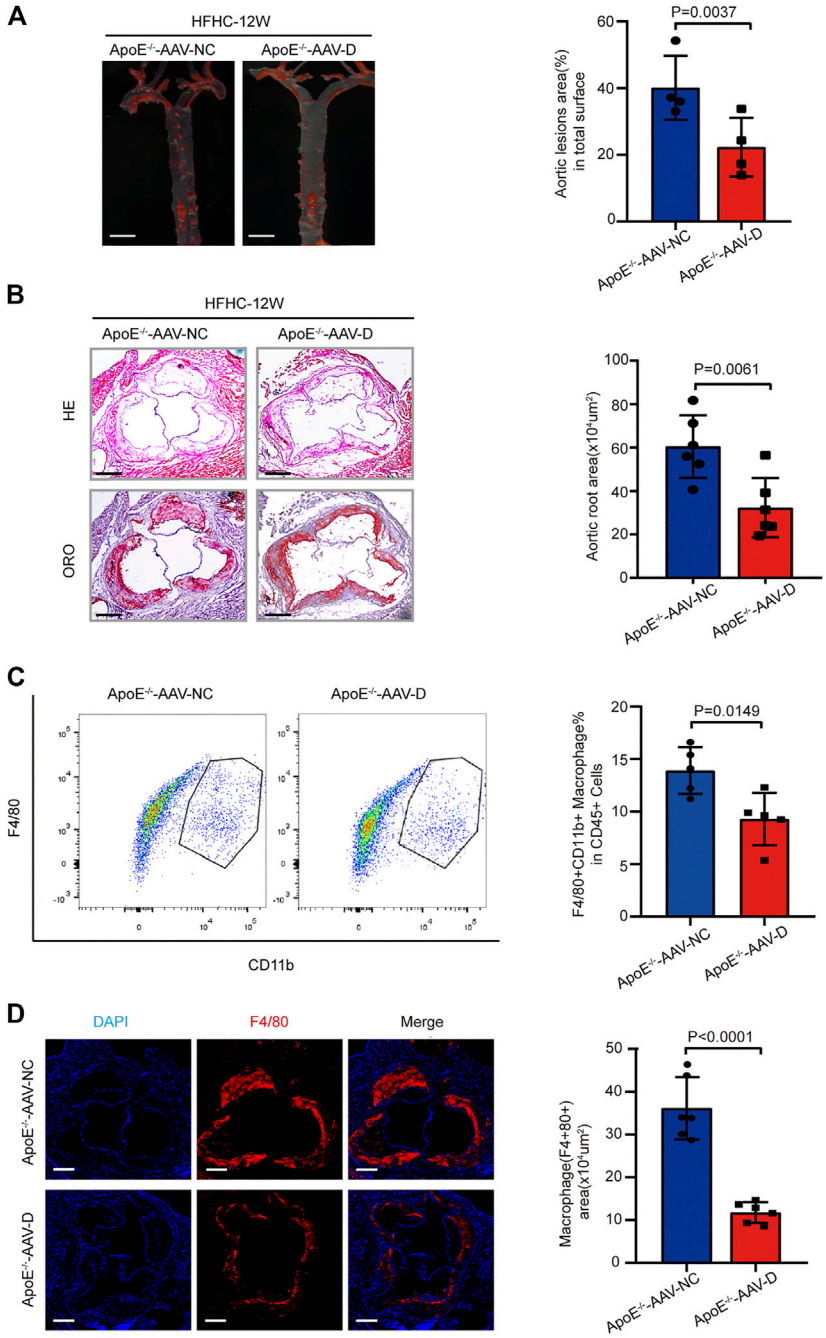

FIGURE 5 | Suppression of gasdermin D attenuated atherosclerosis plaque progression and macrophage infiltration in ApoE$^{-/-}$ mice. **(A)** Left, overall comparison of representative whole-aortas stained with Oil-Red-O staining (n = 5 mice per group; scale bar, 1 mm). Right, quantitative results of the stained area in the entire aortas of ApoE$^{-/-}$ mice administered with vector AAV-gasdermin D or the control vector AAV-control after 12 weeks of HFHC diet treatment. **(B)** Left, histological analysis of aortic root sections stained with H&E and ORO staining in the aortic root sections of ApoE$^{-/-}$ mice administered with vector AAV-GSDMD or the control vector AAV-control after 12 weeks of HFHC diet treatment (n = 4 mice per group; scale bar, 100 μm). Right, statistical analysis of the stained atherosclerotic lesion area in the aortic root sections by ORO staining in the indicated groups ($n \geq 20$ fields per group). **(C)** Left, flow cytometric analysis of aortic macrophage content, determined as F4/80 and CD11b positive cells in ApoE$^{-/-}$ mice administered vector AAV-GSDMD or the control vector AAV-control after 12 weeks of HFHC diet treatment (n = 4 mice per group). Right, statistical analysis of macrophage content in the indicated groups. **(D)** Left, representative images of F4/80 (red) and DAPI (blue) in aortic root sections of the F4/80 positive area of aortic root sections in ApoE$^{-/-}$ mice administered vector AAV-GSDMD or the control vector AAV-control after 12 weeks of HFHC diet treatment (n = 4 mice per group; scale bar, 100 μm). Right, quantification analysis of the F4/80 positive area and aortic area ratio in the indicated groups ($n \geq 20$ fields per group). Data shown are mean ± SD **(A–D)**. Data were first analyzed and passed normality test (Shapiro-Wilk test). p values were shown and assessed by Mann-Whitney test **(A–D)**. All of the p values were labelled in the figure and $p < 0.05$ was considered to indicate statistical significance. AAV-D, AAV-5-gasdermin D; GSDMD, gasdermin D.

occurs partly via caspase-11-gasdermin D-mediated pyroptosis in macrophages. Therefore, targeting caspase 11-gasdermin D could serve as an alternative strategy for the treatment of atherosclerosis.

Atherosclerosis is a disease with low-grade chronic inflammation that can be caused by lipids and other factors, including elevated blood pressure, tobacco use, metabolic disorder, and insulin resistance (Libby et al., 2019; Lu et al., 2020). The accumulation of lipids and proinflammatory cells in the arterial intima is regarded as the main cause of the initiation and progression of atherosclerosis (Back et al., 2019; Cai et al., 2020). Lipoproteins less than 70 nm in diameter can pass through the endothelial barrier and enter the arterial intima from the circulation, becoming retained lipoproteins through the interaction with intimal extracellular proteoglycans (Nordestgaard et al., 1995). Retained lipoproteins are susceptible to modification by intimal oxidizing agents, proteases, and lipases, which leads to the generation of lipid mediators that further increase inflammation and atherogenesis in the arterial intima (Houde and Van Eck, 2018). Canonical inflammasomes NLRP3 is activated by various endogenous danger signals, such as oxidized low-density lipoprotein and cholesterol crystals, and is abundantly presented in atherosclerotic lesions, which contributes to the vascular inflammatory response accelerating atherogenesis development and progression (Duewell et al., 2010; Zhang et al., 2018). The uptake of oxidized, proteolyzed or lipolyzed lipoproteins by macrophages and dendritic cells induces the activation of the canonical Nlrp3 inflammasome (Westerterp et al., 2017).

The recent discovered the non-canonical inflammasome Caspase-11 is a cytosolic LPS receptor that directly binds to lipid A on LPS and mediates cell pyroptosis (Deng et al., 2018; Wu et al., 2018). Human caspase-4/5 and mouse caspase-11 are homologues. Recent studies have revealed that ox-PAPC and stearoyl lysophosphatidylcholine have structural similarities with lipid A, which can bind to caspase-11 (Zanoni et al., 2016). As lipoproteins are cargo proteins for a large variety of fatty acids and cholesterol, we were the first to identify that lipid toxicity triggers noncanonical caspase-11 inflammasome activation in macrophages and promotes the progression of atherosclerosis. Given the evidence, activation of caspase-11 non-canonical inflammasomes by intracellular lipidprotein is distinct from canonical inflammasome activation and provides a new paradigm in macrophage-mediated inflammatory responses.

It has been proven that gasdermin D, a generic substrate for inflammatory caspases, such as caspase-1, caspase-4, caspase-5 and caspase-11, plays a specific role in inflammatory caspase-mediated pyroptosis and acts as a downstream effector of multiple inflammasomes (Shi et al., 2015). Mechanistically, we found that gasdermin D was downstream of caspase-11 activation and induced pyroptosis in lipid-loaded macrophages and that caspase-11 deficiency blocked the activation of gasdermin D in atherosclerosis. Previous studies reported that inflammasome activation and its triggered pyroptosis occurs in endothelial cells (Wu et al., 2018), macrophages (Zheng et al., 2011), and vascular smooth muscle cells (VSMCs) (Bauriedel et al., 1998; Cai et al., 2015) during the pathogenesis of numerous cardiovascular diseases (Pan et al., 2018; Li et al., 2019). Our novel findings indicated that ox-LDL induced caspase-11-gasdermin D-mediated macrophages pyroptosis and inflammation is a critical mechanism promoting atherosclerosis. This study was not able to conclude that pyroptosis in other cell types is also involved in the pathogenesis of atherosclerosis. Recent studies found that caspase-1 associated pyroptosis occurs in VSMCs and its activation potentiated the progression of atherosclerosis (Li et al., 2020). However, the role of caspase-11-gasdermin D-mediated pyroptosis of VSMCs and other cells in atherosclerosis warrant to be investigated in further studies.

Based on previous findings focusing on the mechanism of atherosclerosis, antilipoprotein therapies, anti-inflammatory therapies, and immunomodulatory therapies have been tested or are currently being tested in clinical trials (Cai et al., 2017; Zhao and Mallat, 2019). Antilipoprotein therapies are represented by statins, which target HMG-CoA reductase (Jain and Ridker, 2005). In addition, anti-proprotein convertase subtilisin/kexin type 9 (PCSK9) antibodies reduce plasma LDL-C levels by prolonging the lifespan of low-density lipoprotein receptor (LDLR) and inhibiting its degradation (Sabatine et al., 2017). Anti-inflammatory therapies include antibodies or inhibitors targeting ox-LDL, lipoprotein-associated phospholipase A2, secretory phospholipase A, 2/5-lipoxygenase, and 5-lipoxygenase activating protein (Hakonarson et al., 2005; Tardif et al., 2010; Nicholls et al., 2014; O'Donoghue et al., 2014; Lehrer-Graiwer et al., 2015). Inhibitors of the NLRP3 inflammasome and Il-1β pathway (colchicine, MCC950, anakinra, etc.) are the main drugs applied as immunomodulatory therapies (Fuster et al., 2017). Our discovery provides new perspectives on immunomodulatory therapies for vascular inflammation and atherosclerosis.

CONCLUSION

Caspase-11-gasdermin D-mediated pyroptosis and the subsequent proinflammatory response in macrophages participate in the pathogenesis of atherosclerosis. Therefore, targeting the caspase 11-gasdermin D pathway may serve as an alternative strategy for the treatment of atherosclerosis.

DATA AVAILABILITY STATEMENT

The datasets presented in this study can be found in online repositories. The names of the repository/repositories and accession number(s) can be found below: NCBI GEO; GSE171413.

ETHICS STATEMENT

The studies involving human participants were reviewed and approved by the Ethics Committee of the Third Xiangya Hospital

of Central South University. The patients/participants provided their written informed consent to participate in this study. The animal study was reviewed and approved by the Animal Care and Use Committee of the Third Xiangya Hospital of Central South University and Hunan Normal University.

AUTHOR CONTRIBUTIONS

MJ and XS perform and validated the major experiment, draft the manuscript. SL provided some statistical analysis and visualization. YT, YS, YB and YW provided valuable suggestions and edited manuscript. WJ and HY reviewed and edited the manuscript and provided constructive suggestions to the project design. QZY carried out cellular experiments. QY made critical revision to manuscript and corrected typos. QJ and JC managed and took the responsibility for the research activity planning and execution, designed the project, edited the manuscript, and supervised the study, reviewed and edited the manuscript and acquired funding.

FUNDING

This work was supported in part by the National Natural Science Foundation of China 81870171 (to JC), 81770403, 81974054 (to HY), the National Key Research and Development Projects 2019YFF0216305 (to JC), 2016YFC0900802 (to HY) and 2018YFC1311300 (to WJ), the Hunan Distinguished Young Scholars 2018JJ1048 (to JC), the Hunan Young Scholars 2018JJ3805 (to QY), the Independent Exploration and Innovation Project for Graduate Students of Central South University 1053320184264 (to MJ), the Scientific research project of health and Health Committee of Changning District 20194Y003 (to QX).

SUPPLEMENTARY MATERIAL

The Supplementary Material for this article can be found online at: https://www.frontiersin.org/articles/10.3389/fphar.2021.657486/full#supplementary-material

REFERENCES

Bäck, M., Yurdagul, A., Jr., Tabas, I., Öörni, K., and Kovanen, P. T. (2019). Inflammation and its Resolution in Atherosclerosis: Mediators and Therapeutic Opportunities. *Nat. Rev. Cardiol.* 16 (7), 389–406. doi:10.1038/s41569-019-0169-2

Bauriedel, G., Schluckebier, S., Hutter, R., Welsch, U., Kandolf, R., Lüderitz, B., et al. (1998). Apoptosis in Restenosis versus Stable-Angina Atherosclerosis. *Arterioscler Thromb. Vasc. Biol.* 18 (7), 1132–1139. doi:10.1161/01.atv.18.7.1132

Bruikman, C. S., Stoekenbroek, R. M., Hovingh, G. K., and Kastelein, J. P. (2017). New Drugs for Atherosclerosis. *Can. J. Cardiol.* 33 (3), 350–357. doi:10.1016/j.cjca.2016.09.010

Cai, J., Deng, J., Gu, W., Ni, Z., Liu, Y., Kamra, Y., et al. (2020). Impact of Local Alloimmunity and Recipient Cells in Transplant Arteriosclerosis. *Circ. Res.* 127 (8), 974–993. doi:10.1161/CIRCRESAHA.119.316470

Cai, J., Yuan, H., Wang, Q., Yang, H., Al-Abed, Y., Hua, Z., et al. (2015). HMGB1-Driven Inflammation and Intimal Hyperplasia after Arterial Injury Involves Cell-specific Actions Mediated by TLR4. *Arterioscler Thromb. Vasc. Biol.* 35 (12), 2579–2593. doi:10.1161/ATVBAHA.115.305789

Cai, J., Zhong, H., Wu, J., Chen, R.-F., Yang, H., Al-Abed, Y., et al. (2017). Cathepsin L Promotes Vascular Intimal Hyperplasia after Arterial Injury. *Mol. Med.* 23, 92–100. doi:10.2119/molmed.2016.00222

Deng, M., Tang, Y., Li, W., Wang, X., Zhang, R., Zhang, X., et al. (2018). The Endotoxin Delivery Protein HMGB1 Mediates Caspase-11-dependent Lethality in Sepsis. *Immunity* 49 (4), 740–753. doi:10.1016/j.immuni.2018.08.016

Duewell, P., Kono, H., Rayner, K. J., Sirois, C. M., Vladimer, G., Bauernfeind, F. G., et al. (2010). NLRP3 Inflammasomes Are Required for Atherogenesis and Activated by Cholesterol Crystals. *Nature* 464 (7293), 1357–1361. doi:10.1038/nature08938

Eren, E., Planès, R., Bagayoko, S., Bordignon, P. J., Chaoui, K., Hessel, A., et al. (2020). Irgm2 and Gate-16 Cooperatively Dampen Gram-negative Bacteria-induced Caspase-11 Response. *EMBO Rep.* 21 (11), e50829. doi:10.15252/embr.202050829

Fuster, J. J., MacLauchlan, S., Zuriaga, M. A., Polackal, M. N., Ostriker, A. C., Chakraborty, R., et al. (2017). Clonal Hematopoiesis Associated with TET2 Deficiency Accelerates Atherosclerosis Development in Mice. *Science* 355 (6327), 842–847. doi:10.1126/science.aag1381

Grebe, A., Hoss, F., and Latz, E. (2018). NLRP3 Inflammasome and the IL-1 Pathway in Atherosclerosis. *Circ. Res.* 122 (12), 1722–1740. doi:10.1161/CIRCRESAHA.118.311362

Hakonarson, H., Thorvaldsson, S., Helgadottir, A., Gudbjartsson, D., Zink, F., Andresdottir, M., et al. (2005). Effects of a 5-Lipoxygenase-Activating Protein Inhibitor on Biomarkers Associated with Risk of Myocardial Infarction. *JAMA* 293 (18), 2245–2256. doi:10.1001/jama.293.18.2245

Houde, M., and Van Eck, M. (2018). Escaping the Atherogenic Trap: Preventing LDL Fusion and Binding in the Intima. *Atherosclerosis* 275, 376–378. doi:10.1016/j.atherosclerosis.2018.05.032

Jain, M. K., and Ridker, P. M. (2005). Anti-inflammatory Effects of Statins: Clinical Evidence and Basic Mechanisms. *Nat. Rev. Drug Discov.* 4 (12), 977–987. doi:10.1038/nrd1901

Karmakar, M., Minns, M., Greenberg, E. N., Diaz-Aponte, J., Pestonjamasp, K., Johnson, J. L., et al. (2020). N-GSDMD Trafficking to Neutrophil Organelles Facilitates IL-1β Release Independently of Plasma Membrane Pores and Pyroptosis. *Nat. Commun.* 11 (1), 2212. doi:10.1038/s41467-020-16043-9

Kayagaki, N., Stowe, I. B., Lee, B. L., O'Rourke, K., Anderson, K., Warming, S., et al. (2015). Caspase-11 Cleaves Gasdermin D for Non-canonical Inflammasome Signalling. *Nature* 526 (7575), 666–671. doi:10.1038/nature15541

Lehrer-Graiwer, J., Singh, P., Abdelbaky, A., Vucic, E., Korsgren, M., Baruch, A., et al. (2015). FDG-PET Imaging for Oxidized LDL in Stable Atherosclerotic Disease: a Phase II Study of Safety, Tolerability, and Anti-inflammatory Activity. *JACC: Cardiovasc. Imaging* 8 (4), 493–494. doi:10.1016/j.jcmg.2014.06.021

Li, N., Zhou, H., Wu, H., Wu, Q., Duan, M., Deng, W., et al. (2019). STING-IRF3 Contributes to Lipopolysaccharide-Induced Cardiac Dysfunction, Inflammation, Apoptosis and Pyroptosis by Activating NLRP3. *Redox Biol.* 24, 101215. doi:10.1016/j.redox.2019.101215

Li, Y., Niu, X., Xu, H., Li, Q., Meng, L., He, M., et al. (2020). VX-765 Attenuates Atherosclerosis in ApoE Deficient Mice by Modulating VSMCs Pyroptosis. *Exp. Cel Res.* 389 (1), 111847. doi:10.1016/j.yexcr.2020.111847

Libby, P., Buring, J. E., Badimon, L., Hansson, G. K., Deanfield, J., Bittencourt, M. S., et al. (2019). Atherosclerosis. *Nat. Rev. Dis. Primers* 5 (1), 56. doi:10.1038/s41572-019-0106-z

Lopategi, A., Flores-Costa, R., Rius, B., López-Vicario, C., Alcaraz-Quiles, J., Titos, E., et al. (2019). Frontline Science: Specialized Proresolving Lipid Mediators Inhibit the Priming and Activation of the Macrophage NLRP3 Inflammasome. *J. Leukoc. Biol.* 105 (1), 25–36. doi:10.1002/JLB.3HI0517-206RR

Lu, Y., Sun, X., Peng, L., Jiang, W., Li, W., Yuan, H., et al. (2020). Angiotensin II-Induced Vascular Remodeling and Hypertension Involves Cathepsin L/V-MEK/ERK Mediated Mechanism. *Int. J. Cardiol.* 298, 98–106. doi:10.1016/j.ijcard.2019.09.070

Nicholls, S. J., Kastelein, J. J. P., Schwartz, G. G., Bash, D., Rosenson, R. S., Cavender, M. A., et al. (2014). Varespladib and Cardiovascular Events in

Patients with an Acute Coronary Syndrome. *JAMA* 311 (3), 252–262. doi:10.1001/jama.2013.282836

Nordestgaard, B. G., Wootton, R., and Lewis, B. (1995). Selective Retention of VLDL, IDL, and LDL in the Arterial Intima of Genetically Hyperlipidemic Rabbits *In Vivo*. *Atvb* 15 (4), 534–542. doi:10.1161/01.atv.15.4.534

O'Donoghue, M. L., Braunwald, E., White, H. D., Steen, D. P., Lukas, M. A., Tarka, E., et al. (2014). Effect of Darapladib on Major Coronary Events after an Acute Coronary Syndrome: the SOLID-TIMI 52 Randomized Clinical Trial. *JAMA* 312 (10), 1006–1015. doi:10.1001/jama.2014.11061

Pan, J., Han, L., Guo, J., Wang, X., Liu, D., Tian, J., et al. (2018). AIM2 Accelerates the Atherosclerotic Plaque Progressions in ApoE−/− Mice. *Biochem. Biophysical Res. Commun.* 498 (3), 487–494. doi:10.1016/j.bbrc.2018.03.005

Sabatine, M. S., Giugliano, R. P., Keech, A. C., Honarpour, N., Wiviott, S. D., Murphy, S. A., et al. (2017). Evolocumab and Clinical Outcomes in Patients with Cardiovascular Disease. *N. Engl. J. Med.* 376 (18), 1713–1722. doi:10.1056/NEJMoa1615664

Schroder, K., Zhou, R., and Tschopp, J. (2010). The NLRP3 Inflammasome: a Sensor for Metabolic Danger? *Science* 327 (5963), 296–300. doi:10.1126/science.1184003

Shi, J., Zhao, Y., Wang, K., Shi, X., Wang, Y., Huang, H., et al. (2015). Cleavage of GSDMD by Inflammatory Caspases Determines Pyroptotic Cell Death. *Nature* 526 (7575), 660–665. doi:10.1038/nature15514

Shi, J., Zhao, Y., Wang, Y., Gao, W., Ding, J., Li, P., et al. (2014). Inflammatory Caspases Are Innate Immune Receptors for Intracellular LPS. *Nature* 514 (7521), 187–192. doi:10.1038/nature13683

Tardif, J.-C., L'Allier, P. L., Ibrahim, R., Grégoire, J. C., Nozza, A., Cossette, M., et al. (2010). Treatment with 5-lipoxygenase Inhibitor VIA-2291 (Atreleuton) in Patients with Recent Acute Coronary Syndrome. *Circ. Cardiovasc. Imaging* 3 (3), 298–307. doi:10.1161/CIRCIMAGING.110.937169

Westerterp, M., Gautier, E. L., Ganda, A., Molusky, M. M., Wang, W., Fotakis, P., et al. (2017). Cholesterol Accumulation in Dendritic Cells Links the Inflammasome to Acquired Immunity. *Cel Metab.* 25 (6), 1294–1304. doi:10.1016/j.cmet.2017.04.005

Wu, X., Zhang, H., Qi, W., Zhang, Y., Li, J., Li, Z., et al. (2018). Nicotine Promotes Atherosclerosis via ROS-NLRP3-Mediated Endothelial Cell Pyroptosis. *Cell Death Dis* 9 (2), 171. doi:10.1038/s41419-017-0257-3

Zanoni, I., Tan, Y., Di Gioia, M., Broggi, A., Ruan, J., Shi, J., et al. (2016). An Endogenous Caspase-11 Ligand Elicits Interleukin-1 Release from Living Dendritic Cells. *Science* 352 (6290), 1232–1236. doi:10.1126/science.aaf3036

Zhang, Y., Liu, X., Bai, X., Lin, Y., Li, Z., Fu, J., et al. (2018). Melatonin Prevents Endothelial Cell Pyroptosis via Regulation of Long Noncoding RNA MEG3/miR-223/NLRP3 axis. *J. Pineal Res.* 64 (2), e12449. doi:10.1111/jpi.12449

Zhao, T. X., and Mallat, Z. (2019). Targeting the Immune System in Atherosclerosis. *J. Am. Coll. Cardiol.* 73 (13), 1691–1706. doi:10.1016/j.jacc.2018.12.083

Zhaolin, Z., Guohua, L., Shiyuan, W., and Zuo, W. (2019). Role of Pyroptosis in Cardiovascular Disease. *Cell Prolif* 52 (2), e12563. doi:10.1111/cpr.12563

Zheng, Y., Gardner, S. E., and Clarke, M. C. H. (2011). Cell Death, Damage-Associated Molecular Patterns, and Sterile Inflammation in Cardiovascular Disease. *Arterioscler Thromb. Vasc. Biol.* 31 (12), 2781–2786. doi:10.1161/ATVBAHA.111.224907

Conflict of Interest: The authors declare that the research was conducted in the absence of any commercial or financial relationships that could be construed as a potential conflict of interest.

frontiers in Pharmacology

REVIEW
published: 07 July 2021
doi: 10.3389/fphar.2021.714483

Comparisons of Underlying Mechanisms, Clinical Efficacy and Safety Between Anti-PD-1 and Anti-PD-L1 Immunotherapy: The State-of-the-Art Review and Future Perspectives

Yating Zhao[1,2], *Liu Liu*[3] *and Liang Weng*[4,5,6]*

[1]Institute of Pharmaceutical Science, King's College London, London, United Kingdom, [2]Clinical Pharmacology, BeiGene Ltd., Shanghai, China, [3]Ruikang Hospital Affiliated to Guangxi University of Chinese Medicine, Nanning, China, [4]Key Laboratory of Molecular Radiation Oncology, Changsha, China, [5]Xiangya Cancer Center, Xiangya Hospital, Central South University, Changsha, China, [6]Xiangya Lung Cancer Center, Xiangya Hospital, Central South University, Changsha, China

OPEN ACCESS

Edited by:
Annalisa Bruno,
University of Studies G. d'Annunzio Chieti and Pescara, Italy

Reviewed by:
Nuray Bayar Muluk,
Kırıkkale University, Turkey
Yuan Tian,
Shandong First Medical University and Shandong Academy of Medical Sciences, China

***Correspondence:**
Liang Weng
wengliang@csu.edu.cn

Specialty section:
This article was submitted to Inflammation Pharmacology, a section of the journal Frontiers in Pharmacology

Received: 25 May 2021
Accepted: 24 June 2021
Published: 07 July 2021

Citation:
Zhao Y, Liu L and Weng L (2021) Comparisons of Underlying Mechanisms, Clinical Efficacy and Safety Between Anti-PD-1 and Anti-PD-L1 Immunotherapy: The State-of-the-Art Review and Future Perspectives. Front. Pharmacol. 12:714483. doi: 10.3389/fphar.2021.714483

Over the past decade, diverse PD-1/PD-L1 blockades have demonstrated significant clinical benefit in across a wide range of tumor and cancer types. With the increasing number of PD-1/PD-L1 blockades available in the market, differences between the clinical performance of each of them started to be reported. Here, we provide a comprehensive historical and biological perspective regarding the underlying mechanism and clinical performance of PD-1/PD-L1 blockades, with an emphasis on the comparisons of their clinical efficacy and safety. The real-world evidence indicated that PD-1 blockade may be more effective than the PD-L1, though no significant differences were found as regards to their safety profiles. Future head-to-head studies are warranted for direct comparison between them. Finally, we summarize the yet to be elucidated questions and future promise of anti-PD-1/PD-L1 immunotherapy, including a need to explore novel biomarkers, novel combinatorial strategies, and their clinical use on chronic infection.

Keywords: immunotherapy, PD-1/PD-L1, nivolumab, pembrolizumab, tislelizumab, atezolizumab, efficacy, safety

INTRODUCTION

Programmed cell death protein 1 (PD-1), also known as CD279, is a surface co-inhibitory protein that belongs to the immunoglobulin superfamily and is encoded by the PDCD1 gene in human. It was originally discovered being expressed in activated T lymphocytes (Alsaab et al., 2017). When PD-1 binds to its ligands, known as PD-L1 (B7-H1) and PD-L2 (B7-DC), it will trigger a dual mechanism of stimulating apoptosis in PD-1 expressed T-cells while simultaneously reducing apoptosis in regulatory T-cells, resulting in down-regulation of the immune system (McDermott and Atkins, 2013). The down-regulating immune response can protect healthy tissues from damage induced by excessive inflammation in the physiological environment, while in the tumor microenvironment, the significant over-expression of PD-1/PD-L1 protects tumor cells from apoptosis (Mahoney et al., 2015).

The understanding of PD-1/PD-L1 pathway provided evidence supporting the development of antibodies that inhibit the pathway, so called PD-1/PD-L1 blockades. Over the past few years, many

PD-1/PD-L1 blockades have made a remarkable journey from the bench to the bedside and have led to significant clinical benefits to antitumor therapies (Makuku et al., 2021). With the increasing approved use of anti-PD-1/PD-L1 therapy in tumor immunotherapy, disparities between their clinical performance have attracted widespread attention by clinicians (Duan et al., 2020). Understanding the similarities and differences between PD-1 and PD-L1 blockade is needed to contribute ultimate benefits to patients with cancer.

In this review, we firstly introduce the PD-1/PD-L1 signaling pathway in normal immune function and in tumor microenvironment. The clinical use, efficacy and safety of marketing PD-1/PD-L1 blockades are then summarized, with the focus on their comparative clinical outcomes reported by several recent meta-analyses. Finally, we discuss future perspectives of PD-1/PD-L1 blockades in not only tumor/cancer immunotherapy but anti-chronic infections.

PD-1/PD-L1 SIGNALING PATHWAY

PD-1 is expressed on activated T cells, B cells, monocytes, and natural killer T cells, including cluster of differentiation (CD)8 + cytotoxic T lymphocytes and $CD4^+$ T-helper lymphocytes (McDermott and Atkins, 2013). The two known ligands of PD-1: PD-L1 and PD-L2, both of which are expressed by antigen-presenting cells (APCs) and other immune cells, and can also be expressed on nonimmune cells, including tumor cells (Keir et al., 2008; Dong et al., 1999). PD-L1 is thought to be the principal mediator of PD-1-dependent immunosuppression (Brahmer et al., 2010). When a T cell recognizes the antigen expressed by the major histocompatibility complex (MHC) on the target cell, inflammatory cytokines are produced, initiating the inflammatory process. Upon T cell activation, PD-1 expression is induced. After PD-1 binding with PD-L1, the immunoreceptor tyrosine-based switch motif (ITSM) of PD-1 is phosphorylated to activate intracellular pathways to exert immunosuppression activities: on one hand, the TCR activation signals ZAP70 and CD3δ are immediately dephosphorylated, leading to downstream PI3K/Akt pathway repression and then decreases the cell apoptosis-related gene Bcl-xl and promotes T cell apoptosis (Hofmeyer et al., 2011); on the other hand, Ras/MEK/ERK pathway is inhibited to repress T cell proliferation (Patsoukis et al., 2012). Alternatively, PD-1/PD-L1 pathway impairs the cytokine secretion released by T cells (Hofmeyer et al., 2011). Altogether, PD-L1 signals through T-cell PD-1 to negatively regulates the T-cell receptor and attenuates T-cell proliferation and functional activities, leading to T-cell exhaustion (**Figure 1**). Nevertheless, the inhibitory mechanism of PD-1/PD-L1 pathway differs between T and B cells. In B cells, following PD-1 activation, BCR pathway molecules, such as Igα/β and SγK, are dephosphorylated via SHP-2 being recruited to PD-1, therefore inhibiting PI3K, ERK and PLCγ2 pathway, leading to Ca2+ disorder and B cell growth stagnation (Okazaki et al., 2001; Nicholas et al., 2013). Physiologically, the PD-1/PD-L1 signaling pathway control the degree of inflammation at locations expressing the antigen, minimizing damage to healthy tissue (Mahoney et al., 2015).

However, this protective mechanism triggered by PD-1/PD-L1 is perverted in certain tumors. In the tumor microenvironment, the expression of PD-L1 can be markedly upregulated on tumor cells in the presence of interferon-gamma (IFN-γ), while the expression of PD-1 is significantly lifted on tumor-infiltrating lymphocytes. The engagement of PD-L1 with PD-1 of T cells leads to T-cell dysfunction, exhaustion, neutralization, and interleukin-10 (IL-10) production in a tumor mass (Sun et al., 2015). As a result, T cells unable to destroy the tumor, further enabling tumor cell evasion of immune destruction (Alsaab et al., 2017) (**Figure 1**). The function of PD-1 in B-cells have also become apparent for tumor immunosuppression (Thibult et al., 2013). Furthermore, it has been reported that PD-L1 can increase the expression of Foxp3 (the transcription factor controlling regulatory T-cell [Treg] development) and convert naive $CD4^+$ T cells to Tregs through the downregulation of Akt, mTOR and ERK2 and the simultaneous upregulation of PTEN (Francisco et al., 2010). The expansion of Tregs further execute their immunosuppressive abilities in the tumor microenvironment through maintaining the expression of PD-1 on its surface (Francisco et al., 2010).

It is found that a variety of tumors, including renal cell cancer (RCC), melanoma (MEL), as well as stomach, breast, ovarian, pancreatic, and lung cancers, express PD-L1, potentially contributing to immune suppression and evasion (Zou and Chen, 2008). Consequently, therapies that inhibit the PD-1/PD-L1 pathway can restore the antitumor immune responses and be particularly beneficial to patients with PD-L+ tumors, which has been proved in many clinical studies of checkpoint inhibitors (Duan et al., 2020). However, it has been noted that not all tumor PD-L1 expression confers a worse prognosis (Taube et al., 2012), and further work on this question is ongoing.

CLINICAL USE, EFFICACY AND SAFETY

Numbers of PD-1 and PD-L1 inhibitors were developed and widely used in a wide ranges of tumor types. In 2014, the humanized anti-PD-1 monoclonal antibody nivolumab became the first FDA-approved anti-PD-1 regimen for unresectable or metastatic melanoma (Weber et al., 2015; Robert et al., 2015a). In the same year, pembrolizumab was also approved for unresectable or metastatic melanoma (Robert et al., 2014). In the upcoming years, several novel monoclonal antibodies against PD-1, toripalimab, sintilimab, camrelizumab, tislelizumab and cemiplimab received approval for marketing consecutively. Further clinical trials succeeded and indications expanded to non-small cell lung cancer (NSCLC), renal cell cancer (RCC), urothelial carcinoma (UC), squamous cell carcinoma of the head and neck (HNSCC) and hepatocellular carcinoma (HCC) (**Table 1**). In 2016, first anti-PD-L1 antibody atezolizumab was approved for locally advanced or metastatic UC based on an improved objective response rate (ORR) (Rosenberg et al., 2016). Following that, durvalumab and avelumab, two specific antibodies against PD-L1 were approved to enter the market.

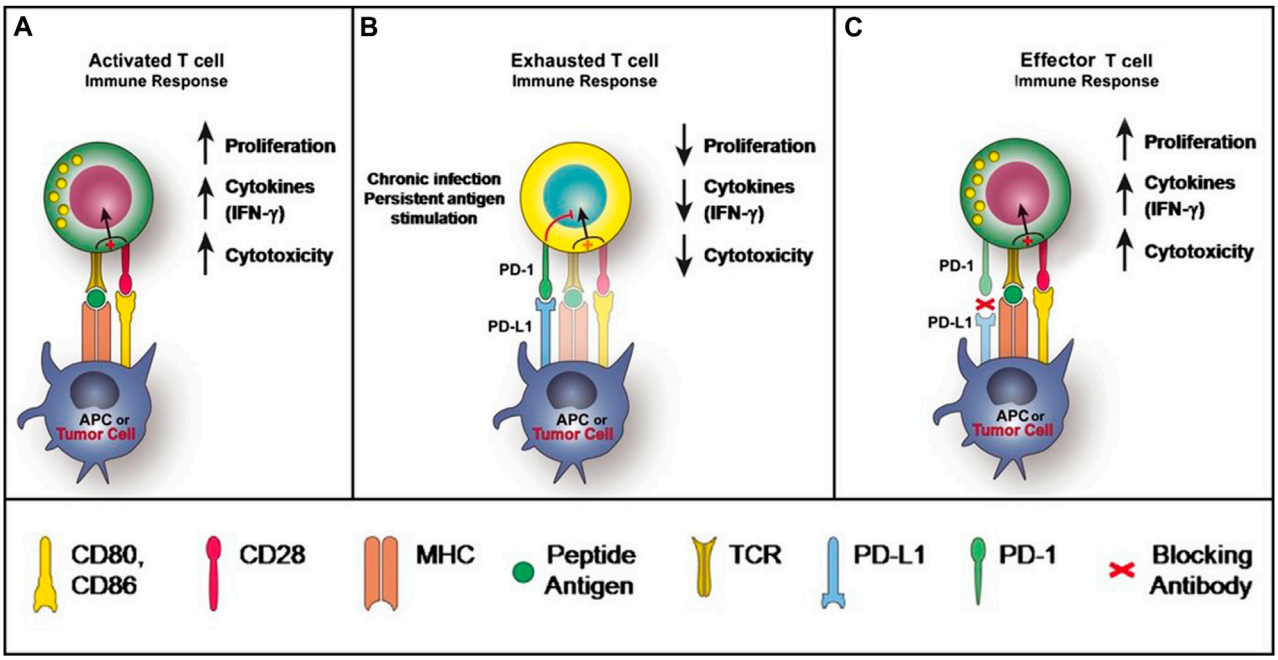

FIGURE 1 | PD-1 and PD-L1 Signaling Pathway McDermott and Atkins (2013).

Similar to anti-PD-1 antibodies, anti-PD-L1 antibodies have been effective in some difficult-to-treat cancer (**Table 2**).

Nivolumab

The clinical development of nivolumab was initiated in 2010. In a phase 1 trial, nivolumab (MDX-1106) exhibited an evidence of antitumor activity and was well tolerated (Brahmer et al., 2010). Further clinical trial that assessed the activity and safety of nivolumab (previous known as BMS-936558) demonstrated anti-PD-1 antibody produced antitumor responses in melanoma, NSCLC and RCC (Topalian et al., 2012). In the phase 3 trials, nivolumab showed a higher rate of objective response than chemotherapy regimens in patients with advanced melanoma who had disease progression after ipilimumab or a BRAF inhibitor (Weber et al., 2015) and a better overall survival (OS) of 72.9% at 1 year compared with 42.1% in the dacarbazine group as a first-line treatment (Robert et al., 2015a). Moreover, clinical trial of combination therapy demonstrated nivolumab combined with ipilimumab had a longer free-progression survival (PFS) than nivolumab alone or ipilimumab alone (11.5, 6.9 and 2.9 months respectively) in advanced melanoma (Larkin et al., 2015). In 2014, FDA granted nivolumab approval for treatment of unresectable or metastatic melanoma. And several months later, nivolumab was approved for NSCLC with progression after chemotherapy. In the phase 3 trials of NSCLC, nivolumab provided a 3.2 months increase of OS in squamous (SQ) NSCLC and 2.8 months increase in nonsquamous (NSQ) NSCLC compared with docetaxel (Borghaei et al., 2015; Brahmer et al., 2015). Regardless of PD-L1 expression, nivolumab plus ipilimumab with or without chemotherapy provided OS benefit compared with chemotherapy alone in untreated metastatic NSCLC (Hellmann et al., 2019; Paz-Ares et al., 2021). As neoadjuvant therapy in NSCLC, nivolumab plus chemotherapy demonstrated superior efficacy with a pCR of 24% comparing to chemotherapy alone (Janjigian et al., 2018) and it will be a new way of treating resectable NSCLC. Based on successful clinical trials, the use of nivolumab has been expanded to small-cell lung cancer (SCLC) (Ready et al., 2019), RCC (Motzer et al., 2015; Motzer et al., 2018), Hodgkin lymphoma (Younes et al., 2016), HNSCC (Ferris et al., 2016), colorectal cancer (Overman et al., 2017; Overman et al., 2018), HCC (El-Khoueiry et al., 2017), esophageal squamous cell cancer (ESCC) (Kato et al., 2019), UC (Sharma et al., 2017) and pleural mesothelioma (Scherpereel et al., 2019).

Pembrolizumab

The clinical development of pembrolizumab (previously known as lambrolizumab or MK-3475) started with advanced melanoma (Hamid et al., 2013). In the phase 1 trial, pembrolizumab showed an ORR of 26% at both low-dosage (2 mg/kg q3w) and high-dosage (10 mg/kg q3w) in patients with advanced melanoma after treatment of ipilimumab (Robert et al., 2015b). In head-to-head comparison with ipilimumab it increased ORR and prolonged PFS and OS in patients with advanced melanoma (Ribas et al., 2015). Further phase 1b trials demonstrated that pembrolizumab exhibited antitumor activity in advanced triple-negative breast cancer (TNBC) (Nanda et al., 2016), advanced gastric cancer (GC) (Muro et al., 2016), HNSCC (Seiwert et al., 2016) and UC (Plimack et al., 2017). In 2014, FDA approved pembrolizumab for the second-line treatment of melanoma. Pembrolizumab was also approved for the treatment in patients with PD-L1-expressing NSCLC

TABLE 1 | Clinical use of anti-PD-1 antibodies.

Drugs	Indication	Regimens	
		Monotherapy	**Combination therapy**
Nivolumab			
	Melanoma, NSCLC, SCLC, renal cell carcinoma, Hodgkin's lymphoma, HNSCC, colorectal cancer, HCC, urothelial cancer	Nivolumab 3 mg/kg q2w	
	Esophageal squamous cell cancer	Nivolumab 240 mg q2w	
	Melanoma without BRAF mutation for 1st line		Nivolumab 1 mg/kg + ipilimumab 3 mg/kg q3w, 4 doses, then nivolumab 3 mg/kg q2w
	NSCLC (PD-L1 ≥ 1%) for 1st line		Nivolumab 360 mg q3w + ipilimumab 1 mg/kg q6w
	NSCLC for 1st line		Nivolumab 360 mg q3w + ipilimumab 1 mg/kg q6w + platinum doublet chemotherapy q3w, 2 cycles
	Renal cell carcinoma for 1st line, colorectal cancer		Nivolumab 3 mg/kg q3w + ipilimumab 1 mg/kg q3w, 4 doses, then nivolumab 3 mg/kg q2w
	Pleural mesothelioma		Nivolumab 3 mg/kg q2w + ipilimumab 1 mg/kg q6w
Pembrolizumab			
	Melanoma, NSCLC (PD-L1 ≥ 1%), NSCLC (PD-L1 ≥ 50%), SCLC, HNSCC, Hodgkin's lymphoma, primary mediastinal B-cell lymphoma, urothelial cancer, colorectal cancer, gastric cancer, esophageal cancer, cervical cancer, HCC, Merkel cell carcinoma, cutaneous squamous cell carcinoma	Pembrolizumab 200 mg q3w	
	NSCLC without EGFR or ALK mutation		Pembrolizumab 200 mg q3w + (pemetrexed + platinum-based drug) q3w, 4 cycles, then pembrolizumab + pemetrexed maintenance
	HNSCC		Pembrolizumab + 5-fluorouracil + platinum
	Renal cell carcinoma		Pembrolizumab 200 mg q3w + axitinib 5 mg bid
Toripalimab			
	Melanoma	Toripalimab 3 mg/kg q2w	
Sintilimab			
	Hodgkin lymphoma	Sintilimab 200 mg q3w	—
Camrelizumab			
	Hodgkin lymphoma, esophageal cancer	Camrelizumab 200 mg q2w	
	HCC	Camrelizumab 3 mg/kg q3w	
	NSQ NSCLC		Camrelizumab 200 mg q3w + (carboplatin + pemetrexed) q3w 4–6 cycles, then pemetrexed with/without camrelizumab maintenance
Tislelizumab			
	Hodgkin lymphoma, urothelial cancer	Tislelizumab 200 mg q3w	
Cemiplimab			
	Cutaneous squamous cell carcinoma	Cemiplimab 3 mg/kg q2w	

TABLE 2 | Clinical use of anti-PD-L1 antibodies.

Drugs	Indication	Regimens	
		Monotherapy	**Combination therapy**
Atezolizumab			
	Urothelial cancer, NSCLC	Atezolizumab 1200 mg q3w	
	NSCLC		Atezolizumab + carboplatin + paclitaxel
	SCLC		Atezolizumab + carboplatin + etoposide
	Breast cancer		Atezolizumab + nab-paclitaxel
	HCC		Atezolizumab + bevacizumab
	Melanoma		Atezolizumab + cobimetinib + vemurafenib
Durvalumab			
	Urothelial cancer, stage III NSCLC	Durvalumab 10 mg/kg q2w	
	ES-SCLC		Durvalumab 1500 mg + etoposide + carboplatin or cisplatin
Avelumab			
	Merkel cell carcinoma, urothelial cancer	Avelumab 10 mg/kg q2w	
	Urothelial cancer		Gemcitabine + cisplatin or carboplatin 4 cycles, then maintenance avelumab
	RCC		Avelumab 10 mg/kg q2w + axitinib 5 mg bid

(Herbst et al., 2016; Reck et al., 2016) and increased expression of PD-L1 on tumor cells was associated with improved efficacy (Garon et al., 2015). Moreover, the addition of pembrolizumab to standard chemotherapy resulted in a significantly longer OS than chemotherapy alone as first-line therapy, which supported to be a standard treatment for metastatic NSQ NSCLC (Gandhi et al., 2018). Similar to nivolumab, the indications of pembrolizumab have been extended to SCLC (Gadgeel et al., 2018), HNSCC (Cohen et al., 2019), Hodgkin's lymphoma (Chen et al., 2017), primary mediastinal B-cell lymphoma (PMBCL) (Armand et al., 2019), UC (Balar et al., 2017; Bellmunt et al., 2017), colorectal cancer (Andre et al., 2020; Le et al., 2020), GC (Fuchs et al., 2018), esophageal cancer (Kojima et al., 2020), cervical cancer (Chung et al., 2019), HCC (Finn et al., 2020a), Merkel cell carcinoma (Nghiem et al., 2019), cutaneous squamous cell carcinoma (cSCC) (Grob et al., 2020) and RCC (Rini et al., 2019). Moreover, pembrolizumab became the first drug to be approved for advanced MSI-H/dMMR-positive solid tumors based on a tumor-specific biomarker instead of the cancer location (Boyiadzis et al., 2018).

Toripalimab

The humanized IgG4 anti-PD-1 mAb toripalimab (previous known as JS001) is developed by Shanghai Junshi Bioscience Co., Ltd. in China. The phase 1 trial demonstrated antitumor activity in UC, RCC and melanoma, especially in previous underexplored acral and mucosal melanoma subtypes (Tang et al., 2019). Further clinical trial revealed toripalimab provided an OS of 22.2 months in patients with acral and mucosal melanoma (Tang et al., 2020). Based on the positive efficacy of this trial, toripalimab received conditional approval for second-line treatment of metastatic melanoma in China. Plenty of clinical trials are ongoing, including monotherapy for treatment of advanced GC (Wang et al., 2019), neuroendocrine neoplasms (Lu et al., 2020) and NSCLC (Wang et al., 2020a), as well as combination therapy for mucosal melanoma (Sheng et al., 2019) and ESCC (Xing et al., 2020).

Sintilimab

Sintilimab is a fully humanized mAb against PD-1 receptor which is co-developed by Innovent Biologics and Eli Lilly Company. In 2018, sintilimab was approved for the treatment of relapsed or refractory classical Hodgkin lymphoma after two lines or more chemotherapy because it provided a high ORR of 80.4% (Shi et al., 2019). The phase 3 trial of sintilimab provided a longer 5.3 months of OS than docetaxel in patients with NSCLC whose disease progressed after chemotherapy (Yang et al., 2020). Besides of monotherapy, sintilimab combined with either chemotherapy or anlotinib as the first-line treatment demonstrated encouraging antitumor activities (Chu et al., 2021; Jiang et al., 2021) and combined with anlotinib, it showed a longer PFS of 15 months representing a novel chemotherapy-free regimen of NSCLC (Zhang et al., 2021). The addition of sintilimab to chemotherapy also revealed promising efficacy and manageable safety in untreated gastric/gastroesophageal junction (GEJ) adenocarcinoma (Jiang et al., 2020).

Camrelizumab

Camrelizumab, previous known as SHR-1210, is developed by Jiangsu Hengrui Medicine Co., Ltd. The phase 1 trial of camrelizumab exhibited promising antitumor activity with two

complete responses (in GC and bladder carcinoma) (Mo et al., 2018). Camrelizumab showed an ORR of 76.0% and controllable safety in patients with classical Hodgkin lymphoma after at least two lines of treatment, leading to the approval for treatment of classical Hodgkin lymphoma in China (Song et al., 2019b). In combination with chemotherapy, it provided a 4-months increased in PFS compared with chemotherapy alone in untreated patients with NSQ NSCLC (Zhou et al., 2021). At present, the clinical use of camrelizumab has been expanded to HCC (Qin et al., 2020) and esophageal cancer (Huang et al., 2020). It is still being investigated for the treatment of B-cell lymphoma (Mei et al., 2020), gastric/GEJ carcinoma (Huang et al., 2019) and nasopharyngeal carcinoma (Fang et al., 2018).

Tislelizumab

Tislelizumab which was developed by BeiGene has been investigated in solid tumors and hematological cancers since 2015. The phase 1/2 studies of tislelizumab demonstrated an acceptable safety and antitumor activity in patients with advanced solid tumors (Desai et al., 2020; Shen et al., 2020). In the treatment of classical Hodgkin lymphoma, tislelizumab was well tolerated with a high ORR of 87.1% (Song et al., 2019a). It also provided an OS of 9.8 months in patients with UC (Ye et al., 2021). Those results led to its approval for classical Hodgkin lymphoma and UC in China. Recent studies in patients with NSCLC progressed after chemotherapy, tislelizumab showed a 3.54 months increase of OS and a 1.51 months increase of PFS comparing to docetaxel. In addition to monotherapy, clinical trials of tislelizumab plus chemotherapy as first-line treatment are investigated in ESCC and gastric/GEJ adenocarcinoma (Xu et al., 2020) and lung cancer (Wang et al., 2020b) are ongoing.

Cemiplimab

In 2018 cemiplimab became the first FDA-approved PD-1-targeted therapeutics for advanced cutaneous squamous cell carcinoma that no systemic therapy has been approved. Among patients with advanced cSCC, almost half of patients responded to cemiplimab (Migden et al., 2018; Migden et al., 2020). Further clinical trials demonstrated cemiplimab produced substantial antitumor activity at either weight-based dose (3 mg/kg q2w) or fixed-dose (350 mg q3w) (Rischin et al., 2020). In NSCLC with PD-L1 expression at least 50%, cemiplimab provided a longer PFS than platinum-doublet chemotherapy, although median OS has not reached with cemiplimab (Sezer et al., 2021).

Atezolizumab

Atezolizumab (previously known as MPDL3280A) is the first-approved PD-L1 blockade for treatment of UC. An ORR of 15% was significantly improved compared with a historical control data (Rosenberg et al., 2016). However, additional clinical data indicated that atezolizumab could not provide survival benefit compared with chemotherapy in UC (Powles et al., 2018), while addition of atezolizumab to platinum-based chemotherapy prolonged PFS as first-line treatment (Galsky et al., 2020). Atezolizumab revealed promising antitumor activity in NSCLC. It provided 7.1 months longer in OS than platinum-based chemotherapy in PD-L1 high-expression patients with NSCLC (Herbst et al., 2020), resulting in its approval as first-line monotherapy for adults with metastatic NSCLC whose tumors are EGFR and ALK wild-type but have PD-L1 stained ≥50% of tumor cells or PD-L1 stained tumor-infiltrating immune cells covering ≥10% of the tumor area in 2020 (FDA). The OS was also improved compared with chemotherapy regardless of PD-L1 expression in previous treated NSCLC (Rittmeyer et al., 2017). Consequently, atezolizumab has also been approved for NSCLC regardless of PD-L1 expression either alone or in combination with chemotherapy. Indications of atezolizumab have been expanded to SCLC (Horn et al., 2018), TNBC (Schmid et al., 2018), HCC (Finn et al., 2020b) and melanoma (Gutzmer et al., 2020).

Durvalumab

Durvalumab with or without tremelimumab demonstrated antitumor responses in multiple forms of solid tumors. At present, durvalumab is used for stage III NSCLC (Antonia et al., 2017), ES-SCLC (Paz-Ares et al., 2019) and UC (Powles et al., 2017). The phase 1/2 trial of advanced UC showed an ORR of 17.8% regardless of PD-L1 expression (Powles et al., 2017). Similar to atezolizumab, further study data has not demonstrated that durvalumab has survival benefit beyond chemotherapy in UC (Powles et al., 2020a). What's more, durvalumab plus tremelimumab showed antitumor activity in NSCLC in a phase 1b study (Antonia et al., 2016). Later study data indicated durvalumab alone or combined with tremelimumab improved OS and PFS compared with standard of care as third-line or later treatment (Planchard et al., 2020). Numerous clinical trials are investigated in HNSCC (Ferris et al., 2020), TNBC (Loibl et al., 2019), HER2-positive breast cancer (Chia et al., 2019), gastric and GEJ adenocarcinoma (Kelly et al., 2020), lymphoma (Herrera et al., 2020) and pleural mesothelioma (Nowak et al., 2020).

Avelumab

The phase 1 clinical trial that assessed the activity and safety of avelumab (MSB0010718C) demonstrated PD-L1 blockade produced antitumor responses in NSCLC (Gulley et al., 2017), UC (Apolo et al., 2017), breast cancer (Dirix et al., 2018), adrenocortical carcinoma (Le Tourneau et al., 2018), melanoma (Keilholz et al., 2019), mesothelioma (Hassan et al., 2019), ovarian cancer (Disis et al., 2019), RCC (Vaishampayan et al., 2019). Based on an ORR of 31.8% in patients with Merkel cell carcinoma in phase 2 study, avelumab became the first-approved anti-PD-L1 antibody for this rare and aggressive skin cancer (Kaufman et al., 2016). Avelumab has been approved for UC and RCC as well. The phase 1b trial of UC demonstrated avelumab provided an OS of 13.7 months and OS rate of 54.3% at 1 year (Apolo et al., 2017) and as maintenance therapy of first-line chemotherapy, OS was significantly longer than best supportive care (Powles et al., 2020b). In RCC, avelumab monotherapy showed clinical activity in both first-line and second-line treatment (Vaishampayan et al., 2019). Avelumab combined

with axitinib provided a 5.4 months increase in PFS vs. sunitinib and was more effective than sunitinib among patients with untreated RCC (Motzer et al., 2019).

Comparison of Efficacy Between PD-1 and PD-L1 Inhibitors

Immune checkpoint inhibitors targeting PD-1/PD-L1 pathway represent the new standard of care in wide spectrum of solid tumors and hematological cancers. While it remains controversial whether anti-PD-1 and anti-PD-L1 antibodies have comparative efficacy and safety in different forms of tumor.

Although in absence of head-to-head comparisons, some systematic reviews and meta-analyses have been done to access the difference between PD-1 and PD-L1 inhibitors through indirect comparisons. In patients with previous treated NSCLC, one meta-analysis data demonstrated nivolumab and pembrolizumab increased ORR compared with atezolizumab but no significant difference in OS and PFS was observed (Passiglia et al., 2018). Other reported the similar result that anti-PD-1 antibodies achieved better efficacy compared with anti-PD-L1 antibody as monotherapy in patients with pre-treated NSCLC (Almutairi et al., 2019). In combination with chemotherapy, pembrolizumab may have superior efficacy compared to atezolizumab in advanced squamous NSCLC as first-line treatment (Zhang et al., 2018). Besides of NSCLC, patients with HNSCC seemed to benefit more from anti-PD-1 therapy than from durvalumab based on an indirect analysis (Zhu et al., 2021). A meta-analysis based on mirror principle suggested patients obtained survival benefit from anti-PD-1 antibodies compared with anti-PD-L1 antibodies across different forms of tumor (NSCLC, GC, UC and RCC) in either monotherapy or combination therapy (Duan et al., 2020). However, in UC the clinical outcomes of PD-1 and PD-L1 inhibitors were similar when patients progressed after a platinum-based chemotherapy (Niglio et al., 2019). Others also suggested the efficacy was similar between anti-PD-1 and anti-PD-L1 across different tumor types (Weng et al., 2018). Few clinical data is available for inclusion, the lack of comparability and systematic bias might be potential limitations of some systematic reviews and meta-analyses.

Real-world evidence is necessary to complement trial evidence and crucial for helping clinicians tailor novel immunotherapy. After failure of anti-PD-1 antibodies, retreatment with atezolizumab revealed limited efficacy in most retreated patients in NSCLC, however it was no correlation between efficacy of prior anti-PD-1 treatment and efficacy of retreatment with atezolizumab (Furuya et al., 2021). And in real-world head-to-head comparison in metastatic melanoma for frontline therapy, efficacy of nivolumab was similar to that of pembrolizumab and no significant difference in OS was observed (Moser et al., 2020). Furthermore, a meta-analysis that enrolled 32 studies of daily clinical practice demonstrated anti-PD-1 and anti-PD-L1 immunotherapy provided survival benefits as sconed-line treatment of NSCLC, in which the median PFS and OS were 3.35 and 9.98 months, respectively (Mencoboni et al., 2021). Although most patients enrolled in this meta-analysis were treated with nivolumab, the efficacy in clinical practice is comparable to that in clinical trials. It might be difficult to determine a better treatment of either anti-PD-1 or anti-PD-L1. Clinical practice of choosing either drugs is based on patients and clinician preference as well as adverse events.

Comparison of Safety and Tolerability Between PD-1 and PD-L1 Inhibitors

Anti-PD-1/PD-L1 have provoked a total paradigm shift in the treatment of oncological malignancies, thus a different pattern of toxicity has arisen in comparison with traditional chemotherapy agents. Main adverse events related to anti-PD-1/anti-PD-L1 agents are immune-related, with multiple organ and system being involved, such as hematology, cardiology, respiratory, ophthalmology, et al. (Baraibar et al., 2019). The immune-related adverse events are usually manageable, but toxicities may sometimes lead to treatment withdrawal, and fulminant and fatal events can also occur (Wang et al., 2019). Similarly, no head-to-head trial has been conducted to compare the difference of safety and tolerability between PD-1 and PD-L1. Until now, only two systematic review and meta-analyses reported the comparative incidence of immune-related adverse events of PD-1/PD-L1 via real-world data and indirect comparisons. Wang et al. (2019) conducted the meta-analysis of 112 trials involving 19,217 patients and reported toxicity-related fatality rates of 0.36% for anti–PD-1, and 0.38% for anti–PD-L1. Following that, Duan et al. (2020) found no significant difference in safety profiles between anti-PD-1 and anti-PD-L1 via the meta-analysis of 19 randomized clinical trials involving 11,379 patients.

Without a randomized, head-to-head trial of anti-PD-1 vs. anti-PD-L1 agents, no conclusive statements can be made regarding the comparative efficacy and safety of them. It appears, however, that targeting only PD-L1 may be less effective than targeting PD-1. One possible reason for the possibly superior efficacy of anti-PD-1 is that it can block signaling via both PD-L1 and PD-L2, while anti-PD-L1 only inhibit the binding the PD-1 to PD-L1. Another reason could be that anti-PD-L1 is overconsumed owing to extra PD-L1 expression following chemotherapy, leading to the inhibition of T-cell activation (Duan et al., 2020). In addition, the tumor burden, tumor growth kinetics, and tumor heterogeneity play important roles in drug resistance in cancer (Vasan et al., 2019), which has been proved by the inevitable emergence of drug resistance observed in many targeted cancer therapies (Lim et al., 2019). Therefore, the anti-PD-L1 targeting to the PD-L1 on tumor cells may be more easily resisted in comparison with anti-PD-1 targeting to the PD-1 on immune cells, which needs to be explored in future studies.

FUTURE PERSPECTIVES

Identification of Novel Biomarkers

It has been noted that discovering novel predictive, diagnostic, and prognostic pharmacological biomarkers is beneficial to better

clinical outcomes and fewer adverse effects for immunotherapy (Ribas et al., 2015). As an example, Higgs et al. (2018) proposed that T cell infiltration assessment or IFN-γ gene signature could be a promising predictive biomarker of PD-1/PD-L1 therapy. It has triggered the development of various assays to monitor T cell infiltration and detect novel biomarkers, such as PD-1/L1-targeted positron emission tomography-(PET-) based imaging biomarkers (Abousaway et al., 2021; Wei et al., 2018), single-cell sequencing technologies (Yu et al., 2016), Cytometry by Time-Of-Flight (CyTOF) (Kay et al., 2016), and genomic approaches (Hellmann et al., 2019), et al. Other potential biomarkers that have been recently found to be correlated to the clinical outcomes of PD-1/L1 include the gut microbiome (e.g. Akkermansia muciniphila), peripheral blood biomarkers (e.g. pretreatment neutrophil to lymphocyte ratio [NLR]), circulating microRNAs. However, their exact mechanisms are not clearly understood (Makuku et al., 2021).

Combination Therapies

In 2018, Mahoney et al. divided tumor immune-cell infiltration into three types: 1) "immune-desert" or noninflamed, 2) "hot" or inflamed, and 3) immune-excluded. Following that, several agents have been reported to be effective to turn "cold" tumors to "hot" T cell infiltrative tumors, improving the effectiveness of anti-PD-1/PD-L1 immunotherapy. For example, anti-cytotoxic T-lymphocyte-associated protein 4 (CTLA-4) agents improve T cell infiltration into the tumor microenvironment, which provides an opportunity for PD-1 blockade agents to work more efficiently, and their synergic combination has been proved to be more efficacious and safer compared with PD-1 blockade or anti-CTLA-4 monotherapy (Wu et al., 2019). The research on other effective approaches to induce effector T cell infiltration into the tumors and improve the therapeutic efficacy of PD-1 is gaining more and more attentions, such as amalgamating PD-1 blockade with oncolytic viruses, cancer vaccines, and local ablation, et al. (Makuku et al., 2021).

Combination of PD-1/PD-L1 blockade with new blockades that inhibit a wider spectrum of inhibitory receptors is the current focus of immunotherapeutic research. In addition to PD-1 and CTLA-4, the inhibitory receptors leading to the failure of cancer elimination known until now include T-cell immunoglobulin mucin-3 (TIM-3), and lymphocyte activation gene 3 (LAG-3), T cell immunoglobulin and ITIM domain (TIGIT), and Band T-lymphocyte-associated protein (BTLA) receptors associated with T cell exhaustion as well as V-domain immunoglobulin suppressor of T cell activation (VISTA). Many clinical trials investigating their combinatorial strategies are ongoing, with the aim to yield better outcomes for cancer patients (Song et al., 2017).

Treatment of Chronic Infections

As mentioned earlier, PD-1 and PD-L1 also play a key role in the failure to eliminate pathogens during chronic infections. Upregulation of PD-1 has been reported on T cells that are specific to tuberculosis (TB) (Jurado et al., 2008), human immunodeficiency virus (HIV) (Trautmann et al., 2006; Paris et al., 2015), hepatitis B virus (HBV) (Boni et al., 2007), and human T-cell leukemia virus type 1 (HTLV-1) (Kozako et al., 2009; Kozako et al., 2011). Also, the upregulation of PD-L1 has been reported on human gastric epithelial cells during a *Helicobacter pylori* infection (Das et al., 2006). It indicates that the PD-1 pathway also appears to result in insufficient clearance during specific bacterial infection. Therefore, anti-PD-1/PD-L1 therapy holds promise as adjunctive therapy for chronic infectious diseases, which, however, must be tested in randomized clinical trials. A phase I trial investigating the safety and tolerability of pembrolizumab with initial viral and immunologic outcome assessment is ongoing (NCT03239899). In addition, a pilot study has shown that nivolumab is safe and effective for the treatment of virally suppressed patients with chronic hepatitis B infection (Gane et al., 2019).

CONCLUSION

Anti PD-1/PD-L1 therapies have demonstrated their promising antitumor effects in cancer immunotherapy of many different solid and hematologic malignancies. Based on the different underlying mechanism of PD-1 and PD-L1 blockade, with the evidence from real-world data, the former may be more effective than the latter, though no significant differences were found as regards to their safety profiles. However, no conclusion can be made without a randomized, head-to-head comparison between them. Future head-to-head studies are warranted for direct comparison between PD-1 and PD-L1 blockade. Moreover, with increasing understanding on the tumor microenvironment, reports to the primary and adaptive resistance to anti-PD-1/PD-L1 therapy, and *in vitro*/*ex vivo* research demonstrating the role of PD-1/PD-L1 pathway in chronic infection, there is a need to explore novel biomarkers, novel combinatorial strategies, and implement clinical trials evaluating the efficacy of PD-1/PD-L1 blockade on chronic infection, to broaden its clinical applicability in the future.

AUTHOR CONTRIBUTIONS

YZ and LL summarized the literature and drafted the manuscript. YZ and LW revised and edited the manuscript. YZ finalized and submitted the manuscript. YZ and LW initiated and supervised the work.

FUNDING

This work was funded by the National Multidisciplinary Cooperative Diagnosis and Treatment Capacity Building Project for Major Diseases (Lung Cancer), National Natural Science Foundations of China (81974465 and 81900199), Hunan province Natural Science Funds for Excellent Young Scholars (2019JJ30043) and the recruitment program for Huxiang Talents (2019RS1009).

REFERENCES

Abousaway, O., Rakhshandehroo, T., Van den Abbeele, A. D., Kircher, M. F., and Rashidian, M. (2021). Noninvasive Imaging of Cancer Immunotherapy. *Nano*, 5, 90–112.

Almutairi, A. R., Alkhatib, N., Martin, J., Babiker, H. M., Garland, L. L., McBride, A., et al. (2019). Comparative Efficacy and Safety of Immunotherapies Targeting the Pd-1/Pd-L1 Pathway for Previously Treated Advanced Non-Small Cell Lung Cancer: A Bayesian Network Meta-Analysis. *Crit. Rev. Oncol. Hematol.* 142, 16–25. doi:10.1016/j.critrevonc.2019.07.004

Alsaab, H. O., Sau, S., Alzhrani, R., Tatiparti, K., Bhise, K., Kashaw, S. K., et al. (2017). PD-1 and PD-L1 Checkpoint Signaling Inhibition for Cancer Immunotherapy: Mechanism, Combinations, and Clinical Outcome. *Front. Pharmacol.* 8, 561. doi:10.3389/fphar.2017.00561

André, T., Shiu, K.-K., Kim, T. W., Jensen, B. V., Jensen, L. H., Punt, C., et al. (2020). Pembrolizumab in Microsatellite-Instability-High Advanced Colorectal Cancer. *N. Engl. J. Med.* 383 (23), 2207–2218. doi:10.1056/NEJMoa2017699

Antonia, S., Goldberg, S. B., Balmanoukian, A., Chaft, J. E., Sanborn, R. E., Gupta, A., et al. (2016). Safety and Antitumour Activity of Durvalumab Plus Tremelimumab in Non-Small Cell Lung Cancer: A Multicentre, Phase 1b Study. *Lancet Oncol.* 17 (3), 299–308. doi:10.1016/s1470-2045(15)00544-6

Antonia, S. J., Villegas, A., Daniel, D., Vicente, D., Murakami, S., Hui, R., et al. (2017). Durvalumab after Chemoradiotherapy in Stage Iii Non-Small-Cell Lung Cancer. *N. Engl. J. Med.* 377 (20), 1919–1929. doi:10.1056/NEJMoa1709937

Apolo, A. B., Infante, J. R., Balmanoukian, A., Patel, M. R., Wang, D., Kelly, K., et al. (2017). Avelumab, an Anti-Programmed Death-Ligand 1 Antibody, in Patients with Refractory Metastatic Urothelial Carcinoma: Results from a Multicenter, Phase Ib Study. *J. Clin. Oncol.* 35 (19), 2117–2124. doi:10.1200/JCO.2016.71.6795

Armand, P., Rodig, S., Melnichenko, V., Thieblemont, C., Bouabdallah, K., Tumyan, G., et al. (2019). Pembrolizumab in Relapsed or Refractory Primary Mediastinal Large B-Cell Lymphoma. *J. Clin. Oncol.* 37 (34), 3291–3299. doi:10.1200/JCO.19.01389

Balar, A. V., Castellano, D., O'Donnell, P. H., Grivas, P., Vuky, J., Powles, T., et al. (2017). First-Line Pembrolizumab in Cisplatin-Ineligible Patients with Locally Advanced and Unresectable or Metastatic Urothelial Cancer (Keynote-052): A Multicentre, Single-Arm, Phase 2 Study. *Lancet Oncol.* 18 (11), 1483–1492. doi:10.1016/s1470-2045(17)30616-2

Bellmunt, J., de Wit, R., Vaughn, D. J., Fradet, Y., Lee, J.-L., Fong, L., et al. (2017). Pembrolizumab as Second-Line Therapy for Advanced Urothelial Carcinoma. *N. Engl. J. Med.* 376 (11), 1015–1026. doi:10.1056/NEJMoa1613683

Boni, C., Fisicaro, P., Valdatta, C., Amadei, B., Di Vincenzo, P., Giuberti, T., et al. (2007). Characterization of Hepatitis B Virus (HBV)-specific T-Cell Dysfunction in Chronic HBV Infection. *J. Virol.* 81 (8), 4215–4225. doi:10.1128/jvi.02844-06

Borghaei, H., Paz-Ares, L., Horn, L., Spigel, D. R., Steins, M., Ready, N. E., et al. (2015). Nivolumab Versus Docetaxel in Advanced Nonsquamous Non-Small-Cell Lung Cancer. *N. Engl. J. Med.* 373 (17), 1627–1639. doi:10.1056/NEJMoa1507643

Boyiadzis, M. M., Kirkwood, J. M., Marshall, J. L., Pritchard, C. C., Azad, N. S., and Gulley, J. L. (2018). Significance and Implications of Fda Approval of Pembrolizumab for Biomarker-Defined Disease. *J. Immunother. Cancer* 6 (1), 35. doi:10.1186/s40425-018-0342-x

Brahmer, J. R., Drake, C. G., Wollner, I., Powderly, J. D., Picus, J., Sharfman, W. H., et al. (2010). Phase I Study of Single-Agent Anti-Programmed Death-1 (MDX-1106) in Refractory Solid Tumors: Safety, Clinical Activity, Pharmacodynamics, and Immunologic Correlates. *J. Clin. Oncol.* 28 (19), 3167–3175. doi:10.1200/JCO.2009.26.7609

Brahmer, J., Reckamp, K. L., Baas, P., Crinò, L., Eberhardt, W. E. E., Poddubskaya, E., et al. (2015). Nivolumab Versus Docetaxel in Advanced Squamous-Cell Non-Small-Cell Lung Cancer. *N. Engl. J. Med.* 373 (2), 123–135. doi:10.1056/NEJMoa1504627

Chen, R., Zinzani, P. L., Fanale, M. A., Armand, P., Johnson, N. A., Brice, P., et al. (2017). Phase Ii Study of the Efficacy and Safety of Pembrolizumab for Relapsed/Refractory Classic Hodgkin Lymphoma. *J. Clin. Oncol.* 35 (19), 2125–2132. doi:10.1200/JCO.2016.72.1316

Chia, S., Bedard, P. L., Hilton, J., Amir, E., Gelmon, K., Goodwin, R., et al. (2019). A Phase Ib Trial of Durvalumab in Combination with Trastuzumab in HER2-Positive Metastatic Breast Cancer (CCTG IND.229). *Oncol.* 24 (11), 1439–1445. doi:10.1634/theoncologist.2019-0321

Chu, T., Zhong, R., Zhong, H., Zhang, B., Zhang, W., Shi, C., et al. (2021). Phase 1b Study of Sintilimab Plus Anlotinib as First-Line Therapy in Patients with Advanced Nsclc. *J. Thorac. Oncol.* 16 (4), 643–652. doi:10.1016/j.jtho.2020.11.026

Chung, H. C., Ros, W., Delord, J.-P., Perets, R., Italiano, A., Shapira-Frommer, R., et al. (2019). Efficacy and Safety of Pembrolizumab in Previously Treated Advanced Cervical Cancer: Results from the Phase Ii Keynote-158 Study. *J. Clin. Oncol.* 37 (17), 1470–1478. doi:10.1200/JCO.18.01265

Cohen, E. E. W., Soulières, D., Le Tourneau, C., Dinis, J., Licitra, L., Ahn, M.-J., et al. (2019). Pembrolizumab Versus Methotrexate, Docetaxel, or Cetuximab for Recurrent or Metastatic Head-And-Neck Squamous Cell Carcinoma (Keynote-040): A Randomised, Open-Label, Phase 3 Study. *The Lancet* 393 (10167), 156–167. doi:10.1016/s0140-6736(18)31999-8

Das, S., Suarez, G., Beswick, E. J., Sierra, J. C., Graham, D. Y., and Reyes, V. E. (2006). Expression of B7-H1 on Gastric Epithelial Cells: Its Potential Role in Regulating T Cells duringHelicobacter pyloriInfection. *J. Immunol.* 176 (5), 3000–3009. doi:10.4049/jimmunol.176.5.3000

Desai, J., Deva, S., Lee, J. S., Lin, C.-C., Yen, C.-J., Chao, Y., et al. (2020). Phase Ia/Ib Study of Single-Agent Tislelizumab, an Investigational Anti-Pd-1 Antibody, in Solid Tumors. *J. Immunother. Cancer* 8 (1), e000453. doi:10.1136/jitc-2019-000453

Dirix, L. Y., Takacs, I., Jerusalem, G., Nikolinakos, P., Arkenau, H.-T., Forero-Torres, A., et al. (2018). Avelumab, an Anti-Pd-L1 Antibody, in Patients with Locally Advanced or Metastatic Breast Cancer: A Phase 1b Javelin Solid Tumor Study. *Breast Cancer Res. Treat.* 167 (3), 671–686. doi:10.1007/s10549-017-4537-5

Disis, M. L., Taylor, M. H., Kelly, K., Beck, J. T., Gordon, M., Moore, K. M., et al. (2019). Efficacy and Safety of Avelumab for Patients with Recurrent or Refractory Ovarian Cancer. *JAMA Oncol.* 5 (3), 393–401. doi:10.1001/jamaoncol.2018.6258

Dong, H., ZhuTamada, G. K., Tamada, K., and Chen, L. (1999). B7-H1, a Third Member of the B7 Family, Co-stimulates T-Cell Proliferation and Interleukin-10 Secretion. *Nat. Med.* 5, 1365–1369. doi:10.1038/70932

Duan, J., Cui, L., Zhao, X., Bai, H., Cai, S., Wang, G., et al. (2020). Use of Immunotherapy with Programmed Cell Death 1 vs Programmed Cell Death Ligand 1 Inhibitors in Patients with Cancer. *JAMA Oncol.* 6 (3), 375–384. doi:10.1001/jamaoncol.2019.5367

El-Khoueiry, A. B., Sangro, B., Yau, T., Crocenzi, T. S., Kudo, M., Hsu, C., et al. (2017). Nivolumab in Patients with Advanced Hepatocellular Carcinoma (Checkmate 040): An Open-Label, Non-Comparative, Phase 1/2 Dose Escalation and Expansion Trial. *The Lancet* 389 (10088), 2492–2502. doi:10.1016/s0140-6736(17)31046-2

Fang, W., Yang, Y., Ma, Y., Hong, S., Lin, L., He, X., et al. (2018). Camrelizumab (Shr-1210) Alone or in Combination with Gemcitabine Plus Cisplatin for Nasopharyngeal Carcinoma: Results from Two Single-Arm, Phase 1 Trials. *Lancet Oncol.* 19 (10), 1338–1350. doi:10.1016/s1470-2045(18)30495-9

Ferris, R. L., Blumenschein, G., Jr., Fayette, J., Guigay, J., Colevas, A. D., Licitra, L., et al. (2016). Nivolumab for Recurrent Squamous-Cell Carcinoma of the Head and Neck. *N. Engl. J. Med.* 375 (19), 1856–1867. doi:10.1056/NEJMoa1602252

Ferris, R. L., Haddad, R., Even, C., Tahara, M., Dvorkin, M., Ciuleanu, T. E., et al. (2020). Durvalumab with or without Tremelimumab in Patients with Recurrent or Metastatic Head and Neck Squamous Cell Carcinoma: Eagle, a Randomized, Open-Label Phase Iii Study. *Ann. Oncol.* 31 (7), 942–950. doi:10.1016/j.annonc.2020.04.001

Finn, R. S., Qin, S., Ikeda, M., Galle, P. R., Ducreux, M., Kim, T.-Y., et al. (2020a). Atezolizumab Plus Bevacizumab in Unresectable Hepatocellular Carcinoma. *N. Engl. J. Med.* 382 (20), 1894–1905. doi:10.1056/NEJMoa1915745

Finn, R. S., Ryoo, B.-Y., Merle, P., Kudo, M., Bouattour, M., Lim, H. Y., et al. (2020b). Pembrolizumab as Second-Line Therapy in Patients with Advanced Hepatocellular Carcinoma in Keynote-240: A Randomized, Double-Blind, Phase Iii Trial. *J. Clin. Oncol.* 38 (3), 193–202. doi:10.1200/JCO.19.01307

Francisco, L. M., Sage, P. T., and Sharpe, A. H. (2010). The PD-1 Pathway in Tolerance and Autoimmunity. *Immunol. Rev.* 236, 219–242. doi:10.1111/j.1600-065X.2010.00923.x

Fuchs, C. S., Doi, T., Jang, R. W., Muro, K., Satoh, T., Machado, M., et al. (2018). Safety and Efficacy of Pembrolizumab Monotherapy in Patients with Previously Treated Advanced Gastric and Gastroesophageal Junction Cancer. *JAMA Oncol.* 4 (5), e180013. doi:10.1001/jamaoncol.2018.0013

Furuya, N., Nishino, M., Wakuda, K., Ikeda, S., Sato, T., Ushio, R., et al. (2021). Real-world Efficacy of Atezolizumab in Non-small Cell Lung Cancer: A Multicenter Cohort Study Focused on Performance Status and Retreatment after Failure of Anti- PD -1 Antibody. *Thorac. Cancer* 12 (5), 613–618. doi:10.1111/1759-7714.13824

Gadgeel, S. M., Pennell, N. A., Fidler, M. J., Halmos, B., Bonomi, P., Stevenson, J., et al. (2018). Phase Ii Study of Maintenance Pembrolizumab in Patients with Extensive-Stage Small Cell Lung Cancer (Sclc). *J. Thorac. Oncol.* 13 (9), 1393–1399. doi:10.1016/j.jtho.2018.05.002

Galsky, M. D., Arija, J. Á. A., Bamias, A., Davis, I. D., De Santis, M., Kikuchi, E., et al. (2020). Atezolizumab with or without Chemotherapy in Metastatic Urothelial Cancer (Imvigor130): A Multicentre, Randomised, Placebo-Controlled Phase 3 Trial. *The Lancet* 395 (10236), 1547–1557. doi:10.1016/s0140-6736(20)30230-0

Gandhi, L., Rodríguez-Abreu, D., Gadgeel, S., Esteban, E., Felip, E., De Angelis, F., et al. (2018). Pembrolizumab Plus Chemotherapy in Metastatic Non-Small-Cell Lung Cancer. *N. Engl. J. Med.* 378 (22), 2078–2092. doi:10.1056/NEJMoa1801005

Gane, E., Verdon, D. J., Brooks, A. E., Gaggar, A., Nguyen, A. H., Subramanian, G. M., et al. (2019). Anti-PD-1 Blockade with Nivolumab with and without Therapeutic Vaccination for Virally Suppressed Chronic Hepatitis B: A Pilot Study. *J. Hepatol.* 71 (5), 900–907. doi:10.1016/j.jhep.2019.06.028

Garon, E. B., Rizvi, N. A., Hui, R., Leighl, N., Balmanoukian, A. S., Eder, J. P., et al. (2015). Pembrolizumab for the Treatment of Non-Small-Cell Lung Cancer. *N. Engl. J. Med.* 372 (21), 2018–2028. doi:10.1056/NEJMoa1501824

Grob, J.-J., Gonzalez, R., Basset-Seguin, N., Vornicova, O., Schachter, J., Joshi, A., et al. (2020). Pembrolizumab Monotherapy for Recurrent or Metastatic Cutaneous Squamous Cell Carcinoma: A Single-Arm Phase Ii Trial (Keynote-629). *J. Clin. Oncol.* 38 (25), 2916–2925. doi:10.1200/JCO.19.03054

Gulley, J. L., Rajan, A., Spigel, D. R., Iannotti, N., Chandler, J., Wong, D. J. L., et al. (2017). Avelumab for Patients with Previously Treated Metastatic or Recurrent Non-Small-Cell Lung Cancer (Javelin Solid Tumor): Dose-Expansion Cohort of a Multicentre, Open-Label, Phase 1b Trial. *Lancet Oncol.* 18 (5), 599–610. doi:10.1016/s1470-2045(17)30240-1

Gutzmer, R., Stroyakovskiy, D., Gogas, H., Robert, C., Lewis, K., Protsenko, S., et al. (2020). Atezolizumab, Vemurafenib, and Cobimetinib as First-Line Treatment for Unresectable Advanced Brafv600 Mutation-Positive Melanoma (Imspire150): Primary Analysis of the Randomised, Double-Blind, Placebo-Controlled, Phase 3 Trial. *The Lancet* 395 (10240), 1835–1844. doi:10.1016/s0140-6736(20)30934-x

Hamid, O., Robert, C., Daud, A., Hodi, F. S., Hwu, W.-J., Kefford, R., et al. (2013). Safety and Tumor Responses with Lambrolizumab (Anti-Pd-1) in Melanoma. *N. Engl. J. Med.* 369 (2), 134–144. doi:10.1056/NEJMoa1305133

Hassan, R., Thomas, A., Nemunaitis, J. J., Patel, M. R., Bennouna, J., Chen, F. L., et al. (2019). Efficacy and Safety of Avelumab Treatment in Patients with Advanced Unresectable Mesothelioma. *JAMA Oncol.* 5 (3), 351–357. doi:10.1001/jamaoncol.2018.5428

Hellmann, M. D., Paz-Ares, L., Bernabe Caro, R., Zurawski, B., Kim, S.-W., Carcereny Costa, E., et al. (2019). Nivolumab Plus Ipilimumab in Advanced Non-Small-Cell Lung Cancer. *N. Engl. J. Med.* 381 (21), 2020–2031. doi:10.1056/NEJMoa1910231

Herbst, R. S., Baas, P., Kim, D.-W., Felip, E., Pérez-Gracia, J. L., Han, J.-Y., et al. (2016). Pembrolizumab Versus Docetaxel for Previously Treated, Pd-L1-Positive, Advanced Non-Small-Cell Lung Cancer (Keynote-010): A Randomised Controlled Trial. *The Lancet* 387 (10027), 1540–1550. doi:10.1016/s0140-6736(15)01281-7

Herbst, R. S., Giaccone, G., de Marinis, F., Reinmuth, N., Vergnenegre, A., Barrios, C. H., et al. (2020). Atezolizumab for First-Line Treatment of Pd-L1-Selected Patients with Nsclc. *N. Engl. J. Med.* 383 (14), 1328–1339. doi:10.1056/NEJMoa1917346

Herrera, A. F., Goy, A., Mehta, A., Ramchandren, R., Pagel, J. M., Svoboda, J., et al. (2020). Safety and Activity of Ibrutinib in Combination with Durvalumab in Patients with Relapsed or Refractory Follicular Lymphoma or Diffuse Large B-cell Lymphoma. *Am. J. Hematol.* 95 (1), 18–27. doi:10.1002/ajh.25659

Hofmeyer, K. A., Jeon, H., and Zang, X. (2011). The PD-1/PD-L1 (B7-H1) Pathway in Chronic Infection-Induced Cytotoxic T Lymphocyte Exhaustion. *J. Biomed. Biotechnol.* 2011, 1–9. doi:10.1155/2011/451694

Horn, L., Mansfield, A. S., Szczęsna, A., Havel, L., Krzakowski, M., Hochmair, M. J., et al. (2018). First-Line Atezolizumab Plus Chemotherapy in Extensive-Stage Small-Cell Lung Cancer. *N. Engl. J. Med.* 379 (23), 2220–2229. doi:10.1056/NEJMoa1809064

Huang, J., Mo, H., Zhang, W., Chen, X., Qu, D., Wang, X., et al. (2019). Promising Efficacy of SHR-1210, a Novel Anti-programmed Cell Death 1 Antibody, in Patients with Advanced Gastric and Gastroesophageal junction Cancer in China. *Cancer* 125 (5), 742–749. doi:10.1002/cncr.31855

Huang, J., Xu, J., Chen, Y., Zhuang, W., Zhang, Y., Chen, Z., et al. (2020). Camrelizumab Versus Investigator's Choice of Chemotherapy as Second-Line Therapy for Advanced or Metastatic Oesophageal Squamous Cell Carcinoma (Escort): A Multicentre, Randomised, Open-Label, Phase 3 Study. *Lancet Oncol.* 21 (6), 832–842. doi:10.1016/s1470-2045(20)30110-8

Jiang, H., Zheng, Y., Qian, J., Mao, C., Xu, X., Li, N., et al. (2020). Safety and Efficacy of Sintilimab Combined with Oxaliplatin/Capecitabine as First-Line Treatment in Patients with Locally Advanced or Metastatic Gastric/Gastroesophageal Junction Adenocarcinoma in a Phase Ib Clinical Trial. *BMC Cancer* 20 (1), 760. doi:10.1186/s12885-020-07251-z

Jiang, H., Zheng, Y., Qian, J., Mao, C., Xu, X., Li, N., et al. (2021). Efficacy and Safety of Sintilimab in Combination with Chemotherapy in Previously Untreated Advanced or Metastatic Nonsquamous or Squamous Nsclc: Two Cohorts of an Open-Label, Phase 1b Study. *Cancer Immunol. Immunother.* 70 (3), 857–868. doi:10.1007/s00262-020-02738-x

Jurado, J. O., Alvarez, I. B., Pasquinelli, V., Martínez, G. J., Quiroga, M. F., Abbate, E., et al. (2008). Programmed Death (PD)-1:PD-ligand 1/PD-Ligand 2 Pathway Inhibits T Cell Effector Functions during Human Tuberculosis. *J. Immunol.* 181, 116–125. doi:10.4049/jimmunol.181.1.116

Kato, K., Cho, B. C., Takahashi, M., Okada, M., Lin, C.-Y., Chin, K., et al. (2019). Nivolumab Versus Chemotherapy in Patients with Advanced Oesophageal Squamous Cell Carcinoma Refractory or Intolerant to Previous Chemotherapy (Attraction-3): A Multicentre, Randomised, Open-Label, Phase 3 Trial. *Lancet Oncol.* 20 (11), 1506–1517. doi:10.1016/s1470-2045(19)30626-6

Kaufman, H. L., Russell, J., Hamid, O., Bhatia, S., Terheyden, P., D'Angelo, S. P., et al. (2016). Avelumab in Patients with Chemotherapy-Refractory Metastatic Merkel Cell Carcinoma: A Multicentre, Single-Group, Open-Label, Phase 2 Trial. *Lancet Oncol.* 17 (10), 1374–1385. doi:10.1016/s1470-2045(16)30364-3

Kay, A. W., Strauss-Albee, D. M., and Blish, C. A. (2016). Application of Mass Cytometry (CyTOF) for Functional and Phenotypic Analysis of Natural Killer Cells. *Methods Mol. Biol.(Clifton, N.J.)*, 1441, 13–26. doi:10.1007/978-1-4939-3684-7_2

Keilholz, U., Mehnert, J. M., Bauer, S., Bourgeois, H., Patel, M. R., Gravenor, D., et al. (2019). Avelumab in Patients with Previously Treated Metastatic Melanoma: Phase 1b Results from the Javelin Solid Tumor Trial. *J. Immunother. Cancer* 7 (1), 12. doi:10.1186/s40425-018-0459-y

Keir, M. E., Butte, M. J., Freeman, G. J., and Sharpe, A. H. (2008). PD-1 and its Ligands in Tolerance and Immunity. *Annu. Rev. Immunol.* 26, 677–704. doi:10.1146/annurev.immunol.26.021607.090331

Kelly, R. J., Lee, J., Bang, Y.-J., Almhanna, K., Blum Murphy, M., Catenacci, D. V. T., et al. (2020). Safety and Efficacy of Durvalumab and Tremelimumab Alone or in Combination in Patients with Advanced Gastric and Gastroesophageal Junction Adenocarcinoma. *Clin. Cancer Res.* 26 (4), 846–854. doi:10.1158/1078-0432.CCR-19-2443

Kojima, T., Shah, M. A., Muro, K., Francois, E., Adenis, A., Hsu, C.-H., et al. (2020). Randomized Phase Iii Keynote-181 Study of Pembrolizumab Versus Chemotherapy in Advanced Esophageal Cancer. *J. Clin. Oncol.* 38 (35), 4138–4148. doi:10.1200/JCO.20.01888

Kozako, T., Yoshimitsu, M., Fujiwara, H., Masamoto, I., Horai, S., White, Y., et al. (2009). PD-1/PD-L1 Expression in Human T-Cell Leukemia Virus Type 1 Carriers and Adult T-Cell Leukemia/lymphoma Patients. *Leukemia* 23 (2), 375–382. doi:10.1038/leu.2008.272

Kozako, T., Yoshimitsu, M., Akimoto, M., White, Y., Matsushita, K., Soeda, S., et al. (2011). Programmed Death-1 (PD-1)/PD-1 Ligand Pathway-Mediated Immune Responses against Human T-Lymphotropic Virus Type 1 (HTLV-1) in HTLV-1-Associated Myelopathy/tropical Spastic Paraparesis and Carriers with Autoimmune Disorders. *Hum. Immunol.* 72 (11), 1001–1006. pmid: 21851845. doi:10.1016/j.humimm.2011.07.308

Larkin, J., Chiarion-Sileni, V., Gonzalez, R., Grob, J. J., Cowey, C. L., Lao, C. D., et al. (2015). Combined Nivolumab and Ipilimumab or Monotherapy in Untreated Melanoma. *N. Engl. J. Med.* 373 (1), 23–34. doi:10.1056/NEJMoa1504030

Le, D. T., Kim, T. W., Van Cutsem, E., Geva, R., Jäger, D., Hara, H., et al. (2020). Phase II Open-Label Study of Pembrolizumab in Treatment-Refractory, Microsatellite Instability-High/Mismatch Repair-Deficient Metastatic Colorectal Cancer: KEYNOTE-164. *J. Clin. Oncol.* 38 (1), 11–19. doi:10.1200/JCO.19.02107

Le Tourneau, C., Hoimes, C., Zarwan, C., Wong, D. J., Bauer, S., Claus, R., et al. (2018). Avelumab in Patients with Previously Treated Metastatic Adrenocortical Carcinoma: Phase 1b Results from the Javelin Solid Tumor Trial. *J. Immunother. Cancer* 6 (1), 111. doi:10.1186/s40425-018-0424-9

Loibl, S., Untch, M., Burchardi, N., Huober, J., Sinn, B. V., Blohmer, J.-U., et al. (2019). A Randomised Phase Ii Study Investigating Durvalumab in Addition to an Anthracycline Taxane-Based Neoadjuvant Therapy in Early Triple-Negative Breast Cancer: Clinical Results and Biomarker Analysis of Geparnuevo Study. *Ann. Oncol.* 30 (8), 1279–1288. doi:10.1093/annonc/mdz158/5490226

Lu, M., Zhang, P., Zhang, Y., Li, Z., Gong, J.-f., Li, J., et al. (2020). Efficacy, Safety and Biomarkers of Toripalimab in Patients with Recurrent or Metastatic Neuroendocrine Neoplasms: a Multiple-center Phase Ib Trial. *Clin. Cancer Res.* 26 (10), 2337–2345. doi:10.1158/1078-0432.CCR-19-4000

Mahoney, K. M., Rennert, P. D., and Freeman, G. J. (2015). Combination Cancer Immunotherapy and New Immunomodulatory Targets. *Nat. Rev. Drug Discov.* 14, 561–584. doi:10.1038/nrd4591

Makuku, R., Khalili, N., Razi, S., Keshavarz-Fathi, M., and Rezaei, N. (2021). Current and Future Perspectives of PD-1/PDL-1 Blockade in Cancer Immunotherapy. *J. Immunol. Res.*, 6661406. doi:10.1155/2021/6661406

McDermott, D. F., and Atkins, M. B. (2013). PD -1 as a Potential Target in Cancer Therapy. *Cancer Med.* 2 (5), 662–673. doi:10.1002/cam4.106

Mei, Q., Zhang, W., Liu, Y., Yang, Q., Rasko, J. E. J., Nie, J., et al. (2020). Camrelizumab Plus Gemcitabine, Vinorelbine, and Pegylated Liposomal Doxorubicin in Relapsed/Refractory Primary Mediastinal B-Cell Lymphoma: A Single-Arm, Open-Label, Phase Ii Trial. *Clin. Cancer Res.* 26 (17), 4521–4530. doi:10.1158/1078-0432.CCR-20-0514

Mencoboni, M., Ceppi, M., Bruzzone, M., Taveggia, P., Cavo, A., Scordamaglia, F., et al. (2021). Effectiveness and Safety of Immune Checkpoint Inhibitors for Patients with Advanced Non Small-Cell Lung Cancer in Real-World: Review and Meta-Analysis. *Cancers* 13 (6), 1388. doi:10.3390/cancers13061388

Migden, M. R., Rischin, D., Schmults, C. D., Guminski, A., Hauschild, A., Lewis, K. D., et al. (2018). Pd-1 Blockade with Cemiplimab in Advanced Cutaneous Squamous-Cell Carcinoma. *N. Engl. J. Med.* 379 (4), 341–351. doi:10.1056/NEJMoa1805131

Migden, M. R., Khushalani, N. I., Chang, A. L. S., Lewis, K. D., Schmults, C. D., Hernandez-Aya, L., et al. (2020). Cemiplimab in Locally Advanced Cutaneous Squamous Cell Carcinoma: Results from an Open-Label, Phase 2, Single-Arm Trial. *Lancet Oncol.* 21 (2), 294–305. doi:10.1016/s1470-2045(19)30728-4

Mo, H., Huang, J., Xu, J., Chen, X., Wu, D., Qu, D., et al. (2018). Safety, Anti-Tumour Activity, and Pharmacokinetics of Fixed-Dose Shr-1210, an Anti-Pd-1 Antibody in Advanced Solid Tumours: A Dose-Escalation, Phase 1 Study. *Br. J. Cancer* 119 (5), 538–545. doi:10.1038/s41416-018-0100-3

Moser, J. C., Wei, G., Colonna, S. V., Grossmann, K. F., Patel, S., and Hyngstrom, J. R. (2020). Comparative-Effectiveness of Pembrolizumab Vs. Nivolumab for Patients with Metastatic Melanoma. *Acta Oncologica* 59 (4), 434–437. doi:10.1080/0284186X.2020.1712473

Motzer, R. J., Escudier, B., McDermott, D. F., George, S., Hammers, H. J., Srinivas, S., et al. (2015). Nivolumab Versus Everolimus in Advanced Renal-Cell Carcinoma. *N. Engl. J. Med.* 373 (19), 1803–1813. doi:10.1056/NEJMoa1510665

Motzer, R. J., Tannir, N. M., McDermott, D. F., Arén Frontera, O., Melichar, B., Choueiri, T. K., et al. (2018). Nivolumab Plus Ipilimumab Versus Sunitinib in Advanced Renal-Cell Carcinoma. *N. Engl. J. Med.* 378 (14), 1277–1290. doi:10.1056/NEJMoa1712126

Motzer, R. J., Penkov, K., Haanen, J., Rini, B., Albiges, L., Campbell, M. T., et al. (2019). Avelumab Plus Axitinib Versus Sunitinib for Advanced Renal-Cell Carcinoma. *N. Engl. J. Med.* 380 (12), 1103–1115. doi:10.1056/NEJMoa1816047

Muro, K., Chung, H. C., Shankaran, V., Geva, R., Catenacci, D., Gupta, S., et al. (2016). Pembrolizumab for Patients with Pd-L1-Positive Advanced Gastric Cancer (Keynote-012): A Multicentre, Open-Label, Phase 1b Trial. *Lancet Oncol.* 17 (6), 717–726. doi:10.1016/s1470-2045(16)00175-3

Nanda, R., Chow, L. Q. M., Dees, E. C., Berger, R., Gupta, S., Geva, R., et al. (2016). Pembrolizumab in Patients with Advanced Triple-Negative Breast Cancer: Phase Ib Keynote-012 Study. *J. Clin. Oncol.* 34 (21), 2460–2467. doi:10.1200/JCO.2015.64.8931

Nghiem, P., Bhatia, S., Lipson, E. J., Sharfman, W. H., Kudchadkar, R. R., Brohl, A. S., et al. (2019). Durable Tumor Regression and Overall Survival in Patients with Advanced Merkel Cell Carcinoma Receiving Pembrolizumab as First-Line Therapy. *J. Clin. Oncol.* 37 (9), 693–702. doi:10.1200/JCO.18.01896

Niglio, S. A., Jia, R., Ji, J., Ruder, S., Patel, V. G., Martini, A., et al. (2019). Programmed Death-1 or Programmed Death Ligand-1 Blockade in Patients with Platinum-Resistant Metastatic Urothelial Cancer: A Systematic Review and Meta-Analysis. *Eur. Urol.* 76 (6), 782–789. doi:10.1016/j.eururo.2019.05.037

Nicholas, K. J., Zern, E. K., Barnett, L., Smith, R. M., Lorey, S. L., and Copeland, C. A. (2013). B Cell Responses to HIV ANTIGen are A Potent Correlate of Viremia in HIV-1 Infection and Improve With PD-1 Blockade. *PLoS One*, 8, e84185. doi:10.1371/journal.pone.0084185

Nowak, A. K., Lesterhuis, W. J., Kok, P.-S., Brown, C., Hughes, B. G., Karikios, D. J., et al. (2020). Durvalumab with First-Line Chemotherapy in Previously Untreated Malignant Pleural Mesothelioma (Dream): A Multicentre, Single-Arm, Phase 2 Trial with a Safety Run-In. *Lancet Oncol.* 21 (9), 1213–1223. doi:10.1016/s1470-2045(20)30462-9

Okazaki, T., Maeda, A., Nishimura, H., Kurosaki, T., and Honjo, T. (2001). PD-1 Immunoreceptor Inhibits B Cell Receptor-Mediated Signaling by Recruiting Src Homology 2-Domain-Containing Tyrosine Phosphatase 2 to Phosphotyrosine. *Proc. Natl. Acad. Sci.* 98 (24), 13866–13871. doi:10.1073/pnas.231486598

Overman, M. J., McDermott, R., Leach, J. L., Lonardi, S., Lenz, H.-J., Morse, M. A., et al. (2017). Nivolumab in Patients with Metastatic DNA Mismatch Repair-Deficient or Microsatellite Instability-High Colorectal Cancer (Checkmate 142): An Open-Label, Multicentre, Phase 2 Study. *Lancet Oncol.* 18 (9), 1182–1191. doi:10.1016/s1470-2045(17)30422-9

Overman, M. J., Lonardi, S., Wong, K. Y. M., Lenz, H.-J., Gelsomino, F., Aglietta, M., et al. (2018). Durable Clinical Benefit with Nivolumab Plus Ipilimumab in DNA Mismatch Repair-Deficient/Microsatellite Instability-High Metastatic Colorectal Cancer. *J. Clin. Oncol.* 36 (8), 773–779. doi:10.1200/JCO.2017.76.9901

Paris, R. M., Petrovas, C., Ferrando-Martinez, S., Moysi, E., Boswell, K. L., Archer, E., et al. (2015). PD-1 Expression on HIV-specific T Cells Is Associated with T-Cell Exhaustion and Disease Progression. *PLoS One* 10 (12), e0144767. doi:10.1371/journal.pone.0144767

Passiglia, F., Galvano, A., Rizzo, S., Incorvaia, L., Listì, A., Bazan, V., et al. (2018). Looking for the Best Immune-Checkpoint Inhibitor in Pre-Treated Nsclc Patients: An Indirect Comparison between Nivolumab, Pembrolizumab and Atezolizumab. *Int. J. Cancer* 142 (6), 1277–1284. doi:10.1002/ijc.31136

Patsoukis, N., Brown, J., Petkova, V., Liu, F., Li, L., and Boussiotis, V. A. (2012). Selective Effects of PD-1 on Akt and Ras Pathways Regulate Molecular Components of the Cell Cycle and Inhibit T Cell Proliferation. *Sci. Signal.* 5, 46. doi:10.1126/scisignal.2002796

Paz-Ares, L., Dvorkin, M., Chen, Y., Reinmuth, N., Hotta, K., Trukhin, D., et al. (2019). Durvalumab Plus Platinum-Etoposide versus Platinum-Etoposide in First-Line Treatment of Extensive-Stage Small-Cell Lung Cancer (CASPIAN): a Randomised, Controlled, Open-Label, Phase 3 Trial. *Lancet* 394 (10212), 1929–1939. doi:10.1016/S0140-6736(19)32222-6

Paz-Ares, L., Ciuleanu, T.-E., Cobo, M., Schenker, M., Zurawski, B., Menezes, J., et al. (2021). First-Line Nivolumab Plus Ipilimumab Combined with Two Cycles of Chemotherapy in Patients with Non-Small-Cell Lung Cancer

(Checkmate 9la): An International, Randomised, Open-Label, Phase 3 Trial. *Lancet Oncol.* 22 (2), 198–211. doi:10.1016/S1470-2045(20)30641-0

Planchard, D., Reinmuth, N., Orlov, S., Fischer, J. R., Sugawara, S., Mandziuk, S., et al. (2020). Arctic: Durvalumab with or without Tremelimumab as Third-Line or Later Treatment of Metastatic Non-Small-Cell Lung Cancer. *Ann. Oncol.* 31 (5), 609–618. doi:10.1016/j.annonc.2020.02.006

Plimack, E. R., Bellmunt, J., Gupta, S., Berger, R., Chow, L. Q. M., Juco, J., et al. (2017). Safety and Activity of Pembrolizumab in Patients with Locally Advanced or Metastatic Urothelial Cancer (Keynote-012): A Non-Randomised, Open-Label, Phase 1b Study. *Lancet Oncol.* 18 (2), 212–220. doi:10.1016/s1470-2045(17)30007-4

Powles, T., O'Donnell, P. H., Massard, C., Arkenau, H.-T., Friedlander, T. W., Hoimes, C. J., et al. (2017). Efficacy and Safety of Durvalumab in Locally Advanced or Metastatic Urothelial Carcinoma. *JAMA Oncol.* 3 (9), e172411. doi:10.1001/jamaoncol.2017.2411

Powles, T., Durán, I., van der Heijden, M. S., Loriot, Y., Vogelzang, N. J., De Giorgi, U., et al. (2018). Atezolizumab Versus Chemotherapy in Patients with Platinum-Treated Locally Advanced or Metastatic Urothelial Carcinoma (Imvigor211): A Multicentre, Open-Label, Phase 3 Randomised Controlled Trial. *The Lancet* 391 (10122), 748–757. doi:10.1016/s0140-6736(17)33297-x

Powles, T., van der Heijden, M. S., Castellano, D., Galsky, M. D., Loriot, Y., Petrylak, D. P., et al. (2020a). Durvalumab Alone and Durvalumab Plus Tremelimumab Versus Chemotherapy in Previously Untreated Patients with Unresectable, Locally Advanced or Metastatic Urothelial Carcinoma (Danube): A Randomised, Open-Label, Multicentre, Phase 3 Trial. *Lancet Oncol.* 21 (12), 1574–1588. doi:10.1016/s1470-2045(20)30541-6

Powles, T., Park, S. H., Voog, E., Caserta, C., Valderrama, B. P., Gurney, H., et al. (2020b). Avelumab Maintenance Therapy for Advanced or Metastatic Urothelial Carcinoma. *N. Engl. J. Med.* 383 (13), 1218–1230. doi:10.1056/NEJMoa2002788

Qin, S., Ren, Z., Meng, Z., Chen, Z., Chai, X., Xiong, J., et al. (2020). Camrelizumab in Patients with Previously Treated Advanced Hepatocellular Carcinoma: A Multicentre, Open-Label, Parallel-Group, Randomised, Phase 2 Trial. *Lancet Oncol.* 21 (4), 571–580. doi:10.1016/s1470-2045(20)30011-5

Ready, N., Farago, A. F., de Braud, F., Atmaca, A., Hellmann, M. D., Schneider, J. G., et al. (2019). Third-Line Nivolumab Monotherapy in Recurrent Sclc: Checkmate 032. *J. Thorac. Oncol.* 14 (2), 237–244. doi:10.1016/j.jtho.2018.10.003

Reck, M., Rodríguez-Abreu, D., Robinson, A. G., Hui, R., Csőszi, T., Fülöp, A., et al. (2016). Pembrolizumab Versus Chemotherapy for Pd-L1-Positive Non-Small-Cell Lung Cancer. *N. Engl. J. Med.* 375 (19), 1823–1833. doi:10.1056/NEJMoa1606774

Ribas, A., Puzanov, I., Dummer, R., Schadendorf, D., Hamid, O., Robert, C., et al. (2015). Pembrolizumab Versus Investigator-Choice Chemotherapy for Ipilimumab-Refractory Melanoma (Keynote-002): A Randomised, Controlled, Phase 2 Trial. *Lancet Oncol.* 16 (8), 908–918. doi:10.1016/s1470-2045(15)00083-2

Rini, B. I., Plimack, E. R., Stus, V., Gafanov, R., Hawkins, R., Nosov, D., et al. (2019). Pembrolizumab Plus Axitinib Versus Sunitinib for Advanced Renal-Cell Carcinoma. *N. Engl. J. Med.* 380 (12), 1116–1127. doi:10.1056/NEJMoa1816714

Rischin, D., Migden, M. R., Lim, A. M., Schmults, C. D., Khushalani, N. I., Hughes, B. G. M., et al. (2020). Phase 2 Study of Cemiplimab in Patients with Metastatic Cutaneous Squamous Cell Carcinoma: Primary Analysis of Fixed-Dosing, Long-Term Outcome of Weight-Based DosingLid - 10.1136/Jitc-2020-000775 [Doi] Lid - E000775. *J. Immunother. Cancer* 8 (1), e000775. doi:10.1136/jitc-2020-000775

Rittmeyer, A., Barlesi, F., Waterkamp, D., Park, K., Ciardiello, F., von Pawel, J., et al. (2017). Atezolizumab Versus Docetaxel in Patients with Previously Treated Non-Small-Cell Lung Cancer (Oak): A Phase 3, Open-Label, Multicentre Randomised Controlled Trial. *The Lancet* 389 (10066), 255–265. doi:10.1016/s0140-6736(16)32517-x

Robert, C., Ribas, A., Wolchok, J. D., Hodi, F. S., Hamid, O., Kefford, R., et al. (2014). Anti-Programmed-Death-Receptor-1 Treatment with Pembrolizumab in Ipilimumab-Refractory Advanced Melanoma: A Randomised Dose-Comparison Cohort of a Phase 1 Trial. *The Lancet* 384 (9948), 1109–1117. doi:10.1016/s0140-6736(14)60958-2

Robert, C., Long, G. V., Brady, B., Dutriaux, C., Maio, M., Mortier, L., et al. (2015a). Nivolumab in Previously Untreated Melanoma without BRAF Mutation. *N. Engl. J. Med.* 372 (4), 320–330. doi:10.1056/NEJMoa1412082

Robert, C., Schachter, J., Long, G. V., Arance, A., Grob, J. J., Mortier, L., et al. (2015b). Pembrolizumab Versus Ipilimumab in Advanced Melanoma. *N. Engl. J. Med.* 372 (26), 2521–2532. doi:10.1056/NEJMoa1503093

Rosenberg, J. E., Hoffman-Censits, J., Powles, T., van der Heijden, M. S., Balar, A. V., Necchi, A., et al. (2016). Atezolizumab in Patients with Locally Advanced and Metastatic Urothelial Carcinoma Who Have Progressed Following Treatment with Platinum-Based Chemotherapy: A Single-Arm, Multicentre, Phase 2 Trial. *The Lancet* 387 (10031), 1909–1920. doi:10.1016/s0140-6736(16)00561-4

Scherpereel, A., Mazieres, J., Greillier, L., Lantuejoul, S., Dô, P., Bylicki, O., et al. (2019). Nivolumab or Nivolumab Plus Ipilimumab in Patients with Relapsed Malignant Pleural Mesothelioma (Ifct-1501 Maps2): A Multicentre, Open-Label, Randomised, Non-Comparative, Phase 2 Trial. *Lancet Oncol.* 20 (2), 239–253. doi:10.1016/s1470-2045(18)30765-4

Schmid, P., Adams, S., Rugo, H. S., Schneeweiss, A., Barrios, C. H., Iwata, H., et al. (2018). Atezolizumab and Nab-Paclitaxel in Advanced Triple-Negative Breast Cancer. *N. Engl. J. Med.* 379 (22), 2108–2121. doi:10.1056/NEJMoa1809615

Seiwert, T. Y., Burtness, B., Mehra, R., Weiss, J., Berger, R., Eder, J. P., et al. (2016). Safety and Clinical Activity of Pembrolizumab for Treatment of Recurrent or Metastatic Squamous Cell Carcinoma of the Head and Neck (Keynote-012): An Open-Label, Multicentre, Phase 1b Trial. *Lancet Oncol.* 17 (7), 956–965. doi:10.1016/s1470-2045(16)30066-3

Sezer, A., Kilickap, S., Gümüş, M., Bondarenko, I., Özgüroğlu, M., Gogishvili, M., et al. (2021). Cemiplimab Monotherapy for First-Line Treatment of Advanced Non-Small-Cell Lung Cancer with Pd-L1 of at Least 50%: A Multicentre, Open-Label, Global, Phase 3, Randomised, Controlled Trial. *Lancet* 397 (10274), 592–604. doi:10.1016/S0140-6736(21)00228-2

Sharma, P., Retz, M., Siefker-Radtke, A., Baron, A., Necchi, A., Bedke, J., et al. (2017). Nivolumab in Metastatic Urothelial Carcinoma after Platinum Therapy (Checkmate 275): A Multicentre, Single-Arm, Phase 2 Trial. *Lancet Oncol.* 18 (3), 312–322. doi:10.1016/s1470-2045(17)30065-7

Shen, L., Guo, J., Zhang, Q., Pan, H., Yuan, Y., Bai, Y., et al. (2020). Tislelizumab in Chinese Patients with Advanced Solid Tumors: An Open-Label, Non-Comparative, Phase 1/2 Study. *J. Immunother. Cancer* 8 (1), e000437. doi:10.1136/jitc-2019-000437

Sheng, X., Yan, X., Chi, Z., Si, L., Cui, C., Tang, B., et al. (2019). Axitinib in Combination with Toripalimab, a Humanized Immunoglobulin G4 Monoclonal Antibody against Programmed Cell Death-1, in Patients with Metastatic Mucosal Melanoma: An Open-Label Phase Ib Trial. *J. Clin. Oncol.* 37 (32), 2987–2999. doi:10.1200/JCO.19.00210

Shi, Y., Su, H., Song, Y., Jiang, W., Sun, X., Qian, W., et al. (2019). Safety and Activity of Sintilimab in Patients with Relapsed or Refractory Classical Hodgkin Lymphoma (Orient-1): A Multicentre, Single-Arm, Phase 2 Trial. *Lancet Haematol.* 6 (1), e12–e19. doi:10.1016/s2352-3026(18)30192-3

Song, Y., Gao, Q., Zhang, H., Fan, L., Zhou, J., Zou, D., et al. (2019a). Treatment of Relapsed or Refractory Classical Hodgkin Lymphoma with the Anti-Pd-1, Tislelizumab: Results of a Phase 2, Single-Arm, Multicenter Study. *Leukemia* 34 (2), 533–542. doi:10.1038/s41375-019-0545-2

Song, Y., Wu, J., Chen, X., Lin, T., Cao, J., Liu, Y., et al. (2019b). A Single-Arm, Multicenter, Phase Ii Study of Camrelizumab in Relapsed or Refractory Classical Hodgkin Lymphoma. *Clin. Cancer Res.* 25 (24), 7363–7369. doi:10.1158/1078-0432.ccr-19-1680

Sun, Z., Fourcade, J., Pagliano, O., Chauvin, J. M., Sander, C., and Kirkwood, J. M. (2015). IL10 and PD-1 Cooperate to Limit the Activity of Tumor-specific D8+ T Cells. *Cancer Res.* 75, 1635–1644. doi:10.1158/0008-5472.CAN-14-3016

Tang, B., Yan, X., Sheng, X., Si, L., Cui, C., Kong, Y., et al. (2019). Safety and Clinical Activity with an Anti-Pd-1 Antibody Js001 in Advanced Melanoma or Urologic Cancer Patients. *J. Hematol. Oncol.* 12 (1), 7. doi:10.1186/s13045-018-0693-2

Tang, B., Chi, Z., Chen, Y., Liu, X., Wu, D., Chen, J., et al. (2020). Safety, Efficacy, and Biomarker Analysis of Toripalimab in Previously Treated Advanced Melanoma: Results of the Polaris-01 Multicenter Phase Ii Trial. *Clin. Cancer Res.* 26 (15), 4250–4259. doi:10.1158/1078-0432.CCR-19-3922

Taube, J. M., Anders, R. A., Young, G. D., Xu, H., Sharma, R., McMiller, T. L., et al. (2012). Colocalization of Inflammatory Response with B7-H1 Expression in Human Melanocytic Lesions Supports an Adaptive Resistance Mechanism of Immune Escape. *Sci. Translational Med.* 4, 127ra37. doi:10.1126/scitranslmed.3003689

Thibult, M.-L., Mamessier, E., Gertner-Dardenne, J., Pastor, S., Just-Landi, S., Xerri, L., et al. (2013). PD-1 Is a Novel Regulator of Human B-Cell Activation. *Int.Immunol.* 25, 129–137. doi:10.1093/intimm/dxs098

Topalian, S. L., Hodi, F. S., Brahmer, J. R., Gettinger, S. N., Smith, D. C., McDermott, D. F., et al. (2012). Safety, Activity, and Immune Correlates of Anti-Pd-1 Antibody in Cancer. *N. Engl. J. Med.* 366 (26), 2443–2454. doi:10.1056/NEJMoa1200690

Trautmann, L., Janbazian, L., Chomont, N., Said, E. A., Gimmig, S., Bessette, B., et al. (2006). Upregulation of PD-1 Expression on HIV-specific CD8+ T Cells Leads to Reversible Immune Dysfunction. *Nat. Med.* 12 (10), 1198–1202. doi:10.1038/nm1482

Vaishampayan, U., Schöffski, P., Ravaud, A., Borel, C., Peguero, J., Chaves, J., et al. (2019). Avelumab Monotherapy as First-Line or Second-Line Treatment in Patients with Metastatic Renal Cell Carcinoma: Phase Ib Results from the Javelin Solid Tumor Trial. *J. Immunother. Cancer* 7 (1), 275. doi:10.1186/s40425-019-0746-2

Wang, F., Wei, X. L., Wang, F. H., Xu, N., Shen, L., Dai, G. H., et al. (2019). Safety, Efficacy and Tumor Mutational Burden as a Biomarker of Overall Survival Benefit in Chemo-Refractory Gastric Cancer Treated with Toripalimab, a Pd-1 Antibody in Phase Ib/Ii Clinical Trial Nct02915432. *Ann. Oncol.* 30 (9), 1479–1486. doi:10.1093/annonc/mdz197

Wang, Z., Ying, J., Xu, J., Yuan, P., Duan, J., Bai, H., et al. (2020a). Safety, Antitumor Activity, and Pharmacokinetics of Toripalimab, a Programmed Cell Death 1 Inhibitor, in Patients with Advanced Non-Small Cell Lung Cancer. *JAMA Netw. Open* 3 (10), e2013770. doi:10.1001/jamanetworkopen.2020.13770

Wang, Z., Zhao, J., Ma, Z., Cui, J., Shu, Y., Liu, Z., et al. (2020b). A Phase 2 Study of Tislelizumab in Combination with Platinum-Based Chemotherapy as First-Line Treatment for Advanced Lung Cancer in Chinese Patients. *Lung Cancer* 147, 259–268. doi:10.1016/j.lungcan.2020.06.007

Weber, J. S., D'Angelo, S. P., Minor, D., Hodi, F. S., Gutzmer, R., Neyns, B., et al. (2015). Nivolumab Versus Chemotherapy in Patients with Advanced Melanoma Who Progressed after Anti-Ctla-4 Treatment (Checkmate 037): A Randomised, Controlled, Open-Label, Phase 3 Trial. *Lancet Oncol.* 16 (4), 375–384. doi:10.1016/s1470-2045(15)70076-8

Weng, Y. M., Peng, M., Hu, M. X., Yao, Y., and Song, Q. B. (2018). Clinical and Molecular Characteristics Associated with the Efficacy of Pd-1/Pd-L1 Inhibitors for Solid Tumors: A Meta-Analysis. *Onco. Targets Ther.* 11, 7529–7542. doi:10.2147/OTT.S167865

Xing, W., Zhao, L., Zhao, L., Fu, X., Liang, G., Zhang, Y., et al. (2020). A Phase Ii, Single-Centre Trial of Neoadjuvant Toripalimab Plus Chemotherapy in Locally Advanced Esophageal Squamous Cell Carcinoma. *J. Thorac. Dis.* 12 (11), 6861–6867. doi:10.21037/jtd-20-2198

Xu, J., Bai, Y., Xu, N., Li, E., Wang, B., Wang, J., et al. (2020). Tislelizumab Plus Chemotherapy as First-Line Treatment for Advanced Esophageal Squamous Cell Carcinoma and Gastric/Gastroesophageal Junction Adenocarcinoma. *Clin. Cancer Res.* 26 (17), 4542–4550. doi:10.1158/1078-0432.CCR-19-3561

Yang, Y., Wang, Z., Fang, J., Yu, Q., Han, B., Cang, S., et al. (2020). Efficacy and Safety of Sintilimab Plus Pemetrexed and Platinum as First-Line Treatment for Locally Advanced or Metastatic Nonsquamous NSCLC: a Randomized, Double-Blind, Phase 3 Study (Oncology pRogram by InnovENT Anti-PD-1-11). *J. Thorac. Oncol.* 15 (10), 1636–1646. doi:10.1016/j.jtho.2020.07.014

Ye, D., Liu, J., Zhou, A., Zou, Q., Li, H., Fu, C., et al. (2021). Tislelizumab in Asian Patients with Previously Treated Locally Advanced or Metastatic Urothelial Carcinoma. *Cancer Sci.* 112 (1), 305–313. doi:10.1111/cas.14681

Younes, A., Santoro, A., Shipp, M., Zinzani, P. L., Timmerman, J. M., Ansell, S., et al. (2016). Nivolumab for Classical Hodgkin's Lymphoma after Failure of Both Autologous Stem-Cell Transplantation and Brentuximab Vedotin: A Multicentre, Multicohort, Single-Arm Phase 2 Trial. *Lancet Oncol.* 17 (9), 1283–1294. doi:10.1016/s1470-2045(16)30167-x

Yu, Y., Tsang, J. C., Wang, C., Clare, S., Wang, J., and Chen, X. (2016). Single-Cell RNA-seq Identifies a PD-1hi ILC Progenitor and Defines its Development Pathway. *Trends Cancer*, Nature, 102–106. doi:10.1038/nature20105

Wei, W., Jiang, D., Ehlerding, E. B., Luo, Q., and Cai, W. (2018). Noninvasive PET Imaging of T Cells. *Trends Cancer*, 4, 359–3731.

Zhang, Y., Zhou, H., and Zhang, L. (2018). Which Is the Optimal Immunotherapy for Advanced Squamous Non-Small-Cell Lung Cancer in Combination with Chemotherapy: Anti-Pd-1 or Anti-Pd-L1?. *J. Immunother. Cancer* 6 (1), 135. doi:10.1186/s40425-018-0427-6

Zhang, X., Zeng, L., Li, Y., Xu, Q., Yang, H., Lizaso, A., et al. (2021). Anlotinib Combined with PD-1 Blockade for the Treatment of Lung Cancer: a Real-World Retrospective Study in China. *Cancer Immunol. Immunother.*. doi:10.1007/s00262-021-02869-9

Zhou, C., Chen, G., Huang, Y., Zhou, J., Lin, L., Feng, J., et al. (2021). Camrelizumab Plus Carboplatin and Pemetrexed Versus Chemotherapy Alone in Chemotherapy-Naive Patients with Advanced Non-Squamous Non-Small-Cell Lung Cancer (Camel): A Randomised, Open-Label, Multicentre, Phase 3 Trial. *Lancet Respir. Med.* 9 (3), 305–314. doi:10.1016/s2213-2600(20)30365-9

Zhu, P., Wang, Y., Zhang, W., and Liu, X. (2021). Anti-PD1/PD-L1 Monotherapy vs Standard of Care in Patients with Recurrent or Metastatic Head and Neck Squamous Cell Carcinoma. *Medicine (Baltimore)* 100 (4), e24339. doi:10.1097/MD.0000000000024339

Zou, W., and Chen, L. (2008). Inhibitory B7-Family Molecules in the Tumour Microenvironment. *Nat. Rev. Immunol.* 8, 467–477. doi:10.1038/nri2326

Conflict of Interest: YZ was employed by BeiGene Ltd.

The remaining authors declare that the research was conducted in the absence of any commercial or financial relationships that could be construed as a potential conflict of interest.

frontiers in Pharmacology

ORIGINAL RESEARCH
published: 09 July 2021
doi: 10.3389/fphar.2021.711772

T-Cell Exhaustion Status Under High and Low Levels of Hypoxia-Inducible Factor 1α Expression in Glioma

Shuai Liu[1,2], *Xing Liu*[2], *Chuanbao Zhang*[3], *Wei Shan*[4]* and *Xiaoguang Qiu*[2]*

[1]Department of Radiation Oncology, Beijing Tiantan Hospital, Capital Medical University, Beijing, China, [2]Beijing Neurosurgical Institute, Capital Medical University, Beijing, China, [3]Department of Neurosurgery, Beijing Tiantan Hospital, Capital Medical University, Beijing, China, [4]Department of Neurology, Beijing Tiantan Hospital, Capital Medical University, Beijing, China

Background: Hypoxia-inducible factor 1α (HIF1A), the principal regulator of hypoxia, is involved in the suppression of antitumor immunity. We aimed to describe the T-cell exhaustion status of gliomas under different levels of HIF1A expression.

Methods: In this study, 692 patients, whose data were collected from the Chinese Glioma Genome Atlas (CGGA) database, and 669 patients, whose data were collected from The Cancer Genome Atlas database, were enrolled. We further screened the data of a cohort of paired primary and recurrent patients from the CGGA dataset (n = 50). The abundance of immune cells was calculated using the transcriptome data. The association between HIF1A and T-cell exhaustion-related genes and immune cells was investigated.

Results: According to the median value of HIF1A expression, gliomas were classified into low-HIF1A-expression and high-HIF1A-expression groups. The expression levels of PDL1 (CD274), FOXO1, and PRDM1 in the high-HIF1A-expression group were significantly higher in both glioblastoma (GBM) and lower-grade glioma. The abundance of exhausted T cells and B cells was significantly higher in the high-HIF1A-expression group, while that of macrophage, monocyte, and natural killer cell was significantly higher in the low-HIF1A-expression group in both GBM and lower-grade glioma. After tumor recurrence, the expression of HIF1A significantly increased, and the correlation between HIF1A expression levels and exhausted T cells and induced regulatory T cells became stronger.

Conclusion: In diffuse gliomas, the levels of T-cell exhaustion-associated genes and the abundance of immune cells were elevated under high HIF1A expression. Reversing hypoxia may improve the efficacy of immunotherapy.

Keywords: T-cell, HIF1A, exhaustion status, glioma, levels of hypoxia

OPEN ACCESS

Edited by:
Liang Weng,
Central South University, China

Reviewed by:
Changlin Yang,
University of Florida, United States
Wang Yu,
Peking Union Medical College Hospital (CAMS), China

***Correspondence:**
Xiaoguang Qiu
qiuxiaoguang@bjtth.org
Wei Shan
weishanns@gmail.com

Specialty section:
This article was submitted to Inflammation Pharmacology, a section of the journal Frontiers in Pharmacology

Received: *19 May 2021*
Accepted: *28 June 2021*
Published: *09 July 2021*

Citation:
Liu S, Liu X, Zhang C, Shan W and Qiu X (2021) T-Cell Exhaustion Status Under High and Low Levels of Hypoxia-Inducible Factor 1α Expression in Glioma. Front. Pharmacol. 12:711772. doi: 10.3389/fphar.2021.711772

Abbreviations: CGGA, chinese glioma genome atlas; DC, dendritic cell; gamma-delta, γδ T cell; HIF1A, hypoxia-inducible factor 1α; iTreg, induced regulatory T cell; NK, natural killer cell; nTreg, natural regulatory T cell; TCGA, the cancer genome atlas; Tr1, type 1 regulator T cell; Th17, T helper 17 cell; Th2, T helper 2 cell; WHO, world health organization.

INTRODUCTION

As the most common primary brain tumor, the prognosis of gliomas remains dismal (Wen and Kesari, 2008). The recent advances in the treatment of glioma are mainly based on the patient's diagnosis determined using molecular pathology (Louis et al., 2016). This makes it possible to develop a more precise treatment strategy. However, no breakthroughs in surgery, radiotherapy, or chemotherapy have been achieved.

The success of immunotherapy in treating extracranial tumors brings light to gliomas. Many pioneer studies have evaluated different strategies, including immune checkpoint blockers, vaccines, and chimeric antigen receptor T cells, for treating glioma (Garcia-Fabiani et al., 2020). To some disappointment, the results were not so inspiring. One important obstacle is T-cell dysfunction, induced by multiple immunosuppressive mechanisms, such as the expression of immunosuppressive factors and immune checkpoint molecules by tumors. When T cells lose their normal functions, including polyfunctionality and renewal capacity, they reach a terminally differentiated state, termed as T-cell exhaustion. A high proportion of exhausted T cells in tumors developed resistance to immunotherapy.

Hypoxia, a hallmark of most solid tumors, is reported to have a negative impact on antitumor immunity (Chouaib et al., 2017). Reversing the hypoxic state in tumors improves the efficacy of immunotherapy (Jayaprakash et al., 2018; Lan et al., 2018; Ni et al., 2020). The rapid induction of T-cell exhaustion by hypoxia is an important mechanism (Scharping et al., 2021). However, these findings were mainly observed in tumors outside the central nervous system, and the association between hypoxia and T-cell exhaustion in glioma needs to be clarified further.

Hypoxia-inducible factor 1α (HIF1A) is a principal regulator of hypoxia and is involved in multiple biological processes of antitumor immunity. Investigating the specific role of HIF1A in T-cell exhaustion in gliomas is an important issue, which could help to improve the efficacy of immunotherapy. In this study, the transcriptome data of gliomas from two large independent datasets were analyzed. We aimed to determine the T-cell exhaustion status in high- and low-HIF1A-expression groups in different grades of gliomas and in paired primary and recurrent tumors.

MATERIALS AND METHODS

Patients and Datasets

In this study, the RNA-seq data of pathologically confirmed diffuse glioma [World Health Organization (WHO) grades II–IV] obtained from the Chinese Glioma Genome Atlas (CGGA) dataset (http://www.cgga.org.cn) (n = 692) and The Cancer Genome Atlas (TCGA) dataset (http://cancergenome.nih.gov/) (n = 669) were included. We further screened the data of a cohort of paired primary and recurrent patients from the CGGA dataset (n = 50). WHO grade II and III gliomas were classified as lower-grade gliomas. For the CGGA dataset, the process of clinical specimen collection and sequencing was described in detail in our previous work (Zhao et al., 2021). Specifically, the RNA-seq data was processed as recommended by TCGA. In brief, the fastq data were aligned to the human genome reference (hg19) with STAR. RSEM was used for the quantification of genes. The expression of the genes in the two datasets were all normalized as FPKM.

All participants provided informed consent for the research use of their data collected from these two public datasets; this study was approved by the Ethics Committee of Beijing Tiantan Hospital.

T-Cell Exhaustion-Related Genes

We reviewed the recent literature and screened 39 genes associated with T-cell exhaustion. A list of these genes is shown in **Supplementary Table S1**.

Estimating the Abundance of Immune Cells

The abundance of 24 types of immune cells, including 18 T-cell subsets, was estimated using ImmuCellAI (Miao et al., 2020) (http://bioinfo.life.hust.edu.cn/ImmuCellAI). This tool uses a gene set signature-based method with tumor RNA-seq data.

Statistical Analysis

For the CGGA and TCGA datasets, the HIF1A expression levels were determined to be high or low based on their median values. The Wilcoxon rank sum test was used to compare the numerical variables, and the *p*-values were adjusted by using the Benjamini-Hochberg procedure. The Wilcoxon signed-rank test was used to compare the numerical variables between paired primary and recurrent patients. A Pearson correlation analysis was conducted to determine correlation between the parameters. All statistical analyses were performed using R software (https://www.r-project.org/). A p-value of < 0.05 was considered significant.

RESULTS

HIF1A Expression Level in Different Grades of Gliomas

First, we compared the expression levels of HIF1A between primary GBM (IDH wild-type) and lower-grade glioma. The expression of HIF1A was higher in GBM than in lower-grade glioma in the CGGA ($p = 0.008$) and TCGA ($p < 0.001$) datasets. In addition, we made comparisons of HIF1A expression in lower grade glioma grouped by IDH and 1p/19q codeletion status in the two datasets. Only significant difference of the HIF1A expression was found by IDH status ($p = 0.012$) in the CGGA dataset.

Differences of T-cell Exhaustion-Related Genes in the High-and Low-HIF1A-Expression Groups

In the CGGA and TCGA datasets, the levels of T-cell exhaustion-related genes were compared separately in the GBM and lower-grade glioma groups. The data of differentially expressed genes in both datasets were retained. In GBM, the expression of T-cell exhaustion-related genes including PDL1 (CD274), B7H3 (CD276),

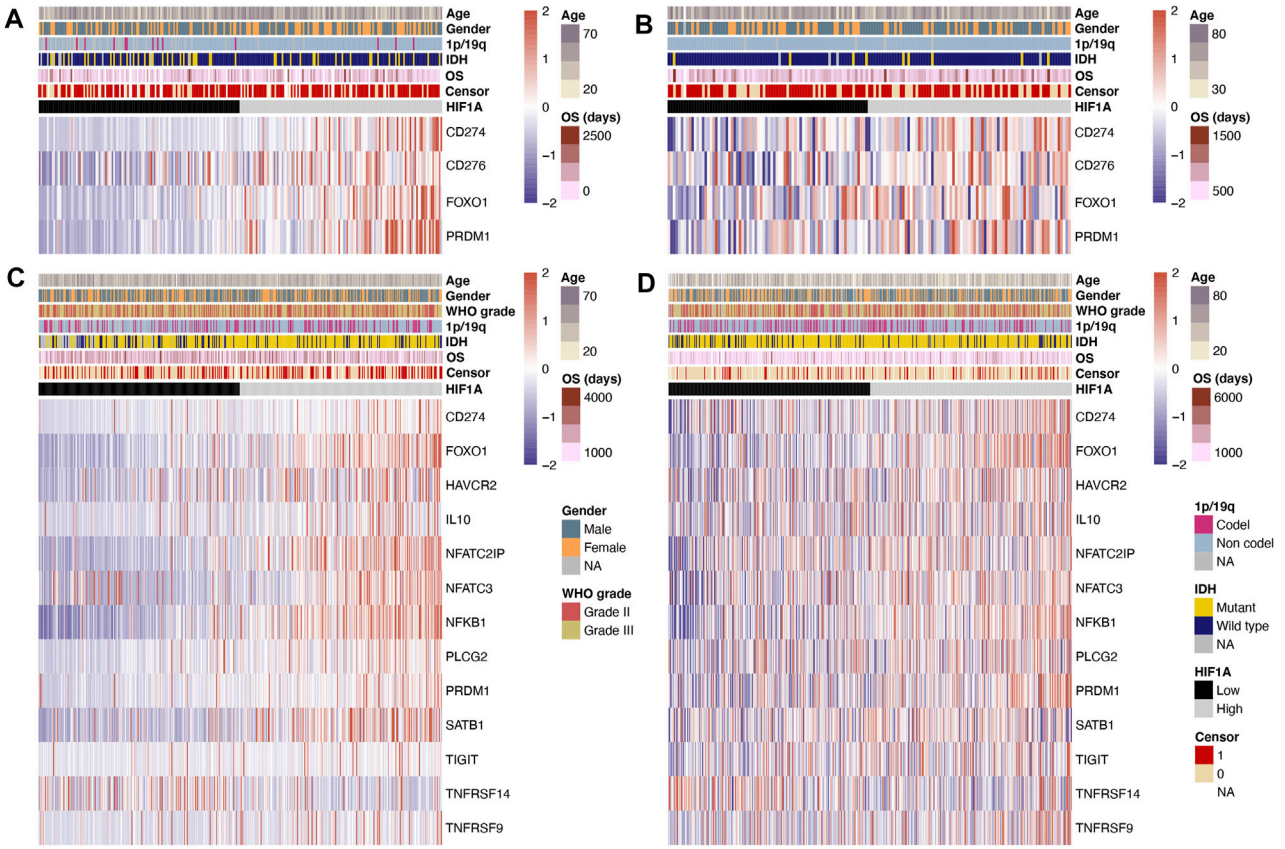

FIGURE 1 | Heatmap of T-cell exhaustion-related genes under high- and low-HIF1A-expression levels: **(A)** Data of GBM from the CGGA dataset, **(B)** data of GBM from the TCGA dataset, **(C)** data of lower-grade glioma from the CGGA dataset, and **(D)** data of lower-grade glioma from the TCGA dataset.

FOXO1, and PRDM1 (all $p < 0.05$) in the high-HIF1A-expression group was higher than that in the low-HIF1A-expression group (**Figures 1A,B**).

In lower-grade glioma, the data of differentially expressed genes in the CGGA and TCGA datasets are shown in **Figures 1C,D**. The expression levels of T-cell exhaustion-related genes including PDL1 (CD274), FOXO1, TIM3 (HAVCR2), IL10, NFATC2IP, NFATC3, NFKB1, PLCG2, PRDM1, SATB1, TIGIT, and TNFRSF9 (all $p < 0.05$) were significantly higher in the high-HIF1A-expression group; meanwhile, the expression level of TNFRSF14 ($p < 0.05$) was significantly lower in the high-HIF1A-expression group.

Differences in the Abundance of Immune Cells in the High-and Low-HIF1A-Expression Groups

Similar to the comparison of genes, we separately investigated the differences in the abundance of immune cells in GBM and lower-grade glioma, and obtained significant results in both the CGGA and TCGA datasets. In GBM, the abundance of B cell and exhausted T cell was significantly higher in the high-HIF1A-expression tumors, while that of macrophage, monocyte, and natural killer cell (NK) was significantly higher in the low-HIF1A-expression tumors (all $p < 0.05$; **Figures 2A,B**).

The abundance of B cell and exhausted cell in lower-grade glioma was similar to that in GBM and was significantly higher in the high-HIF1A-expression group; meanwhile, the abundance of macrophage, monocyte, NK, natural regulatory T cell (nTreg), and type 1 regulator T cell (Tr1) was significantly higher in the low-HIF1A-expression group (all $p < 0.05$; **Figures 2C,D**).

Differences in the Level of T-Cell Exhaustion-Related Genes After Tumor Recurrence

First, we compared the expression levels of HIF1A, and a significant elevation was observed in the recurrent group (**Figure 3A**). In addition, we found that the expression levels of T-cell exhaustion-related genes including CD40, GRB2, MKI67, NFATC3, PRDM1, TCF7, and TGFB1 were significantly higher, while those of CXCR5 and TOX were significantly lower after tumor recurrence (all $p < 0.05$; **Figures 3B,C**).

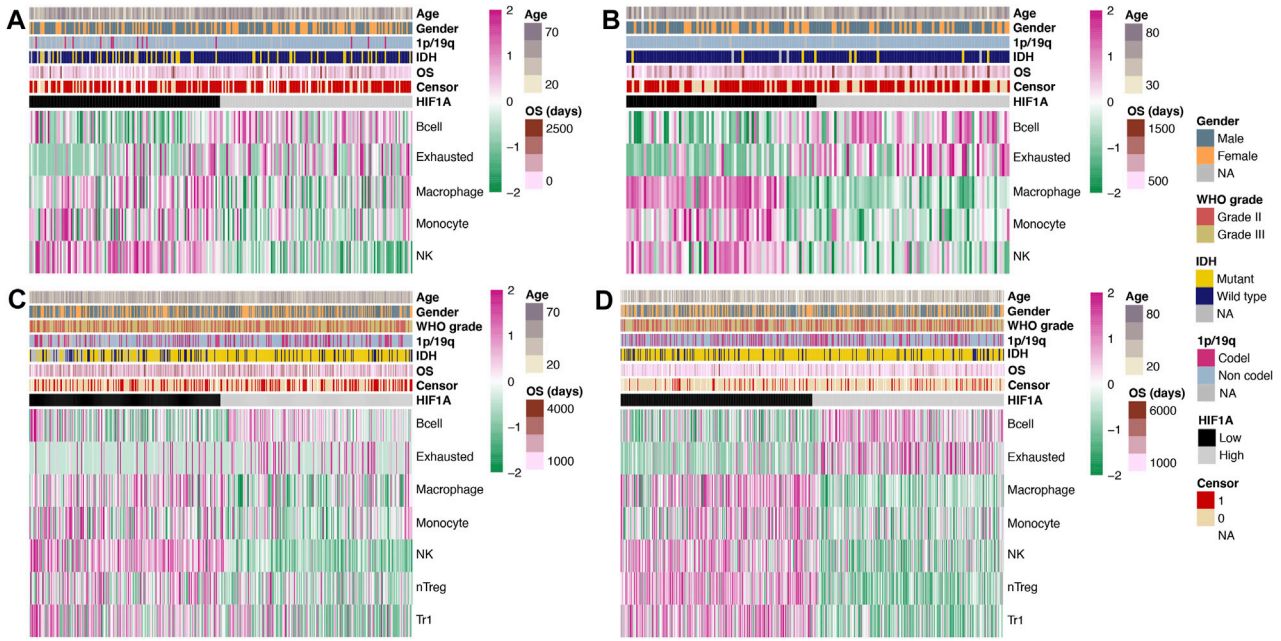

FIGURE 2 | Heatmap of the abundance of immune cells under high- and low-HIF1A-expression levels: **(A)** Data of GBM from the CGGA dataset, **(B)** data of GBM from the TCGA dataset, **(C)** data of lower-grade glioma from the CGGA dataset, and **(D)** data of lower-grade glioma from the TCGA dataset.

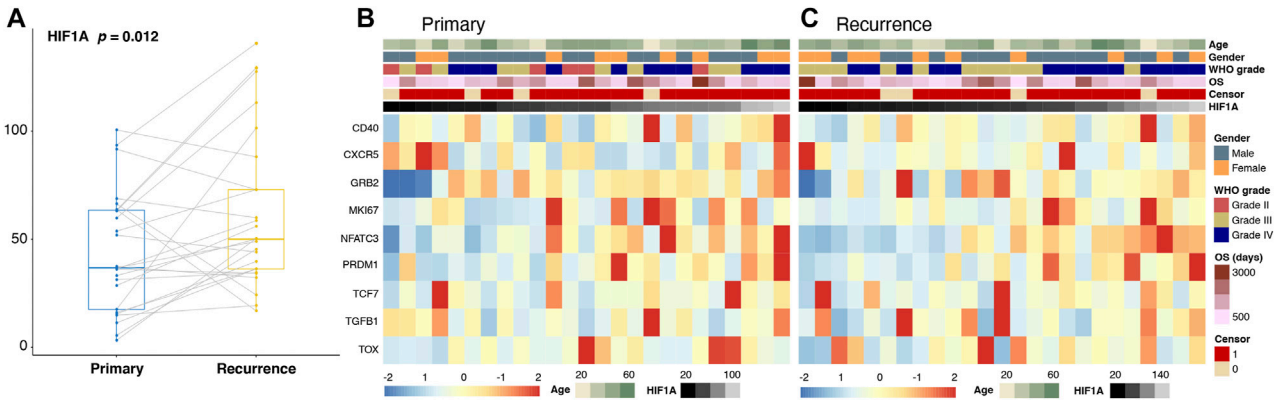

FIGURE 3 | Changes in the expression levels of HIF1A **(A)** and T-cell exhaustion-related genes **(B,C)** in paired primary and recurrence gliomas.

Differences in the Level of Immune Cells After Tumor Recurrence

Among various immune cells, only the level of T helper 17 cell (Th17) (p = 0.034) was elevated after tumor recurrence.

Correlation Between HIF1A and T-Cell Function-Associated Genes Before/After Tumor Recurrence

A Person correlation analysis was performed to investigate the association of HIF1A with T-cell exhaustion-related genes, and the Pearson R remained >0.5 or < −0.4. Before and after recurrence, most of the genes were positively correlated with HIF1A; only BAG6 was negatively correlated with HIF1A and other genes (**Figures 4A,B**).

Correlation Between HIF1A and Immune Cells Before/After Tumor Recurrence

Immune cells were found to be correlated with HIF1A expression with Pearson R > 0.3 or < −0.4 before and after recurrence. Before tumor recurrence, we found that the levels of exhausted, dendritic cell (DC), T helper 2 cell (Th2), and induced regulatory T cell (iTreg) were positively correlated with HIF1A expression, while those of NK, natural killer T cell (NKT), CD8_T, CD8-naive, and

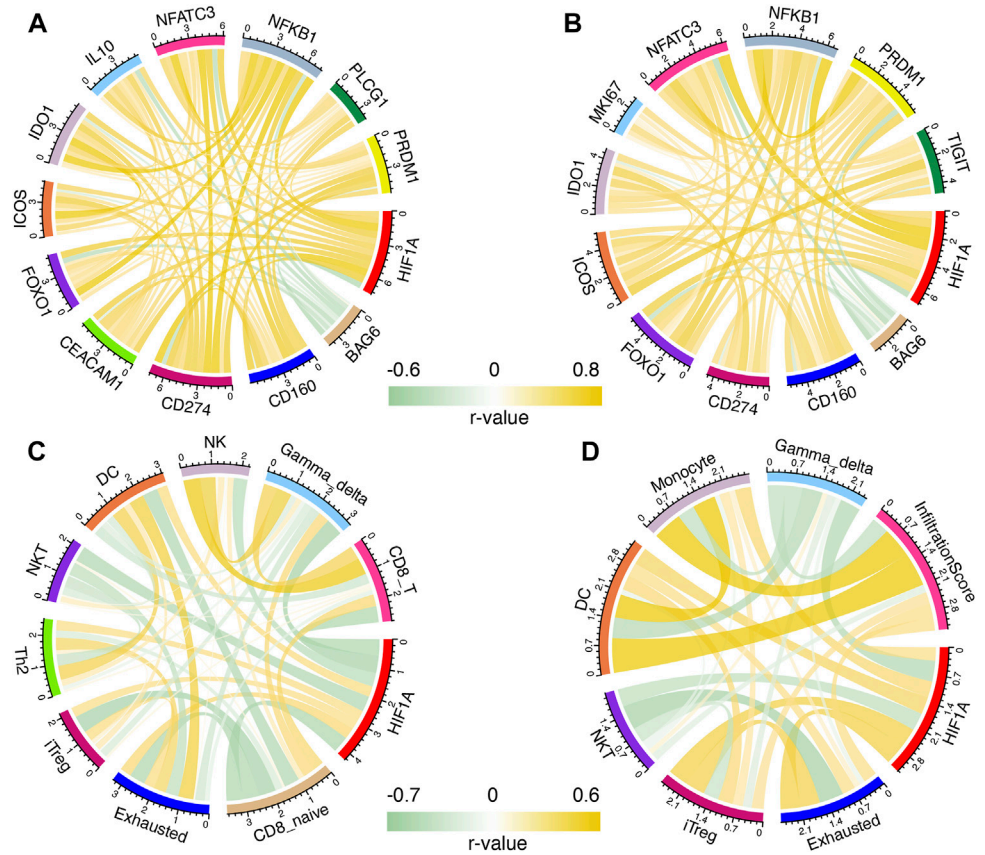

FIGURE 4 | Correlation of HIF1A and T-cell exhaustion-related genes in primary **(A)** and recurrent **(B)** gliomas; correlation of HIF1A and abundance of immune cells in primary **(C)** and recurrent **(D)** gliomas.

γδ T cell (gamma-delta) were negatively correlated with HIF1A expression (**Figure 4C**). After tumor recurrence, iTreg, exhaustion, DC, monocyte, and infiltration scores were positively correlated with HIF1A expression, while the NKT and gamma-delta were negatively correlated with HIF1A expression (**Figure 4D**).

DISCUSSION

In this study, we evaluated the T-cell exhaustion-related profile under hypoxic conditions in glioma. We found that many T-cell exhaustion-related genes and immune cells were associated with HIF1A expression. Importantly, we investigated the changes in the abundance of these genes and immune cells before and after tumor recurrence. Our findings described the T-cell exhaustion status in low and high levels of HIF1A.

Genes regulating the T-cell function are not isolated but interact with each other like a network. Some molecules stand in a more vital place and are potential targets for drug development. The PD1/PDL1 pathway is a promising target for treating various solid tumors (Wu et al., 2019), and the striking results shed light on the effect immunotherapy. Importantly, PD1/PDL1 plays a central role in regulating T-cell exhaustion (Pauken and Wherry, 2015), which may be affected by hypoxic conditions. Previous studies revealed that HIF1A can increase the expression of PDL1 (Noman et al., 2014). Similarly, in patients with GBM and lower-grade glioma, we found that high-HIF1A-expression tumors expressed higher levels of PDL1. In addition, FOXO1, a transcription factor that regulates PD1 expression in antigen-activated T cells, was also highly expressed in the high-HIF1A-expression tumors. Higher expression of NFKB1 and SATB1, which are involved in regulating PD1 expression (Nixon and Li, 2017; Antonangeli et al., 2020) was only observed in patients with lower-grade gliomas. Other immune checkpoints that are targeted by drugs for clinical use (Dempke et al., 2017), including B7H3 (CD276) and TIM3 (HAVCR2), were also found to be highly expressed in patients with high-HIF1A-expression gliomas. These findings indicate that hypoxia upregulates pivotal T-cell exhaustion-related genes, and drugs that target these genes, along with the inhibition of HIF1A, may reverse T-cell exhaustion.

Other molecules, including PRDM1 (BLIMP1), NFAT, and IL10, are involved in T-cell activation and contribute to T-cell exhaustion in cancer (Wherry and Kurachi, 2015). Higher levels of PRDM1 were observed in high-HIF1A-expression GBM and lower-grade glioma, while higher levels of NFAT and IL10 were only observed in lower-grade glioma. Notably, we found that the TNFRSF14 (HVEM) level was higher in low-HIF1A-expression lower-grade glioma. This negative association could be explained by the fact that TNFRSF14 is involved in the activation and proliferation of T cells (Steinberg

et al., 2011), and higher hypoxia is an unfavorable environment for T cells to perform normal functions.

Benefitting from the development of the algorithm, we can now determine the abundance of immune cells using the RNA-seq data. We found that the levels of exhausted T cell and B cell were higher in high-HIF1A-expression tumors in both GBM and lower-grade glioma groups. This finding more directly indicates that hypoxia promotes the transformation of exhausted T cells, which could help explain the limited effect of immunotherapy in glioma. Interestingly, B cells were found to be elevated under hypoxic conditions. This phenomenon was also observed in pancreatic neoplasia (Lee et al., 2016). However, how these B cells affect the antitumor immunity remains unclear and needs further study. The abundance of other immune cells, including macrophage, monocyte, NK cells, nTreg, and Tr1, was decreased in high-HIF1A-expression tumors.

After tumor recurrence, the levels of HIF1A and immune-related genes started to increase. As there are antibodies targeting CD40, GRB2, and TGFB1 for clinical trials or usage, it is reasonable to treat recurrent tumors with these drugs. However, no significant changes were found in the abundance of immune cells after tumor recurrence. We further evaluated the association between HIF1A levels and these immune cells before and after tumor recurrence. The correlation between HIF1A expression and exhausted T cell and iTreg became stronger after tumor recurrence. A previous study on colon cancer also found that regulatory T cell increased under hypoxic condition (Westendorf et al., 2017). As exhausted T cell and iTreg (Paluskievicz et al., 2019) are involved in suppressing antitumor immunity, our findings indicate that improving the hypoxic condition of glioma could relieve the immunosuppression state, thus making the immunotherapy more effective.

CONCLUSION

We investigated the association between HIF1A and T-cell exhaustion-related genes and immune cells in different grades of glioma and in recurrent glioma. These findings help describe the immune state under hypoxic conditions and guide new immunotherapy strategy for glioma.

DATA AVAILABILITY STATEMENT

Publicly available datasets were analyzed in this study. This data can be found here: The Chinese Glioma Genome Atlas (CGGA) dataset (http://www.cgga.org.cn) and The Cancer Genome Atlas (TCGA) dataset (http://cancergenome.nih.gov/).

ETHICS STATEMENT

All participants provided informed consent for the research use of their data collected from these two public datasets; this study was approved by the Ethics Committee of Beijing Tiantan Hospital.

AUTHOR CONTRIBUTIONS

XQ and SL designed the current study and revised the manuscript. SL and WS performed analysis and interpretation of the data and drafted the manuscript. XL and CZ involved in data analysis and manuscript revision.

FUNDING

This work was supported by grants from the National Natural Science Foundation of China (Grant Numbers: 82001778, 81902533, 81802483), the project Genomics Platform Construction for Chinese Major Brain Disease-Germ cell tumor (Grant Number: PXM2019_026280_000002), and the Beijing Hospitals Authority Youth Program (Grant Number: QML20190507).

SUPPLEMENTARY MATERIAL

The Supplementary Material for this article can be found online at: https://www.frontiersin.org/articles/10.3389/fphar.2021.711772/full#supplementary-material

REFERENCES

Antonangeli, F., Natalini, A., Garassino, M. C., Sica, A., Santoni, A., and Di Rosa, F. (2020). Regulation of PD-L1 Expression by NF-kappaB in Cancer. *Front. Immunol.* 11, 584626. doi:10.3389/fimmu.2020.584626

Chouaib, S., Noman, M. Z., Kosmatopoulos, K., and Curran, M. A. (2017). Hypoxic Stress: Obstacles and Opportunities for Innovative Immunotherapy of Cancer. *Oncogene* 36, 439–445. doi:10.1038/onc.2016.225

Dempke, W. C. M., Fenchel, K., Uciechowski, P., and Dale, S. P. (2017). Second- and Third-Generation Drugs for Immuno-Oncology Treatment-The More the Better? *Eur. J. Cancer* 74, 55–72. doi:10.1016/j.ejca.2017.01.001

Garcia-Fabiani, M. B., Ventosa, M., Comba, A., Candolfi, M., Nicola Candia, A. J., Alghamri, M. S., et al. (2020). Immunotherapy for Gliomas: Shedding Light on Progress in Preclinical and Clinical Development. *Expert Opin. Investig. Drugs* 29, 659–684. doi:10.1080/13543784.2020.1768528

Jayaprakash, P., Ai, M., Liu, A., Budhani, P., Bartkowiak, T., Sheng, J., et al. (2018). Targeted Hypoxia Reduction Restores T Cell Infiltration and Sensitizes Prostate Cancer to Immunotherapy. *J. Clin. Invest.* 128, 5137–5149. doi:10.1172/jci96268

Lan, G., Ni, K., Xu, Z., Veroneau, S. S., Song, Y., and Lin, W. (2018). Nanoscale Metal-Organic Framework Overcomes Hypoxia for Photodynamic Therapy Primed Cancer Immunotherapy. *J. Am. Chem. Soc.* 140, 5670–5673. doi:10.1021/jacs.8b01072

Lee, K. E., Spata, M., Bayne, L. J., Buza, E. L., Durham, A. C., Allman, D., et al. (2016). Hif1a Deletion Reveals Pro-neoplastic Function of B Cells in Pancreatic Neoplasia. *Cancer Discov.* 6, 256–269. doi:10.1158/2159-8290.cd-15-0822

Louis, D. N., Perry, A., Reifenberger, G., Von Deimling, A., Figarella-Branger, D., Cavenee, W. K., et al. (2016). The 2016 World Health Organization Classification of Tumors of the Central Nervous System: a Summary. *Acta Neuropathol.* 131, 803–820. doi:10.1007/s00401-016-1545-1

Miao, Y. R., Zhang, Q., Lei, Q., Luo, M., Xie, G. Y., Wang, H., et al. (2020). ImmuCellAI: A Unique Method for Comprehensive T-Cell Subsets Abundance Prediction and its Application in Cancer Immunotherapy. *Adv. Sci.* 7, 1902880. doi:10.1002/advs.201902880

Ni, K., Lan, G., Song, Y., Hao, Z., and Lin, W. (2020). Biomimetic Nanoscale Metal-Organic Framework Harnesses Hypoxia for Effective Cancer Radiotherapy and Immunotherapy. *Chem. Sci.* 11, 7641–7653. doi:10.1039/d0sc01949f

Nixon, B. G., and Li, M. O. (2017). Satb1: Restraining PD1 and T Cell Exhaustion. *Immunity* 46, 3–5. doi:10.1016/j.immuni.2017.01.002

Noman, M. Z., Desantis, G., Janji, B., Hasmim, M., Karray, S., Dessen, P., et al. (2014). PD-L1 Is a Novel Direct Target of HIF-1α, and its Blockade under Hypoxia Enhanced MDSC-Mediated T Cell Activation. *J. Exp. Med.* 211, 781–790. doi:10.1084/jem.20131916

Paluskievicz, C. M., Cao, X., Abdi, R., Zheng, P., Liu, Y., and Bromberg, J. S. (2019). T Regulatory Cells and Priming the Suppressive Tumor Microenvironment. *Front. Immunol.* 10, 2453. doi:10.3389/fimmu.2019.02453

Pauken, K. E., and Wherry, E. J. (2015). Overcoming T Cell Exhaustion in Infection and Cancer. *Trends Immunol.* 36, 265–276. doi:10.1016/j.it.2015.02.008

Scharping, N. E., Rivadeneira, D. B., Menk, A. V., Vignali, P. D. A., Ford, B. R., Rittenhouse, N. L., et al. (2021). Mitochondrial Stress Induced by Continuous Stimulation under Hypoxia Rapidly Drives T Cell Exhaustion. *Nat. Immunol.* 22, 205–215. doi:10.1038/s41590-020-00834-9

Steinberg, M. W., Cheung, T. C., and Ware, C. F. (2011). The Signaling Networks of the Herpesvirus Entry Mediator (TNFRSF14) in Immune Regulation. *Immunological Rev.* 244, 169–187. doi:10.1111/j.1600-065x.2011.01064.x

Wen, P. Y., and Kesari, S. (2008). Malignant Gliomas in Adults. *N. Engl. J. Med.* 359, 492–507. doi:10.1056/nejmra0708126

Westendorf, A. M., Skibbe, K., Adamczyk, A., Buer, J., Geffers, R., Hansen, W., et al. (2017). Hypoxia Enhances Immunosuppression by Inhibiting CD4+ Effector T Cell Function and Promoting Treg Activity. *Cell Physiol Biochem* 41, 1271–1284. doi:10.1159/000464429

Wherry, E. J., and Kurachi, M. (2015). Molecular and Cellular Insights into T Cell Exhaustion. *Nat. Rev. Immunol.* 15, 486–499. doi:10.1038/nri3862

Wu, Y., Chen, W., Xu, Z. P., and Gu, W. (2019). PD-L1 Distribution and Perspective for Cancer Immunotherapy—Blockade, Knockdown, or Inhibition. *Front. Immunol.* 10, 2022. doi:10.3389/fimmu.2019.02022

Zhao, Z., Zhang, K. N., Wang, Q., Li, G., Zeng, F., Zhang, Y., et al. (2021). Chinese Glioma Genome Atlas (CGGA): A Comprehensive Resource with Functional Genomic Data from Chinese Gliomas. *Genomics Proteomics Bioinformatics*. doi:10.1016/j.gpb.2020.10.005

Conflict of Interest: The authors declare that the research was conducted in the absence of any commercial or financial relationships that could be construed as a potential conflict of interest.

frontiers in Pharmacology

ORIGINAL RESEARCH
published: 28 July 2021
doi: 10.3389/fphar.2021.715302

Atrial Natriuretic Peptide Inhibited ABCA1/G1-dependent Cholesterol Efflux Related to Low HDL-C in Hypertensive Pregnant Patients

*Yubing Dong†, Yi Lin†, Wanyu Liu, Wei Zhang, Yinong Jiang and Wei Song**

Department of Hypertension, The First Affiliated Hospital of Dalian Medical University, DaLian, China

Objective: It has been reported that atrial natriuretic peptide (ANP) regulates lipid metabolism by stimulating adipocyte browning, lipolysis, and lipid oxidation, and by impacting the secretion of adipokines. In our previous study, we found that the plasma ANP concentration of hypertensive disorders of pregnancy (HDP) was significantly increased in comparison to that of normotensive pregnancy patients. Thus, this study's objective was to investigate the lipid profile in patients with HDP and determine the effects of ANP on the cholesterol efflux in THP-1 macrophages.

Methods: A total of 265 HDP patients and 178 normotensive women as the control group were recruited. Clinical demographic characteristics and laboratory profile data were collected. Plasma total triglycerides (TGs), total cholesterol (TC), low-density cholesterol (LDL-C), and high-density cholesterol (HDL-C) were compared between the two groups. THP-1 monocytes were incubated with different concentrations of ANP. ATP-binding cassette transporter A1 (ABCA1) and ATP-binding cassette transporter G1 (ABCG1) mRNA and protein were evaluated. ABCA1- and ABCG1-mediated cholesterol efflux to apolipoprotein A-I (apoA-I) and HDL, respectively, were measured by green fluorescent labeled NBD cholesterol. Natriuretic peptide receptor A (NPR-A) siRNA and specific agonists of the peroxisome proliferator–activated receptor-γ (PPAR-γ) and liver X receptor α (LXRα) were studied to investigate the mechanism involved.

Results: Plasma TG, TC, LDL-C, and LDL-C/HDL-C were significantly increased, and HDL-C was significantly decreased in the HDP group in comparison to the control (all $p < 0.001$). ANP inhibited the expression of ABCA1 and ABCG1 at both the mRNA and protein levels in a dose-dependent manner. The functions of ABCA1- and ABCG1-mediated cholesterol efflux to apoA-I and HDL were significantly decreased. NPR-A siRNA further confirmed that ANP binding to its receptor inhibited ABCA1/G1 expression through the PPAR-γ/LXRα pathway.

Conclusions: ABCA1/G1 was inhibited by the stimulation of ANP when combined with NPR-A through the PPAR-γ/LXRα pathway in THP-1 macrophages. The ABCA1/G1-mediated cholesterol efflux was also impaired by the stimulation of ANP. This may provide a new explanation for the decreased level of HDL-C in HDP patients.

Keywords: atrial natriuretic peptide, ATP-binding cassette transporter A1, ATP-binding cassette transporter G1, cholesterol efflux, hypertensive disorders of pregnancy

OPEN ACCESS

Edited by:
Liang Weng,
Central South University, China

Reviewed by:
TingTing Hong,
University of Utah, United States
Dawei Zhang,
University of Alberta, Canada

****Correspondence:***
Wei Song
songwei8124@163.com

†These authors have contributed equally to this work and share first authorship

Specialty section:
This article was submitted to Inflammation Pharmacology, a section of the journal Frontiers in Pharmacology

Received: *26 May 2021*
Accepted: *24 June 2021*
Published: *28 July 2021*

Citation:
Dong Y, Lin Y, Liu W, Zhang W, Jiang Y and Song W (2021) Atrial Natriuretic Peptide Inhibited ABCA1/G1-dependent Cholesterol Efflux Related to Low HDL-C in Hypertensive Pregnant Patients. Front. Pharmacol. 12:715302. doi: 10.3389/fphar.2021.715302

INTRODUCTION

Hypertensive disorders of pregnancy (HDP) is one of the leading causes of placental abruption, stroke, multiple organ failure, disseminated intravascular coagulation, intrauterine growth retardation, and intrauterine death (Anonymous, 2020). Although the etiology is multifactorial, changes in metabolism are also related to the prognosis of HDP. Turgay Emet et al. found that plasma total cholesterol (TC), triglyceride (TG), and low-density lipoprotein cholesterol (LDL-C) levels were significantly increased as pregnancy progressed (Emet et al., 2013). The plasma TG, TC, and LDL-C levels were higher in preeclampsia patients in a study with a southwestern India population (Bhat et al., 2019). Furthermore, maternal plasma TG increase and high-density lipoprotein cholesterol (HDL-C) decrease at late-stage gestation were associated with macrosomia risk and preterm delivery (Wang et al., 2018; Niyaty et al., 2020).

Atrial natriuretic peptide (ANP), which belongs to the natriuretic peptide family, is a polypeptide hormone that is mainly synthesized, stored, and secreted by the heart (Nakagawa et al., 2019). ANP was first recognized by de Bold et al. when a rapid and potent natriuretic response to intravenous injection of the atrial myocardial extract was observed in rats (de Bold et al., 1981). Pro-ANP was hydrolyzed by serine protease corin and released the same amount of N-terminal pro-atrial natriuretic peptide (NT-pro-ANP) and ANP when the blood pressure and volume increased (Nakagawa et al., 2019). There are three kinds of natriuretic peptide receptors in mammals. Natriuretic peptide receptor-A (NPR-A) is the principal receptor for ANP and brain natriuretic peptide. Natriuretic peptide receptor-B is the principal receptor for C-type natriuretic peptide. Natriuretic peptide receptor-C acts as a clearance receptor when binding with ANP. ANP contributes to maintaining blood pressure and body fluid homeostasis through diuresis, vasodilation, and inhibition of the renin–angiotensin system (Nakagawa et al., 2019). ANP knockout in adult male mice induced salt-sensitive hypertension (John et al., 1995). NPR-A knockout caused hypertension in mice (Oliver et al., 1997), indicating that ANP binding to NPR-A plays an important role in the regulation of blood pressure. Our previous study showed that the plasma NT–pro-ANP level was also significantly increased in HDP patients (Lin et al., 2021).

Recently, several lines of evidence have suggested that ANP is involved in lipid metabolism in different ways. Gabriella Garruti et al. found that ANP was expressed in and secreted from subcutaneous and visceral adipose tissue and pre-adipocytes (Garruti et al., 2007). ANP inhibited the proliferation of human visceral mature adipocytes and pre-adipocytes cultured *in vitro* (Sarzani et al., 2008). ANP was also expressed in and secreted from brown adipocytes (Bae and Kim, 2019), which induced thermogenic action (Kimura et al., 2017), and promoted adipose tissue browning (Bordicchia et al., 2012). Meanwhile, ANP accelerated lipolysis by phosphorylating hormone-sensitive lipase *in vitro* and *in vivo* (Sengenès et al., 2003; Birkenfeld et al., 2005) and induced lipid oxidation in humans (Birkenfeld et al., 2008).

ATP-binding cassette transporter A1 and G1 (ABCA1/G1) were transmembrane proteins that mediated cholesterol efflux to apolipoprotein A-I (apoA-I) and HDL-C. It was the first and rate-limiting step of reverse cholesterol transport (RCT). ABCA1 deficiency in patients (known as Tangier's disease) demonstrated a high incidence of early-onset cardiovascular disease because of the extremely low HDL-C levels (Bodzioch et al., 1999). Harmen Wiersma et al. found that the plasma HDL-C level was significantly reduced in ABCG1 knockout mice treated with a high-cholesterol diet (Wiersma et al., 2009).

Our previous study demonstrated that ANP was increased in HDP (Lin et al., 2021); however, whether it affects the lipid profile remains unknown. Therefore, this study aimed to investigate whether ANP is involved in cholesterol metabolism.

MATERIALS AND METHODS

Study Subjects

A total of 265 patients with HDP were enrolled in the HDP group from April 2014 to April 2017 at First Affiliated Hospital of Dalian Medical University (Dalian, China). A total of 178 normotensive women with gestational age >20 weeks were enrolled at the same time as the control group. The registration number for this clinical registration study was ChiCTR-ROC-17011468. Ethical approval for the study was obtained from the Human Ethics Committee of First Affiliated Hospital of Dalian Medical University. All the patients provided written informed consent before participating in the study.

The diagnostic criteria of HDP were in accordance with the guidelines published by the European Society of Cardiology in 2018 (Regitz-Zagrosek et al. (2018)), including preexisting hypertension, gestational hypertension, preeclampsia, preexisting hypertension plus superimposed gestational hypertension with proteinuria, and antenatally unclassifiable hypertension. The exclusion criteria were 1) gestational age <20 weeks; 2) malignant tumor or cancer, immune system disease, blood system disease, taking glucocorticoid drugs within two weeks, and taking immunosuppressants; 3) acute or chronic kidney disease, and taking diuretics; 4) secondary hypertension, severe liver dysfunction, and diabetes diagnosed before pregnancy; and 5) hyperthyroidism or hypothyroidism.

Clinical Assessments

The clinical data, including age, height, prepregnancy body mass index (BMI), history of hypertension, past medical history, and blood pressure, were recorded in each patient's prenatal health records. We selected the maximum blood pressure in the medical history for grouping because some of the patients were taking antihypertensive drugs. Fasting blood samples were collected during hospitalization before delivery, and serum creatinine, TC, TG, HDL-C, and LDL-C were measured using the Hitachi 7170 automatic biochemical analyzer in our Clinical laboratory Center (WEI RIKANG Bioengineering Co. Ltd., China). Urine was collected for urinalysis. Prepregnancy BMI and estimated glomerular filtration rate (eGFR) were calculated according to the formula BMI = height (kg)/weight^2 (cm^2), and eGFR = $(186 \times \mathrm{Scr})^{-1.154} \times \mathrm{age}^{-0.203} \times 0.742$.

THP-1 Culture and Treatment

Human THP-1 macrophages (Procell, Wuhan, China) were cultured in RPMI-1640 supplemented with 0.05 nM β-mercaptoethanol, and 10% fetal bovine serum in 5% CO_2 at 37°C. The cells were differentiated into macrophages by incubation with 100 ng/ml phorbol myristate acetate for 72 h. ANP was dissolved in basic RPMI-1640 to obtain the required concentrations (ranging from 10^{-9} to 10^{-5} mmol/L). The macrophages were cultured in medium containing different concentrations of ANP for 72 h. Total mRNA and protein were extracted for ABCA1 and ABCG1 detection. Liver X receptor α (LXRα) agonist 22-(R)-OH-cholesterol and proliferator-activated receptor-γ (PPARγ) agonist rosiglitazone were used to detect whether LXRα and PPARγ were involved in ABCA1 and ABCG1 expression mediated by ANP. NPR-A small interfering RNA (siRNA) was used to investigate whether NPR-A as a receptor was involved in ABCA1 and ABCG1 expression mediated by ANP. The macrophages were transfected with NPR-A siRNA and then coincubated with 10^{-5} mmol/L ANP for 72 h. Agonists of 22-(R)-OH-cholesterol (1 μM) and rosiglitazone (100 nM) were incubated with macrophages for another 48 h. Total protein was harvested for ABCA1, ABCG1, LXRα, and PPARγ detection.

Quantitative Real-Time PCR (qRT-PCR)

Total RNA was extracted from the cells using TRIZOL reagent (BioTeke, Beijing, China) and then converted into cDNA by M-MLV reverse transcriptase (BioTeke, Beijing, China). The resulting cDNAs were subjected to qRT-PCR with SYBR™ green detection chemistry on an Exicycler™ real-time PCR system (Bioneer, Daejeon, Korea).

The following sequences of the real-time PCR primers were used: ABCA1 forward, 5′-TCACCACTTCGGTCTCC-3′ and reverse 5′- CCACCTTCATCCCATCT-3′; ABCG1 forward, 5′-GGGTCGCTCCATCATTT-3′ and reverse 5′- TGTGGTAGG TTGGGCAGT-3′; β-actin forward, 5′-CACTGTGCCCATCTA CGAGG-3′, and reverse 5′- TAATGTCACGCACGATTTCC. The specificity of all the PCR products was assessed using the melting curve analysis. Relative gene expression was analyzed using the $2^{-\Delta\Delta Ct}$ method and normalized against β-actin as the internal control.

Immunoblotting

The protein samples were loaded onto an 8% or 11% sodium dodecyl sulfate–polyacrylamide gel electrophoresis (SDS-PAGE) system for electrophoresis and blotting. The following antibodies were used: rabbit anti-ABCA1, anti-ABCG1 antibody (Sangon Biotech, Shanghai, China), rabbit anti–NPR-A, anti-LXRα antibody (ABclonal Technology, Wuhan, China), and rabbit anti-PPARγ, and β-actin antibody (Wanleibio, Shenyang, China). After incubation with the horseradish peroxidase–conjugated secondary antibody, the protein bands were visualized by enhanced chemiluminescence (ECL) (Wanleibio, Shenyang, China).

Cellular Cholesterol Efflux Assays

THP-1 macrophages were incubated with 10^{-5} mol/L ANP for 72 h and then labeled with 5 μmol/L 22-NBD-cholesterol for 4 h. Afterward, the 22-NBD cholesterol labeled cells were rinsed with phosphate-buffered saline (PBS) and incubated in the presence of apoA-Ⅰ (15 μg/ml) or HDL (50 μg/ml) for 4 h. The fluorescence intensity (FI) of the medium and lysate was measured at 469 nm wavelengths for excitation and 537 nm for emission using a multimode microplate reader (BioTek, Winooski, VT, United States). Finally, the percent efflux was calculated using the following equation: FI (efflux medium)/[FI (efflux medium) + FI (cell lysate)] × 100%.

SiRNA Transfection

Specific siRNAs against NPR-A (sense, 5′- GGCCGAGUUAUC UACAUCUTT-3′; antisense, 5′-AGAUGUAGAUAACUCGGC CTT-3′), and scramble negative control siRNA (sense, 5′-UUC UCCGAACGUGUCACGUTT-3′; antisense, 5′-ACGUGACAC GUUCGGAGAATT-3′) were synthesized by Jintuosi Company (Wuhan, China). The macrophages were transfected with siRNA duplexes (100 pM final concentration) using Lipofectamine™ RNAiMAX reagent (Invitrogen, Carlsbad, CA, United States). After 48 h, Western blot analysis was performed to determine the transfection efficiency.

Statistical Analysis

Data were represented as the mean ± standard deviation. Clinical data were analyzed using SPSS software, version 17.0 (SPSS Inc., Chicago, IL, United States). The independent *t*-test was used if the distribution was normal; otherwise, the Mann–Whitney *U* test was used. Experimental data were presented using GraphPad Prism 8 (GraphPad Software, San Diego, CA, United States). One-way ANOVA and two-way ANOVA were used. $p < 0.05$ was considered to be statistically significant difference.

RESULTS

Demographic Characteristics of the Two Groups

There were no significant differences in age, height, or prepregnancy BMI between the HDP group and the control group (each $p > 0.05$). The creatinine was significantly higher in the HDP group than in the control group ($p < 0.01$). The eGFR was significantly lower in the HDP group than in the control group ($p < 0.01$) (**Table 1**).

Maternal Plasma Lipid Profile of the Two Groups

The plasma concentration of TC was dramatically higher in the HDP group than that in the control group (6.23 ± 0.10 mmol/L vs. 5.69 ± 0.10 mmol/L, $p < 0.01$) (**Figure 1A**). The plasma concentration of TG was significantly increased in the HDP group in comparison to the control group (3.79 ± 0.11 mmol/L vs. 3.25 ± 0.10 mmol/L, $p < 0.01$) (**Figure 1B**). The plasma concentration of HDL-C was much lower in the HDP group than that in the control group (1.69 ± 0.02 mmol/L vs. 1.86 ± 0.04 mmol/L, $p < 0.01$) (**Figure 1C**). The plasma concentration of LDL-C was significantly higher in the HDP group than that in the control group (3.39 ± 1.03 mmol/L vs. 3.18 ± 0.78 mmol/L, $p < 0.01$) (**Figure 1D**). The plasma LDL-C/HDL-C ratio was markedly increased in the HDP group in comparison to the control group (2.07 ± 0.04 vs. 1.83 ± 0.04, $p < 0.01$) (**Figure 1E**).

TABLE 1 | Demographic characteristics of the two groups.

	Control group (n = 178)	HDP group (n = 265)	p Value
Age (year)	31.06 ± 4.13	31.36 ± 4.62	0.542
Height (cm)	162.99 ± 5.17	163.03 ± 5.26	0.882
Prepregnancy BMI(kg/m^2)	25.11 ± 3.08	25.51 ± 4.22	0.778
Creatinine (umol/L)	44.82 ± 0.59	51.98 ± 0.79	< 0.01[a]
eGFR (mL/min×1.73 m^2)	140.77 ± 1.83	124.03 ± 1.73	< 0.01[a]

HDP, hypertensive disorders of pregnancy; BMI, body mass index; eGFR, estimated glomerular filtration rate.
[a]*p < 0.01, compared with the control group.*

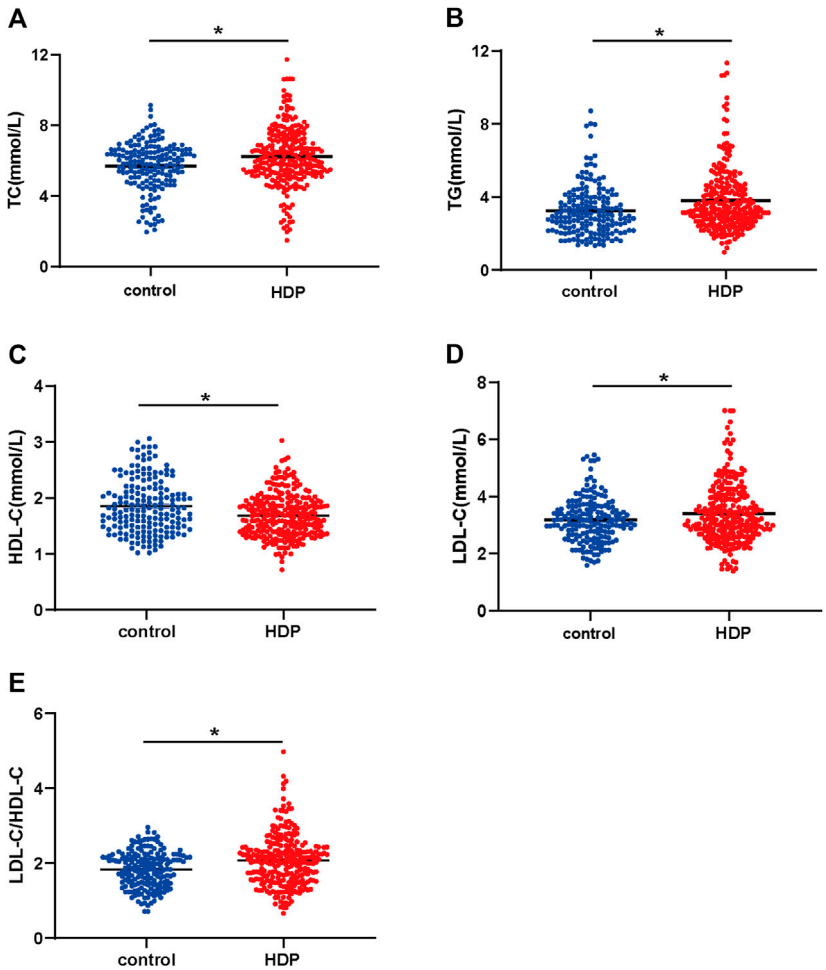

FIGURE 1 | Maternal plasma lipid profile of the two groups. Plasma concentrations of TC (A), TG (B), LDL-C (C), HDL-C (D), and LDL-C/HDL-C ratio (E) were compared in the HDP group (n = 265) and the control group (n = 178). HDP, hypertensive disorders of pregnancy; TC, total cholesterol; TG, total triglycerides; HDL-C, high-density lipoprotein cholesterol; LDL-C, low-density lipoprotein cholesterol. *p < 0.01, compared with the control group.

ABCA1 and ABCG1 Were Inhibited by the Stimulation of ANP in THP-1 Macrophages

ABCA1 and ABCG1 were dramatically inhibited in a dose-dependent manner at both the transcriptional (**Figure 2A, B**) and translational (**Figure 2C–F**) levels by the stimulation of ANP at concentrations ranging between 10^{-9} and 10^{-5} mol/L. Therefore, 10^{-5} mol/L was chosen as the optimal concentration in the subsequent experiments.

ABCA1- and ABCG1-Mediated Cholesterol Efflux Was Impaired by ANP

ABCA1-mediated cholesterol efflux to apoA-I was markedly decreased by ANP treatment in comparison to the control group (p < 0.01) (**Figure 3A**). And ABCG1-mediated cholesterol efflux to HDL was also significantly inhibited by ANP treatment in comparison to the control group (p < 0.01) (**Figure 3B**).

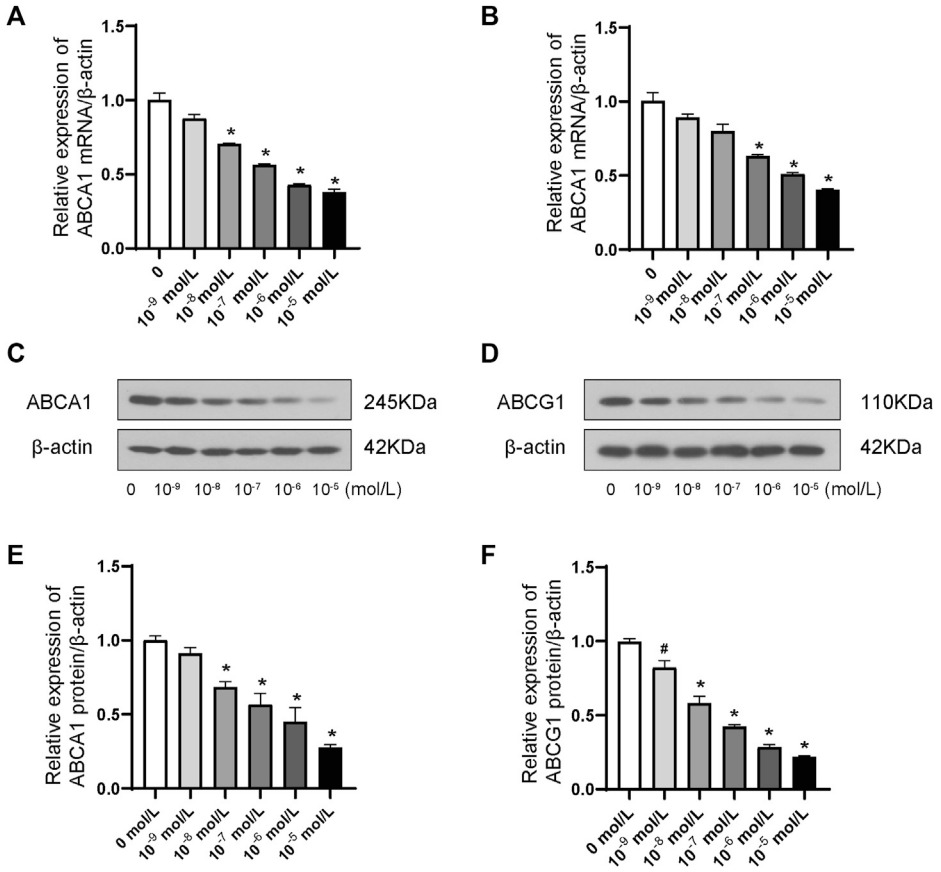

FIGURE 2 | Dose-dependent effects of ANP downregulated ABCA1 and ABCG1 in THP-1 macrophages. A: ANP in concentrations ranging from 10^{-9} to 10^{-5} mol/L inhibited the ABCA1 mRNA expression in a dose-dependent manner ($n = 3$). B: ANP in concentrations ranging from 10^{-9} to 10^{-5} mol/L suppressed ABCG1 mRNA expression in a dose-dependent manner. C and E: ANP in concentrations ranging from 10^{-9} to 10^{-5} mol/L inhibited the ABCA1 protein expression in a dose-dependent manner. D and F: ANP in concentrations ranging from 10^{-9} to 10^{-5} mol/L suppressed ABCG1 protein expression in a dose-dependent manner. $^{\#}p < 0.05$, compared with the control group. $^{*}p < 0.01$, compared with the control group.

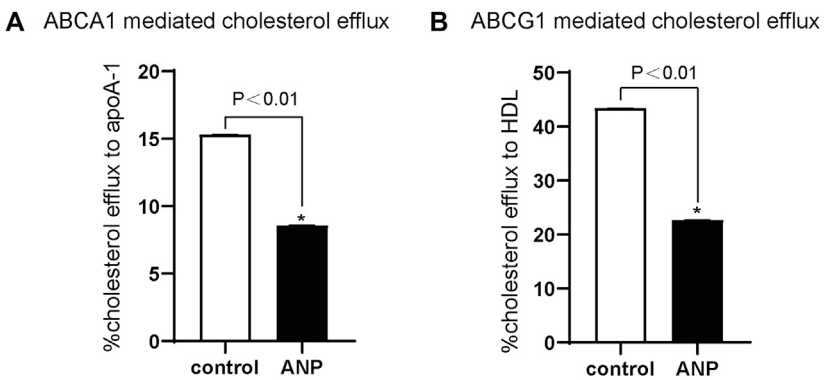

FIGURE 3 | ANP inhibited ABCA1- and ABCG1-mediated cholesterol efflux. THP-1 cells were treated with the absence or presence of 10^{-5} mol/L ANP for 72 h. Cholesterol efflux was measured using apoA-I (15 μg/ml) and HDL (50 μg/ml) as lipid acceptors. A: ABCA1-mediated cholesterol efflux to apoA-I was attenuated in the ANP group. B: ABCG1-mediated cholesterol efflux to HDL was decreased in the ANP group. $^{*}p < 0.01$, compared with the control group. Data are expressed as mean ± SEM of three independent experiments.

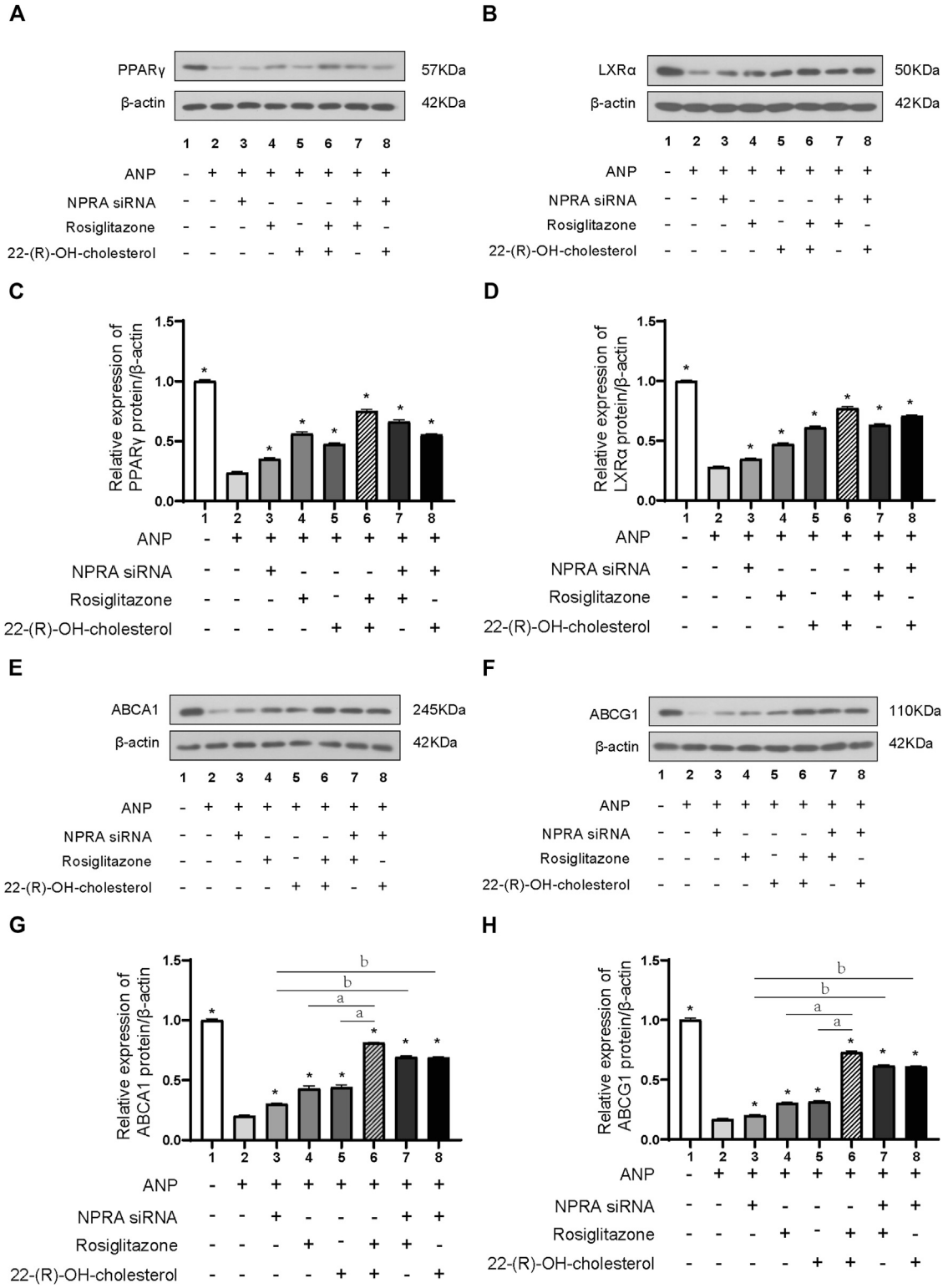

FIGURE 4 | ANP inhibited the expression of ABCA1 and ABCG1 through the PPARγ/LXRα pathway. THP-1 cells were transfected with or without NPR-A siRNA and pretreated with or without ANP (10^{-5} mol/L) for 72h, and then incubated with or without rosiglitazone (100 nM) or 22-(R)-OH-cholesterol (1 μM) for another 24 h. The protein expressions of PPARγ **(A)**, LXRα **(B)**, ABCA1 (E), and ABCG1 (H) were examined by Western immunoblotting assays. β-actin was used as an endogenous control. The protein expressions of PPARγ **(C)**, LXRα **(D)**, ABCA1 **(G)**, and ABCG1 (H) were quantified by densitometric analysis of Western immunoblotting. *$p <$ 0.01 vs. the ANP alone group. $^{a}P < 0.01$ vs. the ANP + rosiglitazone+22-(R)-OH-cholesterol group. $^{b}P < 0.01$ vs. the ANP + NPR-A siRNA group. Data are expressed as mean ± SEM of three independent experiments.

ANP Combined with NPR-A Inhibited ABCA1/G1 Through the PPARγ/Lxrα Pathway

NPR-A expression was dramatically downregulated after NPR-A siRNA transfection (**Supplementary Figure S1**). PPARγ protein expression was decreased by ANP stimulation ($p < 0.01$) (**Figures 4A, C** lane 1 and lane 2). ANP also induced a significant decreased in LXRα protein expression ($p < 0.01$) (Figures 4B, D lane 1 and lane 2). PPARγ and LXRα protein expression was reversed by the treatment of NPR-A siRNA (lane 3), PPARγ agonist (lane 4), and LXRα agonist (lane 5) in comparison to ANP (lane 2) ($p < 0.01$) (Figures 4A–D). PPARγ and LXRα protein expression was further reversed by the combined treatment of NPR-A siRNA, PPARγ, and LXRα agonist ($p < 0.01$) (Figures 4A–D lanes 6–8). These results indicated ANP inhibited the PPARγ and LXRα expression by binding to NPR-A, and PPARγ and LXRα agonists can partially reverse the inhibition of PPARγ and LXRα induced by ANP.

ABCA1 and ABCG1 protein expression was partly reversed by the treatment of NPR-A siRNA (lane 3), PPARγ agonist (lane 4), and LXRα agonist (lane 5) in comparison to the ANP group (lane 2); they were almost totally reversed by the combination of PPARγ and LXRα agonists (lane 6) ($p < 0.01$) (**Figures 4E–H**). We inhibited NPR-A by siRNA and found that both the PPARγ agonist and the LXRα agonist abolished the inhibition of ABCA1 and ABCG1 induced by ANP (**Figures 4E–H**, lane 7 and lane 8). These results demonstrated that ABCA1 and ABCG1 were inhibited by ANP when combined with NPR-A through the PPARγ/LXRα pathway.

DISCUSSION

We found that the plasma concentrations of TG, TC, LDL-C, and LDL-C/HDL-C were increased, and the concentration of HDL-C was decreased in HDP patients. These results were consistent with a previous study of preeclampsia patients with a southwestern Indian population (Bhat et al., 2019). The plasma TG level in early pregnancy was positively associated with preeclampsia (Adank et al., 2019). These lipid profile alterations at late-stage gestation were associated with a neonatal adverse prognosis, such as macrosomia risk and preterm delivery (Wang et al., 2018; Niyaty et al., 2020). Furthermore, the maternal early-stage pregnancy plasma TC level was correlated to the TC and LDL-C levels of a mother's 5- to 6-year-old offspring (van Lieshout et al., 2017). Therefore, alterations of the maternal blood lipid profile were related to the short- and long-term prognoses of the mother's offspring. Thus, we should monitor the lipid profile in HDP patients. However, the mechanism of blood lipid profile changes in HDP is unclear.

Our previous study found that the plasma NT-proANP level in HDP patients was significantly increased (Lin et al., 2021). Dedoussis et al. found that ANP gene G664A polymorphism was associated with lower levels of apoA-I and HDL-C in familial hypercholesterolemia patients (Dedoussis et al., 2006). HDL-C was found to be decreased in patients with coronary artery disease (CAD) when ANP was increased (Osajima et al., 2001). We found that NT-proANP levels were negatively correlated with HDL-C in the HDP group ($r = -0.10$, $p < 0.05$) (**Supplementary Figure S2**). Therefore, the increase in the plasma ANP found in the HDP patients may be related to low levels of HDL-C.

Hepatic ABCA1 plays an essential role in maintaining plasma HDL-C levels (Timmins et al., 2005). Mutations in the ABCA1 gene cause an extremely low plasma HDL-C level (Bodzioch et al., 1999). A study pointed out that the deficiency of ABCA1 in macrophages was probably reflected in its level in the liver, which resulted in low plasma HDL-C levels in CAD patients (Song et al., 2015). Therefore, we found that the deficiency of ABCA1 expression and function in macrophages induced by ANP stimulation may provide an explanation for the low plasma HDL-C level in HDP patients.

The effect of ABCG1 on the plasma HDL-C level remains controversial. Yan Xu et al. demonstrated that ABCG1 promoter region rs57137919 polymorphism caused the reduction of ABCG1 expression which promoted the occurrence of CAD but was not associated with the plasma HDL-C level (Xu et al., 2011). Harmen Wiersma et al. found that the plasma HDL-C level was significantly reduced in ABCG1 knockout mice treated with a high-cholesterol diet (Wiersma et al., 2009). Our study indicated that ANP inhibited the expression and function of ABCG1; however, more evidence is needed to determine if it is related to the low HDL-C level in HDP patients.

Although there may be other mechanisms, we found that the inhibition of ABCA1/G1 by ANP may be partially due to its binding to the NPR-A receptor. A previous study demonstrated that ANP had the highest affinity with NPR-A, which was consistent with our data (Nakagawa et al., 2019). Furthermore, we investigated the transcriptional regulation mechanism of ABCA1. Previous research showed that LXRα promoted RCT in human macrophages by upregulation of ABCA1 and ABCG1 expressions because four nucleotides (from −70 to −55 base pairs) located in the ABCA1 promoter were the binding sites to LXRα that promoted transcription (Costet et al., 2000). LXRα was also found to upregulate the transcription and expression of ABCG1 in macrophages (Ishibashi et al., 2013). Therefore, we thought that this key regulatory mechanism was also involved in the regulation of ANP on ABCA1. We found that the expression of PPARγ was enhanced by LXRα-specific agonists, and *vice versa*. This phenomenon was similar to the finding reported by Chawla et al., which showed that PPARγ stimulated the transcription of LXRα in macrophages (Chawla et al., 2001). Furthermore, there was other evidence which demonstrated that LXRα antagonist inhibited the transcription of PPARγ (Tsuboi et al., 2020). They proposed that LXRα and PPARγ formed a loop pathway to amplify the signals, which was further confirmed by our results. Thus, we concluded that ABCA1 and ABCG1 were inhibited by ANP when binding to its receptor NPR-A dependent on the PPARγ/LXRα pathway, which may be one of the mechanisms involved in the low HDL-C levels in HDP (**Figure 5**).

Andrew C. Li et al. found that the plasma LDL-C increased and the plasma HDL-C decreased in female mice but not in male mice after administration of PPARγ agonists (rosiglitazone or GW7845) to mice (Li et al., 2000). Therefore, the regulation of

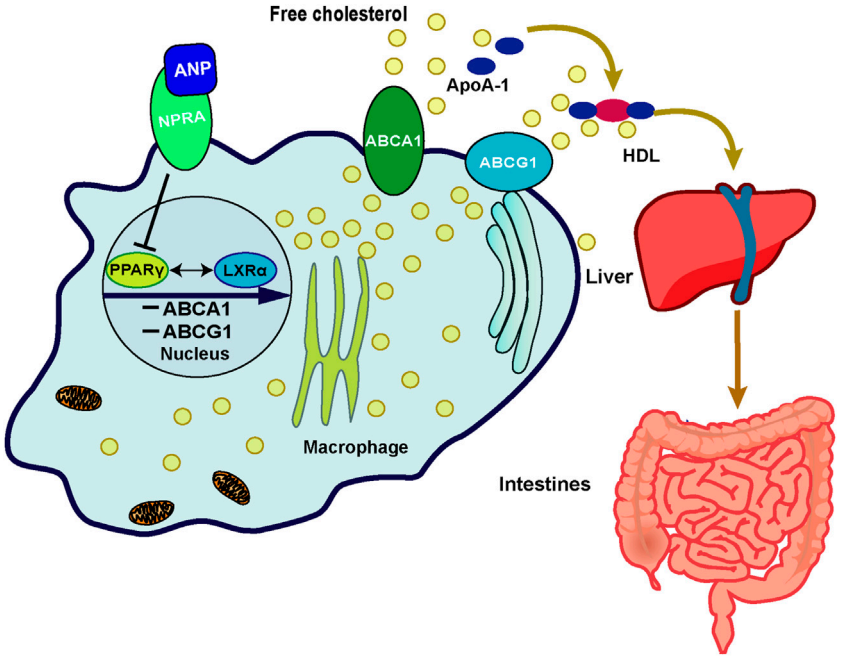

FIGURE 5 | Schematic representation of the possible mechanism of ANP on the cholesterol efflux mediated by the PPARγ/LXRα–ABCA1/ABCG1 signaling pathway in macrophages. In the THP-1 derived macrophages, ANP inhibited the transcription of PPARγ and LXRα, then the expression of ABCA1 and ABCG1 was inhibited, thereby inhibiting cholesterol efflux from macrophages to apoA-I and HDL mediated by ABCA1 and ABCG1.

PPARγ on a lipid profile may be related to pregnancy in females. The safety of statins in pregnant women remains controversial. An obvious teratogenic effect was found in an animal study. There were case series studies which also demonstrated congenital anomalies associated with statin exposure, while some observational research works did not find an increased risk of congenital anomalies with statin therapy in pregnancy (Karalis et al., 2016). The possible reason for this was that the concentration of drugs used was higher for animals than for pregnant women. PPARγ agonists may become a new therapeutic target for clinical treatment for pregnant women.

Our study demonstrated for the first time that ANP binding to NPR-A inhibited ABCA1/ABCG1-mediated cholesterol efflux through the PPARγ/LXRα pathway. This mechanism may be involved in low HDL-C levels in HDP patients. These findings provide updated evidence that ANP may be involved in abnormal lipid metabolism in HDP.

DATA AVAILABILITY STATEMENT

The original contributions presented in the study are included in the article/**Supplementary Material**; further inquiries can be directed to the corresponding author.

ETHICS STATEMENT

The studies involving human participants were reviewed and approved by the Human Ethics Committee of First Affiliated Hospital of Dalian Medical University. The patients/participants provided their written informed consent to participate in this study.

AUTHOR CONTRIBUTIONS

YD and YL performed most of the experimental procedures and carried out the statistical analyses. WL and WZ were in charge of patients' recruitment and clinical data collection. YD, YL, WL, WZ, YJ, and WS contributed to the data analysis interpretation and discussion of the results. YD and WS drafted the manuscript. WS conceived the study and designed the protocols. All authors contributed to the article and approved the submitted version.

FUNDING

This research was supported by the National Natural Science Foundation of China (Grant 81800379) and the National Natural Science Foundation of Liaoning (Grant 20180550577).

SUPPLEMENTARY MATERIAL

The Supplementary Material for this article can be found online at: https://www.frontiersin.org/articles/10.3389/fphar.2021.715302/full#supplementary-material

REFERENCES

Anonymous (2020). Gestational Hypertension and Preeclampsia: ACOG Practice Bulletin, Number 222. *Obstet. Gynecol.* 135 (6), e237–e260. doi:10.1097/AOG.0000000000003891

Adank, M. C., Benschop, L., Peterbroers, K. R., Smak Gregoor, A. M., Kors, A. W., Mulder, M. T., et al. (2019). Is Maternal Lipid Profile in Early Pregnancy Associated with Pregnancy Complications and Blood Pressure in Pregnancy and Long Term Postpartum? *Am. J. Obstet. Gynecol.* 221 (2), e1–e150. doi:10.1016/j.ajog.2019.03.025

Bae, I.-S., and Kim, S. H. (2019). Expression and Secretion of an Atrial Natriuretic Peptide in Beige-like 3T3-L1 Adipocytes. *Int. J. Mol. Sci.* 20 (24), 6128. doi:10.3390/ijms20246128

Bhat, P. V., Vinod, V., Priyanka, A. N., and Kamath, A. (2019). Maternal Serum Lipid Levels, Oxidative Stress and Antioxidant Activity in Pre-eclampsia Patients from Southwest India. *Pregnancy Hypertens.* 15, 130–133. doi:10.1016/j.preghy.2018.12.010

Birkenfeld, A. L., Boschmann, M., Moro, C., Adams, F., Heusser, K., Franke, G., et al. (2005). Lipid Mobilization with Physiological Atrial Natriuretic Peptide Concentrations in Humans. *J. Clin. Endocrinol. Metab.* 90 (6), 3622–3628. doi:10.1210/jc.2004-1953

Birkenfeld, A. L., Budziarek, P., Boschmann, M., Moro, C., Adams, F., Franke, G., et al. (2008). Atrial Natriuretic Peptide Induces Postprandial Lipid Oxidation in Humans. *Diabetes* 57 (12), 3199–3204. doi:10.2337/db08-0649

Bodzioch, M., Orsó, E., Klucken, J., Langmann, T., Böttcher, A., Diederich, W., et al. (1999). The Gene Encoding ATP-Binding Cassette Transporter 1 Is Mutated in Tangier Disease. *Nat. Genet.* 22 (4), 347–351. doi:10.1038/11914

Bordicchia, M., Liu, D., Amri, E.-Z., Ailhaud, G., Dessì-Fulgheri, P., Zhang, C., et al. (2012). Cardiac Natriuretic Peptides Act via P38 MAPK to Induce the Brown Fat Thermogenic Program in Mouse and Human Adipocytes. *J. Clin. Invest.* 122 (3), 1022–1036. doi:10.1172/JCI59701

Chawla, A., Boisvert, W. A., Lee, C.-H., Laffitte, B. A., Barak, Y., Joseph, S. B., et al. (2001). A PPARγ-LXR-ABCA1 Pathway in Macrophages Is Involved in Cholesterol Efflux and Atherogenesis. *Mol. Cel.* 7 (1), 161–171. doi:10.1016/s1097-2765(01)00164-2

Costet, P., Luo, Y., Wang, N., and Tall, A. R. (2000). Sterol-dependent Transactivation of theABC1 Promoter by the Liver X Receptor/Retinoid X Receptor. *J. Biol. Chem.* 275 (36), 28240–28245. doi:10.1074/jbc.m003337200

de Bold, A. J., Borenstein, H. B., Veress, A. T., and Sonnenberg, H. (1981). A Rapid and Potent Natriuretic Response to Intravenous Injection of Atrial Myocardial Extract in Rats. *Life Sci.* 28 (1), 89–94. doi:10.1016/0024-3205(81)90370-2

Dedoussis, G. V. Z., Maumus, S., Skoumas, J., Choumerianou, D. M., Pitsavos, C., Stefanadis, C., et al. (2006). Natriuretic Peptide Val7Met Substitution and Risk of Coronary Artery Disease in Greek Patients with Familial Hypercholesterolemia. *J. Clin. Lab. Anal.* 20 (3), 98–104. doi:10.1002/jcla.20108

Emet, T., Üstüner, I., Güven, S. G., Balık, G., Ural, Ü. M., Tekin, Y. B., et al. (2013). Plasma Lipids and Lipoproteins during Pregnancy and Related Pregnancy Outcomes. *Arch. Gynecol. Obstet.* 288 (1), 49–55. doi:10.1007/s00404-013-2750-y

Garruti, G., Giusti, V., Nussberger, J., Darimont, C., Verdumo, C., Amstutz, C., et al. (2007). Expression and Secretion of the Atrial Natriuretic Peptide in Human Adipose Tissue and Preadipocytes*. *Obesity* 15 (9), 2181–2189. doi:10.1038/oby.2007.259

Ishibashi, M., Filomenko, R., Rébé, C., Chevriaux, A., Varin, A., Derangère, V., et al. (2013). Knock-down of the Oxysterol Receptor LXRα Impairs Cholesterol Efflux in Human Primary Macrophages: Lack of Compensation by LXRβ Activation. *Biochem. Pharmacol.* 86 (1), 122–129. doi:10.1016/j.bcp.2012.12.024

John, S., Krege, J., Oliver, P., Hagaman, J. R., Hodgin, J., Pang, S., et al. (1995). Genetic Decreases in Atrial Natriuretic Peptide and Salt-Sensitive Hypertension. *Science* 267 (5198), 679–681. doi:10.1126/science.7839143

Karalis, D. G., Hill, A. N., Clifton, S., and Wild, R. A. (2016). The Risks of Statin Use in Pregnancy: A Systematic Review. *J. Clin. Lipidol.* 10 (5), 1081–1090. doi:10.1016/j.jacl.2016.07.002

Kimura, H., Nagoshi, T., Yoshii, A., Kashiwagi, Y., Tanaka, Y., Ito, K., et al. (2017). The Thermogenic Actions of Natriuretic Peptide in Brown Adipocytes: The Direct Measurement of the Intracellular Temperature Using a Fluorescent Thermoprobe. *Sci. Rep.* 7 (1), 12978. doi:10.1038/s41598-017-13563-1

Li, A. C., Brown, K. K., Silvestre, M. J., Willson, T. M., Palinski, W., and Glass, C. K. (2000). Peroxisome Proliferator-Activated Receptor γ Ligands Inhibit Development of Atherosclerosis in LDL Receptor-Deficient Mice. *J. Clin. Invest.* 106 (4), 523–531. doi:10.1172/jci10370

Lin, Y., Dong, Y.-B., Liu, Y.-R., Zhang, Y., Li, H.-Y., and Song, W. (2021). Correlation between Corin, N-Terminal Pro-atrial Natriuretic Peptide and Neonatal Adverse Prognostic in Hypertensive Disorders of Pregnancy. *Pregnancy Hypertens.* 23, 73–78. doi:10.1016/j.preghy.2020.11.007

Nakagawa, Y., Nishikimi, T., and Kuwahara, K. (2019). Atrial and Brain Natriuretic Peptides: Hormones Secreted from the Heart. *Peptides* 111, 18–25. doi:10.1016/j.peptides.2018.05.012

Niyaty, S., Moghaddam-Banaem, L., Sourinejad, H., and Mokhlesi, S. (2020). Are Maternal Metabolic Syndrome and Lipid Profile Associated with Preterm Delivery and Preterm Premature Rupture of Membranes?. *Arch. Gynecol. Obstet.* 303, 113–119. doi:10.1007/s00404-020-05738-5

Oliver, P. M., Fox, J. E., Kim, R., Rockman, H. A., Kim, H.-S., Reddick, R. L., et al. (1997). Hypertension, Cardiac Hypertrophy, and Sudden Death in Mice Lacking Natriuretic Peptide Receptor A. *Proc. Natl. Acad. Sci.* 94 (26), 14730–14735. doi:10.1073/pnas.94.26.14730

Osajima, A., Okazaki, M., Kato, H., Anai, H., Tsuda, Y., Segawa, K., et al. (2001). Clinical Significance of Natriuretic Peptides and Cyclic GMP in Hemodialysis Patients with Coronary Artery Disease. *Am. J. Nephrol.* 21 (2), 112–119. doi:10.1159/000046233

Regitz-Zagrosek, V., Roos-Hesselink, J. W., Bauersachs, J., Blomstrom-Lundqvist, C., Cifkova, R., De Bonis, M., et al. (2018). 2018 ESC Guidelines for the Management of Cardiovascular Diseases during Pregnancy. *Eur. Heart J.* 39 (34), 3165–3241. doi:10.1093/eurheartj/ehy34010.1093/eurheartj/ehy478

Sarzani, R., Marcucci, P., Salvi, F., Bordicchia, M., Espinosa, E., Mucci, L., et al. (2008). Angiotensin II Stimulates and Atrial Natriuretic Peptide Inhibits Human Visceral Adipocyte Growth. *Int. J. Obes.* 32 (2), 259–267. doi:10.1038/sj.ijo.0803724

Sengenès, C., Bouloumié, A., Hauner, H., Berlan, M., Busse, R., Lafontan, M., et al. (2003). Involvement of a cGMP-dependent Pathway in the Natriuretic Peptide-Mediated Hormone-Sensitive Lipase Phosphorylation in Human Adipocytes. *J. Biol. Chem.* 278 (49), 48617–48626. doi:10.1074/jbc.m303713200

Song, W., Wang, W., Dou, L.-Y., Wang, Y., Xu, Y., Chen, L.-F., et al. (2015). The Implication of Cigarette Smoking and Cessation on Macrophage Cholesterol Efflux in Coronary Artery Disease Patients. *J. lipid Res.* 56 (3), 682–691. doi:10.1194/jlr.P055491

Timmins, J. M., Lee, J.-Y., Boudyguina, E., Kluckman, K. D., Brunham, L. R., Mulya, A., et al. (2005). Targeted Inactivation of Hepatic Abca1 Causes Profound Hypoalphalipoproteinemia and Kidney Hypercatabolism of apoA-I. *J. Clin. Invest.* 115 (5), 1333–1342. doi:10.1172/jci200523915

Tsuboi, T., Lu, R., Yonezawa, T., Watanabe, A., Woo, J.-T., Abe-Dohmae, S., et al. (2020). Molecular Mechanism for Nobiletin to Enhance ABCA1/G1 Expression in Mouse Macrophages. *Atherosclerosis* 297, 32–39. doi:10.1016/j.atherosclerosis.2020.01.024

van Lieshout, N., Oostvogels, A. J. J. M., Gademan, M. G. J., and Vrijkotte, T. G. M. (2017). Maternal Early Pregnancy Lipid Profile and Offspring's Lipids and Glycaemic Control at Age 5-6 Years: The ABCD Study. *Clin. Nutr.* 36 (6), 1628–1634. doi:10.1016/j.clnu.2016.10.010

Wang, X., Guan, Q., Zhao, J., Yang, F., Yuan, Z., Yin, Y., et al. (2018). Association of Maternal Serum Lipids at Late Gestation with the Risk of Neonatal Macrosomia in Women without Diabetes Mellitus. *Lipids Health Dis.* 17 (1), 78. doi:10.1186/s12944-018-0707-7

Wiersma, H., Nijstad, N., de Boer, J. F., Out, R., Hogewerf, W., Van Berkel, T. J., et al. (2009). Lack of Abcg1 Results in Decreased Plasma HDL Cholesterol Levels and Increased Biliary Cholesterol Secretion in Mice Fed a High Cholesterol Diet. *Atherosclerosis* 206 (1), 141–147. doi:10.1016/j.atherosclerosis.2009.02.022

Xu, Y., Wang, W., Zhang, L., Qi, L.-P., Li, L.-Y., Chen, L.-F., et al. (2011). A Polymorphism in the ABCG1 Promoter Is Functionally Associated with

Coronary Artery Disease in a Chinese Han Population. *Atherosclerosis* 219 (2), 648–654. doi:10.1016/j.atherosclerosis.2011.05.043

Conflict of Interest: The authors declare that the research was conducted in the absence of any commercial or financial relationships that could be construed as a potential conflict of interest.

Publisher's Note: All claims expressed in this article are solely those of the authors and do not necessarily represent those of their affiliated organizations, or those of the publisher, the editors and the reviewers. Any product that may be evaluated in this article, or claim that may be made by its manufacturer, is not guaranteed or endorsed by the publisher.

frontiers in Pharmacology

ORIGINAL RESEARCH
published: 30 July 2021
doi: 10.3389/fphar.2021.728368

A Novel Integrated Metabolism-Immunity Gene Expression Model Predicts the Prognosis of Lung Adenocarcinoma Patients

Songming Chen[1,2†], *Yumei Duan*[3†], *Yanhao Wu*[4], *Desong Yang*[5] *and Jian An*[4,6,7,8*]

[1]Key Laboratory of Molecular Radiation Oncology Hunan Province, Xiangya Hospital, Central South University, Changsha, China, [2]Xiangya Cancer Center, Xiangya Hospital, Central South University, Changsha, China, [3]Department of Pathology, Xiangya Hospital, Central South University, Changsha, China, [4]Department of Respiratory Medicine, Xiangya Hospital, Central South University, Changsha, China, [5]Thoracic Surgery Department II, Hunan Cancer Hospital & the Affiliated Cancer Hospital of Xiangya School of Medicine, Central South University, Changsha, China, [6]National Key Clinical Specialty, Branch of National Clinical Research Center for Respiratory Disease, Xiangya Hospital, Central South University, Changsha, China, [7]Xiangya Lung Cancer Center, Xiangya Hospital, Central South University, Changsha, China, [8]Hunan Provincial Clinical Research Center for Respiratory Diseases, Changsha, China

OPEN ACCESS

Edited by:
Ning Hou,
Guangzhou Medical University, China

Reviewed by:
Jieqiong Liu,
Sun Yat-Sen Memorial Hospital, China
Jia Xu,
Icahn School of Medicine at Mount Sinai, United States

***Correspondence:**
Jian An
175162349@qq.com

[†]*These authors have contributed equally to this work*

Specialty section:
This article was submitted to Inflammation Pharmacology, a section of the journal Frontiers in Pharmacology

Received: *21 June 2021*
Accepted: *19 July 2021*
Published: *30 July 2021*

Citation:
Chen S, Duan Y, Wu Y, Yang D and An J (2021) A Novel Integrated Metabolism-Immunity Gene Expression Model Predicts the Prognosis of Lung Adenocarcinoma Patients. Front. Pharmacol. 12:728368. doi: 10.3389/fphar.2021.728368

Background: Although multiple metabolic pathways are involved in the initiation, progression, and therapy of lung adenocarcinoma (LUAD), the tumor microenvironment (TME) for immune cell infiltration that is regulated by metabolic enzymes has not yet been characterized.

Methods: 517 LUAD samples and 59 non-tumor samples were obtained from The Cancer Genome Atlas (TCGA) database as the training cohort. Kaplan-Meier analysis and Univariate Cox analysis were applied to screen the candidate metabolic enzymes for their role in relation to survival rate in LUAD patients. A prognostic metabolic enzyme signature, termed the metabolic gene risk score (MGRS), was established based on multivariate Cox proportional hazards regression analysis and was verified in an independent test cohort, GSE31210. In addition, we analyzed the immune cell infiltration characteristics in patients grouped by their Risk Score. Furthermore, the prognostic value of these four enzymes was verified in another independent cohort by immunohistochemistry and an optimized model of the metabolic-immune protein risk score (MIPRS) was constructed.

Results: The MGRS model comprising 4 genes (*TYMS, NME4, LDHA*, and *SMOX*) was developed to classify patients into high-risk and low-risk groups. Patients with a high-risk score had a poor prognosis and exhibited activated carbon and nucleotide metabolism, both of which were associated with changes to TME immune cell infiltration characteristics. In addition, the optimized MIPRS model showed more accurate predictive power in prognosis of LUAD.

Conclusion: Our study revealed an integrated metabolic enzyme signature as a reliable prognostic tool to accurately predict the prognosis of LUAD.

Keywords: lung adenocarcinoma, tumor microenvironment, TYMS, NME4, LDHA, SMOX, CD19, CD68

INTRODUCTION

Lung cancer, one of the most prominent malignant tumors, has the highest mortality rate in humans worldwide. A previous study demonstrated that approximately 80% of lung cancers are non-small cell lung cancer (NSCLC), 50–55% of which are lung adenocarcinoma (LUAD) (Relli et al., 2019). Despite improvements in primary prevention gaining more attention in recent years, LUAD is still difficult to diagnose at an early stage due to the delayed occurrence of symptoms. Recently, an accumulating collection of research indicates that abnormal cancer metabolism has a critical role in cancer metastasis, immune escape, and drug resistance. Proteins, lipids, and nucleic acids are the most common macromolecular classes affected in cancer metabolism, as biosynthesis of all three classes is activated in tumorigenesis (Bader et al., 2020; Bose et al., 2020; Dong et al., 2020; Navas and Carnero, 2021; Yang et al., 2021). Thus, the regulatory mechanisms that regulate cancer metabolism have attracted great attention as a prognostic marker and a potential therapeutic target.

Tumor microenvironment (TME) is closely related to tumor progression. At present, more and more studies show that the changes of tumor microenvironment may be related to abnormal tumor metabolism. Immunotherapy targeting immune checkpoint proteins, such as CTLA-4 and PD-1/L1, has benefited a growing number of patients (Kordbacheh et al., 2018; Zhao et al., 2019; Liu and Zheng, 2020). The infiltration of immune cells into TMEs is a key factor in determining the efficiency of immunotherapy. Furthermore, the production of immune-suppressive metabolites can dampen the antitumor activity of immune cells and promote tumor immunity escape by affecting the expression of cell surface markers (Marin-Acevedo et al., 2021; Memmott et al., 2021; Qiao et al., 2021). Immune checkpoint blockades, such as PD1 and B7-H3, can restore glucose in the TME and permit T cell glycolysis and cytokine production. Immune responses can also be fostered by targeting tumor-intrinsic metabolism (Noël et al., 2018). Although targeting metabolism, such as glutamine metabolism and hexosamine biosynthesis, cannot suppress or activate the immune system completely as it still selectively regulates immune responses (Byun et al., 2020; Lam et al., 2021). Immune checkpoint inhibitors combined with targeting metabolism might be a novel strategy to overcome the immune resistance in immunotherapy. Therefore, comprehensively understanding the effect of tumor metabolism on immune cell infiltration within TME will be helpful for the development of new therapy.

In previous studies, all prediction models were constructed based on RNA-seq data, which focused on only single metabolic genes or immune-related genes, failing to consider the influence of multiple factors. In this study, we used Multivariate Cox Proportional Hazards Regression Analysis to construct an optimized metabolic-immune protein risk score (MIPRS) model based on the protein expression of metabolic and immune proteins to classify LUAD into two subtypes with discrete survival rates. Compared to previous biomarkers, MIPRS is a technically simple and reliable tool to predict the prognosis of LUAD patients.

MATERIALS AND METHODS

Data Acquisition

We downloaded the gene expression matrix and clinical information of 517 LUAD samples and 59 non-tumor samples from The Cancer Genome Atlas (TCGA) database (https://portal.gdc.cancer.gov/repository) as the training set. We then downloaded 266 LUAD samples from the microarray dataset GSE31210 (http://www.ncbi.nlm.nih.gov/geo/) as the first validation set. GSE135222, produced by Illumina HiSeq 2500, was also downloaded from GEO for pharmacodynamic evaluation. In addition, we used 50 LUAD patients from the Xiangya Hospital Central South University as the second validation set, the clinical information of which is shown in **Supplementary Table S1**. The data of metabolizing enzyme genes was downloaded from the KEGG PATHWAY database (https://www.genome.jp/kegg/pathway.html). The abundance of 22 immune cells infiltration were calculated by CIBERSORT.

Multivariate Cox Proportional Hazards Regression Analysis

Multivariate Cox proportional hazards regression analysis utilized by the R package "survival" and "survminer" was performed to screen suitable biomarkers. Subsequently, TYMS, NME4, LDHA and SMOX were finally selected as four key metabolic enzyme genes. According to the regression coefficients of four genes, we established a model in the training set to calculate the risk score of LUAD patients. The formula of risk score (metabolic genes risk score (MGRS)) is as follows:

$$\mathbf{MGRS} = 0.28 \times \mathbf{TYMS} + 0.25 \times \mathbf{NME4} + 0.41 \times \mathbf{LDHA} + 0.20 \times \mathbf{SMOX}$$

Immunohistochemical Assay

Paraffin-embedded lung tissue sections (5-μm) were prepared. After conventional dewaxed to water, the sections were boiled in a pressure cooker with EDTA buffer (pH 8.0) for 2.5 min at 125°C. We then incubated the sections in 5% BSA for 1 h at 37°C. Sections were incubated with primary rabbit anti-LDHA antibody (19987-1-AP; dilution, 1:100; proteintech), anti-TYMS antibody (15047-1-AP; dilution, 1:100; proteintech), anti-SMOX antibody (15047-1-AP; dilution, 1:100; proteintech), anti-NME4 antibody (a8350; dilution, 1:100; ABclonal), anti-CD19 (MAB-0705, MaiXin Biotechnologies, Fuzhou, China) andCD68 (Kit-0026, MaiXin Biotechnologies, Fuzhou, China) at 4°C overnight. The expression of the four enzymes was shown in brown. In order to achieve the purpose

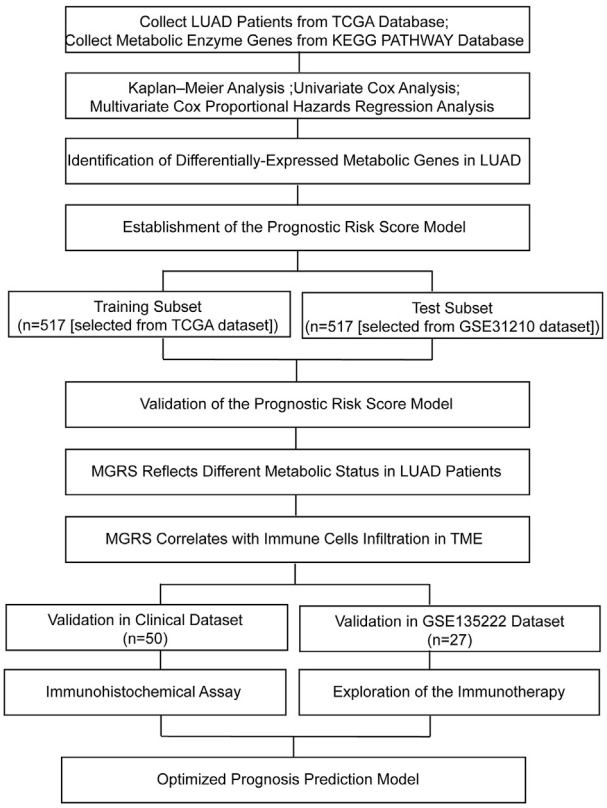

FIGURE 1 | Flow chart of this study. LUAD, lung adenocarcinoma; MGRS, metabolic genes risk score; TME, tumor microenvironment.

of semi quantitative staining, the number of positive cells in each section and their staining intensity were converted into corresponding values. The Mantra™ quantitative pathology workstation, with inForm® image analysis software, were used to analyze the results of immunohistochemistry. The scores of 0, 1, 2 and 3 represent no staining, weak staining, moderate staining and strong staining of target cells, respectively. The sum of percentage of staining scores was calculated to get histochemical score (H-SCORE). Each slice were randomly observed three horizons to calculate the score and took the average as the final score. The median value of H-score was used to distinguish high expression and low expression samples.

Statistical Analysis

All the analysis process was performed by the Strawberry Perl (version 5.32.1.1) software and R (version 4.0.4) software. We have log2 transformed all the data before all of the analysis. The Wilcoxon test and chi-square test were performed for comparisons between two groups and three or more groups respectively. We used both the Kaplan-Meier analysis and Univariate Cox analysis to screen the metabolic enzyme genes negatively correlated with the overall survival (OS). Kyoto Encyclopedia of Genes and Genomes (KEGG) pathway analysis and Gene Ontology (GO) analysis were performed to find differentiation of metabolic pathways in low and high risk groups.

RESULTS

Identification of Differentially-Expressed Metabolic Genes in Lung Adenocarcinoma

The overview of the process used in our study is shown in **Figure 1**. First, we downloaded the expression profile datasets from the TCGA database; 517 LUAD samples and 59 non-tumor samples were included. A total of 1399 metabolic enzyme genes, which were based on the list from the KEGG PATHWAY database, were selected to analyze the distinct expression between LUAD and the adjacent normal samples. 282 metabolizing enzyme genes, with a threshold P-value < 0.05 and $|\log FC| > 1$, were distinguished by using 3 R packages "DESeq2," "edgeR," and "limma," among which 165 genes were determined to be upregulated and 117 downregulated. The R package "pheatmap" and "ggplot2" were performed to draw the heatmap, volcano plots and Venn Diagram, which were shown in **Figures 2A,B** respectively.

Establishment and Validation of the Prognostic Risk Score Model

Kaplan-Meier analysis and Univariate Cox analysis utilized by the R package "survival" and "survminer" was performed to screen 165 upregulated metabolic genes. We used Log Rank test to evaluate the results of survival analysis. There were significant differences in the genes with $p < 0.05$ by Log Rank test. The number of significant genes was 31 by Kaplan-Meier analysis and 24 by univariate Cox analysis. We finally selected the union of the two analysis results, and a total of 34 valid genes were identified as risk factors of overall survival rate in LUAD patients. After checking the immunohistochemical results of the HPA database (https://www.proteinatlas.org/), only 16 genes, which showed significant overexpression in cancer tissues, were extracted for further Multivariate Cox Proportional Hazards Regression Analysis (**Figure 2C**). Four metabolic genes with statistically significant differences, namely TYMS, NME4, LDHA, and SMOX, were finally identified. We extracted these four genes separately for another Multivariate Cox Proportional Hazards Regression Analysis and get their regression coefficients from the forest map (**Supplementary Figure S1A**). According to the regression coefficients of these four genes, we established a model in the TCGA training set to calculate the risk score of LUAD patients. This risk score, referred to hereafter as the metabolic gene risk score (MGRS), was calculated as follows:

$$\mathbf{MGRS} = 0.28 \times \mathbf{TYMS} + 0.25 \times \mathbf{NME4} + 0.41 \times \mathrm{LDHA} + 0.20 \times \mathbf{SMOX}$$

The median risk scores were considered as the cutoff value to classify patients into low-risk and high-risk groups. To test the

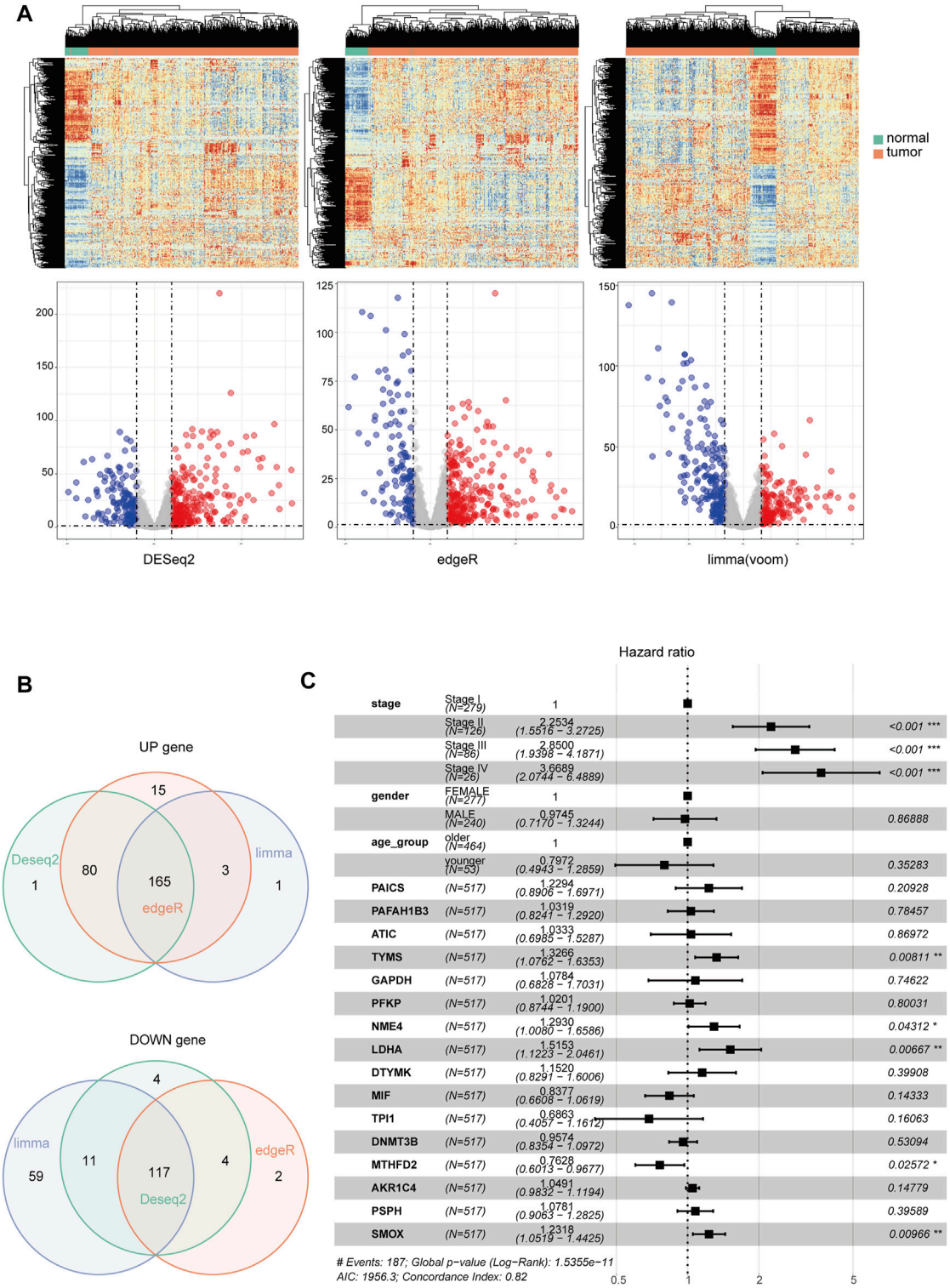

FIGURE 2 | The identification of differentially-expressed metabolic genes. Heatmap and Volcano Plot **(A)**, Venn Diagram **(B)** compared the results of 3 R packages 'DESeq2,' 'edgeR,' and 'limma'. respectively. **(C)** A forest map showed 16 metabolic enzyme genes identified by Multivariate Cox Proportional Hazards Regression analysis. Significance codes: <0.001 = ***, <0.01 = **, and <0.05 = *.

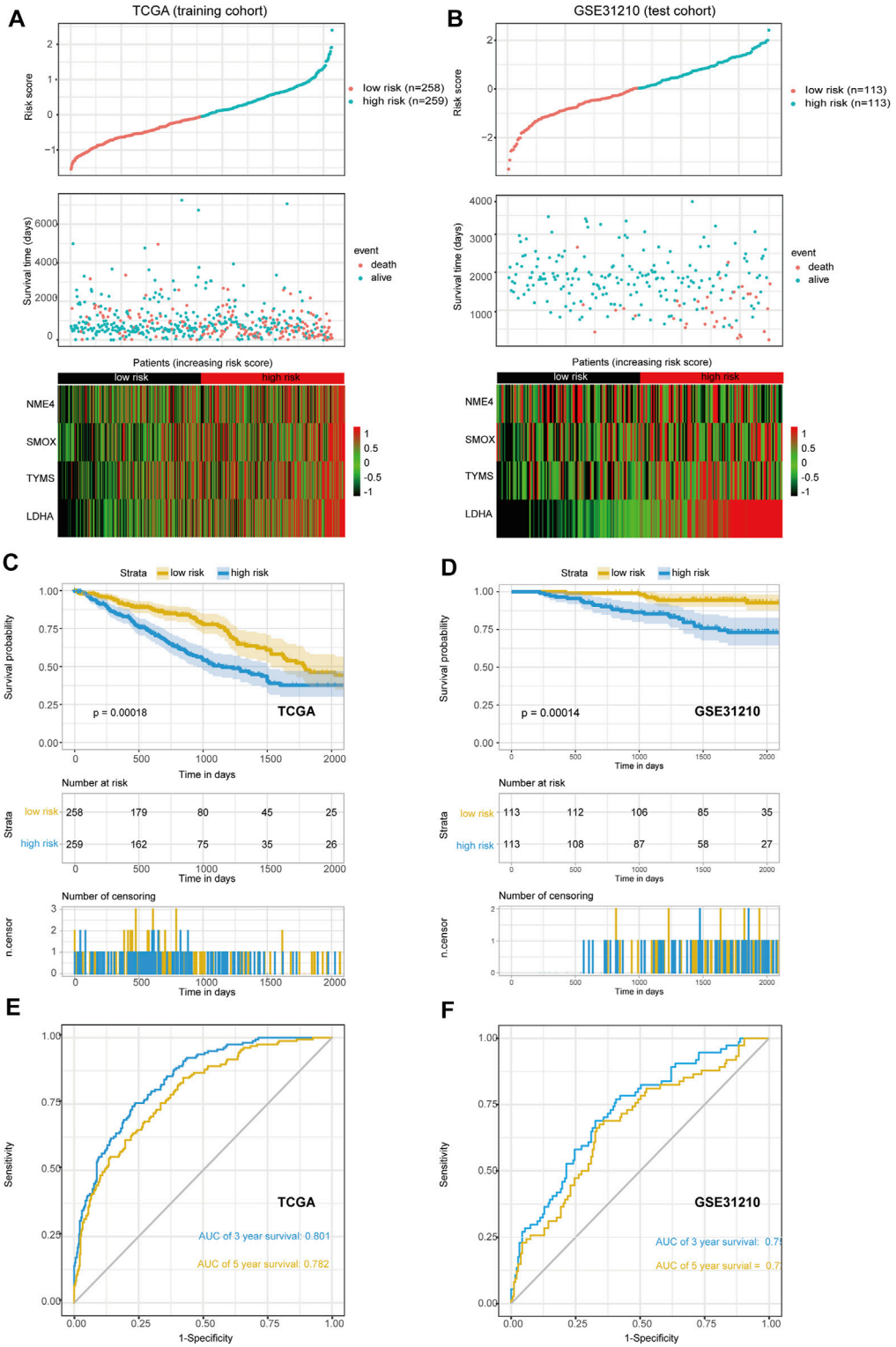

FIGURE 3 | The scatter plot of risk score and heat map of four prognostic genes. **(A,B)** The training set **(A)** and the first validation set **(B)** are shown. **(C,D)** Kaplan-Meier curves of overall survival (OS) for patients with LUAD based on the risk score. The training set **(C)** and the first validation set **(D)** are shown **(E,F)** The 3-, and 5-years ROC of the risk model. The training set **(E)** and the first validation set **(F)** are shown.

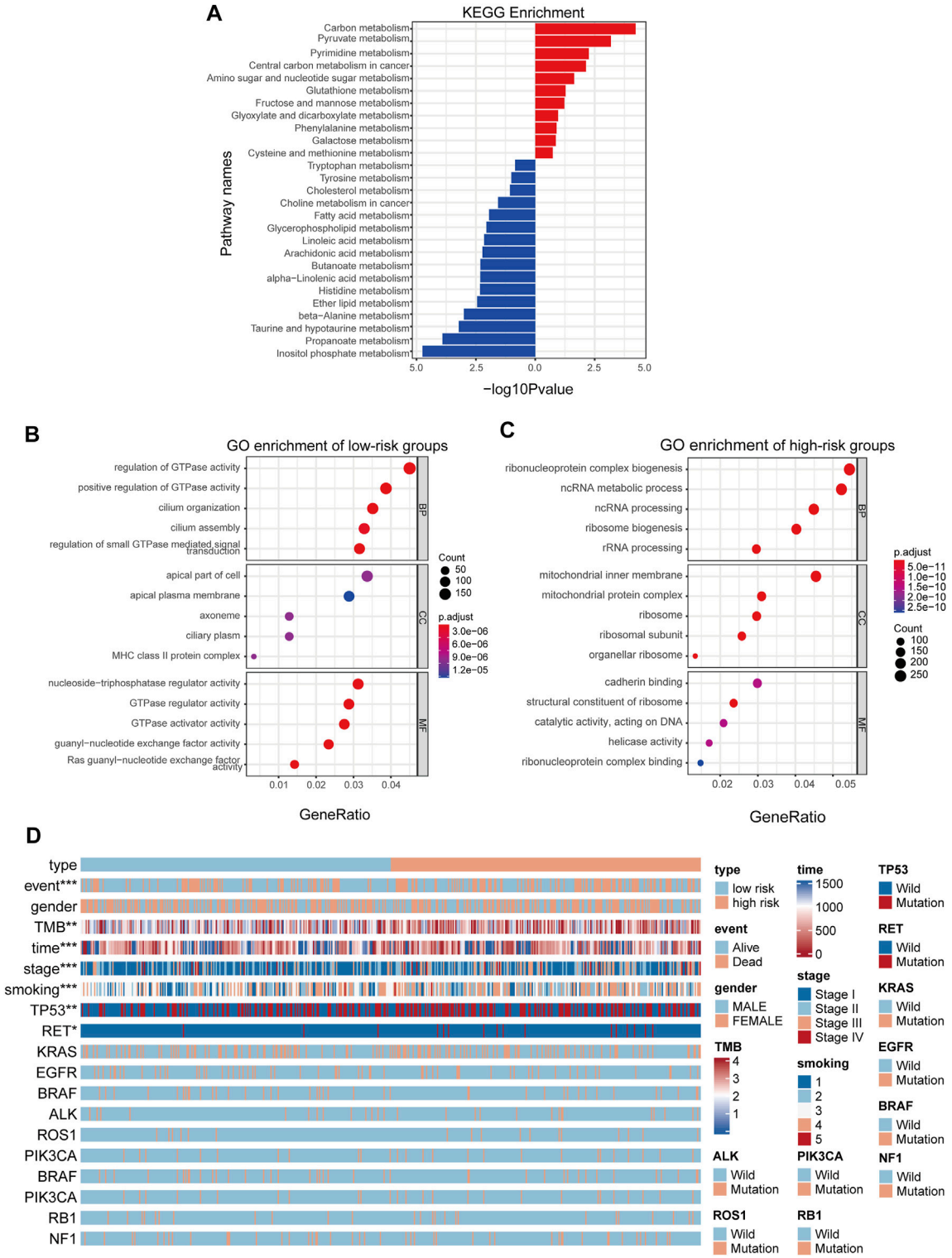

FIGURE 4 | MGRS can identify the survival status of different patients. **(A)** KEGG pathway enrichment analyses for differentially-expressed metabolic genes **(B,C)** GO pathway enrichment analyses for differentially-expressed genes. Pathways activated in low-risk groups **(B)** Pathways activated in high-risk groups **(C)** are shown. All enriched pathways were significant. **(D)** A heatmap showed that clinical stage, survival status, smoking status, Tumor Mutational Burden (TMB), and gene mutations in TP53 and RET were significantly associated with risk.

model predictions, we used scatter plots and heat maps to determine a rough estimate of whether the score of this formula can distinguish the prognosis of patients (**Figures 3A,B**) in both the training and test cohorts. The results suggested that all of the prognostic genes are risky genes and people with high scores from our model might be associated with poor outcomes. We then performed a Kaplan-Meier analysis to validate this cut-off point and show the survival difference between the high-risk and low-risk groups (**Figures 3C,D**). We also performed time-dependent receiver operating characteristic (ROC) curve analysis using the R package "survivalROC" both in the training and first validation set. The areas under the ROC curve at 3 and 5 years were 0.801 and 0.782in the training set and 0.750 and 0.721 in the first validation set, respectively (**Figures 3E,F**). These results showed that the MGRS had a powerful prognostic performance of survival value for LUAD.

Metabolic Gene Risk Score Reflects Different Metabolic Status in Lung Adenocarcinoma Patients

As the prognostic value of the MGRS indicated that this 4-genes-based signature might reflect the distinct metabolic status of LUAD progression, we next performed Kyoto Encyclopedia of Genes and Genomes (KEGG) pathway analysis via the R package "clusterProfiler" to identify differences in metabolic pathway enrichment in low- and high-risk groups. We found that carbon metabolism and nucleotide metabolism were significantly activated in high-risk groups, while some pathways such as inositol phosphate metabolism and propanoate metabolism were inhibited (**Figure 4A**). In order to further study the effects of metabolic differences on the molecular pathways of tumor cells, we used Gene Ontology (GO) to analyze the differentially expressed genes between the two groups. The results showed that GTPase pathway was activated in low-risk group (**Figure 4B**), while ribonucleoprotein complex biogenesis pathways were activated in high-risk groups (**Figure 4C**). To assess the clinical application value of the constructed model, a Wilcoxon test and chi-square test of clinicopathological characteristics were performed and visualized by a heat map, labeled as $p < 0.001$ = ***, $p < 0.01$ = **, and $p < 0.05$ = *. The results showed that clinical stage, survival status, smoking status, Tumor Mutational Burden (TMB), and gene mutation of TP53 and RET were significantly correlated with the level of LUAD risk (**Figure 4D**). Patient's original clinical information and individual p-value for each clinical character are shown in **Supplementary Tables S2, S3**.

Metabolic Gene Risk Score Correlates With Immune Cells Infiltration in Tumor Microenvironment

Due to the crucial role of tumor metabolism in remodeling the TME, we analyzed the abundance of infiltration by 22 types of immune cells by CIBERSORT to evaluate the correlation of MRGS and immune cell infiltration in TME. Differential distribution of immune cells in all patients is shown in **Figures 5A,B**. We found that the high-risk group exhibited significantly decreased B cell and increased M2 macrophage infiltration (**Figure 5C**). To analyze the relationship between the model and immunotherapy, we calculated the IC50 of the immune checkpoint inhibitor PD1 obtained from the microarray dataset GSE135222. A Wilcoxon test was performed to analyze differentiation of the IC50 of anti-PD-1/L1 antibody in the low- and high-risk groups (**Figure 5D**). We found that patients with high-risk scores exhibited low therapeutic efficacy compared to low-risk patients, although these results were not statistically significant due to the limited sample size.

Optimized Prognosis Prediction Model Based on Immunohistochemistry

To further validate the prognostic power of these four metabolic enzymes in LUAD and to create a technically simple tool applied in clinical diagnosis, we performed immunohistochemical analysis to verify the expression levels of the proteins encoded by these four genes, as well as that of the markers of B cells (CD19) and macrophages (CD68) in a second validation set. The representative IHC positive and negative images are shown in **Figure 6A**. The resulting H-score is shown in **Supplementary Table S4**. According to the MGRS model formula and H-score of four metabolic genes, the samples were also divided into low-risk (n = 25) and high-risk groups (n = 25) that exhibited a significantly different survival rate. Furthermore, we found that the level of CD19 and CD68 were significantly correlated with the risk score (**Figures 6B,C**). Therefore, we included CD19 and CD68 in Multivariate Cox Proportional Hazards Regression Analysis as well (**Supplementary Figure S1B**). We constructed an optimized model (the metabolic-immune protein risk score (MPIRS)) by combining the expression data of the four metabolic genes and immune cells as follows:

$$\mathbf{MPIRS} = 0.12 \times \mathbf{TYMS} + 0.09 \times \mathbf{NME4} + 0.23 \times \mathbf{LDHA} + 0.12 \times \mathbf{SMOX} + 0.12 \times \mathbf{CD68} - 0.04 \times \mathbf{CD19}$$

Kaplan Meier and ROC curve analyses were performed using the original model and optimized model, respectively (**Figures 6D–F**). The results show that the optimized model can evaluate the survival prognosis of patients more accurately, which indicated that these models are useful for clinical diagnosis.

DISCUSSION

In this study, a metabolic enzyme signature model referred to as MGRS was constructed to predict the overall survival of LUAD patients and distinguish patients into low-risk and high-risk groups. Using multivariate Cox proportional hazards regression analysis, four metabolic enzymes (*TYMS, NME4, LDHA, and SMOX*) were identified as ideal prognostic markers. Kaplan Meier analysis and ROC curve analysis were performed both in the training set and the first validation set. We revealed the ribonucleoprotein complex biogenesis pathway was

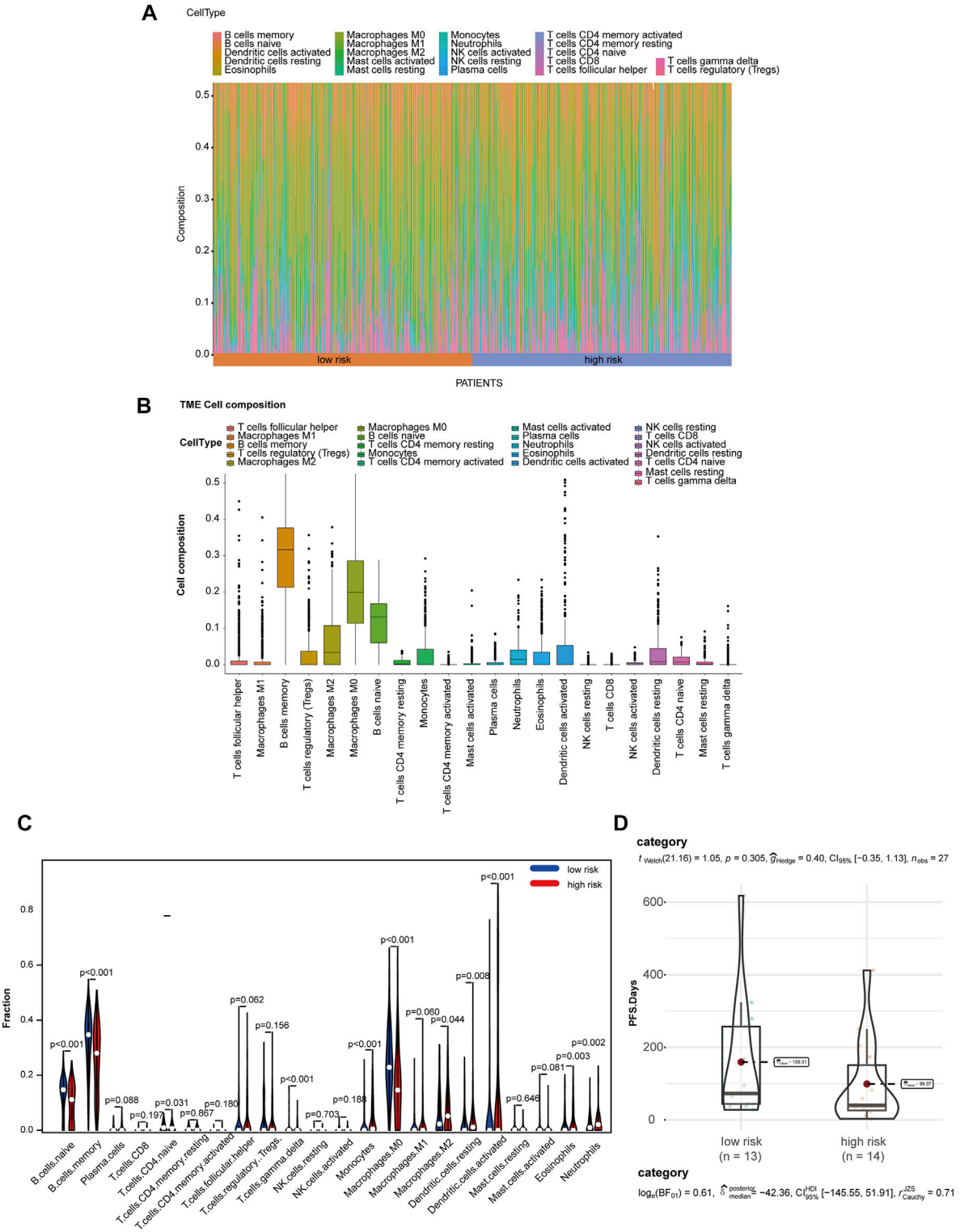

FIGURE 5 | MGRS was associated with TME immune cell infiltration. **(A)** Differential distribution of immune cells in each patient. **(B)** Differential distribution of immune cells in all patients. **(C)** Differential distribution of immune cells in low- and high-risk groups. **(D)** Box/violin plots showing the differentiation of the IC50 of anti-PD-1/L1 antibodyin low- and high-risk groups.

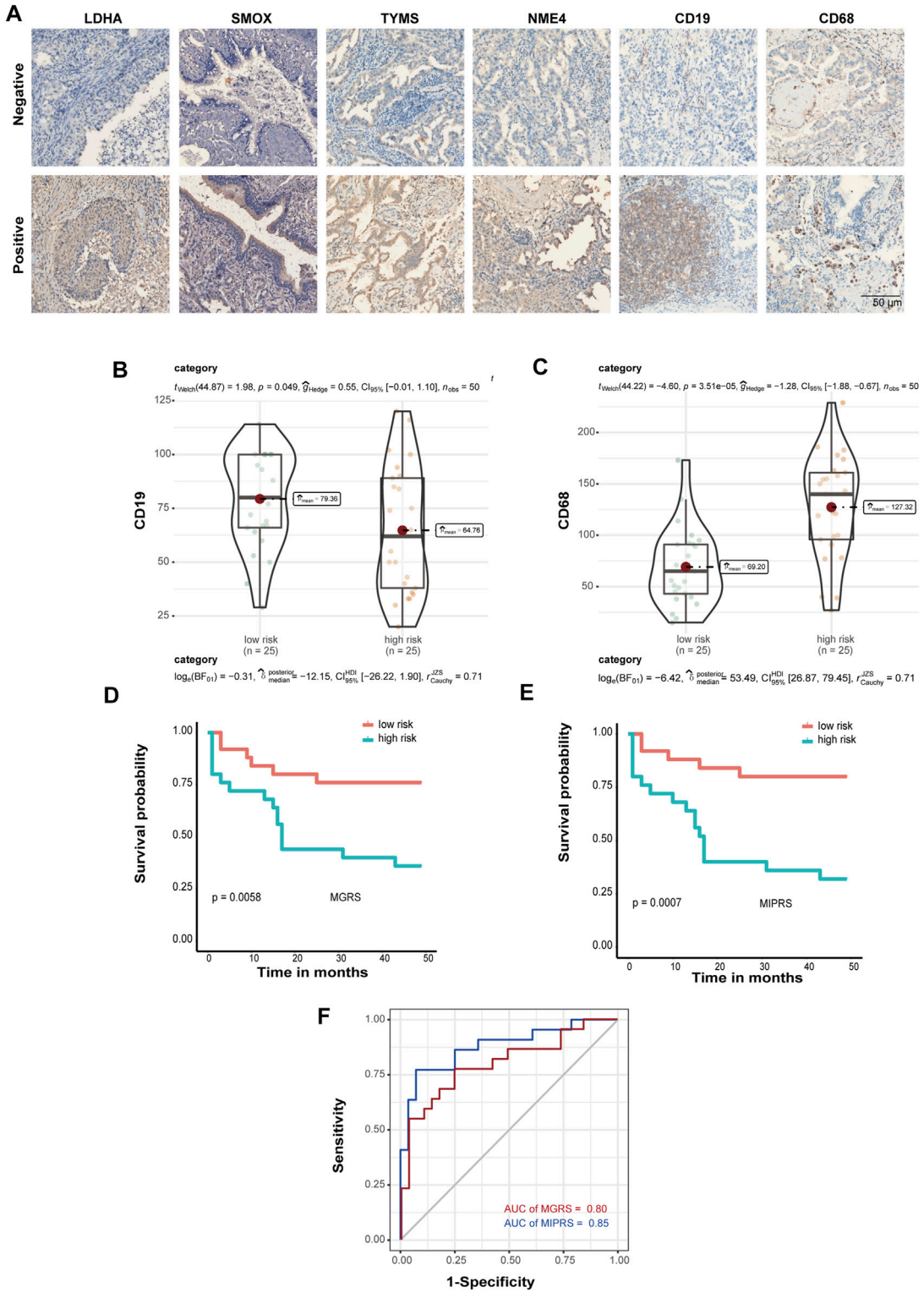

FIGURE 6 | Prediction model optimization based on immunohistochemistry. **(A)** The representative IHC positive and negative images of four prognostic proteins, as well as markers of B cells (CD19) and macrophages (CD68). Box/violin plot showing that the expression of CD19 **(B)** and CD68 **(C)** was significantly correlated with the risk score. **(D,E)** Kaplan-Meier curves of the prediction model. The original model **(D)** and the optimized model **(E)** are shown. **(F)** ROC curves of the original model and the optimized model.

activated in high-risk patients while GTPases were up-regulated in low-risk groups, which may mediate immune escape and confer different outcomes in patients. To evaluate the model in the immune-cell infiltration, we performed the Wilcoxon test to analyze the infiltration of 22 immune cells via CIBERSORT. These results show that high-risk patients suffered a lower survival rate with significantly decreased B cells and increased macrophages M2 infiltration of the TME. In the subsequent analysis, we calculated the risk scores in a cohort with anti-PD-L1immunotherapy. The predictive accuracy of the signature was also confirmed by immunohistochemical assays. We finally constructed an optimized MIPRS model based on the expression of metabolic and immune proteins, which is useful for accurately predicting patient prognosis and should serve as a useful tool in clinical diagnosis.

In recent years, the role of abnormal metabolism in tumor progression has attracted more and more attention. Studies have demonstrated that compared to traditional biomarkers, metabolic enzymes are superior as predictive biomarkers for various cancers (Dong et al., 2015; Xu et al., 2021). Metabolic alteration has wide-ranging effects, such as angiogenesis, metastasis, and immune escape, which has provided opportunities to solve immunotherapy resistance and poor clinical outcomes (Broadfield et al., 2021; Jones et al., 2021; Zanotelli et al., 2021). To date, the expression patterns of metabolic enzymes have been widely studied in different cancer types, such as liver, gastric, colorectal, breast, and prostate cancer (Lavorgna et al., 2018; Zinger et al., 2019; Rivello et al., 2020; Sun et al., 2020; Xu et al., 2020; Jiang et al., 2021). With the development of next-generation sequencing, we can use multiple appropriate statistical methods to analyze TME cell infiltration mediated by metabolic enzymes. However, most of these metabolism-related gene signatures included one or two key molecules and TME infiltration cells, ignoring the fact that metabolic regulation is a complex and interdependent network. In addition, these signatures are based on mRNA levels, which made application to clinical diagnoses difficult. To identify the comprehensive role of metabolic enzymes in heterogeneous and complex processes such as TME cell infiltration, the construction of an integrated metabolic enzyme signature based on immunohistochemical analysis might address the aforementioned limitations.

Metabolic enzymes in our study have been investigated in various cancers. A previous study demonstrated that Lactate dehydrogenase A (LDHA) functions as a sensor for overloaded ROS to enhance antioxidant capacity and sustain cell proliferation by producing α-HB in the nucleus (Liu et al., 2018). Another study showed that the loss of DNA methylation of LDHA was associated with certain malignant clinicopathological features such as a high glycolytic phenotype in gliomas (Ruiz-Rodado et al., 2020). LDHA was also associated with a poor prognosis in pancreatic cancer by regulating the expression of L-2 hydroxyglutarate, an epigenetic modifier, which can inhibit T cell proliferation and migration and thereby contribute to immune escape (Gupta et al., 2021). Thymidylate synthase (TYMS) is a key dNTP synthesizing enzyme and regulates nucleotide metabolism through a YBX1-RRM2-TYMS-TK1 axis in the liver, breast, and lung cancer (Gandhi et al., 2020). The expression of TYMS can be suppressed by inhibiting the synthesis of hydrogen sulfide (H2S) and might be used as a potential therapeutic target to reverse the acquired resistance to 5-FU in colon cancer cells (Ahn et al., 2015). Nucleoside Diphosphate Kinase 4 (NME4) is an enzyme regulating nucleotide metabolism and ATP/ITP metabolism as well (Lu et al., 2014). NME4 is involved in apoptosis and inflammatory reactions through an NME4/NDPK-D-based CL-transfer pathway (Schlattner et al., 2018). Since there are no reports of NME4 associated with the development of any cancer, it might be a novel prognostic signature in LUAD. Spermine oxidase (SMOX) is potentially associated with oxidative DNA damage in gastric cancer by catabolizing polyamine spermine and producing H_2O_2 (Chaturvedi et al., 2014; Chaturvedi et al., 2015; Murray-Stewart et al., 2016; Sierra et al., 2020). Although no studies have reported the role of SMOX in LUAD, it has a significant correlation with chronic inflammation, such as in ulcerative colitis, prostatic intraepithelial neoplasia (PIN), and *Helicobacter* pylori-associated gastritis (Goodwin et al., 2008; Hong et al., 2010; Chaturvedi et al., 2014). Accordingly, all of these enzymes are involved in tumor-related biological processes.

The results of KEGG and GO pathway enrichment analyses in our study show that the formula determined by these four metabolic genes can effectively distinguish different types of patients, high-risk and low risk patients have significant differences in metabolic pathway. GO enrichment results showed that GTPase pathway was activated in low risk group, while ribonucleoprotein complex biosynthesis pathway was activated in high risk group. GTPase-activating protein (GAP), also known as RGS protein or RGS protein, plays an important role in controlling the activity of G protein, involving in cell proliferation, differentiation, survival and movement (Moon and Zheng, 2003; Gray et al., 2020). GTPase activating protein can bind to the activated G protein and stimulate its GTPase activity, thus terminating the signal. Mutations in GTPase are closely related to carcinogenesis (Thaker et al., 2019; Zhou et al., 2020). Similar to the results of KEGG analysis, the increase of ribonucleoprotein complex biogenesis was the main factor in the high risk group. In the KEGG analysis, we also found that carbon metabolism, ribonucleoprotein complex biogenesis pathways and sugar metabolism are activated in the LUAD high-risk group. Carbon metabolism is crucial for oxidative phosphorylation in cells (Ciccarone et al., 2017). Current studies have shown that cancer cells are more active in anaerobic glycolysis while the tricarboxylic acid (TCA) cycle plays an important role in regulating energy production in normal cells (Montal et al., 2015; Anderson et al., 2018; Cai et al., 2020). One of our candidate enzymes, LDHA, is key for anaerobic respiration and catalyzes the inter-conversion of pyruvate and L-lactate using NADH (Ooi and Gomperts, 2015). Our study also found that the frequency of TP53 gene mutation in high-risk score patients is significantly higher than that in low-risk score patients. TP53 can inhibit tumor growth and development by not only downregulating glucose transporters (GLUT1 and GLUT4) but suppressing the activity of glycolytic enzymes, which was verified in the constructed model (Duffy et al.,

2020; Huang, 2021; Liu et al., 2021). Except for carbohydrate metabolism, nucleotide metabolism is involved in the progression of various tumors as well. The carbon metabolism mentioned above also plays an important role in nucleotide synthesis and biomethylation(Newman et al., 2021). Folate mediated carbon metabolism transfers a part of carbon (methyl) to many biological reactions and plays a variety of important roles in normal and abnormal cell division. For example, the synthesis of purine bases, adenine and guanine requires the participation of 10-formyltetrahydrofolate(Hong et al., 2020). Another enzyme of our model, TYMS, served as a key enzyme in pyrimidine metabolism, provides the sole *de novo* pathway for the production of deoxythymidine monophosphate (dTMP), which is a component of DNA (Rosmarin et al., 2015). Mutant TP53 also controls the abundance of deoxyribonucleotides by regulating the abundance of ribonucleotide reductase (RNR) (Xue et al., 2003; Zhou et al., 2003; Link et al., 2008). Although SMOX is a key enzyme of polyamine metabolism, it may still indirectly regulate pyrimidine metabolism by consuming purine during polyamine synthesis (Fan J. et al., 2019). Meanwhile, photoaffinity polyamines can change the helical twist of DNA in nucleosomes by regulating their affinity for DNA, which may, in turn, trigger tumor development (Amarantos and Kalpaxis, 2000). At present, there are few studies on the abnormal metabolism of B cells in tumor, but B cells may also affect the metabolism of tumor immune microenvironment by cooperating with T cells and NK cells.

To evaluate our model of immune-cell infiltration, we performed the Wilcoxon test to analyze the infiltration of 22 types of immune cells using CIBERSORT. These results showed that the high-risk group suffered a poor survival rate and had significantly decreased B cell and increased M2 macrophage infiltration. M2 macrophages are associated with malignant transformation and metastasis in many cancers (Fan CS. et al., 2019), indicating the poor prognosis of the high-risk group. Compared with other inflammatory macrophages, tumor M2 macrophages prefer unique arginine metabolism. Arginine metabolism is the key pathway of innate and adaptive immune response (Luo et al., 2018; Das et al., 2019). After the death of immune cells, they are released from phagocytic lysosomes and consume arginine in the microenvironment, thus inhibiting the proliferation of T cells and natural killer (NK) cells and the secretion of cytokines(Munder, 2009). Arginase 1 (ARG1) is a key enzyme in the urea cycle, which converts L-arginine into urea and L-ornithine. Tumor M2 macrophages produce more polyamines and consume arginine by increasing ARG1 expression(De Santo et al., 2018; Baier et al., 2020). The spermine oxidase (SMOX) in our model is also one of the key enzymes in arginine metabolism, which can decompose polyamine and spermine, and may also participate in the metabolism of M2 macrophages. In most cases, B cells serve as anticancer cells by inducing antigen-specific $CD4^+$ and $CD8^+$ T-cell responses as antigen-presenting cells, with the exception of B-cell lymphoma (Menon et al., 2021; Michaud et al., 2021). In the subsequent analysis, we calculated the risk scores in a cohort treated with anti-PDL1 immunotherapy. PD-L1 (Programmed cell death 1 ligand 1), a ligand of PD-1 (Programmed cell death-1) expressed mainly on tumor cells in the TME, can suppress the function of cytotoxic T cells (Doroshow et al., 2021). In our study, patients with high-risk scores exhibited low therapeutic efficacy compared to low-risk patients, although these results were not statistically significant due to the limited sample size. Although previous reports have shown that anti-PDL1 immunotherapy mostly regulates T cells, tumor-infiltrating B cells (TIL-B) are also involved in the regulation of this process. Compared to spleen B cells, the expression of PD-L1 in TIL-B cells was significantly increased, which might be due to the reduction of calcium signaling (Ou et al., 2014) (Schwartz et al., 2016). TIL-B cells may inhibit the proliferation and immune response of T cells by increasing the expression of PDL1 (Zhang et al., 2016; Nus et al., 2020). Studies have shown that PDL1 antibodies have a promising therapeutic effect on EMT-6 mammary carcinoma with significantly infiltrated B cells (Schwartz et al., 2016). Therefore, the sensitivity of low-risk patients to PDL1 therapy may be attributed to the increased numbers of TIL-B cells.

Finally, we optimized our predictive model (MIPRS) based on the protein level of metabolic enzymes and immune cell markers, by which we can stratify patients into two types according to their calculated risk score. Compared to previous biomarkers, MIPRS is technically simple and might be more accurate in predicting LUAD prognoses. Accordingly, the predictive power of this signature should be assessed in more cases in the future.

DATA AVAILABILITY STATEMENT

The original contributions presented in the study are included in the article/**Supplementary Material**, further inquiries can be directed to the corresponding author.

AUTHOR CONTRIBUTIONS

SC and YD carried out the experiment, SC wrote the manuscript with support from YD DY, and JA. JA supervised the project. YW revised the manuscript.

FUNDING

This work was funded by National Multidisciplinary Cooperative Diagnosis and Treatment Capacity Building Project for Major Diseases (Lung Cancer).

SUPPLEMENTARY MATERIAL

The Supplementary Material for this article can be found online at: https://www.frontiersin.org/articles/10.3389/fphar.2021.728368/full#supplementary-material

REFERENCES

Ahn, J. Y., Lee, J. S., Min, H. Y., and Lee, H. Y. (2015). Acquired Resistance to 5-fluorouracil via HSP90/Src-Mediated Increase in Thymidylate Synthase Expression in colon Cancer. *Oncotarget* 6, 32622–32633. doi:10.18632/oncotarget.5327

Amarantos, I., and Kalpaxis, D. L. (2000). Photoaffinity Polyamines: Interactions with AcPhe-tRNA Free in Solution or Bound at the P-Site of *Escherichia coli* Ribosomes. *Nucleic Acids Res.* 28, 3733–3742. doi:10.1093/nar/28.19.3733

Anderson, N. M., Mucka, P., Kern, J. G., and Feng, H. (2018). The Emerging Role and Targetability of the TCA Cycle in Cancer Metabolism. *Protein Cell* 9, 216–237. doi:10.1007/s13238-017-0451-1

Bader, J. E., Voss, K., and Rathmell, J. C. (2020). Targeting Metabolism to Improve the Tumor Microenvironment for Cancer Immunotherapy. *Mol. Cel* 78, 1019–1033. doi:10.1016/j.molcel.2020.05.034

Baier, J., Gänsbauer, M., Giessler, C., Arnold, H., Muske, M., Schleicher, U., et al. (2020). Arginase Impedes the Resolution of Colitis by Altering the Microbiome and Metabolome. *J. Clin. Invest.* 130, 5703–5720. doi:10.1172/JCI126923

Bose, S., Allen, A. E., and Locasale, J. W. (2020). The Molecular Link from Diet to Cancer Cell Metabolism. *Mol. Cel* 80, 554–1044. doi:10.1016/j.molcel.2020.10.006

Broadfield, L. A., Pane, A. A., Talebi, A., Swinnen, J. V., and Fendt, S. M. (2021). Lipid Metabolism in Cancer: New Perspectives and Emerging Mechanisms. *Dev. Cel* 56, 1363–1393. doi:10.1016/j.devcel.2021.04.013

Byun, J. K., Park, M., Lee, S., Yun, J. W., Lee, J., Kim, J. S., et al. (2020). Inhibition of Glutamine Utilization Synergizes with Immune Checkpoint Inhibitor to Promote Antitumor Immunity. *Mol. Cel* 80, 592–e8. doi:10.1016/j.molcel.2020.10.015

Cai, Z., Li, C. F., Han, F., Liu, C., Zhang, A., Hsu, C. C., et al. (2020). Phosphorylation of PDHA by AMPK Drives TCA Cycle to Promote Cancer Metastasis. *Mol. Cel* 80, 263–e7. doi:10.1016/j.molcel.2020.09.018

Chaturvedi, R., Asim, M., Piazuelo, M. B., Yan, F., Barry, D. P., Sierra, J. C., et al. (2014). Activation of EGFR and ERBB2 by *Helicobacter pylori* Results in Survival of Gastric Epithelial Cells with DNA Damage. *Gastroenterology* 146, 1739–e14. doi:10.1053/j.gastro.2014.02.005

Chaturvedi, R., de Sablet, T., Asim, M., Piazuelo, M. B., Barry, D. P., Verriere, T. G., et al. (2015). Increased Helicobacter Pylori-Associated Gastric Cancer Risk in the Andean Region of Colombia Is Mediated by Spermine Oxidase. *Oncogene* 34, 3429–3440. doi:10.1038/onc.2014.273

Ciccarone, F., Vegliante, R., Di Leo, L., and Ciriolo, M. R. (2017). The TCA Cycle as a Bridge between Oncometabolism and DNA Transactions in Cancer. *Semin. Cancer Biol.* 47, 50–56. doi:10.1016/j.semcancer.2017.06.008

Das, L. M., Binko, A. M., Traylor, Z. P., Peng, H., and Lu, K. Q. (2019). Vitamin D Improves Sunburns by Increasing Autophagy in M2 Macrophages. *Autophagy* 15, 813–826. doi:10.1080/15548627.2019.1569298

De Santo, C., Cheng, P., Beggs, A., Egan, S., Bessudo, A., and Mussai, F. (2018). Metabolic Therapy with PEG-Arginase Induces a Sustained Complete Remission in Immunotherapy-Resistant Melanoma. *J. Hematol. Oncol.* 11, 68. doi:10.1186/s13045-018-0612-6

Dong, G., He, X., Chen, Y., Cao, H., Wang, J., Liu, X., et al. (2015). Genetic Variations in Genes of Metabolic Enzymes Predict Postoperational Prognosis of Patients with Colorectal Cancer. *Mol. Cancer* 14, 171. doi:10.1186/s12943-015-0442-x

Dong, Y., Tu, R., Liu, H., and Qing, G. (2020). Regulation of Cancer Cell Metabolism: Oncogenic MYC in the Driver's Seat. *Signal. Transduct Target. Ther.* 5, 124. doi:10.1038/s41392-020-00235-2

Doroshow, D. B., Bhalla, S., Beasley, M. B., Sholl, L. M., Kerr, K. M., Gnjatic, S., et al. (2021). PD-L1 as a Biomarker of Response to Immune-Checkpoint Inhibitors. *Nat. Rev. Clin. Oncol.* 18, 345–362. doi:10.1038/s41571-021-00473-5

Duffy, M., Synnott, N., O'Grady, S., and Crown, J. (2020). Targeting P53 for the Treatment of Cancer. *Semin. Cancer Biol.* [Preprint]. doi:10.1016/j.semcancer.2020.07.005

Fan, C. S., Chen, L. L., Hsu, T. A., Chen, C. C., Chua, K. V., Li, C. P., et al. (2019a). Endothelial-mesenchymal Transition Harnesses HSP90α-Secreting M2-Macrophages to Exacerbate Pancreatic Ductal Adenocarcinoma. *J. Hematol. Oncol.* 12, 138. doi:10.1186/s13045-019-0826-2

Fan, J., Chen, M., Wang, X., Tian, Z., Wang, J., Fan, D., et al. (2019b). Targeting Smox Is Neuroprotective and Ameliorates Brain Inflammation in Cerebral Ischemia/Reperfusion Rats. *Toxicol. Sci.* 168, 381–393. doi:10.1093/toxsci/kfy300

Gandhi, M., Groß, M., Holler, J. M., Coggins, S. A., Patil, N., Leupold, J. H., et al. (2020). The lncRNA lincNMR Regulates Nucleotide Metabolism via a YBX1 - RRM2 axis in Cancer. *Nat. Commun.* 11, 3214. doi:10.1038/s41467-020-17007-9

Goodwin, A. C., Jadallah, S., Toubaji, A., Lecksell, K., Hicks, J. L., Kowalski, J., et al. (2008). Increased Spermine Oxidase Expression in Human Prostate Cancer and Prostatic Intraepithelial Neoplasia Tissues. *Prostate* 68, 766–772. doi:10.1002/pros.20735

Gray, J. L., von Delft, F., and Brennan, P. E. (2020). Targeting the Small GTPase Superfamily through Their Regulatory Proteins. *Angew. Chem. Int. Ed. Engl.* 59, 6342–6366. doi:10.1002/anie.201900585

Gupta, V., Sharma, N., Durden, B., Garrido, V., Kesh, K., Edwards, D., et al. (2021). Hypoxia-driven Oncometabolite L-2HG Maintains Stemness-Differentiation Balance and Facilitates Immune Evasion in Pancreatic Cancer. *Cancer Res.* [Preprint].

Hong, S. K., Chaturvedi, R., Piazuelo, M. B., Coburn, L. A., Williams, C. S., Delgado, A. G., et al. (2010). Increased Expression and Cellular Localization of Spermine Oxidase in Ulcerative Colitis and Relationship to Disease Activity. *Inflamm. Bowel Dis.* 16, 1557–1566. doi:10.1002/ibd.21224

Hong, Y., Ren, J., Zhang, X., Wang, W., and Zeng, A. P. (2020). Quantitative Analysis of glycine Related Metabolic Pathways for One-Carbon Synthetic Biology. *Curr. Opin. Biotechnol.* 64, 70–78. doi:10.1016/j.copbio.2019.10.001

Huang, J. (2021). Current Developments of Targeting the P53 Signaling Pathway for Cancer Treatment. *Pharmacol. Ther.* 220, 107720. doi:10.1016/j.pharmthera.2020.107720

Jiang, X., Qian, H., and Ding, W. (2021). *New Glance at the Role of TM6SF2 in Lipid Metabolism and Liver Cancer*. (Baltimore, Md): Hepatology.

Jones, C. L., Inguva, A., and Jordan, C. T. (2021). Targeting Energy Metabolism in Cancer Stem Cells: Progress and Challenges in Leukemia and Solid Tumors. *Cell stem cell* 28, 378–393. doi:10.1016/j.stem.2021.02.013

Kordbacheh, T., Honeychurch, J., Blackhall, F., Faivre-Finn, C., and Illidge, T. (2018). Radiotherapy and Anti-PD-1/pd-L1 Combinations in Lung Cancer: Building Better Translational Research Platforms. *Ann. Oncol.* 29, 301–310. doi:10.1093/annonc/mdx790

Lam, C., Low, J. Y., Tran, P. T., and Wang, H. (2021). The Hexosamine Biosynthetic Pathway and Cancer: Current Knowledge and Future Therapeutic Strategies. *Cancer Lett.* 503, 11–18. doi:10.1016/j.canlet.2021.01.010

Lavorgna, G., Montorsi, F., and Salonia, A. (2018). Re: Jinjing Chen, Ilaria Guccini, Diletta Di Mitri, et al. Compartmentalized Activities of the Pyruvate Dehydrogenase Complex Sustain Lipogenesis in Prostate Cancer. Nat Genet 2018;50:219-28. *Eur. Urol.* 74, e20–e21. Nat Genet 2018;50:219-e21: Lipid Metabolism in Prostate Cancer: Expanding Patient Therapeutic Opportunities. doi:10.1016/j.eururo.2018.03.005

Link, P. A., Baer, M. R., James, S. R., Jones, D. A., and Karpf, A. R. (2008). p53-inducible Ribonucleotide Reductase (p53R2/RRM2B) Is a DNA Hypomethylation-independent Decitabine Gene Target that Correlates with Clinical Response in Myelodysplastic Syndrome/acute Myelogenous Leukemia. *Cancer Res.* 68, 9358–9366. doi:10.1158/0008-5472.CAN-08-1860

Liu, Y., Guo, J. Z., Liu, Y., Wang, K., Ding, W., Wang, H., et al. (2018). Nuclear Lactate Dehydrogenase A Senses ROS to Produce α-hydroxybutyrate for HPV-Induced Cervical Tumor Growth. *Nat. Commun.* 9, 4429. doi:10.1038/s41467-018-06841-7

Liu, Y., Leslie, P. L., and Zhang, Y. (2021). Life and Death Decision-Making by P53 and Implications for Cancer Immunotherapy. *Trends Cancer* 7, 226–239. doi:10.1016/j.trecan.2020.10.005

Liu, Y., and Zheng, P. (2020). Preserving the CTLA-4 Checkpoint for Safer and More Effective Cancer Immunotherapy. *Trends Pharmacol. Sci.* 41, 4–12. doi:10.1016/j.tips.2019.11.003

Lu, Y. C., Chang, J. T., Liao, C. T., Kang, C. J., Huang, S. F., Chen, I. H., et al. (2014). OncomiR-196 Promotes an Invasive Phenotype in Oral Cancer through the NME4-JNK-TIMP1-MMP Signaling Pathway. *Mol. Cancer* 13, 218. doi:10.1186/1476-4598-13-218

Luo, Y., Shao, L., Chang, J., Feng, W., Liu, Y. L., Cottler-Fox, M. H., et al. (2018). M1 and M2 Macrophages Differentially Regulate Hematopoietic Stem Cell Self-Renewal and *Ex Vivo* Expansion. *Blood Adv.* 2, 859–870. doi:10.1182/bloodadvances.2018015685

Marin-Acevedo, J. A., Kimbrough, E. O., and Lou, Y. (2021). Next Generation of Immune Checkpoint Inhibitors and beyond. *J. Hematol. Oncol.* 14, 45. doi:10.1186/s13045-021-01056-8

Memmott, R., Wolfe, A., Carbone, D., and Williams, T. (2021). Predictors of Response, Progression-free Survival, and Overall Survival in Patients with Lung Cancer Treated with Immune Checkpoint Inhibitors. *J. Thorac. Oncol.* 16 (7), 1086–1098. doi:10.1016/j.jtho.2021.03.017

Menon, M., Hussell, T., and Ali Shuwa, H. (2021). Regulatory B Cells in Respiratory Health and Diseases. *Immunol. Rev.* 299, 61–73. doi:10.1111/imr.12941

Michaud, D., Steward, C. R., Mirlekar, B., and Pylayeva-Gupta, Y. (2021). Regulatory B Cells in Cancer. *Immunol. Rev.* 299, 74–92. doi:10.1111/imr.12939

Montal, E. D., Dewi, R., Bhalla, K., Ou, L., Hwang, B. J., Ropell, A. E., et al. (2015). PEPCK Coordinates the Regulation of Central Carbon Metabolism to Promote Cancer Cell Growth. *Mol. Cel* 60, 571–583. doi:10.1016/j.molcel.2015.09.025

Moon, S. Y., and Zheng, Y. (2003). Rho GTPase-Activating Proteins in Cell Regulation. *Trends Cel Biol* 13, 13–22. doi:10.1016/s0962-8924(02)00004-1

Munder, M. (2009). Arginase: an Emerging Key Player in the Mammalian Immune System. *Br. J. Pharmacol.* 158, 638–651. doi:10.1111/j.1476-5381.2009.00291.x

Murray-Stewart, T., Sierra, J. C., Piazuelo, M. B., Mera, R. M., Chaturvedi, R., Bravo, L. E., et al. (2016). Epigenetic Silencing of miR-124 Prevents Spermine Oxidase Regulation: Implications for Helicobacter Pylori-Induced Gastric Cancer. *Oncogene* 35, 5480–5488. doi:10.1038/onc.2016.91

Navas, L. E., and Carnero, A. (2021). NAD+ Metabolism, Stemness, the Immune Response, and Cancer. *Signal. Transduct Target. Ther.* 6, 2. doi:10.1038/s41392-020-00354-w

Newman, A. C., Falcone, M., Huerta Uribe, A., Zhang, T., Athineos, D., Pietzke, M., et al. (2021). Immune-regulated Ido1-dependent Tryptophan Metabolism Is Source of One-Carbon Units for Pancreatic Cancer and Stellate Cells. *Mol. Cel* 81, 2290–e7. doi:10.1016/j.molcel.2021.03.019

Noël, G., Langouo Fontsa, M., and Willard-Gallo, K. (2018). The Impact of Tumor Cell Metabolism on T Cell-Mediated Immune Responses and Immuno-Metabolic Biomarkers in Cancer. *Semin. Cancer Biol.* 52, 66–74. doi:10.1016/j.semcancer.2018.03.003

Nus, M., Basatemur, G., Galan, M., Cros-Brunsó, L., Zhao, T. X., Masters, L., et al. (2020). NR4A1 Deletion in Marginal Zone B Cells Exacerbates Atherosclerosis in Mice-Brief Report. *Arterioscler Thromb. Vasc. Biol.* 40, 2598–2604. doi:10.1161/ATVBAHA.120.314607

Ooi, A. T., and Gomperts, B. N. (2015). Molecular Pathways: Targeting Cellular Energy Metabolism in Cancer via Inhibition of SLC2A1 and LDHA. *Clin. Cancer Res.* 21, 2440–2444. doi:10.1158/1078-0432.CCR-14-1209

Ou, X., Xu, S., Li, Y. F., and Lam, K. P. (2014). Adaptor Protein DOK3 Promotes Plasma Cell Differentiation by Regulating the Expression of Programmed Cell Death 1 Ligands. *Proc. Natl. Acad. Sci. U S A.* 111, 11431–11436. doi:10.1073/pnas.1400539111

Qiao, M., Jiang, T., Liu, X., Mao, S., Zhou, F., Li, X., et al. (2021). Immune Checkpoint Inhibitors in EGFR-Mutated NSCLC: Dusk or Dawn?, *J. Thorac. Oncol.* S1556-0864(21)02113–02114. doi:10.1016/j.jtho.2021.04.003

Relli, V., Trerotola, M., Guerra, E., and Alberti, S. (2019). Abandoning the Notion of Non-small Cell Lung Cancer. *Trends Mol. Med.* 25, 585–594. doi:10.1016/j.molmed.2019.04.012

Rivello, F., Matuła, K., Piruska, A., Smits, M., Mehra, N., and Huck, W. T. S. (2020). Probing Single-Cell Metabolism Reveals Prognostic Value of Highly Metabolically Active Circulating Stromal Cells in Prostate Cancer. *Sci. Adv.* 6. doi:10.1126/sciadv.aaz3849

Rosmarin, D., Palles, C., Pagnamenta, A., Kaur, K., Pita, G., Martin, M., et al. (2015). A Candidate Gene Study of Capecitabine-Related Toxicity in Colorectal Cancer Identifies New Toxicity Variants at DPYD and a Putative Role for ENOSF1 rather Than TYMS. *Gut* 64, 111–120. doi:10.1136/gutjnl-2013-306571

Ruiz-Rodado, V., Malta, T. M., Seki, T., Lita, A., Dowdy, T., Celiku, O., et al. (2020). Metabolic Reprogramming Associated with Aggressiveness Occurs in the G-CIMP-High Molecular Subtypes of IDH1mut Lower Grade Gliomas. *Neuro Oncol.* 22, 480–492. doi:10.1093/neuonc/noz207

Schlattner, U., Tokarska-Schlattner, M., Epand, R. M., Boissan, M., Lacombe, M. L., and Kagan, V. E. (2018). NME4/nucleoside Diphosphate Kinase D in Cardiolipin Signaling and Mitophagy. *Lab. Invest.* 98, 228–232. doi:10.1038/labinvest.2017.113

Schwartz, M., Zhang, Y., and Rosenblatt, J. D. (2016). B Cell Regulation of the Anti-tumor Response and Role in Carcinogenesis. *J. Immunother. Cancer* 4, 40. doi:10.1186/s40425-016-0145-x

Sierra, J. C., Piazuelo, M. B., Luis, P. B., Barry, D. P., Allaman, M. M., Asim, M., et al. (2020). Spermine Oxidase Mediates Helicobacter Pylori-Induced Gastric Inflammation, DNA Damage, and Carcinogenic Signaling. *Oncogene* 39, 4465–4474. doi:10.1038/s41388-020-1304-6

Sun, L., Wan, A., Zhou, Z., Chen, D., Liang, H., Liu, C., et al. (2020). RNA-binding Protein RALY Reprogrammes Mitochondrial Metabolism via Mediating miRNA Processing in Colorectal Cancer. *Gut*, 2020:320652. doi:10.1136/gutjnl-2020-320652

Thaker, Y. R., Raab, M., Strebhardt, K., and Rudd, C. E. (2019). GTPase-Activating Protein Rasal1 Associates with ZAP-70 of the TCR and Negatively Regulates T-Cell Tumor Immunity. *Nat. Commun.* 10, 4804. doi:10.1038/s41467-019-12544-4

Xu, D., Shao, F., Bian, X., Meng, Y., Liang, T., and Lu, Z. (2021). The Evolving Landscape of Noncanonical Functions of Metabolic Enzymes in Cancer and Other Pathologies. *Cel Metab.* 33, 33–50. doi:10.1016/j.cmet.2020.12.015

Xu, Q., Li, Y., Gao, X., Kang, K., Williams, J. G., Tong, L., et al. (2020). HNF4α Regulates Sulfur Amino Acid Metabolism and Confers Sensitivity to Methionine Restriction in Liver Cancer. *Nat. Commun.* 11, 3978. doi:10.1038/s41467-020-17818-w

Xue, L., Zhou, B., Liu, X., Qiu, W., Jin, Z., and Yen, Y. (2003). Wild-type P53 Regulates Human Ribonucleotide Reductase by Protein-Protein Interaction with p53R2 as Well as hRRM2 Subunits. *Cancer Res.* 63, 980–986.

Yang, W., Qiu, Y., Stamatatos, O., Janowitz, T., and Lukey, M. (2021), Enhancing the Efficacy of Glutamine Metabolism Inhibitors in Cancer Therapy. *Trends Cancer* 7(21); 790–804. doi:10.1016/j.trecan.2021.04.003

Zanotelli, M., Zhang, J., and Reinhart-King, C. (2021). Mechanoresponsive Metabolism in Cancer Cell Migration and Metastasis. *Cel Metab.* 33(7): 1307–1321. doi:10.1016/j.cmet.2021.04.002

Zhang, Y., Morgan, R., Chen, C., Cai, Y., Clark, E., Khan, W. N., et al. (2016). Mammary-tumor-educated B Cells Acquire LAP/TGF-β and PD-L1 Expression and Suppress Anti-tumor Immune Responses. *Int. Immunol.* 28, 423–433. doi:10.1093/intimm/dxw007

Zhao, P., Li, L., Jiang, X., and Li, Q. (2019). Mismatch Repair Deficiency/microsatellite Instability-High as a Predictor for Anti-PD-1/pd-L1 Immunotherapy Efficacy. *J. Hematol. Oncol.* 12, 54. doi:10.1186/s13045-019-0738-1

Zhou, B., Liu, X., Mo, X., Xue, L., Darwish, D., Qiu, W., et al. (2003). The Human Ribonucleotide Reductase Subunit hRRM2 Complements p53R2 in Response to UV-Induced DNA Repair in Cells with Mutant P53. *Cancer Res.* 63, 6583–6594.

Zhou, Y., Qi, C., Xiao, M. Z., Cai, S. L., and Chen, B. J. (2020). RASAL2-RET: a Novel RET Rearrangement in a Patient with High-Grade Sarcoma of the Chest. *Ann. Oncol.* 31, 659–661. doi:10.1016/j.annonc.2020.01.073

Zinger, L., Merenbakh-Lamin, K., Klein, A., Elazar, A., Journo, S., Boldes, T., et al. (2019). Ligand-binding Domain-Activating Mutations of ESR1 Rewire Cellular Metabolism of Breast Cancer Cells. *Clin. Cancer Res.* 25, 2900–2914. doi:10.1158/1078-0432.CCR-18-1505

Conflict of Interest: The authors declare that the research was conducted in the absence of any commercial or financial relationships that could be construed as a potential conflict of interest.

Publisher's Note: All claims expressed in this article are solely those of the authors and do not necessarily represent those of their affiliated organizations, or those of the publisher, the editors and the reviewers. Any product that may be evaluated in this article, or claim that may be made by its manufacturer, is not guaranteed or endorsed by the publisher.

frontiers in Pharmacology

ORIGINAL RESEARCH
published: 03 August 2021
doi: 10.3389/fphar.2021.721471

ZnT8 Deficiency Protects From APAP-Induced Acute Liver Injury by Reducing Oxidative Stress Through Upregulating Hepatic Zinc and Metallothioneins

*Wen Su[1], Mingji Feng[1], Yuan Liu[1], Rong Cao[2], Yiao Liu[1], Junyao Tang[1], Ke Pan[3], Rongfeng Lan[4] and Zhuo Mao[1]**

[1]School of Basic Medical Sciences, Shenzhen University Medical Center, Shenzhen University Health Science Center, Shenzhen, China, [2]Department of Nephrology, The First Affiliated Hospital of Shenzhen University, Shenzhen, China, [3]Institute for Advanced Study, Shenzhen University, Shenzhen, China, [4]Department of Cell Biology and Medical Genetics, School of Basic Medical Sciences, Shenzhen University Health Science Center, Shenzhen, China

OPEN ACCESS

Edited by:
Yao Lu,
Central South University, China

Reviewed by:
Yu An,
University of Texas Southwestern Medical Center, United States
Olfat Ali Hammam,
Theodor Bilharz Research Institute, Egypt
Jingjing Cai,
Central South University, China

***Correspondence:**
Zhuo Mao
maoz@szu.edu.cn

Specialty section:
This article was submitted to Inflammation Pharmacology, a section of the journal Frontiers in Pharmacology

Received: *07 June 2021*
Accepted: *19 July 2021*
Published: *03 August 2021*

Citation:
Su W, Feng M, Liu Y, Cao R, Liu Y, Tang J, Pan K, Lan R and Mao Z (2021) ZnT8 Deficiency Protects From APAP-Induced Acute Liver Injury by Reducing Oxidative Stress Through Upregulating Hepatic Zinc and Metallothioneins. Front. Pharmacol. 12:721471. doi: 10.3389/fphar.2021.721471

Zinc transporter 8 (ZnT8) is an important zinc transporter highly expressed in pancreatic islets. Deficiency of ZnT8 leads to a marked decrease in islet zinc, which is thought to prevent liver diseases associated with oxidative stress. Herein, we aimed to investigate whether loss of islet zinc affects the antioxidant capacity of the liver and acute drug-induced liver injury. To address this question, we treated ZnT8 knockout (KO) or wild-type control mice with 300 mg/ kg acetaminophen (APAP) or phosphate-buffered saline (PBS). Unexpectedly, we found that loss of ZnT8 in mice ameliorated APAP-induced injury and was accompanied by inhibition of c-Jun N-terminal kinase (JNK) activation, reduced hepatocyte death, and decreased serum levels of alanine aminotransferase (ALT) and aspartate aminotransferase (AST). An increase in hepatic glutathione (GSH) was observed, corresponding to a decrease in malondialdehyde (MDA) and 4-hydroxynonenal (4-HNE) levels. APAP-induced inflammation and glycogen depletion were alleviated. In contrast, no significant changes were observed in cytochrome P450 family 2 subfamily E member 1 (CYP2E1), the main enzyme responsible for drug metabolism. Elevated levels of hepatic zinc and metallothionein (MT) were also observed, which may contribute to the hepatoprotective effect in ZnT8 KO mice. Taken together, these results suggest that ZnT8 deficiency protects the liver from APAP toxicity by attenuating oxidative stress and promoting hepatocyte proliferation. This study provides new insights into the functions of ZnT8 and zinc as key mediators linking pancreatic and hepatic functions.

Keywords: ZnT8, acetaminophen, hepatotoxicity, metallothionein, oxidative stress

INTRODUCTION

Zinc transporter 8 (ZnT8), encoded by the human SLC30A8 gene, is a zinc transporter closely associated with type 1 and type 2 diabetes (Barragán-Álvarez et al., 2021). ZnT8 is expressed almost exclusively in pancreatic β cells and is responsible for the uptake of zinc ions into insulin granules. Zinc ions in the pancreas are co-secreted with insulin into the portal vein and the liver to assist in primary insulin

clearance. Previous studies in rodent models have shown that ZnT8 deficiency leads to a significant decrease in zinc levels in the pancreatic islets, resulting in degradation of insulin by the liver due to the lack of zinc (Tamaki et al., 2013). The pancreas is closely related to the liver in term of anatomy and function. Zinc may act as an important messenger mediating the pancreas-liver cross-talk. Therefore, we hypothesized that dysregulation of zinc homeostasis in ZnT8 knockout (KO) mice may contribute to altered liver function.

The liver is a vital multifunctional organ that secretes bile acids, regulates lipid and glucose hemostasis, and metabolizes drugs and xenobiotics (Trefts et al., 2017). Zinc is important for the oxidative status and metabolism of drug toxicity in the liver. (Prasad and Bao, 2019). Acetaminophen (APAP) overdose is the leading cause of drug-induced liver failure in the Western world (Lee, 2017). The mechanisms of APAP hepatotoxicity are complex and have been substantially investigated. Briefly, APAP is metabolized by cytochrome P450 enzymes to N-acetyl-p-benzoquinone imine (NAPQI), a highly reactive and toxic metabolite. NAPQI is detoxified by glutathione (GSH); however, if GSH is depleted, excess NAPQI can lead to toxicity and cell necrosis (Yan et al., 2018). Further, genetic predisposition may play a significant role in the sensitivity of individuals to drug-induced hepatotoxicity.

In this study, we aimed to investigate whether pancreatic-enriched ZnT8 affects hepatic drug toxicity. Interestingly, ZnT8-deficient mice were more resilient, rather than more sensitive, to APAP-induced liver injury. Both hepatic oxidative stress and inflammation were significantly reduced in the livers of ZnT8 KO mice. Further investigation showed that the zinc content in the liver of APAP-treated ZnT8 KO mice was significantly increased compared to wild-type control mice. Moreover, the expression levels of metallothioneins (MTs), proteins involved in metal detoxification, were substantially increased. These results suggest that genetic changes in the pancreas play an unexpected role in hepatic metabolism.

MATERIALS AND METHODS

Animals

Eight-week-old male ZnT8 KO mice and wild-type control mice were placed at 20–25°C and maintained on a 12-h light/dark cycle. APAP was freshly dissolved in warm (55–60°C) distilled phosphate-buffered saline (PBS) and cooled to 37°C. Prior to APAP treatment, mice were fasted overnight and allowed to drink ad libitum. Mice were administered APAP intraperitoneally at a dose of 300 mg/ kg body weight, or PBS. Mice were sacrificed at various time points after injection. Serum and liver samples were harvested for analysis. All animal experiments were performed in accordance with the National Institute of Health Guide for the Care and Use of Laboratory Animals and were approved by the Scientific Investigation Board of Health Science Center of Shenzhen University (Shenzhen, Guangdong, China).

Antibodies and Chemicals

CYP2E, CYP4A, CDK2, CDK4, and MT antibodies were purchased from Abcam (Cambridge, MA, United States). Phospho-JNK (pJNK), JNK, and F4/80 antibodies were from Cell Signaling Technology, Inc. (Beverly, MA, United States). PCNA, GAPDH, and tubulin antibodies were from Proteintech Group (Wuhan, China). APAP was obtained from Sigma-Aldrich (St Louis, MO, United States).

Biochemical Analysis

Liver GSH assay kit was purchased from Oxford Biomedical Research Company (Rochester Hills, MI). Malondialdehyde (MDA) assay kit, superoxide dismutase (SOD) kit, serum alanine aminotransferase (ALT) assay kit, and aspartate aminotransferase (AST) assay kits were purchased from Nanjing Jiancheng Bioengineering Institute (Nanjing, China).

Histological and Immunohistochemical Staining

Liver samples were fixed in 4% paraformaldehyde and embedded in paraffin, and then section into 4–6 μm thick slices. Sections were stained with hematoxylin and eosin (H and E) to analyze hepatic pathological damage. Images were obtained using a Nikon Eclipse Ti microscope. Immunohistochemical staining was performed as previously described (Mao et al., 2019).

Oil Red O, Periodic Acid-Schiff, and TUNEL Staining

Frozen liver sections were washed once in PBS and fixed with 4% paraformaldehyde (PFA) in PBS for 15 min at room temperature, followed by three washes in PBS. Sections were incubated in 60% isopropanol and then stained with filtered Oil Red O solution (1.5 mg/ ml) for 30 min and rinsed twice with distilled water. PAS staining of glycogen was performed using a commercial kit according to the manufacturer's instructions (Solarbio, Beijing, China). TUNEL assays were performed according to the *In Situ* Cell Death Detection Kit, Fluorescein (Roche, Basel, Switzerland).

Timm's Staining

Liver tissue sections fixed in 4% (w/v) PFA/PBS were immersed in 0.1% Na_2S in 0.1 M PBS for 1 h, 3% glutaraldehyde in 0.15 M PBS for 1 h, and then 0.1% Na_2S in 0.1 M PBS for 1 h. The sections were then incubated for 60 min in developing solution (30 ml 50% gum arabic, 5 ml 2 M citrate buffer pH 3.7, 15 ml 5.67% hydroquinone, and 0.25 ml 17% $AgNO_3$) protected from light and stirred gently. The slides were then rinsed several times in water and observed under a stereomicroscope.

Measurement of Zn^{2+} Using Flame Atomic Absorption Spectroscopy

Liver tissues were lyophilized and weighed prior to zinc concentration measurement. Tissue and serum were then digested with concentrated nitric acid (70%, Fisher Scientific, Waltham, MA) and heated in an auto-regulated heating block at 110°C for 48 h. All completely digested samples were diluted, and Zn^{2+} concentrations were quantified using a Perkin-Elmer

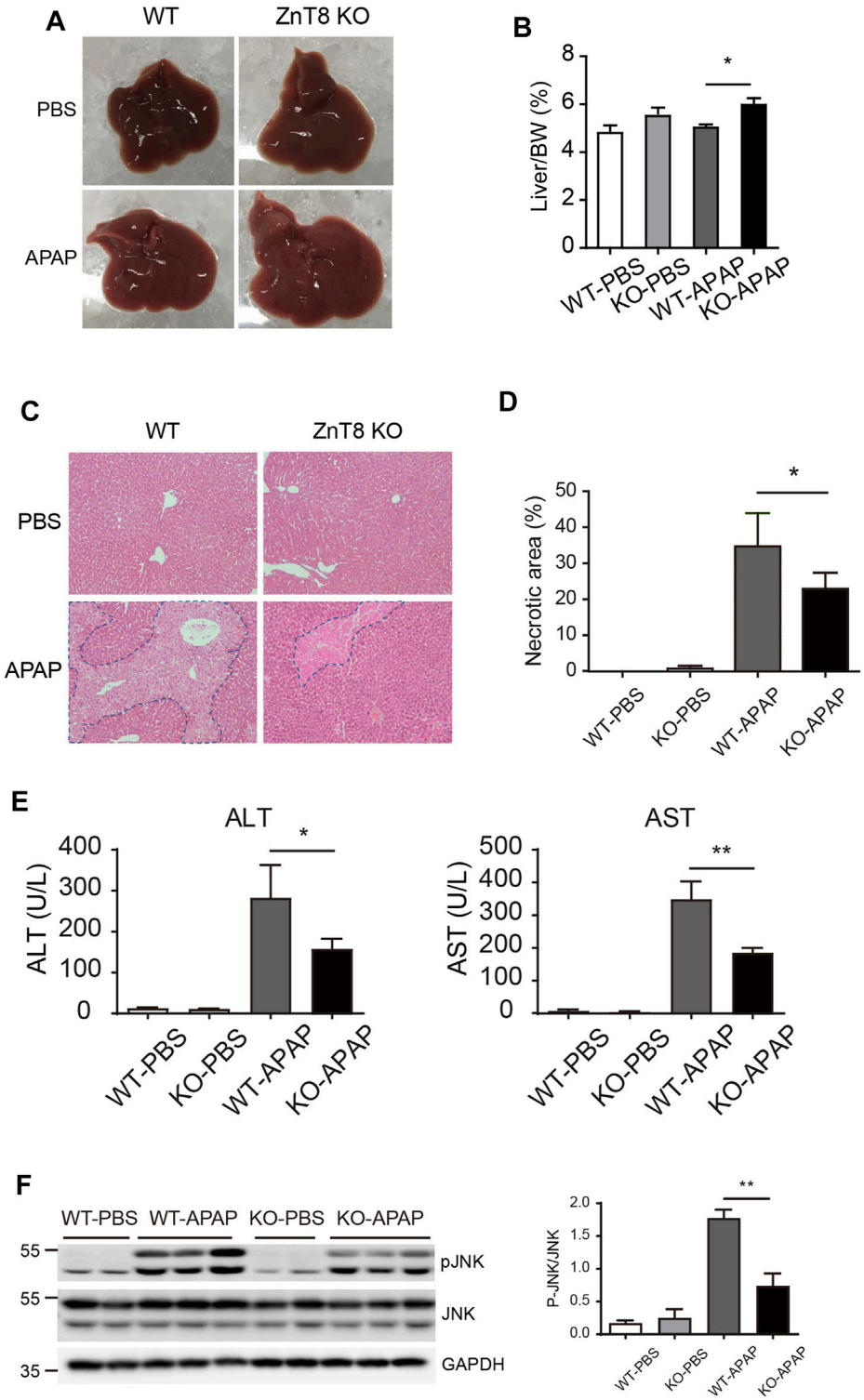

FIGURE 1 | ZnT8 deficiency ameliorates APAP-induced liver injury. Mice were treated with 300 mg/ kg APAP and sacrificed 24 h after APAP treatment. **(A)** Gross morphology of the livers. **(B)** Liver weights. **(C)** Representative H and E stained images. **(D)** Quantification of necrotic area. **(E)** Serum ALT and AST activities. **(F)** Immunoblotting and quantification of pJNK and total JNK in the liver. Data are represented as mean ± SEM. *, $p < 0.05$, **, $p < 0.01$ by the two-way ANOVA and post hoc Bonferroni's multiple comparison test.

Analyst 800 atomic absorption spectrometer. The recoveries of Zn^{2+} in standard reference material ranged between 95 and 110%.

Western Blotting, RNA Extraction and qRT-PCR

Western blotting was performed with 40 μg of protein lysate as described previously (Mao et al., 2021). Total RNA was extracted from mouse tissues, and cDNA synthesis and SYBR green gene expression assays were performed as previously described (Mao et al., 2021).

Statistical Analysis

All data are presented as mean ± standard error of the mean (SEM). Statistical differences between paired groups were measured by the unpaired Student's t-test or two-way analysis of variance (ANOVA) followed by Bonferroni's multiple comparisons test. All statistical analyses were performed using Prism software (GraphPad 8.0). p-values < 0.05 were considered statistically significant.

RESULTS

ZnT8 KO Mice Are Protected From APAP-Induced Liver Injury

To investigate whether ZnT8 plays a role in drug-induced hepatotoxicity, we injected APAP intraperitoneally into ZnT8 KO and wild-type mice. The mice were sacrificed and analyzed 24 h after injection. The liver mass, expressed as a percentage of total body weight, was heavier in ZnT8 KO mice than in wild-type mice (**Figures 1A,B**). Histological analysis showed that ZnT8 KO mice had less typical bridging necrosis within the centrilobular region and smaller areas of necrosis compared with wild-type controls (**Figure 1C**). Quantification of APAP-induced liver damage after 24 h indicated that approximately 22% of the liver was necrotic in ZnT8 KO mice compared to approximately 33% in wild-type mice (**Figure 1D**). APAP treatment resulted in wild-type mice with a significant increase in liver injury markers ALT and AST after 24 h, while ZnT8 KO mice showed a lesser increase (**Figure 1E**).

Activation of JNK, a marker of APAP-induced liver injury, is activated by phosphorylation of JNK protein in response to APAP treatment. The level of activation correlates with the degree of injury. We measured total and activated (phosphorylated) JNK levels by western blotting. Treatment of wild-type mice with APAP for 6 h strongly induced activation of JNK in the liver, whereas ZnT8 KO mice were resistant to APAP-stimulated JNK activation in the liver (**Figure 1F**). These results suggest that the lack of ZnT8 protects mice from APAP-induced hepatotoxicity.

Oxidative Stress Was Reduced in APAP-Treated ZnT8 KO Mice

GSH depletion and oxidative stress have been shown to play a key role in APAP-induced hepatotoxicity. APAP is bioactivated by cytochrome P450 to form NAPQI, which then binds to cellular proteins, forming APAP-protein adducts and leading to GSH depletion and oxidative stress (Yan et al., 2018). To investigate whether the attenuated APAP-induced liver injury in ZnT8 KO mice is the result of altered APAP metabolism, we examined GSH consumption and APAP metabolism. Hepatocellular GSH loss was reduced in ZnT8 KO mice compared to wild-type mice 6 h after APAP treatment (**Figure 2A**), suggesting that ZnT8 deficiency has a lesser bioactivating effect on APAP and consumes less GSH.

Lipid peroxidation is a key indicator of APAP-mediated oxidative damage in the liver (Saito et al., 2010b). The lipid peroxidation product MDA was decreased in APAP-treated ZnT8 KO livers compared to control livers. Consistently, the antioxidant enzyme SOD was increased in ZnT8 KO livers (**Figures 2B,C**). Another marker of lipid peroxidation is 4-Hydroxynonenal (4-HNE). Consistently, APAP induced a significant decrease in 4-HNE levels in the livers of ZnT8 KO mice (**Figure 2D**).

Cytochrome P450 (CYP) enzymes are the predominant enzymes involved in hepatic drug metabolism, and CYP2E1 is the major enzyme responsible for metabolizing APAP (Tracy et al., 2016). We examined CYP2E1 protein expression but detected no difference between ZnT8 KO mice and control mice (**Figure 2E**). In contrast, CYP4A, another important oxidative metabolism enzyme, was markedly increased, which is consistent with our recent study showing that CYP4A has a protective effect in bile duct ligation (BDL) induced liver injury (**Figure 2E**) (Li et al., 2021). We also compared the gene expression levels of other major APAP-metabolizing enzymes and transporters in the livers. However, we did not detect any significant changes in these genes (**Supplementary Figure 1**). Together, these results suggest that ZnT8 deficiency prevents APAP-induced liver injury by inducing CYP4A, reducing GSH depletion, and suppressing lipid peroxidation.

Hepatic Proliferation Is Accelerated in ZnT8 KO Mice

APAP-induced hepatotoxicity also depends on the balance between hepatocyte death and regeneration. The increased liver weight in APAP-treated ZnT8 KO mice compared to control wild-type mice (**Figure 1B**) suggests that this process may also be affected. We labeled apoptotic cells with the TUNEL assay, but there were no differences between ZnT8 KO mice and wild-type mice (**Figure 3A**). Proliferating cell nuclear antigen (PCNA) is a marker of cells with proliferative potential, while cyclin-dependent kinases (CDKs) are important regulators of cell cycle control. Hepatic PCNA and CDK2 protein levels were significantly increased in APAP-treated ZnT8 KO mice (**Figure 3B**). These results suggest that the increase in hepatocyte proliferation may ameliorate APAP-induced liver injury in ZnT8 KO mice.

Inflammation Is Reduced in ZnT8 KO Mice

Altered inflammatory responses and cytokine levels were observed in APAP-induced injury. Macrophage marker F4/80 staining showed a significant reduction in macrophage

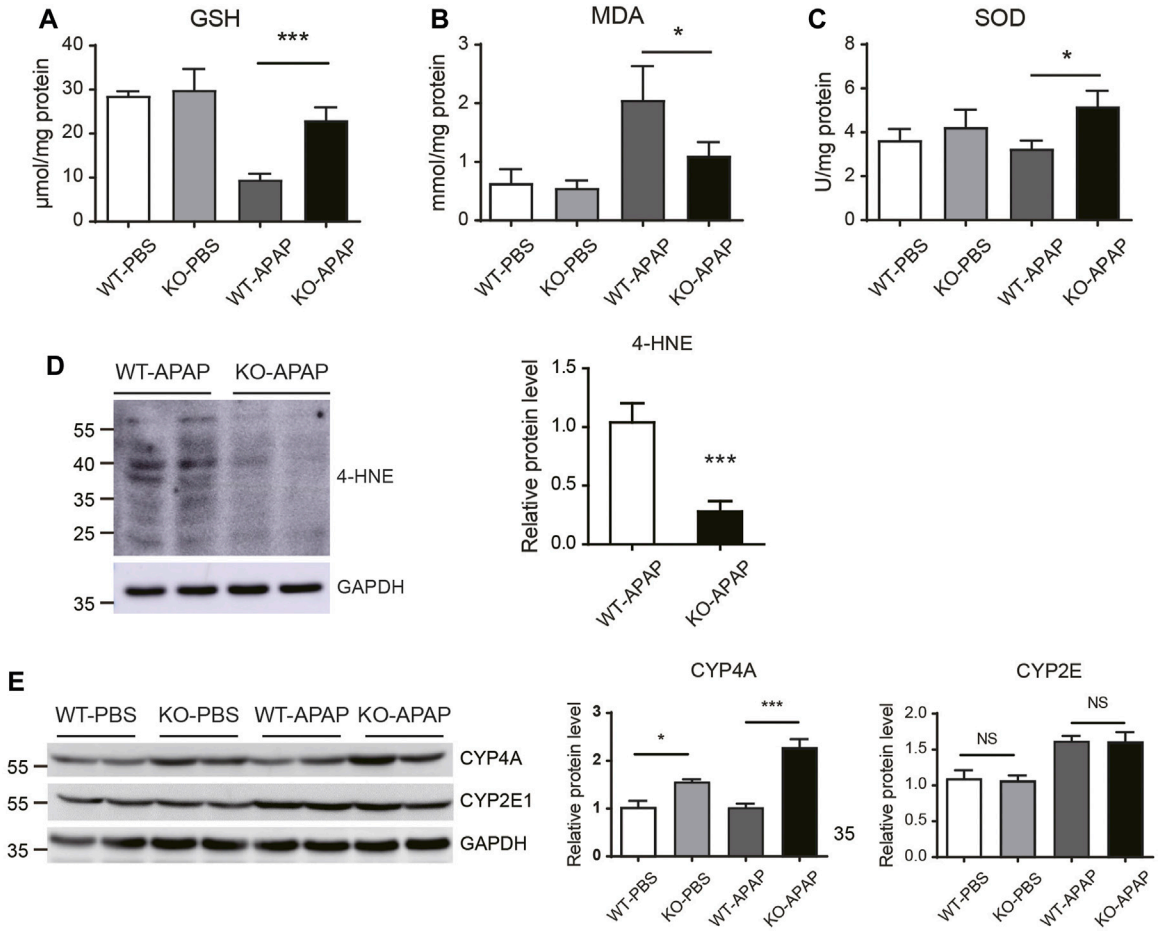

FIGURE 2 | Oxidative stress is reduced in the liver of APAP-treated ZnT8 KO mice. Hepatic levels of GSH **(A)**, MDA **(B)**, and SOD **(C)**. **(D)** Immunoblotting and quantification of 4-HNE in the liver. **(E)** Immunoblotting and quantification of CYP4A and CYP2E1 in liver. GAPDH was used as an internal control. Data are represented as mean ± SEM. *, $p < 0.05$, ***, $p < 0.001$ by the one-way ANOVA test or unpaired Student's *t*-test. NS, not significant.

infiltration in ZnT8 KO mice, suggesting an attenuated inflammatory state (**Figure 4A**). Consistently, the mRNA levels of the liver inflammatory markers interleukin 1 beta (Il1b) and tumor necrosis factor alpha (Tnfa) were also significantly reduced in ZnT8 KO mice (**Figures 4B–D**). Interestingly, mRNA expression of interleukin-6 (Il6) was increased in ZnT8 KO mice (**Figure 4E**). IL6 is known to play an important role in liver regeneration and acute liver injury (Gewiese-Rabsch et al., 2010; Schmidt-Arras and Rose-John, 2016), and IL-6 trans-signaling also significantly affects glycogen depletion in liver injury (Gewiese-Rabsch et al., 2010). Notably, APAP treatment, even as short as 6 h, causes glycogen depletion. We previously showed that ZnT8 deficient mice have more glycogen stored in the liver than wild-type mice (Mao et al., 2019). Here, ZnT8 KO mice also had larger glycogen stores than wild-type mice following APAP treatment (**Supplementary Figure 2**). These findings suggest that the inflammatory status and glycogen metabolism of ZnT8 KO mice are altered after APAP-induced liver damage.

The Level of Hepatic Zinc Is Increased in ZnT8 KO Mice

Zinc levels are associated with hepatic stress and inflammation status (Prasad and Bao, 2019). We analyzed liver and serum zinc levels using FAAS. There was an increase in liver zinc levels but no difference in serum zinc levels after APAP treatment (**Figures 5A,B**). Timm's sulfide silver staining has been used to visualize various metals in the brain and other tissues. To confirm the observed zinc levels, we stained the liver tissue using Timm's staining. Consistently, we found that the zinc levels, shown by brown signals, were remarkably increased in the centrilobular area, which correlated with the necrotic area of H&E staining (**Figure 5C**).

The mRNA Expression Levels of Zinc Transporters Are Changed and MTs Is Increased in ZnT8 KO Mice

Zinc homeostasis is balanced mainly by two major zinc transporter families, the zinc influx ZIP (SLC39) proteins and

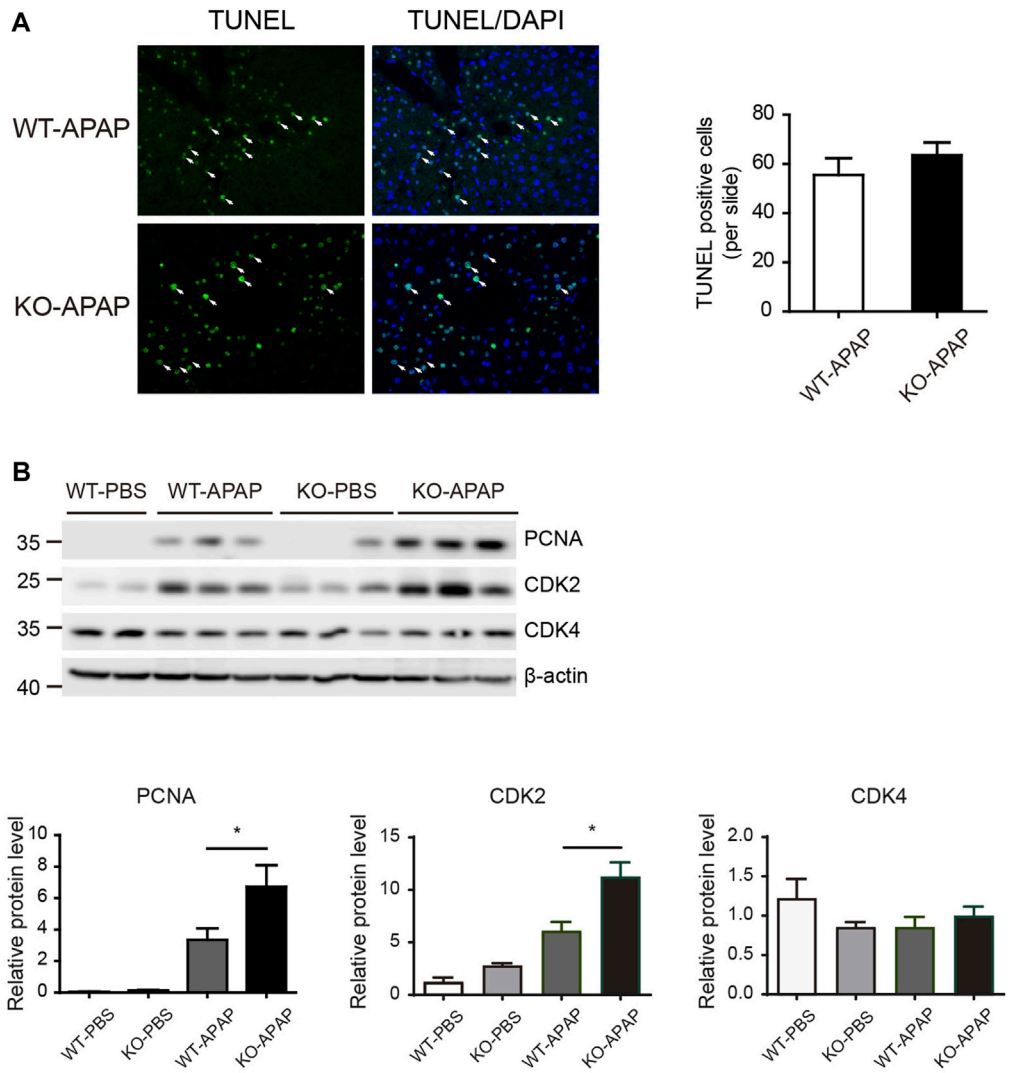

FIGURE 3 | Increased proliferation in APAP-treated ZnT8 KO livers. **(A)** Representative TUNEL staining images and quantification of TUNEL-positive cells. **(B)** Immunoblotting and quantification of PCNA, CDK2, and CDK4 in liver. β-tubulin was used as an internal control. Data are expressed as mean ± SEM. *, $p < 0.05$ by the one-way ANOVA test or unpaired Student's *t*-test. NS, not significant.

the efflux ZnT (SLC30) proteins (Bafaro et al., 2017). We analyzed the mRNA expression levels of ZIPs and ZnTs in the liver. Under basal conditions, most ZIPs, including Slc39a4, Slc39a7, Slc39a11, and Slc39a13, were mildly induced in ZnT8 KO mice. Several ZnTs, including Slc30a1, Slc30a5, and Slc30a6, were induced in ZnT8 KO mice, indicating that zinc metabolism was more active in the livers of ZnT8 KO mice (**Figures 6A,B**, and **Supplementary Figure 3**). Following APAP treatment, *Slc39a4* and *Slc39a14* were the most highly upregulated zinc uptake transporters in the livers of APAP-treated ZnT8 KO mice, whereas the expression levels of most ZnTs were unchanged except for a slight increase in Slc39a6 levels (**Figures 6A,B**). These results suggest that ZIP4 and ZIP14 may contribute to the elevated zinc levels in the livers of ZnT8 KO mice.

Zinc levels are also regulated by a group of buffer proteins called MTs, which directly scavenge reactive oxygen species (ROS) and interact with GSH to enhance SOD activity (Formigari et al., 2007; Chiaverini and De Ley, 2010). Zinc may protect tissues from oxidative stress by inducing the expression of MTs. Indeed, in the liver of ZnT8 KO mice, both mRNA and protein levels of MTs were significantly increased (**Figures 6C,D**). Immunostaining showed that after APAP treatment, MTs were mainly enriched around the pericentral venous area, correlating with the positively stained zinc area. We also noted that hepatic MT levels were significantly elevated in both basal and APAP-treated livers of ZnT8 KO mice (**Figure 6E**). These results suggest that elevated hepatic zinc and MTs in ZnT8 KO mice may confer protection against oxidative stress and hepatic injury.

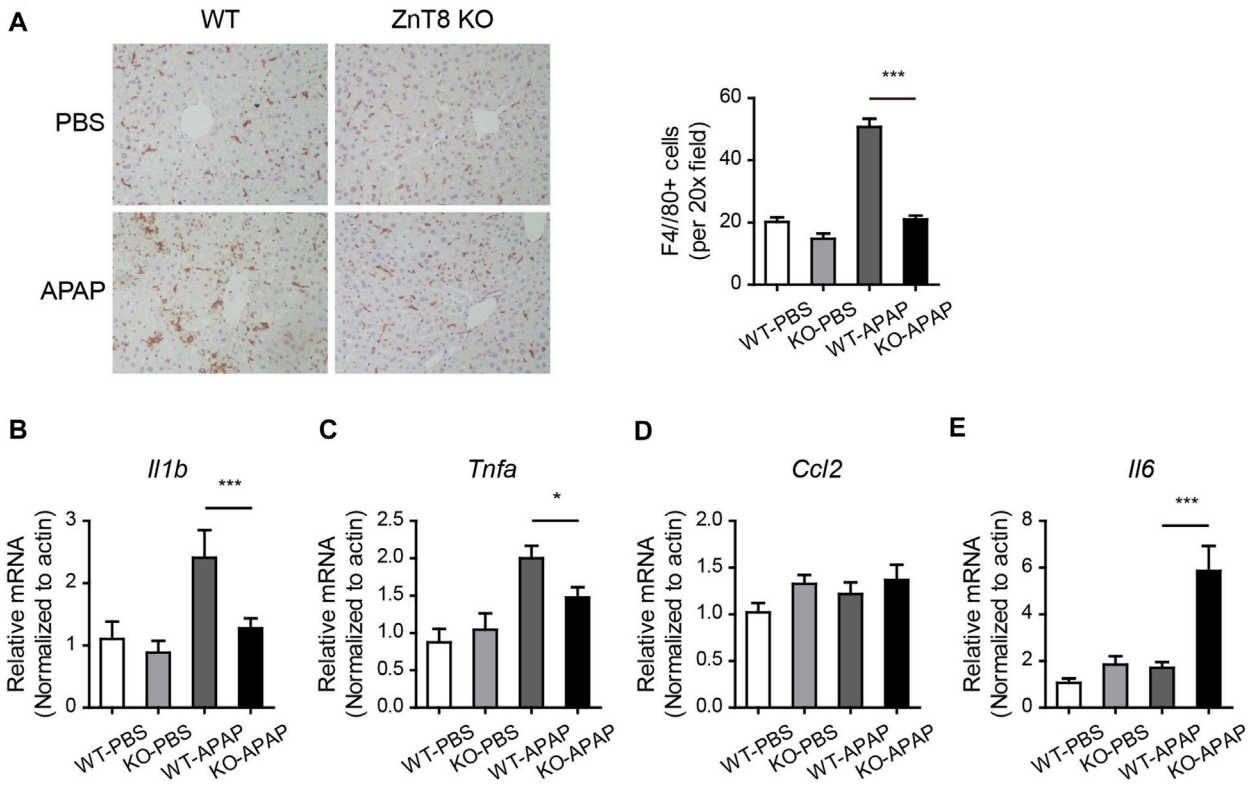

FIGURE 4 | Reduced inflammation in APAP-treated ZnT8 KO livers. **(A)** Representative IHC staining images and quantitative analysis of F4/80 in the liver. **(B–E)** Relative transcript levels of liver inflammatory genes Il1b **(B)**, Tnfa **(C)**, Ccl2 **(D)**, and Il6 **(E)**. Data are represented as mean ± SEM. *, $p < 0.05$, ***, $p < 0.001$. By tested one-way ANOVA.

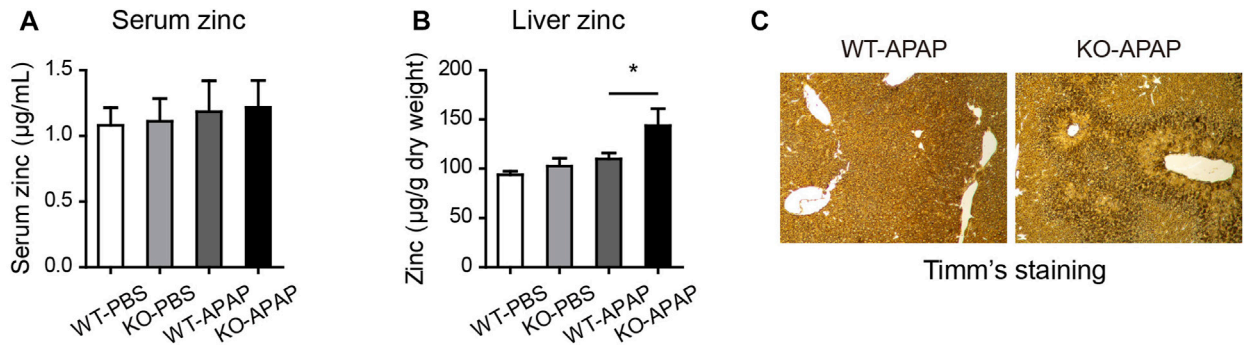

FIGURE 5 | Elevated zinc levels in the liver of ZnT8 KO mice. **(A)** Serum zinc levels. **(B)** Liver zinc levels. **(C)** Representative images of Timm's staining of the liver. Data are represented as mean ± SEM. *, $p < 0.05$ as tested by one-way ANOVA.

DISCUSSION

In this study, we initially hypothesized that ZnT8-deficient mice contain lower levels of pancreatic zinc than wild-type mice, which may deteriorate the antioxidant and detoxification functions of the liver. Unexpectedly, we observed ameliorated hepatic injury in APAP-treated ZnT8 KO mice. Mice were injected intraperitoneally with APAP and were sacrificed to examine the liver injury. ZnT8 KO mice exhibited decreased serum levels of hepatic enzymes ALT and AST. Histopathological examination revealed a significant decrease in the hepatocellular necrosis area in injured livers of ZnT8 KO mice. Consistently, oxidative stress was reduced in ZnT8 KO mice, and an increase in hepatic GSH was observed, along with a decreased in the levels of MDA and 4-HNE. No significant changes were observed in CYP2E1, the main enzyme

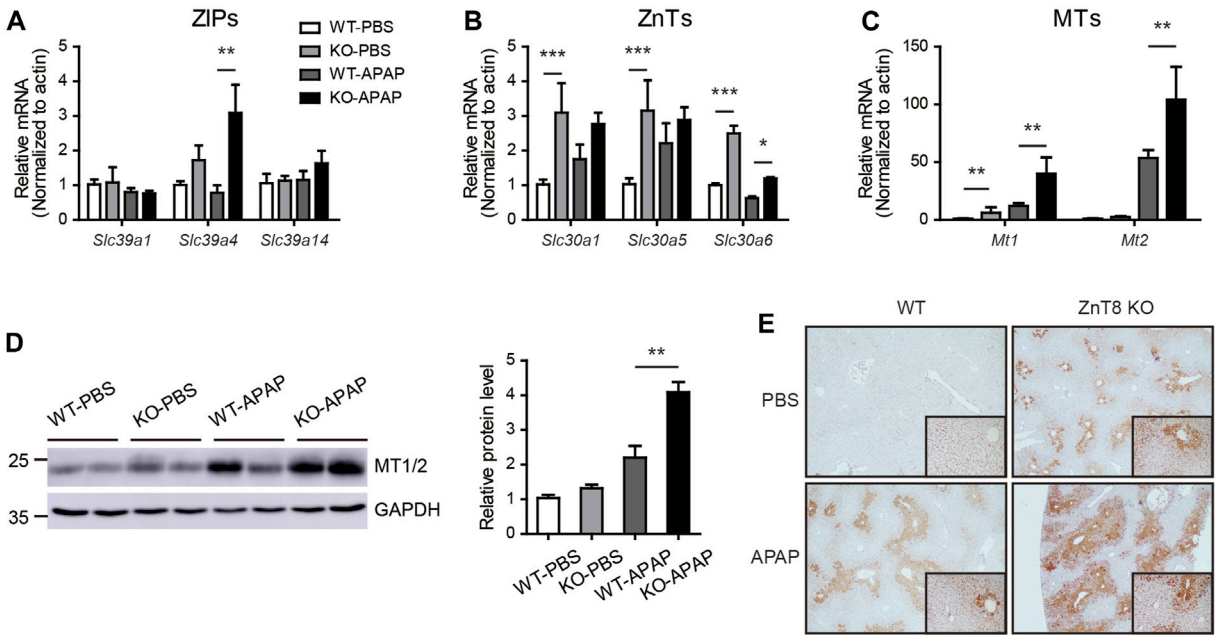

FIGURE 6 | Altered mRNA expression profile of zinc transporters and increased MTs in ZnT8 KO mice livers. **(A–C)** The mRNA expression levels of ZIP **(A)**, ZnT **(B)**, and MT genes in the liver. **(D)** Immunoblotting and quantification of MT1/2 in liver. GAPDH was used as an internal control. **(E)** Representative immunohistochemical staining of MT1/2 proteins in liver. Data are represented as mean ± SEM, and analyzed by the one-way ANOVA test.

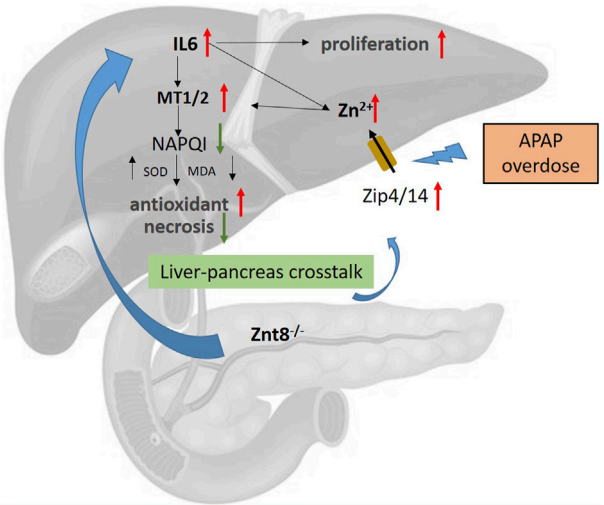

FIGURE 7 | Potential mechanism of ZnT8 KO protection against APAP-induced liver injury. Zip4 and Zip14 are localized to the plasma membrane of hepatocytes and are dramatically upregulated after APAP treatment. ZnT8 KO mice displayed higher levels of hepatic IL6, Zip4, and Zip14 expression than wild-type mice after APAP overdose, accompanied by increased zinc uptake. Accumulation of hepatic Zn^{2+} and IL6 upregulates the antioxidant proteins MT1/2. Accumulation of MT1/2 attenuates APAP-induced inflammation, ROS, and necrosis. Zip4 and Zip14 may play a major role in the mechanisms responsible for the protective effects of ZnT8 KO mice. In addition, higher levels of IL6 also lead to enhanced hepatocyte proliferation in ZnT8 KO mice.

responsible for drug biotransformation. APAP-induced inflammation and glycogen depletion were also alleviated. The increased levels of hepatic zinc and MTs may contribute to the hepatoprotective effect of ZnT8 KO mice. Taken together, our findings suggest that ZnT8 KO mice showed an unexpected improvement in antioxidant activity against APAP hepatotoxicity (**Figure 7**).

The initial aim of our study was to investigate whether alterations in pancreatic genetics could affect liver function. ZnT8, encoded by the SLC30A8 gene, is a pancreatic-enriched zinc transporter primarily responsible for transporting zinc into insulin granules. Genetic ZnT8 polymorphisms have been associated with defective β-cell zinc levels and diabetes mellitus (Sladek et al., 2007; Rutter and Chimienti, 2015). Previous studies have shown that zinc, which is secreted in concert with insulin, suppresses hepatic insulin clearance. In the absence of ZnT8, a substantial amount of insulin is degraded in the liver, resulting in low peripheral insulin levels (Tamaki et al., 2013). Zinc is known to be an important antioxidant that protects the liver from drug toxicity. Therefore, we hypothesized that altered zinc flow from the pancreas to the liver might affect hepatic injury associated with oxidative stress.

In Western countries, APAP-induced liver injury remains the leading cause of drug-induced liver injury (Lee, 2017). The pathogenesis of APAP hepatotoxicity is complex. Briefly, APAP is metabolized in the liver by CYP2E1 to form NAPQI, which is then conjugated and detoxified with GSH.

Upon exhausting hepatic GSH, excess NAPQI eventually leads to mitochondrial damage and hepatocyte death (Yan et al., 2018).

Under normal conditions, zinc levels in the liver are relatively low. Zinc plays an important role in hepatic antioxidant and drug-metabolizing activities by preventing the formation of toxic cellular ROS and mitochondrial stress. Mechanisms of zinc in hepatic drug metabolism include: 1) direct binding of zinc to drugs; 2) zinc as a cofactor for most CYP450 family members; 3) zinc-induces the expression of MTs (Prasad and Bao, 2019). MTs are a family of low molecular mass, cysteine-rich metal-binding proteins, which buffer free zinc in the cytoplasm and protect it against toxic and oxidative stress-inducing effects. MTs are protective against APAP-induced liver injury through scavenging NAPQI after GSH depletion and preventing covalent binding to cellular proteins (Saito et al., 2010a). The expression of MTs is highly regulated by zinc levels, oxidative stress, inflammation, or cytokines such as IL6 (Babula et al., 2012). In our study, we unexpectedly found that basal liver and serum zinc levels were unaltered in ZnT8 KO mice. However, acute treatment with APAP in ZnT8 KO mice significantly increased hepatic zinc and MT1/2 protein levels. The protective effect of zinc and MTs against APAP injury or acute liver injury has been well demonstrated in previous reports (Chen et al., 2001; Saito et al., 2010a; Babula et al., 2012). Since our mouse model is deficient in a zinc transporter, we hypothesize that changes in zinc content and distribution are responsible for the protective effect against the acute liver injury. The lack of islet zinc flux may sensitize the liver to increase the expression of zinc transporters. When stimulated, the liver transports more zinc and defends against oxidative stress. Serum zinc levels were unaltered in ZnT8 KO mice. Therefore, it is unlikely that systemic zinc status affects the expression of hepatic MTs. The most likely alteration is zinc transport in the portal vein from the pancreas.

CYP2E1 is thought to be the major CYP responsible for NAPQI metabolism; however, no change in CYP2E1 expression was observed in ZnT8 KO mice. We hypothesized that the main protective mechanism occurred via zinc/MT signaling. CYP4A was upregulated under basal conditions and after APAP treatment in ZnT8 KO mice. In our previous study, we showed that ZnT8 KO mice exhibited a significant increase in hepatic lipid accumulation (Mao et al., 2019). We also noticed that several PPARα targeting genes were upregulated in the livers of ZnT8 KO mice, suggesting an activated PPAR signaling pathway. CYP4A is under the transcriptional control of PPARα in the liver. Therefore, one would suspect that enhanced PPARα activity is responsible for the increased CYP4A expression at the basal level. In addition, our recent paper showed that CYP4A exerts a protective effect in BDL-induced inflammation and liver injury, supporting the possibility that the increased CYP4A in the ZnT8 KO mice in this study may be participate in the attenuation of APAP-induced liver injury (Li et al., 2021).

In this study, we observed an increase in liver weight following APAP treatment, suggesting increased proliferation. The liver has a strong regenerative capacity after injury. We observed a significant increase in the number of proliferating hepatocytes in the transition zone between necrotic and healthy cells. PCNA and the cell cycle protein CDK2 were also elevated in ZnT8 KO mice livers. Previous reports have suggested that IL6 can make hepatocytes more responsive to growth factors and encourage proliferation (Kovalovich et al., 2000; Schmidt-Arras and Rose-John, 2016). In addition, IL6 is important for hepatocyte regeneration after APAP overdose in mice (James et al., 2003). Therefore, we speculate that IL6 may contribute to the increased proliferation in our ZnT8 KO model. Furthermore, IL6 induces hepatic ZIP14 expression and zinc accumulation (Liuzzi et al., 2005). In this study, Tnfa expression was reduced in ZnT8 KO mice compared to Il6, which may be a reflection of attenuated TNF-α/NFκB signaling and reduced inflammation. Increased IL6 levels and hyperactive IL6 signaling in ZnT8 KO livers may contribute to the increased hepatocyte proliferation, which may also attenuate APAP-induced liver injury by increasing the capacity of liver repair.

ZnT8 is expressed almost exclusively in pancreatic islets and is not found in the liver. ZnT8 deficiency stimulates rescue factors or reduces/inhibits pro-injury factors in an, as yet, unknown manner to maintain hepatocyte viability and reduce liver injury. We recently found that ZnT8 is also expressed in enteroendocrine cells and affects the intestinal microenvironment and microbiota (Mao et al., 2019). These factors may also influence the liver status and xenobiotic metabolism. In the present study, it was not possible to distinguish whether pancreatic or intestinal alterations affecting ZnT8 KO mice resulted in effects on the liver. Tissue-specific ZnT8 KO mice would be an option to address this question.

Interestingly, studies in humans have shown that ZnT8 loss-of-function mutants are associated with increased insulin secretion capacity and lower risk of developing type 2 diabetes (Flannick et al., 2014; Dwivedi et al., 2019). In this study, we also observed that ZnT8 deficiency protects against hepatic drug injury. Therefore, ZnT8 remains an attractive target for antidiabetic therapy, which may also confer antioxidant protection.

In conclusion, we have demonstrated that mice deficient in ZnT8 partially prevent APAP-induced liver injury. The resistance to APAP-induced liver injury is likely due to compensatory changes in zinc transporter expression, increased zinc accumulation, and increased expression of MTs.

DATA AVAILABILITY STATEMENT

The raw data supporting the conclusions of this article will be made available by the authors, without undue reservation.

ETHICS STATEMENT

The animal study was reviewed and approved by the Scientific Investigation Board of Health Science Center of Shenzhen University.

AUTHOR CONTRIBUTION

ZM and WS developed the study rationale, designed the experiments, and wrote the manuscript. WS, MF, RC, YiL, JT, YuL, KP, and RL performed the experiments and assisted with data analysis. ZM supervised the study and served as the guarantor.

FUNDING

This work was funded by National Natural Science Foundation of China (82070557, 81870405), the Guangdong Medical Science and Technology Research Fund Project (A2019422), the Shenzhen Science and Technology Project (JCYJ20190808144203802) and Shenzhen Key Laboratory of Metabolism and Cardiovascular Homeostasis (ZDSYS20190902092903237).

SUPPLEMENTARY MATERIAL

The Supplementary Material for this article can be found online at: https://www.frontiersin.org/articles/10.3389/fphar.2021.721471/full#supplementary-material

REFERENCES

Babula, P., Masarik, M., Adam, V., Eckschlager, T., Stiborova, M., Trnkova, L., et al. (2012). Mammalian Metallothioneins: Properties and Functions. *Metallomics* 4 (8), 739–750. doi:10.1039/c2mt20081c

Bafaro, E., Liu, Y., Xu, Y., and Dempski, R. E. (2017). The Emerging Role of Zinc Transporters in Cellular Homeostasis and Cancer. *Sig Transduct Target. Ther.* 2, 17029. doi:10.1038/sigtrans.2017.29

Barragán-Álvarez, C. P., Padilla-Camberos, E., Díaz, N. F., Cota-Coronado, A., Hernández-Jiménez, C., Bravo-Reyna, C. C., et al. (2021). Loss of Znt8 Function in Diabetes Mellitus: Risk or Benefit?. *Mol. Cel Biochem.* 476, 2703–2718. doi:10.1007/s11010-021-04114-4

Chen, H., Carlson, E. C., Pellet, L., Moritz, J. T., and Epstein, P. N. (2001). Overexpression of Metallothionein in Pancreatic β-Cells Reduces Streptozotocin-Induced DNA Damage and Diabetes. *Diabetes* 50 (9), 2040–2046. doi:10.2337/diabetes.50.9.2040

Chiaverini, N., and De Ley, M. (2010). Protective Effect of Metallothionein on Oxidative Stress-Induced DNA Damage. *Free Radic. Res.* 44 (6), 605–613. doi:10.3109/10715761003692511

Dwivedi, O. P., Lehtovirta, M., Hastoy, B., Chandra, V., Krentz, N. A. J., Kleiner, S., et al. (2019). Loss of ZnT8 Function Protects against Diabetes by Enhanced Insulin Secretion. *Nat. Genet.* 51 (11), 1596–1606. doi:10.1038/s41588-019-0513-9

Flannick, J., Thorleifsson, G., Thorleifsson, G., Beer, N. L., Jacobs, S. B. R., Grarup, N., et al. (2014). Loss-of-function Mutations in SLC30A8 Protect against Type 2 Diabetes. *Nat. Genet.* 46 (4), 357–363. doi:10.1038/ng.2915

Formigari, A., Irato, P., and Santon, A. (2007). Zinc, Antioxidant Systems and Metallothionein in Metal Mediated-Apoptosis: Biochemical and Cytochemical Aspects. *Comp. Biochem. Physiol. C: Toxicol. Pharmacol.* 146 (4), 443–459. doi:10.1016/j.cbpc.2007.07.010

Gewiese-Rabsch, J., Drucker, C., Malchow, S., Scheller, J., and Rose-John, S. (2010). Role of IL-6 Trans-signaling in CCl4 Induced Liver Damage. *Biochim. Biophys. Acta (Bba) - Mol. Basis Dis.* 1802 (11), 1054–1061. doi:10.1016/j.bbadis.2010.07.023

James, L. P., Lamps, L. W., McCullough, S., and Hinson, J. A. (2003). Interleukin 6 and Hepatocyte Regeneration in Acetaminophen Toxicity in the Mouse. *Biochem. Biophysical Res. Commun.* 309 (4), 857–863. doi:10.1016/j.bbrc.2003.08.085

Kovalovich, K., DeAngelis, R. A., Li, W., Furth, E. E., Ciliberto, G., and Taub, R. (2000). Increased Toxin-Induced Liver Injury and Fibrosis in Interleukin-6-Deficient Mice. *Hepatology* 31 (1), 149–159. doi:10.1002/hep.510310123

Lee, W. M. (2017). Acetaminophen (APAP) Hepatotoxicity-Isn't it Time for APAP to Go Away? *J. Hepatol.* 67 (6), 1324–1331. doi:10.1016/j.jhep.2017.07.005

Li, S., Wang, C., Zhang, X., and Su, W. (2021). Cytochrome P450 omega-hydroxylase 4a14 Attenuates Cholestatic Liver Fibrosis. *Front. Physiol.* 12, 688259. doi:10.3389/fphys.2021.688259

Liuzzi, J. P., Lichten, L. A., Rivera, S., Blanchard, R. K., Aydemir, T. B., Knutson, M. D., et al. (2005). Interleukin-6 Regulates the Zinc Transporter Zip14 in Liver and Contributes to the Hypozincemia of the Acute-phase Response. *Proc. Natl. Acad. Sci.* 102 (19), 6843–6848. doi:10.1073/pnas.0502257102

Mao, Z., Feng, M., Li, Z., Zhou, M., Xu, L., Pan, K., et al. (2021). ETV5 Regulates Hepatic Fatty Acid Metabolism through PPAR Signaling Pathway. *Diabetes* 70 (1), 214–226. doi:10.2337/db20-0619

Mao, Z., Lin, H., Su, W., Li, J., Zhou, M., Li, Z., et al. (2019). Deficiency of ZnT8 Promotes Adiposity and Metabolic Dysfunction by Increasing Peripheral Serotonin Production. *Diabetes* 68 (6), 1197–1209. doi:10.2337/db18-1321

Prasad, A. S., and Bao, B. (2019). Molecular Mechanisms of Zinc as a Pro-antioxidant Mediator: Clinical Therapeutic Implications. *Antioxidants* 8 (6), 164. doi:10.3390/antiox8060164

Rutter, G. A., and Chimienti, F. (2015). SLC30A8 Mutations in Type 2 Diabetes. *Diabetologia* 58 (1), 31–36. doi:10.1007/s00125-014-3405-7

Saito, C., Yan, H.-M., Artigues, A., Villar, M. T., Farhood, A., and Jaeschke, H. (2010a). Mechanism of protection by Metallothionein against Acetaminophen Hepatotoxicity. *Toxicol. Appl. Pharmacol.* 242 (2), 182–190. doi:10.1016/j.taap.2009.10.006

Saito, C., Zwingmann, C., and Jaeschke, H. (2010b). Novel Mechanisms of protection against Acetaminophen Hepatotoxicity in Mice by Glutathione and N-Acetylcysteine. *Hepatology* 51 (1), 246–254. doi:10.1002/hep.23267

Schmidt-Arras, D., and Rose-John, S. (2016). IL-6 Pathway in the Liver: from Physiopathology to Therapy. *J. Hepatol.* 64 (6), 1403–1415. doi:10.1016/j.jhep.2016.02.004

Sladek, R., Rocheleau, G., Rung, J., Dina, C., Shen, L., Serre, D., et al. (2007). A Genome-wide Association Study Identifies Novel Risk Loci for Type 2 Diabetes. *Nature* 445 (7130), 881–885. doi:10.1038/nature05616

Tamaki, M., Fujitani, Y., Hara, A., Uchida, T., Tamura, Y., Takeno, K., et al. (2013). The Diabetes-Susceptible Gene SLC30A8/ZnT8 Regulates Hepatic Insulin Clearance. *J. Clin. Invest.* 123 (10), 4513–4524. doi:10.1172/jci68807

Tracy, T. S., Chaudhry, A. S., Prasad, B., Thummel, K. E., Schuetz, E. G., Zhong, X.-B., et al. (2016). Interindividual Variability in Cytochrome P450-Mediated Drug Metabolism. *Drug Metab. Disposition* 44 (3), 343–351. doi:10.1124/dmd.115.067900

Trefts, E., Gannon, M., and Wasserman, D. H. (2017). The Liver. *Curr. Biol.* 27 (21), R1147–R1151. doi:10.1016/j.cub.2017.09.019

Yan, M., Huo, Y., Yin, S., and Hu, H. (2018). Mechanisms of Acetaminophen-Induced Liver Injury and its Implications for Therapeutic Interventions. *Redox Biol.* 17, 274–283. doi:10.1016/j.redox.2018.04.019

Conflict of Interest: The authors declare that the research was conducted in the absence of any commercial or financial relationships that could be construed as a potential conflict of interest.

Publisher's Note: All claims expressed in this article are solely those of the authors and do not necessarily represent those of their affiliated organizations, or those of the publisher, the editors and the reviewers. Any product that may be evaluated in this article, or claim that may be made by its manufacturer, is not guaranteed or endorsed by the publisher.

frontiers in Pharmacology

ORIGINAL RESEARCH
published: 27 August 2021
doi: 10.3389/fphar.2021.696456

Cardio- and Cerebrovascular Outcomes of Postoperative Acute Kidney Injury in Noncardiac Surgical Patients With Hypertension

Yan Guangyu[1,2], *Lou Jingfeng*[1], *Liu Xing*[3], *Yuan Hong*[1]* and *Lu Yao*[1,4,5]*

[1]Center of Clinical Research, The Third Xiangya Hospital, Central South University, Changsha, China, [2]Department of General Surgery, The Third Xiangya Hospital, Central South University, Changsha, China, [3]Department of Anesthesia, The Third Xiangya Hospital, Central South University, Changsha, China, [4]Department of Life Science and Medicine, King's College London, London, United Kingdom, [5]Key Laboratory of Medical Information Research(Central South University), College of Hunan Province, Changsha, China

OPEN ACCESS

Edited by:
Annalisa Capuano,
University of Campania Luigi Vanvitelli, Italy

Reviewed by:
Niccolò Lombardi,
University of Florence, Italy
Mahmood Khan,
The Ohio State University, United States
Ylenia Ingrasciotta,
University of Messina, Italy

***Correspondence:**
Yuan Hong
yuanhong01@csu.edu.cn
Lu Yao
luyao0719@163.com

Specialty section:
This article was submitted to Cardiovascular and Smooth Muscle Pharmacology, a section of the journal Frontiers in Pharmacology

Received: 19 April 2021
Accepted: 05 July 2021
Published: 27 August 2021

Citation:
Guangyu Y, Jingfeng L, Xing L, Hong Y and Yao L (2021) Cardio- and Cerebrovascular Outcomes of Postoperative Acute Kidney Injury in Noncardiac Surgical Patients With Hypertension. Front. Pharmacol. 12:696456. doi: 10.3389/fphar.2021.696456

Background: The cardiovascular and cerebrovascular risk of postoperative acute kidney injury (AKI) in surgical patients is poorly described, especially in the hypertensive population.

Methods: We conducted a retrospective cohort study among all hypertensive patients who underwent elective noncardiac surgery from January 1st, 2012 to August 1st, 2017 at the Third Xiangya Hospital. The primary outcomes were fatal stroke and fatal myocardial infarction (MI). The secondary outcomes were all-cause mortality.

Results: The postoperative cumulative mortality within 3 months, 6 months, 1 year, 2 years, and 5 years were 1.27, 1.48, 2.15, 2.15, and 5.36%, for fatal stroke, and 2.05, 2.27, 2.70, 3.37, and 5.61% for fatal MI, respectively, in patients with postoperative AKI. Compared with non-AKI patients, those with postoperative AKI had a significantly higher risk of fatal stroke and fatal MI within 3 months [hazard ratio (HR): 5.49 (95% CI: 1.88–16.00) and 11.82 (95% CI: 4.56–30.62), respectively], 6 months [HR: 3.58 (95% CI: 1.43–8.97) and 9.23 (95% CI: 3.89–21.90), respectively], 1 year [HR: 3.64 (95% CI: 1.63–8.10) and 5.14 (95% CI: 2.50–10.57), respectively], 2 years [HR: 2.21 (95% CI: 1.03–4.72) and 3.06 (95% CI: 1.66–5.64), respectively], and 5 years [HR: 2.27 (95% CI: 1.30–3.98) and 1.98 (95% CI: 1.16–3.20), respectively]. In subgroup analysis of perioperative blood pressure (BP) lowering administration, postoperative AKI was significantly associated with 1-year and 5-year risk of fatal stroke [HR: 9.46 (95% CI: 2.85–31.40) and 3.88 (95% CI: 1.67–9.01), respectively] in patients with ACEI/ARB, and MI [HR: 6.62 (95% CI: 2.23–19.62) and 2.44 (95% CI: 1.22–4.90), respectively] in patients with CCB.

Conclusion: Hypertensive patients with postoperative AKI have a significantly higher risk of fatal stroke and fatal MI, as well as all-cause mortality, within 5 years after elective noncardiac surgery. In patients with perioperative administration of ACEI/ARB and CCB, postoperative AKI was significantly associated with higher risk of fatal stroke and MI, respectively.

Keywords: acute kidney injury, noncardiac surgery, cardiovascular and cerebrovascular outcomes, hypertension, mortality

INTRODUCTION

Acute kidney injury (AKI) affects millions of patients worldwide, which has become an increasing health problem (Susantitaphong et al., 2013). As a major postoperative complication, AKI happens in 1.8–39.3% of all surgical patients (O'Connor et al., 2016). Despite renal function recovering in the majority of AKI cases, still, AKI has been confirmed as an important risk factor of CKD or end-stage renal disease (ESRD) (Ishani et al., 2009; Chawla and Kimmel, 2012; Kline and Rachoin, 2013), increased mortality after discharge, and longer length of stay (LOS) in all type of surgery (Kork et al., 2015; Lau et al., 2020; Gameiro et al., 2020). In addition to renal impairment, the current evidence supports the notion that acute cardiovascular damage due to AKI, as characterized as type 3 cardiorenal syndrome (Ronco et al., 2008), leads to other poor outcomes (Ronco et al., 2018). The postoperative AKI was found to be associated with an increased risk of cardiovascular events, such as myocardial infarction (MI) (Hansen et al., 2013), heart failure (James et al., 2011), and other major adverse cardiac events (MACE) (Anzai et al., 2010).

Besides, as a well-known risk factor for cardio- and cerebrovascular diseases, hypertension has also been found to increase the risk of postoperative AKI (Ikehata et al., 2016). There are 25% of noncardiac and 80% of cardiac surgical patients being found hypertensive before surgery (Dix and Howell, 2001; Haas and LeBlanc, 2004). Moreover, patients with a history of hypertension have a higher risk of cardiovascular events after AKI (Arias-Cabrales et al., 2018). Thus, it is of great importance to understand the cardiovascular prognosis in hypertensive surgical patients with postoperative AKI.

However, there is a shortage of studies on clinical outcomes, especially of cardio- and cerebrovascular events, in hypertensive patients with postoperative AKI. Therefore, in this retrospective cohort study, we sought to determine the risk of fatal stroke and fatal MI, as well as all-cause mortality, within 5 years after elective noncardiac surgery in hypertensive patients with postoperative AKI, and cardiovascular and cerebrovascular outcomes in patients with or without certain type of perioperative administration of blood pressure (BP) lowering medication.

METHODS

Design and Setting

This was a retrospective cohort study. All patients were recruited from January 1st, 2012 to August 1st, 2017 at the Third Xiangya Hospital, Central South University, Changsha, China. It provides medical care for all residents living in central south China. The present study was following the guidelines of the Declaration of Helsinki and was approved by the Medical Ethics Committee of the Third Xiangya Hospital (Approval ID: R18030). All the participants have signed an informed consent form at admission and agreed to share their health information for medical research.

Inclusion and Exclusion

During the period from January 1st, 2012 to August 1st, 2017, a total of 105,589 surgical patient records of elective surgery with hypertension diagnosis were retrospectively collected in the database of the Third Xiangya Hospital. Inclusions criteria were as follows: 1) age ≥18 years, 2) elective noncardiac surgery (surgery performed more than 2 days after planning the procedure), and 3) confirmed diagnosis of hypertension. Exclusion criteria were as follows: 1) severe preexisting chronic kidney disease (estimated glomerular filtration rate (EGFR) < 15 ml/min/1.73 m^2); 2) previous renal transplant surgery or admission for renal transplant surgery, 3) no serum creatinine within 30 days before surgery; 4) admission for cardiac, obstetric surgery, and procedures of percutaneous puncture; 5) no records of resident ID card numbers or non-Hunan residents by ID card numbers; and 6) admission for multiple surgeries.

Definition of AKI

Serum creatinine was used to identify whether the patients developed postoperative AKI or not. According to the serum creatinine criteria in the KDIGO classification, a serum creatinine increase greater than 26.5 mmol/L within 48 h or a 1.5-fold increase in serum creatinine within 7 days after surgery indicates that the patients have developed AKI (Palevsky et al., 2013). Urine output criteria were not included due to the lack of data. For each patient, records of preoperative serum creatinine measured 30 days before surgery were collected, and averaged values of those records were determined as baseline creatinine. The peak postoperative measurement of creatinine 48 h and/or 7 days after surgery was compared to baseline creatinine to assign postoperative AKI status.

Outcomes and Definitions

The primary outcomes were fatal stroke and fatal MI within 5 years after the elective noncardiac surgery. The secondary outcomes were all-cause mortality. Time points of 3 months, 6 months, 1 year, 2 years, and 5 years were also included in the analysis of primary and secondary outcomes.

Date and cause of death were obtained through linkage to the death dataset in the Chinese National Death Surveillance (Liu et al., 2016) by matching the resident ID card numbers of each patient. In China, unique resident ID card numbers are assigned to every Chinese citizen at birth, in which the date of birth and location of birth are coded in. The dataset in the Chinese National Death Surveillance includes date and cause of death, which is electronically updated by multiple surveillance points. Causes of death were obtained as the International Classification of Diseases 10th revision (ICD-10) (**Supplementary Table 1**). Patients with a concurrent diagnosis of acute stroke or MI at admission were excluded from the concerned analysis.

Covariates

Information on potential confounding factors was obtained from electronic medical records. The included covariates were gender; age; smoking status (yes or no); body mass index (BMI); BP at admission; baseline serum creatinine (an averaged value of 30 days before surgery); surgical type; concurrent diagnosis (yes or no) of diabetes, stroke, coronary heart disease (CHD), heart failure, chronic kidney disease (CKD), chronic obstructive pulmonary disease (COPD), and anemia; and perioperative administration of BP-lowering drugs (yes or no).

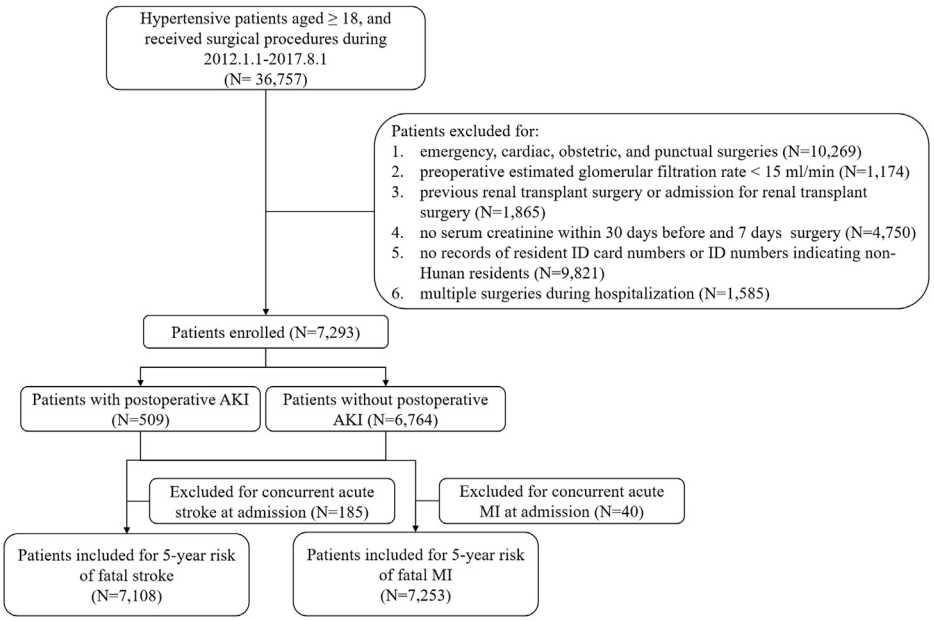

FIGURE 1 | Flowchart. AKI, acute kidney injury; MI, myocardial infarction.

Statistical Analyses

Analyses were performed using Stata® 14.0 package (Stata Corp LP, College Station, TX, United States). The cumulative incidence method was used to compute the absolute risk of all-cause mortality, fatal stroke, fatal MI, and composite cardiovascular and cerebrovascular mortality. Unadjusted and adjusted hazard ratios (HRs) of mortality were computed using a Cox proportional hazards regression model. Covariates adjusted include age, gender, BMI, BP at admission, baseline serum creatinine, comorbidities, type of surgery, and perioperative administration of BP-lowering drugs. Besides, a subgroup analysis of association between postoperative AKI and risk of fatal stroke and fatal MI within 1 year and 5 years was conducted, which was subgrouped by perioperative administration (yes or no) of angiotensin-converting enzyme inhibitor/angiotensin receptor blocker (ACEI/ARB), β-blocker, and calcium channel blocker (CCB) that is commonly used in our study (more than 10% of usage). Statistical significance was determined as p-value < 0.001 in group comparisons of baseline characteristics and p-value < 0.05 in Cox proportional hazards regression analysis.

RESULTS

Postoperative episodes of AKI were found in 509 hypertensive patients (6.98%) during the first 7 postoperative days among 7,293 patients (**Figure 1**). Compared with non-AKI patients, AKI patients were older, more likely to be male (67.19 vs. 54.78%, $p < 0.001$), had a higher level of systolic blood pressure (SBP) (median, 137.70 vs. 132.00 mmHg, $p < 0.001$) and preoperative serum creatinine (109.00 vs. 72.00 μmol/L, $p < 0.001$), more likely to have a history of CKD (23.97 vs. 1.30%, $p < 0.001$) and anemia (34.58 vs. 8.34%, $p < 0.001$), less likely to have a history of CHD (21.81 vs. 32,95%, $p < 0.001$), less likely to have undergone neurological surgery (12.18 vs. 20.92%, $p < 0.001$), more likely to have undergone urological surgery (34.18 vs. 6.00%, $p < 0.001$), and more likely to have perioperative administration of β-blocker (42.83 vs. 30.82%, $p < 0.001$), calcium channel blocker (CCB) (56.58 vs. 41.17%, $p < 0.001$), and α-blocker (9.04 vs. 1.37%, $p < 0.001$) (**Table 1**).

Total follow-up time was 400,802 person-months with a duration of 5 years (**Supplementary Table 2**). 970 patients died during the 5 years (109 AKI patients and 861 non-AKI patients) (**Supplementary Table 3**). The specific cause of death within 5 years after elective noncardiac surgery is shown in **Figure 2**. MI was found as the cause of death in 20.00% of AKI patients and 16.86% of non-AKI patients. Stroke was found as the cause of death in 16.19% of AKI patients and 11.74% of non-AKI patients.

Fatal Stroke and Fatal MI After Elective Noncardiac Surgery

165 non-AKI patients and 20 AKI patients were excluded due to the diagnosis of concurrent acute stroke at admission when analyzing the risk of fatal stroke after elective noncardiac surgery. And 33 non-AKI patients and 7 AKI patients were excluded due to the diagnosis of concurrent acute MI at admission in the analysis for risk of fatal MI.

Kaplan–Meier curves showed that patients with postoperative AKI have higher cumulative risks of fatal stroke and fatal MI within 5 years (**Figure 3**). Within 3 months, 6 months, 1 year,

TABLE 1 | Baseline characteristics of hypertensive patients with or without postoperative AKI.

Variable	Postoperative AKI patients (*n* = 509)	Postoperative non-AKI patients (*n* = 6,764)	*p*-value
Age (year)	61.00 (50.00, 69.00)	56.00 (40.00, 68.00)	<0.001
Gender, male, *n* (%)	342 (67.19%)	3,705 (54.78%)	<0.001
BMI (kg/m^2)	21.84 (19.23, 24.49)	23.42 (20.93, 25.95)	<0.001
Smoking, *n* (%)	86 (16.9%)	1,224 (18.90%)	0.500
Drinking, *n* (%)	54 (10.61%)	885 (13.09%)	0.108
SBP (mmHg)	137.70 (122.00, 151.96)	132.00 (120.00, 145.72)	<0.001
DBP (mmHg)	81.00 (71.50, 91.33)	80.00 (72.50, 88.00)	0.001
Preoperative serum creatinine (μmol/L)	109.00 (76.00, 217.41)	72.00 (58.75, 88.46)	<0.001
Comorbidities, *n* (%)			
Diabetes	100 (19.65)	1,392 (20.58)	0.616
Stroke	91 (17.88)	932 (13.78)	0.010
CHD	111 (21.81)	2,229 (32.95)	<0.001
Cardiac insufficiency	89 (17.49)	848 (12.54)	0.001
CKD	122 (23.97)	88 (1.30)	<0.001
COPD	43 (8.45)	431 (6.37)	0.067
Anemia	176 (34.58)	564 (8.34)	<0.001
Surgical type, *n* (%)			
Neurological	62 (12.18)	1,414 (20.92)	<0.001
Endocrinological	0 (0)	13 (0.19)	0.323
ENT	11 (2.16)	350 (5.17)	0.003
Respiratory	10 (1.96)	323 (4.77)	0.007
Vascular	69 (13.56)	1,136 (16.80)	0.057
Lymphatic and hemopoietic	3 (0.59)	63 (0.93)	0.436
Digestive	113(22.2)	1786 (26.39)	0.030
Urological	174 (34.18)	106 (6.00)	<0.001
Male genital	19 (3.73)	191 (2.83)	0.241
Female genital	15 (2.95)	459 (6.78)	0.001
Muscular and skeleton	29 (5.7)	530 (7.84)	0.080
Dermatological	4 (0.79)	114 (1.68)	0.123
Perioperative BP-lowering medication, *n* (%)			
ACEI/ARB	156 (30.65)	2,261 (33.43)	0.199
β-blocker	218 (42.83)	2,085 (30.82)	<0.001
CCB	288 (56.58)	2,785 (41.17)	<0.001
Diuretics	38 (7.47)	356 (5.26)	0.034
α-blocker	46 (9.04)	93 (1.37)	<0.001

AKI, acute kidney injury; BMI, body mass index; SBP, systolic blood pressure; DBP, diastolic blood pressure; CHD, coronary heart disease; CKD, chronic kidney disease; COPD, chronic pulmonary disease; ENT, ear, nose, and throat; BP, blood pressure; ACEI, angiotensin-converting enzyme inhibitor; ARB, angiotensin receptor blocker; CCB, calcium channel blocker.
All continuous variables were summarized as median (interquartile range) and tested by the Kruskal–Wallis test.
All categorical variables were summarized as number (proportion) and tested by chi-square test.

2 years, and 5 years after surgery, the cumulative risks of fatal stroke were 1.27, 1.48, 2.15, 2.15, and 5.36%, respectively, among AKI patients, and 0.23, 0.41, 0.52, 0.86, and 2.33%, respectively, among non-AKI patients (**Supplementary Table 3**). And the cumulative risks of fatal MI were 2.05, 2.27, 2.70, 3.37, and 5.61% among AKI patients, and 0.19, 0.28, 0.54, 1.08, and 3.42% among non-AKI patients, at the corresponding time points mentioned above (**Supplementary Table 3**).

Kaplan–Meier curves for cumulative risks of fatal stroke and fatal MI are shown in **Figure 3**. HRs for all outcomes were decreased by the follow-up time from 3 months to 5 years (**Figure 4**). The fully adjusted HRs of fatal stoke for AKI patients compared with non-AKI patients were 5.49 (95% CI: 1.88–16.00, $p = 0.002$) within 3 months, 3.58 (95% CI: 1.43–8.97, $p = 0.006$) within 6 months, 3.64 (95% CI: 1.63–8.10, $p = 0.002$) within 1 year, 2.21 (95% CI: 1.03–4.72, $p = 0.041$) within 2 years, and 2.27 (95% CI: 1.30–3.98, $p = 0.004$) within 5 years (**Figure 4** and **Table 2**). The fully adjusted HRs of fatal MI for AKI patients compared with non-AKI patients were 11.82 (95% CI: 4.56–30.62, $p < 0.001$) within 3 months, 9.23 (95% CI: 3.89–21.90, $p < 0.001$) within 6 months, 5.14 (95% CI: 2.50–10.57, $p < 0.001$) within 1 year, 3.06 (95% CI: 1.66–5.64, $p < 0.001$) within 2 years, and 1.93 (95% CI: 1.16–3.20, $p = 0.011$) within 5 years (**Figure 4** and **Table 2**). There were closer associations between postoperative AKI and fatal MI within 2 years than fatal stroke (**Figure 4**).

All-Cause Mortality and Composite Cardiovascular and Cerebrovascular Mortality After Elective Noncardiac Surgery

There were 7,293 patients included in the analysis of all-cause mortality. Kaplan–Meier curves showed that patients with postoperative AKI have higher cumulative risks of all-cause mortality within 5 years (**Figure 3**). The cumulative risks of all-cause mortality within 3 months, 6 months, 1 year, 2 years, and 5 years among AKI patients were 7.86, 9.23, 11.59, 14.73,

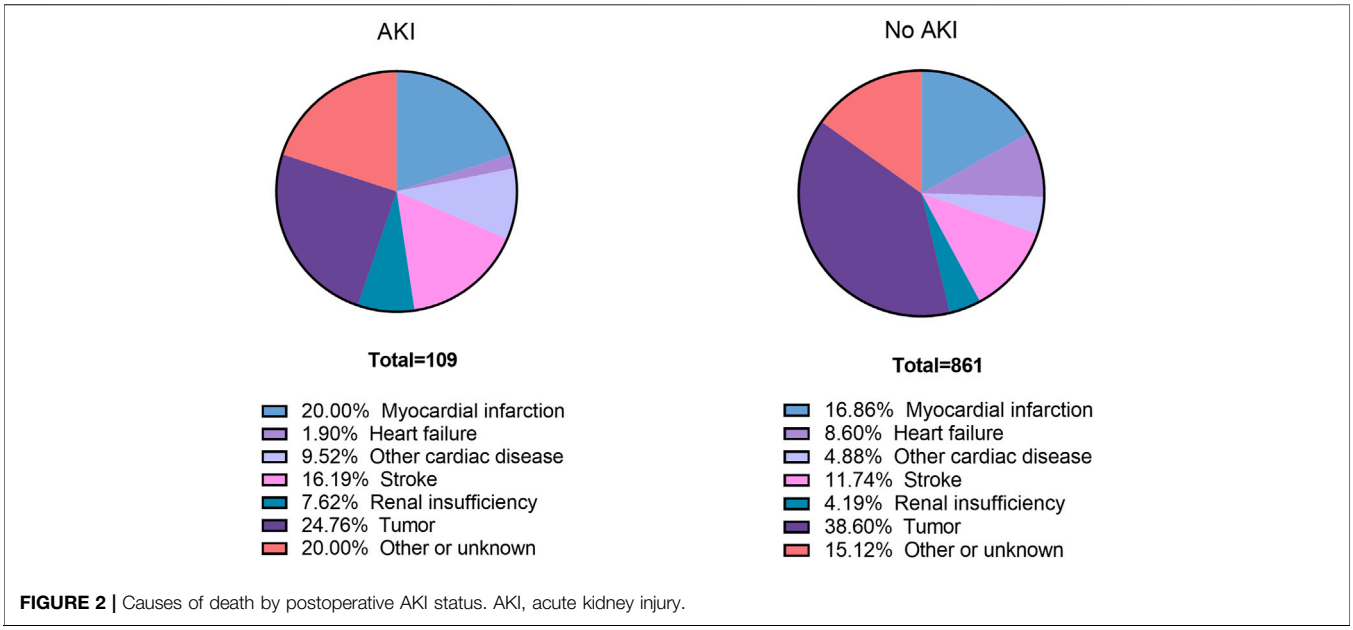

FIGURE 2 | Causes of death by postoperative AKI status. AKI, acute kidney injury.

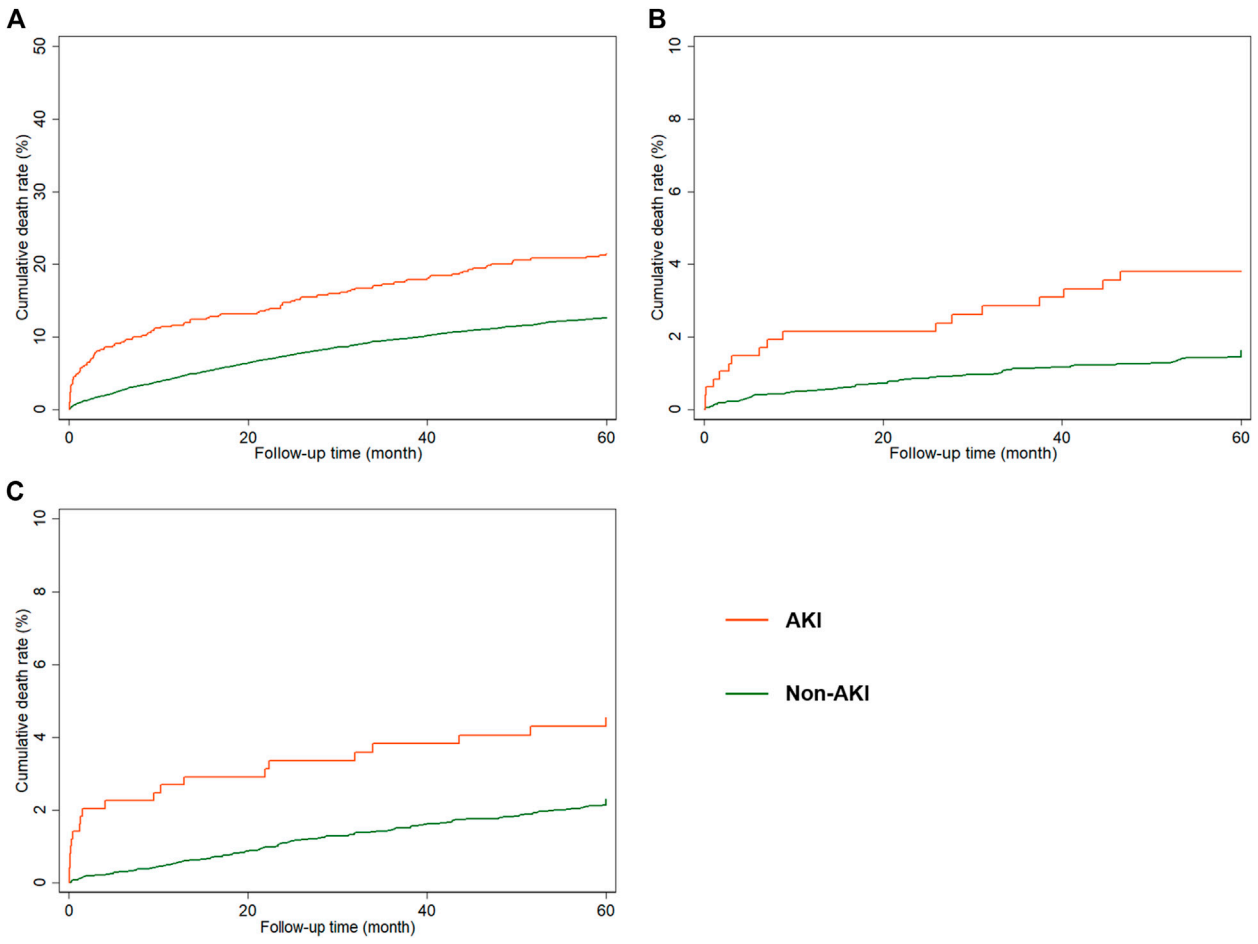

FIGURE 3 | Kaplan–Meier curves for cumulative risks of 5-year mortality. **(A)** Cumulative risk of all-cause mortality. **(B)** Cumulative risk of fatal MI. **(C)** Cumulative risk of fatal stroke. AKI, acute kidney injury.

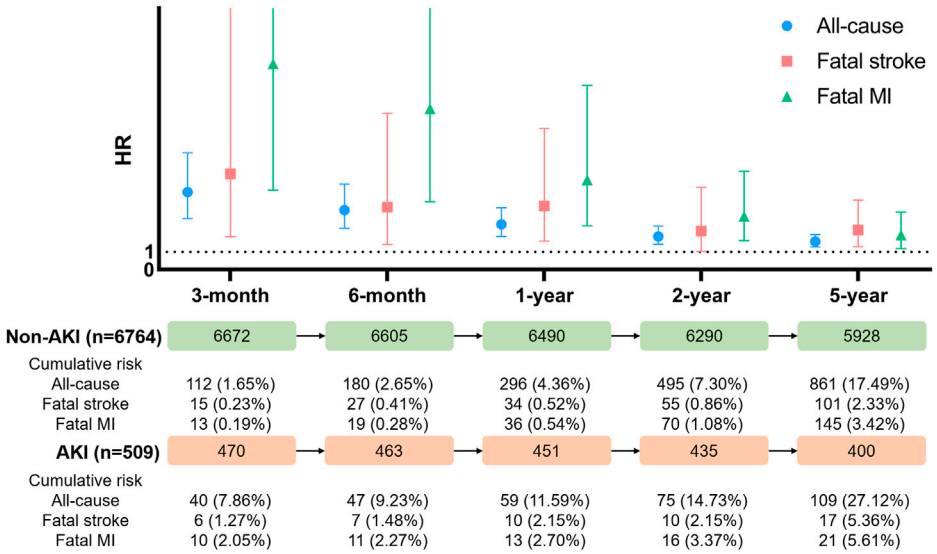

FIGURE 4 | Hazard ratio for all-cause mortality, fatal stoke, and fatal myocardial infarction. AKI, acute kidney injury; MI, myocardial infarction; HR, hazard ratio.

TABLE 2 | Cox proportional hazard regression analysis of association between postoperative AKI and all-cause mortality, fatal stroke, and fatal MI risk in hypertensive patients after elective surgery.

Follow-up time	Unadjusted			Adjusted[a]		
	HR	95% CI	*p*-value	HR	95% CI	*p*-value
3 Months						
All-cause mortality (*n* = 7,293)	4.89	3.41-7.03	<0.001	4.44	2.93-6.71	<0.001
Fatal stroke (*n* = 7,108)	5.60	2.17-14.42	<0.001	5.49	1.88-16.00	0.002
Fatal MI (*n* = 7,253)	10.72	4.70-24.44	<0.001	11.82	4.56-30.62	<0.001
6 Months						
All-cause mortality (*n* = 7,293)	3.65	2.65-5.03	<0.001	3.41	2.37-0.4.90	<0.001
Fatal stroke (*n* = 7,108)	3.67	1.60-8.43	0.002	3.58	1.43-8.97	0.006
Fatal MI (*n* = 7,253)	8.13	3.87-17.09	<0.001	9.23	3.89-21.90	<0.001
1 Year						
All-cause mortality (*n* = 7,293)	2.74	2.07-3.62	<0.001	2.59	1.89-3.55	<0.001
Fatal stroke (*n* = 7,108)	4.19	2.07-8.48	<0.001	3.64	1.63-8.10	0.002
Fatal MI (*n* = 7,253)	5.01	2.66-9.42	<0.001	5.14	2.50-10.57	<0.001
2 Years						
All-cause mortality (*n* = 7,293)	2.16	1.69-2.75	<0.001	1.89	1.44-2.49	<0.001
Fatal stroke (*n* = 7,108)	2.65	1.35-5.21	0.005	2.21	1.03-4.72	0.041
Fatal MI (*n* = 7,253)	3.29	1.91-5.66	<0.001	3.06	1.66-5.64	<0.001
5 Years						
All-cause mortality (*n* = 7,293)	1.82	1.49-2.22	<0.001	1.56	1.25-1.95	<0.001
Fatal stroke (*n* = 7,108)	2.45	1.46-4.09	0.001	2.27	1.30-3.98	0.004
Fatal MI (*n* = 7,253)	2.11	1.34-3.34	0.001	1.93	1.16-3.20	0.011

[a]*Adjusted for age, gender, body mass index, preoperative creatinine, comorbidities, blood pressure at admission, location of surgery, and perioperative administration of blood pressure lowering drugs.*

HR, hazard ratio; CI, confidence interval; MI, myocardial infarction.

and 27.12%, respectively, compared with 1.65, 2.65, 4.36, 7.30, and 17.49%, among non-AKI patients (**Supplementary Table 3**).

The fully adjusted HRs were 4.44 (95% CI: 2.93–6.71, $p < 0.001$), 3.41 (95% CI: 2.73–4.90, $p < 0.001$), 2.59 (95% CI: 1.89–3.55, $p < 0.001$), 1.89 (95% CI: 1.44–2.49, $p < 0.001$), and 1.56 (95% CI: 1.25–1.95, $p < 0.001$) within 3 months, 6 months, 1 year, 2 years, and 5 years, respectively (**Table 2**).

Subgroup Analysis of Association Between Postoperative AKI and Risk of Fatal Stroke and Fatal MI by Perioperative Administration of ACEI/ARB, β-blocker, and CCB

Significance of association between postoperative AKI and 1-year risk of fatal stroke was found in patients only with perioperative

TABLE 3 | Subgroup analysis of association between postoperative AKI and risk of fatal stroke and fatal MI in 1-year and 5-years by perioperative administration of ACEI/ARB, β-blocker, and CCB.

Outcomes	Follow-up time	With administration			Without administration		
		HR[a]	95% CI	*p*-value	HR[a]	95% CI	*p*-value
Fatal stroke	1 year						
	ACEI/ARB	9.46	2.85-31.40	<0.001	3.19	1.05-9.66	0.040
	β-blocker	4.28	0.93-19.60	0.061	4.10	1.58-10.63	0.004
	CCB	1.78	0.47-6.74	0.393	6.40	2.23-18.36	0.001
	5 years						
	ACEI/ARB	3.88	1.67-9.01	0.002	1.15	0.68-3.35	0.308
	β-blocker	1.38	0.42-4.46	0.594	2.64	1.38-5.05	0.003
	CCB	2.19	0.97-4.94	0.058	2.02	0.91-4.47	0.082
Fatal MI	1 year						
	ACEI/ARB	4.03	1.36-11.97	0.012	8.36	3.00-23.25	<0.001
	β-blocker	7.23	2.43-21.55	<0.001	3.87	1.22-12.29	0.022
	CCB	6.62	2.23-19.62	0.001	5.34	1.97-14.48	0.001
	5 years						
	ACEI/ARB	1.78	0.83-3.82	0.140	1.95	0.99-3.86	0.055
	β-blocker	1.64	0.73-3.68	0.231	1.89	0.95-3.76	0.069
	CCB	2.44	1.22-4.90	0.012	1.64	0.76-3.58	0.210

[a]*Adjusted for age, gender, body mass index, preoperative creatinine, comorbidities, blood pressure at admission, location of surgery, and perioperative administration of blood pressure lowering drugs.*

AKI, acute kidney injury; ACEI, angiotensin converting enzyme inhibitor; ARB, angiotensin receptor blocker; CCB, calcium channel blocker. HR, hazard ratio; CI, confidence interval; MI, myocardial infarction.

administration of ACEI/ARB (HR: 9.46, 95% CI: 2.85–31.40) (**Table 3**). However, significance of associations between postoperative AKI and 1-year risk of fatal MI was found in patients with perioperative administration of ACEI/ARB (HR: 4.03, 95% CI: 1.36–11.97), β-blocker (HR: 7.23, 95% CI: 2.43–21.55), and CCB (HR: 6.62, 95% CI: 2.23–19.62) (**Table 3**).

Moreover, in patients without perioperative administration of ACEI/ARB (HR: 3.19, 95% CI: 1.05–9.66), β-blocker (HR: 4.10, 95% CI: 1.58–10.63), and CCB (HR: 6.40, 95% CI: 2.23–18.36), postoperative AKI also significantly increased the 1-year risk of fatal stroke (**Table 3**). Likely, significance of association between postoperative AKI and 1-year risk of fatal MI was found in patients without perioperative administration of ACEI/ARB (HR: 3.19, 95% CI: 1.05–9.66), β-blocker (HR: 4.10, 95% CI: 1.58–10.63), and CCB (HR: 6.40, 95% CI: 2.23–18.36) (**Table 3**).

Meanwhile, postoperative AKI significantly increased the 5-year risk of fatal stroke in patients with ACEI/ARB (HR: 3.88, 95% CI: 1.67–9.01), and without perioperative administration of β-blocker (HR: 2.64, 95% CI: 1.38–5.05) (**Table 3**). While it only increased the 5-year risk of fatal MI in patients with perioperative administration of CCB (HR: 2.44, 95% CI: 1.22–4.90) (**Table 3**).

DISCUSSION

As far as we know, this is the first study in hypertensive patients, which concentrates on the association between postoperative AKI and 5-year all-cause mortality, fatal stroke, and fatal MI after elective noncardiac surgery. In the current retrospective cohort study, 6.98% of adult elective noncardiac surgical patients with hypertension and without preexisting severe kidney impairment developed AKI. Compared with fatal MI, fatal stroke had a higher cumulative risk within 2 years after elective noncardiac surgery. Besides, there was a closer association between postoperative AKI and fatal MI within 2 years than that between postoperative AKI and fatal stroke. In patients with perioperative administration of ACEI/ARB, postoperative AKI was significantly associated with 1-year and 5-year risk of fatal stroke. And in patients with perioperative administration of CCB, postoperative AKI was significantly associated with 1-year and 5-year risk of fatal MI. Our findings should encourage more concerns on prevention strategies for hypertensive patients who develop reductions in kidney function after surgery.

Prognosis after postoperative AKI in hypertensive patients is not well described in previous studies that only included the general population. Patients with AKI have a 2-fold risk of death and a 2-day longer LOS when undergoing all types of surgery, and a 5-fold risk of death and a 3-day longer LOS when undergoing noncardiac surgery, than normal patients (Kork et al., 2015). In a pooled analysis including 1,817,999 participants from 70 studies, long-term risk of death was found to be associated with AKI, with the pooled crude mortality of an additional risk of 5.93 deaths per 100 years (See et al., 2019). In a British study concentrating on mortality 1 year after major noncardiac surgery, AKI was associated with an adjusted HR for death of 2.96 (95% CI: 1.86–4.71) (O'Connor et al., 2017). Also, the mortality climbs with the severity of AKI, in which a 37.1 times higher risk of death was found in patients who need dialysis after experiencing postoperative AKI (Lau et al., 2020).

This study also indicated that postoperative AKI was found to be associated with an increased risk of 5-year fatal stroke and fatal MI in hypertensive patients. Multiple studies have been conducted exploring the association between AKI and long-term cardiovascular events in the general population. In a prospective study of cardiac surgery (Hansen et al., 2013), postoperative AKI was found to be associated with a higher

risk of 5-year all-cause mortality (26.5 vs. 12.1%) and insignificant increased risk of MI (5.0 vs. 3.3%). In contrary to our study, they did not find an association with the risk of stroke, which can be explained by less hypertensive subjects (56.8% in the total cohort). However, in 2017, a meta-analysis of 25 studies involving 254,408 adults confirmed that AKI associates with an elevated risk of cardiovascular mortality (RR: 1.86, 95% CI: 1.72–2.01), major cardiovascular events (RR: 1.38, 95% CI: 1.23–1.55), acute MI (RR: 1.40, 95% CI: 1.23–1.59), and stroke (RR: 1.15, 95% CI: 1.03–1.28) (Odutayo et al., 2017), which supports the result in our study.

Our finding indicated that postoperative AKI had a higher incidence of fatal MI than stroke. The current understanding of pathophysiology may explain the elevated risk of cardiovascular events after AKI (Legrand and Rossignol, 2020). AKI increases certain circulating inflammatory mediators in animal models, which exert direct cardiodepressant effects (Dépret et al., 2017; Bartekova et al., 2018). In human studies, neutrophil gelatinase–associated lipocalin (NGAL), as a predictor of AKI, was reported to be associated with the development of cardiac remodeling and vascular pro-fibrosis (Tarjus et al., 2015; Martínez-Martínez et al., 2017). Still, the pathophysiology of cardiovascular damage after acute kidney injury needs further exploration.

In subgroup analysis in our study, postoperative AKI was significantly associated with 1-year and 5-year risk of fatal stroke, as well as 1-year risk of fatal MI, in patients with perioperative administration of ACEI/ARB. In patients with perioperative administration of CCB, postoperative AKI was significantly associated with 1-year and 5-year risk of fatal MI. And postoperative AKI was significantly associated with only 1-year risk of fatal MI in patients with perioperative β-blocker. Studies reported that perioperative use of ACEI/ARB was associated with an increased incidence of intraoperative hypotension (Hollmann et al., 2018) and resulted in increased odds of postoperative AKI and mortality (Yacoub et al., 2013). A meta-analysis indicated that perioperative β-blocker was associated with an increased incidence of bradycardia (OR: 3.49; 95% CI: 2.4–5.9) and congestive heart failure (OR: 1.68; 95% CI: 1.00–2.8) after surgical procedure (Beattie et al., 2008). CCB is considered as a safe agent that can be continued during the perioperative period (Sanders et al., 2019). However, few studies focused on the association between CCB and postoperative outcomes, which were inadequate in patients with postoperative AKI.

Limitations of our work to date include the following. First, 1-year mortality is relatively low (4.98%) in our study, compared with the previous British study (7.5%) (O'Connor et al., 2017), which can be explained by the misreported deaths in the Chinese National Death Surveillance. Second, due to the limitation of the enrollment, the prognosis of postoperative AKI between hypertensive and normotensive patients did not be compared in this study. Third, patients with missing data in our study might increase bias in the subject's enrollment.

CONCLUSION

Hypertensive patients with postoperative AKI have a significantly higher risk of fatal stroke and fatal MI, as well as all-cause mortality, within 5 years after elective noncardiac surgery. In patients with perioperative administration of ACEI/ARB and CCB, postoperative AKI was significantly associated with higher risk of fatal stroke and MI, respectively.

DATA AVAILABILITY STATEMENT

The raw data supporting the conclusion of this article will be made available by the authors, without undue reservation.

ETHICS STATEMENT

Written informed consent was obtained from the individual(s) for the publication of any potentially identifiable images or data included in this article.

AUTHOR CONTRIBUTIONS

YL and HY participated in the general design of this study, XL and JL collected the dataset, and GY conducted the statistical analysis in this study. All authors have participated in manuscript writing.

FUNDING

The study was funded by the National Key Research and Development Project of China (2019YFF0216304 and 2019YFF0216305), the National Natural Science Foundation of China (81800393, 82170437 and 81901842), the China Primary Health Care Foundation (YLGX-WS-2020003), the Outstanding Young Investigator of Hunan province (2020JJ2056), the National Key Research and Development Project of China (2018YFC1311302), and the Hunan Youth Talent Project (2019RS2014).

ACKNOWLEDGMENTS

We acknowledge the invaluable support of the staff in the Hunan Center of Disease Control.

SUPPLEMENTARY MATERIAL

The Supplementary Material for this article can be found online at: https://www.frontiersin.org/articles/10.3389/fphar.2021.696456/full#supplementary-material

REFERENCES

Anzai, A., Anzai, T., Naito, K., Kaneko, H., Mano, Y., Jo, Y., et al. (2010). Prognostic Significance of Acute Kidney Injury After Reperfused ST-Elevation Myocardial Infarction: Synergistic Acceleration of Renal Dysfunction and Left Ventricular Remodeling. *J. Card. Fail.* 16, 381–389. doi:10.1016/j.cardfail.2009.12.020

Arias-Cabrales, C., Rodríguez, E., Bermejo, S., Sierra, A., Burballa, C., Barrios, C., et al. (2018). Short- and Long-Term Outcomes after Non-severe Acute Kidney Injury. *Clin. Exp. Nephrol.* 22, 61–67. doi:10.1007/s10157-017-1420-y

Bartekova, M., Radosinska, J., Jelemensky, M., and Dhalla, N. S. (2018). Role of Cytokines and Inflammation in Heart Function during Health and Disease. *Heart Fail. Rev.* 23, 733–758. doi:10.1007/s10741-018-9716-x

Beattie, W. S., Wijeysundera, D. N., Karkouti, K., McCluskey, S., and Tait, G. (2008). Does Tight Heart Rate Control Improve Beta-Blocker Efficacy? An Updated Analysis of the Noncardiac Surgical Randomized Trials. *Anesth. Analgesia* 106, 1039–1048. doi:10.1213/ane.0b013e318163f6a9

Chawla, L. S., and Kimmel, P. L. (2012). Acute Kidney Injury and Chronic Kidney Disease: an Integrated Clinical Syndrome. *Kidney Int.* 82, 516–524. doi:10.1038/ki.2012.208

Dépret, F., Prud'homme, M., and Legrand, M. (2017). A Role of Remote Organs Effect in Acute Kidney Injury Outcome. *Nephron* 137, 273–276. doi:10.1159/000476077

Dix, P., and Howell, S. (2001). Survey of Cancellation Rate of Hypertensive Patients Undergoing Anaesthesia and Elective Surgery. *Br. J. Anaesth.* 86, 789–793. doi:10.1093/bja/86.6.789

Gameiro, J., Duarte, I., Marques, F., Fonseca, J. A., Jorge, S., Rosa, R., et al. (2020). Transient and Persistent AKI and Outcomes in Patients Undergoing Major Abdominal Surgery. *Nephron* 144, 236–244. doi:10.1159/000506397

Haas, C. E., and LeBlanc, J. M. (2004). Acute Postoperative Hypertension: A Review of Therapeutic Options. *Am. J. Health-System Pharm.* 61, 1661–1673. doi:10.1093/ajhp/61.16.1661

Hansen, M. K., Gammelager, H., Mikkelsen, M. M., Hjortdal, V. E., Layton, J. B., Johnsen, S. P., et al. (2013). Post-operative Acute Kidney Injury and Five-Year Risk of Death, Myocardial Infarction, and Stroke Among Elective Cardiac Surgical Patients: a Cohort Study. *Crit. Care* 17, R292. doi:10.1186/cc13158

Hollmann, C., Fernandes, N. L., and Biccard, B. M. (2018). A Systematic Review of Outcomes Associated with Withholding or Continuing Angiotensin-Converting Enzyme Inhibitors and Angiotensin Receptor Blockers Before Noncardiac Surgery. *Anesth. Analgesia* 127, 678–687. doi:10.1213/ane.0000000000002837

Ikehata, Y., Tanaka, T., Ichihara, K., Kobayashi, K., Kitamura, H., Takahashi, S., et al. (2016). Incidence and Risk Factors for Acute Kidney Injury after Radical Cystectomy. *Int. J. Urol.* 23, 558–563. doi:10.1111/iju.13104

Ishani, A., Xue, J. L., Himmelfarb, J., Eggers, P. W., Kimmel, P. L., Molitoris, B. A., et al. (2009). Acute Kidney Injury Increases Risk of ESRD Among Elderly. *J. Am. Soc. Nephrol.* 20, 223–228. doi:10.1681/asn.2007080837

James, M. T., Ghali, W. A., Knudtson, M. L., Ravani, P., Tonelli, M., Faris, P., et al. (2011). Associations Between Acute Kidney Injury and Cardiovascular and Renal Outcomes After Coronary Angiography. *Circulation* 123, 409–416. doi:10.1161/circulationaha.110.970160

Kline, J., and Rachoin, J.-S. (2013). Acute Kidney Injury and Chronic Kidney Disease: It's a Two-Way Street. *Ren. Fail.* 35, 452–455. doi:10.3109/0886022x.2013.766572

Kork, F., Balzer, F., Spies, C. D., Wernecke, K.-D., Ginde, A. A., Jankowski, J., et al. (2015). Minor Postoperative Increases of Creatinine Are Associated with Higher Mortality and Longer Hospital Length of Stay in Surgical Patients. *Anesthesiology* 123, 1301–1311. doi:10.1097/aln.0000000000000891

Lau, D., Pannu, N., James, M. T., Hemmelgarn, B. R., Kieser, T. M., Meyer, S. R., et al. (2020). Costs and Consequences of Acute Kidney Injury after Cardiac Surgery: A Cohort Study. *J. Thorac. Cardiovasc. Surg.* S0022-5223, 30516. doi:10.1016/j.jtcvs.2020.01.101

Legrand, M., and Rossignol, P. (2020). Cardiovascular Consequences of Acute Kidney Injury. *N. Engl. J. Med.* 382, 2238–2247. doi:10.1056/nejmra1916393

Liu, S., Wu, X., Lopez, A. D., Wang, L., Cai, Y., Page, A., et al. (2016). An Integrated National Mortality Surveillance System for Death Registration and Mortality Surveillance, China. *Bull. World Health Organ.* 94, 46–57. doi:10.2471/blt.15.153148

Martínez-Martínez, E., Buonafine, M., Boukhalfa, I., Ibarrola, J., Fernández-Celis, A., Kolkhof, P., et al. (2017). Aldosterone Target NGAL (Neutrophil Gelatinase-Associated Lipocalin) Is Involved in Cardiac Remodeling After Myocardial Infarction through NFκB Pathway. *Hypertension* 70, 1148–1156. doi:10.1161/hypertensionaha.117.09791

O'Connor, M. E., Kirwan, C. J., Pearse, R. M., and Prowle, J. R. (2016). Incidence and Associations of Acute Kidney Injury after Major Abdominal Surgery. *Intensive Care Med.* 42, 521–530. doi:10.1007/s00134-015-4157-7

O'Connor, M. E., Hewson, R. W., Kirwan, C. J., Ackland, G. L., Pearse, R. M., and Prowle, J. R. (2017). Acute Kidney Injury and Mortality 1 Year after Major Non-cardiac Surgery. *Br. J. Surg.* 104, 868–876. doi:10.1002/bjs.10498

Odutayo, A., Wong, C. X., Farkouh, M., Altman, D. G., Hopewell, S., Emdin, C. A., et al. (2017). AKI and Long-Term Risk for Cardiovascular Events and Mortality. *J. Am. Soc. Nephrol.* 28, 377–387. doi:10.1681/asn.2016010105

Palevsky, P. M., Liu, K. D., Brophy, P. D., Chawla, L. S., Parikh, C. R., Thakar, C. V., et al. (2013). KDOQI US Commentary on the 2012 KDIGO Clinical Practice Guideline for Acute Kidney Injury. *Am. J. Kidney Dis.* 61, 649–672. doi:10.1053/j.ajkd.2013.02.349

Ronco, C., Bellasi, A., and Di Lullo, L. (2018). Cardiorenal Syndrome: An Overview. *Adv. Chronic Kidney Dis.* 25, 382–390. doi:10.1053/j.ackd.2018.08.004

Ronco, C., Haapio, M., House, A. A., Anavekar, N., and Bellomo, R. (2008). Cardiorenal Syndrome. *J. Am. Coll. Cardiol.* 52, 1527–1539. doi:10.1016/j.jacc.2008.07.051

Sanders, R. D., Hughes, F., Shaw, A., Thompson, A., Bader, A., Hoeft, A., et al. (2019). Perioperative Quality Initiative Consensus Statement on Preoperative Blood Pressure, Risk and Outcomes for Elective Surgery. *Br. J. Anaesth.* 122, 552–562. doi:10.1016/j.bja.2019.01.018

See, E. J., Jayasinghe, K., Glassford, N., Bailey, M., Johnson, D. W., Polkinghorne, K. R., et al. (2019). Long-term Risk of Adverse Outcomes after Acute Kidney Injury: a Systematic Review and Meta-Analysis of Cohort Studies Using Consensus Definitions of Exposure. *Kidney Int.* 95, 160–172. doi:10.1016/j.kint.2018.08.036

Susantitaphong, P., Cruz, D. N., Cerda, J., Abulfaraj, M., Alqahtani, F., Koulouridis, I., et al. (2013). World Incidence of AKI: A Meta-Analysis. *Clin. J. Am. Soc. Nephrol.* 8, 1482–1493. doi:10.2215/cjn.00710113

Tarjus, A., Martínez-Martínez, E., Amador, C., Latouche, C., El Moghrabi, S., Berger, T., et al. (2015). Neutrophil Gelatinase-Associated Lipocalin, a Novel Mineralocorticoid Biotarget, Mediates Vascular Profibrotic Effects of Mineralocorticoids. *Hypertension* 66, 158–166. doi:10.1161/hypertensionaha.115.05431

Yacoub, R., Patel, N., Lohr, J. W., Rajagopalan, S., Nader, N., and Arora, P. (2013). Acute Kidney Injury and Death Associated with Renin Angiotensin System Blockade in Cardiothoracic Surgery: a Meta-Analysis of Observational Studies. *Am. J. Kidney Dis.* 62, 1077–1086. doi:10.1053/j.ajkd.2013.04.018

Conflict of Interest: The authors declare that the research was conducted in the absence of any commercial or financial relationships that could be construed as a potential conflict of interest.

frontiers in Pharmacology

REVIEW
published: 01 September 2021
doi: 10.3389/fphar.2021.728458

Sulfonylureas for Treatment of Periodontitis-Diabetes Comorbidity-Related Complications: Killing Two Birds With One Stone

Luxi Yang[1†], Qing Ge[1†], Zhitong Ye[1], Lijing Wang[1,2], Liping Wang[1], Mubarak Ahmed Mashrah[1] and Janak L. Pathak[1]**

[1]Guangzhou Key Laboratory of Basic and Applied Research of Oral Regenerative Medicine, Affiliated Stomatology Hospital of Guangzhou Medical University, Guangzhou, China, [2]School of Life Sciences and Biopharmaceutics, Vascular Biology Research Institute, Guangdong Pharmaceutical University, Guangzhou, China

OPEN ACCESS

Edited by:
Liang Weng,
Central South University, China

Reviewed by:
Chengcheng Liu,
Sichuan University, China
Astrid Parenti,
University of Florence, Italy

***Correspondence:**
Mubarak Ahmed Mashrah
mubarak198226@gmail.com
Janak L. Pathak
j.pathak@gzhmu.edu.cn

[†]These authors have contributed equally to this work and share first authorship

Specialty section:
This article was submitted to Inflammation Pharmacology, a section of the journal Frontiers in Pharmacology

Received: 21 June 2021
Accepted: 19 August 2021
Published: 01 September 2021

Citation:
Yang L, Ge Q, Ye Z, Wang L, Wang L, Mashrah MA and Pathak JL (2021) Sulfonylureas for Treatment of Periodontitis-Diabetes Comorbidity-Related Complications: Killing Two Birds With One Stone. Front. Pharmacol. 12:728458. doi: 10.3389/fphar.2021.728458

Periodontitis is one of the most prevalent oral inflammatory diseases leading to teeth loss and oral health problems in adults. Periodontitis mainly affects periodontal tissue by affecting the host immune system and bone homeostasis. Moreover, periodontitis is associated with various systemic diseases. Diabetes is a metabolic disease with systemic effects. Both periodontitis and diabetes are common inflammatory diseases, and comorbidity of two diseases is linked to exacerbation of the pathophysiology of both diseases. Since bacterial dysbiosis is mainly responsible for periodontitis, antibiotics are widely used drugs to treat periodontitis in clinics. However, the outcomes of antibiotic treatments in periodontitis are not satisfactory. Therefore, the application of anti-inflammatory drugs in combination with antibiotics could be a treatment option for periodontitis-diabetes comorbidity. Anti-diabetic drugs usually have anti-inflammatory properties and have shown beneficial effects on periodontitis. Sulfonylureas, insulin secretagogues, are the earliest and most widely used oral hypoglycemic drugs used for type-2 diabetes. Studies have found that sulfonylurea drugs can play a certain role in the mitigation of periodontitis and inflammation. This article reviews the effects of sulfonylurea drugs on the mitigation of periodontitis-diabetes comorbidity-related inflammation, bone loss, and vascular growth as well as the involved molecular mechanisms. We discuss the possibility of a new application of sulfonylureas (old drug) to treat periodontitis-diabetes comorbidity.

Keywords: periodontitis-diabetes comorbidity, sulfonylureas, inflammation, bone metabolism, angiogenesis

Abbreviations: PI3K, phosphatidylinositol-4,5-bisphosphate3-kinase; MMP, matrix metalloproteinase; PECAM-1, platelet endothelial cell adhesion molecule-1; MAPK, mitogen-activated protein (MAP) kinase; sICAM-1, soluble intercellular adhesion molecule-1; hsCRP, high-sensitivity C-reactive protein; SUR1-TRPM, sulfonylurea receptor 1-transient receptor potential melastatin 4; NLRP3, NLR family pyrin domain containing 3; THP-1, human monocytic leukemia cell line; BMDM, bone marrow-derived macrophages; Ca2+/CamKII, Ca^{2+}/calcium calmodulin-dependent kinase II; IGF-1, insulin-like growth factor 1; TGF-β, transforming growth factor-β; IL-10, interleukin-10; HCAECs, human coronary artery endothelial cells; HASMCs, human aortic smooth muscle cells; VSMC, vascular smooth muscle cell; VEGF, vascular endothelial growth factor; MCAO, middle cerebral artery occlusion; KATP, ATP sensitive potassium (K) channel; oxLDL, oxidized low-density lipoprotein; AGE, advanced glycation end-products; PKC, protein kinase C; MAPK, mitogen-activated protein kinase; NF-κB, nuclear factor kappa B; HUVECs, human umbilical vein endothelial cells; ECs, endothelial cells

INTRODUCTION

Periodontitis refers to the chronic inflammation of tooth-supporting tissues. The loss of periodontal attachment, surrounding bone, and teeth are clinical features of periodontitis (Gasner and Schure, 2020). According to the fourth national oral health epidemiological survey, almost 90% of Chinese adults suffered from periodontal disease of various severities and >30% of them had severe periodontitis (Jiao et al., 2021). Periodontitis has a high incidence rate and the prevalence of severe periodontitis in the world has reached approximately 10% (Frencken et al., 2017). In 2019, there were 1.1 billion (95% uncertainty interval: 0.8–1.4 billion) prevalent cases of severe periodontitis globally. From 1990 to 2019, the age-standardized prevalence rate of severe periodontitis increased by 8.44% (6.62–10.59%) worldwide (Chen et al., 2021). Shreds of evidence indicate that periodontitis is associated with many systemic diseases, including cardiovascular disease, type 2 diabetes mellitus (T2DM), rheumatoid arthritis, inflammatory bowel disease (IBD), Alzheimer's disease, nonalcoholic fatty liver disease, and certain cancers (Hajishengallis and Chavakis, 2021). Periodontitis leads to a 19% increase in the risk of cardiovascular disease (Nazir, 2017). Oral inflammatory diseases aggravate chronic inflammatory lung diseases such as asthma and chronic obstructive pulmonary disease (COPD) (Coffee and Sockrider, 2019). There are many common risk factors between periodontitis and osteoporosis, and the two influence each other (Wang and McCauley, 2016). Periodontitis is also associated with maternal infections, premature birth, low birth weight, and pre-eclampsia (Nazir, 2017). Therefore, periodontitis is not only an oral health problem but has a direct systemic connection and aggravates systemic inflammatory diseases. Due to the unique comorbidities and exacerbation relation between periodontitis and various systemic inflammatory diseases, periodontitis has become a huge public health burden.

Plaque microorganisms play an indispensable role in the pathogenesis of periodontitis, but their existence alone does not mean that periodontitis will inevitably occur. The combined action of some risk factors eventually leads to the occurrence of periodontitis (Darveau, 2010; Hajishengallis, 2014). In periodontitis, oral microbiome dysbiosis triggers host response inducing inflammatory mediators in oral tissues. This effect causes the periodontitis and oral tissue degeneration. Oral bacteria and inflammatory mediators enter the circulation exerting systemic effects. Moreover, oral microbiome can directly enter to oropharyngeal and orogastrointestinal route that further causes systemic effect as indicated in **Figure 1**. Over the past 30 years, a large number of research results have proved the host's defense response, or the host's susceptibility to periodontal disease as a necessary condition to develop disease (Darveau, 2010). The multi-microbial synergy and biological disorders of susceptible hosts are the initiation events of periodontitis. The host's defense barrier and defense cells have anti-inflammatory or pro-inflammatory. As the host's first line of defense against pathogenic microorganisms, neutrophils not only engulf bacteria through their Fc receptor-binding antibodies but also release collagenase, which has a destructive effect on tissues (Hajishengallis, 2020). *Porphyromonas gingivalis*, the main pathogen of periodontitis, polarizes macrophages to the M1 phenotype and their penetration into the gum tissue also leads to alveolar bone resorption (Zhu et al., 2019). Compared with healthy tissues, the proportion of monocytes observed in periodontitis tissue is significantly higher, and these monocytes overexpress human leukocyte antigen-DR (HLA-DR) and programmed cell death 1 ligand-1 (PDL-1) molecules, indicating that monocytes are in an inflammatory state during periodontitis. The ratio of M1/M2 macrophages is also significantly higher at the site of periodontal infection, indicating an imbalance between inflammation and repair mechanisms (Almubarak et al., 2020). Actinobacillus actinomycetemcomitans, a Gram-negative anaerobic microorganism that causes periodontitis in humans, activates $CD4^+$ cells in periodontitis tissues and cause local alveolar bone destruction (Teng et al., 2000). Immune cells release a large number of cytokines, such as interleukin-1β (IL-1β), IL-6, IL-8, tumor necrosis factor-α (TNF-α), prostaglandin-E2 (PGE2),

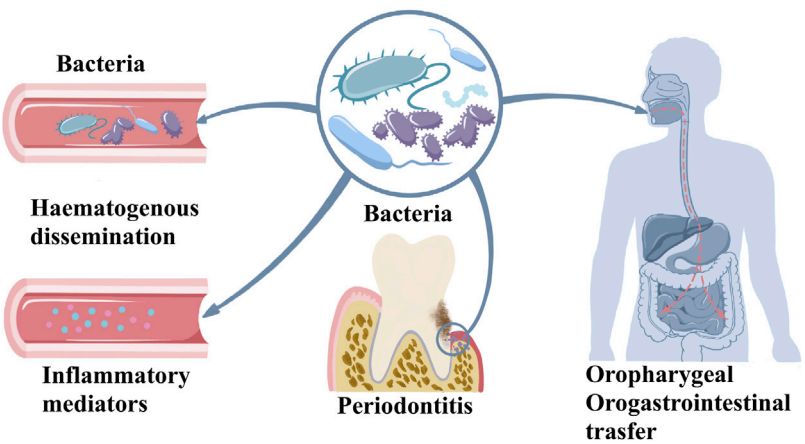

FIGURE 1 | The possible route of systemic effects of periodontitis.

matrix metalloproteinases (MMPs), interferon-γ (IFN-γ), and receptor activator of nuclear factor-κB ligand (RANKL) in response to bacterial invasion. These cytokines respective effects causing tissue damage to the periodontal region (Ramadan et al., 2020). Under physiological conditions, bone remodeling is the result of coordination between bone formation and resorption. The balance between osteoblast-mediated bone formation and osteoclast-mediated bone resorption ensures bone homeostasis. In an inflammatory state, excessive activation of the immune system and increased pro-inflammatory factors promote RANKL-mediated osteoclast formation, leading to bone resorption (Jung et al., 2014; Renn et al., 2018). At the same time, the host's susceptibility factors, including genetic factors, endocrine, immune function, psychological regulation, and certain diseases such as diabetes, are important in the development and aggravation of periodontitis (Badran et al., 2015). Both diabetes and periodontitis are systemic inflammatory diseases that accelerate the development and progression of each other. Comorbidity of the two diseases is associated with poor health and quality of life.

DIABETES

Diabetes is a chronic metabolic disease. In the past few decades, the prevalence of diabetes has increased significantly in the world. More than 422 million adults worldwide had diabetes in 2014 (Collaboration, 2016). Diabetes is categorized as type 1 diabetes mellitus (T1DM), T2DM, and pregnancy diabetes. T1DM is an autoimmune disease characterized by the destruction of pancreatic β-cells. T2DM is characterized by insulin resistance and impaired insulin secretion. The ability of T2DM patients to produce insulin in the body is not completely lost, and this type of diabetes treated with certain oral drugs that stimulate insulin secretion in the body. Gestational diabetes refers to a situation where women without a history of diabetes have elevated blood sugar during pregnancy. In this case, the baby has a high risk of developing diabetes in adulthood (Lovic et al., 2020). The global burden of diabetes is increasing with the increasing incidence rate of the disease.

DIABETES AND PERIODONTITIS COMORBIDITY

The prevalence of diabetes-affected people worldwide is expected to be 642 million by 2040 (Ogurtsova et al., 2017). Periodontitis is closely related to the progression of diabetes. There was sufficient evidence in the mid-1990s that regards periodontitis as the sixth complication of diabetes (Loe, 1993). New consensus indicates periodontal disease and diabetes as comorbidity (American Diabetes, 2018). Periodontitis is closely related to the aggravation of diabetes and T2DM is regarded as the risk factor of periodontitis (Chávarry et al., 2009). Similarly, the severity of periodontitis affects the blood sugar control of diabetic patients and exacerbates diabetes-related complications (Lalla and Papapanou, 2011). Multiple meta-analysis studies have shown that periodontal treatment alone can have a beneficial effect on glycemic control (Simpson et al., 2010; Teeuw et al., 2010; Sgolastra et al., 2013). On the other hand, anti-diabetic drugs not only play an indirect role in treating inflammation due to diabetes control but also have a direct anti-inflammatory effect (Kothari et al., 2016). The anti-inflammatory properties of anti-diabetic drugs have the potential to ameliorate periodontitis. At the same time, prospective studies had shown that patients with moderate or severe periodontitis have a significantly increased risk of diabetes in the future (Morita et al., 2012). Therefore, the exploration of a drug that can treat periodontitis-diabetes comorbidity could be of clinical significance.

As aforementioned, the clinical observation that periodontitis and diabetes can interact with each other is well researched. The mechanism of the association between these two diseases is still under study, but there are some accepted theories. It is generally believed that diabetes affects periodontitis in four ways. Diabetes causes a hyperinflammatory response to infection, oxidative stress, bone metabolism disorders, and increased expression of advanced glycation end products (AGEs) and their receptors (RAGE) (Lalla and Papapanou, 2011). Hyperglycemia predisposes to exaggerated inflammatory response, primes leukocytes for marginalization and superoxide production, as well as increases the free radical load in the gingival microvasculature (Gyurko et al., 2006). Cytokine dysregulation also represents the mechanism by which bacteria may induce destructive inflammatory responses in diabetic individuals (Naguib et al., 2004). Hyperglycemia can modulate the ratio of RANKL to osteoprotegerin (OPG) in periodontal tissue (Wu et al., 2014). Increased the ratio of RANKL/OPG and the secretion of AGEs, reactive oxygen species (ROS), TNF-α, IL-1β, and IL-6 in diabetes enhance periodontal ligament (PDL) and osteoblast apoptosis, induces osteoclastogenesis, and reduces bone formation (Pacios et al., 2013; Wu et al., 2015). AGEs increase IL-6 and intercellular adhesion molecule-1 (ICAM-1) expression via the RAGE, MAPK, and nuclear factor-κB (NF-κB) pathways in human gingival fibroblasts and exacerbate the progression of the pathogenesis of periodontal diseases (Nonaka et al., 2018). The AGE-RAGE interaction induces the production of ROS, the production of inflammatory cytokines such as TNF-α, and the activation of NF-κB (Brownlee, 2001). AGE-RAGE also serves as a promoting factor to regulate osteoclast formation (Ding et al., 2006).

Oxidative stress plays a critical role in diabetes complications. Inflammation induced by increased intracellular ROS also contributes to diabetes complications (Pitocco et al., 2010). The upregulation of ROS play important role in the establishment and progression of periodontitis through the development of oxidative stress (Sczepanik et al., 2020). The increase in superoxide production activates the increase in AGE formation and RAGE expression, as well as the protein kinase C (PKC) and hexosamine pathways. Through these pathways, increased intracellular ROS cause defective angiogenesis in response to ischemia activates many proinflammatory pathways (Giacco and Brownlee, 2010). Regarding the effect of periodontitis on diabetes, it is generally believed that periodontitis induced periodontal microbiota dysbiosis. The disease

concomitantly impacts the regional and systemic immune response impairing glucose metabolism (Su et al., 2013; Ilievski et al., 2015; Huang et al., 2016; Blasco-Baque et al., 2017). Inflammation markers such as c-reactive protein (CRP) and IL-6 are involved in insulin resistance, which positively correlates with the progress of diabetes (Pradhan et al., 2001). NAcht Leucine-rich repeat protein 3 (NLRP3), a pathogen recognition molecule, activates caspase-1. Activated caspase-1 cleaves and promotes the maturation of IL-1β that induces pancreatic inflammation, β-cell death, T2DM progression, and insulin-dependent diabetes development (Zhou et al., 2010). NLRP3 inflammasome-mediated effector adipose tissue T cells activation also leads to a decrease in insulin sensitivity. These cells regulate insulin resistance by releasing IFN-γ (Vandanmagsar et al., 2011). Pieces of literature had indicated that periodontitis causes an increase in systemic oxidative stress which could influence diabetes (Allen et al., 2011; Bastos et al., 2012). In addition, the microbiota plays a critical role in the connection between diabetes and periodontitis. T2DM patients are more susceptible to subgingival microbiome dysbiosis, potentially due to impaired host metabolic and immune regulation (Shi et al., 2020). Hypoglycemic therapy reconstructs the salivary microbiota of diabetes patients (Sun et al., 2020). Periodontitis affects diabetes through oral and gut microbiota dysbiosis. Gut microbial shifting driven by periodontitis contributes to systemic inflammation and metabolic dysfunction during the progression of T2DM (Li et al., 2020). Effective periodontal therapy reduced insulin resistance and improved periodontal health status and insulin sensitivity in patients with T2DM and chronic periodontitis (Mammen et al., 2017). The anti-diabetic drugs not only play an indirect role in treating inflammation due to diabetes control but also have a direct anti-inflammatory effect (Kothari et al., 2016). **Figure 2** illustrates the mechanisms of two-way relationship of periodontitis and diabetes that intensify the severity of both diseases. Antibacterial drugs are often used as adjuvant treatments for patients with diabetes and periodontitis. A prospective clinical study showed the adjunct of doxycycline (Doxy) to conventional periodontal therapy provides an additional benefit in reducing the glycemic level and improves periodontal health (Das et al., 2019). Photodynamic therapy + Doxy possesses the best efficacy in lowering HbA1c% of non-smoking chronic periodontitis patients with diabetes (Cao et al., 2019). The adjunctive use of systemic metronidazole and amoxicillin improves the microbiological and clinical outcomes of scaling and root planing in subjects with chronic periodontitis and T2DM (Tamashiro et al., 2016). Adjunctive omega-3 polyunsaturated fatty acids (ω-3 PUFA) and low-dose aspirin (ASA) after periodontal debridement provides clinical and immunological benefits to periodontitis patients with T2DM (Castro Dos Santos et al., 2020). Metformin, a traditional hypoglycemic drug, has been found to have anti-inflammatory effects. Metformin reduces the activity of NLRP3 inflammasomes by inhibiting the expression of Nek7, and significantly reduces experimental diabetic periodontitis *in vivo* and *in vitro* (Zhou et al., 2019). Hypoglycemic therapy has the potential to reconstruct the salivary microbiota and improve the localized conditions of diabetes patients with periodontitis (Sun et al., 2020). There are also some uncommon drugs used to treat periodontitis-diabetes comorbidities. A double-blind clinical trial study showed that melatonin supplementation in adjunct with non-surgical periodontal therapy improves inflammatory and periodontal status in T2DM with chronic periodontitis (Bazyar et al., 2019). Locally delivered atorvastatin was found to be effective in the treatment of intrabony defects in chronic periodontitis patients with T2DM (Kumari et al., 2016). Propolis can also be used as an adjuvant drug for scaling and root planning that significantly reduces the levels of fasting plasma glucose, and serum N-(carboxymethyl) lysine, and improves the periodontal treatment effect in patients with T2DM and chronic periodontitis (El-Sharkawy et al., 2016). The above clinical studies have not clarified whether the treatment effects are through unilateral benefit to diabetes or periodontitis that indirectly affects the other side. However, it is predictable that the drugs that mitigate the inflammation or reconstruct the microbiome could be beneficial to treat periodontitis-diabetes comorbidity.

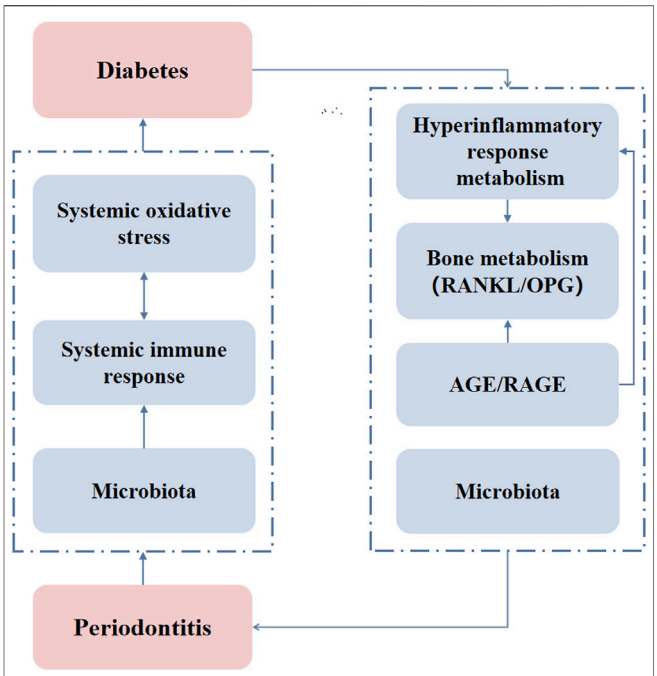

FIGURE 2 | The mechanisms of the two-way relationship of periodontitis and diabetes. AGE/RAGE: advanced glycation end product/receptor of advanced glycation end products.

SULFONYLUREAS

Sulfonylurea is currently one of the most common diabetes drugs. French scientist Marcel J. Janbon discovered the hypoglycemic effect of sulfa drugs in 1842. Since then, sulfonylurea has been extensively researched and developed to treat diabetes (Loubatieres-Mariani, 2007). Sulfonylurea drugs have been developed into more than ten kinds of oral hypoglycemic drugs, which are usually divided into two generations. Various

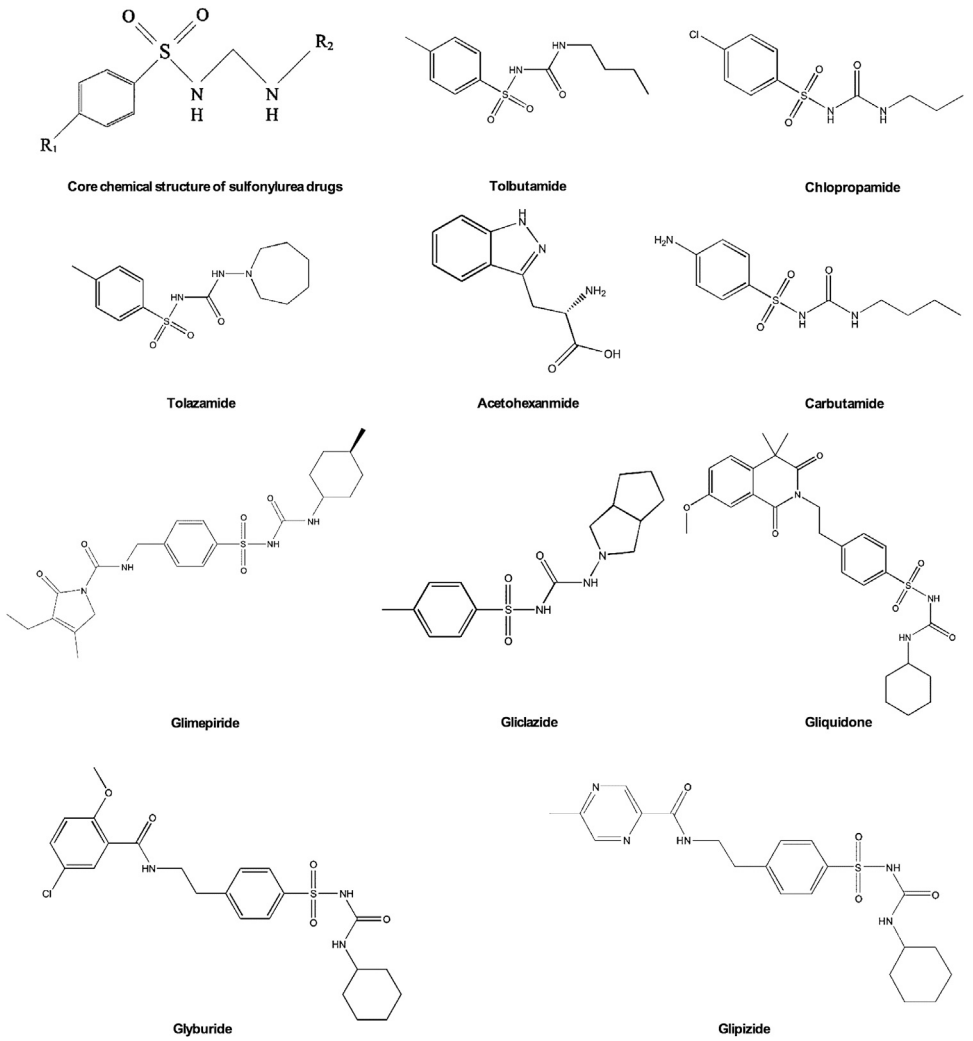

FIGURE 3 | Chemical structures of sulfonylureas.

sulfonylureas are derived by changing the nitrogen of the urea group and the para substituent of the benzene ring structure (**Figure 3**). In the first generation of sulfonylurea drugs chlorpropamide, tolbutamide, tolazamide, acetohexamide, and carbutamide the urea substituents are smaller and more polar, thus making the aryl-sulfonylurea more soluble in water. In the second generation of sulfonylurea drugs glyburide, glipizide, Gliclazide, glisoxepide, and glimepiride the substituents are large with nonpolar lipophilic groups that are easier to penetrate cell membranes and are therefore more effective (Doyle and Egan, 2003). The pancreatic β-cell membrane contains sulfonylurea receptors coupled with adenosine triphosphate (ATP)-sensitive potassium current IK(ATP) as well as voltage-dependent calcium channels. After binding with receptors sulfonylurea drugs block IK(ATP) and prevent potassium outflow, resulting in depolarization of cell membranes, enhancing voltage-dependent calcium channel opening, and extracellular calcium influx. The increased intracellular free calcium concentration triggers exocytosis and insulin release (Ashcroft and Rorsman, 2012; Lv et al., 2020). Therefore, sulfonylurea drugs only exert an effect on patients with T2DM who still have functional pancreatic β-cells in the body.

MECHANISMS OF PERIODONTITIS-DIABETES COMORBIDITY

Periodontitis-related systemic diseases are likely induced by three ways: hematogenous dissemination of periodontal bacteria, transfer of inflammatory mediators from periodontal tissue to blood, and oropharyngeal or oral-intestinal transfer of periodontal bacteria (**Figure 1**) (Teles and Wang, 2011; Mammen et al., 2020). Structural equation modeling was used to evaluate periodontal treatment effects on oral and systemic inflammation, and researchers found that diabetes and periodontitis together appear to increase systemic inflammation, with evidence of inflammation reduction

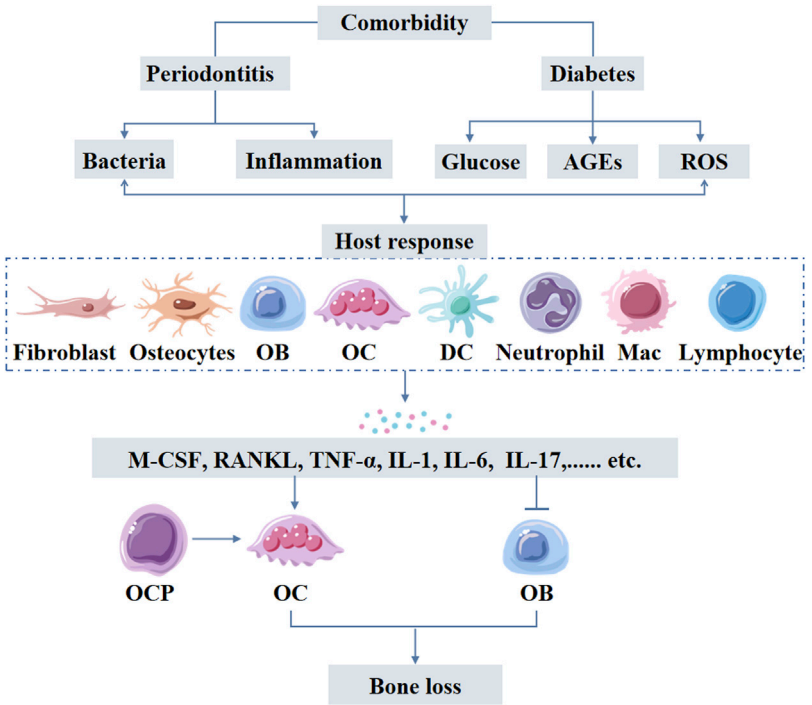

FIGURE 4 | Periodontitis-diabetes comorbidity induces host response triggering the release of inflammatory mediators form variety of cells including immune cells. Elevated levels of inflammatory mediators cause both local and systemic effects. Inflammatory mediator-induced osteoclastogenesis and compromised osteoblast function are the main causes of excessive alveolar bone loss in periodontitis-diabetes comorbidity. AGEs: advanced glycation end products; ROS: reactive oxygen species; OB: osteoblasts, OCP: osteoclast precursors; OC: osteoclasts; DC: dendritic cells; Mac: Macrophages.

following periodontal treatment (Preshaw et al., 2020). Diabetes increases inflammation in the periodontium, which causes changes in bacterial composition. Diabetes results in increased inflammation reflected by an increase in leukocytes and increased cytokine expression as well as a change in bacterial composition that enhances the overall pathogenicity of the microbiota (Graves et al., 2020).

Hematopoietic stem cells and progenitor cells sense systemic infections or inflammation in the bone marrow through inflammatory cytokine receptors, thereby differentiate into infection-resistant cells such as neutrophils and monocytes (Teitelbaum and Ross, 2003). This process relies on IL-6 serum levels, which increase during *Porphyromonas gingivalis* (Zhao et al., 2020). Monocytic lineage is the precursor of osteoclasts and differentiates into osteoclasts by further stimulation of macrophage colony-stimulating factor (M-CSF) and RANKL (Teitelbaum and Ross, 2003). Diabetes increases the levels of glucose, AGEs, and ROS in periodontal tissues leading to increased inflammation. Intensified inflammation further impacts the oral microbiota dysbiosis and stimulates periodontal ligament fibroblasts, osteoblasts, and osteocytes to produce pro-osteoclastogenic factors. The inflammation also affects these cells to reduce bone formation, resulting in greater net bone loss (**Figure 4**) (Graves et al., 2020).

Vascular inflammation is attributed to periodontitis-induced activation and adhesion of circulating monocytes to aortic endothelial cells via NF-κB/p65 nuclear translocation and upregulation of VCAM1 (Miyajima et al., 2014). Local treatment of periodontitis attenuates vascular inflammation and atherosclerosis in experimental models of periodontitis (Hasturk et al., 2015). *Porphyromonas gingivalis* is the most abundant bacterial species detected in non-diseased vascular tissue of patients with atherosclerosis (Mougeot et al., 2017). Gingipains are important for the virulence of *Porphyromonas gingivalis* in extra-oral sites. *Porphyromonas gingivalis* induces edema by increasing vascular permeability, which is attributed to gingipain-dependent degradation of platelet endothelial cell adhesion molecule (PECAM1) and vascular endothelial cadherin disrupting the endothelial barrier (Farrugia et al., 2021). Periodontitis-associated insulin resistance and hyperglycemia also induce the formation of AGEs, which is involved in several metabolic disorders, including vascular inflammation (Chavakis et al., 2003), and atherosclerosis (Ruiz et al., 2020) in experimental periodontitis in diabetic mice (**Figure 5**) (Lalla et al., 2000).

ANTI-INFLAMMATORY EFFECT OF SULFONYLUREAS

Sulfonylureas have shown the potential to alleviate inflammation. Insulin stimulation leads to the activation of different pathways involved in metabolic regulation, including the phosphatidylinositol-3-kinase (PI3K) cascade (Kumar and Dey,

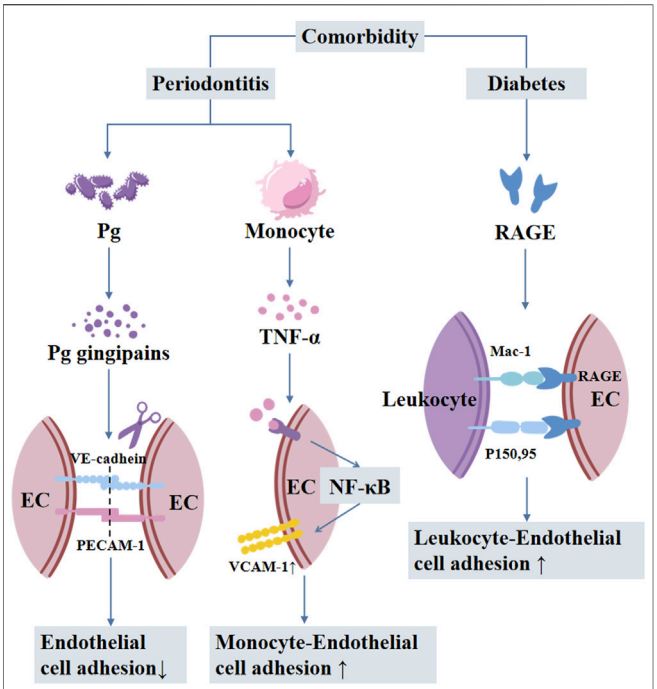

FIGURE 5 | The mechanisms involved in periodontitis-diabetes comorbidity-mediated vascular inflammation and atherosclerosis. Pg: Porphyromonas gingivalis; EC: endothelial cells; RAGE: receptor of advanced glycation end products.

2002). Compared to the healthy gingival tissue, PI3K expression is increased in periodontal tissues affected by periodontitis (Ozcan et al., 2017) (Sarkar et al., 2012). Gliclazide reduces oxidative stress, blocks PI3K signal transmission, and reduces matrix metalloproteinase 2 (MMP-2), cathepsin K, and RANKL levels in the rat periodontitis model. Gliclazide treatment alleviates periodontitis and alveolar bone resorption (Araújo et al., 2019).

MMPs, as a class of zinc-dependent endopeptidases, are produced in large quantities when host reactions occur in a variety of pathological conditions. MMPs degrade extracellular matrix and basement membrane destroying periodontal tissue (Sorsa et al., 2006). The researchers had reported the elevated levels of MMP in the serum of patients with inflammatory periodontal tissue and gingival crevicular fluid of periodontitis patients (Silosi et al., 2015). Glyburide has been reported to reduce plasma MMP-9 levels (Sheth et al., 2016). Reducing the elevated MMP levels could mitigate the periodontitis-induced oral tissue destruction. However, the ability of various sulfonylureas to reduce the MMPs level during periodontitis still needs to be investigated.

Macrophages and monocytes are key regulators of the inflammatory process. During inflammation, IL-1β is mainly secreted by mononuclear cells and macrophages (Koh and DiPietro, 2011). Cryopyrin/NALP3/NLRP3 is an essential component of inflammasomes triggered by microbial ligands, danger-associated molecular patterns (DAMPs), and crystals. Glyburide is the first identified compound to prevent cryopyrin activation and microbial ligand-, DAMPs-, and crystal-induced IL-1β secretion (Lamkanfi et al., 2009; Masters et al., 2010). Nine different sulfonylureas have been reported to inhibit the activation of NLRP3 in mouse bone marrow-derived macrophages in a dose-dependent manner. Nano molar concentration of MCC950, glyburide, sulofenur, glimepiride, gliquidone, or glisoxepide inhibits NLRP3 activation and stimulates insulin secretion in mouse pancreatic cells, indicating the dual effects (Hill et al., 2017). Chronic inflammation often causes delayed wound healing in diabetes. Mitigation of inflammation is part of the treatment of diabetes-related complications. Glyburide promotes the inflammatory regulator-140 receptor-interacting protein ubiquitin degradation by activating Ca^{2+}/calmodulin dependent protein kinase II (CamKII) that leads to anti-inflammatory M2 macrophage polarization (Lin et al., 2018). Glyburide and glimepiride have been shown to inhibit the release of IL-1β in macrophage-like THP-1 cells by targeting the activity of NLRP3 inflammasomes. Similarly, the rat model of periodontitis has shown the inhibitory effect of glyburide on inflammatory cell infiltration and alveolar bone osteoclast formation during the development of periodontitis (Kawahara et al., 2020). Glyburide inhibits NLRP3 formation, and induces the expression of pro-healing growth factors insulin-like growth factor-1 (IGF-1), TGF-β and IL-10, thereby promotes wound healing in diabetic mice (Mirza et al., 2014).

CRP is an acute-phase reactive protein and a non-specific marker of inflammation. Cross-sectional studies have shown that periodontitis and poor oral hygiene are associated with elevated serum CRP levels (Torrungruang et al., 2019). Glyburide reduces CRP level during treating diabetes (Putz et al., 2004). Clinical studies have shown that gliclazide reduces soluble ICAM-1 (sICAM-10, serum soluble E-selectin (sE-selectin), and hsCRP in diabetic patients (Räkel et al., 2007). Moreover, gliclazide blocks insulin-mediated neutrophil migration through endothelial cells and the expression of PECAM-1 by inhibiting the activation of MAPK (Okouchi et al., 2004).

There is a clear connection between diabetes and inflammation, and sulfonylurea drugs have obvious positive effects on inflammation mitigation. The literature had reported the various mechanisms of action of different sulfonylurea drugs during inflammation mitigation (**Table 1**).

THE EFFECT OF SULFONYLUREA DRUGS ON BONE METABOLISM

Periodontitis eventually destroys periodontal tissues and alveolar bone leading to tooth looseness and even loss. The main reason for alveolar bone loss in periodontitis is the imbalance of bone metabolism, mainly due to the increased osteoclasts' number and activity (Straka et al., 2015). Activation of nuclear factor-kappa B receptor activator (RANK) signaling in osteoclasts precursors during bacterial infection is a key driver of enhanced osteoclast number and activity in periodontitis. Bacterial components induce the production of proinflammatory cytokines TNF-α

TABLE 1 | Effect of sulfonylureas in pathophysiology of inflammatory diseases.

Sulfonylurea	Disease	Model used	Mechanism	Reference
Gliclazide	Periodontitis	Rat periodontitis model	-Reduces oxidative stress via inhibition of PI3K signaling, MMP-2, cathepsin K, and RANKL level	Kumar and Dey, (2002); Araújo et al., (2019)
	Coronary artherosclerosis	*In vitro*	-Blocks insulin-mediated neutrophil migration through endothelial cells	Okouchi et al. (2004)
		Model of neutrophils transmigration across umbilical vein endothelial cells	-Inhibits the expression of PECAM-1 via inhibition of MAPK	
	Diabetes	Clinical trial	-Reduces sICAM-1, sE-selectin, and hsCRP	Räkel et al. (2007)
Glyburide	Brian swelling	Clinical trial	-Blocks SUR1-TRPM4 channel in neurons, astrocytes, and endothelium -Reduces MMP-9 plasma level	Sheth et al. (2016)
	The inflammation in diabetes	*In vitro* THP-1	-Inhibits NLRP3 inflammasomes -Activates Ca^{2+}/CamKII -Induce the expression of pro-healing growth factors: IGF-1, TGF-β, and IL-10	Mirza et al. (2014); Hill et al. (2017); Kawahara et al. (2020)
	Diabetes	Clinical trial	- Reduces CRP level	Putz et al. (2004)
MCC950	—	*In vitro* BMDM	-Inhibits NLRP3 at nanomolar concentrations	Hill et al. (2017)
Sulofenur	—	*In vitro* BMDM	-Inhibits NLRP3 at nanomolar concentrations	Hill et al. (2017)
Glimepiride	—	*In vitro* BMDM	-Inhibits NLRP3 at nanomolar concentrations	Hill et al. (2017)
Gliquidone	—	*In vitro* BMDM	-Inhibits NLRP3 at nanomolar concentrations	Hill et al. (2017)
Glisoxepide	—	*In vitro* BMDM	-Inhibits NLRP3 at nanomolar concentrations	Hill et al. (2017)

BMDM: bone marrow derived macrophages.

and IL-1β, which enhance the activation of RANK by RANKL and down-regulating OPG signaling (Darveau, 2010).

In the rat periodontitis model, oral administration of glyburide significantly inhibits the infiltration of inflammatory cells and osteoclasts in the periodontal tissue (Kawahara et al., 2020). MCC950, a diarylsulfonylurea compound, which is the most specific inhibitor of NLRP3 inflammasome (Laliberte et al., 2003), inhibits the classical and non-classical pathways of NLRP3 inflammasome activation (Coll et al., 2015). The administration of MCC950 prevents alveolar bone loss in aging mice, but not in young mice. *In vitro* studies have shown that MCC950 treatment directly inhibits osteoclast differentiation (Zang et al., 2020). These effects are achieved through the inhibition of NLRP3 inflammasome and IL-1β expression by sulfonylurea drugs. **Table 2** summarizes the effect of sulfonylureas on bone metabolism.

Sulfonylurea drugs stimulate pancreatic β-cells to increase insulin secretion. Insulin is a bone anabolic factor that acts through insulin receptor substrate (IRS) signaling and glucose uptake. *In vivo* studies suggest that the absence of IRS gene decreases bone mass, reduces osteoblast/osteoclast function, and impairs bone turnover (Ogata et al., 2000). IRS-2 signal maintains the tendency of bone formation to exceed bone resorption, and IRS-1 signal maintains bone renewal. The integration of these two signals leads to strong bone anabolic effects of insulin and IGF-1 (Akune et al., 2002). The reduction of bone mass in most diabetic patients is related to the function of β-cells. Moreover, *in vitro* studies have shown that insulin regulates bone metabolism by stimulating osteoblast proliferation and inhibiting osteoclast activity (Kalaitzoglou et al., 2019). Therefore, the sulfonylureas that can stimulate insulin secretion may also play a role in making bone metabolism tend to the direction of bone formation.

Many studies have proven that bone metabolism and energy metabolism are mutually regulated by closely related mechanisms. OPG induces islet β-cell replication by regulating CREB and GSK3 pathways (Kondegowda et al., 2015). Under the same pathological conditions, hyperglycemia has various adverse effects on glucose metabolism. Diabetes affects bone through glucose metabolism disorders, destruction of bone microvascular function, and muscle endocrine function, which is also a unique bone feature in diabetes (Lecka-Czernik, 2017). Hyperglycemia interferes with the proliferation and mineralization of osteoblasts. Studies have shown that hyperglycemia inhibits the PI3K/Akt/eNOS pathway in rat osteoblasts, thereby interfering with the osteoblast transcription factors such as RUNX2, which have an important effect on osteoblast differentiation. Glimepiride stimulates the proliferation and differentiation of rat osteoblasts through the PI3K/Akt/eNOS signaling pathway

TABLE 2 | Sulfonylurea-mediated effects on bone metabolism and vascular functions.

Sulfonylurea	Effect	Model used	Mechanism	Reference
MCC950	Suppress alveolar bone loss in aged mice	Aged mice and *In vitro* BMDM culture	Reduces caspase-1 activation	Zang et al. (2020)
Glimepiride	Protect estrogen deficiency- mediated bone loss	Ovariectomized rats	Reverses the inhibitory effect of high glucose on the PI3K/Akt/eNOS pathway	Ma et al. (2011); Ma et al. (2014)
	Inhibits the formation of atheromatous plaques in high-cholesterol fed rabbits	*In vitro* HCAECs culture	Induces the production of NO in HCAEC by activating PI3K/Akt resulting vasodilation	Ueba et al. (2005)
	Improves the proliferation and migration of VSMC	*In vitro* HASMC culture	KATP channels	Zhang et al. (2019)
Glyburide	Significantly suppresses the infiltration of the number of osteoclasts in the alveolar bone	Periodontitis rat model	Suppresses activation of the NLRP3 inflammasome	Kawahara et al. (2020)
	Changes the circulating bone biomarkers	Clinical trial	Reduces osteoclast markers	Zinman et al. (2010)
	Enhances long-term brain repair and improves behavioral recovery	MCAO rat model	Acute blockade of SUR1 and enhanced angiogenesis	Ortega et al. (2013)
	Improves the proliferation and migration of VSMC	*In vitro* HASMC culture	KATP channels	Zhang et al. (2019)
Gliclazide	Inhibits the retinal endothelial cell proliferation and VEGF expression	*In vitro* BREC culture	Inhibits AGE-induced activation of PKC-, MAPK- and NF-κB signaling	Mamputu and Renier, (2004)
	Protects vascular endothelial cells from apoptosis	*In vitro* HUVECs culture	Attenuate oxidative stress induced by high glucose in HUVECs	Corgnali et al. (2008)
	Attenuates the sustained inflammatory process that occurs in the atherosclerotic plaque	*In vitro*	-Reduces oxLDL-, and AGEs-induced monocyte adhesion to ECs	Renier et al. (2003)
		Model of neutrophils transmigration across HUVECs	-Inhibits EC adhesion molecule expression and NF-κB activation	
	Reduces oxidative stress in patients with T2DM	Clinical trial	Improves plasma antioxidant status related to NO-mediated vasodilation enhancement	Fava et al. (2002)
	Prevents vascular obstructive diseases in T2DM	*In vitro* HASMCs culture	Shows an inhibitory effect on VSMC	Zhang et al. (2019)
Glipizide	Inhibits the growth and metastasis of cancer	TRAMP transgenic mouse model	Reduces microvessel density in PC tumor tissues	Qi et al. (2016)
		In vitro HUVECs culture	-inhibits the tubular structure formation of HUVECs by regulating the HMGIY/Angiopoietin-1 signaling pathway	

BMDM: bone marrow derived macrophages; NO: nitric oxide.

(Ma et al., 2014). Glimepiride reverses the inhibitory effect of high glucose on the PI3K/Akt/eNOS pathway, enhances osteoblast proliferation, expression of RUNX2, osteocalcin, and alkaline phosphatase mRNA, and protects rat mandibular osteoblast-apoptosis from high concentrations of glucose (Ma et al., 2011).

Studies have shown that glimepiride alleviates the skeletal damage caused by estrogen deficiency in ovariectomized rats and promotes bone formation (Fronczek-Sokol and Pytlik, 2014). There is also a gender-wise difference in the effect of glyburide on bone metabolism. The results of clinical sampling and the diabetes endpoint progression test showed that after glyburide treatment, bone resorption marker type I collagen c-terminal peptide (CTX) is significantly reduced in women but not in men. Glyburide alters the bone formation markers: type 1 procollagen amino-terminal peptide (P1NP), and bone alkaline phosphatase (bsALP). The effect of glyburide had been reported as changes of +0.2% P1NP in males and −11.6% bsALP in females (Zinman et al., 2010).

There is still considerable disagreement about the association of sulfonylurea drugs with fracture risk. Some studies have shown that compared with thiazolidinediones, sulfonylurea-treated patients have a lower fracture risk (Vestergaard et al., 2005; Dormuth et al., 2009; Solomon et al., 2009), and the same results have been obtained in cross-sectional surveys in postmenopausal populations (Kanazawa et al., 2010). However, some studies have found that there is no significant correlation between sulfonylurea treatment and fracture risk (Melton et al., 2008; Colhoun et al., 2012). These controversial results may be due to differences in study design, patient age/sex, drug concentration, and treatment duration. Multicenter clinical studies using the same protocol are needed to confirm the inconsistent outcome of these studies.

THE EFFECT OF SULFONYLUREA DRUGS ON ANGIOGENESIS

Angiogenesis is an important process that occurs under physiological and pathological conditions. Inflammatory diseases are one of the angiogenesis-dependent diseases.

Inflammation-induced angiogenesis affects many diseases, and periodontitis is one of them (Carmeliet, 2003). The formation of blood vessels is strictly regulated and this process involves the synergistic effect between various cells, cytokines, growth factors, and extracellular matrix components (Andreuzzi et al., 2017). Among them, vascular endothelial growth factor (VEGF) is the essential factor for vascular endothelium, which is also an important factor in the pathogenesis of invasive periodontitis and chronic periodontitis (Unlü et al., 2003). Gingival tissue, gingival crevicular fluid, and serum show a high expression trend of VEGF in periodontitis (Noguchi et al., 2011; Pradeep et al., 2011). VEGF also interacts with factors that regulate bone homeostasis and bone development, affecting bone metabolism (Peng et al., 2002). Under high glucose conditions, VEGF inhibits insulin secretion of pancreatic β-cells, sulfonylurea receptor expression, and inwardly rectifying potassium channel gene 6.2 (Kir6.2) expression (An et al., 2017). Gliclazide reduces protein kinase C (PKC) translocation, extracellular signal-regulated protein kinase 1/2, and NF-κB induced by AGEs in the bovine retinal endothelial cell (BREC), inhibiting BREC proliferation and VEGF expression (Mamputu and Renier, 2004).

H_2S and C-type Natriuretic Peptide (CNP) also act as vasoactive agents and induce angiogenic responses. H_2S enhances EC migration through a KATPchannel/p38/hsp27 pathway. Blockade of KATP channels in ECs by glibenclamide blocked H2S-induced EC migration (Papapetropoulos et al., 2009). Similarly, CNP mediates angiogenesis via KATP activation. Subsequent research pointed out that ATP-sensitive potassium channel activation induces angiogenesis effects *in vitro* and *in vivo* (Khambata et al., 2011). KATP activation and the expression of the Kir6.1 KATP subunit may underpin angiogenesis to a variety of vasoactive stimuli, including H2S, VEGF, and CNP (Umaru et al., 2015). Sulfonylurea drugs may have inhibitory effects on angiogenesis via targeting Kir6.1 KATP subunit.

The effects of sulfonylurea drugs on angiogenesis have been proven by multiple animal experiments. **Table 2** summarizes the effect of sulfonylureas on vascular functions. Male Wistar rats treated with low-dose glyburide simulate stroke after middle cerebral artery occlusion treatment. Histological evaluation showed that glyburide treatment enhances angiogenesis in the hippocampus (Ortega et al., 2013). Under the stimulation of angiogenesis, MMP-9 degrades multimerin 2 (MMRN2). The decreased MMRN2 acts as a negative feedback regulator to promote the expression of VEGFA and angiogenesis (Andreuzzi et al., 2017). In periodontitis, MMP-9 is up-regulated in serum and gingival crevicular fluid (Yang et al., 2019). Intravenous glyburide shows a decrease in plasma MMP-9 during a clinical study on the safety and efficacy of glyburide in the treatment of brain swelling after cerebral infarction (Sheth et al., 2016). These reports suggest that glyburide may have an inhibitory effect on angiogenesis by reducing the MMP-9 and modulating MMRN2/VEGFA pathway.

Anti-diabetes drugs also have a direct effect on tumor growth. The second-generation sulfonylurea glipizide has obvious vascular inhibitory effects and inhibits tumor-induced angiogenesis by up-regulating natriuretic peptide that inhibits tumor growth and metastasis (Qi et al., 2014; Qi et al., 2016). The results of the studies on the effects of sulfonylurea drugs on angiogenesis are not consistent. Some studies have shown that glyburide inhibits vascular function. However, the anabolic effect of sulfonylurea drugs on vascular function cannot be denied (Matsuzawa et al., 2015). Different sulfonylurea drugs have different effects on vascular function. The different study models and drugs used might be responsible for the contradictory results.

Gliclazide attenuates oxidative stress induced by high glucose in human umbilical vein endothelial cells and protect vascular endothelial cells from apoptosis (Corgnali et al., 2008). Gliclazide also reduces the adhesion of monocytes and endothelial cells induced by oxidized low-density lipoprotein (oxLDL) and AGEs *in vitro*. This effect reduces the ability of monocytes adhesion in the blood vessel walls and the continuous inflammatory process that occurs in atherosclerotic plaques (Renier et al., 2003). Similar events might occur during periodontitis. However, future studies are needed to support this hypothesis.

Glimepiride induces the production of nitric oxide (NO) in human coronary artery endothelial cells by activating PI3K/Akt, and more NO release will play a role in vasodilation (Ueba et al., 2005). Gliclazide reduces oxidative stress in patients with T2DM by improving plasma antioxidant status, and this effect is also related to NO-mediated vasodilation enhancement (Fava et al., 2002). Sulfonylurea receptors are also present in vascular smooth muscle cells (VSMC), and KATP channels play an important role in the proliferation and migration of VSMC induced by glyburide and glimepiride. In contrast, gliclazide has an inhibitory effect on VSMC, which makes gliclazide a potential therapeutic to prevent vascular obstructive diseases in T2DM (Zhang et al., 2019).

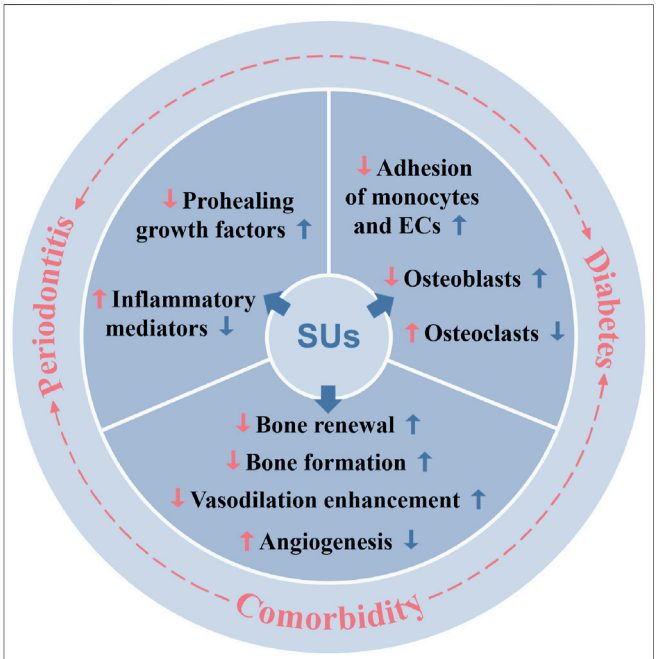

FIGURE 6 | Periodontitis, diabetes, and periodontitis-diabetes comorbidity affects various local and systemic functions, and sulfonylureas had shown potential to alleviate those effects. SUs: sulfonylureas; ECs: endothelial cells.

SUMMARY

In summary, sulfonylurea drugs have multiple therapeutic potential other than the traditional treatment of diabetes. The occurrence and development of periodontal disease are closely related to inflammatory factors, bone metabolism balance, and neovascularization. Affected by systemic metabolic changes, periodontitis combined with diabetes aggravates the pathology of both diseases. Sulfonylurea drugs alleviate periodontitis possibly via direct mitigation of inflammation or indirectly via anti-diabetic effect (**Figure 6**). The above-mentioned studies indicated that sulfonylurea drugs are likely to have a therapeutic effect by directly acting on periodontitis suggesting its possible application to treat periodontitis alone. Moreover, sulfonylureas can be used as a "one stone two birds" to treat periodontitis-diabetes comorbidity. However, more *in vitro* and *in vivo* studies are needed to test the efficacy of sulfonylureas on periodontitis or periodontitis-diabetes comorbidity and to unravel the underlying mechanisms of action.

AUTHOR CONTRIBUTIONS

JP and MM: study design and manuscript final editing; LY and QG: literature survey and manuscript writing; ZY, LjW, and LpW: Figure preparation and manuscript editing.

FUNDING

This study was supported by the project of Guangzhou Science and Technology Bureau (202002030301), Department of Education of Guangdong Province (2018KTSCX186), and highlevel university construction funding of Guangzhou Medical University (02-412-B205002-1003018, 02-410-B205001293, B185006003014, B195002003017, and 02-412-B205002-1003017). The funding bodies played no role in the design of the study and collection, analysis, and interpretation of data, and in writing the manuscript.

REFERENCES

Akune, T., Ogata, N., Hoshi, K., Kubota, N., Terauchi, Y., Tobe, K., et al. (2002). Insulin Receptor Substrate-2 Maintains Predominance of Anabolic Function over Catabolic Function of Osteoblasts. *J. Cel Biol* 159, 147–156. doi:10.1083/jcb.200204046

Allen, E. M., Matthews, J. B., O' Halloran, D. J., Griffiths, H. R., and Chapple, I. L. (2011). Oxidative and Inflammatory Status in Type 2 Diabetes Patients with Periodontitis. *J. Clin. Periodontol.* 38, 894–901. doi:10.1111/j.1600-051X.2011.01764.x

Almubarak, A., Tanagala, K. K. K., Papapanou, P. N., Lalla, E., and Momen-Heravi, F. (2020). Disruption of Monocyte and Macrophage Homeostasis in Periodontitis. *Front. Immunol.* 11, 330. doi:10.3389/fimmu.2020.00330

American Diabetes, A. (2018). 3. Comprehensive Medical Evaluation and Assessment of Comorbidities: Standards of Medical Care in Diabetes-2018. *Diabetes Care* 41, S28–S37. doi:10.2337/dc18-S003

An, S. Y., Lee, Y. J., Neupane, S., Jun, J. H., Kim, J. Y., Lee, Y., et al. (2017). Effects of Vascular Formation during Alveolar Bone Process Morphogenesis in Mice. *Histochem. Cel Biol* 148, 435–443. doi:10.1007/s00418-017-1584-2

Andreuzzi, E., Colladel, R., Pellicani, R., Tarticchio, G., Cannizzaro, R., Spessotto, P., et al. (2017). The Angiostatic Molecule Multimerin 2 Is Processed by MMP-9 to Allow Sprouting Angiogenesis. *Matrix Biol.* 64, 40–53. doi:10.1016/j.matbio.2017.04.002

Araújo, A. A., Morais, H. B., Medeiros, C. A. C. X., Brito, G. A. C., Guedes, P. M. M., Hiyari, S., et al. (2019). Gliclazide Reduced Oxidative Stress, Inflammation, and Bone Loss in an Experimental Periodontal Disease Model. *J. Appl. Oral Sci.* 27, e20180211. doi:10.1590/1678-7757-2018-0211

Ashcroft, F. M., and Rorsman, P. (2012). Diabetes Mellitus and the β Cell: the Last Ten Years. *Cell* 148, 1160–1171. doi:10.1016/j.cell.2012.02.010

Badran, Z., Struillou, X., Verner, C., Clee, T., Rakic, M., Martinez, M. C., et al. (2015). Periodontitis as a Risk Factor for Systemic Disease: Are Microparticles the Missing Link? *Med. Hypotheses* 84, 555–556. doi:10.1016/j.mehy.2015.02.013

Bastos, A. S., Graves, D. T., Loureiro, A. P., Rossa Júnior, C., Abdalla, D. S., Faulin, T. E. S., et al. (2012). Lipid Peroxidation Is Associated with the Severity of Periodontal Disease and Local Inflammatory Markers in Patients with Type 2 Diabetes. *J. Clin. Endocrinol. Metab.* 97, E1353–E1362. doi:10.1210/jc.2011-3397

Bazyar, H., Gholinezhad, H., Moradi, L., Salehi, P., Abadi, F., Ravanbakhsh, M., et al. (2019). The Effects of Melatonin Supplementation in Adjunct with Non-surgical Periodontal Therapy on Periodontal Status, Serum Melatonin and Inflammatory Markers in Type 2 Diabetes Mellitus Patients with Chronic Periodontitis: a Double-Blind, Placebo-Controlled Trial. *Inflammopharmacology* 27, 67–76. doi:10.1007/s10787-018-0539-0

Blasco-Baque, V., Garidou, L., Pomié, C., Escoula, Q., Loubieres, P., Le Gall-David, S., et al. (2017). Periodontitis Induced by Porphyromonas Gingivalis Drives Periodontal Microbiota Dysbiosis and Insulin Resistance via an Impaired Adaptive Immune Response. *Gut* 66, 872–885. doi:10.1136/gutjnl-2015-309897

Brownlee, M. (2001). Biochemistry and Molecular Cell Biology of Diabetic Complications. *Nature* 414, 813–820. doi:10.1038/414813a

Cao, R., Li, Q., Wu, Q., Yao, M., Chen, Y., and Zhou, H. (2019). Effect of Non-surgical Periodontal Therapy on Glycemic Control of Type 2 Diabetes Mellitus: a Systematic Review and Bayesian Network Meta-Analysis. *BMC Oral Health* 19, 176. doi:10.1186/s12903-019-0829-y

Carmeliet, P. (2003). Angiogenesis in Health and Disease. *Nat. Med.* 9, 653–660. doi:10.1038/nm0603-653

Castro Dos Santos, N. C., Andere, N. M. R. B., Araujo, C. F., De Marco, A. C., Kantarci, A., Van Dyke, T. E., et al. (2020). Omega-3 PUFA and Aspirin as Adjuncts to Periodontal Debridement in Patients with Periodontitis and Type 2 Diabetes Mellitus: Randomized Clinical Trial. *J. Periodontol.* 91, 1318–1327. doi:10.1002/JPER.19-0613

Chávarry, N. G., Vettore, M. V., Sansone, C., and Sheiham, A. (2009). The Relationship between Diabetes Mellitus and Destructive Periodontal Disease: a Meta-Analysis. *Oral Health Prev. Dent* 7, 107–127. doi:10.3290/j.ohpd.a15518

Chavakis, T., Bierhaus, A., Al-Fakhri, N., Schneider, D., Witte, S., Linn, T., et al. (2003). The Pattern Recognition Receptor (RAGE) Is a Counterreceptor for Leukocyte Integrins: a Novel Pathway for Inflammatory Cell Recruitment. *J. Exp. Med.* 198, 1507–1515. doi:10.1084/jem.20030800

Chen, M. X., Zhong, Y. J., Dong, Q. Q., Wong, H. M., and Wen, Y. F. (2021). Global, Regional, and National burden of Severe Periodontitis, 1990-2019: An Analysis of the Global Burden of Disease Study 2019. *J. Clin. Periodontol.* 48,1165–1188. doi:10.1111/jcpe.13506

Coffee, L., and Sockrider, M. (2019). Dental Health and Lung Disease. *Am. J. Respir. Crit. Care Med.* 199, P9–P10. doi:10.1164/rccm.1995P9

Colhoun, H. M., Livingstone, S. J., Looker, H. C., Morris, A. D., Wild, S. H., Lindsay, R. S., et al. (2012). Hospitalised Hip Fracture Risk with Rosiglitazone and Pioglitazone Use Compared with Other Glucose-Lowering Drugs. *Diabetologia* 55, 2929–2937. doi:10.1007/s00125-012-2668-0

Coll, R. C., Robertson, A. A., Chae, J. J., Higgins, S. C., Muñoz-Planillo, R., Inserra, M. C., et al. (2015). A Small-Molecule Inhibitor of the NLRP3 Inflammasome for the Treatment of Inflammatory Diseases. *Nat. Med.* 21, 248–255. doi:10.1038/nm.3806

Collaboration, N. C. D. R. F. (2016). Worldwide Trends in Diabetes since 1980: a Pooled Analysis of 751 Population-Based Studies with 4.4 Million Participants. *Lancet* 387, 1513–1530. doi:10.1016/S0140-6736(16)00618-8

Corgnali, M., Piconi, L., Ihnat, M., and Ceriello, A. (2008). Evaluation of Gliclazide Ability to Attenuate the Hyperglycaemic 'memory' Induced by High Glucose in

Isolated Human Endothelial Cells. *Diabetes Metab. Res. Rev.* 24, 301–309. doi:10.1002/dmrr.804

Darveau, R. P. (2010). Periodontitis: a Polymicrobial Disruption of Host Homeostasis. *Nat. Rev. Microbiol.* 8, 481–490. doi:10.1038/nrmicro2337

Das, A. C., Das, S. J., Panda, S., Sharma, D., Taschieri, S., and Fabbro, M. D. (2019). Adjunctive Effect of Doxycycline with Conventional Periodontal Therapy on Glycemic Level for Chronic Periodontitis with Type 2 Diabetes Mellitus Subjects. *J. Contemp. Dent Pract.* 20, 1417–1423. doi:10.5005/jp-journals-10024-2722

Ding, K. H., Wang, Z. Z., Hamrick, M. W., Deng, Z. B., Zhou, L., Kang, B., et al. (2006). Disordered Osteoclast Formation in RAGE-Deficient Mouse Establishes an Essential Role for RAGE in Diabetes Related Bone Loss. *Biochem. Biophys. Res. Commun.* 340, 1091–1097. doi:10.1016/j.bbrc.2005.12.107

Dormuth, C. R., Carney, G., Carleton, B., Bassett, K., and Wright, J. M. (2009). Thiazolidinediones and Fractures in Men and Women. *Arch. Intern. Med.* 169, 1395–1402. doi:10.1001/archinternmed.2009.214

Doyle, M. E., and Egan, J. M. (2003). Pharmacological Agents that Directly Modulate Insulin Secretion. *Pharmacol. Rev.* 55, 105–131. doi:10.1124/pr.55.1.7

El-Sharkawy, H. M., Anees, M. M., and Van Dyke, T. E. (2016). Propolis Improves Periodontal Status and Glycemic Control in Patients with Type 2 Diabetes Mellitus and Chronic Periodontitis: A Randomized Clinical Trial. *J. Periodontol.* 87, 1418–1426. doi:10.1902/jop.2016.150694

Farrugia, C., Stafford, G. P., Potempa, J., Wilkinson, R. N., Chen, Y., Murdoch, C., et al. (2021). Mechanisms of Vascular Damage by Systemic Dissemination of the Oral Pathogen Porphyromonas Gingivalis. *FEBS J.* 288, 1479–1495. doi:10.1111/febs.15486

Fava, D., Cassone-Faldetta, M., Laurenti, O., De Luca, O., Ghiselli, A., and De Mattia, G. (2002). Gliclazide Improves Anti-oxidant Status and Nitric Oxide-Mediated Vasodilation in Type 2 Diabetes. *Diabet Med.* 19, 752–757. doi:10.1046/j.1464-5491.2002.00762.x

Frencken, J. E., Sharma, P., Stenhouse, L., Green, D., Laverty, D., and Dietrich, T. (2017). Global Epidemiology of Dental Caries and Severe Periodontitis - a Comprehensive Review. *J. Clin. Periodontol.* 44 Suppl 18 (Suppl. 18), S94–S105. doi:10.1111/jcpe.12677

Fronczek-Sokół, J., and Pytlik, M. (2014). Effect of Glimepiride on the Skeletal System of Ovariectomized and Non-ovariectomized Rats. *Pharmacol. Rep.* 66, 412–417. doi:10.1016/j.pharep.2013.12.013

Gasner, N. S., and Schure, R. S. (2020). "Periodontal Disease," in StatPearls. *(Treasure Island (FL)*. StatPearls Publishing LLC. Copyright © 2020.

Giacco, F., and Brownlee, M. (2010). Oxidative Stress and Diabetic Complications. *Circ. Res.* 107, 1058–1070. doi:10.1161/CIRCRESAHA.110.223545

Graves, D. T., Ding, Z., and Yang, Y. (2020). The Impact of Diabetes on Periodontal Diseases. *Periodontol. 2000* 82, 214–224. doi:10.1111/prd.12318

Gyurko, R., Siqueira, C. C., Caldon, N., Gao, L., Kantarci, A., and Van Dyke, T. E. (2006). Chronic Hyperglycemia Predisposes to Exaggerated Inflammatory Response and Leukocyte Dysfunction in Akita Mice. *J. Immunol.* 177, 7250–7256. doi:10.4049/jimmunol.177.10.7250

Hajishengallis, G., and Chavakis, T. (2021). Local and Systemic Mechanisms Linking Periodontal Disease and Inflammatory Comorbidities. *Nat. Rev. Immunol.* 21, 426–440. doi:10.1038/s41577-020-00488-6

Hajishengallis, G. (2014). Immunomicrobial Pathogenesis of Periodontitis: Keystones, Pathobionts, and Host Response. *Trends Immunol.* 35, 3–11. doi:10.1016/j.it.2013.09.001

Hajishengallis, G. (2020). New Developments in Neutrophil Biology and Periodontitis. *Periodontol. 2000* 82, 78–92. doi:10.1111/prd.12313

Hasturk, H., Abdallah, R., Kantarci, A., Nguyen, D., Giordano, N., Hamilton, J., et al. (2015). Resolvin E1 (RvE1) Attenuates Atherosclerotic Plaque Formation in Diet and Inflammation-Induced Atherogenesis. *Arterioscler Thromb. Vasc. Biol.* 35, 1123–1133. doi:10.1161/ATVBAHA.115.305324

Hill, J. R., Coll, R. C., Sue, N., Reid, J. C., Dou, J., Holley, C. L., et al. (2017). Sulfonylureas as Concomitant Insulin Secretagogues and NLRP3 Inflammasome Inhibitors. *ChemMedChem* 12, 1449–1457. doi:10.1002/cmdc.201700270

Huang, Y., Zeng, J., Chen, G., Xie, X., Guo, W., and Tian, W. (2016). Periodontitis Contributes to Adipose Tissue Inflammation through the NF-B, JNK and ERK Pathways to Promote Insulin Resistance In a rat Model. *Microbes Infect.* 18, 804–812. doi:10.1016/j.micinf.2016.08.002

Ilievski, V., Cho, Y., Katwala, P., Rodriguez, H., Tulowiecka, M., Kurian, D., et al. (2015). TLR4 Expression by Liver Resident Cells Mediates the Development of Glucose Intolerance and Insulin Resistance in Experimental Periodontitis. *PLoS One* 10, e0136502. doi:10.1371/journal.pone.0136502

Jiao, J., Jing, W., Si, Y., Feng, X., Tai, B., Hu, D., et al. (2021). The Prevalence and Severity of Periodontal Disease in Mainland China: Data from the Fourth National Oral Health Survey (2015-2016). *J. Clin. Periodontol.* 48, 168–179. doi:10.1111/jcpe.13396

Jung, S. M., Kim, K. W., Yang, C. W., Park, S. H., and Ju, J. H. (2014). Cytokine-mediated Bone Destruction in Rheumatoid Arthritis. *J. Immunol. Res.* 2014, 263625. doi:10.1155/2014/263625

Kalaitzoglou, E., Fowlkes, J. L., Popescu, I., and Thrailkill, K. M. (2019). Diabetes Pharmacotherapy and Effects on the Musculoskeletal System. *Diabetes Metab. Res. Rev.* 35, e3100. doi:10.1002/dmrr.3100

Kanazawa, I., Yamaguchi, T., Yamamoto, M., and Sugimoto, T. (2010). Relationship between Treatments with Insulin and Oral Hypoglycemic Agents versus the Presence of Vertebral Fractures in Type 2 Diabetes Mellitus. *J. Bone Miner Metab.* 28, 554–560. doi:10.1007/s00774-010-0160-9

Kawahara, Y., Kaneko, T., Yoshinaga, Y., Arita, Y., Nakamura, K., Koga, C., et al. (2020). Effects of Sulfonylureas on Periodontopathic Bacteria-Induced Inflammation. *J. Dent Res.* 99, 830–838. doi:10.1177/0022034520913250

Khambata, R. S., Panayiotou, C. M., and Hobbs, A. J. (2011). Natriuretic Peptide Receptor-3 Underpins the Disparate Regulation of Endothelial and Vascular Smooth Muscle Cell Proliferation by C-type Natriuretic Peptide. *Br. J. Pharmacol.* 164, 584–597. doi:10.1111/j.1476-5381.2011.01400.x

Koh, T. J., and Dipietro, L. A. (2011). Inflammation and Wound Healing: the Role of the Macrophage. *Expert Rev. Mol. Med.* 13, e23. doi:10.1017/S1462399411001943

Kondegowda, N. G., Fenutria, R., Pollack, I. R., Orthofer, M., Garcia-Ocaña, A., Penninger, J. M., et al. (2015). Osteoprotegerin and Denosumab Stimulate Human Beta Cell Proliferation through Inhibition of the Receptor Activator of NF-Kb Ligand Pathway. *Cell Metab* 22, 77–85. doi:10.1016/j.cmet.2015.05.021

Kothari, V., Galdo, J. A., and Mathews, S. T. (2016). Hypoglycemic Agents and Potential Anti-inflammatory Activity. *J. Inflamm. Res.* 9, 27–38. doi:10.2147/JIR.S86917

Kumar, N., and Dey, C. S. (2002). Gliclazide Increases Insulin Receptor Tyrosine Phosphorylation but Not P38 Phosphorylation in Insulin-Resistant Skeletal Muscle Cells. *J. Exp. Biol.* 205, 3739–3746. doi:10.1242/jeb.205.23.3739

Kumari, M., Martande, S. S., Pradeep, A. R., and Naik, S. B. (2016). Efficacy of Subgingivally Delivered 1.2% Atorvastatin in the Treatment of Chronic Periodontitis in Patients with Type 2 Diabetes Mellitus: A Randomized Controlled Clinical Trial. *J. Periodontol.* 87, 1278–1285. doi:10.1902/jop.2016.130227

Laliberte, R. E., Perregaux, D. G., Hoth, L. R., Rosner, P. J., Jordan, C. K., Peese, K. M., et al. (2003). Glutathione S-Transferase omega 1-1 Is a Target of Cytokine Release Inhibitory Drugs and May Be Responsible for Their Effect on Interleukin-1beta Posttranslational Processing. *J. Biol. Chem.* 278, 16567–16578. doi:10.1074/jbc.M211596200

Lalla, E., and Papapanou, P. N. (2011). Diabetes Mellitus and Periodontitis: a Tale of Two Common Interrelated Diseases. *Nat. Rev. Endocrinol.* 7, 738–748. doi:10.1038/nrendo.2011.106

Lalla, E., Lamster, I. B., Feit, M., Huang, L., Spessot, A., Qu, W., et al. (2000). Blockade of RAGE Suppresses Periodontitis-Associated Bone Loss in Diabetic Mice. *J. Clin. Invest.* 105, 1117–1124. doi:10.1172/JCI8942

Lamkanfi, M., Mueller, J. L., Vitari, A. C., Misaghi, S., Fedorova, A., Deshayes, K., et al. (2009). Glyburide Inhibits the Cryopyrin/Nalp3 Inflammasome. *J. Cel Biol* 187, 61–70. doi:10.1083/jcb.200903124

Lecka-Czernik, B. (2017). Diabetes, Bone and Glucose-Lowering Agents: Basic Biology. *Diabetologia* 60, 1163–1169. doi:10.1007/s00125-017-4269-4

Li, J., Lu, H., Wu, H., Huang, S., Chen, L., Gui, Q., et al. (2020). Periodontitis in Elderly Patients with Type 2 Diabetes Mellitus: Impact on Gut Microbiota and Systemic Inflammation. *Aging (Albany NY)* 12, 25956–25980. doi:10.18632/aging.202174

Lin, Y. W., Liu, P. S., Pook, K. A., and Wei, L. N. (2018). Glyburide and Retinoic Acid Synergize to Promote Wound Healing by Anti-inflammation and RIP140 Degradation. *Sci. Rep.* 8, 834. doi:10.1038/s41598-017-18785-x

Löe, H. (1993). Periodontal Disease. The Sixth Complication of Diabetes Mellitus. *Diabetes Care* 16, 329–334. doi:10.2337/diacare.16.1.329

Loubatières-Mariani, M.-M. (2007). La découverte des sulfamides hypoglycémiants. *J. Soc. Biol.* 201, 121–125. doi:10.1051/jbio:2007014

Lovic, D., Piperidou, A., Zografou, I., Grassos, H., Pittaras, A., and Manolis, A. (2020). The Growing Epidemic of Diabetes Mellitus. *Curr. Vasc. Pharmacol.* 18, 104–109. doi:10.2174/1570161117666190405165911

Lv, W., Wang, X., Xu, Q., and Lu, W. (2020). Mechanisms and Characteristics of Sulfonylureas and Glinides. *Curr. Top. Med. Chem.* 20, 37–56. doi:10.2174/1568026620666191224141617

Ma, P., Xiong, W., Liu, H., Ma, J., Gu, B., and Wu, X. (2011). Extrapancreatic Roles of Glimepiride on Osteoblasts from Rat Manibular Bone *In Vitro*: Regulation of Cytodifferentiation through PI3-kinases/Akt Signalling Pathway. *Arch. Oral Biol.* 56, 307–316. doi:10.1016/j.archoralbio.2010.10.009

Ma, P., Gu, B., Xiong, W., Tan, B., Geng, W., Li, J., et al. (2014). Glimepiride Promotes Osteogenic Differentiation in Rat Osteoblasts via the PI3K/Akt/eNOS Pathway in a High Glucose Microenvironment. *PLoS One* 9, e112243. doi:10.1371/journal.pone.0112243

Mammen, J., Vadakkekuttical, R. J., George, J. M., Kaziyarakath, J. A., and Radhakrishnan, C. (2017). Effect of Non-surgical Periodontal Therapy on Insulin Resistance in Patients with Type II Diabetes Mellitus and Chronic Periodontitis, as Assessed by C-Peptide and the Homeostasis Assessment Index. *J. Investig. Clin. Dent.* 8. e12221. doi:10.1111/jicd.12221

Mammen, M. J., Scannapieco, F. A., and Sethi, S. (2020). Oral-lung Microbiome Interactions in Lung Diseases. *Periodontol. 2000* 83, 234–241. doi:10.1111/prd.12301

Mamputu, J. C., and Renier, G. (2004). Signalling Pathways Involved in Retinal Endothelial Cell Proliferation Induced by Advanced Glycation End Products: Inhibitory Effect of Gliclazide. *Diabetes Obes. Metab.* 6, 95–103. doi:10.1111/j.1462-8902.2004.00320.x

Masters, S. L., Dunne, A., Subramanian, S. L., Hull, R. L., Tannahill, G. M., Sharp, F. A., et al. (2010). Activation of the NLRP3 Inflammasome by Islet Amyloid Polypeptide Provides a Mechanism for Enhanced IL-1β in Type 2 Diabetes. *Nat. Immunol.* 11, 897–904. doi:10.1038/ni.1935

Matsuzawa, Y., Guddeti, R. R., Kwon, T. G., Lerman, L. O., and Lerman, A. (2015). Treating Coronary Disease and the Impact of Endothelial Dysfunction. *Prog. Cardiovasc. Dis.* 57, 431–442. doi:10.1016/j.pcad.2014.10.004

Melton, L. J., 3rd, Leibson, C. L., Achenbach, S. J., Therneau, T. M., and Khosla, S. (2008). Fracture Risk in Type 2 Diabetes: Update of a Population-Based Study. *J. Bone Miner Res.* 23, 1334–1342. doi:10.1359/jbmr.080323

Mirza, R. E., Fang, M. M., Weinheimer-Haus, E. M., Ennis, W. J., and Koh, T. J. (2014). Sustained Inflammasome Activity in Macrophages Impairs Wound Healing in Type 2 Diabetic Humans and Mice. *Diabetes* 63, 1103–1114. doi:10.2337/db13-0927

Miyajima, S., Naruse, K., Kobayashi, Y., Nakamura, N., Nishikawa, T., Adachi, K., et al. (2014). Periodontitis-activated Monocytes/macrophages Cause Aortic Inflammation. *Sci. Rep.* 4, 5171. doi:10.1038/srep05171

Morita, I., Inagaki, K., Nakamura, F., Noguchi, T., Matsubara, T., Yoshii, S., et al. (2012). Relationship between Periodontal Status and Levels of Glycated Hemoglobin. *J. Dent Res.* 91, 161–166. doi:10.1177/0022034511431583

Mougeot, J. C., Stevens, C. B., Paster, B. J., Brennan, M. T., Lockhart, P. B., and Mougeot, F. K. (2017). Porphyromonas Gingivalis Is the Most Abundant Species Detected in Coronary and Femoral Arteries. *J. Oral Microbiol.* 9, 1281562. doi:10.1080/20002297.2017.1281562

Naguib, G., Al-Mashat, H., Desta, T., and Graves, D. T. (2004). Diabetes Prolongs the Inflammatory Response to a Bacterial Stimulus through Cytokine Dysregulation. *J. Invest. Dermatol.* 123, 87–92. doi:10.1111/j.0022-202X.2004.22711.x

Nazir, M. A. (2017). Prevalence of Periodontal Disease, its Association with Systemic Diseases and Prevention. *Int. J. Health Sci. (Qassim)* 11, 72–80.

Noguchi, K., Miwa, Y., Sunohara, M., and Sato, I. (2011). Analysis of Vascular Distribution and Growth Factors in Human Gingival Tissue Associated with Periodontal Probing Depth. *Okajimas Folia Anat. Jpn.* 88, 75–83. doi:10.2535/ofaj.88.75

Nonaka, K., Kajiura, Y., Bando, M., Sakamoto, E., Inagaki, Y., Lew, J. H., et al. (2018). Advanced Glycation End-Products Increase IL-6 and ICAM-1 Expression via RAGE, MAPK and NF-Kb Pathways in Human Gingival Fibroblasts. *J. Periodontal Res.* 53, 334–344. doi:10.1111/jre.12518

Ogata, N., Chikazu, D., Kubota, N., Terauchi, Y., Tobe, K., Azuma, Y., et al. (2000). Insulin Receptor Substrate-1 in Osteoblast Is Indispensable for Maintaining Bone Turnover. *J. Clin. Invest.* 105, 935–943. doi:10.1172/JCI9017

Ogurtsova, K., Da Rocha Fernandes, J. D., Huang, Y., Linnenkamp, U., Guariguata, L., Cho, N. H., et al. (2017). IDF Diabetes Atlas: Global Estimates for the Prevalence of Diabetes for 2015 and 2040. *Diabetes Res. Clin. Pract.* 128, 40–50. doi:10.1016/j.diabres.2017.03.024

Okouchi, M., Okayama, N., Omi, H., Imaeda, K., Fukutomi, T., Nakamura, A., et al. (2004). The Antidiabetic Agent, Gliclazide, Reduces High Insulin-Enhanced Neutrophil-Transendothelial Migration through Direct Effects on the Endothelium. *Diabetes Metab. Res. Rev.* 20, 232–238. doi:10.1002/dmrr.444

Ortega, F. J., Jolkkonen, J., Mahy, N., and Rodríguez, M. J. (2013). Glibenclamide Enhances Neurogenesis and Improves Long-Term Functional Recovery after Transient Focal Cerebral Ischemia. *J. Cereb. Blood Flow Metab.* 33, 356–364. doi:10.1038/jcbfm.2012.166

Özcan, E., Saygun, N. I., Ilıkçı, R., Karslıoğlu, Y., Muşabak, U., and Yeşillik, S. (2017). Increased Visfatin Expression Is Associated with Nuclear Factor-Kappa B and Phosphatidylinositol 3-kinase in Periodontal Inflammation. *Clin. Oral Investig.* 21, 1113–1121. doi:10.1007/s00784-016-1871-7

Pacios, S., Andriankaja, O., Kang, J., Alnammary, M., Bae, J., De Brito Bezerra, B., et al. (2013). Bacterial Infection Increases Periodontal Bone Loss in Diabetic Rats through Enhanced Apoptosis. *Am. J. Pathol.* 183, 1928–1935. doi:10.1016/j.ajpath.2013.08.017

Papapetropoulos, A., Pyriochou, A., Altaany, Z., Yang, G., Marazioti, A., Zhou, Z., et al. (2009). Hydrogen Sulfide Is an Endogenous Stimulator of Angiogenesis. *Proc. Natl. Acad. Sci. U S A.* 106, 21972–21977. doi:10.1073/pnas.0908047106

Peng, H., Wright, V., Usas, A., Gearhart, B., Shen, H. C., Cummins, J., et al. (2002). Synergistic Enhancement of Bone Formation and Healing by Stem Cell-Expressed VEGF and Bone Morphogenetic Protein-4. *J. Clin. Invest.* 110, 751–759. doi:10.1172/JCI15153

Pitocco, D., Zaccardi, F., Di Stasio, E., Romitelli, F., Santini, S. A., Zuppi, C., et al. (2010). Oxidative Stress, Nitric Oxide, and Diabetes. *Rev. Diabet Stud.* 7, 15–25. doi:10.1900/RDS.2010.7.15

Pradeep, A. R., Prapulla, D. V., Sharma, A., and Sujatha, P. B. (2011). Gingival Crevicular Fluid and Serum Vascular Endothelial Growth Factor: Their Relationship in Periodontal Health, Disease and after Treatment. *Cytokine* 54, 200–204. doi:10.1016/j.cyto.2011.02.010

Pradhan, A. D., Manson, J. E., Rifai, N., Buring, J. E., and Ridker, P. M. (2001). C-reactive Protein, Interleukin 6, and Risk of Developing Type 2 Diabetes Mellitus. *Jama* 286, 327–334. doi:10.1001/jama.286.3.327

Preshaw, P. M., Taylor, J. J., Jaedicke, K. M., De Jager, M., Bikker, J. W., Selten, W., et al. (2020). Treatment of Periodontitis Reduces Systemic Inflammation in Type 2 Diabetes. *J. Clin. Periodontol.* 47, 737–746. doi:10.1111/jcpe.13274

Putz, D. M., Goldner, W. S., Bar, R. S., Haynes, W. G., and Sivitz, W. I. (2004). Adiponectin and C-Reactive Protein in Obesity, Type 2 Diabetes, and Monodrug Therapy. *Metabolism* 53, 1454–1461. doi:10.1016/j.metabol.2004.06.013

Qi, C., Zhou, Q., Li, B., Yang, Y., Cao, L., Ye, Y., et al. (2014). Glipizide, an Antidiabetic Drug, Suppresses Tumor Growth and Metastasis by Inhibiting Angiogenesis. *Oncotarget* 5, 9966–9979. doi:10.18632/oncotarget.2483

Qi, C., Bin Li, L., Yang, Y., Yang, Y., Li, J., Zhou, Q., et al. (2016). Glipizide Suppresses Prostate Cancer Progression in the TRAMP Model by Inhibiting Angiogenesis. *Sci. Rep.* 6, 27819. doi:10.1038/srep27819

Räkel, A., Renier, G., Roussin, A., Buithieu, J., Mamputu, J. C., and Serri, O. (2007). Beneficial Effects of Gliclazide Modified Release Compared with Glibenclamide on Endothelial Activation and Low-Grade Inflammation in Patients with Type 2 Diabetes. *Diabetes Obes. Metab.* 9, 127–129. doi:10.1111/j.1463-1326.2006.00571.x

Ramadan, D. E., Hariyani, N., Indrawati, R., Ridwan, R. D., and Diyatri, I. (2020). Cytokines and Chemokines in Periodontitis. *Eur. J. Dent* 14, 483–495. doi:10.1055/s-0040-1712718

Renier, G., Mamputu, J. C., and Serri, O. (2003). Benefits of Gliclazide in the Atherosclerotic Process: Decrease in Monocyte Adhesion to Endothelial Cells. *Metabolism* 52, 13–18. doi:10.1016/s0026-0495(03)00212-9

Renn, T. Y., Huang, Y. K., Feng, S. W., Wang, H. W., Lee, W. F., Lin, C. T., et al. (2018). Prophylactic Supplement with Melatonin Successfully Suppresses the Pathogenesis of Periodontitis through Normalizing RANKL/OPG Ratio and Depressing the TLR4/MyD88 Signaling Pathway. *J. Pineal Res.* 64, e12464. doi:10.1111/jpi.12464

Ruiz, H. H., Ramasamy, R., and Schmidt, A. M. (2020). Advanced Glycation End Products: Building on the Concept of the "Common Soil" in Metabolic Disease. *Endocrinology* 161, bqz006. doi:10.1210/endocr/bqz006

Sarkar, A., Hellberg, L., Bhattacharyya, A., Behnen, M., Wang, K., Lord, J. M., et al. (2012). Infection with Anaplasma Phagocytophilum Activates the Phosphatidylinositol 3-Kinase/Akt and NF-Kb Survival Pathways in Neutrophil Granulocytes. *Infect. Immun.* 80, 1615–1623. doi:10.1128/IAI.05219-11

Sczepanik, F. S. C., Grossi, M. L., Casati, M., Goldberg, M., Glogauer, M., Fine, N., et al. (2020). Periodontitis Is an Inflammatory Disease of Oxidative Stress: We Should Treat it that Way. *Periodontol. 2000* 84, 45–68. doi:10.1111/prd.12342

Sgolastra, F., Severino, M., Pietropaoli, D., Gatto, R., and Monaco, A. (2013). Effectiveness of Periodontal Treatment to Improve Metabolic Control in Patients with Chronic Periodontitis and Type 2 Diabetes: a Meta-Analysis of Randomized Clinical Trials. *J. Periodontol.* 84, 958–973. doi:10.1902/jop.2012.120377

Sheth, K. N., Elm, J. J., Molyneaux, B. J., Hinson, H., Beslow, L. A., Sze, G. K., et al. (2016). Safety and Efficacy of Intravenous Glyburide on Brain Swelling after Large Hemispheric Infarction (GAMES-RP): a Randomised, Double-Blind, Placebo-Controlled Phase 2 Trial. *Lancet Neurol.* 15, 1160–1169. doi:10.1016/S1474-4422(16)30196-X

Shi, B., Lux, R., Klokkevold, P., Chang, M., Barnard, E., Haake, S., et al. (2020). The Subgingival Microbiome Associated with Periodontitis in Type 2 Diabetes Mellitus. *ISME J.* 14, 519–530. doi:10.1038/s41396-019-0544-3

Silosi, I., Cojocaru, M., Foia, L., Boldeanu, M. V., Petrescu, F., Surlin, P., et al. (2015). Significance of Circulating and Crevicular Matrix Metalloproteinase-9 in Rheumatoid Arthritis-Chronic Periodontitis Association. *J. Immunol. Res.* 2015, 218060. doi:10.1155/2015/218060

Simpson, T. C., Needleman, I., Wild, S. H., Moles, D. R., and Mills, E. J. (2010). Treatment of Periodontal Disease for Glycaemic Control in People with Diabetes. *Cochrane Database Syst Rev.* 5, Cd004714. doi:10.1002/14651858.cd004714.pub2

Solomon, D. H., Cadarette, S. M., Choudhry, N. K., Canning, C., Levin, R., and Stürmer, T. (2009). A Cohort Study of Thiazolidinediones and Fractures in Older Adults with Diabetes. *J. Clin. Endocrinol. Metab.* 94, 2792–2798. doi:10.1210/jc.2008-2157

Sorsa, T., Tjäderhane, L., Konttinen, Y. T., Lauhio, A., Salo, T., Lee, H. M., et al. (2006). Matrix Metalloproteinases: Contribution to Pathogenesis, Diagnosis and Treatment of Periodontal Inflammation. *Ann. Med.* 38, 306–321. doi:10.1080/07853890600800103

Straka, M., Straka-Trapezanlidis, M., Deglovic, J., and Varga, I. (2015). Periodontitis and Osteoporosis. *Neuro Endocrinol. Lett.* 36, 401–406.

Su, Y., Wang, D., Xuan, D., Ni, J., Luo, S., Xie, B., et al. (2013). Periodontitis as a Novel Contributor of Adipose Tissue Inflammation Promotes Insulin Resistance in a Rat Model. *J. Periodontol.* 84, 1617–1626. doi:10.1902/jop.2013.120442

Sun, X., Li, M., Xia, L., Fang, Z., Yu, S., Gao, J., et al. (2020). Alteration of Salivary Microbiome in Periodontitis with or without Type-2 Diabetes Mellitus and Metformin Treatment. *Sci. Rep.* 10, 15363. doi:10.1038/s41598-020-72035-1

Tamashiro, N. S., Duarte, P. M., Miranda, T. S., Maciel, S. S., Figueiredo, L. C., Faveri, M., et al. (2016). Amoxicillin Plus Metronidazole Therapy for Patients with Periodontitis and Type 2 Diabetes: A 2-year Randomized Controlled Trial. *J. Dent Res.* 95, 829–836. doi:10.1177/0022034516639274

Teeuw, W. J., Gerdes, V. E., and Loos, B. G. (2010). Effect of Periodontal Treatment on Glycemic Control of Diabetic Patients: a Systematic Review and Meta-Analysis. *Diabetes Care* 33, 421–427. doi:10.2337/dc09-1378

Teitelbaum, S. L., and Ross, F. P. (2003). Genetic Regulation of Osteoclast Development and Function. *Nat. Rev. Genet.* 4, 638–649. doi:10.1038/nrg1122

Teles, R., and Wang, C. Y. (2011). Mechanisms Involved in the Association between Periodontal Diseases and Cardiovascular Disease. *Oral Dis.* 17, 450–461. doi:10.1111/j.1601-0825.2010.01784.x

Teng, Y. T., Nguyen, H., Gao, X., Kong, Y. Y., Gorczynski, R. M., Singh, B., et al. (2000). Functional Human T-Cell Immunity and Osteoprotegerin Ligand Control Alveolar Bone Destruction in Periodontal Infection. *J. Clin. Invest.* 106, R59–R67. doi:10.1172/jci10763

Torrungruang, K., Katudat, D., Mahanonda, R., Sritara, P., and Udomsak, A. (2019). Periodontitis Is Associated with Elevated Serum Levels of Cardiac Biomarkers-Soluble ST2 and C-Reactive Protein. *J. Clin. Periodontol.* 46, 809–818. doi:10.1111/jcpe.13149

Ueba, H., Kuroki, M., Hashimoto, S., Umemoto, T., Yasu, T., Ishikawa, S. E., et al. (2005). Glimepiride Induces Nitric Oxide Production in Human Coronary Artery Endothelial Cells via a PI3-Kinase-Akt Dependent Pathway. *Atherosclerosis* 183, 35–39. doi:10.1016/j.atherosclerosis.2005.01.055

Umaru, B., Pyriochou, A., Kotsikoris, V., Papapetropoulos, A., and Topouzis, S. (2015). ATP-sensitive Potassium Channel Activation Induces Angiogenesis *In Vitro* and *In Vivo*. *J. Pharmacol. Exp. Ther.* 354, 79–87. doi:10.1124/jpet.114.222000

Unlü, F., Güneri, P. G., Hekimgil, M., Yeşilbek, B., and Boyacioğlu, H. (2003). Expression of Vascular Endothelial Growth Factor in Human Periodontal Tissues: Comparison of Healthy and Diabetic Patients. *J. Periodontol.* 74, 181–187. doi:10.1902/jop.2003.74.2.181

Vandanmagsar, B., Youm, Y. H., Ravussin, A., Galgani, J. E., Stadler, K., Mynatt, R. L., et al. (2011). The NLRP3 Inflammasome Instigates Obesity-Induced Inflammation and Insulin Resistance. *Nat. Med.* 17, 179–188. doi:10.1038/nm.2279

Vestergaard, P., Rejnmark, L., and Mosekilde, L. (2005). Relative Fracture Risk in Patients with Diabetes Mellitus, and the Impact of Insulin and Oral Antidiabetic Medication on Relative Fracture Risk. *Diabetologia* 48, 1292–1299. doi:10.1007/s00125-005-1786-3

Wang, C. J., and Mccauley, L. K. (2016). Osteoporosis and Periodontitis. *Curr. Osteoporos. Rep.* 14, 284–291. doi:10.1007/s11914-016-0330-3

Wu, Y., Liu, F., Zhang, X., and Shu, L. (2014). Insulin Modulates Cytokines Expression in Human Periodontal Ligament Cells. *Arch. Oral Biol.* 59, 1301–1306. doi:10.1016/j.archoralbio.2014.07.002

Wu, Y. Y., Xiao, E., and Graves, D. T. (2015). Diabetes Mellitus Related Bone Metabolism and Periodontal Disease. *Int. J. Oral Sci.* 7, 63–72. doi:10.1038/ijos.2015.2

Yang, S., Gu, B., Zhao, L., Shi, Q., Xu, J., and Wen, N. (2019). Meta-analysis of the Association between Serum and Gingival Crevicular Fluid Matrix Metalloproteinase-9 and Periodontitis. *J. Am. Dent Assoc.* 150, 34–41. doi:10.1016/j.adaj.2018.08.025

Zang, Y., Song, J. H., Oh, S. H., Kim, J. W., Lee, M. N., Piao, X., et al. (2020). Targeting NLRP3 Inflammasome Reduces Age-Related Experimental Alveolar Bone Loss. *J. Dent Res.* 99, 1287–1295. doi:10.1177/0022034520933533

Zhang, R., Zou, Z., Zhou, X., Shen, X., Fan, Z., Xie, T., et al. (2019). Comparative Effects of Three Sulfonylureas (Glibenclamide, Glimepiride, and Gliclazide) on Proliferation and Migration of Vascular Smooth Muscle Cells. *Cell Physiol Biochem* 52, 16–26. doi:10.33594/000000002

Zhao, Y., Li, Z., Su, L., Ballesteros-Tato, A., Katz, J., Michalek, S. M., et al. (2020). Frontline Science: Characterization and Regulation of Osteoclast Precursors Following Chronic Porphyromonas Gingivalis Infection. *J. Leukoc. Biol.* 108, 1037–1050. doi:10.1002/JLB.1HI0620-230R

Zhou, R., Tardivel, A., Thorens, B., Choi, I., and Tschopp, J. (2010). Thioredoxin-interacting Protein Links Oxidative Stress to Inflammasome Activation. *Nat. Immunol.* 11, 136–140. doi:10.1038/ni.1831

Zhou, X., Zhang, P., Wang, Q., Ji, N., Xia, S., Ding, Y., et al. (2019). Metformin Ameliorates Experimental Diabetic Periodontitis Independently of Mammalian Target of Rapamycin (mTOR) Inhibition by Reducing NIMA-Related Kinase 7 (Nek7) Expression. *J. Periodontol.* 90, 1032–1042. doi:10.1002/JPER.18-0528

Zhu, L. F., Li, L., Wang, X. Q., Pan, L., Mei, Y. M., Fu, Y. W., et al. (2019). M1 Macrophages Regulate TLR4/AP1 via Paracrine to Promote Alveolar Bone Destruction in Periodontitis. *Oral Dis.* 25, 1972–1982. doi:10.1111/odi.13167

Zinman, B., Haffner, S. M., Herman, W. H., Holman, R. R., Lachin, J. M., Kravitz, B. G., et al. (2010). Effect of Rosiglitazone, Metformin, and Glyburide on Bone Biomarkers in Patients with Type 2 Diabetes. *J. Clin. Endocrinol. Metab.* 95, 134–142. doi:10.1210/jc.2009-0572

Conflict of Interest: The authors declare that the research was conducted in the absence of any commercial or financial relationships that could be construed as a potential conflict of interest.

Publisher's Note: All claims expressed in this article are solely those of the authors and do not necessarily represent those of their affiliated organizations, or those of the publisher, the editors and the reviewers. Any product that may be evaluated in this article, or claim that may be made by its manufacturer, is not guaranteed or endorsed by the publisher.

frontiers in Pharmacology

ORIGINAL RESEARCH
published: 30 September 2021
doi: 10.3389/fphar.2021.706580

Single-Cell Transcriptomic Analysis of Peripheral Blood Reveals a Novel B-Cell Subset in Renal Allograft Recipients With Accommodation

Quan Zhuang[1,2], *Hao Li*[1], *Bo Peng*[1,2], *Yang Liu*[1], *Ying Zhang*[1], *Haozheng Cai*[1], *Shu Liu*[1,2] *and Yingzi Ming*[1,2]*

[1]Transplantation Center, The Third Xiangya Hospital, Central South University, Changsha, China, [2]Research Center of National Health Ministry on Transplantation Medicine, Changsha, China

Background: Kidney transplantation (KTx) is a preeminent treatment for end-stage renal disease (ESRD). After the application of immunosuppressants (IS), renal allograft recipients could reach a state called accommodation which means they are neither rejected nor infected. This study aimed to describe the details of this immune accommodation and reveal a novel mechanism of IS on immune cell subpopulations.

Methods: We analyzed multiple cell subgroups and their gene expression of peripheral T, B, myeloid, and NK cells from renal allograft recipients with accommodation and healthy control (HC) by single-cell transcriptomics sequencing (scRNA-seq) and flow cytometry.

Results: A total of 8,272 cells were isolated and sequenced from three individuals, including 2,758 cells from HC, 2,550 cells from ESRD patient, and 2,964 cells from KTx patient, as well as 396 immune response–related genes were detected during sequencing. 5 T-cell, 4 NK-cell, 5 myeloid, and 4 B-cell clusters were defined. Among them, a B-cell subset ($CD19^{+}IGLC3^{low}IGKC^{high}TCL1A^{-}CD127^{+}$) of renal transplant recipients with accommodation was significantly lower than that of HC and verified by flow cytometry, and this B-cell subset showed an activated potential because of its high expression of CD127. Furthermore, we found that IL32 might be the key cytokine to induce the differentiation of this B-cell cluster.

Conclusion: We found a novel B-cell subset ($CD19^{+}IGLC3^{low}IGKC^{high}TCL1A^{-}CD127^{+}$) which was inhibited and decreased in renal allograft recipients with accommodation. This study might reveal the effect of commonly used IS in clinical practice on B-cell subsets and related mechanism.

Keywords: kidney transplantation, single-cell RNA sequencing, B cell, immune accommodation, flow cytometry

OPEN ACCESS

Edited by:
Ning Hou,
Guangzhou Medical University, China

Reviewed by:
Yiping Jin,
University of California, Los Angeles, United States
Hai Huang,
The Ohio State University, United States

***Correspondence:**
Yingzi Ming
myz_china@aliyun.com

Specialty section:
This article was submitted to Inflammation Pharmacology, a section of the journal Frontiers in Pharmacology

Received: *07 May 2021*
Accepted: *13 August 2021*
Published: *30 September 2021*

Citation:
Zhuang Q, Li H, Peng B, Liu Y, Zhang Y, Cai H, Liu S and Ming Y (2021) Single-Cell Transcriptomic Analysis of Peripheral Blood Reveals a Novel B-Cell Subset in Renal Allograft Recipients With Accommodation. Front. Pharmacol. 12:706580. doi: 10.3389/fphar.2021.706580

INTRODUCTION

Kidney transplantation (KTx) is a preeminent treatment for end-stage renal disease (ESRD) (Parajuli et al., 2018) that effectively improves the quality of life of patients undergoing dialysis. Although the application of immunosuppressants (IS) reduces the risk of rejection in transplant patients and significantly improves the survival rates of transplant grafts and recipients, excessive IS

administration creates higher risks of infection and tumor occurrence (Fishman, 2013). Finding the best balance between rejection and infection is an important issue faced by every transplant doctor. In clinical practice, most transplant recipients can reach a state called accommodation (Garcia de Mattos Barbosa et al., 2018), a state in which neither rejection nor infection occurs post transplantation. However, accommodation is still different from the immune state of healthy people and is a special type of immune homeostasis under immunosuppressive conditions.

Currently, IS commonly used in the clinic (i.e., FK506, mycophenolate mofetil (MMF), and steroids) target the activation and proliferation of T cells (Romano et al., 2019). However, it is not clear whether these IS could affect other immune cells, such as B cells, NK cells, and myeloid cells. In addition, there is little research on the effects of IS on various T-cell subpopulations. Our previous study suggested that compared with healthy controls (HC), renal transplant recipients with accommodation had reduced proportions of γδ and Vδ2 subsets, as well as $CD27^+CD28^+$ subsets in both the $CD4^+$ and $CD8^+$ T-cell compartments, but the programmed cell death protein (PD) 1^+ $CD4^+$ and $CD8^+$ T-cell subsets were increased. Additionally, an increased percentage of $CD4^+$ effector memory T cells and a decreased fraction of $CD8^+$ central memory T cells were found in the renal allograft recipients with accommodation (Zhuang et al., 2019). We also reported that multiple subpopulations of B cells were altered in renal allograft recipients with accommodation, including reduced levels of regulatory B cells (Bregs) ($CD38^{high}CD27^+CD24^+$), transitional B cells ($IgM^+CD38^{high}CD24^{high}$), and marginal zone (MZ) B cells but increased levels of IgD^-CD27^+ and $CD38^{low}CD21^-$ B cells (Zhuang et al., 2020).

Although allograft biopsy is the gold standard for diagnosis of transplant rejection and immune-related problems, it is difficult to scale up in accommodation patients because of its invasive nature (Snijders et al., 2020). At present, peripheral blood is still the most convenient and quickest tissue for sampling in humans, owing to its highly informative populations of immune cells and the relative harmlessness of collection. The immune distribution in the peripheral blood in renal transplant recipients with accommodation definitely varies from that in healthy people because of the application of IS, so a better understanding of the peripheral immune cell profile is needed. With the rapid development of single-cell transcriptomic sequencing (scRNA-seq) in recent years, an increasing number of new immune cell subsets and their new functions of existing immune cells have been revealed (Dulken et al., 2019; Pont et al., 2019; Xiong et al., 2019). This technology compensates for the shortcomings of bulk RNA sequencing and microarrays and can detect and analyze the comprehensive transcriptome of each immune cell subset in different diseases. scRNA-seq can even identify rare cell subpopulations that were overlooked previously (Dulken et al., 2019). scRNA-seq can analyze more than 10,000 single-cell transcriptomes once, distinguish two similar subgroups within one kind of immune cell and trace the trajectory of cell evolution (Pont et al., 2019).

In this study, we analyzed multiple cell subgroups within peripheral T, B, myeloid, and NK-cell populations from renal transplant recipients with accommodation and healthy people by scRNA-seq and flow cytometry and found that the level of a novel B-cell subset ($CD19^+IGLC3^{low}IGKC^{high}TCL1A^-CD127^+$) in the renal transplant recipients with accommodation was significantly lower than that in the healthy people, and this B-cell subset showed an activated potential because of its high expression of CD127. This study might reveal the effect of IS commonly used in clinical practice on B-cell subsets and the related mechanism.

MATERIALS AND METHODS

Human Specimens

Peripheral blood mononuclear cells (PBMCs) from two patients (one KTx patient and one ESRD patient) and one healthy volunteer were sent for scRNA-seq. The patient with KTx was in accommodation at 1 year post transplantation. The patient with ESRD was still undergoing regular hemodialysis. PBMCs from 12 KTx patients and 20 HC with backgrounds similar to those of the patients evaluated by scRNA-seq were recruited for the analysis by flow cytometry. In brief, peripheral blood was collected into EDTA-anticoagulant tubes. After red blood cell lysis, a lymphocyte separation medium (TBD and LTS1077), blood, and 1X phosphate-buffered saline (HyClone and SH30256.01) were slowly added into centrifuge tubes separately at a ratio of 2:1:1. After centrifugation at 450 g for 20 minutes (min), PBMCs were aspirated from the interface in the centrifuge tubes. The study was reviewed and approved by the Institutional Review Board (Ethics Committee) of the Third Xiangya Hospital, Central South University (No. 2018-S347). **Supplementary Tables S1, S2** contain detailed information of the patients and healthy volunteers.

scRNA-Seq Analysis

A BD Rhapsody Single-Cell Analysis System (BD Biosciences) was used for the scRNA-seq analysis. In brief, PBMCs were processed into a single-cell suspension and loaded into a BD Rhapsody cartridge with >200,000 microwells. Then, a bead library was loaded into the microwell cartridge to saturation, and each cell was paired with a microbead. Next, the bead-cell complexes were hybridized with mRNA molecules to capture the barcoded oligos on the beads after lysing the cells in the microwell cartridge. The beads were collected into a single tube to generate a multiplex PCR-based library customized by the BD Rhapsody Immune Response Targeted Panel for Human (BD Biosciences). Fastq files were processed by an Illumina HiSeq 3000 platform and then processed into the expression matrix Fastq by the BD Rhapsody Analysis Pipeline. BD DataView software (BD Biosciences) and the R package Seurat (V 4.01) were used to analyze the expression matrix. The Kyoto Encyclopedia of Genes and Genomes (KEGG) analysis was performed using the R package "enrichplot" (Yu et al., 2012). The raw expression data from these experiments are available at the NCBI Gene Expression Omnibus database, with the following identifier: GSE175429 (https://www.ncbi.nlm.nih.gov/geo/query/acc.cgi?acc=GSE175429).

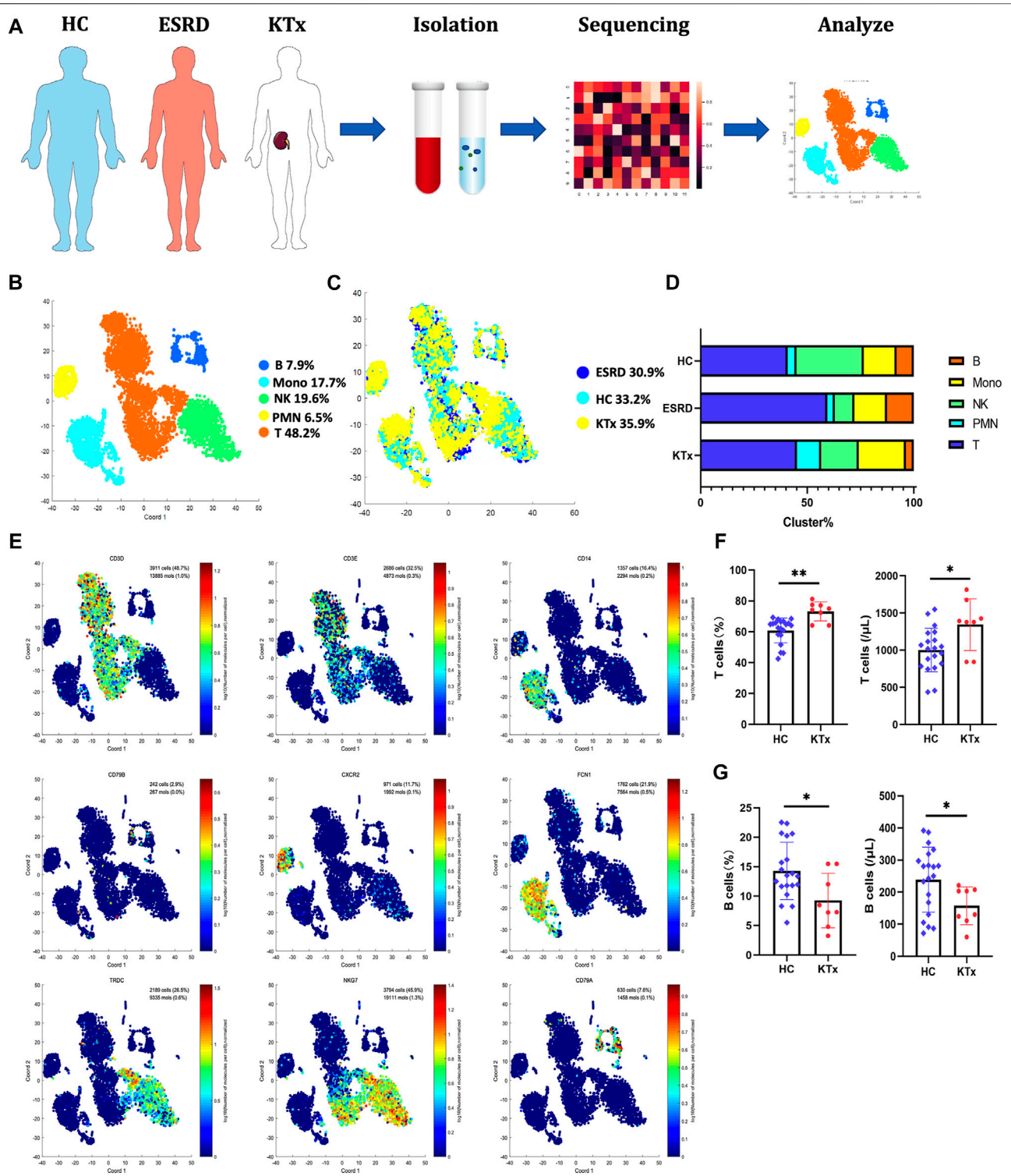

FIGURE 1 | Single-cell transcriptional profiling of PBMCs from HC, ESRD, and KTx. **(A)** Schematic of experimental workflow for defining and comparing PBMCs between three donors. **(B,C)** tSNE of single-cell profile annotated by a sample type and associated cell type. **(D)** Different expressions of marker genes in different clusters above. **(E)** Fraction of cells for 5 cell types in HC, ESRD, and KTx individuals. **(F)** Proportion and absolute counts of $CD3^+$ T cells in HC and KTx groups. **(G)** Ratio and absolute counts of $CD19^+$ B cells in HC and KTx groups. $^*p < 0.05$ $^{**}p < 0.005$.

Leukocyte Staining and Flow Cytometric Analysis

The following antibodies specific for surface antigens were used: anti-human (Hu) lambda light chain-APC (eBioscience, Catalog Number 17-9990-42), anti-Hu kappa light chain-super bright 600 (eBioscience, Catalog Number 63-9970-42), anti-Hu CD3-Alexa Fluor 700 (eBioscience, Catalog Number: 56-0038-42), Anti-Hu CD4-eFluor 450 (eBioscience, Catalog Number: 48-0049-42), anti-Hu CD14-APC/cyanine7 (BioLegend, Catalog Number: 325620), anti-Hu CD19-PerCP-Cyanine5.5 (Invitrogen, Catalog Number:45-0199-42), anti-Hu CD127-PerCP-Cyanine5.5 (Invitrogen, Catalog Number:45-1278-42), Anti-LEF1-Alexa Fluor® 647 (abcam, Catalog Number: ab246715), anti-Hu TCL1-PE-Cyanine7 (Invitrogen, Catalog Number: 2132361), anti-Hu CCL4-Alexa Fluor 488 (eBioscience, Catalog Number: 25-6699-42), BD anti-CD19-PE (BD, Catalog Number: 349209), and BD Multitest 6-Color TBNK (BD, Catalog Number: 662967). For intracellular and nuclear antigens, the FOXP3/Transcription Factor Staining Buffer Set (eBioscience, Catalog Number: 00-5523-00) and a stain for nucleation treatment were used. BD Trucount Tubes (BD, Catalog Number: 340334) were used to determine the absolute cell count. FlowJo V 10.62 was used to analyze flow cytometric data. Based on the FSC-SSC plot, lymphocytes were well separated. CD3 and CD19 were used to distinguish T cells and B cells from total lymphocytes. Then, $IGLC3^{low}IGKC^{high}$ cells were gated, and the TCL1-FMO tube was used as a negative control group to identify $TCL1^{-}IGLC3^{low}IGKC^{high}$ B cells.

Statistical Analysis

The mean ± standard deviation (SD) was used to describe the analyzed data. Differences in $CD19^{+}IGLC3^{low}IGKC^{high}TCL1A^{-}CD127^{+}$ B-cell subset percentages between groups were compared using the Mann–Whitney U-test because not all of the parameters were normally distributed. GraphPad Prism 7.0 (GraphPad Software Inc., La Jolla, CA, United States) was used to perform statistical analyses. Values of $p < 0.05$ were considered statistically significant.

RESULTS

scRNA-Seq Revealed the Landscape of Peripheral Immune Cells and Novel Gene Expression Patterns

A total of 8,272 cells were isolated and sequenced from three individuals including 2,758 cells from the HC, 2,550 cells from the ESRD patient and the 2,964 cells from KTx patient, and 396 immune response-related genes were detected during sequencing (**Figure 1A**). The Seurat package was used to identify 5 distinct cell clusters across all three individuals (**Figures 1B,C**): a T-cell cluster (defined by CD3D and CD3E, 48.2%), a B-cell cluster (defined by CD79A and CD79B, 7.9%), a polymorphonuclear cell (PMN) cluster (defined by CXCR2, 6.5%), a monocyte cluster (defined by FCN and CD14, 17.7%), and an NK-cell cluster (defined by NKG7 and TRDC, 19.6%) (**Figure 1D**; **Supplementary Figure S1A**). Other differentially expressed genes in each patient are displayed in a heat map (**Supplementary Figure S1B**).

T cells are often regarded as the target cells of immunosuppressive agents (Lim et al., 2017), but in our data, B cells, not T cells, were obviously suppressed in the KTx group compared with the HC group (**Figure 1G**). The proportions of NK-cell and myeloid subsets were not significantly different. To verify this, we used flow cytometry to evaluate the percentages and absolute numbers of T cells (defined by $CD3^{+}$), B cells (defined by $CD19^{+}$), and NK cells (defined as $CD16^{+}CD56^{+}$) in the peripheral blood of healthy people and kidney transplant recipients with accommodation at 1 year after transplantation. Compared to those in the HC group, the percentage ($p = 0.019$) and absolute number ($p = 0.042$) of B cells in the transplant group were significantly decreased, while those of T cells were increased (percentage: $p = 0.0006$ and absolute number: $p = 0.0136$) (**Figures 1F,G**). NK-cell data were consistent with the sequencing data and did not show significant differences between the KTx and HC groups (ratio: $p = 0.87$ and absolute number: $p = 0.56$) (**Supplementary Figure S2**).

PBMC scRNA-Seq Identified Five T-Cell Subsets

The T-cell cluster distribution among the three groups is shown (**Figure 2A**). Two $CD8^{+}$, two $CD4^{+}$, and one $CD8^{-}CD4^{-}$ T-cell subpopulations were identified as follows: the T1 cluster ($CD8A^{+}GNLY^{+}GZMH^{+}GZMB^{+}$), T2 cluster ($CD8A^{+}GZMK^{+}NKG7^{+}$), T3 cluster ($CD4^{+}LEF1^{low}NKG7^{-}$), T4 cluster ($CD4^{+}LEF1^{high}CCR7^{+}NKG7^{-}$), and T5 cluster ($CD4^{-}CD8^{-}TRDC^{+}NKG7^{+}$) (**Figures 2B,C**). The specific gene markers and distribution are shown in **Figure 2E**, **Supplementary Figures S3A,B**. Compared with those in the HC group, the percentages of the T3 and T4 subsets in the KTx group were decreased significantly, while the proportion of the T1 and T5 subset in the KTx group was obviously increased (**Figure 2D**). The results of KEGG and GO enrichment analyses of highly expressed genes in the T3 subset showed a positive regulation of lymphocyte activation (**Supplementary Figure S3C**); however, the FOXP3 gene was upregulated in the T3 subset compared to the other T-cell subsets (**Figure 2E**). According to the gene expression pattern of the T5 subset (**Figure 2F**; **Supplementary Figures S3A,B**), we considered the T5 subset to be γδ T cells, and the results of KEGG and GO enrichment analyses of highly expressed genes in the T5 subset showed that this subset was related to the adaptive immune system (**Supplementary Figure S3D**).

PBMC scRNA-Seq Identified Four NK-Cell Subsets

Four NK-cell subpopulations defined by scRNA-seq (**Figures 3A,B**) were as follows: the NK1 cluster ($FCER1G^{+}CCL5^{+}$), NK2 cluster ($IL32^{+}KLRC3^{+}$), NK3 cluster ($FCER1G^{+}CCL5^{-}$), and NK4 cluster ($IL32^{+}KLRB^{+}$) (**Figure 3C**). The specific gene markers and distribution are shown in **Figure 3D**, **Supplementary Figures**

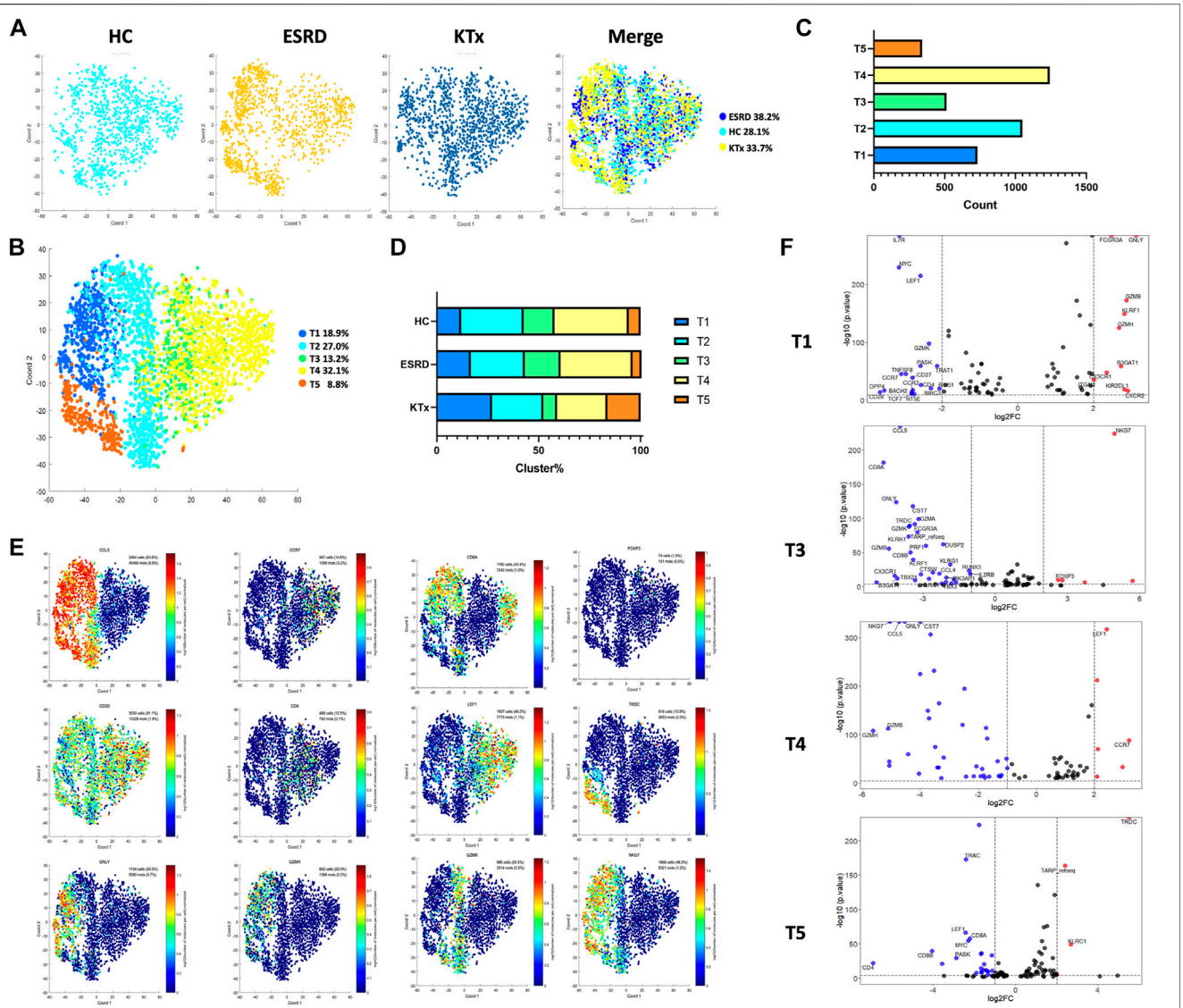

FIGURE 2 | T-cell clusters in PBMCs from HC, ESRD, and KTx. **(A,B)** tSNE of single-cell profile with each cell color coded for T-cell subsets. **(C)** Cell count of 5 T-cell subsets. **(D)** Distribution of 5 T-cell subsets. **(E)** Expression of highly expressed genes in each T-cell cluster. **(F)** Gene fingerprint expression volcano map of T1, T3, T4, and T5 clusters.

S4A,B. **Figure 3E** shows that there was no significant difference in the cell fraction between the KTx and HC groups. The flow cytometry analysis also proved that NK cells ($CD16^+CD56^+$) were not significantly different between these two groups (**Supplementary Figure S2**). In contrast, the ESRD group showed high proportions of the NK1 and NK3 subgroups but a low proportion of the NK2 subgroup compared to the other two groups (**Figure 3E**).

PBMC scRNA-Seq Identified Five Myeloid Cell Subsets

Five myeloid cell subpopulations were defined by scRNA-seq (**Figures 4A,B**) given as follows: M1 cluster ($GZMH^+GNLY^+$), M2 cluster ($S100A12^+S100A9^+$), M3 cluster ($CCL4^+DUSP2^+$), M4 cluster ($FCGR3A^+$), and M5 cluster ($FCER1A^+CD1c^+$) (**Figure 4D**). The gene expression pattern of the M5 cluster was relatively close to that of dendritic cells (DCs) (García-González et al., 2017). The specific marker distribution and the distribution in each cluster are shown in **Figure 4C** and **Supplementary Figures 5A,B**. There was a significant difference in the M3 cluster between the KTx and HC groups (**Figure 4E**), and the results of KEGG and GO enrichment analyses of highly expressed genes in the M3 subset showed that this cluster was related to cytokine-mediated signaling pathways (**Supplementary Figure S5C**). Unfortunately, we did not verify this difference by flow cytometry (**Supplementary Figure S5D**).

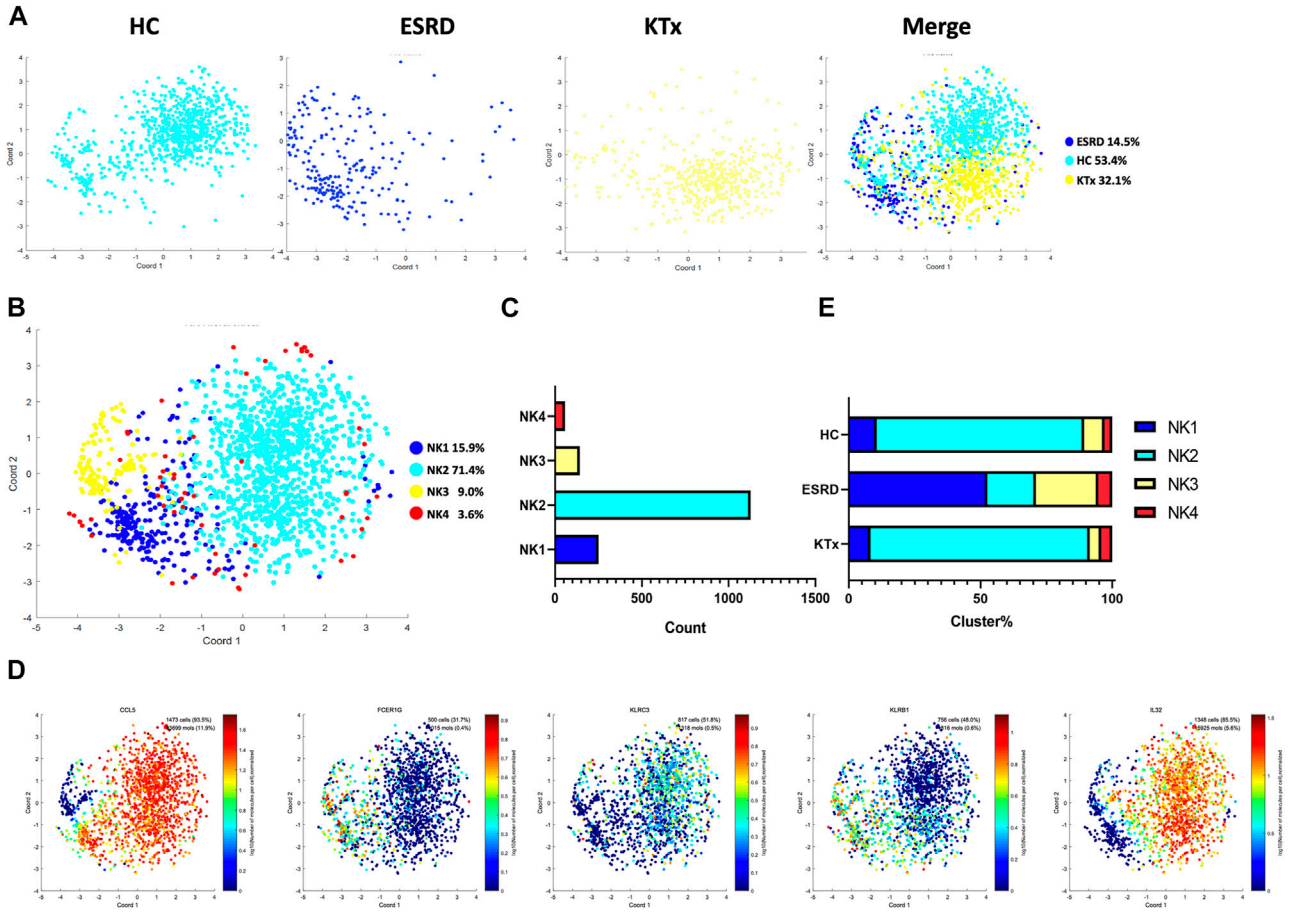

FIGURE 3 | NK-cell clusters in PBMCs from HC, ESRD, and KTx. **(A,B)** tSNE of single-cell profile with each cell color coded for NK-cell subsets. **(C)** Cell count of 4 NK-cell subsets. **(D)** Expression of highly expressed genes in each NK-cell cluster. **(E)** Proportion of 4 NK-cell subsets.

IGLC3^{low}IGKC^{high}TCL1A^{-} B Cells Were Significantly Suppressed in KTx Patients

Four B-cell subpopulations were defined by scRNA-seq (**Figures 5A,B**) given as follows: the B1 cluster (IGLC3^{high}IGKC^{low}TCL1A^{+}), B2 cluster (IGLC3^{high}IGKC^{low}TCL1A^{-}), B3 cluster (IGLC3^{low}IGKC^{high}TCL1A^{+}), and B4 cluster (IGLC3^{low}IGKC^{high}TCL1A^{-}). The specific markers and distribution in each cluster are shown in **Figure 5C,D**, **Supplementary Figures S6A,B**. Interestingly, our analysis showed that the KTx group had a significantly lower B4 percentage than the HC group (**Figure 5E**). To further verify this change, we detected the proportion of B4 cells by flow cytometry and found that the B4 cluster (IGLC3^{low}IGKC^{high}TCL1A^{-}) was significantly reduced in the KTx group compared with the HC group (**Figures 6A,B**). In addition, the B4 cluster highly expressed the characteristic T-cell gene TRAC (**Figure 5F**).

IGLC3^{low}IGKC^{high}TCL1A^{-} B Cells Might Have Potential Activated and Proliferous Effects

To further verify the function of the B4 cluster (IGLC3^{low}IGKC^{high}TCL1A^{-}), we performed the KEGG pathway analysis and found that the B4 cluster was closely related to primary immunodeficiency (**Figure 7A**). Further investigation found that IL7R, also known as CD127, was the key gene (**Figure 7B**). CD127 plays an important role in the development of T cells and B cells, and positively regulate the survival and the response to antigens of T cells (Dooms, 2013). We found that the expression of CD127 on B4 cluster in the KTx group was very obvious compared with that observed for the fluorescence minus one (FMO) control (**Figure 7C**). The high expression of CD127 showed that B4 cluster represented as the activated and proliferous B-cell subset, which is inhibited in kidney recipients caused by immunosuppressant treatment.

The pseudotime analysis was used to analyze the "physical relationship" among the B-cell subsets. B cells could be divided into five fate states (**Figures 7D,E**). Among them, the B4 cluster (IGLC3^{low}IGKC^{high}TCL1A^{-}) was regarded as an end point of the genetic relationship (**Figure 7F**) and was directly differentiated from the B3 cluster (IGLC3^{low}IGKC^{high}TCL1A^{+}) (**Figure 7F**). The BEAM analysis was used to explore the key compartments necessary for B4 cluster differentiation. At the fate decision point 2, IL32 and TRAC were specifically marked as hot genes (**Figure 7G**).

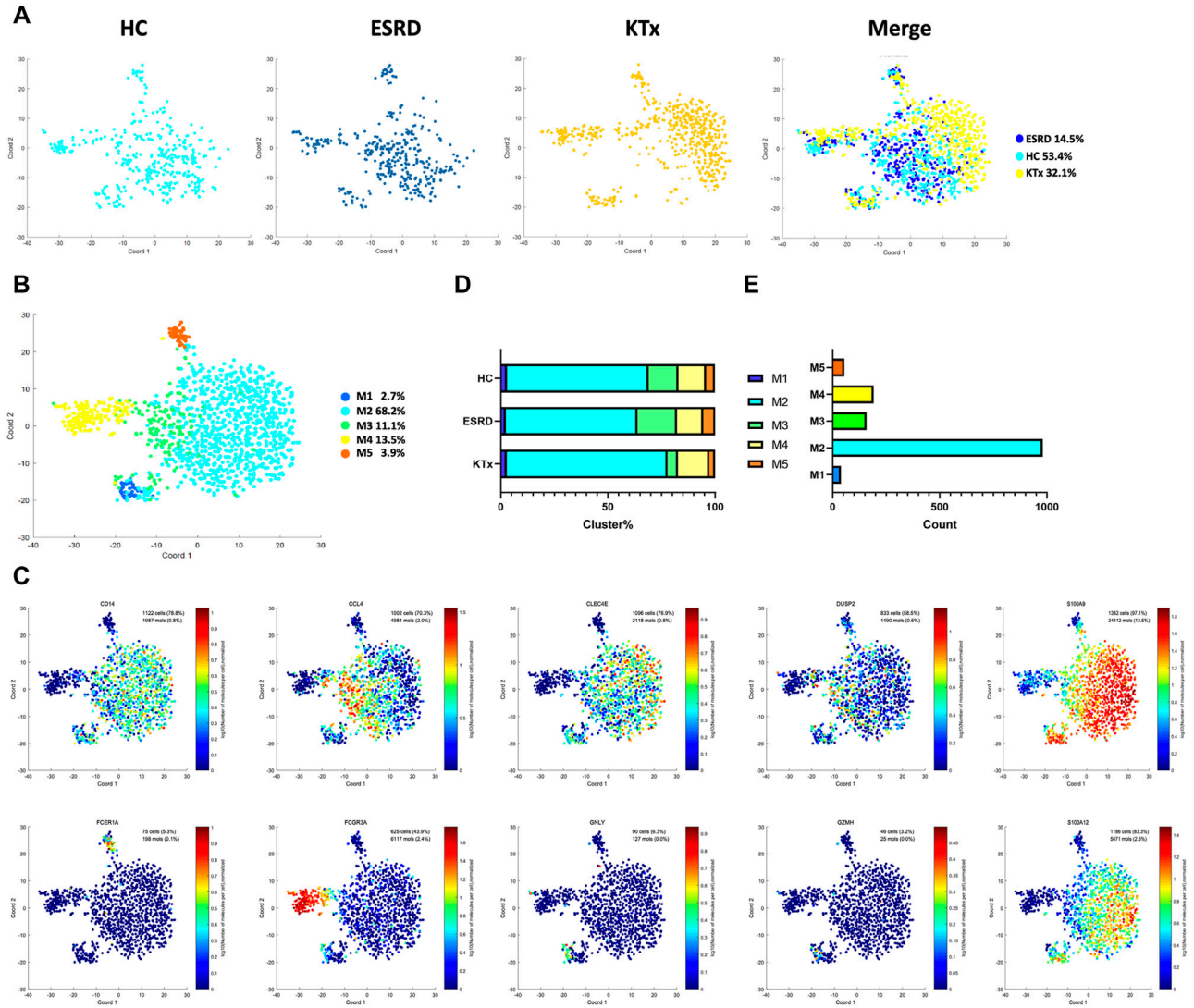

FIGURE 4 | Myeloid clusters in PBMCs from HC, ESRD, and KTx. **(A,B)** tSNE of single-cell profile with each cell color coded for myeloid subsets. **(C)** Expression of highly expressed genes in each myeloid cluster. **(D)** Proportion of 5 myeloid subsets. **(E)** Cell count of 5 myeloid subsets.

DISCUSSION

Using PBMC scRNA-seq, flow cytometric, and bioinformatic analyses, we found that in renal allograft patients with immune accommodation, T, myeloid, and B cells but not NK cells could be affected by immunosuppressants. Among these cell types, a newly identified B-cell subset, the B4 cluster ($CD19^{+}IGLC3^{low}IGKC^{high}TCL1A^{-}CD127^{+}$), was affected the most. More importantly, the expression of IL7R (CD127) in this subgroup showed that the B4 cluster might have an activated potential.

With its high resolution, single-cell sequencing greatly improves the ability to identify rare immune cells and can more comprehensively describe the functions of immune cells (Nguyen et al., 2018). At present, studies have shown the important roles of B-cell subpopulations in inflammatory bowel disease and noted that B cells significantly remodel the phenotype in the course of disease development (Castro-Dopico et al., 2020). In addition, Park et al. (2021) found that in *Dabie bandavirus*–infected individuals, B cells are greatly expanded and that SFTSV infection can suppress the maturation of high-affinity antibodies and inhibit neutralizing antibodies secreted by plasma B cells, leading to a large amount of viral replication and subsequent death. In addition, through the single-cell sequencing technology, Sutton et al. (2021) found that SARS-CoV exists in malaria-infected patients. The phenotypic B-cell subpopulation was characterized by a $CD21^{-}CD27^{-}$ or $CD21^{-}CD27^{+}$ phenotype, which represents an immune-exhausted phenotype. These findings represent the contribution of single-cell sequencing to the understanding of the functional diversity of B cells, especially in immune-related diseases.

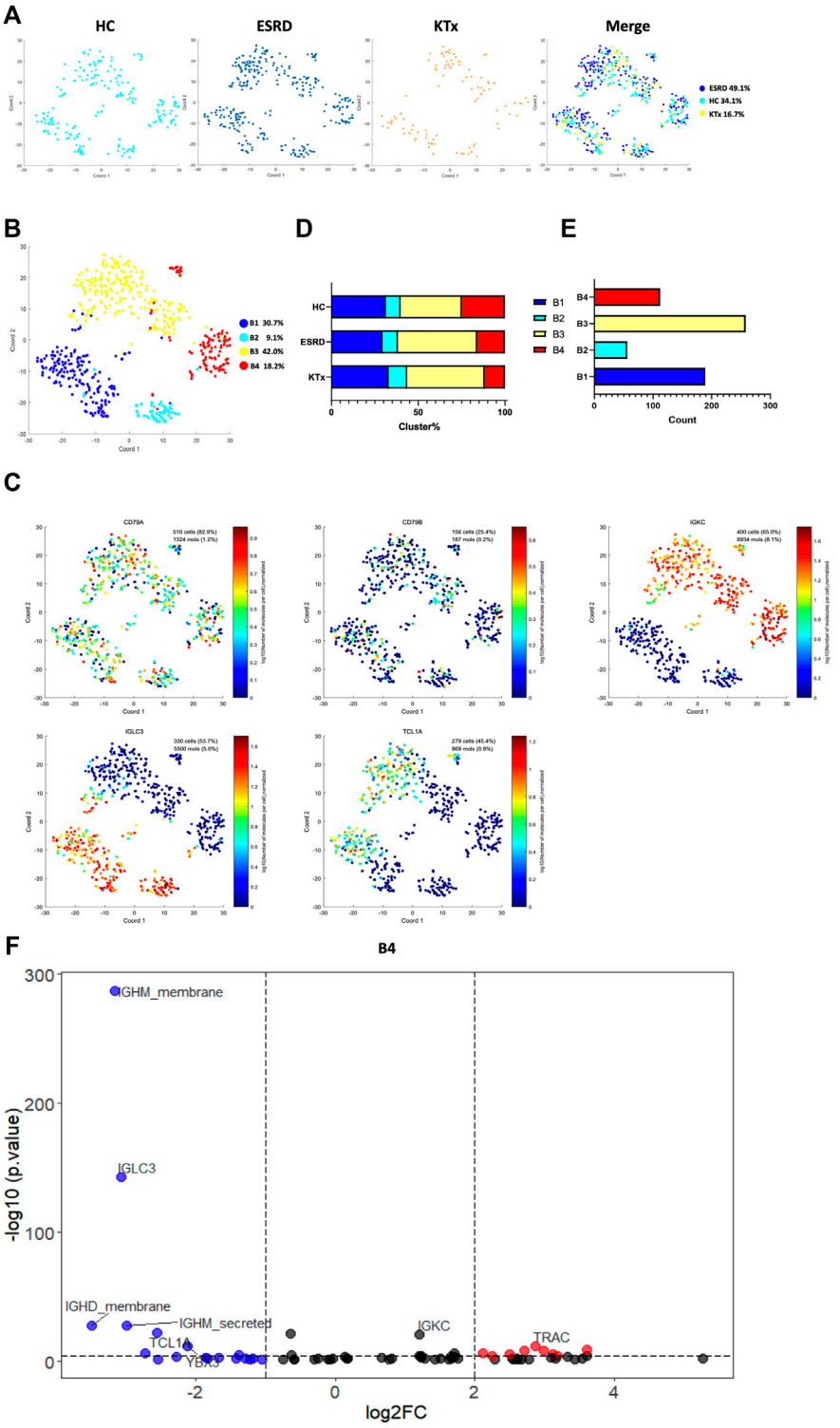

FIGURE 5 | B-cell clusters in PBMCs from HC, ESRD, and KTx. **(A,B)** tSNE of single-cell profile with each cell color coded for B-cell subsets. **(C)** Expression of highly expressed genes in each B-cell cluster. **(D)** Distribution of 5 B-cell subsets. **(E)** Cell count of 4 B-cell subsets. **(F)** Gene fingerprint expression volcano map of B4 cluster.

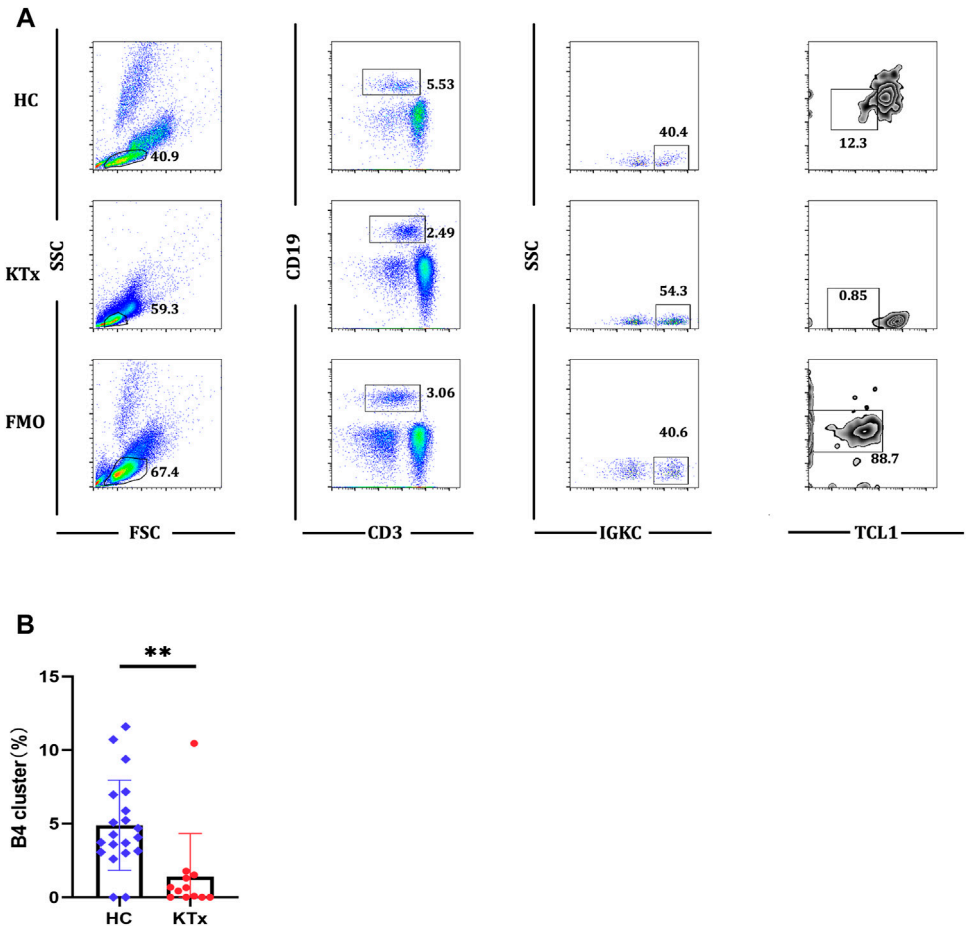

FIGURE 6 | Flow cytometric analysis of B4 cluster in HC and KTx groups. **(A)** Gating strategy and flow cytometric plots of B4 cluster in HC, KTx, and FMO control groups. **(B)** Frequency of $CD19^{+}IGKC^{+}IGLC^{-}$B4 cluster from $CD19^{+}$ B cells in HC and KTx groups. A Mann–Whitney test was used to analyze the differences between two groups. $^{**}p < 0.01$.

Kidney transplantation is the most common solid organ transplantation operation. Due to the implantation of an allograft and the use of immunosuppressive agents, kidney transplantation has a relatively great impact on the recipient's immune system. In fact, some researchers have already used single-cell sequencing to test the immune status of kidney transplant recipients with rejection. Varma et al. (2021) found that in rejected renal allografts, allogeneic infiltrated myeloid cells differentiated from monocytes into proinflammatory macrophages. The trajectory analysis showed a unique interaction with allogeneic renal parenchymal cells, and the Axl expression on myeloid cells played a major role in promoting intragraft myeloid cell and T-cell differentiation. Lei et al. (2020) identified the most important pathogenic effect of cathepsin S (Cat-S)–expressing monocytes by single-cell sequencing. In addition, Liu et al. (2020) found increased collagen- and extracellular matrix component-expressing myofibroblasts in the human kidneys undergoing chronic rejection, which indicates that renal fibrosis plays an important pathological role in rejection. These findings not only deepen our understanding of the immunoregulatory process in allograft rejection but also indicate the great potential of single-cell sequencing technology in investigating rare and novel immune cell subgroups and analyzing the interactions between immune cells and transplant parenchymal cells.

In our study, we focused on the so-called immune accommodation state in kidney transplant recipients to obtain a deeper understanding of the immune status of these recipients. Here, we discovered a new type of B-cell subgroup ($IGLC3^{low}IGKC^{high}TCL1A^{-}$). This subpopulation is characterized by a unique IG chain composition and a low expression of TCL1A, which is considered a stable B-cell marker in kidney transplant patients (Heidt et al., 2015). In addition, IGKC is regarded as a prognostic marker in breast cancer (Pandey et al., 2014), which means that the genotype of the light chain region may be related to the immune status and function of B cells.

In the $IGLC3^{low}IGKC^{high}TCL1A^{-}$ B-cell cluster, a small number of cells were found to express IL7R (CD127). IL7 provides survival signals to T cells and plays an important role in autoimmune diseases. Also, IL7R is indispensable for B-cell

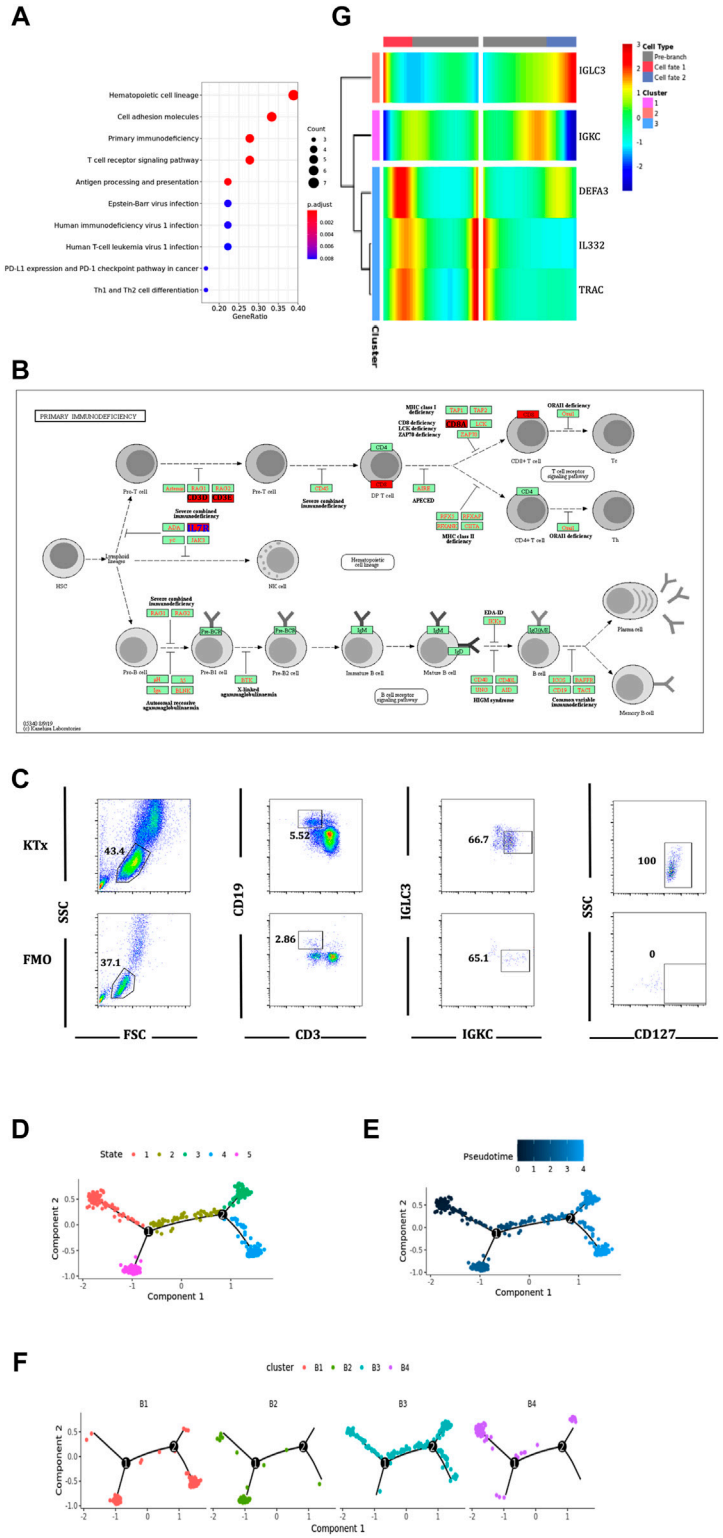

FIGURE 7 | Function and differentiation analysis of B4 cluster. **(A)** KEGG analysis of highly expressed genes on B4 cluster. **(B)** In the primary immunodeficiency pathway, IL7R was the key gene. **(C)** Flow cytometric analysis of $CD19^{+}IGKC^{+}IGLC^{-}CD127^{+}$ B cells from lymphocytes in KTx group. **(D–F)** Packages monocle2 was used for pseudotime analysis of B-cell subset differentiation. **(G)** BEAM analysis of B4 cluster fate point.

lymphopoiesis. Alhaj Hussen et al. (2017) reported the existence of $CD127^+$ early lymphoid progenitors can differentiate into NK cells, ILCs, and B cells but lack the potential to differentiate into T cells. IL7 and IL7Rα–deficient mice showed arrested B-cell development in the bone marrow. An early lymphocyte expansion is severely impaired in IL7R–deficient mice, and lymphopenia in IL7 gene-knockout mice identified IL7 as a nonredundant cytokine. This proved that $CD127^+$ B cells may represent a B-cell subgroup with a proliferation potential and suggest that the suppressive effect of B4 subset may be the reason for the decrease in the proportion and absolute count of B cells in kidney transplant recipients. Furthermore, we explored whether there are interventions that can induce the differentiation of $IGLC3^{low}IGKC^{high}TCL1A^-$ B cells. As mentioned above, through pseudotime and BEAM analysis, we discovered the important roles of IL32 and TRAC in this process. In particular, researchers have reported that IL32γ enhances host immunity to *Mycobacterium tuberculosis* in mice. Besides, increased IL32 was found in giant cell arteritis with enhanced B-cell survival and expansion. Although there is currently no complete evidence to prove the causality between IL32 and B cells, but we predicted that IL32 might be a potential proliferation factor for B cells. Correspondingly, we did not find any reports on TRAC in B cells, so the functions and roles of TRAC in the differentiation and development of B cells need to be further explored.

There were also some limitations to our study. We did not conduct further *in vitro* experiments to verify the activated potential of $CD19^+IGLC3^{low}IGKC^{high}TCL1A^-CD127^+$ B cells and evaluate whether IL32 could induce $CD19^+IGLC3^{low}IGKC^{high}TCL1A^-CD127^+$ B-cell differentiation. We will try to investigate these issues in our future research. In addition, there was only one specimen included in each single-cell sequencing group, but we did verify most of our findings through multiple-sample flow cytometry.

CONCLUSION

By scRNA-seq, flow cytometric, and bioinformatic analyses, we found that the level of a novel B-cell subset ($CD19^+IGLC3^{low}IGKC^{high}TCL1A^-CD127^+$) in renal transplant recipients with accommodation was significantly lower than that in healthy people and that this B-cell subset showed an activated potential because of its high expression of CD127. This study might reveal the effects of IS commonly used in clinical practice on B-cell subsets and the related mechanism.

DATA AVAILABILITY STATEMENT

The data presented in the study are deposited in the NCBI Gene Expression Omnibus database repository (https://www.ncbi.nlm.nih.gov/geo/query/acc.cgi?accGSE175429), accession number (GSE175429).

ETHICS STATEMENT

The studies involving human participants were reviewed and approved by the Institutional Review Board (Ethics Committee) of the Third Xiangya Hospital, Central South University (No. 2018-S347). The patients/participants provided their written informed consent to participate in this study. Written informed consent was obtained from the individual(s) for the publication of any potentially identifiable images or data included in this article.

AUTHOR CONTRIBUTIONS

Study was conceived and designed by QZ and YM. Statistical analyses were performed by HL, BP, and QZ. Software package was prepared by YL and HC. Flow cytometry was performed by YL and YZ. Manuscript was written by QZ, HL, and SL. QZ and HL contributed equally to this study.

FUNDING

This study was supported by grants of the National Natural Science Foundation of China (81700658) and the Hunan Provincial Natural Science Foundation-Outstanding Youth Foundation (2020JJ3058).

SUPPLEMENTARY MATERIAL

The Supplementary Material for this article can be found online at: https://www.frontiersin.org/articles/10.3389/fphar.2021.706580/full#supplementary-material

REFERENCES

Alhaj Hussen, K., Vu Manh, T. P., Guimiot, F., Nelson, E., Chabaane, E., Delord, M., et al. (2017). Molecular and Functional Characterization of Lymphoid Progenitor Subsets Reveals a Bipartite Architecture of Human Lymphopoiesis. *Immunity*. 47 (4), 680–696.e8. doi:10.1016/j.immuni.2017.09.009

Castro-Dopico, T., Colombel, J. F., and Mehandru, S. (2020). Targeting B Cells for Inflammatory Bowel Disease Treatment: Back to the Future. *Curr. Opin. Pharmacol.* 55, 90–98. doi:10.1016/j.coph.2020.10.002

Dooms, H. (2013). Interleukin-7: Fuel for the Autoimmune Attack. *J. Autoimmun.* 45, 40–48. doi:10.1016/j.jaut.2013.06.007

Dulken, B. W., Buckley, M. T., Navarro Negredo, P., Saligrama, N., Cayrol, R., Leeman, D. S., et al. (2019). Single-cell Analysis Reveals T Cell Infiltration in Old Neurogenic Niches. *Nature.* 571 (7764), 205–210. doi:10.1038/s41586-019-1362-5

Fishman, J. A. (2013). Opportunistic Infections-Ccoming to the Limits of Immunosuppression? *Cold Spring Harb Perspect. Med.* 3 (10), a015669. doi:10.1101/cshperspect.a015669

Garcia de Mattos Barbosa, M., Cascalho, M., and Platt, J. L. (2018). Accommodation in ABO-Incompatible Organ Transplants. *Xenotransplantation* 25 (3), e12418. doi:10.1111/xen.12418

García-González, P. A., Schinnerling, K., Sepúlveda-Gutiérrez, A., Maggi, J., Mehdi, A. M., Nel, H. J., et al. (2017). Dexamethasone and Monophosphoryl Lipid A Induce a Distinctive Profile on Monocyte-Derived Dendritic Cells through Transcriptional Modulation of Genes Associated with Essential Processes of the Immune Response. *Front. Immunol.* 8, 1350. doi:10.3389/fimmu.2017.01350

Heidt, S., Vergunst, M., Anholts, J. D., Reinders, M. E., de Fijter, J. W., Eikmans, M., et al. (2015). B Cell Markers of Operational Tolerance Can Discriminate Acute Kidney Allograft Rejection from Stable Graft Function. *Transplantation.* 99 (5), 1058–1064. doi:10.1097/tp.0000000000000465

Lei, Y., Ehle, B., Kumar, S. V., Müller, S., Moll, S., Malone, A. F., et al. (2020). Cathepsin S and Protease-Activated Receptor-2 Drive Alloimmunity and Immune Regulation in Kidney Allograft Rejection. *Front Cel Dev Biol.* 8, 398. doi:10.3389/fcell.2020.00398

Lim, M. A., Kohli, J., and Bloom, R. D. (2017). Immunosuppression for Kidney Transplantation: Where Are We Now and where Are We Going? *Transpl. Rev (Orlando).* 31 (1), 10–17. doi:10.1016/j.trre.2016.10.006

Liu, Y., Hu, J., Liu, D., Zhou, S., Liao, J., Liao, G., et al. (2020). Single-cell Analysis Reveals Immune Landscape in Kidneys of Patients with Chronic Transplant Rejection. *Theranostics.* 10 (19), 8851–8862. doi:10.7150/thno.48201

Nguyen, A., Khoo, W. H., Moran, I., Croucher, P. I., and Phan, T. G. (2018). Single Cell RNA Sequencing of Rare Immune Cell Populations. *Front. Immunol.* 9, 1553. doi:10.3389/fimmu.2018.01553

Pandey, J. P., Kistner-Griffin, E., Black, L., Namboodiri, A. M., Iwasaki, M., Kasuga, Y., et al. (2014). IGKC and FcγR Genotypes and Humoral Immunity to HER2 in Breast Cancer. *Immunobiology.* 219 (2), 113–117. doi:10.1016/j.imbio.2013.08.005

Parajuli, S., Mandelbrot, D. A., Aziz, F., Garg, N., Muth, B., Mohamed, M., et al. (2018). Characteristics and Outcomes of Kidney Transplant Recipients with a Functioning Graft for More Than 25 Years. *Kidney Dis. (Basel).* 4 (4), 255–261. doi:10.1159/000491575

Park, A., Park, S. J., Jung, K. L., Kim, S. M., Kim, E. H., Kim, Y. I., et al. (2021). Molecular Signatures of Inflammatory Profile and B-Cell Function in Patients with Severe Fever with Thrombocytopenia Syndrome. *mBio.* 12 (1), e02583. doi:10.1128/mBio.02583-20

Pont, F., Tosolini, M., and Fournié, J. J. (2019). Single-Cell Signature Explorer for Comprehensive Visualization of Single Cell Signatures across scRNA-Seq Datasets. *Nucleic Acids Res.* 47 (21), e133. doi:10.1093/nar/gkz601

Romano, M., Fanelli, G., Albany, C. J., Giganti, G., and Lombardi, G. (2019). Past, Present, and Future of Regulatory T Cell Therapy in Transplantation and Autoimmunity. *Front. Immunol.* 10, 43. doi:10.3389/fimmu.2019.00043

Snijders, M. L. H., Varol, H., van der Zwan, M., Becker, J. U., Hesselink, D. A., Baan, C. C., et al. (2020). Molecular Analysis of Renal Allograft Biopsies: Where Do We Stand and where Are We Going? *Transplantation.* 104 (12), 2478–2486. doi:10.1097/tp.0000000000003220

Sutton, H. J., Aye, R., Idris, A. H., Vistein, R., Nduati, E., Kai, O., et al. (2021). Atypical B Cells Are Part of an Alternative Lineage of B Cells that Participates in Responses to Vaccination and Infection in Humans. *Cell Rep.* 34 (6), 108684. doi:10.1016/j.celrep.2020.108684

Varma, E., Luo, X., and Muthukumar, T. (2021). Dissecting the Human Kidney Allograft Transcriptome: Single-Cell RNA Sequencing. *Curr. Opin. Organ. Transpl.* 26 (1), 43–51. doi:10.1097/mot.0000000000000840

Xiong, X., Kuang, H., Ansari, S., Liu, T., Gong, J., Wang, S., et al. (2019). Landscape of Intercellular Crosstalk in Healthy and NASH Liver Revealed by Single-Cell Secretome Gene Analysis. *Mol. Cel.* 75 (3), 644–660.e5. doi:10.1016/j.molcel.2019.07.028

Yu, G., Wang, L. G., Han, Y., and He, Q. Y. (2012). clusterProfiler: an R Package for Comparing Biological Themes Among Gene Clusters. *OMICS.* 16 (5), 284–287. doi:10.1089/omi.2011.0118

Zhuang, Q., Li, H., Yu, M., Peng, B., Liu, S., Luo, M., et al. (2020). Profiles of B-Cell Subsets in Immunologically Stable Renal Allograft Recipients and End-Stage Renal Disease Patients. *Transpl. Immunol.* 58, 101249. doi:10.1016/j.trim.2019.101249

Zhuang, Q., Peng, B., Wei, W., Gong, H., Yu, M., Yang, M., et al. (2019). The Detailed Distribution of T Cell Subpopulations in Immune-Stable Renal Allograft Recipients: a Single center Study. *PeerJ.* 7, e6417. doi:10.7717/peerj.6417

Conflict of Interest: The authors declare that the research was conducted in the absence of any commercial or financial relationships that could be construed as a potential conflict of interest.

Publisher's Note: All claims expressed in this article are solely those of the authors and do not necessarily represent those of their affiliated organizations, or those of the publisher, the editors and the reviewers. Any product that may be evaluated in this article, or claim that may be made by its manufacturer, is not guaranteed or endorsed by the publisher.

frontiers in Pharmacology

ORIGINAL RESEARCH
published: 12 October 2021
doi: 10.3389/fphar.2021.714643

Blood Immune Cell Composition Associated with Obesity and Drug Repositioning Revealed by Epigenetic and Transcriptomic Conjoint Analysis

Jia-Chen Liu[1†], Sheng-Hua Liu[1†], Guang Fu[2], Xiao-Rui Qiu[1], Run-Dong Jiang[1], Sheng-Yuan Huang[1], Li-Yong Zhu[3] and Wei-Zheng Li[3]**

[1]Center of Biomedical Informatics and Genomics, Xiangya Medical College of Central South University, Changsha, China, [2]Department of Gastroenterology, The First Affiliated Hospital of University of South, Hengyang, China, [3]Department of General Surgery, Third Xiangya Hospital, Central South University, Changsha, China

OPEN ACCESS

Edited by:
Ning Hou,
Guangzhou Medical University, China

Reviewed by:
Zan Li,
Ludong University, China
Antonio Neme,
National Autonomous University of Mexico, Mexico

***Correspondence:**
Li-Yong Zhu
zly8128@126.com
Wei-Zheng Li
zhnfy-Daniel@csu.edu.cn

[†]These authors have contributed equally to this work

Specialty section:
This article was submitted to Inflammation Pharmacology, a section of the journal Frontiers in Pharmacology

Received: 25 May 2021
Accepted: 13 August 2021
Published: 12 October 2021

Citation:
Liu J-C, Liu S-H, Fu G, Qiu X-R, Jiang R-D, Huang S-Y, Zhu L-Y and Li W-Z (2021) Blood Immune Cell Composition Associated with Obesity and Drug Repositioning Revealed by Epigenetic and Transcriptomic Conjoint Analysis. Front. Pharmacol. 12:714643. doi: 10.3389/fphar.2021.714643

This research was designed to analyze the composition of immune cells in obesity and identify novel and potent drugs for obesity management by epigenetic and transcriptomic conjoint analysis. DNA methylation data set (GSE166611) and mRNA expression microarray (GSE18897) were obtained from the Gene Expression Omnibus database. A total of 72 objects (35 obese samples and 37 controls) were included in the study. Immune cell composition analysis, drug repositioning, and gene set enrichment analysis (GSEA) were performed using CIBERSORT, connectivity map (CMap), and GSEA tools. Besides, we performed a single-cell RNA-seq of the immune cells from whole blood samples obtained from one obese patient and one healthy control. mRNA levels of drug target genes were analyzed by qPCR assay in blood samples from six patients and six healthy controls. Immune cell composition analysis found that CD8 + T cells and NK cells were significantly lower in the obese group. 11 drugs/compounds are considered to possess obesity-control potential, such as atorvastatin. Moreover, the expression of drug targets (*STAT3, MCL1, PMAIP1, SOD2, FOX O 3, FOS, FKBP5*) in obese patients were higher than those in controls. In conclusion, immune cells are potential therapeutic targets for obesity. Our results also contribute to accelerate research on drug development of obesity.

Keywords: obesity, drug repositioning, epigenomics, transcriptomics, immunity, inflammation

INTRODUCTION

Obesity is a chronic metabolic disease caused by the interaction of genetic, environmental, and other factors. Recent data from the 2017–2018 National Health and Nutrition Examination Survey (NHANES) suggest the age-adjusted prevalence of obesity among United States adults was 42.4% and exerted an increasing trend year by year (Fryar and Afful, 2020a; Fryar and Afful, 2020b). As a leading mortality risk factor for Type 2 Diabetes (T2D), coronary heart disease, and other chronic diseases, obesity imposes a considerable economic burden on our medical system and the whole society. For example, a meta-analysis of 97 studies, including 1.8 million participants, suggested that obesity has been linked to an increased risk of coronary heart disease and stroke

(Lu et al., 2014). Besides, Epidemiological surveys show that the annual expenditure on obesity and related conditions in the United States is between 147 and 210 billion United States dollars (Cawley and Meyerhoefer, 2012). Therefore, there is an urgent need to address the substantial social burden caused by obesity.

Obesity is a complex disorder caused by the imbalance between energy intake and expenditure (Leeners et al., 2017). Notably, low-grade inflammation is a crucial characteristic of obesity, resulting in the heterogeneity of immune cell composition and polarization (Hotamisligil, 2006; Han and Levings, 2013). Besides, various studies have indicated that obesity-related inflammation is associated with the occurrence of insulin resistance (Kanda et al., 2006; Weisberg et al., 2006), which is a leading risk for T2D and cardiovascular diseases, and the most common and severe complication of obesity (Kochanek et al., 2020).

The continuity and multi-process of obesity make it more lucid to explain the entire development process of obesity at multiple levels (Conway and Rene, 2004; Yan et al., 2018). Notably, multi-omics analysis (Hasin et al., 2017), including epigenomics, transcriptomics, etc., provides an opportunity to better understand the progression of complex diseases (Lee et al., 2020; Yang et al., 2020). For example, a recent study by Zhang et al. (Zhang et al., 2015) which used integration of biological data across genomics, metabolomics, and microbiomics, found that gut microbiota dysbiosis may be an essential cause of genetic and simple obesity in children.

Given the high prevalence rates, economic burden, and complex pathological mechanism, there has been a surge of interest in the effects of obesity pharmacotherapy. The updated guidelines indicated the limitations of existing weight-loss drugs, which suggested an urgent need for drugs with better efficacy and lower prices (Apovian et al., 2015). Due to the high cost and high-level risk of traditional drug development (DiMasi et al., 2010), multi-omics-based drug repositioning may provide a novel approach to solve the problem (Barh et al., 2020). Since the repositioned drugs usually have completed formulation development and even early clinical development (Ashburn and Thor, 2004), their safety in preclinical models and humans is guaranteed (Nosengo, 2016; Pushpakom et al., 2019).

Based on previous research, in this study, we first downloaded the epigenomes and transcriptomes microarray dataset of obesity from the Gene Expression Omnibus (GEO) database. In GSE166611, the study of Nonino et al. comparing methylation patterns between normal weight (n = 17) and obese women (n = 15) in peripheral blood, which sought to confirm that an obesogenic lifestyle can promote epigenetic changes in the human DNA. In GSE18897, Ghosh et al. (Ghosh et al., 2011) carried out whole-genome expression profiling of whole blood from 60 obese samples and 20 controls. Subsequently, we used EpiDISH and CIBERSORT to reveal the immune cell composition associate with obesity and provide insights into the interplay between host immune response and pathogenesis of obesity. Based on this, drug repositioning screening was performed to identify potential therapeutic agents for obesity, which may shed light in the field of pharmacological intervention of obesity.

METHODS

Microarray Data Source

The gene methylation profiling datasets (GSE166611) and gene expression profiling datasets (GSE18897), were downloaded from Gene Expression Omnibus (https://www.ncbi.nlm.nih.gov/geo) in the National Center for Biotechnology Information (NCBI). In total, whole blood samples from 20 obese samples and 20 controls were enrolled in GSE18897 (platform: GPL570 Affymetrix Human Genome U133 Plus 2.0 Array). In GSE18897 (GPL13534 Illumina HumanMethylation450 BeadChip), out of 32 peripheral blood samples, 15 were obese, and 17 were normal weight.

Data Process

DNA methylation microarray data and gene expression profiles data were pre-processed by R (version 4.0.5) and Biomanger packages [limma (Ritchie et al., 2015)], where raw data were background corrected, log-transformed, and quantile normalized. Finally, differentially expressed genes (DEGs) were screened out with $p < 0.05$ and LogFC > 1 as the cut-off criteria.

Immune Cell Composition Calculation Based on DNA Methylation Data

Immune cell fraction based on DNA methylation data was predicted by EpiDISH algorithm (Teschendorff et al., 2017). The proportion of immune cells between normal samples and obese samples were presented via Bar plots and violin plots, which were all generated in R using ggplot2 package.

Functional Enrichment Analysis and Pathway Enrichment Analysis

Gene ontology (GO) analysis and Kyoto Encyclopedia of Genes and Genomes (KEGG) pathway enrichment analysis were performed using Hiplot (https://hiplot.com.cn/). GSEA was performed using GSEA 4.1.0 (http://www.broadinstitute.org/gsea).

Immune Cell Composition Calculation Based on mRNA Expression Profile Data

Immune cells in obese samples was assessed by applying the "Cell type Identification By Estimating Relative Subsets Of RNA Transcripts" (CIBERSORT) deconvolution algorithm (Newman et al., 2015). We set 100 permutations and $p < 0.05$ as the criteria for the successful deconvolution of a sample. Besides, the gene expression signature matrix of six immune cells was obtained from the CIBERSORT platform (https://cibersortx.stanford.edu/).

Single Cell RNA-Sequencing Analysis

Heparinized blood was mixed with equal volume of PBS buffer (PBS +2% FBS + 2 mm EDTA) and was gently overlaid on density gradient media (Ficoll-Paque Premium 1.073, GE Healthcare, United States) in 15 ml tubes, with volume ratio (blood to media) of 0.75 and Peripheral Blood Mononuclear Cells (PBMCs) were extracted according to manufacturer's

TABLE 1 | The sequences of RT-PCR primers.

	Forward	Reverse	Amplicon size
STAT3	CAGCAGCTTGACACACGGTA	AAACACCAAAGTGGCATGTGA	150
MCL1	TGCTTCGGAAACTGGACATCA	TAGCCACAAAGGCACCAAAAG	135
PMAIP1	ACCAAGCCGGATTTGCGATT	ACTTGCACTTGTTCCTCGTGG	121
SOD2	GGAAGCCATCAAACGTGACTT	CCCGTTCCTTATTGAAACCAAGC	116
FOXO3	CGGACAAACGGCTCACTCT	GGACCCGCATGAATCGACTAT	150
FOS	GGGGCAAGGTGGAACAGTTAT	CCGCTTGGAGTGTATCAGTCA	126
FKBP5	AATGGTGAGGAAACGCCGATG	TCGAGGGAATTTTAGGGAGACT	250
GAPDH	ACAACTTTGGTATCGTGGAAGG	GCCATCACGCCACAGTTTC	—

protocol. Remaining red blood cells were removed by red blood cell lysis buffer (Sigma, United States). PBMC were then resuspended in 1 ml freezing media (Fetal Bovine Serum +10% DMSO), and transferred to cryopreservation tubes, and stored in liquid nitrogen.

Frozen cells were thawed and washed by PBS buffer. And Cell concentration was adjusted to around 1,000 cells/ul. 10X Single Cell 3′ V3 kits were used for scRNA-seq library preparation in the same batch following the manufacturer's protocol (10X Genomics, Pleasanton, CA, United States). We targeted approximately 5,000 cells in each sample and the final libraries were sequenced with pair-end on Illumina platform (Illumina, San Diego, CA, United States), with at least 50,000 reads per cell.

Raw FASTQ data were processed using the 10x Genomics CellRanger pipeline (v3.0.0) to generate a UMI count matrix. After alignment, downstream normalization, scaling and clustering of data were processed using the Seurat package (version 3.0.0) (Fryar and Afful, 2020b) in R (version 3.6.0). Low-quality cells (such as doublets, cells with high expression of mitochondria-associated genes (>20%) were removed. Red blood cells and remaining neutrophils were also removed. t-distributed stochastic neighbor embedding (tSNE) was used for data visualization. The function of FindAllMarkers in Seruat was used to get differentially expressed genes with fold change >0.25 and Bonferroni-adjusted $p < 0.01$ was considered statistically significant.

Drug Repositioning

Potential drugs for the management of obesity were selected using the Connectivity Map (CMap) database (https://www.broadinstitute.org/connectivity-map-cmap). CMap is an online tool to identify molecular drugs highly correlated with diseases; the link between the query genes and chemicals was measured with connectivity score ranged from −1 to one and $p < 0.05$. All of the predicted targets were included for the DGIdb and L1000 FWD databases as no threshold was provided. Drug-target and protein-protein interactions among these targets, collected from the STITCH (https://stitch.embl.de/), were used to construct a drug-target interaction network and visualized using Cytoscape v3.8.2.

RNA Isolation and RT-PCR Analyses

The total RNA was isolated using RNA extraction kit (TIANGEN) and reverse transcribed into cDNA using reverse transcription kit (ABI). Quantitative real-time PCR analysis was performed using real-time PCR kit (ABI). The relative mRNA expression levels of STAT3, MCL1, PMAIP1, SOD2, FOXO3, FOS, and FKBP5were normalized with the GADPH in the same sample. The thermal cycler parameters for the amplification of these genes were as follows: one cycle at 95°C for 10 min followed by 40 cycles at 95°C for 15 s, 60°C for 15 s and 72°C for 30 s. Gene expression was evaluated by the 2−ΔΔCt method. The sequences of RT-PCR primers are the following (5–3′, **Table 1**).

RESULTS

The Identification of Methylated-Differentially Genes and the Composition of Immune Cells in Obesity

Analysis of the methylation profiles by the EpiDISH algorithm was used to estimate the proportion of obesity-related immune cell composition. There was no significant difference in the immune cell composition between normal and obese populations (**Figure 1A**).

Then, we conducted gene set enrichment analysis (GSEA) to determine the biological processes modulated by DNA methylation in obese patients. The results showed the low-density lipoprotein particle remodeling, positive regulation of calcium ion import, and cyclic nucleotide phosphodiesterase activity genes were significantly enriched in the obesity groups (**Figure 1B**). Besides, pathway enrichment analysis revealed a variety of signaling pathways in which fatty acid metabolism and histidine metabolism may be relevant to the pathology of obesity (**Figure 1C**).

The Immune Cell Composition Status From Transcriptomes of the Obese Cohort

The immune composition in obese and control was analyzed by the CIBERSORT algorithm (**Figure 2A**). The results showed that the proportion of immune cells was different in each subgroup. Among these, CD8 + T cells and NK cells was significantly lower in the obese group.

GSEA results showed that arachidonic acid secretion, acyl CoA binding, and phospholipase a2 activity were closely correlated with obesity (**Figure 2B**). Pathway enrichment analysis revealed significant enrichment for the TGF-β signaling pathway and p53 signaling pathway (**Figure 2C**). Besides, enrichment of immune signatures was further analyzed using GSEA, and results showed that immunologic signatures most correlated with NeuromedinU, TGF-β, IL-4 (**Figure 2D**).

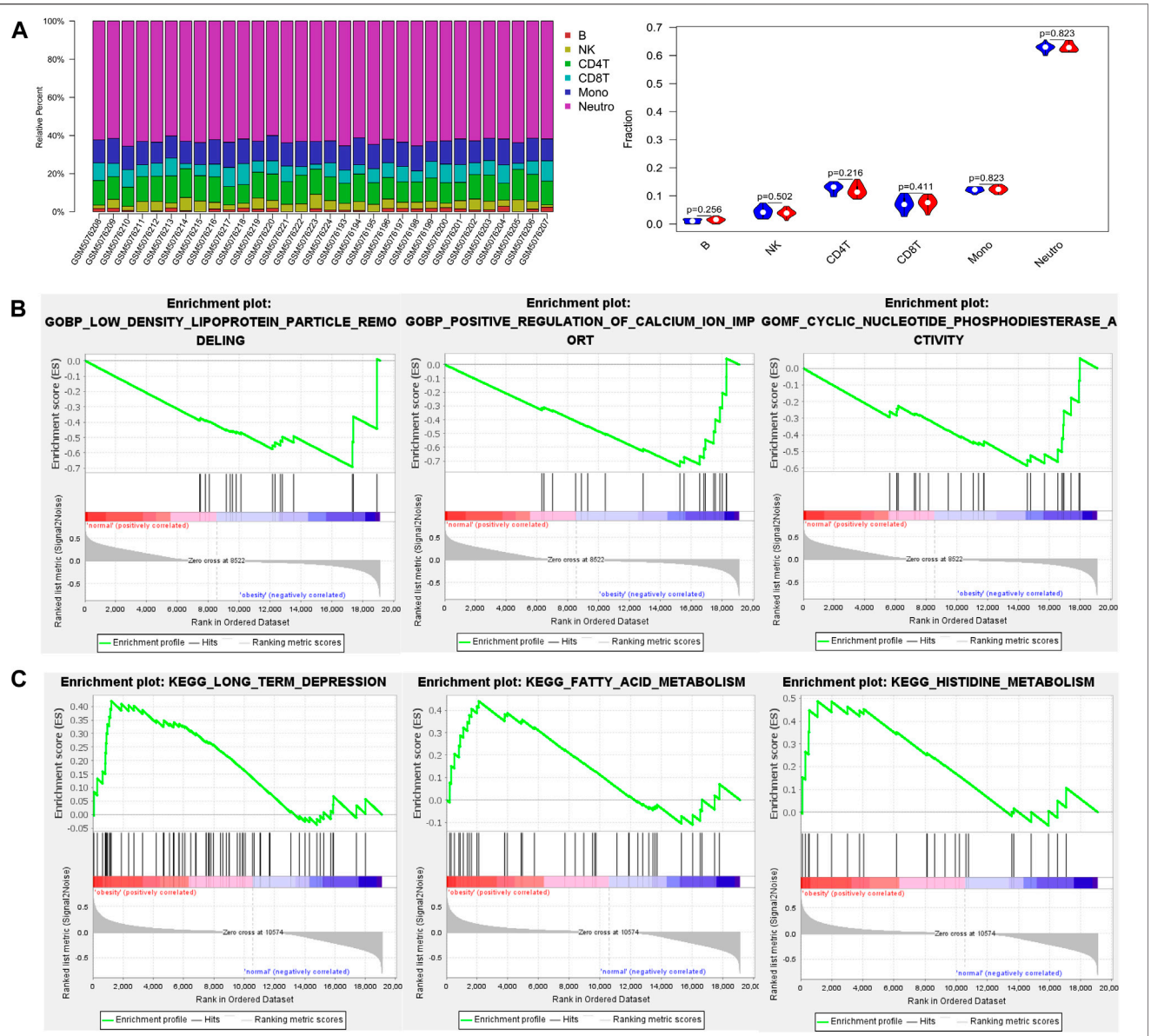

FIGURE 1 | The proportion of immune cells and gene set enrichment analysis (GSEA) results based on DNA methylation profiles between normal and obese samples **(A)** The proportion of immune cells between normal and obese samples. The quantified contrast of the distribution of obesity-related immune cell subtypes and the difference in immune composition in each obesity and control tissues sample **(B)** Enrichment plots from gene set enrichment analysis (GSEA). The low-density lipoprotein particle remodeling, positive regulation of calcium ion import, and cyclic nucleotide phosphodiesterase activity genes were significantly enriched in obesity groups **(C)** Clustering of KEGG pathways identified by GSEA analysis. Pathway enrichment analysis revealed a variety of signaling pathways in which fatty acid metabolism and histidine metabolism may be relevant to the pathology of obesity.

Enrichment Analysis of Immune Cells Using Single-Cell RNA-Sequencing Reference Data

We performed single-cell sequencing of one obese patient and one healthy control. Enrichment analysis of B cells (**Figure 3A**), CD8 + T cells (**Figure 3B**), CD4 + T cells (**Figure 3C**), NK cells (**Figure 3D**), Monocytes (**Figure 3E**) was conducted. The enrichment analysis revealed that some common GO terms, such as MHC protein complex and response to calcium ion, were significantly enriched in various immune cell types. Besides, according to the annotation of KEGG, apoptosis and IL-17 signaling pathway were enriched in NK cells and CD4 + cells, which were negatively associated with obesity based on the above findings.

Drug Repurposing Based on Gene Expression Profile

Identification of Expression Profiles of Obese Patients

A total of 204 obesity-associated genes, including 173 up-regulated genes and 31 down-regulated genes (p-value < 0.05, logFC >1) were extracted from mRNA profiles of 20 obese patients and 20 controls.

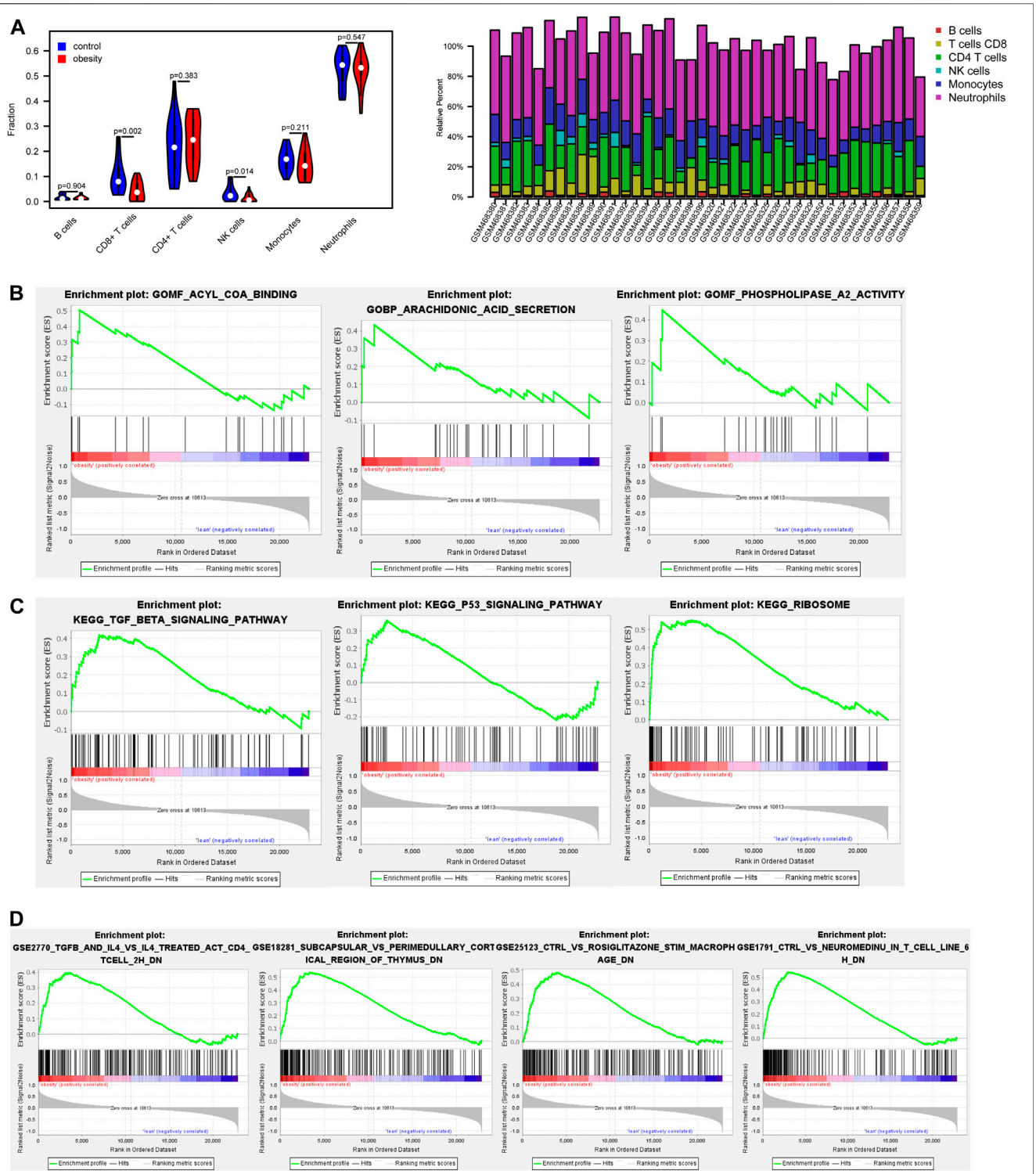

FIGURE 2 | The proportion of immune cells and gene set enrichment analysis (GSEA) results based on gene expression profiles between normal and obese samples **(A)** The proportion of immune cells between normal and obese samples. Among these, CD8 + T cells and NK cells were negatively associated with obesity **(B)** Enrichment plots from gene set enrichment analysis (GSEA). The arachidonic acid secretion, acyl CoA binding, and phospholipase a2 activity were significantly enriched in obesity groups **(C)** Clustering of KEGG pathways identified by GSEA analysis. Pathway enrichment analysis revealed TGF-β signaling pathway and p53 signaling pathway may be relevant to the pathology of obesity **(D)** Enrichment of immune signatures by GSEA analysis. Immunologic signatures most correlated with NeuromedinU, TGF-β, IL-4 in obese patients.

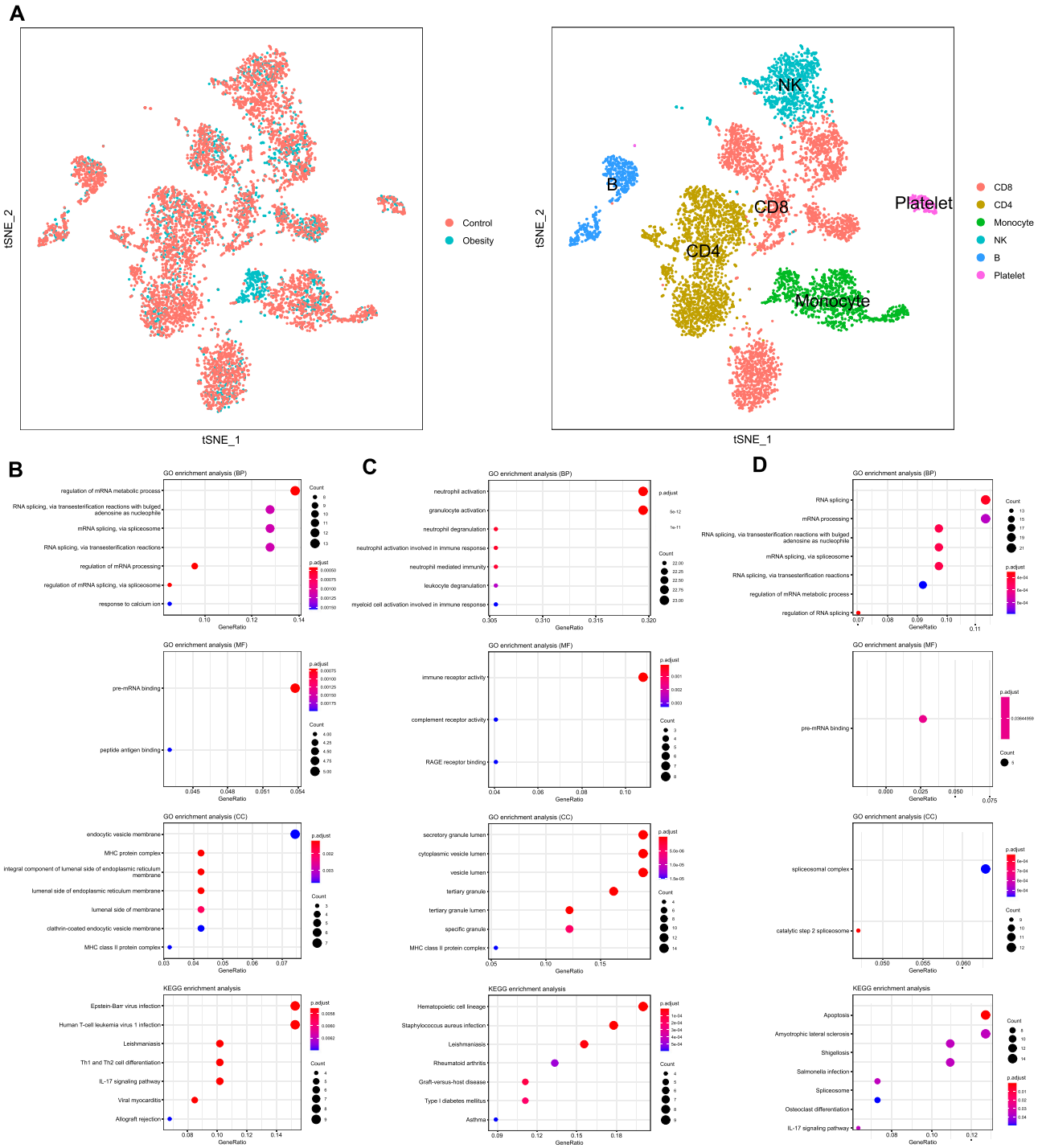

FIGURE 3 | Single-cell RNA sequencing and enrichment analysis of immune cells **(A)** TSNE plot of PBMCs from different groups and different cell type **(B)** Enrichment analysis of B cells **(C)**Enrichment analysis of CD8 + T cells **(D)** Enrichment analysis of CD4 + T cells **(E)** Enrichment analysis of NK cells **(F)** Enrichment analysis of monocytes.

Obesity-Targeted Screening for Candidate Drugs

According to the above results, a total of 11,675 compounds were screened from the CMap, DGIdb and L1000 FWD databases (**Figure 4A**). The overlapping 12 compounds among the three databases were considered as potential drugs of obesity (**Table 2**).

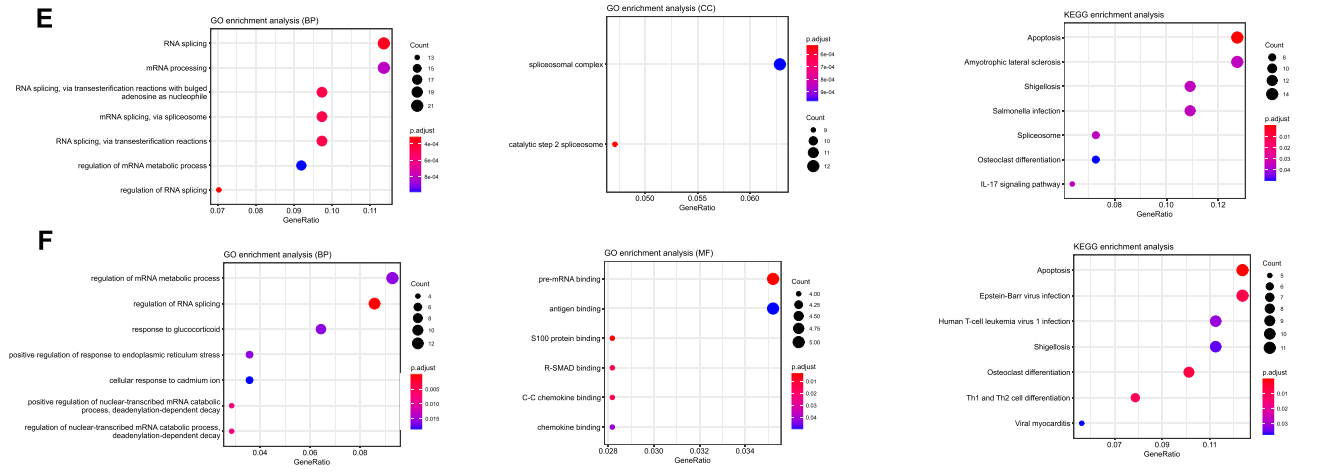

FIGURE 3 | (Continued).

Network Pharmacology Approach to Predicting the Mechanisms of Drugs Counteracts Obesity

The Collection of Pathogenic-Related Genes of Obesity

We comprehensively collected the genes associated with obesity from Online Mendelian Inheritance in Man (OMIM) database, GeneCards, and DisGeNET. Based on this, we created a final list of 2,316 pathogenic-related genes of obesity that were reported in at least two examined databases.

Identification of Drug Targets and Construction of the Drug-Targets Network

A total of 466 genes related to 11 compounds were identified using STITCH prediction (One of the compounds was excluded from the drug candidates owing to a smaller number of targets.) Among these, 201 genes belonged to pathogenic-related genes, as mentioned above. Finally, a network was constructed to display the association between the gene targets and candidate drugs (**Figure 4B**). Notably, atorvastatin was considered the most likely candidate for the treatment of obesity as 43/50 of gene targets were overlapping with pathogenic-related genes. Besides, through consulting literature, atorvastatin is closely related to the progress of obesity. Therefore, the target genes of atorvastatin were further analyzed by GO and KEGG analyses (**Figure 4C**). The results show that atorvastatin may affect the redistribution of lipids, thereby influencing the development of obesity.

Screening and Identification of the Hub Genes

To further examine the drug targets, we focused on 201 drug targets and find that seven genes, *STAT3, MCL1, PMAIP1, SOD2, FOXO3, FOS, FKBP5* were overlapping with differential genes from single-cell sequencing (**Figure 4D**). Expression of selected genes was subjected to real-time quantitative PCR (RT-qPCR) verification from six obese patients and six controls, which revealed that the expression of the corresponding mRNAs was all up-regulated in obese patients (**Figure 4E**).

DISCUSSION

Methylation signals in the blood may serve as surrogate markers for immune cells and provide molecular insight into immune-related diseases such as obesity. In this study, we performed GSEA to determine the different biological functional states of obese and normal samples. In the obesity group, the enriched GO terms were mainly focused on low-density lipoprotein (LDL) particle remodeling, cyclic nucleotide phosphodiesterase activity, and positive regulation of calcium ion import. The result is consistent with those of Roderick FDJ et al. (King et al., 2008), which compared the phenotype and composition changes of LDL-c particles before and after the weight loss of nine obese children. They found that the LDL-c III particles and their relative cholesterol concentration decreased significantly, while the proportion of type II and type I particles increased. In addition, a study by Xue et al. (Xue et al., 2001) indicated that through activating phosphodiesterase activity to promote the degradation of cAMP, calcium ions in fat cells could reduce the phosphorylation of hormone-sensitive lipase, thereby inhibiting lipolysis. Based on the KEGG database, we found the enrichment in various metabolic pathways in the obesity group, such as fatty acid metabolism and histidine metabolism. Many studies have proved that the increase of free fatty acids can enhance insulin resistance and increase the expression of pro-inflammatory cytokines to aggravate obesity (Boden et al., 2002; Itani et al., 2002). Moreover, a vicious cycle may be created by increasing plasma-free fatty acids, which can inhibit the anti-lipolytic effect of insulin and promote the release of free fatty acids (Jensen et al., 1989). Besides, an imbalance in the ratio of n-6/n-3 polyunsaturated fatty acids (PUFAs) may lead to adipose tissue hyperplasia (Ailhaud et al., 2008). Similarly, there is

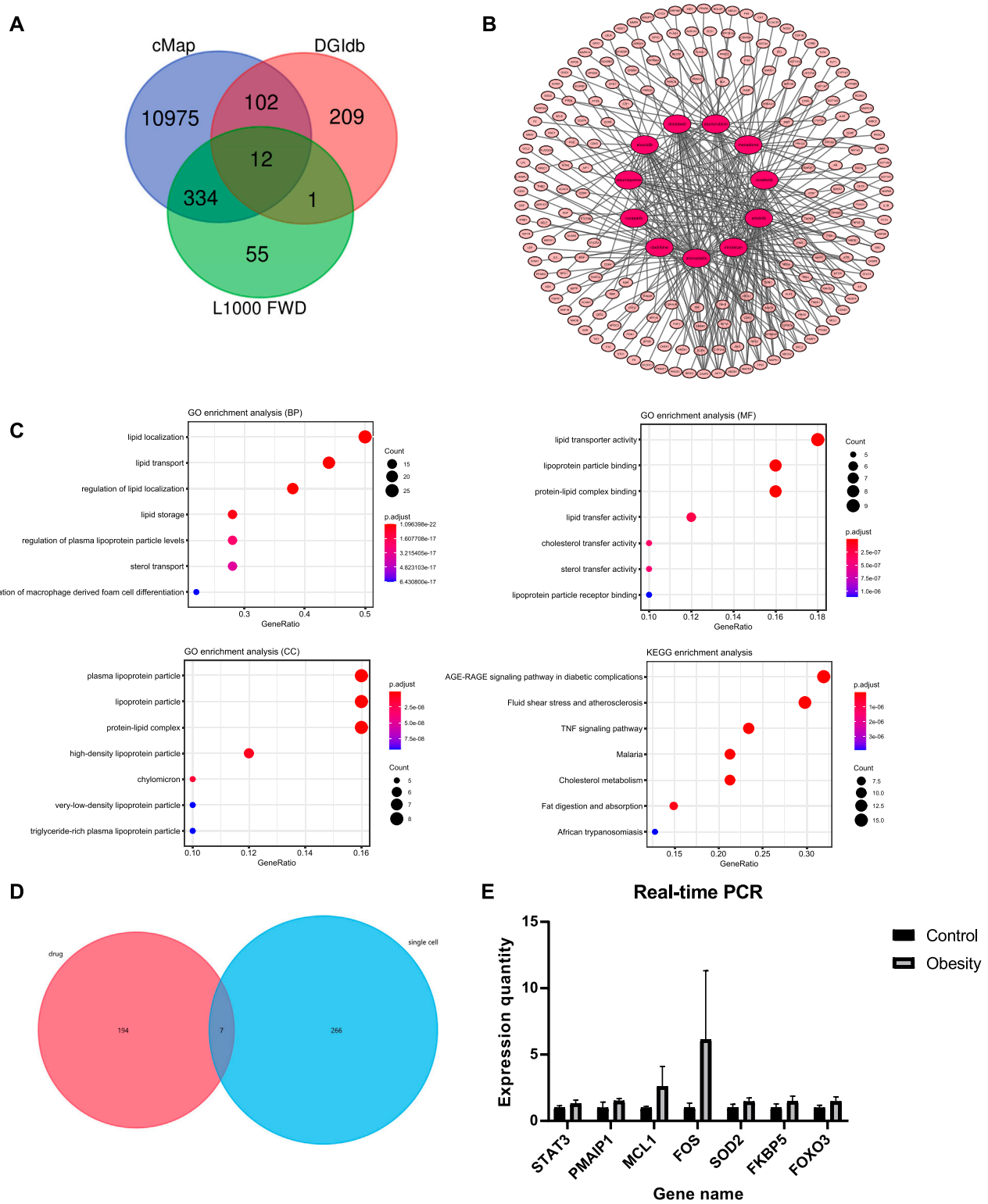

FIGURE 4 | Drug repositioning and network pharmacology analysis **(A)** The screening results in CMap, DGIdb, and L1000 FWD databases; 12 repeated compounds were shared among all three databases **(B)** Pharmacology-network of the "drugs-targets-disease"; The red ellipse represent drugs. The pink ellipse represents drug targets of genes **(C)** GO and KEGG analyses of target genes of atorvastatin **(D)** Screening of the hub genes; seven genes among 201 drug targets (*STAT3, MCL1, PMAIP1, SOD2, FOX O 3, FOS, FKBP5*) were overlapping with differential genes from single-cell sequencing **(E)** Quantitative real-time PCR analysis of hub genes (n = 2 for each group); The expression of the corresponding mRNAs was all up-regulated in obese patient.

TABLE 2 | Eleven chemicals were identified as potential interventions for obesity.

Generic name	Associated conditions	Adverse effects	Price
Daunorubicin	Acute Lymphocytic Leukemia Acute Myeloid Leukemia Acute erythroid leukemia Acute monocytic leukemia Newly diagnosed Therapy-Related Acute Myeloid Leukemia	Sores Trouble swallowing Dry mouth Bad breath Altered sense of taste Nausea	163.01 USD/4 ml
Menadione	Factor II deficiency Vitamin B12 Deficiency	Hemolytic anemia Brain damage	5.59 USD/5 mg
Docetaxel	Esophageal Cancers Ewing's Sarcoma Locally Advanced Breast Cancer Metastatic Bladder Cancer Metastatic Breast Cancer Metastatic Hormone Refractory Prostate Cancer Node Positive Breast Cancer Ovarian Cancer Metastatic Small Cell Lung Cancer	Black, tarry stools Bleeding gums Blood in the urine or stools Chest pain Chills Diarrhea Heartburn Dizziness Hoarseness Irritation	477.37 USD/0.5 vial
Alvocidib (Flavopiridol)	Esophageal cancer Leukemia Lung cancer Liver cancer	Nausea Fatigue Hepatic dysfunction Myelosuppression	11.4 USD/mg
Staurosporine	Acute Myeloid Leukemia (AML) Aggressive Systemic Mastocytosis Systemic Mastocytosis with Associated Hematological Neoplasm	Abdominal or stomach cramps or pain Accumulation of pus Backache Nasal congestion Nausea	156.1 USD/mg
Rucaparib	Advanced Ovarian Cancer Fallopian tube cancer Prostate cancer with an abnormal BRCA gene	Low blood cell counts Shortness of breath Cold symptoms such as stuffy nose, sneezing, Sore throat Stomach pain Nausea Vomiting	21.4 USD/mg
Cladribine	Chronic Lymphocytic Leukaemia Cutaneous T-Cell Lymphoma Hairy Cell Leukemia Non-Hodgkin's Lymphoma	Hives Difficult breathing Headache Fever Unusual bleeding Night sweats	102.78 USD/10 mg
Atorvastatin	Anginal Pain Cardiovascular Disease Coronary Artery Disease Coronary artery thrombosis Dysbetalipoproteinemia Fredrickson Type III lipidemia High Cholesterol Hospitalizations Hypertriglyceridemias Postoperative Thromboembolism Primary Hypercholesterolemia	Joint pain Stuffy nose Sore throat Diarrhea	Tablet: 5.0 USD/20 mg
Irinotecan	Esophageal Cancers Ewing's Sarcoma Glioblastomas Malignant Neoplasm of Pancreas Malignant Neoplasm of Stomach Metastatic Colorectal Carcinoma Non-Small Cell Lung Carcinoma	Fever Mouth sores Low blood cell counts Diarrhea Constipation Nausea Vomiting	138.07 USD/2 ml

(Continued on following page)

TABLE 2 | (*Continued*) Eleven chemicals were identified as potential interventions for obesity.

Generic name	Associated conditions	Adverse effects	Price
	Ovarian Cancer Rhabdomyosarcomas Small Cell Lung Cancer	Stomach pain Loss of appetite Weight loss	
Erlotinib	Locally Advanced Non-Small Cell Lung Cancer Locally Advanced Pancreatic Cancer Metastatic Non-Small Cell Lung Cancer Non-Small Cell Lung Carcinoma Pancreatic Cancer Metastatic	Burning, tingling, numbness or pain in the hands, arms, feet, or legs Cough Hoarseness Diarrhea (severe) Difficult or labored breathing Fever or chills Lower back or side pain Rash (severe) Sensation of pins and needles Stabbing chest pain	Tablet: 163.98 USD/ 150 mg
Sorafenib	Advanced Renal Cell Carcinoma Gastrointestinal Stromal Tumors Hemangiosarcoma Unresectable Hepatocellular Carcinoma Locally recurrent refractory to radioactive iodine treatment Thyroid carcinoma Metastatic refractory to radioactive iodine treatment	Bleeding Feeling tired Vomiting Diarrhea Nausea Stomach pain High blood pressure Rash Weight loss Thinning hair	Tablet: 66.61 USD/ 200 mg

evidence that a diet high in omega-6 fatty acids during the perinatal period would cause accumulation of body fat in offspring (Massiera et al., 2010). On the other hand, histidine is an essential amino acid, which proper supplementation has a positive effect on resisting obesity-related inflammation. Animal-based studies have shown that supplementing histidine can significantly increase the expression of the anti-inflammatory factor adiponectin by activating PPARg. Additionally, another anti-inflammatory mechanism of histidine is manifested in its inhibition of the transfer of the p65 subunit of NF-kB to the nucleus, which can reduce the stimulation of IL-6 and other pro-inflammatory factors, thereby improving the inflammation of obesity (Sun et al., 2014). Thus, histidine metabolism disorder may be associated with the progression of obesity-related inflammation, which is worth exploring.

In the present study, we aimed to clarify potential pathways of obesity development through analyzing transcriptomics data. The GO terms were enriched in arachidonic acid secretion, Acyl CoA binding, and phospholipase A2 activity. Interestingly, they seem to be included in the same story. Acyl-CoA synthase can indirectly enhance the uptake of exogenous arachidonic acid (DiRusso and Black, 1999). The endogenous arachidonic acid is mainly released from cell membrane phospholipids. This process is catalyzed by the phospholipase A2 (PLA2) superfamily of enzymes and is induced by various cell activation signals, including inflammatory stimuli and so on (Dennis et al., 2011). Corresponding to the foregoing, arachidonic acid is an omega-6 polyunsaturated fatty acid, and the instability of its secretion may lead to the massive production of pro-inflammatory eicosanoids and thus aggravate the state of obesity (Saini and Keum, 2018). In the current study, the information of metabolic pathways obtained from the KEGG database revealed that the TGF-β signaling pathway, p53 signaling pathway, and ribosome are enriched in the obese cohort. A recent study by Hariom et al. (Yadav et al., 2011) suggested that blocking the TGF-β/Smad3 pathway would reduce fat mass by down-regulating the expression of adipocyte-specific genes and reducing the infiltration of pro-inflammatory macrophages. Besides, Shjie et al. (Liu et al., 2017) found that the expression of c-MYC was increased in high-fat-fed mice whose RPL11 binding was disrupted, thereby up-regulating the biogenesis of ribosomes and promoting nutrient absorption through the RPL11-MDM2-p53 pathway, resulting in obesity-related metabolic changes. Besides, the composition of immune cells might be related to the state of obesity. The results of GSEA based on immunity and immunology showed that the level and status of immune cells such as macrophages, CD4 + T cells, CD8 + T cells, and B cells have changed during the progress of obesity, which also involves cytokines such as IL-4.

One interesting finding is the immune cell composition status from transcriptomes of the obese cohort. The results showed a significant decrease in CD8 + T cells and NK cells in the obese group compared with the control group. This finding is different from the accepted conclusion that the infiltration of CD8 + T cells and NK cells in the adipose tissue of obese patients is increased (Chatzigeorgiou et al., 2012). The possible reason is the samples we analyzed are blood samples instead of adipose tissue, which may have lost the activation effect of adipose tissue-derived factors on the relevant immune cells.

The results of single-cell sequencing reflected the enrichment of the differentially expressed genes of the five immune cells based on the GO and KEGG databases. The result revealed that B cells is mainly implicated in MHC protein complex, endocytic vesicle

membrane, and clathrin-coated endocytic vesicle membrane. The binding of the antigen to the B cell receptor (BCR) initiates B cell activation, triggers BCR endocytosis, and recruits peripheral vesicles containing MHC class II to the lysosomal-like antigen processing chamber containing the antigen BCR. The internalized antigens are processed into peptides in these compartments and produce peptide-MHC class II complexes (Raposo et al., 1996), transported to the plasma membrane for recognition by CD4 + T cells for subsequent immune response (Lankar et al., 2002). In addition, the process by which IL-23 can stimulate CD4 + T cells to secrete IL-17 pro-inflammatory factors has been confirmed (Harrington et al., 2005), which corresponds to the result of the IL-17 signaling pathway in the KEGG pathway enrichment. Besides, apoptosis is significantly enriched in CD8 + and CD4 + T cells and NK cells. Fas and Fas ligand (FasL) induce apoptosis of immune cells (Restifo, 2000), which are rapidly expressed after the TCR/CD3 complex of primary T cells is activated by the peptide antigen presented by MHC class II or MHC class I. The data taken from Alderson et al. showed that activated CD8 + and CD4 + T cells express high amounts of FasL and are susceptible to Fas antibody-mediated apoptosis, thereby limiting the expansion of the immune response (Alderson et al., 1995). Thus, the results suggested that apoptosis may play a significant role in maintaining immune homeostasis and reducing inflammation in obese patients, which needs future studies to improve knowledge. Furthermore, the enrichment results of KEGG also indicated an association among osteoclast differentiation and CD4 + and CD8 + T cells. A previous study provides strong evidence for this result, which proves that similar to the role of B cells, osteoclasts are professional antigen-presenting cells (APCs), which can present antigens through MHC protein complex and activate CD4 + and CD8 + T cells (Li et al., 2010). Conversely, it seems that CD8 + T cells can inhibit the production of cytokines that stimulate osteoclast differentiation by producing certain inhibitors (John et al., 1996). The complex feedforward and feedback mechanisms between osteoclasts and CD4 + and CD8 + T cells may be one reason for the number of T cells and the secretion of related cytokines.

Furthermore, the results of qPCR analysis validated our bioinformatic analyses that the expression of selected genes was all up-regulated, which significantly reflects the complex regulation of the inflammatory state in obese patients. Recalling previous animal studies that identified macrophage-intrinsic miR-17–92 family miRNAs promote FOS expression by inhibiting the YY1 protein, thereby maintaining the optimum expression of the anti-inflammatory cytokine IL-10 (Zhang et al., 2020). Moreover,a study of animal models suggested that the differentiation of Th17 cells and the production of IL-17 of *Bat f*$^{-/-}$ mice with normal expression of AP-1 transcription factor composed of Jun, Fos, and MAF was inhibited. It provided evidence that FOS has an inhibitory effect on the secretion of pro-inflammatory factors by CD4 + T cells (Schraml et al., 2009). Thus, the high expression of FOS in obese patients may be negative feedback to persistent low-grade inflammation. In the present study, as expected, the increased expression of STAT3 in the obese group promotes obesity through the IL-23/STAT3/Th17 axis. The primary downstream molecule of the IL-23 signal pathway is STAT3 (Parham et al., 2002), which can facilitate the development of Th17 cells by activating RORC, thereby promoting the release of pro-inflammatory cytokines such as IL-17 to induce inflammation (Isono et al., 2014). Besides, since IL-27 can activate STAT3, STAT3 also appears to be contained in the IL-27-mediated up-regulation of IL-10 (Stumhofer et al., 2007).

Due to the lack of effective/safe and less expensive drugs, drug repositioning appears to be the best tool for finding proper targets and predicting latent drugs in the therapy for obesity and related complications. Finally, 12 compounds were predicted to have potential therapeutic effects on obesity (Table 2) Among these, atorvastatin is a class of cholesterol-lowering drugs that inhibit the enzyme 3-hydroxy-3-methylgluteryl CoA reductase, which are the first choices for treating the hyperlipidemia (Shitara and Sugiyama, 2006). In addition, animal-based studies have shown that atorvastatin can restrain adipose tissue inflammation by inhibiting the activation of nuclear factor-κB and its activation inducers (Furuya et al., 2010; Yamada et al., 2017), indicating its pleiotropic effect on obesity control. Furthermore, its low price among these therapeutic agents makes it more conducive to being accepted by patients. As reported in a previous study concerning the effect of alvocidib on preventing inflammation, alvocidib could block the infiltration of leukocytes and their interaction with endothelial cells by preventing the activation of endothelial cells (Schmerwitz et al., 2011).

Concerning the research methods, some limitations need to be acknowledged. One of them was the lack of detection indicators or the small sample size, which may lead to the high probability of negative results in differential DNA methylation. Besides, the limitations of algorithms made an overall conclusion about the relationship between immune cell composition extremely difficult. In addition, the drugs we have found are conclusions based on systems biology methods, which are needed to be validated by animal models or cohort studies in the future. Notwithstanding these limitations, this work offers valuable insights into exploring inflammation during obesity through a multi-omics approach and developing novel clinical management of obesity.

CONCLUSION

The principal findings of this research are that CD8 + T cells and NK cells were significantly lower in the obese group calculated by CIBERSORT. 12 drugs/compounds are considered to possess obesity-control potential, such as atorvastatin. Moreover, *STAT3, MCL1, PMAIP1, SOD2, FOXO3, FOS, FKBP5* may play an essential role in the genesis and growth of obesity and might serve as a possible therapeutic target.

DATA AVAILABILITY STATEMENT

The original contributions presented in the study are publicly available. This data can be found here: https://www.ncbi.nlm.nih.

gov/geo/query/acc.cgi?acc=GSE166611 and https://www.ncbi.nlm.nih.gov/geo/query/acc.cgi?acc=GSE18897

ETHICS STATEMENT

The studies involving human participants were reviewed and approved by IRB of the third Xiangya hospital of central south university expedited approval. The patients/participants provided their written informed consent to participate in this study.

AUTHOR CONTRIBUTIONS

J-CL: Conceptualization, Methodology, Software. S-HL: Writing—Original draft, Writing—Review and Editing. GF: Formal analysis, Validation. X-RQ: Visualization. R-DJ: Software, Resources. S-YH: Writing—Reviewing and Editing. L-YZ: Supervision, W-ZL: Project administration.

FUNDING

This work was supported by a grant from the Natural Science Foundation of Hunan Province (grant number 2020JJ5856), and the National undergraduate innovation training project (2020105330289).

SUPPLEMENTARY MATERIAL

The Supplementary Material for this article can be found online at: https://www.frontiersin.org/articles/10.3389/fphar.2021.714643/full#supplementary-material.

REFERENCES

Ailhaud, G., Guesnet, P., and Cunnane, S. C. (2008). An Emerging Risk Factor for Obesity: Does Disequilibrium of Polyunsaturated Fatty Acid Metabolism Contribute to Excessive Adipose Tissue Development? *Br. J. Nutr.* 100 (3), 461–470. doi:10.1017/s0007114508911569

Alderson, M. R., Tough, T. W., Davis-Smith, T., Braddy, S., Falk, B., Schooley, K. A., et al. (1995). Fas Ligand Mediates Activation-Induced Cell Death in Human T Lymphocytes. *J. Exp. Med.* 181 (1), 71–77. doi:10.1084/jem.181.1.71

Apovian, C. M., Aronne, L. J., Bessesen, D. H., McDonnell, M. E., Murad, M. H., Pagotto, U., et al. (2015). Pharmacological Management of Obesity: an Endocrine Society Clinical Practice Guideline. *J. Clin. Endocrinol. Metab.* 100 (2), 342–362. doi:10.1210/jc.2014-3415

Ashburn, T. T., and Thor, K. B. (2004). Drug Repositioning: Identifying and Developing New Uses for Existing Drugs. *Nat. Rev. Drug Discov.* 3 (8), 673–683. doi:10.1038/nrd1468

Barh, D., Tiwari, S., Weener, M. E., Azevedo, V., Góes-Neto, A., Gromiha, M. M., et al. (2020). Multi-omics-based Identification of SARS-CoV-2 Infection Biology and Candidate Drugs against COVID-19. *Comput. Biol. Med.* 126, 104051. doi:10.1016/j.compbiomed.2020.104051

Boden, G., Cheung, P., Stein, T. P., Kresge, K., and Mozzoli, M. (2002). FFA Cause Hepatic Insulin Resistance by Inhibiting Insulin Suppression of Glycogenolysis. *Am. J. Physiol. Endocrinol. Metab.* 283 (1), E12–E19. doi:10.1152/ajpendo.00429.2001

Cawley, J., and Meyerhoefer, C. (2012). The Medical Care Costs of Obesity: an Instrumental Variables Approach. *J. Health Econ.* 31 (1), 219–230. doi:10.1016/j.jhealeco.2011.10.003

Chatzigeorgiou, A., Karalis, K. P., Bornstein, S. R., and Chavakis, T. (2012). Lymphocytes in Obesity-Related Adipose Tissue Inflammation. *Diabetologia* 55 (10), 2583–2592. doi:10.1007/s00125-012-2607-0

Conway, B., and Rene, A. (2004). Obesity as a Disease: No Lightweight Matter. *Obes. Rev.* 5 (3), 145–151. doi:10.1111/j.1467-789X.2004.00144.x

Dennis, E. A., Cao, J., Hsu, Y. H., Magrioti, V., and Kokotos, G. (2011). Phospholipase A2 Enzymes: Physical Structure, Biological Function, Disease Implication, Chemical Inhibition, and Therapeutic Intervention. *Chem. Rev.* 111 (10), 6130–6185. doi:10.1021/cr200085w

DiMasi, J. A., Feldman, L., Seckler, A., and Wilson, A. (2010). Trends in Risks Associated with New Drug Development: success Rates for Investigational Drugs. *Clin. Pharmacol. Ther.* 87 (3), 272–277. doi:10.1038/clpt.2009.295

DiRusso, C. C., and Black, P. N. (1999). Long-chain Fatty Acid Transport in Bacteria and Yeast. Paradigms for Defining the Mechanism Underlying This Protein-Mediated Process. *Mol. Cel Biochem* 192 (1-2), 41–52. doi:10.1007/978-1-4615-4929-1_5

Fryar, C. D. C. M., and Afful, J. (2020). *Prevalence of Overweight, Obesity, and Severe Obesity Among Adults Aged 20 and over: United States, 1960–1962 through 2017–2018*. NCHS Health E-Stats.

Fryar, C. D. C. M., and Afful, J. (2020). *Prevalence of Overweight, Obesity, and Severe Obesity Among Children and Adolescents Aged 2–19 Years: United States, 1963–1965 through 2017–2018*. NCHS Health E-Stats.

Furuya, D. T., Poletto, A. C., Favaro, R. R., Martins, J. O., Zorn, T. M., and Machado, U. F. (2010). Anti-inflammatory Effect of Atorvastatin Ameliorates Insulin Resistance in Monosodium Glutamate-Treated Obese Mice. *Metabolism* 59 (3), 395–399. doi:10.1016/j.metabol.2009.08.011

Ghosh, S., Dent, R., Harper, M. E., Stuart, J., and McPherson, R. (2011). Blood Gene Expression Reveal Pathway Differences between Diet-Sensitive and Resistant Obese Subjects Prior to Caloric Restriction. *Obesity (Silver Spring)* 19 (2), 457–463. doi:10.1038/oby.2010.209

Han, J. M., and Levings, M. K. (2013). Immune Regulation in Obesity-Associated Adipose Inflammation. *J. Immunol.* 191 (2), 527–532. doi:10.4049/jimmunol.1301035

Harrington, L. E., Hatton, R. D., Mangan, P. R., Turner, H., Murphy, T. L., Murphy, K. M., et al. (2005). Interleukin 17-producing CD4+ Effector T Cells Develop via a Lineage Distinct from the T Helper Type 1 and 2 Lineages. *Nat. Immunol.* 6 (11), 1123–1132. doi:10.1038/ni1254

Hasin, Y., Seldin, M., and Lusis, A. (2017). Multi-omics Approaches to Disease. *Genome Biol.* 18 (1), 83. doi:10.1186/s13059-017-1215-1

Hotamisligil, G. S. (2006). Inflammation and Metabolic Disorders. *Nature* 444 (7121), 860–867. doi:10.1038/nature05485

Isono, F., Fujita-Sato, S., and Ito, S. (2014). Inhibiting RORγt/Th17 axis for Autoimmune Disorders. *Drug Discov. Today* 19 (8), 1205–1211. doi:10.1016/j.drudis.2014.04.012

Itani, S. I., Ruderman, N. B., Schmieder, F., and Boden, G. (2002). Lipid-induced Insulin Resistance in Human Muscle Is Associated with Changes in Diacylglycerol, Protein Kinase C, and IkappaB-Alpha. *Diabetes* 51 (7), 2005–2011. doi:10.2337/diabetes.51.7.2005

Jensen, M. D., Haymond, M. W., Rizza, R. A., Cryer, P. E., and Miles, J. M. (1989). Influence of Body Fat Distribution on Free Fatty Acid Metabolism in Obesity. *J. Clin. Invest.* 83 (4), 1168–1173. doi:10.1172/jci113997

John, V., Hock, J. M., Short, L. L., Glasebrook, A. L., and Galvin, R. J. (1996). A Role for CD8+ T Lymphocytes in Osteoclast Differentiation *In Vitro*. *Endocrinology* 137 (6), 2457–2463. doi:10.1210/endo.137.6.8641199

Kanda, H., Tateya, S., Tamori, Y., Kotani, K., Hiasa, K., Kitazawa, R., et al. (2006). MCP-1 Contributes to Macrophage Infiltration into Adipose Tissue, Insulin Resistance, and Hepatic Steatosis in Obesity. *J. Clin. Invest.* 116, 1494–1505. doi:10.1172/JCI26498

King, R. F., Hobkirk, J. P., Cooke, C. B., Radley, D., and Gately, P. J. (2008). Low-density Lipoprotein Sub-fraction Profiles in Obese Children before and after Attending a Residential Weight Loss Intervention. *J. Atheroscler. Thromb.* 15 (2), 100–107. doi:10.5551/jat.e490

Kochanek, K. D., Murphy, S., Xu, J., and Arias, E. (2020). *Mortality in the United States, 2019*. NCHS Data Brief, (395) 1–8.

Lankar, D., Vincent-Schneider, H., Briken, V., Yokozeki, T., Raposo, G., and Bonnerot, C. (2002). Dynamics of Major Histocompatibility Complex Class II Compartments during B Cell Receptor-Mediated Cell Activation. *J. Exp. Med.* 195 (4), 461–472. doi:10.1084/jem.20011543

Lee, A. J., Einarsson, G. G., Gilpin, D. F., and Tunney, M. M. (2020). Multi-Omics Approaches: The Key to Improving Respiratory Health in People with Cystic Fibrosis? *Front. Pharmacol.* 11, 569821. doi:10.3389/fphar.2020.569821

Leeners, B., Geary, N., Tobler, P. N., and Asarian, L. (2017). Ovarian Hormones and Obesity. *Hum. Reprod. Update* 23 (3), 300–321. doi:10.1093/humupd/dmw045

Li, H., Hong, S., Qian, J., Zheng, Y., Yang, J., and Yi, Q. (2010). Cross Talk between the Bone and Immune Systems: Osteoclasts Function as Antigen-Presenting Cells and Activate CD4+ and CD8+ T Cells. *Blood* 116 (2), 210–217. doi:10.1182/blood-2009-11-255026

Liu, S., Kim, T. H., Franklin, D. A., and Zhang, Y. (2017). Protection against High-Fat-Diet-Induced Obesity in MDM2C305F Mice Due to Reduced P53 Activity and Enhanced Energy Expenditure. *Cell Rep* 18 (4), 1005–1018. doi:10.1016/j.celrep.2016.12.086

Lu, Y., Lu, Y., Hajifathalian, K., Ezzati, M., Woodward, M., Rimm, E. B., et al. (2014). Metabolic Mediators of the Effects of Body-Mass index, Overweight, and Obesity on Coronary Heart Disease and Stroke: a Pooled Analysis of 97 Prospective Cohorts with 1·8 Million Participants. *Lancet* 383 (9921), 970–983. doi:10.1016/s0140-6736(13)61836-x

Massiera, F., Barbry, P., Guesnet, P., Joly, A., Luquet, S., Moreilhon-Brest, C., et al. (2010). A Western-like Fat Diet Is Sufficient to Induce a Gradual Enhancement in Fat Mass over Generations. *J. Lipid Res.* 51 (8), 2352–2361. doi:10.1194/jlr.M006866

Newman, A. M., Liu, C. L., Green, M. R., Gentles, A. J., Feng, W., Xu, Y., et al. (2015). Robust Enumeration of Cell Subsets from Tissue Expression Profiles. *Nat. Methods* 12 (5), 453–457. doi:10.1038/nmeth.3337

Nosengo, N. (2016). Can You Teach Old Drugs New Tricks? *Nature* 534 (7607), 314–316. doi:10.1038/534314a

Parham, C., Chirica, M., Timans, J., Vaisberg, E., Travis, M., Cheung, J., et al. (2002). A Receptor for the Heterodimeric Cytokine IL-23 Is Composed of IL-12Rbeta1 and a Novel Cytokine Receptor Subunit, IL-23R. *J. Immunol.* 168 (11), 5699–5708. doi:10.4049/jimmunol.168.11.5699

Pushpakom, S., Iorio, F., Eyers, P. A., Escott, K. J., Hopper, S., Wells, A., et al. (2019). Drug Repurposing: Progress, Challenges and Recommendations. *Nat. Rev. Drug Discov.* 18 (1), 41–58. doi:10.1038/nrd.2018.168

Raposo, G., Nijman, H. W., Stoorvogel, W., Liejendekker, R., Harding, C. V., Melief, C. J., et al. (1996). B Lymphocytes Secrete Antigen-Presenting Vesicles. *J. Exp. Med.* 183 (3), 1161–1172. doi:10.1084/jem.183.3.1161

Restifo, N. P. (2000). Not so Fas: Re-evaluating the Mechanisms of Immune Privilege and Tumor Escape. *Nat. Med.* 6 (5), 493–495. doi:10.1038/74955

Ritchie, M. E., Phipson, B., Wu, D., Hu, Y., Law, C. W., Shi, W., et al. (2015). Limma powers Differential Expression Analyses for RNA-Sequencing and Microarray Studies. *Nucleic Acids Res.* 43 (7), e47. doi:10.1093/nar/gkv007

Saini, R. K., and Keum, Y. S. (2018). Omega-3 and omega-6 Polyunsaturated Fatty Acids: Dietary Sources, Metabolism, and Significance - A Review. *Life Sci.* 203, 255–267. doi:10.1016/j.lfs.2018.04.049

Schmerwitz, U. K., Sass, G., Khandoga, A. G., Joore, J., Mayer, B. A., Berberich, N., et al. (2011). Flavopiridol Protects against Inflammation by Attenuating Leukocyte-Endothelial Interaction via Inhibition of Cyclin-dependent Kinase 9. *Arterioscler Thromb. Vasc. Biol.* 31 (2), 280–288. doi:10.1161/atvbaha.110.213934

Schraml, B. U., Hildner, K., Ise, W., Lee, W. L., Smith, W. A., Solomon, B., et al. (2009). The AP-1 Transcription Factor Batf Controls T(H)17 Differentiation. *Nature* 460 (7253), 405–409. doi:10.1038/nature08114

Shitara, Y., and Sugiyama, Y. (2006). Pharmacokinetic and Pharmacodynamic Alterations of 3-Hydroxy-3-Methylglutaryl Coenzyme A (HMG-CoA) Reductase Inhibitors: Drug-Drug Interactions and Interindividual Differences in Transporter and Metabolic Enzyme Functions. *Pharmacol. Ther.* 112 (1), 71–105. doi:10.1016/j.pharmthera.2006.03.003

Stumhofer, J. S., Silver, J. S., Laurence, A., Porrett, P. M., Harris, T. H., Turka, L. A., et al. (2007). Interleukins 27 and 6 Induce STAT3-Mediated T Cell Production of Interleukin 10. *Nat. Immunol.* 8 (12), 1363–1371. doi:10.1038/ni1537

Sun, X., Feng, R., Li, Y., Lin, S., Zhang, W., Li, Y., et al. (2014). Histidine Supplementation Alleviates Inflammation in the Adipose Tissue of High-Fat Diet-Induced Obese Rats via the NF-Kb- and PPARγ-Involved Pathways. *Br. J. Nutr.* 112 (4), 477–485. doi:10.1017/s0007114514001056

Teschendorff, A. E., Breeze, C. E., Zheng, S. C., and Beck, S. (2017). A Comparison of Reference-Based Algorithms for Correcting Cell-type Heterogeneity in Epigenome-wide Association Studies. *BMC Bioinformatics* 18 (1), 105. doi:10.1186/s12859-017-1511-5

Weisberg, S. P., Hunter, D., Huber, R., Lemieux, J., Slaymaker, S., Vaddi, K., et al. (2006). CCR2 Modulates Inflammatory and Metabolic Effects of High-Fat Feeding. *J. Clin. Invest.* 116, 115–124. doi:10.1172/JCI24335

Xue, B., Greenberg, A. G., Kraemer, F. B., and Zemel, M. B. (2001). Mechanism of Intracellular Calcium ([Ca2+]i) Inhibition of Lipolysis in Human Adipocytes. *Faseb j* 15 (13), 2527–2529. doi:10.1096/fj.01-0278fje

Yadav, H., Quijano, C., Kamaraju, A. K., Gavrilova, O., Malek, R., Chen, W., et al. (2011). Protection from Obesity and Diabetes by Blockade of TGF-β/Smad3 Signaling. *Cell Metab* 14 (1), 67–79. doi:10.1016/j.cmet.2011.04.013

Yamada, Y., Takeuchi, S., Yoneda, M., Ito, S., Sano, Y., Nagasawa, K., et al. (2017). Atorvastatin Reduces Cardiac and Adipose Tissue Inflammation in Rats with Metabolic Syndrome. *Int. J. Cardiol.* 240, 332–338. doi:10.1016/j.ijcard.2017.04.103

Yan, J., Risacher, S. L., Shen, L., and Saykin, A. J. (2018). Network Approaches to Systems Biology Analysis of Complex Disease: Integrative Methods for Multi-Omics Data. *Brief Bioinform* 19 (6), 1370–1381. doi:10.1093/bib/bbx066

Yang, T. L., Shen, H., Liu, A., Dong, S. S., Zhang, L., Deng, F. Y., et al. (2020). A Road Map for Understanding Molecular and Genetic Determinants of Osteoporosis. *Nat. Rev. Endocrinol.* 16 (2), 91–103. doi:10.1038/s41574-019-0282-7

Zhang, C., Yin, A., Li, H., Wang, R., Wu, G., Shen, J., et al. (2015). Dietary Modulation of Gut Microbiota Contributes to Alleviation of Both Genetic and Simple Obesity in Children. *EBioMedicine* 2 (8), 968–984. doi:10.1016/j.ebiom.2015.07.007

Zhang, X., Liu, J., Wu, L., and Hu, X. (2020). MicroRNAs of the miR-17~9 Family Maintain Adipose Tissue Macrophage Homeostasis by Sustaining IL-10 Expression. *Elife* 9. e55676. doi:10.7554/eLife.55676

Conflict of Interest: The authors declare that the research was conducted in the absence of any commercial or financial relationships that could be construed as a potential conflict of interest.

Publisher's Note: All claims expressed in this article are solely those of the authors and do not necessarily represent those of their affiliated organizations, or those of the publisher, the editors and the reviewers. Any product that may be evaluated in this article, or claim that may be made by its manufacturer, is not guaranteed or endorsed by the publisher.

frontiers in Pharmacology

REVIEW
published: 18 November 2021
doi: 10.3389/fphar.2021.762334

Receptor Interacting Protein Kinases 1/3: The Potential Therapeutic Target for Cardiovascular Inflammatory Diseases

Yiming Leng[1†], *Ying Zhang*[2†], *Xinyu Li*[3], *Zeyu Wang*[3], *Quan Zhuang*[2,4*] *and Yao Lu*[1*]

[1]Clinical Research Center of the 3rd Xiangya Hospital, Central South University, Changsha, China, [2]Transplantation Center of the 3rd Xiangya Hospital, Central South University, Changsha, China, [3]Xiangya School of Medicine, Central South University, Changsha, China, [4]Research Center of National Health Ministry on Transplantation Medicine, Changsha, China

The receptor interacting protein kinases 1/3 (RIPK1/3) have emerged as the key mediators in cell death pathways and inflammatory signaling, whose ubiquitination, phosphorylation, and inhibition could regulate the necroptosis and apoptosis effectually. Recently, more and more studies show great interest in the mechanisms and the regulator of RIPK1/3-mediated inflammatory response and in the physiopathogenesis of cardiovascular diseases. The crosstalk of autophagy and necroptosis in cardiomyocyte death is a nonnegligible conversation of cell death. We elaborated on RIPK1/3-mediated necroptosis, pathways involved, the latest regulatory molecules and therapeutic targets in terms of ischemia reperfusion, myocardial remodeling, myocarditis, atherosclerosis, abdominal aortic aneurysm, and cardiovascular transplantation, etc.

Keywords: RIPK1, RIPK3, cardiovascular diseases, necroptosis, therapeutic

OPEN ACCESS

Edited by:
Chiara Bolego,
University of Padua, Italy

Reviewed by:
Sathish Kumar Natarajan,
University of Nebraska-Lincoln, United States
Fuminori Tokunaga,
Osaka City University, Japan

***Correspondence:**
Quan Zhuang
zhuangquansteven@163.com
Yao Lu
luyao0719@163.com

[†]*These authors have contributed equally to this work.*

Specialty section:
This article was submitted to Inflammation Pharmacology, a section of the journal Frontiers in Pharmacology

Received: *21 August 2021*
Accepted: *26 October 2021*
Published: *18 November 2021*

Citation:
Leng Y, Zhang Y, Li X, Wang Z, Zhuang Q and Lu Y (2021) Receptor Interacting Protein Kinases 1/3: The Potential Therapeutic Target for Cardiovascular Inflammatory Diseases. Front. Pharmacol. 12:762334. doi: 10.3389/fphar.2021.762334

INTRODUCTION

Cardiovascular disease is the major reason of global death, especially in North America, Europe, and Asia (Braunwald, 1997; Breslow, 1997). Classical anti-hypertension and hypolipidemic therapies are usually used for coronary artery disease, atherosclerosis, and heart failure. It has been revealed that certain circulating immune cells could directly induce endothelia injury, or indirectly activate endothelia to express effector molecules to aggravate deterioration in atherosclerosis (Eriksson et al., 2001; Skalen et al., 2002). Recruited by activated/injured endothelia, circulating monocytes could migrate into atherosclerotic plaque and differentiate into macrophages to release inflammatory cytokines and up-regulate pattern-recognition receptors to accelerate the development of atherosclerosis (Peiser et al., 2002). Recent studies also indicated that cardiac hypertrophy, fibrosis, and remodeling could be regulated by several kinds of immune cells, including dendritic cell (Anzai et al., 2012; Choo et al., 2017), T cell (Hofmann et al., 2012; Weirather et al., 2014), and B cell (Guzik et al., 2007), etc.

The receptor interacting protein kinases (RIPK), especially RIPK1 and RIPK3, are key mediators in cell death and inflammation. In RIPK family, 7 members share a homologous kinase domain which have diverse functions (Zhang et al., 2010). The incipiently family member RIPK1 contains a death domain (DD) which can identify and bond with other DD-containing proteins, such as tumor necrosis factor receptor 1 (TNFR1), TNF-related apoptosis-inducing ligand (TRAIL), and CD95 (Fas) (Micheau and Tschopp, 2003). RIPK3 contains N-terminal kinase domain like other members and an intermediary domain (ID) containing RIP homotypic interaction motif (RHIM) on

C-terminus, which can interact with RIPK1 (Sun et al., 1999). The combination of RIPK1 and RIPK3 via RHIM is essential to initiate the necroptosis signaling pathway. RIPK1-RIPK3 interaction in inflammatory and immunological response has attracted much attention in recent years. By mutating RHIM of RIPK1 in mice, Z-DNA-binding protein 1 (ZBP-1) could trigger necroptosis and induce perinatal lethality, skin inflammation, and colitis (Jiao et al., 2020). However, RIPK1 could prevent ZBP-1 activating RIPK3 autophosphorylation on Thr231 and Ser232. Potential mechanism may be closely connected to competitive binding with RIPK3 though RHIM (Newton et al., 2016).

The structure of RIPK1 and whether it is in the kinase active conformation dictate its function. When ubiquitinated, RIPK1's conformation is enclosed, so it is conducive to form a platform which facilitates congregation of multiprotein complexes resulting in nuclear factor κB (NF-κB) and mitogen-activated protein kinase (MAPK) activation (Kelliher et al., 1998). In its kinase-active form, RIPK1 recruits RIPK3 to its RHIM domain and initiates cell death pathways. RIPK1 is constitutively expressed in most tissues, and it can be stimulated by stress signals, DR ligands, or T cell activation (Stanger et al., 1995). When caspase-8 is inhibited or absent, TNF can trigger alternative cell death of necroptosis, which is regulated in execution, but necrotic in morphology (He et al., 2009). These signaling events can occur downstream of various DRs (TNF, Fas, etc.) with some variations (Newton, 2015).

In this review, we discuss the latest progress in this fast-moving field, with a focus on the signaling pathways, and the physiological and pathological implications of RIPK1/3 mediated necroptosis, and the latent therapeutic targets in diverse cardiovascular diseases.

APOPTOSIS AND NECROPTOSIS SIGNALING PATHWAY

TNF and its superfamily members such as factor-related apoptosis ligand (FasL) and TRAIL are potent inducers of cytokines and inflammation which can also lead the caspase activation, DNA fragmentation, chromatin condensation, and ultimately the progress of extrinsic apoptosis (Guicciardi et al., 2013). The binding of TNF and TNFR1 on the surface of the cell leads to the recruitment of RIPK1 and other adaptor proteins, ubiquitin ligases, kinases to form the Complex I. RIPK1 can bind directly to the death domain (DD) in TNFR1 or the DD-containing adaptor TRADD (Pobezinskaya et al., 2008), meanwhile through the TNFR-associated factors, such as TRAF2 and TRAF5 (which are adaptor proteins), the E3 ubiquitin ligases cellular inhibitors of apoptosis (cIAP1/2) and linear ubiquitin chain assembly complex (LUBAC) are recruited to the complex (Gerlach et al., 2011). The ubiquitin ligases complex creates a scaffold for the recruitment of kinase complexes composed of transforming growth factor-b-activated kinase 1 and TAK1-binding proteins 2 and 3 (TAK1/TAB2/TAB3) (Kanayama et al., 2004). The pivotal function of TAK1 in regulating necroptotic myocyte death, myocardial remodeling, and heart failure propensity was initially described by Li et al. (2014). To verify the particular function of TAK1, cardiac-specific ablation of TAK1 mice was generated for apoptosis and necroptosis spontaneously leading to myocardial remodeling. This phenomenon could be rescued by genetic deletion of TNFR1. TAK1 as a nodal regulator of TNFR1-mediated necroptosis was unraveled whereafter. With activation of the downstream IKK-NFκB pathway, TAK1 was bound with RIPK1 through promotion of TNFR1 ligation. When activity of TAK1 was compromised, RIPK1 dissociated from TAK1 and switched its interacting partners to bind caspase 8 and FADD, inducing necroptosis mediated by RIPK1-FADD-caspase 8 and the RIPK1-RIPK3 complexes (Guo et al., 2017). TRAF2 is also a bridging regulator of necroptotic cell death which shows cardioprotective function. Ablation of TRADD could block necroptosis and abrogate the RIPK1-RIPK3 necrosome formation; activation of TAK1 could inhibit the necrosome formation by inhibiting RIPK1-RIPK3-FADD interaction. These results identified TRADD as an upstream regulator and TAK1 as a downstream effector in regulation of RIPK1-RIPK3-MLKL necroptotic signaling by TRAF2 (Guo et al., 2017).

Linear ubiquitin linkages on RIPK1 are important for recruiting NEMO/IKKγ which may inhibit necroptosis as well as apoptosis by binding to ubiquitinated RIPK1 to restrain RIPK1 from engaging the necroptotic death pathway (O'donnell et al., 2012; Shan et al., 2018). Further transformation from Complex I to cytoplasmic complex (Complex II) is required to execute apoptosis or necroptosis depending on the inhibit of cellular caspase-8/FLICE-like inhibitory protein (cFLIP) (Dillon et al., 2012). cFLIP can form heterodimers with caspase-8 in Complex II. In contrast with Complex I, the degradation of cIAPs or LUBAC, and the deubiquitylation of RIPK1 by cylindromatosis (CYLD) induce the formation of Complex II (Gerlach et al., 2011; Moquin et al., 2013) which has the same core components with ripoptosome (RIPK1/FADD/caspase-8). But ripoptosome forms independently of TNFR1 indicates that it cannot constitute Complex II (Feoktistova et al., 2011). Intrinsic apoptosis is triggered by apoptogenic proteins released by mitochondria which interrupts IAPs inhibition of caspases (Yang and Du, 2004) or activates caspase-9 (Li et al., 1997). The apoptosis promoted by Complex II requires the RIPK1, FADD, and caspase-8/cFLIP which lead the cascade of caspases (including caspase 8, 3, and 7) activation to perform apoptosis (Li et al., 1997; Micheau and Tschopp, 2003; Petersen et al., 2007). However, in situations where caspase inhibitors (e.g., z-VAD-fmk) block the activity of caspase-8 (and caspase-8/cFLIP heterodimers), the complex matures into necrosome which contains RIPK3 and MLKL (Holler et al., 2000; Degterev et al., 2005; Dillon et al., 2012). RIPK1 could auto-phosphorylate at Ser166 (Li et al., 2012) and interact with RIPK3 or other RHIM-containing proteins (TRIF for example) and induce downstream signaling pathways activation. RIPK1 binding to RIPK3 is a vital procedure to form necrosome which in turn activates RIPK3 phosphorylation at Ser 227 anthropogenically, or at Thr231 and Ser232 in murine (Li et al., 2012). RIPK3 can be directly activated by TLR3/TLR4-mediated signaling pathways and TRIF which induces RIPK3-mediated necroptosis through ROS without regulation of RIPK1 (He et al., 2011; Mocarski et al., 2011) (**Figure 1**). RIPK3

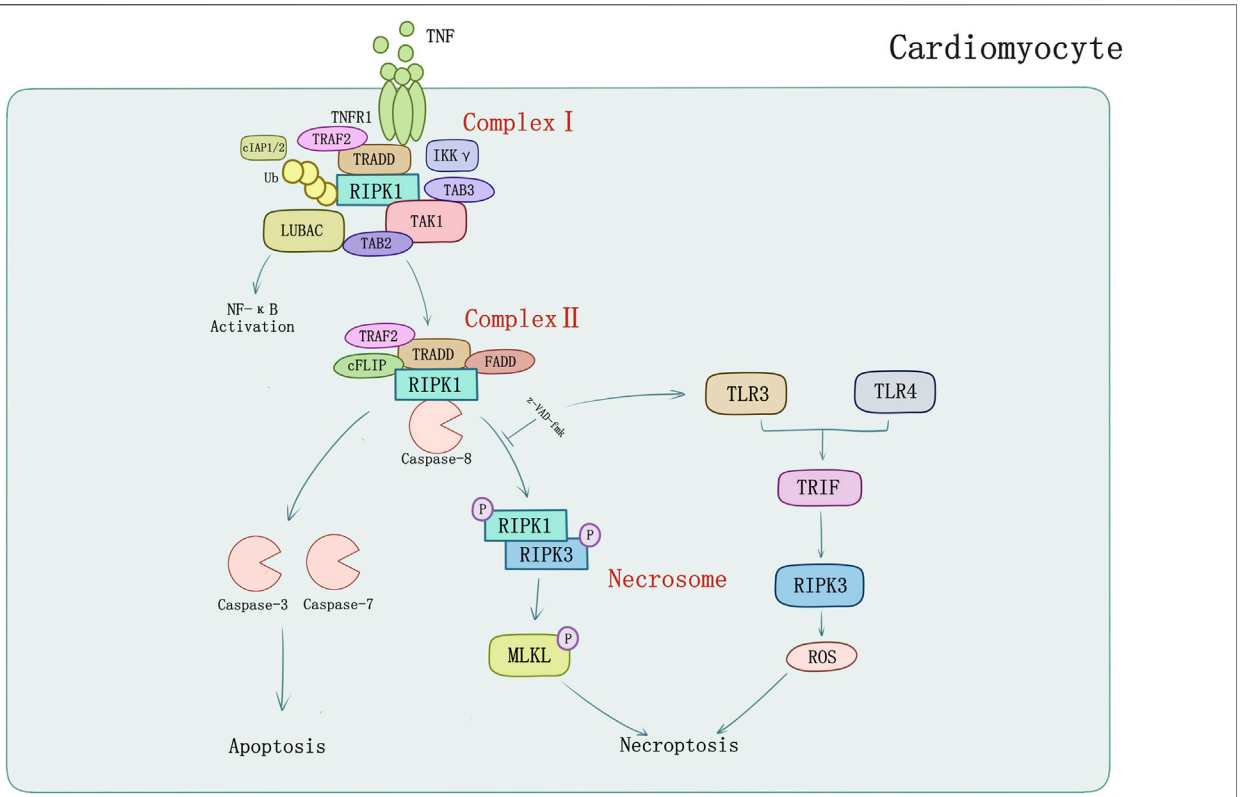

FIGURE 1 | TNFR1-mediated apoptosis and necroptosis in cardiomyocyte. TNF-α binds with TNFR1 to transmit inflammatory signal into cells, and then induces formation of complex I consisting of TRADD, TRAF2, RIPK1, cIAPs, LUBAC, etc. Activated complex II induces caspase-dependent apoptosis which could be inhibited by pan-caspase inhibitor z-VAD-fmk. Z-VAD-fmk could also induce TLR3/TLR4-mediated signaling pathways and TRIF which induces RIPK3-mediated necroptosis through ROS.

activation phosphorylates the pseudokinase MLKL (Sun et al., 2012). MLKL contains an N-terminal effector domain which is kept inactive by its C-terminal region folding in normal condition (Holler et al., 2000; Degterev et al., 2005). Bound with phosphorylated RIPK3, MLKL is phosphorylated thereupon and induces a conformational switch which exposes the N-terminal four-helix bundle of MLKL (Murphy et al., 2013). Oligomerization and translocation to plasma membrane of MLKL is induced, therefore, causing membrane rupture and cell death of which the explicit mechanisms require to be defined (Murphy et al., 2013; Cai et al., 2014; Hildebrand et al., 2014).

RIPK1/3 IN CARDIAC DISEASES

The Crosstalk Between Necroptosis and Autophagy in Myocardial Death

Necroptosis causes cardiomyocyte death in multiple signaling pathways. Luedde et al. (2014) first observed up-regulation of RIPK3 expression in ischemic mouse model. Following discovery argued that RIPK1-RIPK3-mediated necroptosis may play a special role in cardiomyocytes subsistence and death. Inhibiting HMGB1 expression via dexmedetomidine treatment could suppress hypoxia/reoxygenation (H/R)-induced necroptosis (Chen et al., 2019). However, the underlying mechanisms of myocardial death regulated by necroptosis still require thorough understanding. A growing number of new research suggests that crosstalk with autophagy may provide novel perspectives. Autophagy is an evolutionarily conserved mechanism by which cytoplasmic proteins and organelles are degraded intracellularly though lysosomal pathway, which has also emerged as a major regulator of cardiac homeostasis and function (Sciarretta et al., 2018). Autophagy exists in three known types thus far, which are macroautophagy, microautophagy, and chaperone-mediated autophagy (CMA). Subcellular behavior of autophagy contains initiation and maturation of autophagosomes as well as fusion of autophagosomes to lysosomes which is regulated mainly by specific autophagy-related (Atg) genes family (Mizushima and Komatsu, 2011; Schinnerling et al., 2015). Normally, autophagy is adaptive to limit derangements and cell death. However, in some conditions, autophagy facilitates cell death, including apoptosis and necrosis (Choi et al., 2013; Sciarretta et al., 2018). Fast-growing studies on cardiomyocyte death and myocardial infarction substantiate this point. Ad-HGF could induce necroptosis and enhance cardiomyocyte proliferation (You et al., 2016). Liu et al. (2016c) demonstrated that it could also remarkably decrease the

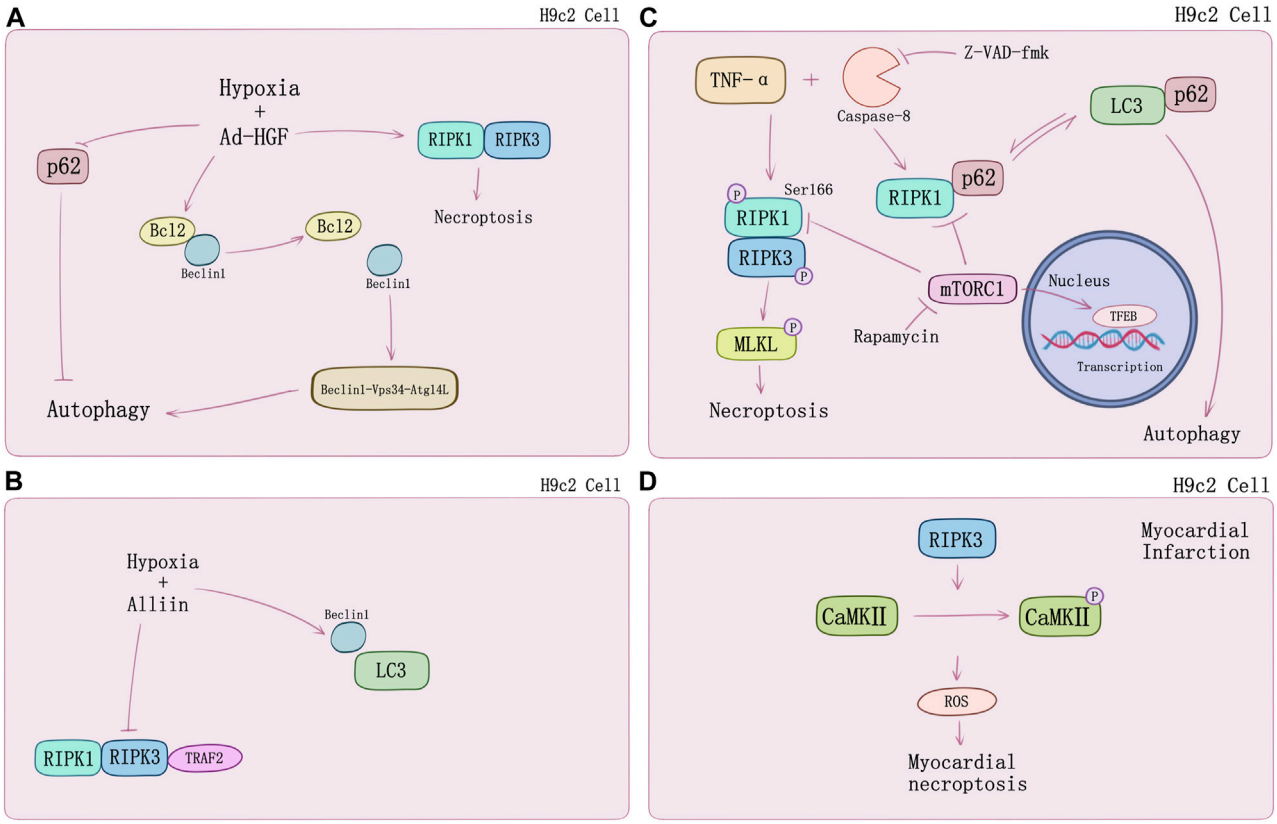

FIGURE 2 | The crosstalk between necroptosis and autophagy in H9c2 cells. **(A)** HGF promotes autophagy and necroptosis in H9c2 cells under hypoxia by decreasing the binding of Bcl2 to Beclin1 and p62. **(B)** Alliin decreases hypoxia-induced necroptosis in H9c2 cells and promotes autophagy by increasing the levels of Beclin1 and LC3. **(C)** TNF-α/zVAD treatment induces necroptosis and switches RIP1-p62 binding to p62-LC3 notably causing suppression of autophagic flux. mTOC1 inhibition by rapamycin would suppress TNF-α/zVAD-mediated activation of IKKα/β and attenuates RIPK1/RIPK3-mediated necroptosis by suppressing RIP1-Ser166 phosphorylation. Rapamycin can induce TFEB nuclear translocation and promote autophagy in a TFEB-dependent manner. **(D)** RIP3-induced CaMKII phosphorylation and the release of ROS.

binding of Bcl-2 to Beclin1 and increase the formation of Beclin1-Vps34-Atg14L complex to promote autophagy in necroptosis process. Additionally, p62 was markedly attenuated rat with Ad-HGF treatment (**Figure 2A**). S-allyl-cysteine sulfoxide (alliin) treatment in H9c2 cells shows necroptosis inhibition and autophagy promotion by down-regulating RIPK1, RIPK3, and TRAF2 expression meanwhile up-regulating Beclin 1 and microtubule-associated protein 1 light chain 3 (LC3) (Yue et al., 2019) (**Figure 2B**). Zhang et al. (2020) found Beclin 1 knockdown genetically would impair autophagy flux, which exacerbated oxygen and glucose deprivation (OGD)-induced necroptotic cardiomyocyte death and cardiac dysfunction but would be alleviated by RIPK3 deletion. TNF-α and pan-caspase inhibitor z-VAD-fmk induced RIPK1-RIPK3-mediated necroptosis in H9c2 cells increased the level of LC3-II, an autophagosome-membrane bound form of LC3, and cannot be attenuated by mitochondrial permeability transition pore (mPTP) inhibitors or GSK-3β inhibitors, that hinted at alternative regulation beyond RIPK3-CaMKII-mPTP myocardial necroptosis pathway. TNF-α/zVAD treatment also increased RIPK1-p62 binding notably and reduced p62-LC3 binding which can be inhibited by rapamycin, while Atg5 knockdown can reduce this effect (Goodall et al., 2016; Ogasawara et al., 2017). Mammalian target of rapamycin (mTOR) is a pivotal kinase regulating cell growth and metabolism via different signaling pathways such as PI3K–AKT and MAPK-IKKα/β, etc. (Saxton and Sabatini, 2017; Mossmann et al., 2018). Regulation of autophagy and potential interaction with necroptosis of mTORC1 may also contribute to cardiomyocyte death. Abe et al. (2019) found that mTOC1 inhibition would suppress TNF-α/zVAD-mediated activation of IKKα/β and attenuate RIPK1/RIPK3-mediated necroptosis. In their study, H9c2 cells were treated by TNF-α/zVAD and determined the level of LDH release for necroptosis. mTORC1 inhibitor rapamycin, and mTORC1/2 inhibitor Ku-0063794 could suppress RIPK1-Ser166 phosphorylation and increase RIPK1-Ser320 phosphorylation, a directly MK2 phosphorylation site (Herranz et al., 2015) compared to TAK1 inhibition. Intracellular localization of transcriptional factor EB (TFEB) suggested that rapamycin and necrostatin-1 can induce TFEB nuclear translocation and promote autophagy in a TFEB-dependent manner (**Figure 2C**).

Suppression of TFEB expression abolished the protective effects of mTORC1 inhibitor on both autophagy and necroptosis (Abe et al., 2019).

In addition, RIPK3-mediated necroptosis regulated by CaMKII can conduct in specific processes of myocardial infarction. RIPK3 phosphorylates CaMKII and increases myocardial ROS production which will cause the myocardial infarction (Zhang et al., 2016) (**Figure 2D**). RIPK3$^{-/-}$ mice undergoing left anterior descending coronary artery ligation developed a myocardial infarction and showed better ejection fraction and less hypertrophy. Inflammation response and ROS activation was restricted by RIPK3 knockout *in vitro* (Luedde et al., 2014). ZYZ-803 is a hybrid molecule of a dual donor for gasotransmitter H2S and NO. Endoplasmic reticulum stress and necroptosis of AMI heart could be attenuated by ZYZ-803 depending on RIPK3-CaMKII signaling pathway regulation (Chang et al., 2019). Evidence suggests that long term xenoestrogen Bisphenol-A exposure would interfere with coronary circulation by activating CaMKII and inducing coronary endothelial necroptosis (Reventun et al., 2020).

Ischemia-Reperfusion Injury

Reperfusion of ischemic myocardium is a critical strategy for rescuing cardiomyocytes from impendent infarction, whereas it can also cause both reversible and irreversible injury performing as expansion of infarct area and coronary artery dysfunction (Bolli, 1992; Przyklenk, 1997). An indisputable fact has been acknowledged with the continuous cognition of the post-conditioning phenomenon that reperfusion could cause irreversible injury, which can be alleviated by reperfusion modification (Ovize et al., 2010). Apoptosis and necrosis are two crucial mechanisms of early research in ischemia-reperfusion (I/R) injury (Skemiene et al., 2013). Increasing findings unravel that RIPK1/RIPK3-mediated necroptosis also manifest a pivotal effect.

Oerlemans et al. (2012) discovered in 2012 that inhibiting RIPK1 may lead to long-term improvements after ischemia-reperfusion *in vivo*. After left coronary artery (LCA) ligation and 24 h of reperfusion of C57Bl/6 mice, the group treating with RIPK1 inhibitor Nec-1 showed reduction of infarction area and attenuation of inflammatory response. Cardiac remodeling measured by cardiac geometry and fibrosis after I/R for 28 days can be remarkably prevented through RIPK1 inhibition. Similarly, ischemia and reperfusion had been conducted on Guinea pig hearts to verify the effect of RIPK1-mediated necroptosis in myocardial ischemia–reperfusion injury, finding that apoptosis and necroptosis are both involved. These findings indicated that cardio-protection could be promoted by the combination of necroptosis and apoptosis inhibition (Koshinuma et al., 2014). Of note, downregulating of oxidative stress genes CYBA and TXNIP of RIPK1 inhibition provides a novel insight of cardiomyocyte I/R injury and myocardial remodeling (Oerlemans et al., 2012).

Non-classical necroptosis pathway mediated directly by RIPK3 rather than RIPK1 has also been found essential in pathophysiological process of myocardial I/R injury, in addition to RIPK1-RIPK3-MLKL pathway. Zhang et al. (2016) revealed a profound mechanism of RIPK3 in ischemia and oxidative stress–induced myocardial necroptosis. Utilizing RIPK3-deficient (Ripk3$^{-/-}$) mice, they observed that RIPK3 deficiency of mice could block I/R-induced and Dox-induced myocardial necrosis, which did not require the participation of RIPK1 or MLKL. A similar result was also found *in vitro*. Phosphorylation of RIPK3 or oxidation could activate CaMKII and subsequently trigger an opening of the mitochondrial permeability transition pore (mPTP) and myocardial necroptosis. CaMKII as a novel substrate of RIPK3 demonstrated a promising therapeutic strategy of I/R injury (Zhang et al., 2016).

Endoplasmic reticulum (ER) stress can induce cellular death by activating intrinsic mitochondrial apoptosis and RIPK3-mediated necroptosis. RIPK3 was evidently upregulated in I/R injury mice, of which ER stress was induced accompanied by Ca level ([Ca]) and xanthine oxidase (XO) increase and mediated mPTP opening by raising reactive oxygen species (ROS), cardiomyocytes necroptosis occurred ultimately (Saveljeva et al., 2015; Zhu et al., 2018). Melatonin can reverse IR-triggered microvascular perfusion defect and sustain microvascular barrier function via suppressing expression of RIPK3 and prevent endothelial necroptosis by inhibiting the RIPK33-PGAM5-CypD-mPTP cascade (Zhou H. et al., 2018). Through inhibiting RIPK3-MLKL/CaMKII necroptosis pathway, melatonin treatment would attenuate the sensibility of cardiomyocytes to I/R injury induced by chronic pain (Yang et al., 2018).

Recently studies also set sights on mitochondrial function. RIPK3 could intensely perform translocation and expression in mitochondria when mouse model undergoes I/R injury. During cardiomyocyte I/R injury, mitochondria suffered hypoxia/reoxygenation damage resulting in RIPK3-depended mitochondrial fragmentation and necrosis-based death, mediated by increasing lactate dehydrogenase release and inhibiting cell viability. Activation of dynamin-related protein 1 (Drp1) by RIPK3 was found participating in this process, together with the ROS elevation and mitochondrial inner membrane potential ($\Delta\Psi m$) decline (Hou et al., 2018).

Tumor necrosis factor receptor (TNFR) plays a key role in necroptosis signaling pathway (Dondelinger et al., 2017). TNFR1 knockout *in vitro* blocked the phosphorylation of RIPK3 and decreased APJ, HIF-1α, and VEGF level. Nε-(carboxymethyl) lysine (CML) is the main component of advanced glycation end products. Acute myocardial infarction patients and MI/R mice were both found elevation of CML. RIPK3 phosphorylation can be induced by CML and be blocked by advanced glycation end product (RAGE) receptor knockout as well as glyoxalase-1 overexpression (Yang J. et al., 2019) suggesting novel sight of necroptosis regulation in MI/R injury (**Figure 3**).

Cardiac Remodeling

Diversified research recently provided wide sights which contribute to understanding the role of necroptosis in myocardial remodeling. Soluble CD74 receptor ectodomain (sCD74) could perform as a modulator of macrophage migration inhibitory factor (MIF) signaling by diminishing MIF-mediated protein kinase B (AKT) activation and triggering p38 activation. sCD74 could induce necroptosis in

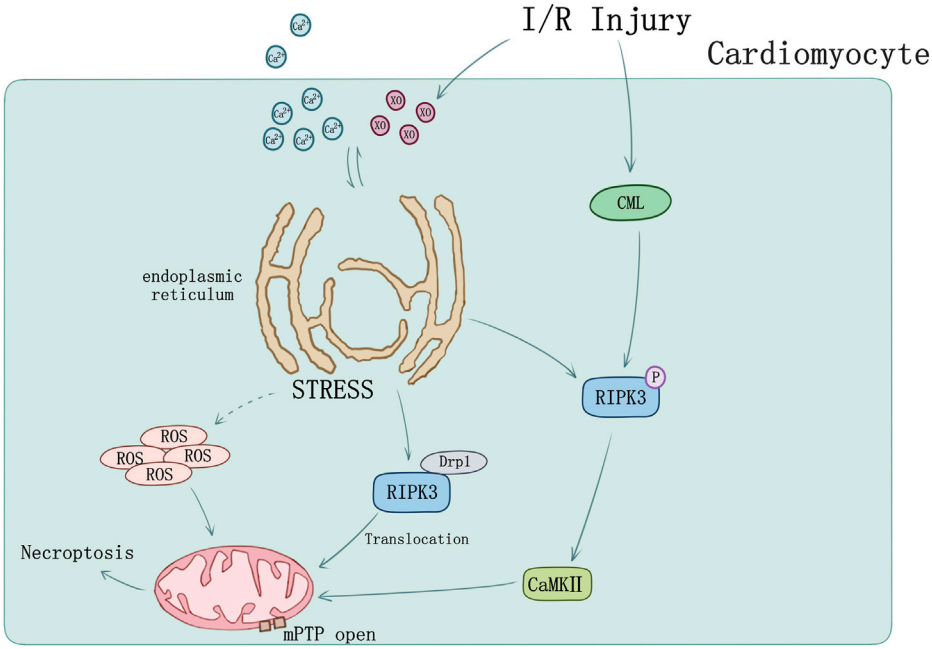

FIGURE 3 | Ischemia-reperfusion injury and ER stress induced myocardial necroptosis. [Ca] and XO influx cause ER stress and mediated mPTP opening by raising ROS. RIPK3 phosphorylation can be induced by CML in I/R injury. Phosphorylation of RIPK3 could activate CaMKII and subsequently trigger opening of the mPTP. I/R could cause RIPK3 and Drp1 translocation from cytoplasm to mitochondrion.

cardiac myofibroblasts via inhibiting MIF-mediated survival pathway through C-X-C chemokine receptor 4/AKT axis (Soppert et al., 2018). Autophagy interacts with necroptotic cell death and is also a participant in myocardial remodeling (Liu et al., 2016b; Zhang et al., 2020). High glucose (HG) status may induce inflammation response and then cause cardiac injury and myocardial fibrosis (Miura et al., 2003; You et al., 2016). HG would increase the expression of TLR4 and RIPK3. ATP-sensitive K+ (KATP) channel opener such as diazoxide and pinacidil would blocked the up-regulation of TLR4 and RIP3, suggesting that KATP channel opening can protect myocardium against HG-induced injury and inflammation by inhibiting ROS-TLR4-necroptosis pathway (Liang et al., 2017b). ROS positively interacted with necroptosis demonstrate a novel damage mechanism in HG-induced cardiac injury and inflammation (Liang et al., 2017a). Stimulation of aldehyde dehydrogenases 2 (ALDH2) in high glucose-induced primary cardiomyocytes injury model prevents the occurrence of fibrosis, apoptosis, and necroptosis via inhibiting oxidative stress and inflammation, together with the increased expression of tissue inhibitors of matrix metalloproteinase 4 (TIMP4) protein and the decreased level of matrix metalloproteinase 14 (MMP14) protein level. The mRNA and protein levels of RIPK1, RIPK3, and MLKL decreased (Kang et al., 2020). These provide a new mechanism for myocardial protection.

Myocarditis

RIPK1/RIPK3-mediated necroptosis regulates inflammatory pathological changing of myocardium. Mouse model of acute viral myocarditis (VMC) induced by Coxsackievirus B3 (CVB3) showed highly expressed of RIPK1/RIPK3, which could be rescued by Nec-1 treatment. Inhibiting the necroptosis pathway may serve as a new therapeutic strategy for acute viral myocarditis (Zhou F. et al., 2018).

Streptococcus pneumoniae (the *pneumococcus*) can invade the heart and then cause myocarditis. Pneumococcal myocardial invasion induces inflammation response and immune cell infiltration. Pneumococci releasing pneumolysin via bacterial strain-specific manner kills infiltrated macrophages by activating necroptosis, which alters the immune response (Gilley et al., 2016). The nonhuman primate (NHP) model was used to investigate whether *S. pneumoniae* can cause heart translocation and induce cardiac toxicity. *S. pneumoniae* was detected in the myocardium of all NHPs with acute severe pneumonia. Necroptosis and apoptosis were detected in the myocardium of both acute and convalescent NHPs. It can be treated as an efficient therapeutic target for treatment of severe pneumonia by inhibiting the necroptosis pathway, especially in patients who experience major adverse cardiac events (Reyes et al., 2017).

The interaction and crosstalk of necroptosis and autophagy can change the way of cell death and reduce damage. Myocardial infarction and ischemia-reperfusion injury are related to RIPK3-dependent necroptosis. The upstream molecules related to TNF-induced necroptosis can inhibit or promote myocardial remodeling. Myocarditis is associated with the increase in RIPK1/3.

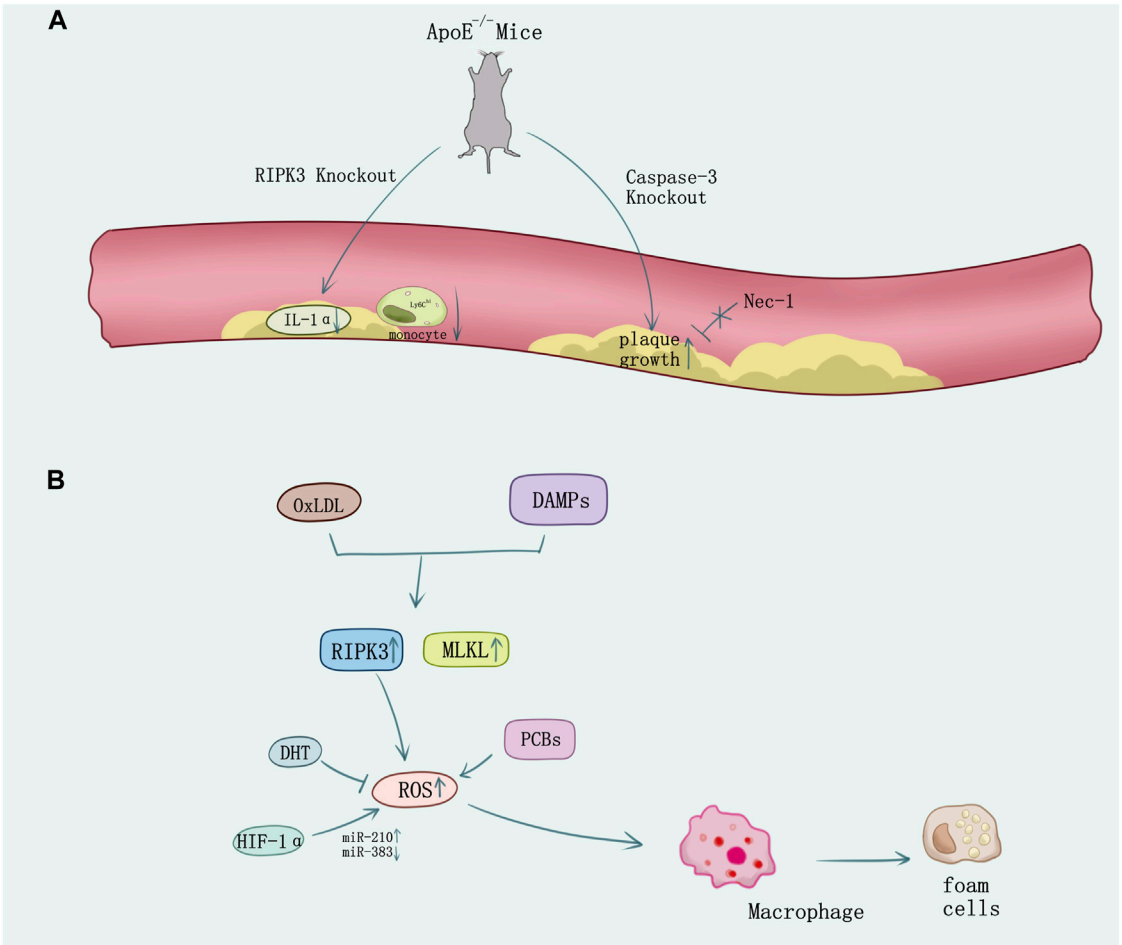

FIGURE 4 | The necroptosis in atherosclerosis. **(A)** In ApoE-knockout-induced spontaneous atherosclerosis mice, knock out RIPK3 causes the decrease of IL-1α and the Ly6C^{hi} monocyte. However, knock out the caspase-3 causes the plaque growth which cannot be reversed by the inhibitor of RIPK1 Nec-1. **(B)** Ox-LDL or DAMPs stimulation released from necrotic cells induces necroptosis in macrophage and the formation of foam cells. ROS overproduction promotes necroptosis which can be suppressed by oxidative stress inhibition using DHT. HIF-1α promotes macrophage necroptosis and ROS production by regulating miR-210 and miR-383.

RIPK1/3 IN VASCULAR DISEASES

Atherosclerosis

Atherosclerosis is a chronic disease of the vessel wall involving inflammation response of multiple cell types driven by lipid deposition. The process of atherosclerosis would hold a huge reserve of latent period. Once atherosclerotic plaque ruptures, urgent life-threatening cardiovascular events would occur such as myocardial infarction (Kavurma et al., 2017). The basic pathophysiological mechanism of atherosclerosis includes incipient subendothelial retention and accumulation of infiltrated LDL, conducting oxidation and aggregation sequentially, and ultimately triggering chronic inflammatory response and immune reaction (Moore and Tabas, 2011; Hansson et al., 2015). Necroptotic cell death found in the necrotic core within atherosclerotic lesions (Lin et al., 2013) provides the possibility of RIPK1/RIPK3-mediate necroptosis signaling pathway investigation in atherosclerosis.

Macrophages perform major immune and inflammatory functions in atherosclerosis, including recruitment, homing, migration, and differentiation of monocytes, phagocytosis of modified cholesterol, proinflammatory cytokines, enzymes, and ROS secretion (Kavurma et al., 2017). These pathophysiological behaviors not only induce cell death and inflammatory response, but also contribute to foam cell transformation and vulnerable plaque formation (Yahagi et al., 2016). Bao et al. (2006) observed that high levels of sitosterol and other plant sterols would induce premature atherothrombotic vascular disease and macrophage death through autophagy and necroptosis. In ApoE-knockout-induced spontaneous atherosclerosis mice model under RIPK3−/−background, inflammation in atherosclerotic plaques was attenuated and the survival time of atherosclerosis mice got prolonged (Lin et al., 2013). The mRNA expression levels of inflammatory cytokines such as IL-1α, TNF-α, and IL-2 were decreased, lymphocyte infiltrations in the adipocyte tissue and in skin lesions were mitigated, and the high percentage of inflammatory monocytes with high serum levels of lymphocyte

antigen 6C (Ly6Chi) which is an inflammatory marker for atherosclerotic risk was greatly decreased in the ApoE/RIPK3 double-knockout mice (**Figure 4A**). The double-knockout mice presented delayed mortality dramatically in addition (Meng et al., 2015). Thus, antagonism of IL-1α would reduce atherosclerotic lesion mediated by necroptosis (Meng et al., 2016). Macrophage's necroptosis and genetic expression increase of RIPK3 and MLKL was induced by OxLDL and DAMPS released from necrotic cells driving ROS activation *in vitro*. Mice experiments showed using small-molecule necroptosis inhibitor Nec-1 could reduce atherosclerosis lesions (Karunakaran et al., 2016). Consistent with studies on RIPK3, recently a study indicates MLKL may directly contribute to atherosclerosis lesion development and necrotic core formation. Administration of antisense oligonucleotides down-regulated MLKL expression in ApoE−/− mice alleviated both programmed cell death and necrotic core in the plaque, whereas the total lesion area remained.

Increasing evidence showed diverse methods on regulation of necroptosis which may mediate the atherosclerosis process. Caspase 3 deletion in ApoE−/− mice promoted plaque growth and plaque necrosis but did not sensitize cells to undergo RIPK1-dependent necroptosis (Grootaert et al., 2016) (**Figure 4A**). However, 5-aminolevulinic acid-mediated sonodynamic therapy would activated the caspase 3 and caspase 8 pathways in foam cells, which is responsible for the switch from necroptosis to apoptosis and may improve the prognosis of atherosclerosis (Tian et al., 2016). Pituitary adenylate cyclase-activating polypeptide (PACAP) plays an important role in cytoprotection, inflammation, and cardiovascular regulation. PACAP/ApoE-deficiency mice showed increasing necroptotic process in atherosclerotic plaques (Leon et al., 2019). Activation of NF-κB in smooth muscle cells (SMCs) is integral to atherosclerosis and involves reversible ubiquitination that activates proteins downstream of pro-atherogenic receptors. TNFR1 activates NF-κB through cascades of polyubiquitination that culminate in the activation of IKK and phosphorylation of IκBα responding to TNF (Peltzer et al., 2016; Jean-Charles et al., 2018), and ubiquitin-specific protease 20 (USP20) would deubiquitinate RIPK1 and alleviate TNF and IL-1β-evoked atherogenic signaling in SMCs accordingly, which add to the evidence demonstrating that SMC-specific gene expression affects atherosclerosis (Subramanian et al., 2010; Liu D. et al., 2016; Jean-Charles et al., 2018). The pathogenesis of atherosclerosis is associated with oxidative stress (Witztum, 1994; Kavurma et al., 2017). Necroptosis plays a vital role in ROS activation (Zhang et al., 2016). Evidence shows that polychlorinated biphenyls (PCBs) promoted the macrophage formation of foam cells, inflammation, and cell necroptosis via ROS overproduction (Yang B. et al., 2019). However, dihydrotanshinone I (DHT) would suppress RIPK3-mediated necroptosis of macrophage to stabilize vulnerable plaque by reducing oxidative stress (Zhao et al., 2021). New findings unveil hypoxia-inducible factor (HIF-1α) upregulates miR-210 and downregulates miR-383 levels in lesioned macrophages and inflammatory bone marrow-derived macrophages. In contrast to miR-210, which inhibited oxidative phosphorylation and enhanced mitochondrial reactive oxygen species production, miR-383 increased ATP levels and inhibited necroptosis by suppressing poly(ADP-ribose) glycohydrolase *(Parg)*, which enhanced atherosclerosis (Karshovska et al., 2020) (**Figure 4B**).

RIPK3 has been identified to have an atherogenic effect (Lin et al., 2013; Karunakaran et al., 2016), athero-protective function in macrophages and endothelial cells have also been reported lately. RIPK3 may play an anti-inflammatory role by suppressing MCP-1 expression in macrophages and E-selectin expression in endothelial cells, rather than classic function of promoting necroptosis or IL-β processing (Weinlich et al., 2017; Colijn et al., 2020). Novel insights about RIPK3 in atherosclerosis emerge endlessly.

Abdominal Aortic Aneurysm

Abdominal aortic aneurysm (AAA), characterized by depletion of SMCs, inflammation, negative extracellular matrix remodeling, and progressive expansion of aorta is a major potentially lethal aortic disease with no available pharmacological treatment (Baxter et al., 2008). The pathophysiology of AAA remains incompletely understood. Studies using human specimens and animal models have shown that the infiltrating inflammatory cells, such as macrophages and mast cells, are the major source of both proinflammatory cytokines and matrix-degrading enzymes accumulated in the aneurysmal aortae (Longo et al., 2002; Shimizu et al., 2006). Levels of RIPK3 as well as RIPK1 are elevated in human tissues affected by various pathological conditions, including ischemic stroke, atherosclerosis, and aortic aneurysm. Wang et al. (2015) recently confirmed increased expression of RIPK3 in AAA. In isolated aortic SMCs, knockdown or knockout RIPK3 attenuated TNFα-induced phosphorylation of p65 serine536 and expression of several proinflammatory cytokines. P65 serine536 is critical for enhancing the transcriptional activity of NF-κB and the cytokines regulated by NF-κB such as IL-6, TNF, and VCAM-1 are changed with the activity of NF-κB signaling pathway. Zhou et al. (2019) demonstrate that in AAA, RIPK3 deficiency inhibits aneurysm formation via suppressing cell necrosis and inflammatory response of aortic SMCs. They screened 1141 kinase inhibitors having abilities to block necroptosis and virtual binding to RIPK3, finding GSK074 showed structural similarity to GSK843, a necroptosis blocker in several cell lines such as mouse SMCs. Besides, GSK074 can be bound by both RIPK1 and RIPK3 rather than cause profound apoptosis. Treating with GSK074 can diminish cell death and macrophage infiltration in mouse SMCs and mouse models of AAA histologically.

Studies also unravel RIPK1 plays an extraordinary role in the progression of AAA. Wang et al. (2017) observed amelioration in mouse abdominal aortic aneurysm model by inhibiting RIPK1 with Nec-1. They treated mouse SMCs and elastase-induced murine AAAs with TNFα and zVAD causing necroptosis and then inhibited RIPK1 by Nec-1. The injection of Nec-1 in hypercholesterolemic ApoE−/− mice 30 min ahead of AAA induction showed significantly alleviated aneurysm formation. Interestingly, after treating Nec-1 for another 7 days, at the 8th day of elastase perfusion, smaller mean aortic expansion and marked reduction of macrophage infiltration and MMP9, which

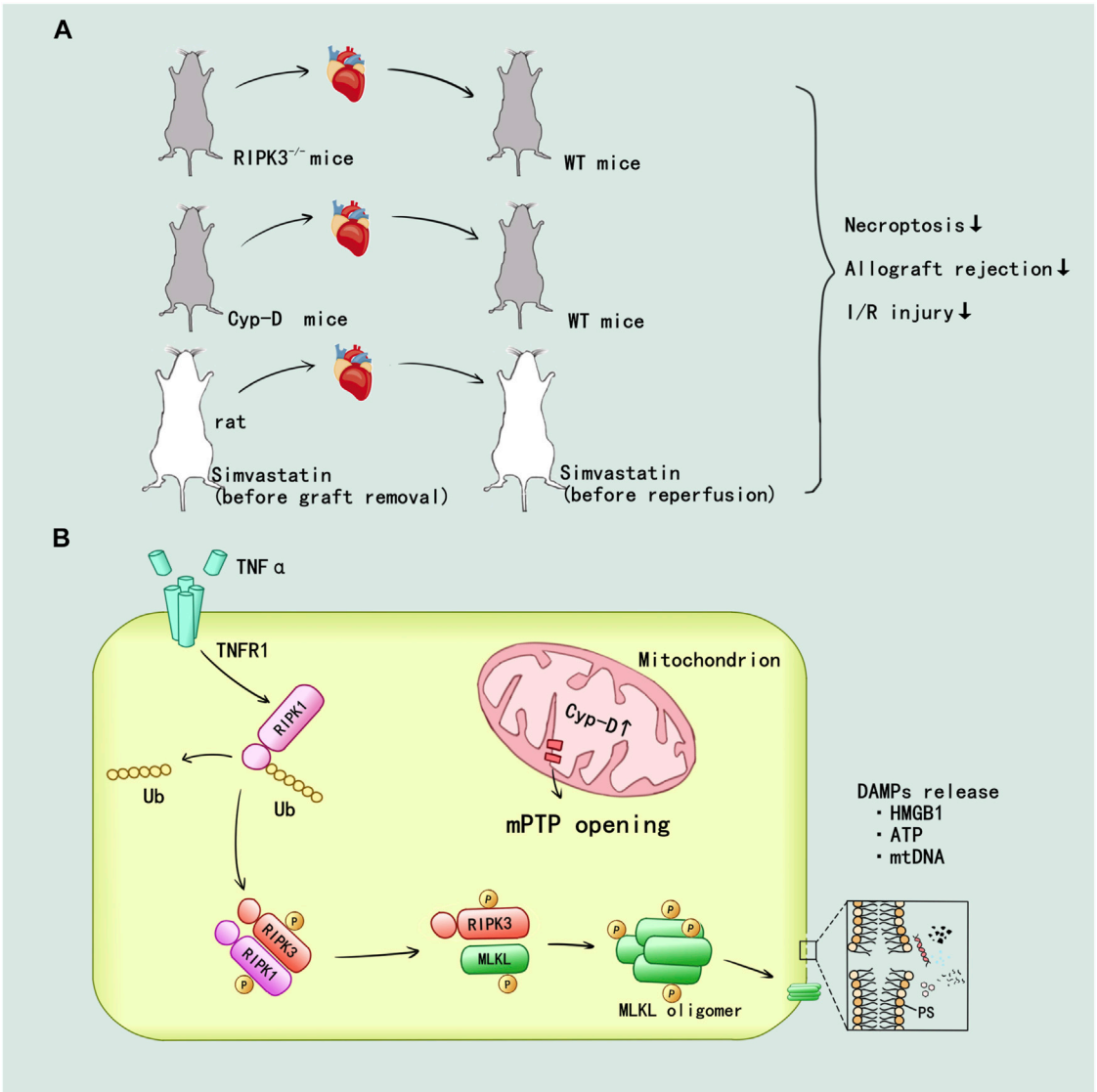

FIGURE 5 | RIPK1/3-mediated necroptosis promoted the inflammatory and I/R injury in heart transplant. **(A)** *In vivo*, the establishment of RIPK3 and Cyp-D knockout have been verified that inhibition of RIPK3 and mitochondrial pathway could alleviate the injury. The simvastatin pretreatment in donor and recipient attenuated the allograft rejection and I/R injury. **(B)** TNF-α can promote the deubiquitination of RIPK1 through TNFR1 mediated intracellular signal transduction. mPTP opening mediated by Cyp-D facilitate the formation of RIPK1/RIPK3/MLKL necrosome and MLKL phosphorylation. Then, MLKL ultimately mediated the cell membrane rupture and released a variety of DAMPs.

was produced primarily by inflammatory cells and plays important roles in aneurysm pathogenesis was observed, suggesting inhibition of RIPK1 can block progression in mice with pre-existing small AAAs.

MLKL expression is also tested in elastase-induced AAA rat model. Within angiotensin AT2 receptor agonist compound 21 (C21) treating, twofold of MLKL expression was decreased as compared with the vehicle group; meanwhile, the expression of other inflammatory mediators such as IL-1β, NF-κB, MMP9, and TGF-β1 were down-regulated likewise (Lange et al., 2018). Histologically, MLKL was found mostly in the media colocalizing with vascular smooth muscle cells and inflammatory cells (Marin et al., 2018). Although changes in genetical and protein levels of MLKL have been verified in AAA, further research remains to better understand the relationship between MLKL and AAA.

Stimulator of interferon genes (STING), a proinflammatory molecule in the cyclic GMP-AMP synthase (cGAS)–STING cytosolic DNA sensor signaling pathway (Ablasser et al., 2013), has previously been shown to promote necroptosis partially through tumor necrosis factor receptor signaling (Sarhan et al., 2019). Novel study shows that DNA damage would activate STING-TBK1-IRF3 pathway and induce necroptosis to promote aortic degeneration, via

phosphorylating RIPK3 directly (Luo et al., 2020). Potential multiple pathway crosstalk with RIPK1/3-mediated necroptosis requires confirmation.

RIPK3 knockout decreased the infiltration of pro-inflammation cytokines and the trend of macrophages transforming to foam cells in arthrosclerosis. Inhibition of RIPK1/3 and MLKL are expected to be the therapeutic targets of AAA.

RIPK1/3 IN CARDIOVASCULAR TRANSPLANTS

Organ transplant injury occurs with ischemia and alloimmunity. Lau et al. (2013) first confirmed the involvement of RIPK1/3 in donor organ necroptosis to promote inflammatory and ischemia-reperfusion (I/R) injury in kidney transplant models. Subsequently, extensive evidence showed that the suppression of RIPK1/3-induced necroptosis can provide major protective benefits in the diverse organ transplant model (Kwok et al., 2017; Kanou et al., 2018; Kim et al., 2018).

Pavlosky et al. (2014) first confirmed the mechanism of RIPK1/3-mediated donor graft rejection in cardiac transplantation: TNFα induced necroptosis in murine cardiac microvascular endothelial cell (MVEC) required expression of TNFR1 and RIPK3. Then RIPK1/3 promoted the necroptotic death and release of the danger molecule HMGB1 in MVEC. The RIPK3−/− mice showed alleviated lymphocyte infiltration and damage in endothelium and myocyte, also RIPK3 deficiency in heart allografts prolongs graft survival after transplantation (**Figure 5A**). $CD4^+$ T cell also could induce MVEC death via released TNFα. The cytotoxicity of $CD4^+$ T cell depended on a RIPK3-induced necroptosis in MVEC, and the loss of RIPK3 could reduce chronic cardiac allograft rejection (Kwok et al., 2017) (**Figure 5A**). In addition, prolonged cold ischemia could significantly enhance expression of RIPK1/3 in cardiac allograft. In addition, the simvastatin pretreatment reduced mRNA expression of RIPK1/3 and protein activity of RIPK1 in cardiac allograft I/R injury as well as prevented necroptotic pathway activation in cardiac allograft (Tuuminen et al., 2016) (**Figure 5A**).

The mitochondrial permeability regulated by cyclophilin D (Cyp-D) has been confirmed to participate in the RIPK3-mediated necroptosis and rejection in donor heart: Cyp-D promoted the phosphorylation of RIPK3-downstream mixed lineage kinase domain-like protein (MLKL), resulting in cell membrane rupture. Cyp-D–deficiency contributed to prolonged survival in cardiac grafts (Gan et al., 2019) (**Figure 5A**). Researchers speculated that CypD-mediated mitochondrial permeability transition pore (mPTP) opening might provide enzymes and ATP for the formation of RIPK1/RIPK3/MLKL necrosome and MLKL phosphorylation, but this idea needed to be further verified. The details of RIPK1/3-mediated necroptosis promoting the inflammatory and I/R injury in heart allograft were displayed in **Figure 5B**.

CONCLUSION

Thus far, cardiovascular disease still is the major reason of global death. Although there are many surgical and medical treatments for cardiovascular diseases, there is no treatment through immunotherapy and inhibition of necroptosis. As a key regulator of necroptosis, RIPK1/3 can participate in the occurrence of cell death and inflammation in cardiovascular diseases. In myocardial infarction, ischemia-reperfusion injury, cardiac remodeling, and myocarditis, inhibiting RIPK1/3 would interrupt the transmission of inflammatory signals, thereby reducing the damage and remodeling of cardiomyocytes. Similarly, in atherosclerosis and abdominal aortic aneurysms, inhibiting RIPK1/3 can reduce the formation of foam cells and the development of small aneurysms. In a variety of inflammatory signaling pathways, the RIPK family is very important and is expected to become a key target for therapy.

AUTHOR CONTRIBUTIONS

Y.M.L., Y.Z., and X.L. collected the literatures and drafted the initial manuscript. Z.W. drew the figures. Q.Z. and Y.L. revised the manuscript and edited the language. Q.Z. and Y.L. conceptualized and guaranteed the review. All authors approved the final manuscript as submitted and agree to be accountable for all aspects of the work. Y.M.L. and Y.Z. contributed to this paper equally.

FUNDING

This study was supported by grants of the National Natural Science Foundation of China (81700658, 81800393, and 82170437), the Hunan Provincial Natural Science Foundation-Outstanding Youth Foundation (2020JJ3058 and 2020JJ 2056), and the Fundamental Research Funds for Central Universities of Central South University (No. 2019zzts106).

REFERENCES

Abe, K., Yano, T., Tanno, M., Miki, T., Kuno, A., Sato, T., et al. (2019). mTORC1 Inhibition Attenuates Necroptosis through RIP1 Inhibition-Mediated TFEB Activation. *Biochim. Biophys. Acta Mol. Basis Dis.* 1865 (12), 165552. doi:10.1016/j.bbadis.2019.165552

Ablasser, A., Goldeck, M., Cavlar, T., Deimling, T., Witte, G., Röhl, I., et al. (2013). cGAS Produces a 2'-5'-linked Cyclic Dinucleotide Second Messenger that Activates STING. *Nature* 498 (7454), 380–384. doi:10.1038/nature12306

Anzai, A., Anzai, T., Nagai, S., Maekawa, Y., Naito, K., Kaneko, H., et al. (2012). Regulatory Role of Dendritic Cells in Postinfarction Healing and Left Ventricular Remodeling. *Circulation* 125 (10), 1234–1245. doi:10.1161/CIRCULATIONAHA.111.052126

Bao, L., Li, Y., Deng, S. X., Landry, D., and Tabas, I. (2006). Sitosterol-containing Lipoproteins Trigger Free Sterol-Induced Caspase-independent Death in ACAT-Competent Macrophages. *J. Biol. Chem.* 281 (44), 33635–33649. doi:10.1074/jbc.M606339200

Baxter, B. T., Terrin, M. C., and Dalman, R. L. (2008). Medical Management of Small Abdominal Aortic Aneurysms. *Circulation* 117 (14), 1883–1889. doi:10.1161/CIRCULATIONAHA.107.735274

Bolli, R. (1992). Myocardial "stunning" in Man. *Circulation* 86 (6), 1671–1691. doi:10.1161/01.cir.86.6.1671

Braunwald, E. (1997). Shattuck Lecture-Ccardiovascular Medicine at the Turn of the Millennium: Triumphs, Concerns, and Opportunities. *N. Engl. J. Med.* 337 (19), 1360–1369. doi:10.1056/NEJM199711063371906

Breslow, J. L. (1997). Cardiovascular Disease burden Increases, NIH Funding Decreases. *Nat. Med.* 3 (6), 600–601. doi:10.1038/nm0697-600

Cai, Z., Jitkaew, S., Zhao, J., Chiang, H. C., Choksi, S., Liu, J., et al. (2014). Plasma Membrane Translocation of Trimerized MLKL Protein Is Required for TNF-Induced Necroptosis. *Nat. Cel Biol* 16 (1), 55–65. doi:10.1038/ncb2883

Chang, L., Wang, Z., Ma, F., Tran, B., Zhong, R., Xiong, Y., et al. (20192019). ZYZ-803 Mitigates Endoplasmic Reticulum Stress-Related Necroptosis after Acute Myocardial Infarction through Downregulating the RIP3-CaMKII Signaling Pathway. *Oxid Med. Cel Longev.* 2019, 6173685. doi:10.1155/2019/6173685

Chen, J., Jiang, Z., Zhou, X., Sun, X., Cao, J., Liu, Y., et al. (2019). Dexmedetomidine Preconditioning Protects Cardiomyocytes against Hypoxia/Reoxygenation-Induced Necroptosis by Inhibiting HMGB1-Mediated Inflammation. *Cardiovasc. Drugs Ther.* 33 (1), 45–54. doi:10.1007/s10557-019-06857-1

Choi, A. M., Ryter, S. W., and Levine, B. (2013). Autophagy in Human Health and Disease. *N. Engl. J. Med.* 368 (19), 1845–1846. doi:10.1056/NEJMc1303158

Choo, E. H., Lee, J. H., Park, E. H., Park, H. E., Jung, N. C., Kim, T. H., et al. (2017). Infarcted Myocardium-Primed Dendritic Cells Improve Remodeling and Cardiac Function after Myocardial Infarction by Modulating the Regulatory T Cell and Macrophage Polarization. *Circulation* 135 (15), 1444–1457. doi:10.1161/CIRCULATIONAHA.116.023106

Colijn, S., Muthukumar, V., Xie, J., Gao, S., and Griffin, C. T. (2020). Cell-specific and Athero-Protective Roles for RIPK3 in a Murine Model of Atherosclerosis. *Dis. Model. Mech.* 13 (1), dmm041962. doi:10.1242/dmm.041962

Degterev, A., Huang, Z., Boyce, M., Li, Y., Jagtap, P., Mizushima, N., et al. (2005). Chemical Inhibitor of Nonapoptotic Cell Death with Therapeutic Potential for Ischemic Brain Injury. *Nat. Chem. Biol.* 1 (2), 112–119. doi:10.1038/nchembio711

Dillon, C. P., Oberst, A., Weinlich, R., Janke, L. J., Kang, T. B., Ben-Moshe, T., et al. (2012). Survival Function of the FADD-CASPASE-8-cFLIP(L) Complex. *Cell Rep* 1 (5), 401–407. doi:10.1016/j.celrep.2012.03.010

Dondelinger, Y., Delanghe, T., Rojas-Rivera, D., Priem, D., Delvaeye, T., Bruggeman, I., et al. (2017). MK2 Phosphorylation of RIPK1 Regulates TNF-Mediated Cell Death. *Nat. Cel Biol* 19 (10), 1237–1247. doi:10.1038/ncb3608

Eriksson, E. E., Xie, X., Werr, J., Thoren, P., and Lindbom, L. (2001). Importance of Primary Capture and L-selectin-dependent Secondary Capture in Leukocyte Accumulation in Inflammation and Atherosclerosis *In Vivo*. *J. Exp. Med.* 194 (2), 205–218. doi:10.1084/jem.194.2.205

Feoktistova, M., Geserick, P., Kellert, B., Dimitrova, D. P., Langlais, C., Hupe, M., et al. (2011). cIAPs Block Ripoptosome Formation, a RIP1/caspase-8 Containing Intracellular Cell Death Complex Differentially Regulated by cFLIP Isoforms. *Mol. Cel* 43 (3), 449–463. doi:10.1016/j.molcel.2011.06.011

Gan, I., Jiang, J., Lian, D., Huang, X., Fuhrmann, B., Liu, W., et al. (2019). Mitochondrial Permeability Regulates Cardiac Endothelial Cell Necroptosis and Cardiac Allograft Rejection. *Am. J. Transpl.* 19 (3), 686–698. doi:10.1111/ajt.15112

Gerlach, B., Cordier, S. M., Schmukle, A. C., Emmerich, C. H., Rieser, E., Haas, T. L., et al. (2011). Linear Ubiquitination Prevents Inflammation and Regulates Immune Signalling. *Nature* 471 (7340), 591–596. doi:10.1038/nature09816

Gilley, R. P., González-Juarbe, N., Shenoy, A. T., Reyes, L. F., Dube, P. H., Restrepo, M. I., et al. (2016). Infiltrated Macrophages Die of Pneumolysin-Mediated Necroptosis Following Pneumococcal Myocardial Invasion. *Infect. Immun.* 84 (5), 1457–1469. doi:10.1128/IAI.00007-16

Goodall, M. L., Fitzwalter, B. E., Zahedi, S., Wu, M., Rodriguez, D., Mulcahy-Levy, J. M., et al. (2016). The Autophagy Machinery Controls Cell Death Switching between Apoptosis and Necroptosis. *Dev. Cel* 37 (4), 337–349. doi:10.1016/j.devcel.2016.04.018

Grootaert, M. O., Schrijvers, D. M., Hermans, M., Van Hoof, V. O., De Meyer, G. R., and Martinet, W. (2016). Caspase-3 Deletion Promotes Necrosis in Atherosclerotic Plaques of ApoE Knockout Mice. *Oxid. Med. Cel Longev.* 2016, 3087469. doi:10.1155/2016/3087469

Guicciardi, M. E., Malhi, H., Mott, J. L., and Gores, G. J. (2013). Apoptosis and Necrosis in the Liver. *Compr. Physiol.* 3 (2), 977–1010. doi:10.1002/cphy.c120020

Guo, X., Yin, H., Li, L., Chen, Y., Li, J., Doan, J., et al. (2017). Cardioprotective Role of Tumor Necrosis Factor Receptor-Associated Factor 2 by Suppressing Apoptosis and Necroptosis. *Circulation* 136 (8), 729–742. doi:10.1161/CIRCULATIONAHA.116.026240

Guzik, T. J., Hoch, N. E., Brown, K. A., Mccann, L. A., Rahman, A., Dikalov, S., et al. (2007). Role of the T Cell in the Genesis of Angiotensin II Induced Hypertension and Vascular Dysfunction. *J. Exp. Med.* 204 (10), 2449–2460. doi:10.1084/jem.20070657

Hansson, G. K., Libby, P., and Tabas, I. (2015). Inflammation and Plaque Vulnerability. *J. Intern. Med.* 278 (5), 483–493. doi:10.1111/joim.12406

He, S., Wang, L., Miao, L., Wang, T., Du, F., Zhao, L., et al. (2009). Receptor Interacting Protein Kinase-3 Determines Cellular Necrotic Response to TNF-Alpha. *Cell* 137 (6), 1100–1111. doi:10.1016/j.cell.2009.05.021

He, S., Liang, Y., Shao, F., and Wang, X. (2011). Toll-like Receptors Activate Programmed Necrosis in Macrophages through a Receptor-Interacting Kinase-3-Mediated Pathway. *Proc. Natl. Acad. Sci. U S A.* 108 (50), 20054–20059. doi:10.1073/pnas.1116302108

Herranz, N., Gallage, S., Mellone, M., Wuestefeld, T., Klotz, S., Hanley, C. J., et al. (2015). Erratum: mTOR Regulates MAPKAPK2 Translation to Control the Senescence-Associated Secretory Phenotype. *Nat. Cel Biol.* 17 (9), 1370–1217. doi:10.1038/ncb322510.1038/ncb3243

Hildebrand, J. M., Tanzer, M. C., Lucet, I. S., Young, S. N., Spall, S. K., Sharma, P., et al. (2014). Activation of the Pseudokinase MLKL Unleashes the Four-helix Bundle Domain to Induce Membrane Localization and Necroptotic Cell Death. *Proc. Natl. Acad. Sci. U S A.* 111 (42), 15072–15077. doi:10.1073/pnas.1408987111

Hofmann, U., Beyersdorf, N., Weirather, J., Podolskaya, A., Bauersachs, J., Ertl, G., et al. (2012). Activation of CD4+ T Lymphocytes Improves Wound Healing and Survival after Experimental Myocardial Infarction in Mice. *Circulation* 125 (13), 1652–1663. doi:10.1161/CIRCULATIONAHA.111.044164

Holler, N., Zaru, R., Micheau, O., Thome, M., Attinger, A., Valitutti, S., et al. (2000). Fas Triggers an Alternative, Caspase-8-independent Cell Death Pathway Using the Kinase RIP as Effector Molecule. *Nat. Immunol.* 1 (6), 489–495. doi:10.1038/82732

Hou, H., Wang, Y., Li, Q., Li, Z., Teng, Y., Li, J., et al. (2018). The Role of RIP3 in Cardiomyocyte Necrosis Induced by Mitochondrial Damage of Myocardial Ischemia-Reperfusion. *Acta Biochim. Biophys. Sin (Shanghai)* 50 (11), 1131–1140. doi:10.1093/abbs/gmy108

Jean-Charles, P. Y., Wu, J. H., Zhang, L., Kaur, S., Nepliouev, I., Stiber, J. A., et al. (2018). USP20 (Ubiquitin-Specific Protease 20) Inhibits TNF (Tumor Necrosis Factor)-Triggered Smooth Muscle Cell Inflammation and Attenuates Atherosclerosis. *Arterioscler Thromb. Vasc. Biol.* 38 (10), 2295–2305. doi:10.1161/ATVBAHA.118.311071

Jiao, H., Wachsmuth, L., Kumari, S., Schwarzer, R., Lin, J., Eren, R. O., et al. (2020). Z-nucleic-acid Sensing Triggers ZBP1-dependent Necroptosis and Inflammation. *Nature* 580 (7803), 391–395. doi:10.1038/s41586-020-2129-8

Kanayama, A., Seth, R. B., Sun, L., Ea, C. K., Hong, M., Shaito, A., et al. (2004). TAB2 and TAB3 Activate the NF-kappaB Pathway through Binding to Polyubiquitin Chains. *Mol. Cel* 15 (4), 535–548. doi:10.1016/j.molcel.2004.08.008

Kang, P., Wang, J., Fang, D., Fang, T., Yu, Y., Zhang, W., et al. (2020). Activation of ALDH2 Attenuates High Glucose Induced Rat Cardiomyocyte Fibrosis and Necroptosis. *Free Radic. Biol. Med.* 146, 198–210. doi:10.1016/j.freeradbiomed.2019.10.416

Kanou, T., Ohsumi, A., Kim, H., Chen, M., Bai, X., Guan, Z., et al. (2018). Inhibition of Regulated Necrosis Attenuates Receptor-Interacting Protein Kinase 1-mediated Ischemia-Reperfusion Injury after Lung Transplantation. *J. Heart Lung Transpl.* 37 (10), 1261–1270. doi:10.1016/j.healun.2018.04.005

Karshovska, E., Wei, Y., Subramanian, P., Mohibullah, R., Geissler, C., Baatsch, I., et al. (2020). HIF-1α (Hypoxia-Inducible Factor-1α) Promotes Macrophage Necroptosis by Regulating miR-210 and miR-383. *Atvb* 40 (3), 583–596. doi:10.1161/ATVBAHA.119.313290

Karunakaran, D., Geoffrion, M., Wei, L., Gan, W., Richards, L., Shangari, P., et al. (2016). Targeting Macrophage Necroptosis for Therapeutic and Diagnostic Interventions in Atherosclerosis. *Sci. Adv.* 2 (7), e1600224. doi:10.1126/sciadv.1600224

Kavurma, M. M., Rayner, K. J., and Karunakaran, D. (2017). The Walking Dead: Macrophage Inflammation and Death in Atherosclerosis. *Curr. Opin. Lipidol.* 28 (2), 91–98. doi:10.1097/MOL.0000000000000394

Kelliher, M. A., Grimm, S., Ishida, Y., Kuo, F., Stanger, B. Z., and Leder, P. (1998). The Death Domain Kinase RIP Mediates the TNF-Induced NF-kappaB Signal. *Immunity* 8 (3), 297–303. doi:10.1016/s1074-7613(00)80535-x

Kim, H., Zamel, R., Bai, X. H., Lu, C., Keshavjee, S., Keshavjee, S., et al. (2018). Ischemia-reperfusion Induces Death Receptor-independent Necroptosis via Calpain-STAT3 Activation in a Lung Transplant Setting. *Am. J. Physiol. Lung Cel Mol Physiol* 315 (4), L595–l608. doi:10.1152/ajplung.00069.2018

Koshinuma, S., Miyamae, M., Kaneda, K., Kotani, J., and Figueredo, V. M. (2014). Combination of Necroptosis and Apoptosis Inhibition Enhances Cardioprotection against Myocardial Ischemia-Reperfusion Injury. *J. Anesth.* 28 (2), 235–241. doi:10.1007/s00540-013-1716-3

Kwok, C., Pavlosky, A., Lian, D., Jiang, J., Huang, X., Yin, Z., et al. (2017). Necroptosis Is Involved in CD4+ T Cell-Mediated Microvascular Endothelial Cell Death and Chronic Cardiac Allograft Rejection. *Transplantation* 101 (9), 2026–2037. doi:10.1097/tp.0000000000001578

Lange, C., Sommerfeld, M., Namsolleck, P., Kintscher, U., Unger, T., and Kaschina, E. (2018). AT2R (Angiotensin AT2 Receptor) Agonist, Compound 21, Prevents Abdominal Aortic Aneurysm Progression in the Rat. *Hypertension* 72 (3), e20–e29. doi:10.1161/HYPERTENSIONAHA.118.11168

Lau, A., Wang, S., Jiang, J., Haig, A., Pavlosky, A., Linkermann, A., et al. (2013). RIPK3-mediated Necroptosis Promotes Donor Kidney Inflammatory Injury and Reduces Allograft Survival. *Am. J. Transpl.* 13 (11), 2805–2818. doi:10.1111/ajt.12447

León, M. A., Palma, C., Hernández, C., Sandoval, M., Cofre, C., Perez-Mateluna, G., et al. (2019). *Helicobacter pylori* Pediatric Infection Changes FcεRI Expression in Dendritic Cells and Treg Profile In vivo and In vitro. *Microbes Infect.* 21 (10), 449–455. doi:10.1016/j.micinf.2019.05.001

Li, P., Nijhawan, D., Budihardjo, I., Srinivasula, S. M., Ahmad, M., Alnemri, E. S., et al. (1997). Cytochrome C and dATP-dependent Formation of Apaf-1/caspase-9 Complex Initiates an Apoptotic Protease cascade. *Cell* 91 (4), 479–489. doi:10.1016/s0092-8674(00)80434-1

Li, J., Mcquade, T., Siemer, A. B., Napetschnig, J., Moriwaki, K., Hsiao, Y. S., et al. (2012). The RIP1/RIP3 Necrosome Forms a Functional Amyloid Signaling Complex Required for Programmed Necrosis. *Cell* 150 (2), 339–350. doi:10.1016/j.cell.2012.06.019

Li, L., Chen, Y., Doan, J., Murray, J., Molkentin, J. D., and Liu, Q. (2014). Transforming Growth Factor β-activated Kinase 1 Signaling Pathway Critically Regulates Myocardial Survival and Remodeling. *Circulation* 130 (24), 2162–2172. doi:10.1161/CIRCULATIONAHA.114.011195

Liang, W., Chen, M., Zheng, D., He, J., Song, M., Mo, L., et al. (2017a). A Novel Damage Mechanism: Contribution of the Interaction between Necroptosis and ROS to High Glucose-Induced Injury and Inflammation in H9c2 Cardiac Cells. *Int. J. Mol. Med.* 40 (1), 201–208. doi:10.3892/ijmm.2017.3006

Liang, W., Chen, M., Zheng, D., Li, J., Song, M., Zhang, W., et al. (2017b). The Opening of ATP-Sensitive K+ Channels Protects H9c2 Cardiac Cells against the High Glucose-Induced Injury and Inflammation by Inhibiting the ROS-TLR4-Necroptosis Pathway. *Cell Physiol Biochem* 41 (3), 1020–1034. doi:10.1159/000461391

Lin, J., Li, H., Yang, M., Ren, J., Huang, Z., Han, F., et al. (2013). A Role of RIP3-Mediated Macrophage Necrosis in Atherosclerosis Development. *Cel Rep* 3 (1), 200–210. doi:10.1016/j.celrep.2012.12.012

Liu, D., Lei, L., Desir, M., Huang, Y., Cleman, J., Jiang, W., et al. (2016a). Smooth Muscle Hypoxia-Inducible Factor 1α Links Intravascular Pressure and Atherosclerosis-Brief Report. *Arterioscler Thromb. Vasc. Biol.* 36 (3), 442–445. doi:10.1161/ATVBAHA.115.306861

Liu, J., Wu, P., Wang, H., Wang, Y., Du, Y., Cheng, W., et al. (2016b). Necroptosis Induced by Ad-HGF Activates Endogenous C-Kit+ Cardiac Stem Cells and Promotes Cardiomyocyte Proliferation and Angiogenesis in the Infarcted Aged Heart. *Cel Physiol. Biochem.* 40 (5), 847–860. doi:10.1159/000453144

Liu, J., Wu, P., Wang, Y., Du, Y., A, N., Liu, S., et al. (2016c). Ad-HGF Improves the Cardiac Remodeling of Rat Following Myocardial Infarction by Upregulating Autophagy and Necroptosis and Inhibiting Apoptosis. *Am. J. Transl Res.* 8 (11), 4605–4627.

Longo, G. M., Xiong, W., Greiner, T. C., Zhao, Y., Fiotti, N., and Baxter, B. T. (2002). Matrix Metalloproteinases 2 and 9 Work in Concert to Produce Aortic Aneurysms. *J. Clin. Invest.* 110 (5), 625–632. doi:10.1172/JCI15334

Luedde, M., Lutz, M., Carter, N., Sosna, J., Jacoby, C., Vucur, M., et al. (2014). RIP3, a Kinase Promoting Necroptotic Cell Death, Mediates Adverse Remodelling after Myocardial Infarction. *Cardiovasc. Res.* 103 (2), 206–216. doi:10.1093/cvr/cvu146

Luo, W., Wang, Y., Zhang, L., Ren, P., Zhang, C., Li, Y., et al. (2020). Critical Role of Cytosolic DNA and its Sensing Adaptor STING in Aortic Degeneration, Dissection, and Rupture. *Circulation* 141 (1), 42–66. doi:10.1161/CIRCULATIONAHA.119.041460

Marín, E., Cuturi, M. C., and Moreau, A. (2018). Tolerogenic Dendritic Cells in Solid Organ Transplantation: Where Do We Stand? *Front. Immunol.* 9, 274. doi:10.3389/fimmu.2018.00274

Meng, L., Jin, W., and Wang, X. (2015). RIP3-mediated Necrotic Cell Death Accelerates Systematic Inflammation and Mortality. *Proc. Natl. Acad. Sci. U S A.* 112 (35), 11007–11012. doi:10.1073/pnas.1514730112

Meng, L., Jin, W., Wang, Y., Huang, H., Li, J., and Zhang, C. (2016). RIP3-dependent Necrosis Induced Inflammation Exacerbates Atherosclerosis. *Biochem. Biophys. Res. Commun.* 473 (2), 497–502. doi:10.1016/j.bbrc.2016.03.059

Micheau, O., and Tschopp, J. (2003). Induction of TNF Receptor I-Mediated Apoptosis via Two Sequential Signaling Complexes. *Cell* 114 (2), 181–190. doi:10.1016/s0092-8674(03)00521-x

Miura, H., Wachtel, R. E., Loberiza, F. R., Jr., Saito, T., Miura, M., Nicolosi, A. C., et al. (2003). Diabetes Mellitus Impairs Vasodilation to Hypoxia in Human Coronary Arterioles: Reduced Activity of ATP-Sensitive Potassium Channels. *Circ. Res.* 92 (2), 151–158. doi:10.1161/01.res.0000052671.53256.49

Mizushima, N., and Komatsu, M. (2011). Autophagy: Renovation of Cells and Tissues. *Cell* 147 (4), 728–741. doi:10.1016/j.cell.2011.10.026

Mocarski, E. S., Upton, J. W., and Kaiser, W. J. (2011). Viral Infection and the Evolution of Caspase 8-regulated Apoptotic and Necrotic Death Pathways. *Nat. Rev. Immunol.* 12 (2), 79–88. doi:10.1038/nri3131

Moore, K. J., and Tabas, I. (2011). Macrophages in the Pathogenesis of Atherosclerosis. *Cell* 145 (3), 341–355. doi:10.1016/j.cell.2011.04.005

Moquin, D. M., Mcquade, T., and Chan, F. K. (2013). CYLD Deubiquitinates RIP1 in the TNFα-Induced Necrosome to Facilitate Kinase Activation and Programmed Necrosis. *PLoS One* 8 (10), e76841. doi:10.1371/journal.pone.0076841

Mossmann, D., Park, S., and Hall, M. N. (2018). mTOR Signalling and Cellular Metabolism Are Mutual Determinants in Cancer. *Nat. Rev. Cancer* 18 (12), 744–757. doi:10.1038/s41568-018-0074-8

Murphy, J. M., Czabotar, P. E., Hildebrand, J. M., Lucet, I. S., Zhang, J. G., Alvarez-Diaz, S., et al. (2013). The Pseudokinase MLKL Mediates Necroptosis via a Molecular Switch Mechanism. *Immunity* 39 (3), 443–453. doi:10.1016/j.immuni.2013.06.018

Newton, K., Wickliffe, K. E., Maltzman, A., Dugger, D. L., Strasser, A., Pham, V. C., et al. (2016). RIPK1 Inhibits ZBP1-Driven Necroptosis during Development. *Nature* 540 (7631), 129–133. doi:10.1038/nature20559

Newton, K. (2015). RIPK1 and RIPK3: Critical Regulators of Inflammation and Cell Death. *Trends Cel Biol.* 25 (6), 347–353. doi:10.1016/j.tcb.2015.01.001

O'donnell, M. A., Hase, H., Legarda, D., and Ting, A. T. (2012). NEMO Inhibits Programmed Necrosis in an NFκB-independent Manner by Restraining RIP1. *PLoS One* 7 (7), e41238. doi:10.1371/journal.pone.0041238

Oerlemans, M. I., Liu, J., Arslan, F., Den Ouden, K., Van Middelaar, B. J., Doevendans, P. A., et al. (2012). Inhibition of RIP1-dependent Necrosis Prevents Adverse Cardiac Remodeling after Myocardial Ischemia-Reperfusion *In Vivo*. *Basic Res. Cardiol.* 107 (4), 270. doi:10.1007/s00395-012-0270-8

Ogasawara, M., Yano, T., Tanno, M., Abe, K., Ishikawa, S., Miki, T., et al. (2017). Suppression of Autophagic Flux Contributes to Cardiomyocyte Death by

Activation of Necroptotic Pathways. *J. Mol. Cel Cardiol.* 108, 203–213. doi:10.1016/j.yjmcc.2017.06.008

Ovize, M., Baxter, G. F., Di Lisa, F., Ferdinandy, P., Garcia-Dorado, D., Hausenloy, D. J., et al. (2010). Postconditioning and protection from Reperfusion Injury: where Do We Stand? Position Paper from the Working Group of Cellular Biology of the Heart of the European Society of Cardiology. *Cardiovasc. Res.* 87 (3), 406–423. doi:10.1093/cvr/cvq129

Pavlosky, A., Lau, A., Su, Y., Lian, D., Huang, X., Yin, Z., et al. (2014). RIPK3-mediated Necroptosis Regulates Cardiac Allograft Rejection. *Am. J. Transpl.* 14 (8), 1778–1790. doi:10.1111/ajt.12779

Peiser, L., Mukhopadhyay, S., and Gordon, S. (2002). Scavenger Receptors in Innate Immunity. *Curr. Opin. Immunol.* 14 (1), 123–128. doi:10.1016/s0952-7915(01)00307-7

Peltzer, N., Darding, M., and Walczak, H. (2016). Holding RIPK1 on the Ubiquitin Leash in TNFR1 Signaling. *Trends Cel Biol* 26 (6), 445–461. doi:10.1016/j.tcb.2016.01.006

Petersen, S. L., Wang, L., Yalcin-Chin, A., Li, L., Peyton, M., Minna, J., et al. (2007). Autocrine TNFalpha Signaling Renders Human Cancer Cells Susceptible to Smac-Mimetic-Induced Apoptosis. *Cancer Cell* 12 (5), 445–456. doi:10.1016/j.ccr.2007.08.029

Pobezinskaya, Y. L., Kim, Y. S., Choksi, S., Morgan, M. J., Li, T., Liu, C., et al. (2008). The Function of TRADD in Signaling through Tumor Necrosis Factor Receptor 1 and TRIF-dependent Toll-like Receptors. *Nat. Immunol.* 9 (9), 1047–1054. doi:10.1038/ni.1639

Przyklenk, K. (1997). Lethal Myocardial "Reperfusion Injury": The Opinions of Good Men. *J. Thromb. Thrombolysis* 4 (1), 5–6. doi:10.1023/a:1017549827004

Reventun, P., Sanchez-Esteban, S., Cook, A., Cuadrado, I., Roza, C., Moreno-Gomez-Toledano, R., et al. (2020). Bisphenol A Induces Coronary Endothelial Cell Necroptosis by Activating RIP3/CamKII Dependent Pathway. *Sci. Rep.* 10 (1), 4190. doi:10.1038/s41598-020-61014-1

Reyes, L. F., Restrepo, M. I., Hinojosa, C. A., Soni, N. J., Anzueto, A., Babu, B. L., et al. (2017). Severe Pneumococcal Pneumonia Causes Acute Cardiac Toxicity and Subsequent Cardiac Remodeling. *Am. J. Respir. Crit. Care Med.* 196 (5), 609–620. doi:10.1164/rccm.201701-0104OC

Sarhan, J., Liu, B. C., Muendlein, H. I., Weindel, C. G., Smirnova, I., Tang, A. Y., et al. (2019). Constitutive Interferon Signaling Maintains Critical Threshold of MLKL Expression to License Necroptosis. *Cell Death Differ.* 26 (2), 332–347. doi:10.1038/s41418-018-0122-7

Saveljeva, S., Mc Laughlin, S. L., Vandenabeele, P., Samali, A., and Bertrand, M. J. (2015). Endoplasmic Reticulum Stress Induces Ligand-independent TNFR1-Mediated Necroptosis in L929 Cells. *Cell Death Dis.* 6, e1587. doi:10.1038/cddis.2014.548

Saxton, R. A., and Sabatini, D. M. (2017). mTOR Signaling in Growth, Metabolism, and Disease. *Cell* 168 (6), 960–976. doi:10.1016/j.cell.2017.02.004

Schinnerling, K., García-González, P., and Aguillón, J. C. (2015). Gene Expression Profiling of Human Monocyte-Derived Dendritic Cells - Searching for Molecular Regulators of Tolerogenicity. *Front. Immunol.* 6, 528. doi:10.3389/fimmu.2015.00528

Sciarretta, S., Maejima, Y., Zablocki, D., and Sadoshima, J. (2018). The Role of Autophagy in the Heart. *Annu. Rev. Physiol.* 80, 1–26. doi:10.1146/annurev-physiol-021317-121427

Shan, B., Pan, H., Najafov, A., and Yuan, J. (2018). Necroptosis in Development and Diseases. *Genes Dev.* 32 (5-6), 327–340. doi:10.1101/gad.312561.118

Shimizu, K., Mitchell, R. N., and Libby, P. (2006). Inflammation and Cellular Immune Responses in Abdominal Aortic Aneurysms. *Arterioscler Thromb. Vasc. Biol.* 26 (5), 987–994. doi:10.1161/01.ATV.0000214999.12921.4f

Skålén, K., Gustafsson, M., Rydberg, E. K., Hultén, L. M., Wiklund, O., Innerarity, T. L., et al. (2002). Subendothelial Retention of Atherogenic Lipoproteins in Early Atherosclerosis. *Nature* 417 (6890), 750–754. doi:10.1038/nature00804

Skemiene, K., Jablonskiene, G., Liobikas, J., and Borutaite, V. (2013). Protecting the Heart against Ischemia/reperfusion-Induced Necrosis and Apoptosis: the Effect of Anthocyanins. *Medicina (Kaunas)* 49 (2), 84–88.

Soppert, J., Kraemer, S., Beckers, C., Averdunk, L., Möllmann, J., Denecke, B., et al. (2018). Soluble CD74 Reroutes MIF/CXCR4/AKT-Mediated Survival of Cardiac Myofibroblasts to Necroptosis. *J. Am. Heart Assoc.* 7 (17), e009384. doi:10.1161/JAHA.118.009384

Stanger, B. Z., Leder, P., Lee, T. H., Kim, E., and Seed, B. (1995). RIP: a Novel Protein Containing a Death Domain that Interacts with Fas/APO-1 (CD95) in Yeast and Causes Cell Death. *Cell* 81 (4), 513–523. doi:10.1016/0092-8674(95)90072-1

Subramanian, V., Golledge, J., Ijaz, T., Bruemmer, D., and Daugherty, A. (2010). Pioglitazone-induced Reductions in Atherosclerosis Occur via Smooth Muscle Cell-specific Interaction with PPAR{gamma}. *Circ. Res.* 107 (8), 953–958. doi:10.1161/CIRCRESAHA.110.219089

Sun, X., Lee, J., Navas, T., Baldwin, D. T., Stewart, T. A., and Dixit, V. M. (1999). RIP3, a Novel Apoptosis-Inducing Kinase. *J. Biol. Chem.* 274 (24), 16871–16875. doi:10.1074/jbc.274.24.16871

Sun, L., Wang, H., Wang, Z., He, S., Chen, S., Liao, D., et al. (2012). Mixed Lineage Kinase Domain-like Protein Mediates Necrosis Signaling Downstream of RIP3 Kinase. *Cell* 148 (1-2), 213–227. doi:10.1016/j.cell.2011.11.031

Tian, F., Yao, J., Yan, M., Sun, X., Wang, W., Gao, W., et al. (2016). 5-Aminolevulinic Acid-Mediated Sonodynamic Therapy Inhibits RIPK1/RIPK3-Dependent Necroptosis in THP-1-Derived Foam Cells. *Sci. Rep.* 6, 21992. doi:10.1038/srep21992

Tuuminen, R., Holmström, E., Raissadati, A., Saharinen, P., Rouvinen, E., Krebs, R., et al. (2016). Simvastatin Pretreatment Reduces Caspase-9 and RIPK1 Protein Activity in Rat Cardiac Allograft Ischemia-Reperfusion. *Transpl. Immunol.* 37, 40–45. doi:10.1016/j.trim.2016.05.001

Wang, Q., Liu, Z., Ren, J., Morgan, S., Assa, C., and Liu, B. (2015). Receptor-interacting Protein Kinase 3 Contributes to Abdominal Aortic Aneurysms via Smooth Muscle Cell Necrosis and Inflammation. *Circ. Res.* 116 (4), 600–611. doi:10.1161/CIRCRESAHA.116.304899

Wang, Q., Zhou, T., Liu, Z., Ren, J., Phan, N., Gupta, K., et al. (2017). Inhibition of Receptor-Interacting Protein Kinase 1 with Necrostatin-1s Ameliorates Disease Progression in Elastase-Induced Mouse Abdominal Aortic Aneurysm Model. *Sci. Rep.* 7, 42159. doi:10.1038/srep42159

Weinlich, R., Oberst, A., Beere, H. M., and Green, D. R. (2017). Necroptosis in Development, Inflammation and Disease. *Nat. Rev. Mol. Cel Biol.* 18 (2), 127–136. doi:10.1038/nrm.2016.149

Weirather, J., Hofmann, U. D., Beyersdorf, N., Ramos, G. C., Vogel, B., Frey, A., et al. (2014). Foxp3+ CD4+ T Cells Improve Healing after Myocardial Infarction by Modulating Monocyte/macrophage Differentiation. *Circ. Res.* 115 (1), 55–67. doi:10.1161/CIRCRESAHA.115.303895

Witztum, J. L. (1994). The Oxidation Hypothesis of Atherosclerosis. *Lancet* 344 (8925), 793–795. doi:10.1016/s0140-6736(94)92346-9

Yahagi, K., Kolodgie, F. D., Otsuka, F., Finn, A. V., Davis, H. R., Joner, M., et al. (2016). Pathophysiology of Native Coronary, Vein Graft, and In-Stent Atherosclerosis. *Nat. Rev. Cardiol.* 13 (2), 79–98. doi:10.1038/nrcardio.2015.164

Yang, Q. H., and Du, C. (2004). Smac/DIABLO Selectively Reduces the Levels of C-IAP1 and C-IAP2 but Not that of XIAP and Livin in HeLa Cells. *J. Biol. Chem.* 279 (17), 16963–16970. doi:10.1074/jbc.M401253200

Yang, Z., Li, C., Wang, Y., Yang, J., Yin, Y., Liu, M., et al. (2018). Melatonin Attenuates Chronic Pain Related Myocardial Ischemic Susceptibility through Inhibiting RIP3-MLKL/CaMKII Dependent Necroptosis. *J. Mol. Cel Cardiol* 125, 185–194. doi:10.1016/j.yjmcc.2018.10.018

Yang, B., Wang, Y., Qin, Q., Xia, X., Liu, Z., Song, E., et al. (2019a). Polychlorinated Biphenyl Quinone Promotes Macrophage-Derived Foam Cell Formation. *Chem. Res. Toxicol.* 32 (12), 2422–2432. doi:10.1021/acs.chemrestox.9b00184

Yang, J., Zhang, F., Shi, H., Gao, Y., Dong, Z., Ma, L., et al. (2019b). Neutrophil-derived Advanced Glycation End Products-Nε-(carboxymethyl) Lysine Promotes RIP3-Mediated Myocardial Necroptosis via RAGE and Exacerbates Myocardial Ischemia/Reperfusion Injury. *FASEB J.* 33 (12), 14410–14422. doi:10.1096/fj.201900115RR

You, Q., Wu, Z., Wu, B., Liu, C., Huang, R., Yang, L., et al. (2016). Naringin Protects Cardiomyocytes against Hyperglycemia-Induced Injuries *In Vitro* and *In Vivo*. *J. Endocrinol.* 230 (2), 197–214. doi:10.1530/JOE-16-0004

Yue, L. J., Zhu, X. Y., Li, R. S., Chang, H. J., Gong, B., Tian, C. C., et al. (2019). Sallylcysteine Sulfoxide (Alliin) Alleviates Myocardial Infarction by Modulating Cardiomyocyte Necroptosis and Autophagy. *Int. J. Mol. Med.* 44 (5), 1943–1951. doi:10.3892/ijmm.2019.4351

Zhang, D., Lin, J., and Han, J. (2010). Receptor-interacting Protein (RIP) Kinase Family. *Cell Mol Immunol.* 7 (4), 243–249. doi:10.1038/cmi.2010.10

Zhang, T., Zhang, Y., Cui, M., Jin, L., Wang, Y., Lv, F., et al. (2016). CaMKII Is a RIP3 Substrate Mediating Ischemia- and Oxidative Stress-Induced Myocardial Necroptosis. *Nat. Med.* 22 (2), 175–182. doi:10.1038/nm.4017

Zhang, H., Yin, Y., Liu, Y., Zou, G., Huang, H., Qian, P., et al. (2020). Necroptosis Mediated by Impaired Autophagy Flux Contributes to Adverse Ventricular Remodeling after Myocardial Infarction. *Biochem. Pharmacol.* 175, 113915. doi:10.1016/j.bcp.2020.113915

Zhao, W., Li, C., Zhang, H., Zhou, Q., Chen, X., Han, Y., et al. (2021). Dihydrotanshinone I Attenuates Plaque Vulnerability in Apolipoprotein E-Deficient Mice: Role of Receptor-Interacting Protein 3. *Antioxid. Redox Signal.* 34 (5), 351–363. doi:10.1089/ars.2019.7796

Zhou, F., Jiang, X., Teng, L., Yang, J., Ding, J., and He, C. (2018a). Necroptosis May Be a Novel Mechanism for Cardiomyocyte Death in Acute Myocarditis. *Mol. Cel Biochem* 442 (1-2), 11–18. doi:10.1007/s11010-017-3188-5

Zhou, H., Li, D., Zhu, P., Ma, Q., Toan, S., Wang, J., et al. (2018b). Inhibitory Effect of Melatonin on Necroptosis via Repressing the Ripk3-PGAM5-CypD-mPTP Pathway Attenuates Cardiac Microvascular Ischemia-Reperfusion Injury. *J. Pineal Res.* 65 (3), e12503. doi:10.1111/jpi.12503

Zhou, T., Wang, Q., Phan, N., Ren, J., Yang, H., Feldman, C. C., et al. (2019). Identification of a Novel Class of RIP1/RIP3 Dual Inhibitors that Impede Cell Death and Inflammation in Mouse Abdominal Aortic Aneurysm Models. *Cel Death Dis* 10 (3), 226. doi:10.1038/s41419-019-1468-6

Zhu, P., Hu, S., Jin, Q., Li, D., Tian, F., Toan, S., et al. (2018). Ripk3 Promotes ER Stress-Induced Necroptosis in Cardiac IR Injury: A Mechanism Involving Calcium overload/XO/ROS/mPTP Pathway. *Redox Biol.* 16, 157–168. doi:10.1016/j.redox.2018.02.019

Conflict of Interest: The authors declare that the research was conducted in the absence of any commercial or financial relationships that could be construed as a potential conflict of interest.

Publisher's Note: All claims expressed in this article are solely those of the authors and do not necessarily represent those of their affiliated organizations, or those of the publisher, the editors and the reviewers. Any product that may be evaluated in this article, or claim that may be made by its manufacturer, is not guaranteed or endorsed by the publisher.

GLOSSARY

APJ angiotensin domain type 1 receptor-associated proteins
ApoE apolipoprotein E
cIAP cellular inhibitors of apoptosis
CML ε-(carboxymethyl) lysine
CypD cyclophilin D
DAMP damage-associated molecular pattern
DD death domain
DR death receptor
Drp1 dynamin-related protein 1
HGF hepatocyte growth factor
HIF-1 hypoxia-inducible factor-1
HMGB1 high mobility group protein 1
LC3 microtubule-associated protein 1 light chain 3
LUBAC linear ubiquitin chain assembly complex
MAPK mitogen-activated protein kinase
MLKL mixed lineage kinase domain-like
mPTP mitochondrial permeability transition pore
NF-κB nuclear factor κB
OxLDL oxidized low-density lipoprotein
RHIM RIP homotypic interaction motif
RIPK1/3 receptor interacting protein kinases 1/3
ROS reactive oxygen species
TAB TAK1-binding proteins
TAK1 transforming growth factor-b-activated kinase 1
TFEB transcriptional factor EB
TLR toll like receptors
TNF tumor necrosis factor
TNFR tumor necrosis factor receptor
TRAF TNFR-associated factors
TRAIL TNF-related apoptosis-inducing ligand
ZBP-1 Z-DNA-binding protein 1

frontiers in Pharmacology

ORIGINAL RESEARCH
published: 01 December 2021
doi: 10.3389/fphar.2021.724777

Intermedin Inhibits the Ox-LDL–Induced Inflammation in RAW264.7 Cells by Affecting Fatty Acid–Binding Protein 4 Through the PKA Pathway

Kai Liu[1†], Rufeng Shi[1,2†], Si Wang[1], Qi Liu[2], Hengyu Zhang[1] and Xiaoping Chen[1*]*

[1]Cardiology Department, West China Hospital, Sichuan University, Chengdu, China, [2]State Key Laboratory of Biotherapy, The Molecular Medicine Research Center, West China Hospital, Sichuan University, Chengdu, China

OPEN ACCESS

Edited by:
Yao Lu,
Central South University, China

Reviewed by:
Yuanli Chen,
Hefei University of Technology, China
Xianwei Wang,
Xinxiang Medical University, China

***Correspondence:**
Hengyu Zhang
Hengyuzhang_scu@126.com
Xiaoping Chen
xiaopingchen11@126.com

[†]These authors have contributed equally to this work and share first authorship

Specialty section:
This article was submitted to Inflammation Pharmacology, a section of the journal Frontiers in Pharmacology

Received: 14 June 2021
Accepted: 29 October 2021
Published: 01 December 2021

Citation:
Liu K, Shi R, Wang S, Liu Q, Zhang H and Chen X (2021) Intermedin Inhibits the Ox-LDL–Induced Inflammation in RAW264.7 Cells by Affecting Fatty Acid–Binding Protein 4 Through the PKA Pathway. Front. Pharmacol. 12:724777. doi: 10.3389/fphar.2021.724777

Objectives: Macrophages stimulated by oxidized low-density lipoprotein (ox-LDL) play an important role in the occurrence and progression of atherosclerosis. Fatty acid–binding protein 4 (FABP4), mainly existing in macrophages and adipocytes, can influence lipid metabolism and inflammation regulated by macrophages. Herein, we first established the connection between intermedin (IMD: a new peptide that has versatile biological activities in the cardiovascular system) and FABP4 and then investigated the influence of IMD on ox-LDL-induced changes in RAW264.7 macrophages line.

Methods: The bioinformatics analysis, such as gene ontology enrichment and protein–protein interactions, was performed. For ox-LDL–stimulated assays, RAW264.7 was first pretreated with IMD and then exposed to ox-LDL. To explore the cell signaling pathways of IMD on inflammatory inhibition, main signaling molecules were tested and then cells were co-incubated with relevant inhibitors, and then exposed/not exposed to IMD. Finally, cells were treated with ox-LDL. The protein and gene expression of FABP4, IL-6, and TNF-α were quantified by WB/ELISA and RT-qPCR.

Results: In the ox-LDL-stimulated assays, exposure of the RAW264.7 macrophages line to ox-LDL reduced cell viability and increased the expression of FABP4, as well as induced the release of IL-6 and TNF-α (all $p < 0.05$). On the other hand, IMD prevented ox-LDL–induced cell toxicity, FABP4 expression, and the inflammatory level in RAW264.7 (all $p < 0.05$) in a dose-dependent manner. The inhibition of FABP4 and the anti-inflammatory effect of IMD were partially suppressed by the protein kinase A (PKA) inhibitor H-89.

Conclusion: IMD can prevent ox-LDL–induced macrophage inflammation by inhibiting FABP4, whose signaling might partially occur via the PKA pathway.

Keywords: intermedin (17-47)/adrenomedullin 2 (17-47), fatty acid–binding protein 4, inflammation, RAW264.7 cells, PKA

INTRODUCTION

Cardiovascular diseases (CVDs) are the leading causes of mortality worldwide, while atherosclerosis (AS) is a major risk factor for CVDs (Taggart, 2010). The World Health Organization has predicted that, by 2030, the total number of deaths from CVDs will increase by 27% (Roger, 2015). Previous studies proved that statin, a cholesterol-lowering drug, could effectively reduce AS development and CVDs outcomes; however, the residual risk remains (Ridker et al., 2010). Besides lipid metabolism, inflammation also has an important role in AS pathogenesis (Yudkin et al., 2000). Thus, exploring an effective anti-inflammatory strategy to reduce inflammation could attenuate AS and CVD prognosis.

Fatty acid–binding protein 4 (FABP4), a member of the fatty acid–binding protein (FABP) family, is a soluble carrier protein with low molecular weight and high affinity with fatty acids that mainly exists in macrophages and adipocytes (Furuhashi et al., 2014). Macrophages uptake oxidizes low-density lipoprotein (ox-LDL) cholesterol by scavenger receptors to form foam cells, which is a main pathological feature of AS (Seidelmann et al., 2014). FABP4 has an important role in both the transport and metabolism of fatty acids and inflammation mediated by macrophages, thus making it a promising target for AS treatment (Furuhashi et al., 2014).

Intermedin (IMD), also known as adrenomedullin 2, is a biologically active peptide that belongs to the calcitonin gene–related peptide (CGRP) superfamily (Roh et al., 2004). Combining different receptors and G protein, IMD has versatile biological activities in organisms, especially in the cardiovascular system (Zhang et al., 2018). Yet, whether IMD has a protective effect on macrophage-regulated inflammation and its mechanism remain unknown. Consequently, the present study aimed to test IMD as an anti-inflammatory treatment in the course of macrophages stimulated by ox-LDL and investigate the potential mechanisms.

MATERIALS AND METHODS

Data Collection and Processing

All data sources that were included in the gene ontology (GO) enrichment analysis and protein–protein interaction (PPI) are publically available, as described below. Google Scholar and PubMed were used as search engines for protein identification. These proteins were proved or predicted to be the functional partners to the target protein. We downloaded the human gene annotations file from the GO website (http://geneontology.org) starting from May 01, 2021. The analysis was performed using STRING 11.0 (http://string-db.org/), g:Profiler (https://biit.cs.ut.ee/gprofiler/gost), and REVIGO (http://revigo.irb.hr/). The names of related proteins were searched in STRING, and codes were extracted. The codes used in STRING for PPI network and in g:Profiler for the GO analysis were molecular functions, cellular components, and biological processes. REVIGO was used for visualized illustration of predicted interactions between target proteins.

Materials

RAW264.7 cells were purchased from American Type Culture Collection. Dulbecco's modified Eagle's medium (DMEM), fetal bovine serum (FBS), and phosphate-buffered saline were obtained from Invitrogen (Carlsbad, CA, United States). Dimethyl sulfoxide (DMSO) and Cell Counting Kit-8 (CCK-8) were from KeyGEN BioTECH (Nanjing, China). IMD was acquired from Phoenix BioTECH (Beijing, China). Ox-LDL was obtained from Peking Union Biology (Beijing, China), and superoxide dismutase (SOD) and malondialdehyde (MDA) assay kits were purchased from Jiancheng Bioengineering Institute (Nanjing, China). Bovine serum albumin was purchased from Sigma-Aldrich (Saint Louis, MO, United States). The protein kinase A inhibitor (PKAI; H-89), protein kinase G inhibitor (PKGI; KT5823), and p38-mitogen–activated protein kinase inhibitor (p38-MAPKI; SB203580) were obtained from Beyotime Biotechnology (Shanghai, China). A PrimeScript™ RT reagent kit with gDNA Eraser and SYBR Premix EX Taq™ II were purchased from TaKaRa Bio (Tokyo, Japan). TNF-α and IL-6 kits for enzyme-linked immunosorbent assay (ELISA) were purchased from Invitrogen, as was 2′,7′-dichlorodihydrofluorescein diacetate. The first antibody for FABP4 (ab92501) and β-actin (ab8226) was bought from Abcam.

Cell Culture and Treatments

Cells were maintained in DMEM (high glucose) supplemented with 10% FBS, 100 U/ml penicillin, and 100 μg/ml streptomycin in 95% air and 5% CO_2 at 37°C. When cells presented monolayer and confluence up to 70%, they were pretreated with various concentrations (0, 20, 40, and 80 nmol/L) of IMD for 24 h and were subsequently incubated with 50 μg/ml ox-LDL for 24 h. To explore the cell signaling pathways of IMD for inhibition of inflammation and oxidative stress, sub-confluence cells were co-incubated/not co-incubated with H-89 (1 μmol/L, PKAI), KT5823 (1 μmol/L, PKGI), and SB203580 (1 μmol/L, p38-MAPKI) for 30 min, and then exposed/not exposed to 80 nmol/L IMD for 24 h. Finally, cells were treated with 50 μg/ml ox-LDL for another 24 h. The cells treated with equal amounts of DMSO were used as controls.

Cell Viability

RAW264.7 cells were plated at a density of 1×10^4 per well in a 96-well plate and incubated at 37°C. The cells were treated with different concentrations of IMD (0, 20, 40, and 80 nmol/L) for 24 h, after which the CCK-8 reagent (Nanjing, China) was added for 4 h. Thereafter, the absorbance at 450 nm was measured using an ELISA microplate reader (Benchmark; BioRad Laboratories, CA, United States). Cell viability was calculated relative to that of the control group. All experiments were performed in triplicate.

SOD Measurement

The cells were scraped and operated according to the SOD detection kit. The cells were centrifuged at 1,500 rpm/min for 10 min, and then precipitated. After the buffer was added, the cells were sonicated. The reagent was added to the cells according to the kit instruction and incubated at 37°C for 20 min. The absorption was read at 450 nm.

TABLE 1 | The sequence-specific primers for RT-PCR.

Gene	Forward primer 5′ to 3′	Reverse primer 5′ to 3′
β-actin	CTAAGGCCAACCGTGAAAG	ACCAGAGGCATACAGGGACA
FABP4	TCACCTGGAAGACAGCTCCT	AATCCCCATTTACGCTGATG
IL-6	AACGATGATGCACTTGCAGA	GAGCATTGGAAATTGGGGTA
TNF-α	ACACTCAGATCATCTTCTCAAAATTCG	GTGTGGGTGAGGAGCACGTAGT

MDA Measurement

The pretreatment of the cells is the same as mentioned in SOD measurement, followed by heating at 95°C for 20 min. The reagents required for the experiment were prepared and tested as the MDA kit instructed. The absorbance was read at 530 nm.

Western Blot

The method was previously described by Liao et al. (2017). In short, cells were lysed by using a 4× Sodium dodecyl sulfate (SDS) sample buffer and then the samples were boiled. 20 μg of the extract was loaded onto 12% SDS–polyacrylamide gel (PAGE) and transferred to polyvinylidene fluoride membranes (Bio-Rad, United States). Immunoblotting was performed using the first antibody overnight at 4°C. β-actin was used as the control protein. The blots were detected using an enhanced chemiluminescence reagent (Thermo, United States). The amount of each target was normalized by the level of β-actin in each sample. The experiments were repeated at least three times.

Enzyme-Linked Immunosorbent Assay

Cell supernatants (100 μl) were used to quantify IL-6 and TNF-α using TaKaRa Bio ELISA kits (TaKaRa, Japan) according to manufacturer's instructions. Briefly, human TNF-α and IL-6 antibodies were coated on 96-well plates followed by incubation for 2 h at room temperature with cell supernatants. Then, 100 μl of biotin-conjugated human TNF-α or IL-6 was added to the solution in each well, followed by incubation for 1 h at room temperature. Then, 100 μl of 1× streptavidin–horseradish peroxidase solution was placed in each well and incubated for 30 min at room temperature. A stabilized chromogen was added to each well, followed by incubation for 30 min in the dark at room temperature. Stop Solution (100 μl) was added to each well. The side of the plate was tapped to allow mixing. Finally, the plate was read, and a standard curve was generated.

Quantitative Real-time polymerase chain reaction (RT-PCR)

Total RNA was extracted from cultured RAW264.7 cells using MiniBEST Universal RNA Extraction Kit (TaKaRa, Japan), followed by reverse transcription into cDNA using the PrimeScript™ preamplification system (TaKaRa, Japan) according to the manufacture's protocol. PCR was then performed to estimate the expression of FABP4, IL-6, and TNF-α. The sequence-specific primers are shown in **Table 1**. After an initial denaturation for 5 min at 94°C, followed by 40 cycles of denaturation (95°C for 1 min), annealing (60°C for 1 min), extension (72°C for 1 min) ensued with a final extension of 72°C for 10 min. The β-actin mRNA amplified from the same samples served as the control.

RNA Interference

Lipofectamine RNAiMAX (Invitrogen, United States) targeting FABP4 and a scramble controlled small interfering RNA (scramble siRNA) were used to transfect RAW264.7 cells (2.5×10^5 per well, 6-well plates) transiently for 4 h. The primer sequences for FABP4 siRNA were sense, 5′-AUACUGAGAUUU CCUUCAU-3′, and antisense, 5′-GGUGGAAUGCGUCAU GAAA-3′.

Statistical Analyses

All experiments were performed at least three times, and the results are expressed as mean ± standard deviation of the mean (SD). One-way analysis of variance was used to analyze the group differences. $p < 0.05$ was considered as a statistically significant difference.

RESULTS

IMD Interacts With FABP4 and Regulates the Inflammatory Response

Data mining suggested the ten most related proteins to IMD, i.e., ADM, CALCRL, RAMP1, RAMP2, RAMP3, CALCA, IAPP, CALCR, CALCB, and POMC (**Supplementary Figure S1A**). Most of them belonged to the CGRP superfamily, which binds its ligand and activates multiple biological processes (**Supplementary Figures S1B,C**). Then, FABP4 was added into the analysis, revealing the interactions between IMD and FABP4 (**Supplementary Figures S2A,B**). Some of their biological processes were associated with lipid metabolism and inflammatory response (**Supplementary Figure S2C**).

IMD Ameliorates Ox-LDL–Induced Cytotoxic Effect in RAW264.7

Compared with the blank control group, the cell viability of 50 mg/L ox-LDL intervention treatment was significantly reduced (**Figure 1A**). However, when cells were pretreated with IMD, the cell viability gradually recovered in a dose-dependent manner compared to the ox-LDL alone intervention group (**Figure 1A**), which was in accordance with

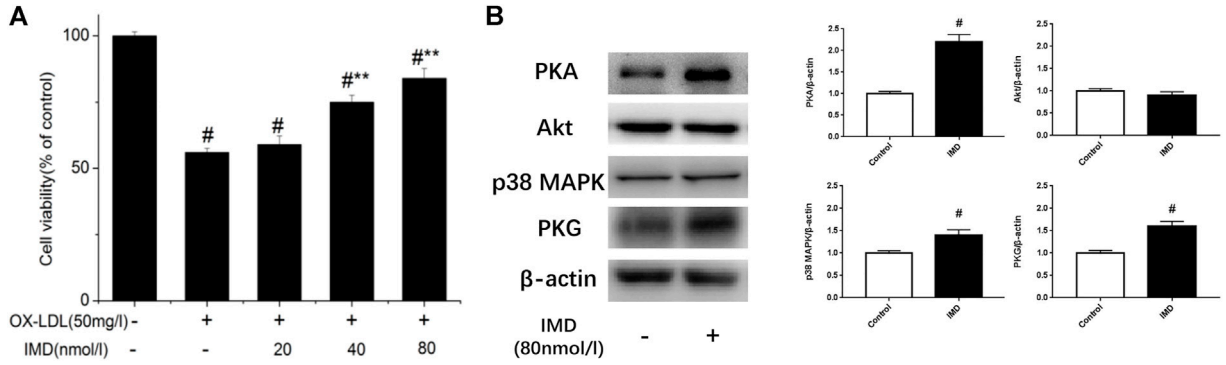

FIGURE 1 | Dose-dependent protective effect of IMD on ox-LDL–induced macrophages and its signaling pathway. # Compared with the control group ($p < 0.05$); ** compared to the ox-LDL alone group ($p < 0.05$).

TABLE 2 | Cell MDA and SOD activity.

Activity	Control group	Ox-LDL group	Ox-LDL + IMD group
SOD (μ/ml)	14.51 ± 1.13	12.47 ± 0.97[a]	13.97 ± 1.07[b]
MDA (nmol/ml)	2.89 ± 0.05	3.73 ± 0.08[a]	3.06 ± 0.09[b]

Control group was added carrier medium, ox-LDL group 50 mg/L ox-LDL; ox-LDL + IMD group 50 mg/L ox-LDL and 40 nmol/L IMD. Values are presented as the mean ± standard error of the mean.

[a]p < *0.01 vs. control group.*

[b]p < *0.01 vs. ox-LDL group.*

the oxidation activity (**Table 2**). Thus, it indicates that IMD could counteract the damage to macrophages that was stimulated by ox-LDL. Among IMD's main signaling molecules, Western blot showed that PKA, p38-mitogen–activated protein kinase, and protein kinase G were altered after IMD intervention (**Figure 1B**). Moreover, when 10 μmol/L H-89 (PKAI) was pretreated with 80 nmol/L IMD, the cytoprotective effect was partially inhibited (**Figure 2A**). Neither the 1 μmol/L KT5823 (p38 inhibitor) group nor the 1 μmol/L SB203580 (PKGI) group showed this phenomenon (**Figures 2B,C**).

IMD Inhibits Upregulated FABP4 in RAW264.7 Stimulated by Ox-LDL

The FABP4 expression was significantly increased in macrophages stimulated with 50 mg/L ox-LDL (**Figure 3A**),

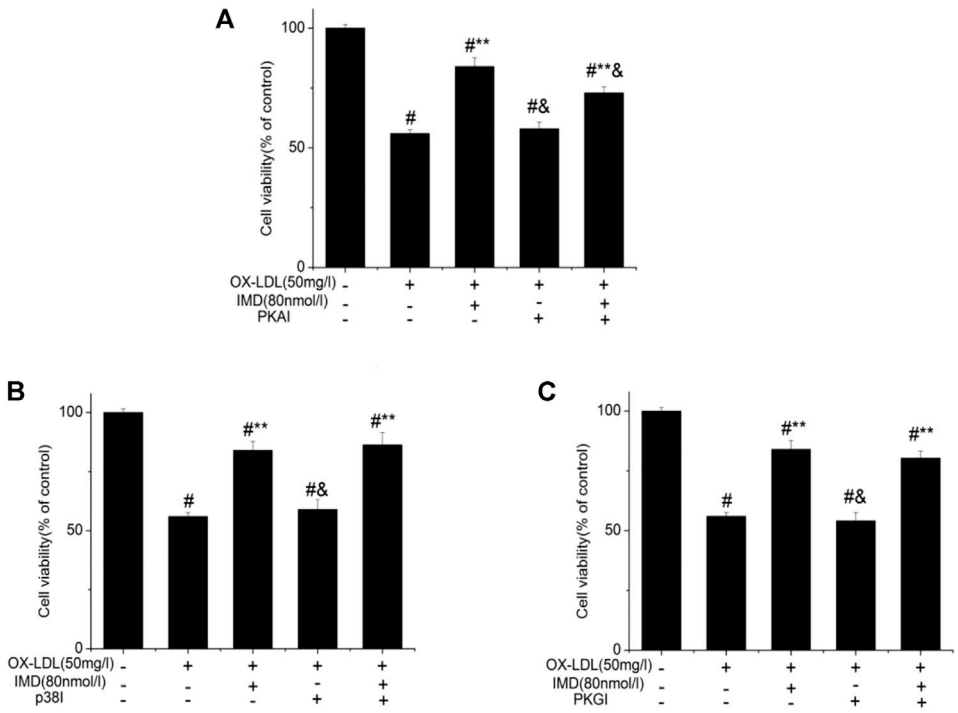

FIGURE 2 | Protective effect of IMD partially through the PKA pathway. # Compared with the control group ($p < 0.05$); ** compared to the ox-LDL alone group ($p < 0.05$); & compared to the ox-LDL + IMD group ($p < 0.05$).

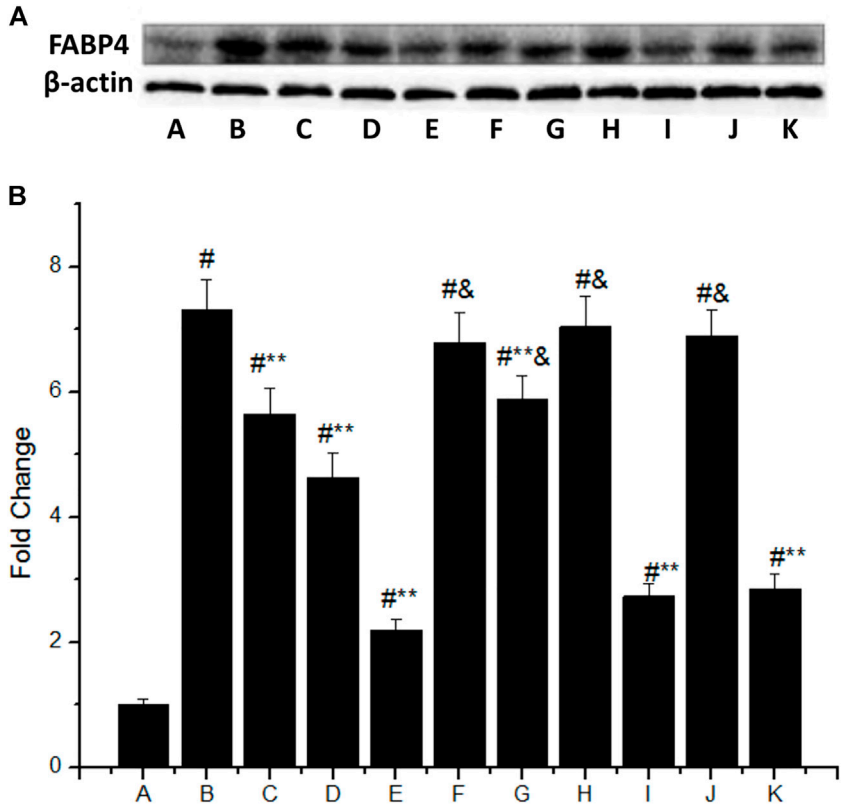

FIGURE 3 | IMD inhibits FABP4 protein expression dose-dependently in ox-LDL–stimulated macrophages partially through the PKA pathway. **(A)** Western blot for FABP4 protein in RAW264.7; **(B)** Quantitative band density analysis according to the gray image scanning, and normalization of all bands to housekeeping protein β-actin. **(A)** control group; **(B)** ox-LDL group; **(C)** ox-LDL+20 nm IMD group; **(D)** ox-LDL+40 nm IMD group; **(E)** ox-LDL+80 nm IMD group; **(F)** ox-LDL + PKAI group; **(G)** ox-LDL + PKAI+80 nm IMD group; **(H)** ox-LDL + p38 inhibitor group; **(I)** ox-LDL + p38 inhibitor+80 nm IMD group; **(J)** ox-LDL + PKGI group; **(K)** ox-LDL + PKGI +80 nm IMD group. $^{\#}$ Compared with group A ($p < 0.05$); ** compared to group B ($p < 0.05$); $^{\&}$ compared to group E ($p < 0.05$).

which was 7.3 times higher than that of the control group (group B vs. group A, $p < 0.05$). However, IMD could downregulate the mentioned incremental FABP4 in a concentration-dependent manner, where the FABP4 expression from low to high IMD concentration was 5.65, 4.63, and 2.2 times compared to the control group (compared with group B, all $p < 0.05$). The 80 nm IMD + PKAI group was 5.89 times compared to the control group (group G vs. group A, $p < 0.05$), while the 80 nm IMD alone group was 2.2 times compared to the control group (group E vs. group A, $p < 0.05$), thus indicating that the PKAI could partially inhibit this effect of IMD, while PKGI and p38 inhibitor did not block such inhibitory effect (**Figure 3B**).

Accordingly, RT-PCR revealed that the mRNA of FABP4 in the ox-LDL group was significantly higher than in the control group ($p < 0.05$). The mRNA of FABP4 in the 40 nmol/L IMD group was lower than in the ox-LDL group (3.27 ± 0.17 vs. 4.66 ± 0.31, $p < 0.05$), while the 80 nmol/L IMD group was lower than in the ox-LDL group (2.25 ± 0.14 vs. 4.66 ± 0.31, $p < 0.05$), which indicated that IMD could reduce the expression of the FABP4 gene (**Figure 4A**).

In addition, the mRNA of FABP4 in the PKAI group was increased compared with the ox-LDL + IMD group (**Figure 4B**; 3.66 ± 0.21 vs. 2.25 ± 0.14, $p < 0.05$), thus indicating that PKAI could partially inhibit IMD downregulation of the FABP4 gene expression. The p38 and PKGI groups had no such changes (**Figures 4C,D**).

IMD Reduced Ox-LDL–Stimulated Production of IL-6 and TNF-α

The anti-inflammatory effects of IMD on ox-LDL–induced production of IL-6 or TNF-α in the RAW264.7 cells were evaluated by ELISA, Western blot (WB), and RT-PCR. The protein and mRNA expression of both IL-6 and TNF-α were obviously increased in the cells treated with ox-LDL alone compared to the unstimulated cells (**Figures 6**, **7**, all $p < 0.05$). By contrast, IMD treatment reduced ox-LDL–stimulated production of IL-6 and TNF-α in a dose-dependent manner (**Figures 5**, **6**, all $p < 0.05$). Considering the protein level, the 40 nmol/L IMD group had significantly decreased IL-6 (**Figure 5A**; 3.23 ± 0.27 vs. 4.47 ± 0.11, by ELISA, $p < 0.05$) and TNF-α (**Figure 5C**; 2.71 ± 0.28 vs. 3.62 ± 0.34, by ELISA, $p < 0.05$) compared with the ox-LDL group, while 80 nmol/L showed a similar but more dramatic effect (**Figures 5A,C**; IL-6: 2.21 ±

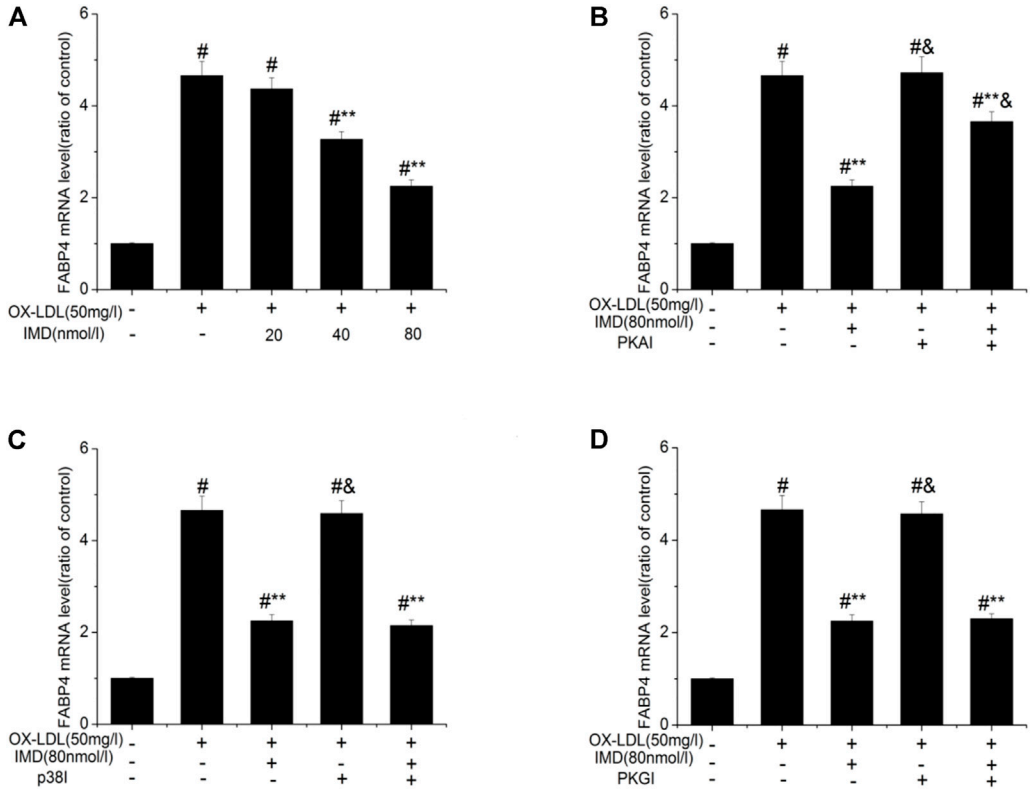

FIGURE 4 | IMD inhibits the mRNA expression of FABP4 in ox-LDL–induced macrophages. # Compared with the control group ($p < 0.05$); ** compared to the ox-LDL alone group ($p < 0.05$); & compared to the ox-LDL +IMD group ($p < 0.05$).

0.21 vs. 4.47 ± 0.11; TNF-α:1.76 ± 0.09 vs. 3.62 ± 0.34, by ELISA, both $p < 0.05$). At the mRNA level, the 40 nmol/L and 80 nmol/L IMD groups had significantly decreased IL-6 (**Figure 7A**; 1.89 ± 0.11 vs. 2.63 ± 0.19 vs. 3.26 ± 0.26, $p < 0.05$) and TNF-α (**Figure 7C**; 1.5 ± 0.1 vs. 2.0 ± 0.12 vs. 2.9 ± 0.13, $p < 0.05$), respectively. Similarly, the anti-inflammatory effect of IMD on the ox-LDL–induced release of IL-6 and TNF-α was inhibited when macrophages were pretreated with PKAI.

IMD Inhibit Inflammation Through FABP4

The FABP4 inhibitor was used to validate whether IMD fulfilled its anti-inflammatory effect via the FABP4 pathway. We used siRNA to knockdown FABP4, and its mRNA expression was significantly decreased (**Supplementary Figure S5**). Compared with the IMD intervention group, the production of IL-6 and TNF-α were almost recovered to the ox-LDL simulated level when FABP4 siRNA was pretreated, thus suggesting that IMD partially inhibited these inflammatory factors via the FABP4 pathway (**Figure 8**).

DISCUSSION

Our study showed that IMD counteracted the ox-LDL–induced injury in RAW264.7 cells by inhibiting FABP4. However, this process was partially inhibited by the PKAI. This data suggested that IMD inhibits the ox-LDL–induced inflammation in RAW264.7 cells by affecting fatty acid–binding protein 4 through the PKA pathway.

AS, one of the main causes of CVDs and cerebrovascular diseases, is considered a chronic inflammatory disease (Bobryshev et al., 2016). Lipid metabolism disorders are the basis of AS, triggering the subsequent inflammatory response regulated by macrophages (Bobryshev et al., 2016). After vascular endothelial cells are damaged, the vascular endothelium secretes adhesion molecules to mediate the adhesion of monocytes and lymphocytes. Once monocytes adhere, they migrate into the subintimal space of the damaged endothelium under the action of chemokines and transform into macrophages. Macrophages engulf ox-LDL-C–based cholesterol through CD36 and scavenger receptor A, promoting monocyte-derived macrophages to transform to foam cells and secrete proinflammatory cytokines, along with atherosclerotic lesions progress. Therefore, macrophages and inflammation that they regulate may be used as a promising target for AS therapy.

IMD and its receptor complex comprise calcitonin receptor-like receptor (CRLR), while receptor activity–modifying protein (RAMP) 1, 2, and 3 are highly expressed in the vasculature (Zhang et al., 2018). Coupling different G proteins, IMD presents diverse biological effects such as anti-inflammatory,

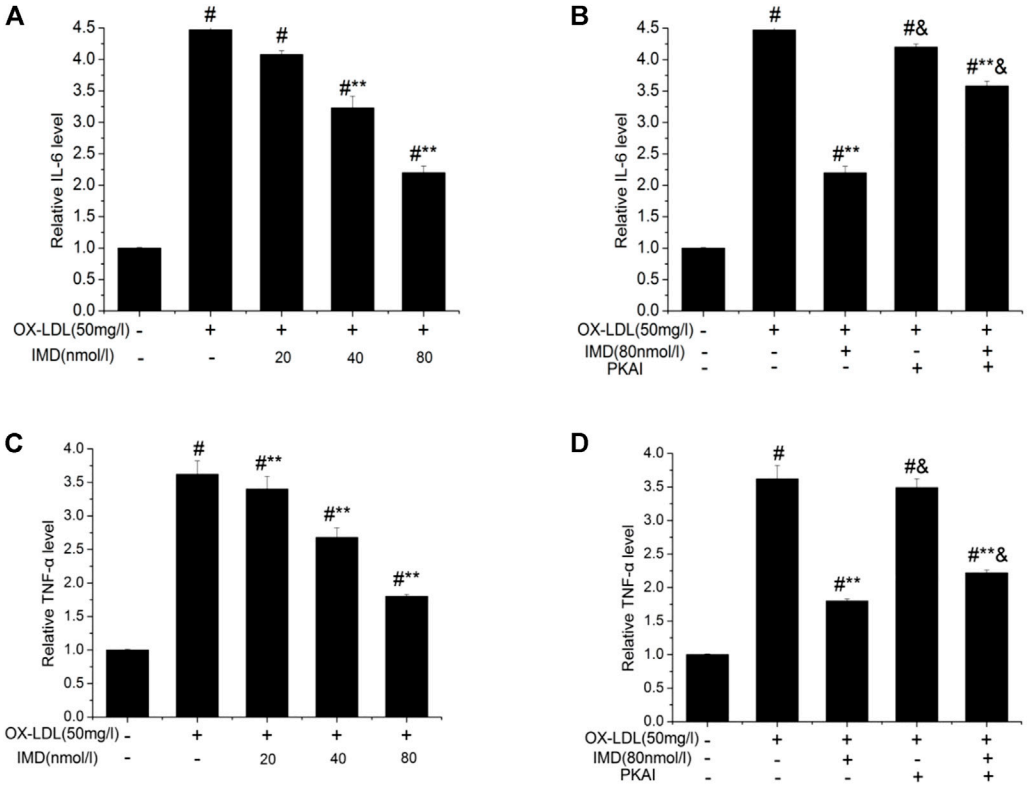

FIGURE 5 | IMD inhibits the protein expression of IL-6 and TNF-α in ox-LDL–induced macrophages (ELISA). # Compared with the control group ($p < 0.05$); ** compared to the ox-LDL alone group ($p < 0.05$); & compared to the ox-LDL +IMD group ($p < 0.05$).

anti-oxidation, and anti-apoptosis via a different signaling pathway. Consequently, IMD has a regulatory effect on cardiovascular homeostasis. Our previous study showed that IMD ameliorates AS in ApoE null mice (Zhang et al., 2012). Besides, a study suggested that IMD could prevent the atherosclerotic lesions progression by inhibiting ERS-CHOP–mediated apoptosis and inflammasome in macrophages (Ren et al., 2021). However, it remains unclear whether other mechanisms are involved.

Previous studies have proved that FABP4 is an important factor in the development of AS due to metaflammation. FABP4 knockout can prevent the development of AS in $ApoE^{-/-}$ mice (Makowski et al., 2001). On the other hand, the FABP4 expression is significantly upregulated during the process of ox-LDL–induced macrophages forming foam cells, which might be because ox-LDL induces FABP4 gene expression by activating the nuclear factor NF-κB and protein kinase C pathway (Fu et al., 2002). Other studies also suggested that peroxidase proliferator–activated receptor γ (PPARγ) might be involved (Fu et al., 2002; Makowski et al., 2005). Bone marrow transplantation studies have confirmed that this effect should be attributed to FABP4 in macrophages rather than to adipocytes for promoting AS lesion formation (Rolph et al., 2006). Our previous study showed that IMD enhanced the expression of ABCA1, a cholesterol efflux pathway–associated protein, and cholesterol efflux in macrophages (Liao et al., 2017), while other studies demonstrated that FABP4 gene deletion could upregulate ABCA1 (Chawla et al., 2001). Therefore, IMD increasing ABCA1 to regulate cholesterol efflux by inhibiting FABP4 expression might explain the alleviation of AS.

The mechanism of FABP4 resulting in AS is due to its direct effect on lipid metabolism and its ability to mediate inflammatory responses. FABP4 binds monounsaturated fatty acids and polyunsaturated fatty acids that prevent the activation of PPARγ. On the other hand, it also links Liver X receptor α, thus disrupting the expression of PPARγ-dependent genes. This reduces the expression of SIRT3 and UCP2, leading to an enhanced production of ROS and inflammatory responses (Korbecki and Bajdak-Rusinek, 2019). *In vitro* study demonstrated that FABP4 knockout significantly reduced the expression of IL-1β, IL-6, TNF-α, and MCP-1 (Fu et al., 2002; Ren et al., 2021). This is consistent with our results revealing that IMD reduced the generation of IL-6 and TNF-α in macrophages stimulated by ox-LDL, which might be another result ensuing the inhibition of FABP4. The mechanism might be based on FABP4 activating IκB kinase and NF-κB activity, which in turn upgrades the expression of cyclooxygenase 2 and inducible NO synthase and the production of inflammatory cytokines (Fu et al., 2002). Another pathway lies in FABP4 that has a positive feedback relationship with JNK and activator protein-1 (AP-1), which promote the inflammatory response induced by lipopolysaccharide (Hui et al., 2010).

A common receptor of the CGRP superfamily is the calcitonin receptor-like receptor/receptor activation–modified protein

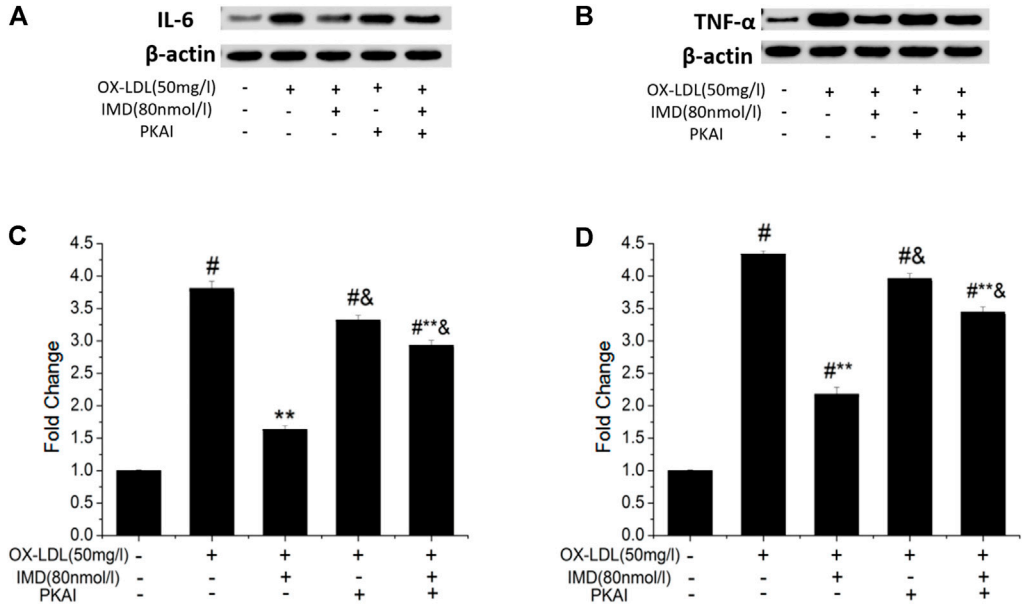

FIGURE 6 | IMD inhibits the protein expression of IL-6 and TNF-α in ox-LDL–induced macrophages (WB). # Compared with the control group ($p < 0.05$); ** compared to the ox-LDL alone group ($p < 0.05$); & compared to the ox-LDL +IMD group ($p < 0.05$).

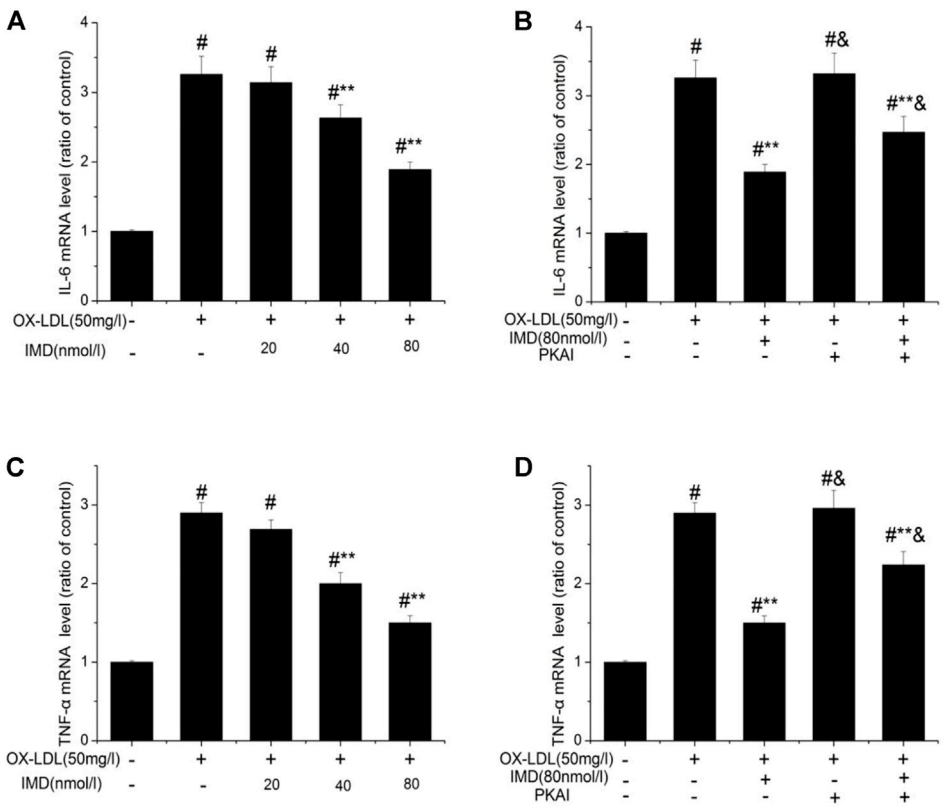

FIGURE 7 | IMD inhibits the mRNA expression of IL-6 and TNF-α in ox-LDL–induced macrophages. # Compared with the control group ($p < 0.05$); ** compared to the ox-LDL alone group ($p < 0.05$); & compared to the ox-LDL +IMD group ($p < 0.05$).

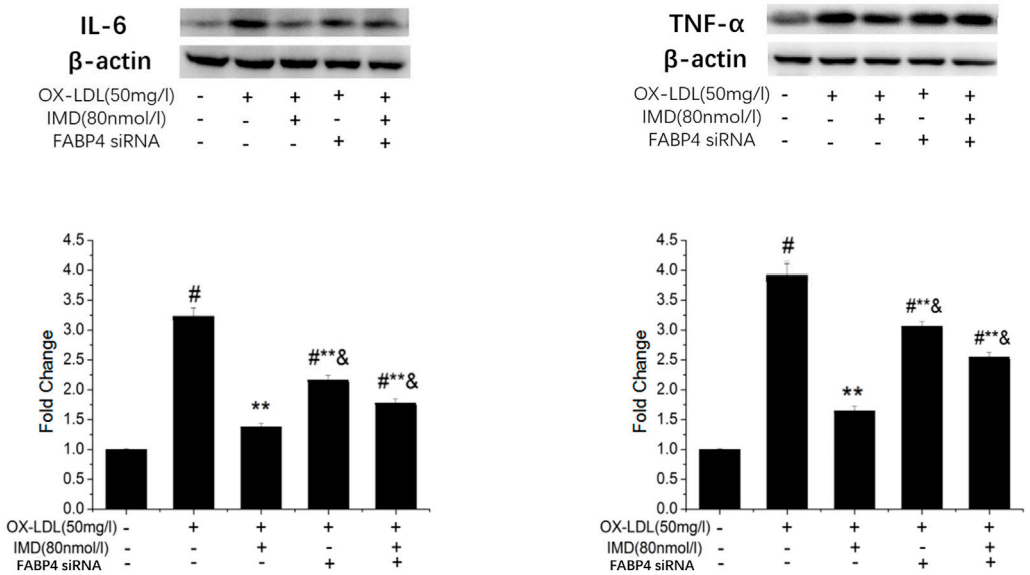

FIGURE 8 | IMD inhibits the protein expression of IL-6 and TNF-α through the FABP4 pathway. # Compared with the control group ($p < 0.05$); ** compared to the ox-LDL alone group ($p < 0.05$); & compared to the ox-LDL +IMD group ($p < 0.05$).

complex (CRLR/RAMP) (Zhang et al., 2018). CRLR belongs to the G protein–coupled receptor superfamily and has complex downstream signaling pathways, such as the AC-cAMP/PKA, L-arginine–NO–cGMP, and Gq/11-PLC (Kandilci et al., 2008; Dai et al., 2012; Li et al., 2013). Nevertheless, the pathway through which IMD inhibits FABP4 and the inflammatory response remains unknown. In our study, three signaling pathways were verified, and only PKAI significantly blocked the above effects, suggesting that IMD exerted these functions through the PKA signaling pathway, which is consistent with our previous findings (Rolph et al., 2006).

This study has a few limitations. First, our data must be confirmed to be *in vivo*. Second, whether IMD causes vascular inflammatory disease and whether other mechanisms are involved needs to be further addressed by future studies.

In conclusion, IMD could prevent ox-LDL–induced macrophages inflammation by inhibiting FABP4, where signaling might partially occur via the PKA pathway.

DATA AVAILABILITY STATEMENT

The raw data supporting the conclusion of this article will be made available by the authors, without undue reservation.

AUTHOR CONTRIBUTIONS

KL contributed to conceptualization and in writing the original draft. RS contributed in performing the experiment, writing, reviewing, and editing. SW contributed in data analysis and visualization. QL contributed in performing the experiment. XC contributed to conceptualization, resources, and supervision. HZ contributed to supervision and project administration.

FUNDING

The study was supported by the Youth Program of National Natural Science Foundation of China (grant number: 82000418), Sichuan Science and Technology Department R&D Key Projects in Key Fields (grant numbers: 2019YFS0348, 2021YJ0460), and Chengdu Scientific Program R&D Key Project (grant number: 2019-YF05-00156-SN).

SUPPLEMENTARY MATERIAL

The Supplementary Material for this article can be found online at: https://www.frontiersin.org/articles/10.3389/fphar.2021.724777/full#supplementary-material

REFERENCES

Bobryshev, Y. V., Ivanova, E. A., Chistiakov, D. A., Nikiforov, N. G., and Orekhov, A. N. (2016). Macrophages and Their Role in Atherosclerosis: Pathophysiology and Transcriptome Analysis. *Biomed. Res. Int.* 2016, 9582430. doi:10.1155/2016/9582430

Chawla, A., Boisvert, W. A., Lee, C. H., Laffitte, B. A., Barak, Y., Joseph, S. B., et al. (2001). A PPAR Gamma-LXR-ABCA1 Pathway in Macrophages Is Involved in Cholesterol Efflux and Atherogenesis. *Mol. Cel* 7, 161–171. doi:10.1016/s1097-2765(01)00164-2

Dai, X. Y., Cai, Y., Mao, D. D., Qi, Y. F., Tang, C., Xu, Q., et al. (2012). Increased Stability of Phosphatase and Tensin Homolog by Intermedin Leading to Scavenger Receptor A Inhibition of Macrophages Reduces Atherosclerosis in Apolipoprotein E-Deficient Mice. *J. Mol. Cel Cardiol* 53, 509–520. doi:10.1016/j.yjmcc.2012.07.006

Fu, Y., Luo, N., Lopes-Virella, M. F., and Garvey, W. T. (2002). The Adipocyte Lipid Binding Protein (ALBP/aP2) Gene Facilitates Foam Cell Formation in

Human THP-1 Macrophages. *Atherosclerosis* 165, 259–269. doi:10.1016/s0021-9150(02)00305-2

Furuhashi, M., Saitoh, S., Shimamoto, K., and Miura, T. (2014). Fatty Acid-Binding Protein 4 (FABP4): Pathophysiological Insights and Potent Clinical Biomarker of Metabolic and Cardiovascular Diseases. *Clin. Med. Insights Cardiol.* 8, 23–33. doi:10.4137/CMC.S17067

Hui, X., Li, H., Zhou, Z., Lam, K. S., Xiao, Y., Wu, D., et al. (2010). Adipocyte Fatty Acid-Binding Protein Modulates Inflammatory Responses in Macrophages through a Positive Feedback Loop Involving C-Jun NH2-terminal Kinases and Activator Protein-1. *J. Biol. Chem.* 285 (14), 10273–10280. doi:10.1074/jbc.M109.097907

Kandilci, H. B., Gumusel, B., and Lippton, H. (2008). Intermedin/adrenomedullin-2 (IMD/AM2) Relaxes Rat Main Pulmonary Arterial Rings via cGMP-dependent Pathway: Role of Nitric Oxide and Large Conductance Calcium-Activated Potassium Channels (BK(Ca)). *Peptides* 29 (8), 1321–1328. doi:10.1016/j.peptides.2008.04.008

Korbecki, J., and Bajdak-Rusinek, K. (2019). The Effect of Palmitic Acid on Inflammatory Response in Macrophages: an Overview of Molecular Mechanisms. *Inflamm. Res.* 68, 915–932. doi:10.1007/s00011-019-01273-5

Li, P., Sun, H. J., Han, Y., Wang, J. J., Zhang, F., Tang, C. S., et al. (2013). Intermedin Enhances Sympathetic Outflow via Receptor-Mediated cAMP/PKA Signaling Pathway in Nucleus Tractus Solitarii of Rats. *Peptides* 47, 1–6. doi:10.1016/j.peptides.2013.05.002

Liao, H., Wan, S., Zhang, X., Shi, D., Zhu, X., and Chen, X. (2017). Intermedin Ameliorates Atherosclerosis by Increasing Cholesterol Efflux through the cAMP-PKA Pathway in Macrophage RAW264.7 Cell Line. *Med. Sci. Monit.* 23, 5462–5471. doi:10.12659/msm.907298

Makowski, L., Boord, J. B., Maeda, K., Babaev, V. R., Uysal, K. T., Morgan, M. A., et al. (2001). Lack of Macrophage Fatty-Acid-Binding Protein aP2 Protects Mice Deficient in Apolipoprotein E against Atherosclerosis. *Nat. Med.* 7 (6), 699–705. doi:10.1038/89076

Makowski, L., Brittingham, K. C., Reynolds, J. M., Suttles, J., and Hotamisligil, G. S. (2005). The Fatty Acid-Binding Protein, aP2, Coordinates Macrophage Cholesterol Trafficking and Inflammatory Activity. *J. Biol. Chem.* 280 (13), 12888–12895. doi:10.1074/jbc.m413788200

Ren, J. L., Chen, Y., Zhang, L. S., Zhang, Y. R., Liu, S. M., Yu, Y. R., et al. (2021). Intermedin 1-53 Attenuates Atherosclerotic Plaque Vulnerability by Inhibiting CHOP-Mediated Apoptosis and Inflammasome in Macrophages. *Cel Death Dis.* 12 (5), 1–6. doi:10.1038/s41419-021-03712-w

Ridker, P. M., Genest, J., Boekholdt, S. M., Libby, P., Gotto, A. M., Nordestgaard, B. G., et al. (2010). HDL Cholesterol and Residual Risk of First Cardiovascular Events after Treatment with Potent Statin Therapy: an Analysis from the JUPITER Trial. *Lancet* 376, 333–339. doi:10.1016/S0140-6736(10)60713-1

Roger, V. L. (2015). Cardiovascular Diseases in Populations: Secular Trends and Contemporary Challenges-Geoffrey Rose Lecture, European Society of Cardiology Meeting 2014. *Eur. Heart J.* 36 (32), 2142–2146. doi:10.1093/eurheartj/ehv220

Roh, J., Chang, C. L., Bhalla, A., Klein, C., and Hsu, S. Y. (2004). Intermedin Is a Calcitonin/calcitonin Gene-Related Peptide Family Peptide Acting through the Calcitonin Receptor-like Receptor/receptor Activity-Modifying Protein Receptor Complexes. *J. Biol. Chem.* 279 (8), 7264–7274. doi:10.1074/jbc.M305332200

Rolph, M. S., Young, T. R., Shum, B. O., Gorgun, C. Z., Schmitz-Peiffer, C., Ramshaw, I. A., et al. (2006). Regulation of Dendritic Cell Function and T Cell Priming by the Fatty Acid-Binding Protein AP2. *J. Immunol.* 177 (11), 7794–7801. doi:10.4049/jimmunol.177.11.7794

Seidelmann, S. B., Lighthouse, J. K., and Greif, D. M. (2014). Development and Pathologies of the Arterial wall. *Cell Mol Life Sci* 71 (11), 1977–1999. doi:10.1007/s00018-013-1478-y

Taggart, M. (2010). Vascular Function in Health and Disease Review Series. *J. Cel Mol Med* 14 (5), 1017. doi:10.1111/j.1582-4934.2010.01050.x

Yudkin, J. S., Kumari, M., Humphries, S. E., and Mohamed-Ali, V. (2000). Inflammation, Obesity, Stress and Coronary Heart Disease: Is Interleukin-6 the Link?: Is Interleukin-6 the Link. *Atherosclerosis* 148 (2), 209–214. doi:10.1016/s0021-9150(99)00463-3

Zhang, S. Y., Xu, M. J., and Wang, X. (2018). Adrenomedullin 2/intermedin: a Putative Drug Candidate for Treatment of Cardiometabolic Diseases. *Br. J. Pharmacolapr* 175 (8), 1230–1240. doi:10.1111/bph.13814

Zhang, X., Gu, L., Chen, X., Wang, S., Deng, X., Liu, K., et al. (2012). Intermedin Ameliorates Atherosclerosis in ApoE Null Mice by Modifying Lipid Profiles. *Peptides* 37 (2), 189–193. doi:10.1016/j.peptides.2012.07.011

Conflict of Interest: The authors declare that the research was conducted in the absence of any commercial or financial relationships that could be construed as a potential conflict of interest.

Publisher's Note: All claims expressed in this article are solely those of the authors and do not necessarily represent those of their affiliated organizations, or those of the publisher, the editors, and the reviewers. Any product that may be evaluated in this article, or claim that may be made by its manufacturer, is not guaranteed or endorsed by the publisher.

frontiers in Pharmacology

SYSTEMATIC REVIEW
published: 10 December 2021
doi: 10.3389/fphar.2021.770861

Effects of Probiotic Supplementation on Inflammatory Markers and Glucose Homeostasis in Adults With Type 2 Diabetes Mellitus: A Systematic Review and Meta-Analysis

Li-Na Ding[1,2†], *Wen-Yu Ding*[1,2†], *Jie Ning*[1,2], *Yao Wang*[1,2], *Yan Yan*[3*] and *Zhi-Bin Wang*[1,2*]

[1]Endocrine and Metabolic Diseases Hospital of Shandong First Medical University, Shandong First Medical University and Shandong Academy of Medical Sciences, Jinan, China, [2]Shandong Institute of Endocrine and Metabolic Diseases, Jinan, China, [3]Department of Surgery, Qilu Hospital of Shandong University, Jinan, China

OPEN ACCESS

Edited by:
Ning Hou,
Guangzhou Medical University, China

Reviewed by:
Simona Gabriela Bungau,
University of Oradea, Romania
Mahdi Sepidarkish,
Babol University of Medical Sciences, Iran

***Correspondence:**
Zhi-Bin Wang
Zhibinking@163.com
Yan Yan
ql-yanyan@163.com

[†]These authors have contributed equally to this work

Specialty section:
This article was submitted to Inflammation Pharmacology, a section of the journal Frontiers in Pharmacology

Received: 05 September 2021
Accepted: 23 November 2021
Published: 10 December 2021

Citation:
Ding L-N, Ding W-Y, Ning J, Wang Y, Yan Y and Wang Z-B (2021) Effects of Probiotic Supplementation on Inflammatory Markers and Glucose Homeostasis in Adults With Type 2 Diabetes Mellitus: A Systematic Review and Meta-Analysis. Front. Pharmacol. 12:770861. doi: 10.3389/fphar.2021.770861

Background: Several studies have revealed the effect of probiotic supplementation in patients with type 2 diabetes (T2DM) on the amelioration of low-grade inflammation, which plays an important role in the pathogenesis of T2DM. However, the effects of the clinical application of probiotics on inflammation in individuals with T2DM remain inconsistent. This study aims to investigate the comprehensive effects of probiotics on inflammatory markers in adults with T2DM.

Methods: PubMed, Embase, Cochrane Library, and the Web of Science were searched to identify randomized controlled trials (RCTs) exploring the effect of probiotic supplementation on inflammatory markers in individuals with T2DM through March 11, 2021. Two reviewers independently screened the literature, extracted data, and assessed the risk of bias of the included studies. We used a random-effects model to calculate the standardized mean difference (SMD) between the probiotic supplementation and control groups.

Results: Seventeen eligible studies were selected with a total of 836 participants, including 423 participants in probiotic supplementation groups and 413 participants in control groups. Our study demonstrated that compared with the control condition, probiotic intake produced a beneficial effect in reducing the levels of plasma inflammation markers, including tumour necrosis factor-α (TNF-α) (SMD [95% CI]; −0.37 [−0.56, −0.19], $p < 0.0001$) and C-reactive protein (CRP) (SMD [95% CI]; −0.21 [−0.42, −0.01], $p = 0.040$), while it had no effect on the plasma interleukin-6 (IL-6) level (SMD [95% CI]; −0.07 [−0.27, 0.13], $p = 0.520$). In addition, our results support the notion that probiotic supplementation improves glycaemic control, as evidenced by a significant reduction in fasting blood glucose (FPG), HbA1c and HOMA-IR (SMD [95% CI]: −0.24

Abbreviations: CRP, C-reactive protein; FPG, fasting plasma glucose; HbA1c, haemoglobin A1c; HOMA-IR, homeostasis model of assessment of insulin resistance; IL-6, interleukin-6; IECs, intestinal epithelial cells; IRS1, Insulin receptor substrate 1; NF-κB, nuclear factor kappa B; RCT, randomized controlled trial; SCFAs, Short-chain fatty acids; SMD, standardized mean difference; TNF-α, tumour necrosis factor-α; T2DM, type 2 diabetes mellitus.

[–0.42, –0.05], p = 0.010; –0.19 [–0.37, –0.00], p = 0.040; –0.36 [–0.62, –0.10], p = 0.006, respectively).

Conclusion: Our study revealed some beneficial effects of probiotic supplementation on improving inflammatory markers and glucose homeostasis in individuals with T2DM. Probiotics might be a potential adjuvant therapeutic approach for T2DM.

Keywords: probiotic, inflammation, type 2 diabetes mellitus, gut microbiota, meta-analysis

Systematic Review Registration: [https://www.crd.york.ac.uk/prospero/], identifier [CRD42021235998].

INTRODUCTION

Type 2 diabetes mellitus (T2DM) is one of the most common endocrine and metabolic diseases and is characterized by impaired pancreatic islet β cell function and insulin resistance in insulin target tissues (Gurung et al., 2020; Arora et al., 2021). Data have shown that the incidence of T2DM has been sharply increasing worldwide and has become one of the most critical public health concerns (Zhang and Gregg, 2017). Moreover, due to diabetes-related complications such as blindness, kidney failure, heart attacks, stroke, and lower-limb amputation, T2DM is a leading cause of morbidity and mortality worldwide (Pearson, 2019).

Currently, there is no simple or effective intervention available to prevent and manage diabetes due to the complex and multifactorial nature of T2DM (Pearson, 2019). In recent years, emerging evidence suggests that the gut microbiota is closely related to the development and progression of T2DM (Tsai et al., 2019; Gurung et al., 2020). Some studies have found that the occurrence of T2DM is associated with gut microbial dysbiosis, which plays a major role in promoting chronic low-grade inflammation and insulin resistance and increases the risk of diabetes (Qin et al., 2012; Karlsson et al., 2013; Harkins et al., 2020). A variety of mechanisms have been proposed to explain the role of the gut microbiota in the onset of T2DM, including alteration of the host's energy homeostasis, intestinal barrier integrity, gastrointestinal peptide hormone secretion, immune response, and inflammatory status (Dongarra et al., 2013; Marchesi et al., 2016; Corb Aron et al., 2021).

Several studies have proposed that T2DM is associated with long-term chronic low-grade inflammation characterized by an increase in circulating levels of pro-inflammatory cytokines and chemokines, such as tumour necrosis factor-α (TNF-α) and interleukin-6 (IL-6) (Coope et al., 2016; Eguchi and Nagai, 2017). Elevated levels of TNF-α and IL-6 could also trigger the synthesis of C-reactive protein (CRP) in the liver, which is a common systemic inflammatory biomarker and invariably correlates with insulin resistance and the pathogenesis of T2DM (Badawi et al., 2010; Lainampetch et al., 2019). These pro-inflammatory factors could interfere with the insulin signalling cascade and impair insulin sensitivity by increasing the serine/threonine phosphorylation ratio of insulin receptor substrate 1 (IRS-1) in insulin target tissues (Chen et al., 2015). Pro-inflammatory signalling can also affect pancreatic β-cell functions and impair insulin secretion. In addition, pro-inflammatory factors disrupt endothelial cell functions and limit insulin access to its target tissues, which also contribute to insulin resistance (**Figure 1**) (Cani et al., 2019; Harkins et al., 2020).

Probiotics play a pivotal role in maintaining the balance of the gut microbiota (Bagarolli et al., 2017; Ardeshirlarijani et al., 2019). Currently, as a potential source of new therapeutics that work by regulating the gut microbiota, probiotics are commonly used to prevent and improve diabetes by altering the gut microbiota and its metabolites (Cani, 2018; Gurung et al., 2020). Among these changes, changes in short-chain fatty acids (SCFAs) and bile acids can improve glucose homeostasis, alleviate insulin resistance, and increase adipose tissue thermogenesis (Descamps et al., 2019; Woldeamlak et al., 2019; Tilg et al., 2020). Interestingly, recent studies have also shown that probiotic supplementation can prevent and improve type 2 diabetes by reducing the levels of pro-inflammatory cytokines,

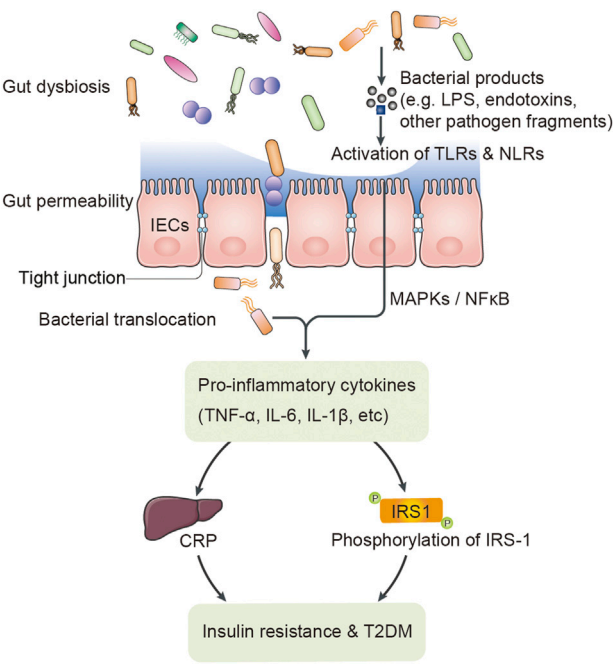

FIGURE 1 | The putative relationship between gut dysbiosis and T2DM.

such as TNF-α, IL-6, and CRP, and regulating the secretion of anti-inflammatory cytokines, such as interleukin-4 (IL-4) and interleukin-10 (IL-10) (Brunkwall and Orho-Melander, 2017; Woldeamlak et al., 2019; Harkins et al., 2020).

T2DM is usually accompanied by chronic low-grade inflammation (Hendijani and Akbari, 2018). Some prospective studies and meta-analyses support the notion that the administration of probiotics could improve glycaemic control (Hu et al., 2017; Wang et al., 2017). However, to our knowledge, the effect of probiotics on inflammatory markers in T2DM patients remains inconsistent. Several RCTs suggest that probiotics reduced the level of chronic systemic inflammatory markers in individuals with T2DM (Tonucci et al., 2017; Raygan et al., 2018; Sabico et al., 2019), while others obtained different conclusions (Feizollahzadeh et al., 2017; Firouzi et al., 2017; Hsieh et al., 2018). No study has simultaneously examined inflammatory biomarkers to capture the interrelation between glycaemic control parameters and inflammatory markers. The aim of the present study is to fill this gap of knowledge.

In the current systematic review and meta-analysis, we aimed to investigate the comprehensive effects of probiotic supplementation on glucose homeostasis and inflammatory markers in adults with T2DM, hoping to obtain more credible evidence-based evidence and provide objective support for the clinical prevention and treatment of T2DM.

METHODS

We conducted the current systematic review and meta-analysis to investigate the comprehensive effects of probiotics on the inflammatory response and glucose homeostasis markers in adults with T2DM according to the PRISMA guidelines (Page et al., 2021a; Page et al., 2021b). This systematic review has been registered in PROSPERO (registration number: CRD42021235998).

Search Strategy

Two reviewers independently executed a systematic search of randomized controlled trials (RCTs) examining the effect of probiotic supplementation on the inflammatory response and glycaemic control markers in T2DM patients from inception to March 2021 using the following databases: PubMed, Embase, Cochrane Library, and Web of Science. The search strategies used for PubMed, Embase, Cochrane Library, and Web of Science, which were based on the controlled vocabulary terms for each concept (e.g., MeSH) and keyword synonyms, are shown in Table S1. We imposed no language or other restrictions on any of the searches. A manual search was also conducted to identify further relevant studies from the references of included studies and previous systematic reviews.

Eligibility Criteria

Studies were selected based on the following criteria: (1) studies with participants with T2DM aged ≥18 years old; (2) RCTs; (3) studies in which the intervention was probiotic supplementation; and (4) studies in which changes in inflammatory markers (TNF-α, IL-6, and CRP) between pre- and posttreatment were outcome variables.

The exclusion criteria were as follows: (1) studies with pregnant or breast-breeding individuals and (2) studies with participants who consumed synbiotics, prebiotics, herbs or other supplements (such as micronutrients and other dietary constituents).

Data Extraction

According to the eligibility criteria, two reviewers independently conducted the literature search and data extraction. The third reviewer resolved any disagreements that occurred between the two data collectors. Details of population characteristics (e.g., sex, age and country), intervention arms (e.g., types of probiotics/placebo, dose, and duration of intervention), study design, and outcomes (e.g., inflammatory markers and glycaemic markers) were extracted from the included studies.

Risk of Bias of Individual Studies

Two investigators independently evaluated the risk of bias within the randomized controlled studies. The risk of biases, including selection bias, performance bias, detection bias, attrition bias, reporting bias, and other biases, of the included studies was classified as low, high, or unclear using the Cochrane Collaboration tool (Higgins et al., 2011).

Statistical Analysis

Statistical analysis of the data was conducted using Review Manager 5.3 and STATA/SE 15.1. p-values less than 0.05 were regarded as statistically significant. The standardized mean difference (SMD) with 95% confidence interval (CI) was used to analyse the effects of probiotics on glycaemic control and inflammatory markers between the probiotic supplementation and control groups. We used a random-effects model to pool SMDs on glycaemic control and inflammatory markers. When the studies did not provide the standard deviations (SDs), the missing SDs of the mean change were calculated based on the CI, standard error (SE), p-value, or correlation coefficient (Corr). The correlation coefficient value was estimated as 0.5 to impute the missing SDs, which were not provided by the authors (Follmann et al., 1992). Heterogeneity among studies was assessed by the Cochrane Q-test. I square (I^2) was used to quantify the magnitude of heterogeneity. I^2 values of 25, 50, and 75% represented low, moderate, and high levels of heterogeneity, respectively (Higgins et al., 2003). To explore the possible source of heterogeneity, subgroup analysis and sensitivity analysis were conducted. Subgroup analysis was carried out according to the potentially influential variables, including the duration of interventions (≤8 vs. >8 weeks), doses of probiotic supplementation ($<10^{10}$ vs. $\geq 10^{10}$ CFU/day), probiotic strains (single-vs. multistrains), and methods of probiotic administration (food vs. powder or capsule). Sensitivity analysis was conducted by the one-study remove (leave-one-out) approach to assess the pooled SMDs for each glycaemic control and inflammatory marker. In

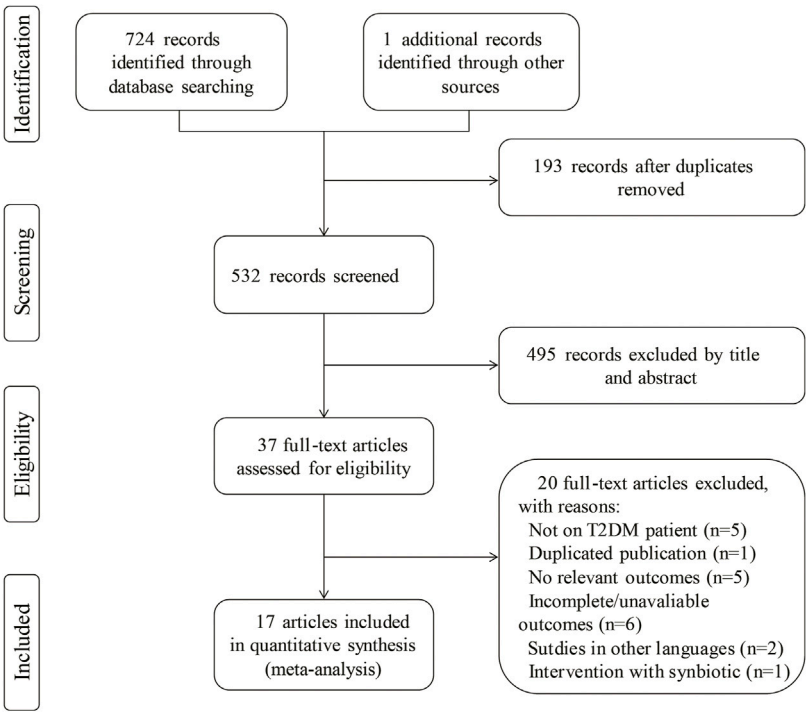

FIGURE 2 | Study flow diagram for study selection.

addition, funnel plots and Egger's test were utilized to evaluate the possible publication bias of the included studies.

RESULTS

Search Results and Characteristics of the Included Studies

A total of 725 studies (75 from Cochrane Library, 484 from Embase, 111 from PubMed, 54 from Web of Science and 1 from references) were identified using the search strategies described in the methods section, of which 193 duplicate records were removed. Two investigators independently screened the titles and abstracts and identified 37 articles according to the eligibility criteria described above. Twenty of these articles were excluded according to the inclusion/exclusion criteria. Finally, 17 RCTs were selected for inclusion in the meta-analysis. A flow diagram presents the study selection, and the reasons articles were excluded (**Figure 2**).

The characteristics of the included studies are summarized in **Table 1**. Overall, 17 relevant studies were conducted in Europe [Ukraine (Kobyliak et al., 2018a; Kobyliak et al., 2018b), Sweden (Mobini et al., 2017), and Denmark (Hove et al., 2015)], South America [Brazil (Tonucci et al., 2017)], and Asia [China (Hsieh et al., 2018; Fang et al., 2020), Saudi Arabia (Sabico et al., 2019), Malaysia (Firouzi et al., 2017), Iran (Mazloom et al., 2013; Mohamadshahi et al., 2014; Tajadadi-Ebrahimi et al., 2014; Bayat et al., 2016; Feizollahzadeh et al., 2017; Raygan et al., 2018), Turkey (Eliuz Tipici et al., 2020), and Japan (Sato et al., 2017)]. A total of 836 participants from 17 RCTs were randomized into probiotic groups (n = 423) and control groups (n = 413). Within the 17 RCTs, eight studies used one single-strain probiotic, eight studies used two-strain or multistrain probiotics, and one trial did not report the species of probiotics. Seven studies used food products, such as fermented milk (n = 3), yogurt (n = 2), soy milk (n = 1), and bread (n = 1), for probiotic delivery, while others were supplemented in the form of powder (n = 5), capsules (n = 3), and tablets (n = 1). The daily dose of probiotics ranged from 2×10^7 to 1×10^{12} colony-forming units (CFU). The median duration of probiotic intervention was 12 weeks, ranging from 4 to 24 weeks.

Risk of Bias in Individual Studies

Two investigators independently assessed the risk of bias of the included studies using the Cochrane collaboration tool. **Figure 3** summarizes the risk of bias, including selection bias, attrition bias, performance bias, detection bias, reporting bias, and other biases, among the included studies. Thirteen studies reported adequate random sequence generation, and ten studies described allocation concealment. In 15 studies, the participants and key researchers were blinded. The dropout rates in 13 RCTs were less than 20%. Selective reporting bias was not found. Two studies may have a high risk of other potential bias, according to the funding, which was supported by the

TABLE 1 | Characteristics of included studies.

Study	Country	Sample size (P/C)	Ages (year) (P/C)	Underlying disorder	Female (%)	ITT/ PP	Study design	Form of probiotics	Probiotics (strain and daily dose)	Duration (weeks)
Tipici et al. (2020)	Turkey	34 (17/17)	30–60	NR	100	ITT	PC	NR	*Lactobacillus GG*, 1 × 10^{10} CFU/day	8
Fang et al. (2020)	China	30 (15/15)	35–68 (57.87 ± 6.31/ 56.67 ± 7.68)	NR	66.33	PP	DB, PC	powder	*Bifidobacterium animalis A6*, 1 × 10^{10} CFU/day	4
Sabico et al. (2019)	Saudi Arabia	61 (31/30)	30–60 (48.00 ± 8.30/ 46.60 ± 5.90)	NR	57.38	PP	DB, PC	powder	2 g probiotics mixture (2 × 10^{9} CFU/g, contains *Bifidobacterium bifidum* W23, *Bifidobacterium lactis* W52, *Lactobacillus acidophilus* W37, *Lactobacillus brevis* W63, *Lactobacillus casei* W56, *Lactobacillus salivarius* W24, *Lactococcus lactis* W19, and *Lactobacillus lactis* W58), twice/day	24
Kobyliak et al. (2018a)	Ukraine	58 (30/28)	18–65 (53.40 ± 9.55/ 57.29 ± 10.45)	NAFLD	NR	ITT	DB, PC	powder	*Lactobacillus* + *Lactococcus* (6 × 10^{10} CFU/g), *Bifidobacterium* (1 × 10^{10} CFU/g), *Propionibacterium* (3 × 10^{10} CFU/g), *Acetobacter* (1 × 10^{6} CFU/g), 10 g/day	8
Kobyliak et al. (2018b)	Ukraine	53 (31/22)	18–75 (52.23 ± 9.69/ 57.18 ± 9.66)	NR	NR	ITT	DB, PC	powder	*Lactobacillus* + *Lactococcus* (6 × 10^{10} CFU/g), *Bifidobacterium* (1 × 10^{10} CFU/g), *Propionibacterium* (3 × 10^{10} CFU/g), *Acetobacter* (1 × 10^{6} CFU/g), 10 g/day	8
Hsieh et al. (2018)	China	44 (22/22)	25–70 (52.32 ± 10.20/ 55.77 ± 8.55)	NR	43.18	PP	DB, PC	capsule	*Lactobacillus reuteri* ADR-1, 4 × 10^{9} CFU/day	24
Raygan et al. (2018)	Iran	60 (30/30)	40–85 (60.70 ± 9.40/ 61.80 ± 9.80)	CHD	NR	ITT	DB, PC	capsule	*Bifidobacterium bifidum* 2 × 10^{9} CFU/day + *Lactobacillus casei* 2 × 10^{9} CFU/day + *Lactobacillus acidophilus* 2 × 10^{9} CFU/day	12
Tonucci et al. (2017)	Brazil	45 (23/22)	35–60 (51.83 ± 6.64/ 50.95 ± 7.20)	NR	42.22	PP	DB, PC	fermented milk	*Lactobacillus acidophilus* La-5, 1 × 10^{9} CFU/day + *Bifidobacterium animalis subsp. lactis* BB-12, 1 × 10^{9} CFU/day	6
Firouzi et al. (2017)	Malaysia	101 (48/53)	30–70 (52.90 ± 9.20/ 54.20 ± 8.30)	NR	51.64	PP	DB, PC	powder	*Lactobacillus acidophilus*, *Lactobacillus casei*, *Lactobacillus lactis, Bifidobacterium bifidum, Bifidobacterium longum, Bifidobacterium infantis,* 3 × 10^{10} CFU, twice/day	12
Mobini et al. (2017)	Sweden	29 (14/15)	NR (64.00 ± 6.00/ 65.00 ± 5.00)	NR	24.14	PP	DB, PC	tablet	*Lactobacillus reuteri* DSM 17938, 1 × 10^{10} CFU/day	12
Feizollahzadeh et al. (2017)	Iran	40 (20/20)	35–68 (56.90 ± 8.09/ 53.60 ± 7.16)	NR	52.50	PP	DB, PC	soy milk	*Lactobacillus planetarum* A7, 2 × 10^{7} CFU/day	8

(Continued on following page)

TABLE 1 | (*Continued*) Characteristics of included studies.

Study	Country	Sample size (P/C)	Ages (year) (P/C)	Underlying disorder	Female (%)	ITT/ PP	Study design	Form of probiotics	Probiotics (strain and daily dose)	Duration (weeks)
Sato et al. (2017)	Japan	68 (34/34)	30–79 (64.00 ± 9.20/ 65.00 ± 8.30)	NR	27.94	ITT	DB, PC	fermented milk	*Lactobacillus casei strain* Shirota, 4×10^{10} CFU/day	16
Bayat et al. (2016)	Iran	40 (20/20)	25–75 (54.10 ± 9.54/ 46.95 ± 9.34)	NR	70.00	ITT	PC	Yogurt	NR	8
Hove et al. (2015)	Denmark	41 (23/18)	40–70 (58.50 ± 7.70/ 60.60 ± 5.20)	NR	0	ITT	DB, PC	fermented milk	*Lactobacillus helveticus* Cardi04	12
Tajadadi-Ebrahimi et al. (2014)	Iran	54 (27/27)	35–70 (52.00 ± 7.20/ 53.40 ± 7.50)	NR	81.48	ITT	DB, PC	bread	*Lactobacillus Sporogenes,* 1×10^8 CFU, 3 times/day	8
Mohamadshahi et al. (2014)	Iran	44 (22/22)	30–60 (53.00 ± 5.90/ 49.00 ± 7.08)	overweight or obesity	76.19	ITT	DB, PC	yogurt	*Lactobacillus acidophilus* 3.7×10^6 CFU/g, *Bifidobacterium lactic* 3.7×10^6 CFU/g, 300 g/day	8
Mazloom et al. (2013)	Iran	34 (16/18)	25–65 (55.40 ± 8.00/ 51.80 ± 10.20)	NR	76.47	PP	SB, PC	capsule	*Lactobacillus acidophilus* + *Lactobacillus bulgaricus* + *Lactobacillus bifidum* + *Lactobacillus casei*	6

CHD, coronary heart disease; P/C, probiotic group/control group; ITT/PP, intention-to-treat/per-protocol; DB, double-blinded; PC, placebo-controlled; SB, single blinded; NR, not reported.

probiotic companies. In summary, no significant bias was detected (**Figure 3**).

Effects of Probiotics Supplementation on the Inflammatory Response and Glycaemic Control Marker Profile

Effects on Pro-Inflammatory Markers (TNF-α, IL-6, and CRP)

Effect on TNF-α

A total of 11 RCTs assessed the effect of probiotic supplementation on TNF-α and involved 498 individuals (258 consuming probiotics and 240 in the placebo group). The pooled effect of probiotic administration showed a significant decrease in TNF-α levels in comparison with the effects in the control groups (SMD [95% CI]; −0.37 [−0.56, −0.19], $p < 0.0001$), and the interstudy heterogeneity was low (I^2 = 6%, p = 0.390) (**Figure 4A**).

Subgroup analysis (**Table 2**) stratified by probiotic dosage, the number of probiotic strains, duration of intervention or method of administration showed that the effects of probiotic supplementation on TNF-α were significantly reduced in studies with the high-dose subgroup (SMD [95% CI]; −0.65 [−0.92, −0.39], I^2 = 0%), multistrain subgroup (SMD [95% CI]; −0.55 [−0.82, −0.27], I^2 = 16.6%), short intervention duration subgroup (SMD [95% CI]; −0.47 [−0.72, −0.22], I^2 = 0%), and administration in the form of powder/capsule subgroup (SMD [95% CI]; −0.56 [−0.81, −0.31], I^2 = 0%).

In the sensitivity analysis, we found that the pooled effect of probiotic supplementation on TNF-α was not significantly changed by omitting the studies one at a time sequentially, suggesting that the meta-analysis results were stable and reliable.

Effect on IL-6

Ten studies involving 456 patients investigated the effect of probiotic intake and placebo on the serum level of IL-6. The pooled effect of probiotic supplementation indicated no significant effect of probiotics in reducing the serum level of IL-6 compared to the effects in the control group (**Figure 4B**) (SMD [95% CI]; −0.07 [−0.27, 0.13], p = 0.520).

Subgroup analysis showed that there was no significant reduction in IL-6 levels in those subgroups stratified by probiotic dosage, the number of probiotic strains, duration of intervention, or method of administration (**Table 3**).

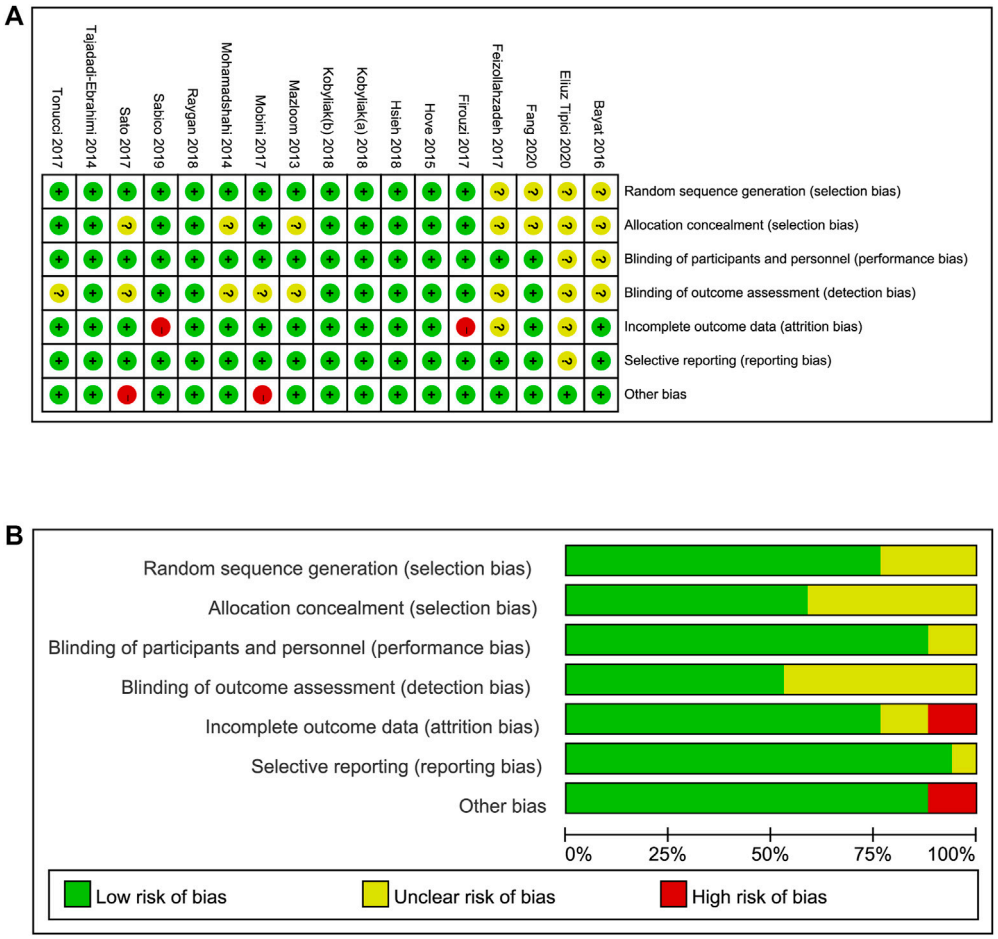

FIGURE 3 | Risk of bias assessment **(A)** details of included studies, **(B)** overall summary.

We also performed sensitivity analysis by sequentially eliminating one study at a time. No particular studies significantly affected the pooled effect of probiotic supplementation on IL-6 levels. However, heterogeneity among studies was eliminated (I^2 = 0%, p = 0.960) when the meta-analysis excluded only the trial of Kobyliak et al. (2018a).

Effect on CRP

The effect of probiotic supplementation on CRP was evaluated in 13 studies including 650 participants. We found a significant effect with a low heterogeneity of probiotic supplementation in reducing serum CRP levels compared to the effects in the control group (SMD [95% CI]; −0.21 [−0.42, −0.01], I^2 = 36%, p = 0.040) (**Figure 4C**).

In the subgroup analysis, significant beneficial effects of probiotic intervention were observed for CRP in the short intervention duration subgroup (SMD [95% CI]; −0.36 [−0.67, −0.05], I^2 = 22.9%) (**Table 4**).

In the sensitivity analysis, we found that the heterogeneity among studies did not significantly change when eliminating the study of Bayat et al. (Bayat et al., 2016), which decreased the interstudy heterogeneity from 36 to 7%.

In this work, eleven studies reported the effect of probiotic supplementation on TNF-α, ten studies described the effect on IL-6, and 13 studies investigated the effect on CRP and were included in the meta-analysis. Compared to the control group, significant beneficial effects of probiotic supplementation were observed for TNF-α (SMD [95% CI]; −0.37 [−0.56, −0.19], $p < 0.0001$) and CRP (SMD [95% CI]; −0.21 [−0.42, −0.01], p = 0.040). However, there was no significant beneficial effect on the IL-6 level (SMD [95% CI]; −0.07 [−0.27, 0.13], p = 0.520). In line with our results, a previous meta-analysis also found that these supplementations significantly decreased the levels of TNF-α and CRP but had no effect on IL-6 levels (Tabrizi et al., 2019; Zheng et al., 2019).

Effect of Probiotics Supplementation on Glucose Homeostasis (FPG, HbA1c, and HOMA-IR)

Effect on FPG

A total of 778 participants in 16 studies were included in the analysis of the effect of probiotic supplementation on the level of FPG. probiotic supplementation resulted in a significant reduction in FPG levels (SMD [95% CI]; −0.24 [−0.42, −0.05], p = 0.010), and the interstudy heterogeneity (I^2 = 39%, p = 0.060) was low (**Figure 5A**).

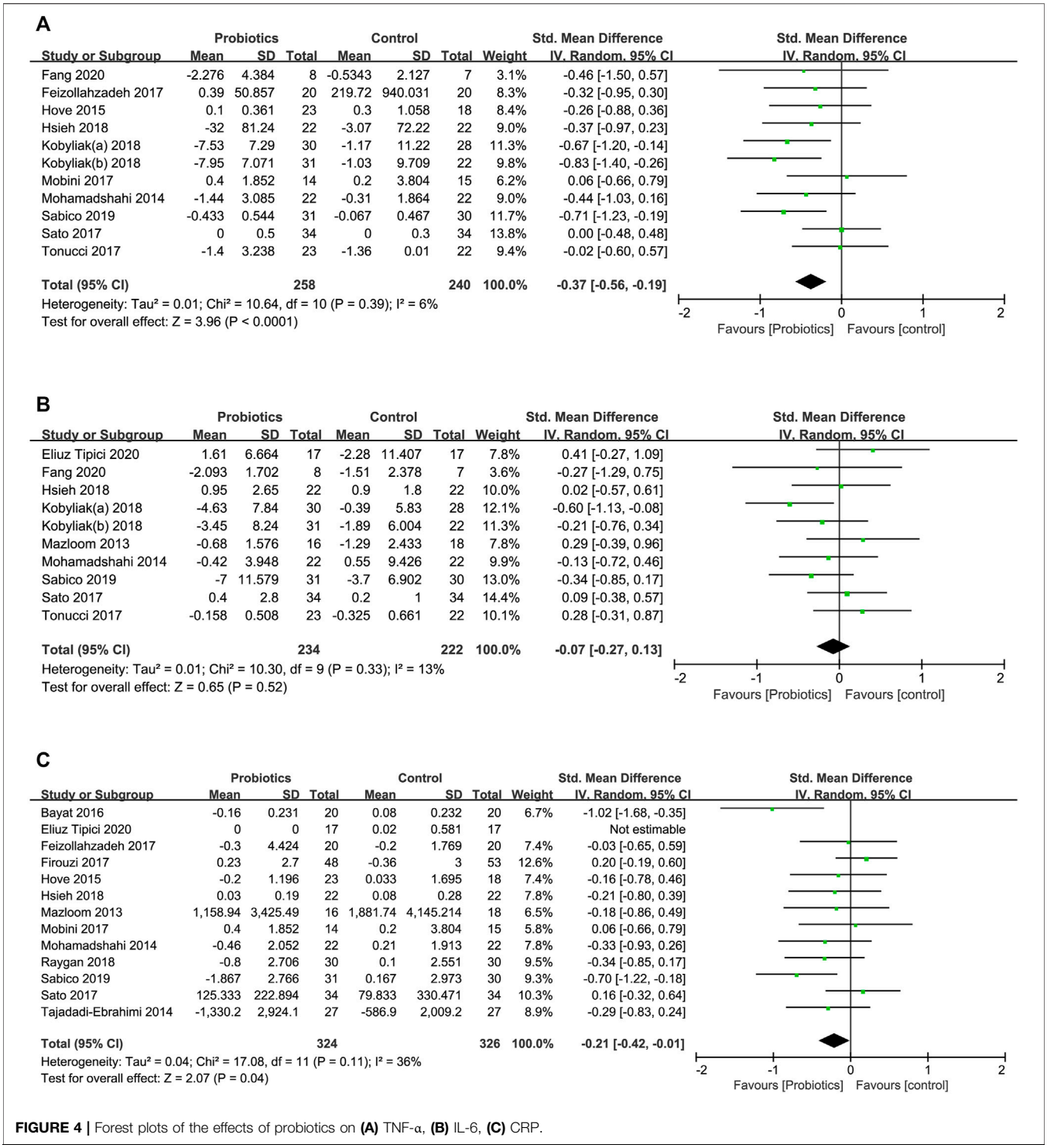

FIGURE 4 | Forest plots of the effects of probiotics on **(A)** TNF-α, **(B)** IL-6, **(C)** CRP.

Subgroup analysis (**Table 5**) showed that the effects of probiotic supplementation on FPG were significantly reduced in the multistrain subgroup (SMD [95% CI]; −0.30 [−0.54, −0.05], I^2 = 33%), long intervention duration subgroup (SMD [95% CI]; −0.34 [−0.60, −0.09], I^2 = 35.5%), and administration in the form of powder/capsule subgroup (SMD [95% CI]; −0.30 [−0.54, −0.06], I^2 = 28.9%).

In the leave-one-out sensitivity analysis, the pooled effect of probiotic supplementation on the FPG level remained significant among studies compared to the effects in the control group. Furthermore, after the removal of a single study (Bayat et al., 2016), the interstudy heterogeneity decreased from 39 to 16%, while the FPG reduction was still significant in the probiotic group.

TABLE 2 | Subgroup analysis for the effects of probiotics on TNF-α.

Subgroup	No. of trials	No. of participants	I^2 (%)	Pooled SMD [95% CI]
Probiotics dose				
≥10^{10} CFU/day	5	231	0	−0.65 [−0.92, −0.39]
<10^{10} CFU/day	5	226	0	−0.12 [−0.38, 0.14]
NR	1	41	0	−0.26 [−0.88, 0.36]
Probiotics strain				
Single	6	237	0	−0.19 [−0.44, 0.07]
Multiple	5	261	16.6	−0.55 [−0.82, −0.27]
Duration of intervention				
≤8 weeks	6	255	0	−0.47 [−0.72, −0.22]
>8 weeks	5	243	19.1	−0.27 [−0.56, 0.01]
Method of administration				
Powder/capsule	6	260	0	−0.56 [−0.81, −0.31]
Food	5	238	0	−0.18 [−0.44, 0.07]

CFU, colony forming unit; SMD, standardized mean difference.

TABLE 3 | Subgroup analysis for the effects of probiotics on IL−6.

Subgroup	No. of trials	No. of participants	I^2 (%)	Pooled SMD [95% CI]
Probiotics dose				
≥10^{10} CFU/day	6	265	10.4	−0.23 [−0.49, 0.03]
<10^{10} CFU/day	3	157	0	0.13 [−0.19, 0.44]
NR	1	34	0	0.29 [−0.39, 0.96]
Probiotics strain				
Single	4	161	0	0.11 [−0.20, 0.42]
Multiple	6	295	29.0	−0.15 [−0.43, 0.12]
Duration of intervention				
≤8 weeks	7	283	30.7	−0.05 [−0.34, 0.24]
>8 weeks	3	173	0	−0.08 [−0.38, 0.22]
Method of administration				
Powder/capsule	6	265	0.8	−0.22 [−0.47, 0.02]
Food	3	157	0	0.08 [−0.23, 0.40]
NR	1	34	0	0.41 [−0.27, 1.09]

TABLE 4 | Subgroup analysis for the effects of probiotics on CRP.

Subgroup	No. of trials	No. of participants	I^2 (%)	Pooled SMD [95% CI]
Probiotics dose				
≥ 10^{10} CFU/day	3	206	74.4	−0.25 [−0.82, 0.31]
< 10^{10} CFU/day	6	295	0	−0.11 [−0.34, 0.12]
NR	3	115	52.9	−0.45 [−1.00, 0.10]
Probiotics strain				
Single	6	276	0	−0.07 [−0.31, 0.17]
Multiple	5	300	50.9	−0.25 [−0.58, 0.09]
NR	1	40	0	-1.02 [-1.68, −0.35]
Duration of intervention				
≤8 weeks	5	212	22.9	−0.36 [−0.67, −0.05]
>8 weeks	7	404	38.8	−0.13 [−0.38, 0.13]
Method of administration				
Powder/capsule	6	329	40.2	−0.19 [−0.48, 0.10]
Food	6	287	41.8	−0.25 [−0.56, 0.06]

Effect on HbA1c

Ten studies described the significant effect of probiotic intake on reducing HbA1c levels in 499 participants (SMD [95% CI]; −0.19 [−0.37, −0.00], $p = 0.040$). The heterogeneity among studies (I^2 = 4%, $p = 0.410$) was low (**Figure 5B**).

In the subgroup analysis, significant beneficial effects of probiotic intervention were observed for HbAlc in the multistrain subgroup (SMD [95% CI]; −0.28 [−0.53, −0.02], I^2 = 0%) and administration in the form of a powder/capsule subgroup (SMD [95% CI]; −0.29 [−0.57, −0.02], I^2 = 6.6%) (**Table 6**).

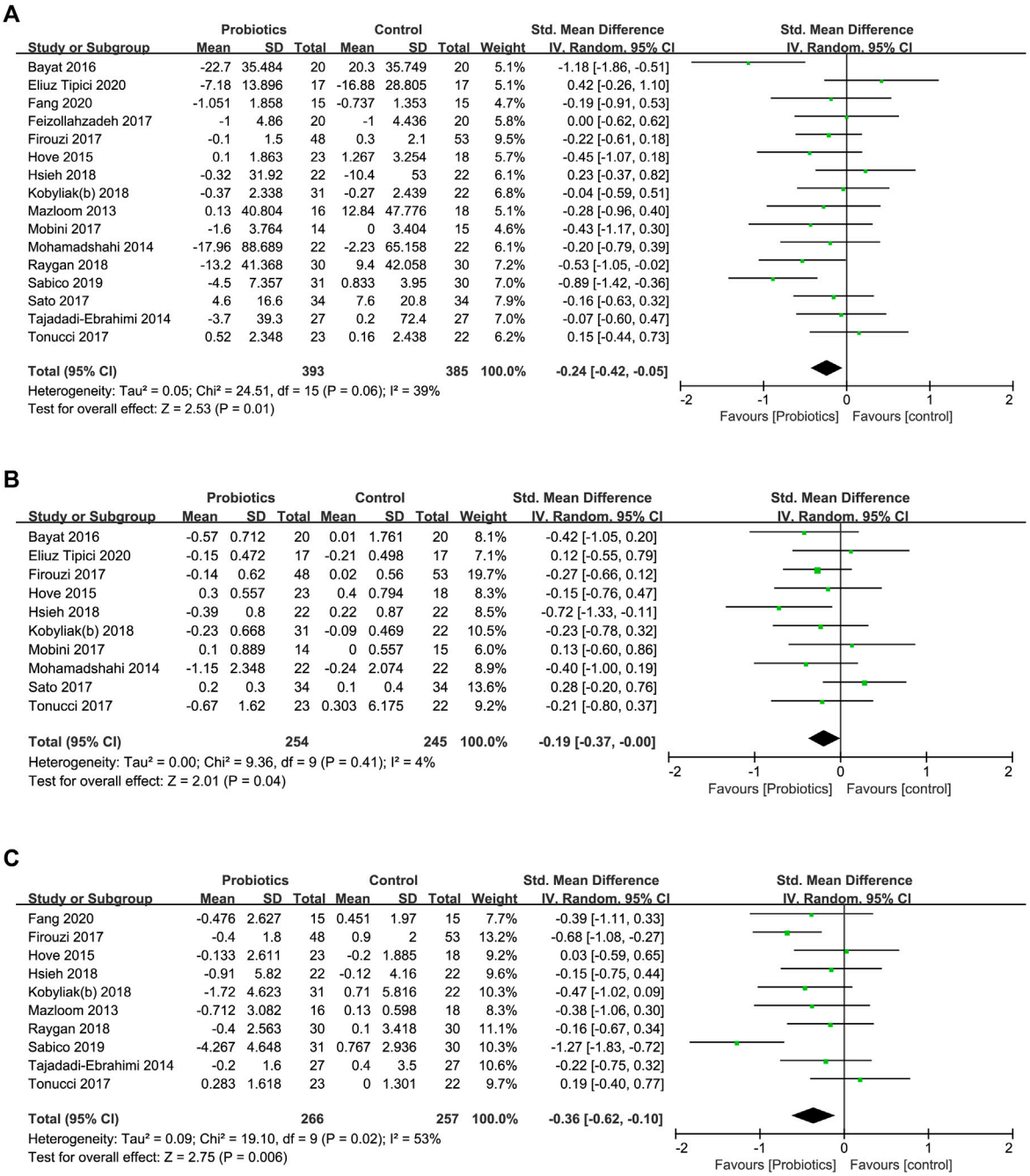

FIGURE 5 | Forest plots of the effects of probiotics on **(A)** FPG, **(B)** HbA1c, **(C)** HOMA-IR.

Sensitivity analysis conducted by sequentially omitting one study at a time confirmed that the pooled effect of probiotic supplementation on HbA1c was stable and reliable.

Effect on HOMA-IR

Ten studies investigated the effect of probiotic supplementation on the HOMA-IR level in a total of 523 participants. Compared to the effect in the control groups, probiotic supplementation significantly reduced the HOMA-IR level (SMD [95% CI]; −0.36 [−0.62, −0.10], $p = 0.006$), with moderate heterogeneity ($I^2 = 53\%$, $p = 0.020$) among studies (**Figure 5C**).

Due to the moderate heterogeneity among studies, we conducted a subgroup analysis for the effect of probiotic administration on HOMA-IR, which is displayed in **Figure 6**. Probiotic supplementation reduced the HOMA-IR level in the high-dose subgroup (SMD [95% CI]; −0.72 [−1.09, −0.35], $I^2 = 45.5\%$), multistrain subgroup (SMD [95% CI]; −0.47 [−0.86, −0.09], $I^2 = 67.5\%$), long intervention duration subgroup (SMD [95% CI];

TABLE 5 | Subgroup analysis for the effects of probiotics on FPG.

Subgroup	No. of trials	No. of participants	I^2 (%)	Pooled SMD [95% CI]
Probiotics dose				
≥ 10^{10} CFU/day	6	323	49.7	−0.21 [−0.54, 0.11]
< 10^{10} CFU/day	7	340	0	−0.12 [−0.34, 0.09]
NR	3	115	49.1	−0.63 [−1.16, −0.10]
Probiotics strain				
Single	8	340	0	−0.08 [−0.29, 0.14]
Multiple	7	398	33.0	−0.30 [−0.54, −0.05]
NR	1	40	0	−1.18 [−1.86, −0.51]
Duration of intervention				
≤8 weeks	9	374	39.6	−0.14 [−0.41, 0.12]
>8 weeks	7	404	35.5	−0.34 [−0.60, −0.09]
Method of administration				
Powder/capsule	8	412	28.9	−0.30 [−0.54, −0.06]
Food	7	332	43.7	−0.24 [−0.54, 0.05]
NR	1	34	0	0.42 [−0.26, 1.10]

TABLE 6 | Subgroup analysis for the effects of probiotics on HbAlc.

Subgroup	No. of trials	No. of participants	I^2 (%)	Pooled SMD [95% CI]
Probiotics dose				
≥ 10^{10} CFU/day	4	232	0	−0.23 [−0.49, 0.03]
< 10^{10} CFU/day	4	186	56.3	−0.12 [−0.57, 0.33]
NR	2	81	0	−0.28 [−0.72, 0.16]
Probiotics strain				
Single	5	216	42.6	−0.06 [−0.42, 0.30]
Multiple	4	243	0	−0.28 [−0.53, −0.02]
NR	1	40	0	−0.42 [−1.05, 0.20]
Duration of intervention				
≤8 weeks	5	216	0	−0.24 [−0.51, 0.03]
>8 weeks	5	283	45.5	−0.14 [−0.47, 0.19]
Method of administration				
Powder/capsule	4	227	6.6	−0.29 [−0.57, −0.02]
Food	5	238	12.0	−0.14 [−0.41, 0.14]
NR	1	34	100.0	0.12 [−0.55, 0.79]

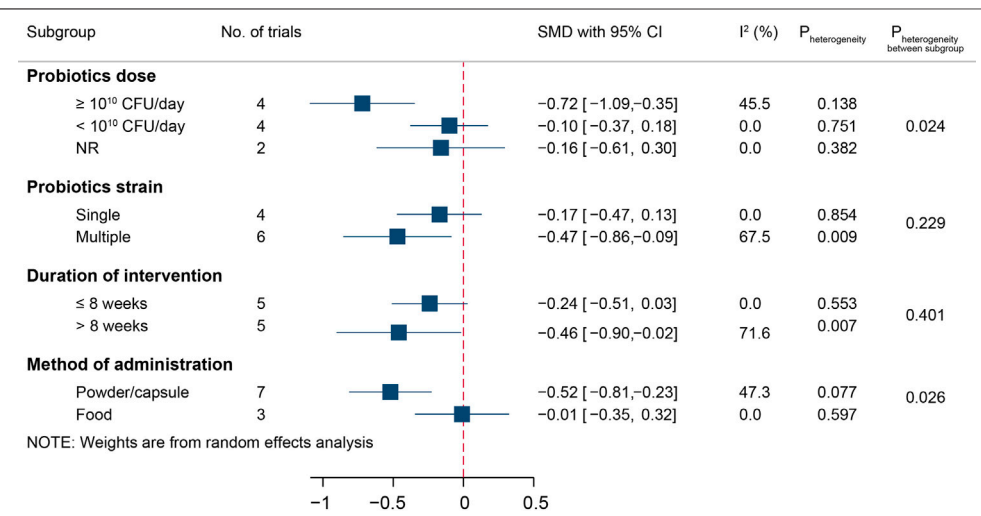

FIGURE 6 | Subgroup analysis for the effects of probiotics on HOMA-IR.

−0.46 [−0.90, −0.02], I^2 = 71.6%), and administration in the form of powder/capsule subgroup (SMD [95% CI]; −0.52 [−0.81, −0.23], I^2 = 47.3%). The interstudy heterogeneity remained similar across all effective subgroups.

Sensitivity analysis confirmed that the HOMA-IR level was not significantly changed compared with that of the control groups. When excluding the study by Sabico et al., we found that the interstudy heterogeneity decreased (I^2 = 2%, p = 0.420), but the effect on HOMA-IR level remained significant (SMD [95% CI]; −0.29 [−0.47, −0.10]).

Publication Bias Analysis

Funnel plots and Egger's test were performed to assess the possible publication bias of the included studies for glycaemic control and inflammatory markers. No evidence of publication bias identified from the funnel plots was found (Figure S1). The results from Egger's tests also showed no evidence of publication bias for FPG (p = 0.990), HbA1c (p = 0.927), HOMA-IR (p = 0.358), TNF-α (p = 0.821), IL-6 (p = 0.500), or CRP (p = 0.161).

DISCUSSION

T2DM is associated with long-term chronic low-grade inflammation characterized by an increase in some inflammatory markers, such as TNF-α, IL-6, and CRP, contributing to insulin resistance and the pathogenesis of T2DM (Coope et al., 2016; Eguchi and Nagai, 2017). In recent years, several studies have reported that probiotic supplementation has a variable effect on the inflammatory response in T2DM (Raygan et al., 2018; Anhê et al., 2020; Harkins et al., 2020). Therefore, we conducted the present meta-analysis to evaluate the effect of probiotic supplementation on inflammatory markers and glucose homeostasis in adults with T2DM, attempting to investigate its potential role in modulating gut microbiota to ameliorate glycaemic control and inflammatory markers.

Accumulating evidence provides support for the notion that the gut microbiota is critical to maintain human health (Arora et al., 2021; Wei et al., 2021). Dysbiosis of the gut microbiota could stimulate an increase in the levels of inflammatory markers, such as TNF-α and CRP, leading to aberrant immune activation and chronic low-grade inflammation in individuals with T2DM (Frost et al., 2021; Rinninella et al., 2019). There was also a growing body of evidence suggesting that elevated levels of pro-inflammatory markers, including TNF-α, IL-6, and CRP, play a vital role in the pathogenesis of T2DM (Liaqat et al., 2021; Hyun et al., 2013). These pro-inflammatory markers could inhibit insulin signalling pathways, leading to insulin resistance, dysfunction of β-cells, hyperglycaemia, and the occurrence of T2DM (Liaqat et al., 2021; Harkins et al., 2020; Descamps et al., 2019). However, probiotics play a vital role in glucose homeostasis, insulin resistance, energy metabolism, and chronic low-grade inflammation (Corb Aron et al., 2021; Namazi et al., 2021; Tilg et al., 2020). Some studies have shown that *Akkermansia muciniphila,* as a probiotic, could benefit T2DM by modulating gut microbiota LPS prevention and intestinal permeability reduction (Corb Aron et al., 2021; Zhang et al., 2021). Probiotics could regulate the balance of the host's gut microbiota by increasing or cross-feeding interactions with other potential beneficial microbes, which could increase insulin secretion, restore insulin sensitivity, and improve glucose homeostasis (Corb Aron et al., 2021; Gurung et al., 2020; Cani et al., 2019). Recent studies have reported that probiotic intake could increase the secretion of hormones, such as GLP-1 and PYY, by regulating the gut microbiota and their metabolites to prevent diabetes (Iorga et al., 2020; Zhang et al., 2020). In addition, probiotics consumed with prebiotics, synbiotics, herbs, micronutrients, or other dietary supplements might enhance the modulation of the gut microbiota and their metabolites, including short-chain fatty acids (SCFAs), neuropeptides, and gastrointestinal peptides (Arora et al., 2021). Moreover, these metabolites could reinforce barrier function, affect gut permeability, suppress chronic low-grade inflammation, and improve insulin resistance and glucose metabolism (**Figure 7**) (Mulders et al., 2018; Tsai et al., 2019; Gurung et al., 2020; Arora et al., 2021). Some studies also revealed that probiotic supplementation could ameliorate T2DM via inhibition of the expression of pro-inflammatory cytokines, chemokines, or inflammatory proteins (Gomes et al., 2017; Sabico et al., 2019; Tilg et al., 2020).

To obtain accurate results of probiotic supplementation on glycaemic control and inflammatory markers, we excluded studies with participants who consumed prebiotics, synbiotics, herbs, micronutrients, or other dietary supplements, which might influence the gut microbiota or interact with probiotics. Eleven studies reported the effect on TNF-α, ten studies described the effect on IL-6, and thirteen studies investigated the effect on CRP were included in the meta-analysis to evaluate the effects of probiotic supplementation on inflammatory markers. In our study, significant effects of probiotic supplementation were observed on TNF-α and CRP. However, there was no significant effect on IL-6 levels. In line with our results, some studies also showed that the participants consumed probiotics and synbiotics, and these supplementations significantly decreased the levels of TNF-α and CRP but had no effect on IL-6 levels. A previous study found that probiotic and synbiotic administration had a significant effect on CRP levels in individuals with diabetes (Zheng et al., 2019). In addition, a similar result was reported: probiotic and synbiotic supplementation decreased the levels of TNF-α and CRP, but there was no significant effect on IL-6 between the diabetes and control groups (Tabrizi et al., 2019). Subgroup analysis was conducted to assess the potentially influential variables, including the duration of interventions, doses of probiotic supplementation, probiotic strains, and methods of probiotic administration. Significant reductions in TNF-α were detected in consuming multiple strains of probiotics, short intervention duration, high probiotic daily doses, and administration in the form of powder/capsule. There were also significant reductions in CRP levels with short intervention durations and the consumption of multiple strain probiotics. In addition, there were no effects on IL-6 levels among those variables.

These meta-analysis results of glycaemic control parameters were also improved significantly in the levels of FPG, HbA1c, and HOMA-IR compared with the control group. Our results relating to FPG and HOMA-IR were similar to those of previous studies, which showed that probiotic intake could reduce the levels of FPG

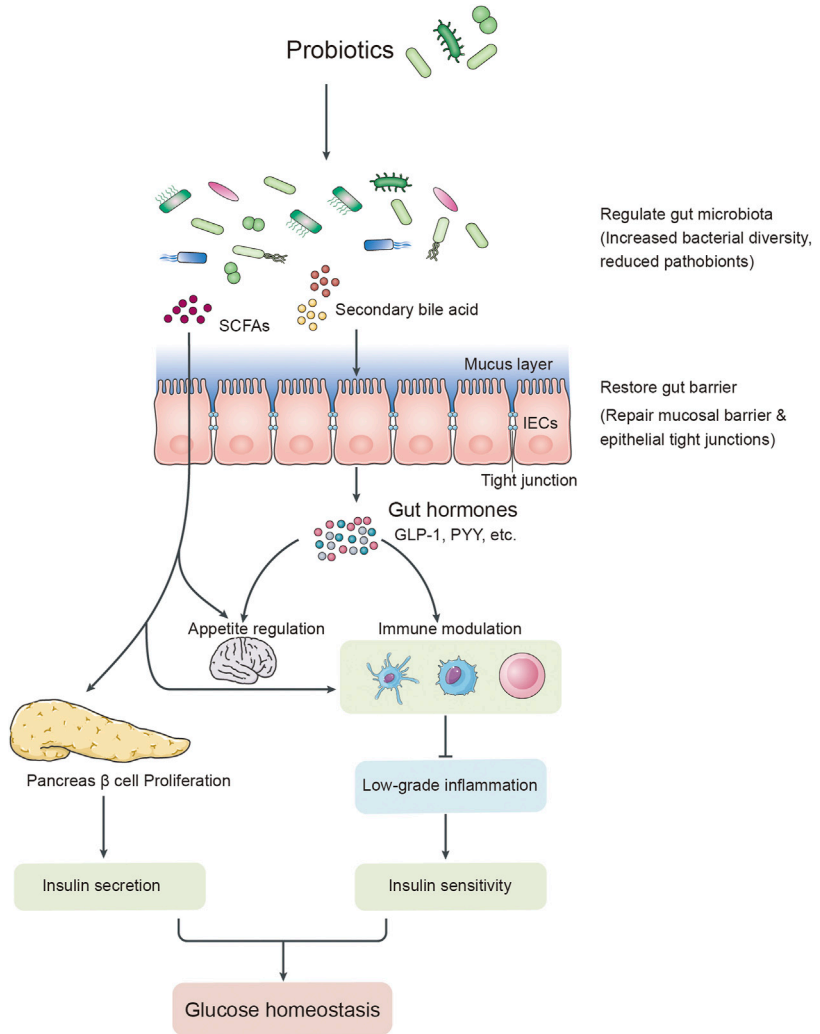

FIGURE 7 | The possible mechanism linking probiotic supplementation and diabetes.

and HOMA-IR in overweight/obese adults (Wang et al., 2019). However, there was no significant effect on HbA1c levels in their study, which might be because the baseline HbA1c level was lower than that in participants with T2DM. Ardeshirlarijani et al. reported that probiotic intake significantly reduced the level of FPG, while it had no effect on HbA1c levels (Ardeshirlarijani et al., 2019). Moreover, Dong et al. reported that probiotic supplementation improved the levels of HbA1c and HOMA-IR, with no effect on FPG (Dong et al., 2019). In view of previous studies, there were inconsistent results regarding the impact of probiotics on the levels of FPG, HbA1c, and HOMA-IR. Therefore, further evidence is needed to confirm these findings. Subgroup analysis and sensitivity analysis were also conducted in our meta-analysis. The subgroup analysis results showed that the invention groups consuming multiple strains of probiotics or administration in the form of powder/capsule had significantly reduced levels of fasting blood glucose. There were significant reductions in HbA1c levels in those subgroups stratified by probiotic dosage, the number of probiotic strains, duration of intervention, or method of administration. In addition, consistent results were also found for the HOMA-IR level in the subgroup analysis.

However, there were also some potential limitations. First, the sample sizes in all included random clinical trials were small (<60 participants per treatment group). Second, two studies (Hove et al., 2015; Bayat et al., 2016) in our meta-analysis did not provide enough information about interventions. In addition, there were also some differences in intervention types among the included studies, such as the species, doses, survivability of probiotics, and method of probiotic administration, which could also affect the outcomes. These limitations could reduce the reliability of the results from the current meta-analysis. Due to these limitations, some RCTs with well-designed, multicentre, and large sample sizes are still needed for future investigations to provide explicit results.

In summary, probiotic supplementation had a positive effect on glycaemic control markers, including FPG, HbA1c, and HOMA-IR, in parallel with the improvement of some inflammatory markers, such as TNF-α and CRP, in adults with T2DM. This result revealed that the glucose-lowering

effect of probiotic supplementation might contribute to its modulation of the gut microbiota, which could exert beneficial effects on glucose homeostasis in patients with T2DM by altering the systemic inflammatory response.

CONCLUSION

The evidence supports that probiotic supplementation had beneficial effects on some inflammatory markers (TNF-α and CRP) in parallel with improving glucose homeostasis (FPG, HbA1c, and HOMA-IR) in adults with T2DM. Probiotic supplementation could be beneficial for T2DM patients due to the attenuation of chronic low-grade inflammation by the gut microbiota, which was modulated by probiotics. Therefore, probiotics might become a potential adjuvant therapeutic method for patients with T2DM. However, more well-designed, multicentre RCTs with large sample sizes are needed to further investigate the potential beneficial effects of probiotics in the management of T2DM.

DATA AVAILABILITY STATEMENT

The original contributions presented in the study are included in the article/**Supplementary Material**, further inquiries can be directed to the corresponding authors.

AUTHOR CONTRIBUTIONS

All authors were involved in conducting the study, interpreting the results, and revising and correcting the manuscript. W-YD and L-ND individually searched the eligible datasets suitable for articles. JN, L-ND, and W-YD reviewed and extracted the data from articles. Z-BW and YW planned and conducted the analysis. Z-BW, W-YD, and YY wrote the manuscript. All authors read and approved the final version of the manuscript.

FUNDING

This work was supported by grants from the Key Research and Development Program of Shandong Province (2018YYSP030), the Natural Science Foundation of Shandong Province (ZR2017YL009, ZR2019PH096), the Innovation Project of Shandong Academy of Medical Sciences, and the Shandong Province "Double-Hundred Talent Plan" on 100 Foreign Experts and 100 Foreign Expert Teams Introduction (WST2018004).

ACKNOWLEDGMENTS

This is a short text to acknowledge the contributions of specific colleagues, institutions, or agencies that aided the efforts of the authors.

SUPPLEMENTARY MATERIAL

The Supplementary Material for this article can be found online at: https://www.frontiersin.org/articles/10.3389/fphar.2021.770861/full#supplementary-material

Supplementary Table S1 | Search strategy.

Supplementary Figure S1 | Funnel plots of the effects of probiotics on **(A)** TNF-α, **(B)** IL-6, **(C)** CRP, **(D)** FPG, **(E)** HbA1c, and **(F)** HOMA-IR.

REFERENCES

Anhê, F. F., Jensen, B. A. H., Varin, T. V., Servant, F., Van Blerk, S., Richard, D., et al. (2020). Type 2 Diabetes Influences Bacterial Tissue Compartmentalisation in Human Obesity. *Nat. Metab.* 2 (3), 233–242. doi:10.1038/s42255-020-0178-9

Ardeshirlarijani, E., Tabatabaei-Malazy, O., Mohseni, S., Qorbani, M., Larijani, B., and Baradar Jalili, R. (2019). Effect of Probiotics Supplementation on Glucose and Oxidative Stress in Type 2 Diabetes Mellitus: a Meta-Analysis of Randomized Trials. *Daru* 27 (2), 827–837. doi:10.1007/s40199-019-00302-2

Arora, A., Behl, T., Sehgal, A., Singh, S., Sharma, N., Bhatia, S., et al. (2021). Unravelling the Involvement of Gut Microbiota in Type 2 Diabetes Mellitus. *Life Sci.* 273, 119311. doi:10.1016/j.lfs.2021.119311

Badawi, A., Klip, A., Haddad, P., Cole, D. E., Bailo, B. G., El-Sohemy, A., et al. (20102010). Type 2 Diabetes Mellitus and Inflammation: Prospects for Biomarkers of Risk and Nutritional Intervention. *Diabetes Metab. Syndr. Obes.* 3, 173–186. doi:10.2147/dmsott.s9089

Bagarolli, R. A., Tobar, N., Oliveira, A. G., Araújo, T. G., Carvalho, B. M., Rocha, G. Z., et al. (20172017). Probiotics Modulate Gut Microbiota and Improve Insulin Sensitivity in DIO Mice. *J. Nutr. Biochem.* 50, 16–25. doi:10.1016/j.jnutbio.2017.08.006

Bayat, A., Azizi-Soleiman, F., Heidari-Beni, M., Feizi, A., Iraj, B., Ghiasvand, R., et al. (2016). Effect of Cucurbita Ficifolia and Probiotic Yogurt Consumption on Blood Glucose, Lipid Profile, and Inflammatory Marker in Type 2 Diabetes. *Int. J. Prev. Med.* 7, 30. doi:10.4103/2008-7802.175455

Brunkwall, L., and Orho-Melander, M. (2017). The Gut Microbiome as a Target for Prevention and Treatment of Hyperglycaemia in Type 2 Diabetes: from Current Human Evidence to Future Possibilities. *Diabetologia* 60 (6), 943–951. doi:10.1007/s00125-017-4278-3

Cani, P. D. (2018). Human Gut Microbiome: Hopes, Threats and Promises. *Gut* 67 (9), 1716–1725. doi:10.1136/gutjnl-2018-316723

Cani, P. D., Van Hul, M., Lefort, C., Depommier, C., Rastelli, M., and Everard, A. (2019). Microbial Regulation of Organismal Energy Homeostasis. *Nat. Metab.* 1 (1), 34–46. doi:10.1038/s42255-018-0017-4

Chen, L., Chen, R., Wang, H., and Liang, F. (2015). Mechanisms Linking Inflammation to Insulin Resistance. *Int. J. Endocrinol.* 2015, 508409–9. doi:10.1155/2015/508409

Coope, A., Torsoni, A. S., and Velloso, L. A. (2016). MECHANISMS IN ENDOCRINOLOGY: Metabolic and Inflammatory Pathways on the Pathogenesis of Type 2 Diabetes. *Eur. J. Endocrinol.* 174 (5), R175–R187. doi:10.1530/EJE-15-1065

Corb Aron, R. A., Abid, A., Vesa, C. M., Nechifor, A. C., Behl, T., Ghitea, T. C., et al. (2021). Recognizing the Benefits of Pre-/Probiotics in Metabolic Syndrome and Type 2 Diabetes Mellitus Considering the Influence of Akkermansia Muciniphila as a Key Gut Bacterium. *Microorganisms* 9 (3), 618. doi:10.3390/microorganisms9030618

Descamps, H. C., Herrmann, B., Wiredu, D., and Thaiss, C. A. (2019). The Path toward Using Microbial Metabolites as Therapies. *EBioMedicine* 44 (2019), 747–754. doi:10.1016/j.ebiom.2019.05.063

Dong, Y., Xu, M., Chen, L., and Bhochhibhoya, A. (2019). Probiotic Foods and Supplements Interventions for Metabolic Syndromes: A Systematic Review and Meta-Analysis of Recent Clinical Trials. *Ann. Nutr. Metab.* 74 (3), 224–241. doi:10.1159/000499028

Dongarrà, M. L., Rizzello, V., Muccio, L., Fries, W., Cascio, A., Bonaccorsi, I., et al. (2013). Mucosal Immunology and Probiotics. *Curr. Allergy Asthma Rep.* 13 (1), 19–26. doi:10.1007/s11882-012-0313-0

Eguchi, K., and Nagai, R. (2017). Islet Inflammation in Type 2 Diabetes and Physiology. *J. Clin. Invest.* 127 (1), 14–23. doi:10.1172/JCI88877

Eliuz Tipici, B., Coskunpinar, E., Altunkanat, D., Cagatay, P., Omer, B., Palanduz, S., et al. (2020). Effects of Lactobacillus GG Supplementation in Type 2 Diabetes: Are Mucin Genes Expressions Important? *Diabetologia* 63 (Suppl. 1), S296. doi:10.1007/s00125-020-05221-5

Fang, B., Zhang, M., Dong, L., Zhou, X., Ren, F., and Ge, S. (2020). *Probiotic Camel Milk Powder Improves Glycemic Control, Dyslipidemia, Adipose Tissue and Skeletal Muscle Function in T2DM Patients: A Randomized Trial.* doi: doi:10.21203/rs.3.rs-34115/v1

Feizollahzadeh, S., Ghiasvand, R., Rezaei, A., Khanahmad, H., Sadeghi, A., and Hariri, M. (2017). Effect of Probiotic Soy Milk on Serum Levels of Adiponectin, Inflammatory Mediators, Lipid Profile, and Fasting Blood Glucose Among Patients with Type II Diabetes Mellitus. *Probiotics Antimicrob. Proteins* 9 (1), 41–47. doi:10.1007/s12602-016-9233-y

Firouzi, S., Majid, H. A., Ismail, A., Kamaruddin, N. A., and Barakatun-Nisak, M. Y. (2017). Effect of Multi-Strain Probiotics (Multi-strain Microbial Cell Preparation) on Glycemic Control and Other Diabetes-Related Outcomes in People with Type 2 Diabetes: a Randomized Controlled Trial. *Eur. J. Nutr.* 56 (4), 1535–1550. doi:10.1007/s00394-016-1199-8

Follmann, D., Elliott, P., Suh, I., and Cutler, J. (1992). Variance Imputation for Overviews of Clinical Trials with Continuous Response. *J. Clin. Epidemiol.* 45 (7), 769–773. doi:10.1016/0895-4356(92)90054-q

Frost, F., Kacprowski, T., Rühlemann, M., Pietzner, M., Bang, C., Franke, A., et al. (2021). Long-term Instability of the Intestinal Microbiome Is Associated with Metabolic Liver Disease, Low Microbiota Diversity, Diabetes Mellitus and Impaired Exocrine Pancreatic Function. *Gut* 70 (3), 522–530. doi:10.1136/gutjnl-2020-322753

Gomes, A. C., de Sousa, R. G., Botelho, P. B., Gomes, T. L., Prada, P. O., and Mota, J. F. (2017). The Additional Effects of a Probiotic Mix on Abdominal Adiposity and Antioxidant Status: A Double-Blind, Randomized Trial. *Obesity (Silver Spring)* 25 (1), 30–38. doi:10.1002/oby.21671

Gurung, M., Li, Z., You, H., Rodrigues, R., Jump, D. B., Morgun, A., et al. (2020). Role of Gut Microbiota in Type 2 Diabetes Pathophysiology. *EBioMedicine* 51 (2020), 102590. doi:10.1016/j.ebiom.2019.11.051

Harkins, C. P., Kong, H. H., and Segre, J. A. (2020). Manipulating the Human Microbiome to Manage Disease. *JAMA* 323 (4), 303–304. doi:10.1001/jama.2019.19602

Hendijani, F., and Akbari, V. (2018). Probiotic Supplementation for Management of Cardiovascular Risk Factors in Adults with Type II Diabetes: A Systematic Review and Meta-Analysis. *Clin. Nutr.* 37 (2), 532–541. doi:10.1016/j.clnu.2017.02.015

Higgins, J. P., Altman, D. G., Gøtzsche, P. C., Jüni, P., Moher, D., Oxman, A. D., et al. (2011). The Cochrane Collaboration's Tool for Assessing Risk of Bias in Randomised Trials. *BMJ* 343, d5928. doi:10.1136/bmj.d5928

Higgins, J. P., Thompson, S. G., Deeks, J. J., and Altman, D. G. (2003). Measuring Inconsistency in Meta-Analyses. *BMJ* 327 (7414), 557–560. doi:10.1136/bmj.327.7414.557

Hove, K. D., Brøns, C., Færch, K., Lund, S. S., Rossing, P., and Vaag, A. (2015). Effects of 12 Weeks of Treatment with Fermented Milk on Blood Pressure, Glucose Metabolism and Markers of Cardiovascular Risk in Patients with Type 2 Diabetes: a Randomised Double-Blind Placebo-Controlled Study. *Eur. J. Endocrinol.* 172 (1), 11–20. doi:10.1530/EJE-14-0554

Hsieh, M. C., Tsai, W. H., Jheng, Y. P., Su, S. L., Wang, S. Y., Lin, C. C., et al. (2018). The Beneficial Effects of Lactobacillus Reuteri ADR-1 or ADR-3 Consumption on Type 2 Diabetes Mellitus: a Randomized, Double-Blinded, Placebo-Controlled Trial. *Sci. Rep.* 8 (1), 16791. doi:10.1038/s41598-018-35014-1

Hu, Y. M., Zhou, F., Yuan, Y., and Xu, Y. C. (2017). Effects of Probiotics Supplement in Patients with Type 2 Diabetes Mellitus: A Meta-Analysis of Randomized Trials. *Med. Clin. (Barc)* 148 (8), 362–370. doi:10.1016/j.medcli.2016.11.036

Hyun, B., Shin, S., Lee, A., Lee, S., Song, Y., Ha, N. J., et al. (2013). Metformin Down-Regulates TNF-α Secretion via Suppression of Scavenger Receptors in Macrophages. *Immune Netw.* 13 (4), 123–132. doi:10.4110/in.2013.13.4.123

Iorga, R. A., Bacalbasa, N., Carsote, M., Bratu, O. G., Stanescu, A. M. A., Bungau, S., et al. (2020). Metabolic and Cardiovascular Benefits of GLP-1 Agonists, besides the Hypoglycemic Effect (Review). *Exp. Ther. Med.* 20 (3), 2396–2400. doi:10.3892/etm.2020.8714

Karlsson, F. H., Tremaroli, V., Nookaew, I., Bergström, G., Behre, C. J., Fagerberg, B., et al. (2013). Gut Metagenome in European Women with normal, Impaired and Diabetic Glucose Control. *Nature* 498 (7452), 99–103. doi:10.1038/nature12198

Kobyliak, N., Abenavoli, L., Mykhalchyshyn, G., Kononenko, L., Boccuto, L., Kyriienko, D., et al. (2018a). A Multi-Strain Probiotic Reduces the Fatty Liver Index, Cytokines and Aminotransferase Levels in NAFLD Patients: Evidence from a Randomized Clinical Trial. *J. Gastrointestin Liver Dis.* 27 (1), 41–49. doi:10.15403/jgld.2014.1121.271.kby

Kobyliak, N., Falalyeyeva, T., Mykhalchyshyn, G., Kyriienko, D., and Komissarenko, I. (2018b). Effect of Alive Probiotic on Insulin Resistance in Type 2 Diabetes Patients: Randomized Clinical Trial. *Diabetes Metab. Syndr.* 12 (5), 617–624. doi:10.1016/j.dsx.2018.04.015

Lainampetch, J., Panprathip, P., Phosat, C., Chumpathat, N., Prangthip, P., Soonthornworasiri, N., et al. (2019). Association of Tumor Necrosis Factor Alpha, Interleukin 6, and C-Reactive Protein with the Risk of Developing Type 2 Diabetes: A Retrospective Cohort Study of Rural Thais. *J. Diabetes Res.* 2019, 9051929–9. doi:10.1155/2019/9051929

Liaqat, I., Ali, N. M., Arshad, N., Sajjad, S., Rashid, F., Hanif, U., et al. (2021). Gut Dysbiosis, Inflammation and Type 2 Diabetes in Mice Using Synthetic Gut Microbiota from Diabetic Humans. *Braz. J. Biol.* 83, e242818. doi:10.1590/1519-6984.242818

Marchesi, J. R., Adams, D. H., Fava, F., Hermes, G. D., Hirschfield, G. M., Hold, G., et al. (2016). The Gut Microbiota and Host Health: a New Clinical Frontier. *Gut* 65 (2), 330–339. doi:10.1136/gutjnl-2015-309990

Mazloom, Z., Yousefinejad, A., and Dabbaghmanesh, M. H. (2013). Effect of Probiotics on Lipid Profile, Glycemic Control, Insulin Action, Oxidative Stress, and Inflammatory Markers in Patients with Type 2 Diabetes: a Clinical Trial. *Iran J. Med. Sci.* 38 (1), 38–43.

Mobini, R., Tremaroli, V., Ståhlman, M., Karlsson, F., Levin, M., Ljungberg, M., et al. (2017). Metabolic Effects of Lactobacillus Reuteri DSM 17938 in People with Type 2 Diabetes: A Randomized Controlled Trial. *Diabetes Obes. Metab.* 19 (4), 579–589. doi:10.1111/dom.12861

Mohamadshahi, M., Veissi, M., Haidari, F., Shahbazian, H., Kaydani, G. A., and Mohammadi, F. (2014). Effects of Probiotic Yogurt Consumption on Inflammatory Biomarkers in Patients with Type 2 Diabetes. *Bioimpacts* 4 (2), 83–88. doi:10.5681/bi.2014.007

Mulders, R. J., de Git, K. C. G., Schéle, E., Dickson, S. L., Sanz, Y., and Adan, R. A. H. (2018). Microbiota in Obesity: Interactions with Enteroendocrine, Immune and central Nervous Systems. *Obes. Rev.* 19 (4), 435–451. doi:10.1111/obr.12661

Page, M. J., Mckenzie, J. E., Bossuyt, P. M., Boutron, I., Hoffmann, T. C., Mulrow, C. D., et al. (2021a). The PRISMA 2020 Statement: an Updated Guideline for Reporting Systematic Reviews. *BMJ* 372, n71. doi:10.1136/bmj.n71

Page, M. J., Mckenzie, J. E., Bossuyt, P. M., Boutron, I., Hoffmann, T. C., Mulrow, C. D., et al. (2021b). Updating Guidance for Reporting Systematic Reviews: Development of the PRISMA 2020 Statement. *J. Clin. Epidemiol.* 134, 103–112. doi:10.1016/j.jclinepi.2021.02.003

Pearson, E. R. (2019). Type 2 Diabetes: a Multifaceted Disease. *Diabetologia* 62 (7), 1107–1112. doi:10.1007/s00125-019-4909-y

Qin, J., Li, Y., Cai, Z., Li, S., Zhu, J., Zhang, F., et al. (2012). A Metagenome-wide Association Study of Gut Microbiota in Type 2 Diabetes. *Nature* 490 (7418), 55–60. doi:10.1038/nature11450

Raygan, F., Rezavandi, Z., Bahmani, F., Ostadmohammadi, V., Mansournia, M. A., Tajabadi-Ebrahimi, M., et al. (2018). The Effects of Probiotic Supplementation on Metabolic Status in Type 2 Diabetic Patients with Coronary Heart Disease. *Diabetol. Metab. Syndr.* 10 (1), 51–58. doi:10.1186/s13098-018-0353-2

Rinninella, E., Raoul, P., Cintoni, M., Franceschi, F., Miggiano, G. A. D., Gasbarrini, A., et al. (2019). What Is the Healthy Gut Microbiota Composition? A Changing Ecosystem across Age, Environment, Diet,

and Diseases. *Microorganisms* 7 (1), 14. doi:10.3390/microorganisms7010014

Sabico, S., Al-Mashharawi, A., Al-Daghri, N. M., Wani, K., Amer, O. E., Hussain, D. S., et al. (2019). Effects of a 6-month Multi-Strain Probiotics Supplementation in Endotoxemic, Inflammatory and Cardiometabolic Status of T2DM Patients: A Randomized, Double-Blind, Placebo-Controlled Trial. *Clin. Nutr.* 38 (4), 1561–1569. doi:10.1016/j.clnu.2018.08.009

Sato, J., Kanazawa, A., Azuma, K., Ikeda, F., Goto, H., Komiya, K., et al. (2017). Probiotic Reduces Bacterial Translocation in Type 2 Diabetes Mellitus: A Randomised Controlled Study. *Sci. Rep.* 7 (1), 12115. doi:10.1038/s41598-017-12535-9

Tabrizi, R., Ostadmohammadi, V., Lankarani, K. B., Akbari, M., Akbari, H., Vakili, S., et al. (2019). The Effects of Probiotic and Synbiotic Supplementation on Inflammatory Markers Among Patients with Diabetes: A Systematic Review and Meta-Analysis of Randomized Controlled Trials. *Eur. J. Pharmacol.* 852, 254–264. doi:10.1016/j.ejphar.2019.04.003

Tajadadi-Ebrahimi, M., Bahmani, F., Shakeri, H., Hadaegh, H., Hijijafari, M., Abedi, F., et al. (2014). Effects of Daily Consumption of Synbiotic Bread on Insulin Metabolism and Serum High-Sensitivity C-Reactive Protein Among Diabetic Patients: a Double-Blind, Randomized, Controlled Clinical Trial. *Ann. Nutr. Metab.* 65 (1), 34–41. doi:10.1159/000365153

Tilg, H., Zmora, N., Adolph, T. E., and Elinav, E. (2020). The Intestinal Microbiota Fuelling Metabolic Inflammation. *Nat. Rev. Immunol.* 20 (1), 40–54. doi:10.1038/s41577-019-0198-4

Tonucci, L. B., Olbrich Dos Santos, K. M., Licursi de Oliveira, L., Rocha Ribeiro, S. M., and Duarte Martino, H. S. (2017). Clinical Application of Probiotics in Type 2 Diabetes Mellitus: A Randomized, Double-Blind, Placebo-Controlled Study. *Clin. Nutr.* 36 (1), 85–92. doi:10.1016/j.clnu.2015.11.011

Tsai, Y. L., Lin, T. L., Chang, C. J., Wu, T. R., Lai, W. F., Lu, C. C., et al. (2019). Probiotics, Prebiotics and Amelioration of Diseases. *J. Biomed. Sci.* 26 (1), 3. doi:10.1186/s12929-018-0493-6

Wang, X., Juan, Q. F., He, Y. W., Zhuang, L., Fang, Y. Y., and Wang, Y. H. (2017). Multiple Effects of Probiotics on Different Types of Diabetes: a Systematic Review and Meta-Analysis of Randomized, Placebo-Controlled Trials. *J. Pediatr. Endocrinol. Metab.* 30 (6), 611–622. doi:10.1515/jpem-2016-0230

Wang, Z. B., Xin, S. S., Ding, L. N., Ding, W. Y., Hou, Y. L., Liu, C. Q., et al. (20192019). The Potential Role of Probiotics in Controlling Overweight/Obesity and Associated Metabolic Parameters in Adults: A Systematic Review and Meta-Analysis. *Evid. Based Complement. Alternat Med.* 2019, 3862971. doi:10.1155/2019/3862971

Wei, R. X., Ye, F. J., He, F., Song, Q., Xiong, X. P., Yang, W. L., et al. (2021). Comparison of Overfeeding Effects on Gut Physiology and Microbiota in Two Goose Breeds. *Poult. Sci.* 100 (3), 100960. doi:10.1016/j.psj.2020.12.057

Woldeamlak, B., Yirdaw, K., and Biadgo, B. (2019). Role of Gut Microbiota in Type 2 Diabetes Mellitus and its Complications: Novel Insights and Potential Intervention Strategies. *Korean J. Gastroenterol.* 74 (6), 314–320. doi:10.4166/kjg.2019.74.6.314

Zhang, J., Ni, Y., Qian, L., Fang, Q., Zheng, T., Zhang, M., et al. (2021). Decreased Abundance of Akkermansia Muciniphila Leads to the Impairment of Insulin Secretion and Glucose Homeostasis in Lean Type 2 Diabetes. *Adv. Sci.* 8 (16), 2100536. doi:10.1002/advs.202100536

Zhang, N., Tao, J., Gao, L., Bi, Y., Li, P., Wang, H., et al. (2020). Liraglutide Attenuates Nonalcoholic Fatty Liver Disease by Modulating Gut Microbiota in Rats Administered a High-Fat Diet. *Biomed. Res. Int.* 2020, 2947549. doi:10.1155/2020/2947549

Zhang, P., and Gregg, E. (2017). Global Economic burden of Diabetes and its Implications. *Lancet Diabetes Endocrinol.* 5 (6), 404–405. doi:10.1016/S2213-8587(17)30100-6

Zheng, H. J., Guo, J., Jia, Q., Huang, Y. S., Huang, W. J., Zhang, W., et al. (20192019). The Effect of Probiotic and Synbiotic Supplementation on Biomarkers of Inflammation and Oxidative Stress in Diabetic Patients: A Systematic Review and Meta-Analysis of Randomized Controlled Trials. *Pharmacol. Res.* 142, 303–313. doi:10.1016/j.phrs.2019.02.016

Conflict of Interest: The authors declare that the research was conducted in the absence of any commercial or financial relationships that could be construed as a potential conflict of interest.

Publisher's Note: All claims expressed in this article are solely those of the authors and do not necessarily represent those of their affiliated organizations, or those of the publisher, the editors, and the reviewers. Any product that may be evaluated in this article, or claim that may be made by its manufacturer, is not guaranteed or endorsed by the publisher.

frontiers in Pharmacology

ORIGINAL RESEARCH
published: 02 February 2022
doi: 10.3389/fphar.2021.795483

Polydextrose Alleviates Adipose Tissue Inflammation and Modulates the Gut Microbiota in High-Fat Diet-Fed Mice

Qiuyue Hu[1†], Yixin Niu[1†], Yanxia Yang[2†], Qianyun Mao[1], Yao Lu[1], Hui Ran[1], Hongmei Zhang[1], Xiaoyong Li[1], Hongxia Gu[2] and Qing Su[1*]*

[1]Department of Endocrinology, Xinhua Hospital, Shanghai Jiao Tong University School of Medicine, Shanghai, China, [2]Department of Endocrinology, Xinhua Hospital Chongming Branch, Shanghai Jiao Tong University School of Medicine, Shanghai, China

The soluble dietary fiber polydextrose (PDX) is a randomly linked glucose oligomer containing small amounts of sorbitol and citric acid and is widely used in the food industry. However, whether PDX can prevent and treat obesity in high-fat diet (HFD)-fed mice has not been directly investigated, and further studies are needed to better understand the complex interactions among PDX, adipose tissue inflammation and the gut microbiota. In the present study, PDX reduced body weight, fasting blood glucose (FBG), adipose tissue accumulation, adipocyte hypertrophy, serum total cholesterol (TC), low-density lipoprotein cholesterol (LDL-C) and high-density lipoprotein cholesterol (HDL-C) levels in HFD-fed mice. Moreover, PDX alleviated serum lipopolysaccharide (LPS) levels and macrophage infiltration in epididymal adipose tissue and resulted in macrophage polarization toward the M2 phenotype. Gut microbiota analysis revealed that PDX promoted the growth of beneficial microbes such as *Bacteroides*, *Parabacteroides*, *Alloprevotella*, *Muribaculum*, *Akkermansia*, *Ruminococcaceae_UCG-014* and *UBA1819* in obese mice, which were negatively correlated with subcutaneous fat, epididymal fat, body weight, FBG, serum TC, HDL-C, LDL-C and LPS levels. Our results indicates that PDX can prevent and treat obesity in HFD-fed mice, specifically in alleviating glucolipid metabolism disorders and adipose tissue inflammation, which may be mediated by modulating the structure of the gut microbiota. Therefore, PDX may become a promising nondrug therapy for obesity.

Keywords: polydextrose, gut microbiota, adipose tissue inflammation, macrophage polarization, glucolipid metabolism

OPEN ACCESS

Edited by:
Yao Lu,
Central South University, China

Reviewed by:
Birsen Yilmaz,
Gazi University, Turkey
Duygu Agagündüz,
Gazi University, Turkey

***Correspondence:**
Hongxia Gu
ghxgjj@163.com
Qing Su
suqing@xinhuamed.com.cn

[†]These authors have contributed equally to this work

Specialty section:
This article was submitted to Inflammation Pharmacology, a section of the journal Frontiers in Pharmacology

Received: *15 October 2021*
Accepted: *22 December 2021*
Published: *02 February 2022*

Citation:
Hu Q, Niu Y, Yang Y, Mao Q, Lu Y, Ran H, Zhang H, Li X, Gu H and Su Q (2022) Polydextrose Alleviates Adipose Tissue Inflammation and Modulates the Gut Microbiota in High-Fat Diet-Fed Mice. Front. Pharmacol. 12:795483. doi: 10.3389/fphar.2021.795483

INTRODUCTION

Obesity is a global health problem that is characterized by weight gain, fat accumulation, insulin resistance, chronic inflammation and gut microbiota dysbiosis (Canfora et al., 2019; Xu et al., 2021). Obesity can lead to a series of comorbidities, including type 2 diabetes mellitus, nonalcoholic fatty liver disease, cancer, cardiovascular diseases, hypertension, neurodegenerative diseases and sleep apnea (Blüher, 2019; Wilding et al., 2019). One study predicted that nearly 1 in 2 adults will have obesity and 1 in 4 adults will have severe obesity by 2030 in the United States (Ward et al., 2019).

Obesity is associated with an increased risk of morbidity and mortality as well as a decrease in life expectancy (Martel et al., 2017; LeBlanc et al., 2018). Recently, many studies have indicated that individuals with obesity are associated with an increased risk of coronavirus disease 2019 (COVID-19) morbidity and mortality, and obese patients with COVID-19 infection should be treated more aggressively (Hamer et al., 2020; Popkin et al., 2020; Sanchis-Gomar et al., 2020; Stefan et al., 2020). Therefore, it is crucial and urgent for us to find effective therapies to prevent and treat obesity.

Dietary fiber is defined as carbohydrate polymers with three or more monomeric units that are neither digested nor absorbed in the small intestine. Dietary fiber is generally categorized into two classes: soluble dietary fiber such as inulin and β-glucan and insoluble dietary fiber such as cellulose. A large number of studies have indicated that dietary fiber intake is negatively correlated with chronic metabolic disorders and promotes health (Makki et al., 2018; Zhao and Zhang, 2018). Previous studies have revealed that obesity is often characterized by an increase in the proportion of *Firmicutes* and a decrease in *Bacteroides* (Ye et al., 2021; Zhai et al., 2021). Notably, dietary fiber can regulate the gut microbiota structure and contribute to fermentation products, in particular, short-chain fatty acids (SCFAs), which are considered important signaling molecules and beneficial for human health (Koh et al., 2016; Makki et al., 2018). Polydextrose (PDX) is a highly branched and randomly bonded glucose polymer that is considered a soluble dietary fiber. PDX is not hydrolyzed in the small intestine and fermented in the colon by endogenous microbiota (do Carmo et al., 2016). Several clinical trials have indicated that PDX can increase fecal bulk, soften stools and increase defecation frequency in healthy or constipated people (Hengst et al., 2009; Costabile et al., 2012). In addition, a galacto-oligosaccharide and PDX mixture can significantly reduce the incidence of viral respiratory tract infections in infants (Luoto et al., 2014; Ranucci et al., 2018). Moreover, PDX can decrease pH and increase SCFA production in the cecum of Wistar rats undergoing Billroth II partial gastrectomy (do Carmo et al., 2018). A previous study also revealed that PDX can modulate the gut microbiota and attenuate serum triglyceride and cholesterol levels in 14-days Western diet-fed mice (Raza et al., 2017).

Adipose tissue inflammation is considered a hallmark of obesity and is closely associated with the development of type 2 diabetes and cardiovascular disease (Kusminski et al., 2016; Oikonomou and Antoniades, 2019). Overnutrition can cause metabolic and structural changes in adipocytes, which initiate an inflammatory program and the subsequent recruitment of proinflammatory macrophages (Reilly and Saltiel, 2017). Moreover, emerging studies have demonstrated that metabolic inflammation is characterized by alterations in gut microbiota structure (Tilg et al., 2020; Chassaing et al., 2021; Shealy et al., 2021).

PDX has been widely used in the food industry, however, whether PDX can prevent and treat obesity in high-fat diet (HFD)-fed mice has not been directly investigated. We aim to investigate the effects of PDX on glucolipid metabolism disorders, adipose tissue inflammation and the gut microbiota in HFD-fed mice, as well as the complex interactions among them.

MATERIALS AND METHODS

Animal Experiment Design

Part 1: Study on prevention of obesity. 4-week-old male C57BL/6 mice were purchased from Shanghai SLAC Laboratory Animal Co. Ltd. After 1 week of quarantine, the mice were randomly divided into three groups (12 mice per group): the chow, HFD and HFD + PDX groups. Mice in the chow group were fed a normal chow diet, while mice in the latter groups were fed a HFD (60% energy from fat; Research Diet, United States) supplemented or not with PDX (10 g/kg/day; Tate & Lyle Group, United Kingdom) for 12 weeks (**Figure 1**).

Part 2: Study on treatment of obesity. 4-week-old male C57BL/6 mice were randomly divided into two groups: the control and obesity groups. Mice in the obesity group were fed a HFD for 12 weeks to establish an obesity model. Then, these obese mice were randomly divided into two groups: the obesity and obesity + PDX groups (10 mice per group). The latter two groups were fed a HFD and left untreated or treated with PDX (10 g/kg/day) for another 12 weeks (**Figure 1**).

All of the mice were housed in the animal facility under a 12 h light/dark cycle and constant temperature (20–23°C). The mice had free access to sterile drinking water and food. Body weight was recorded once weekly, and fasting blood glucose (FBG) was measured every two weeks. At the end of the experiments, the mice were sacrificed under anesthesia. Serum samples and epididymal fat tissue were collected for further assays. Tissue samples were immediately submerged in liquid nitrogen and transferred to −80°C for storage. All procedures were performed in accordance with the National Institutes of Health Guidelines for the Care and Use of Animals and were approved by the Ethics Committee of Xinhua Hospital affiliated to Shanghai Jiao Tong University School of Medicine.

Intraperitoneal Glucose Tolerance Test

The intraperitoneal glucose tolerance test (IPGTT) was conducted 1 week before the end of the experiment. The mice were fasted overnight for 16 h and then intraperitoneally injected with glucose (2 g/kg). Blood glucose was measured at 0, 15, 30, 60 and 120 min using a blood glucose meter (Bayer, Germany).

Intraperitoneal Insulin Tolerance Test

The intraperitoneal insulin tolerance test (IPITT) was conducted at the end of the experiment. The mice were fasted for 6 h and then intraperitoneally injected with insulin (0.75 units/kg; Novo Nordisk, Denmark). Blood glucose was measured at 0, 15, 30, 60 and 120 min using a blood glucose meter (Bayer, Germany).

Histology and Immunohistochemistry

Fresh epididymal adipose tissue samples from all parts of the mice were fixed in 4% paraformaldehyde for 24 h. Then, the tissues were embedded in paraffin wax and cut into 5 μm thick tissue slices. The slices were stained with hematoxylin and eosin (H&E)

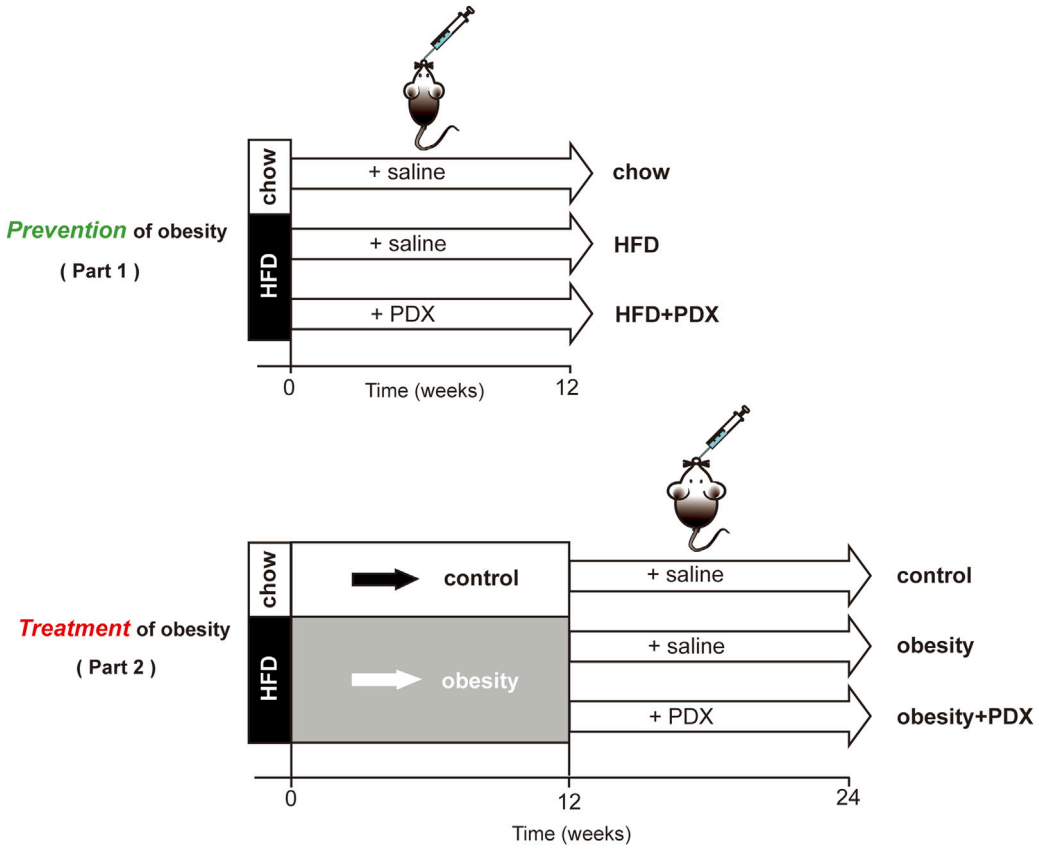

FIGURE 1 | Schematic diagram of the two-part animal experiment design.

TABLE 1 | Sequence of primers for quantitative real-time PCR

Gene	Species	Forward primer (5′→3′)	Reverse primer (5′→3′)
DGAT2	mouse	GCGCTACTTCCGAGACTACTT	GGGCCTTATGCCAGGAAACT
SREBF1	mouse	TGACCCGGCTATTCCGTGA	CTGGGCTGAGCAATACAGTTC
Fasn	mouse	GGAGGTGGTGATAGCCGGTAT	TGGGTAATCCATAGAGCCCAG
PPARα	mouse	TACTGCCGTTTTCACAAGTGC	AGGTCGTGTTCACAGGTAAGA
CPT1α	mouse	TGGCATCATCACTGGTGTGTT	GTCTAGGGTCCGATTGATCTTTG
CD36	mouse	ATGGGCTGTGATCGGAACTG	TTTGCCACGTCATCTGGGTTT
HSL	mouse	CTCACAGTTACCATCTCACCTC	GATTTTGCCAGGCTGTTGAGTA
LPL	mouse	GCCGAGAGCGAGAACATTCC	GCAGTTCTCCGATGTCCACC
Acsl3	mouse	CGGAAATCATGGATCGGATCTA	GTGGAGTACTACACCCTTTTGA
TNF-α	mouse	ATGTCTCAGCCTCTTCTCATTC	GCTTGTCACTCGAATTTTGAGA
IL-1β	mouse	TCGCAGCAGCACATCAACAAGAG	AGGTCCACGGGAAAGACACAGG
IL-6	mouse	CTGCAAGAGACTTCCATCCAG	AGTGGTATAGACAGGTCTGTTGG
IL-10	mouse	TTCTTTCAAACAAAGGACCAGC	GCAACCCAAGTAACCCTTAAAG
MCP1	mouse	TTTTTGTCACCAAGCTCAAGAG	TTCTGATCTCATTTGGTTCCGA
Nos2	mouse	AGGCCACATCGGATTTCACT	TCAATGGCATGAGGCAGGAG
CD11c	mouse	TCATCACTGATGGGAGAAAACA	CCCCAATTGCATAACGAATGAT
F4/80	mouse	TGTCTGCATGATCATCACGATA	CGTGTCCTTGAGTTTAGAGACT
Arg1	mouse	AGACCACAGTCTGGCAGTTGG	AGGTTGCCCATGCAGATTCCC
Fizz1	mouse	CAGCTGATGGTCCCAGTGAAT	CAGTGGAGGGATAGTTAGCTGG
Mrc1	mouse	GGAAGCCCATTCCGGTATCT	CATCGCTTGCTGAGGGAATG
IL-4	mouse	GGACGCCATGCACGGAGATG	CGAAGCACCTTGGAAGCCCTAC
PPARγ	mouse	CCAAGAATACCAAAGTGCGATC	TCACAAGCATGAACTCCATAGT
β-actin	mouse	GTGACGTTGACATCCGTAAAGA	GCCGGACTCATCGTACTCC

and observed with optical microscopy. ImageJ software was used to estimate adipocyte size. Additionally, the slices were deparaffinized and rehydrated. Then, the slices were placed in citric acid antigen repair buffer (pH 6.0), heated in a microwave oven for antigen repair, and incubated with 3% H_2O_2 for 25 min in the dark to block the activity of endogenous peroxidase. The slices were blocked in 3% BSA for 30 min, incubated with primary rabbit anti-mouse F4/80 antibody (Cell Signaling, MA, United States) at 4°C overnight, and then incubated with HRP-conjugated secondary antibody for 50 min at room temperature. Diaminobenzidine substrate was used to develop the color, and the slices were counterstained with hematoxylin. A Leica microscope was used for image acquisition, and ImageJ was used to calculate the percentage of F4/80-positive staining area per slice.

Immunofluorescence

The slices were deparaffinized and rehydrated. Then, the slices were placed in citric acid antigen repair buffer (pH 9.0), heated in a microwave oven for antigen repair, and blocked in 3% BSA for 30 min. Next, the slices were incubated with primary F4/80 antibody (Cell Signaling, MA, United States) at 4°C overnight, followed by incubation with secondary antibody for 50 min at room temperature. Then, the slices were stained with DAPI and mounted.

Biochemical Analyses

Blood samples were centrifuged at 3,000 × g for 10 min, and the supernatant was collected and stored at −80°C before the assay. The serum total triglyceride (TG), total cholesterol (TC), low-density lipoprotein cholesterol (LDL-C) and high-density lipoprotein cholesterol (HDL-C) levels of all the samples were detected with an automatic biochemical analyzer (Hitachi, Japan).

Enzyme-Linked Immunosorbent Assay

Serum lipopolysaccharide (LPS), tumor necrosis factor-alpha (TNF-α), interleukin (IL)-1β, IL-6, IL-10 and fasting insulin (FINS) levels were measured according to the protocol of the corresponding ELISA kit (Westang, China).

Quantitative Real-Time Polymerase Chain Reaction

Total RNA was extracted from epididymal adipose tissues using TRIzol reagent (Takara, Japan) according to the manufacturer's instructions. Then, total RNA was reverse transcribed to complementary deoxyribonucleic acid (cDNA) with a reverse transcription reagent kit (Takara, Japan). The cDNA samples were subsequently amplified with SYBR Green PCR reagent (Takara, Japan) on an Applied Biosystems QuantStudio3 Real-Time PCR System (Thermo Fisher, MA, United States). The relative mRNA expression level of each gene was calculated by the comparative cycle threshold method ($2^{-\Delta\Delta Ct}$), and the results were normalized to the expression level of the housekeeping gene β-actin. The primer sequences are provided in **Table 1**.

Western Blot Analysis

Proteins were extracted from epididymal adipose tissue using RIPA lysis buffer containing protease and phosphatase inhibitor cocktails (Beyotime, China), followed by quantification with a BCA protein quantitative analysis kit (Beyotime, China). Equal amounts of protein samples were separated on an SDS PAGE gel and transferred onto a polyvinylidene fluoride (PVDF) membrane (Millipore, United States). The membranes were then blocked with 5% skim milk powder and incubated with primary antibodies against β-actin, IκBα, p65 and p-p65 (Cell Signaling Technology, MA, United States) at 4°C overnight, followed by incubation with an HRP-conjugated secondary antibody (Beyotime, China) for 60 min at room temperature. Protein bands were visualized using Immobilon western chemiluminescent HRP substrate (Millipore, MA, United States) and then quantified with ImageJ software.

Microbiota Analysis

In the last week of the Part 2 experiment, fresh feces were collected by anal stimulation or abdominal massage into sterile cryopreservation tubes, immediately submerged in liquid nitrogen and transferred to −80°C for storage. Microbial DNA was extracted from the fecal samples using a TIANamp Stool DNA kit (Qiagen, Germany) according to the manufacturer's instructions. The V3-V4 region of the bacterial 16S ribosomal RNA gene was amplified by PCR using primers 343F (TACGGRAGGCAGCAG) and 798R (AGGGTATCTAATCCT). Amplicons were extracted from 2% agarose gels and purified using an AxyPrep DNA Gel Extraction Kit (Axygen Biosciences, CA, United States), followed by quantification using QuantiFluor™-ST (Promega, United States). Equal amounts of purified amplicons were sequenced on an Illumina MiSeq platform (Illumina, MA, United States) according to standard protocols. The raw sequencing data were obtained in FASTQ format. Ambiguous bases of paired-end reads were detected and trimmed using Trimmomatic software, and then paired-end reads were assembled using FLASH software. Clean reads were clustered to generate operational taxonomic units (OTUs) using Vsearch software with 97% identity. All representative reads were annotated and blasted against the Silva database using the RDP classifier (confidence threshold of 70%).

Statistical Analysis

Data are shown as the mean ± standard error of the mean (SEM). Statistical analyses were performed using GraphPad Prism V.7.0. For parametric variables, the unpaired two-tailed Student's t-test was used for comparisons between two groups, and one-way analysis of variance (ANOVA) followed by Bonferroni's post hoc test was used for comparisons of three groups. For nonparametric variables, statistically significant differences were evaluated by the Wilcoxon rank-sum test or Kruskal–Wallis test with Dunn's multiple comparisons test. To compare the body weight and FBG of three groups, two-way ANOVA followed by Bonferroni's post hoc test was performed. The LEfSe method was used to assess the

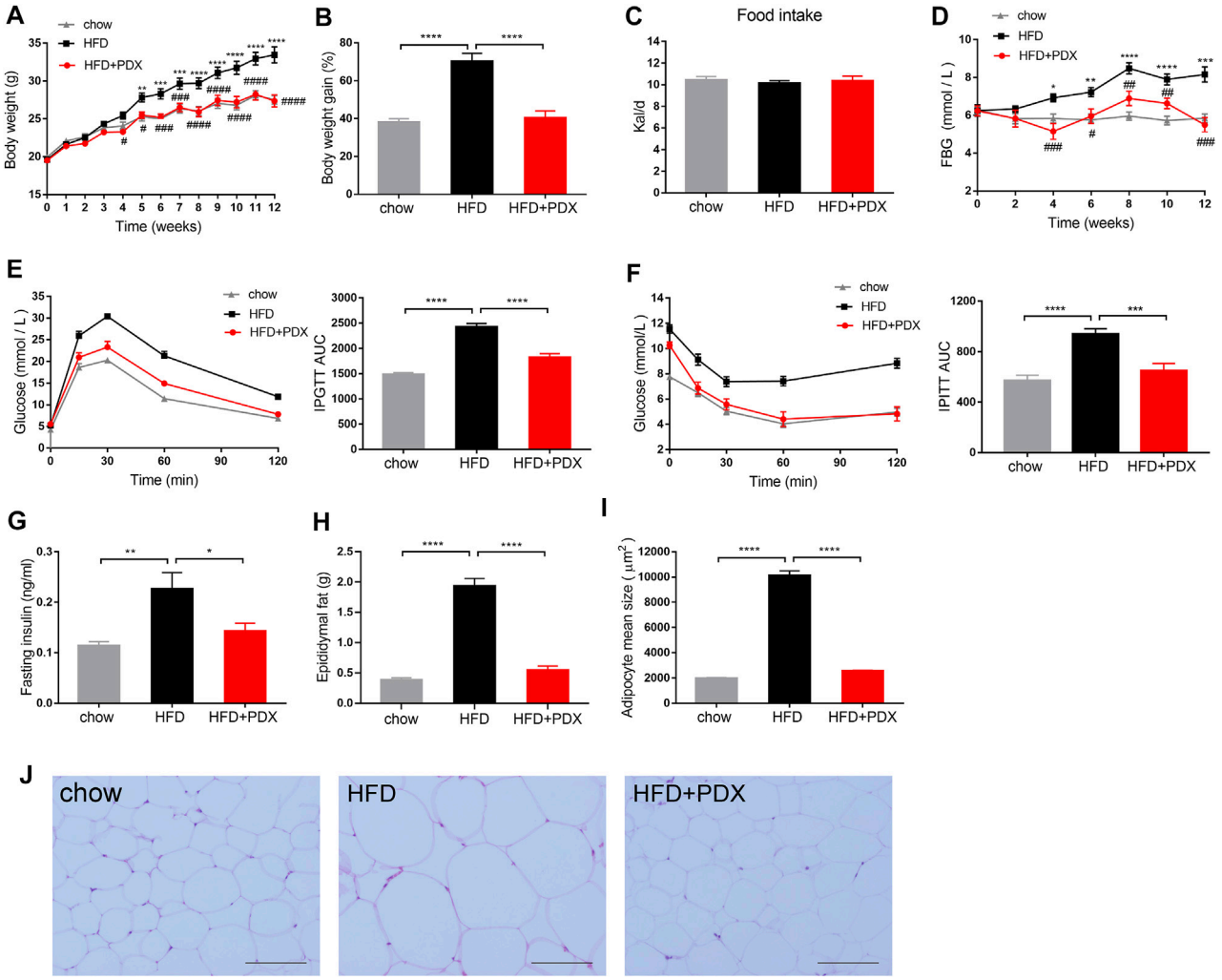

FIGURE 2 | PDX prevented obesity-related traits in HFD-fed mice (Part 1). **(A)** Body weight. **(B)** Body weight gain at week 12. **(C)** Food intake measured as kilocalories per day. **(D)** FBG. **(E)** IPGTT and AUC measured during the IPGTT (mM·min). **(F)** IPITT and AUC measured during the IPITT (mM·min). **(G)** Fasting insulin. **(H)** Epididymal fat accumulation. **(I)** Adipocyte mean size. **(J)** Representative images of H&E-stained epididymal adipose tissues. Scale bar, 100 μm; magnification, x200. AUC, area under the curve. n = 12 per group. *p < 0.05; **p < 0.01; ***p < 0.001; ****p < 0.0001.

statistically significant difference in bacterial species. Spearman's correlation analysis was performed to determine correlation coefficients between bacterial species and obesity traits. $p < 0.05$ was considered statistically significant.

RESULTS

The Role of PDX in the Prevention of Obesity (Part 1)

To investigate the effects of PDX on the prevention of obesity, mice were administered a HFD and PDX supplementation simultaneously for 12 weeks (**Figure 1**). The body weight and FBG of mice in the HFD group were significantly elevated compared with those of mice in the chow group (**Figures 2A,B,D**). In contrast, the HFD mice supplemented with PDX maintained a lower body weight and FBG than those of HFD group (**Figures 2A,B,D**). However, there was no significant difference in food intake among the three groups (**Figure 2C**). We also performed an IPGTT and an IPITT to study the effects of PDX on glucose tolerance and insulin sensitivity, respectively. The results indicated that the HFD decreased glucose tolerance and insulin sensitivity in mice; notably, PDX supplementation increased glucose tolerance and improved HFD-induced insulin resistance (**Figures 2E,F**). The FINS, epididymal fat accumulation and adipocyte size of the HFD group were increased significantly compared with those of the chow group. Additionally, PDX supplementation decreased all these metabolic parameters (**Figures 2G–J**).

We next explored whether PDX supplementation could prevent dyslipidemia in HFD-fed mice. Serum TC, LDL-C and HDL-C levels of the HFD group were increased compared with

those of the chow group. In contrast, all serum lipid profiles as well as TG were reduced significantly in the HFD + PDX group (**Figures 3A–D**). To investigate whether PDX regulates the expression of genes involved in lipid metabolism, we examined genes involved in lipid transport, uptake, lipogenesis and lipolysis in adipose tissue. The results revealed that a HFD increased the expression of sterol regulatory element binding transcription factor 1 (SREBF1), fatty acid synthase (Fasn), and diacylglycerol acyltransferase 2 (DGAT2) in epididymal adipose tissue (**Figure 3E**). Notably, PDX supplementation reduced Fasn and DGAT2 levels in the epididymal adipose tissue of HFD-fed mice (**Figure 3E**).

We further explored whether PDX could maintain a lower inflammation level in HFD-fed mice. The HFD group had a higher level of serum IL-6 compared with the chow group; however, PDX supplementation reduced serum IL-1β and IL-6 levels (**Figures 4C,D**). Moreover, PDX supplementation increased the serum level of the anti-inflammatory cytokine IL-10 (**Figure 4E**), and there was no significant difference in serum LPS and TNF-α levels among the three groups (**Figures 4A,B**).

To investigate whether PDX regulates macrophage infiltration and polarization, F4/80-positive macrophages were quantified by immunohistochemical staining in epididymal adipose tissue. The results revealed that a HFD largely increased the F4/80-positive staining area, and PDX supplementation significantly reversed macrophage infiltration (**Figure 4F**). In addition, the mRNA levels of F4/80 and monocyte chemoattractant protein-1 (MCP1) were increased in epididymal adipose tissue of the HFD group compared with that of the chow group and were reduced in that of the HFD + PDX group (**Figures 4G,H**). We next examined M1 and M2 macrophage markers in epididymal adipose tissue to further explore the regulatory effect of PDX on macrophage polarization. On the one hand, the results revealed that the mRNA levels of CD11c and nitric oxide synthase 2 (Nos2) were significantly increased in the HFD group compared with the chow group, and PDX supplementation reversed the change in the expression of CD11c and Nos2 (**Figure 4I**). On the other hand, the mRNA levels of Fizz1 and peroxisome proliferator-activated receptor γ (PPARγ) were decreased in the HFD group compared with the chow group, and PDX supplementation significantly increased mannose receptor 1 (Mrc1) and PPARγ levels in epididymal adipose tissue compared with a HFD alone (**Figure 4J**). Moreover, the results indicated that PDX supplementation increased IκBα (an inhibitor of the transcription factor NF-κB) levels and reduced p-p65 levels in epididymal adipose tissue of HFD-fed mice (**Figure 4K**).

The Role of PDX in the Treatment of Obesity (Part 2)

To investigate the effects of PDX on the treatment of obesity, an animal model of HFD-induced obesity was applied in our study (**Figure 1**). After 12 weeks of administering a HFD, the body weight and FBG of the obesity group were significantly increased compared with those of the control group (**Figures 5A,B**). Moreover, the IPGTT results showed that the HFD decreased glucose tolerance (**Figure 5C**). Then, obese mice were treated

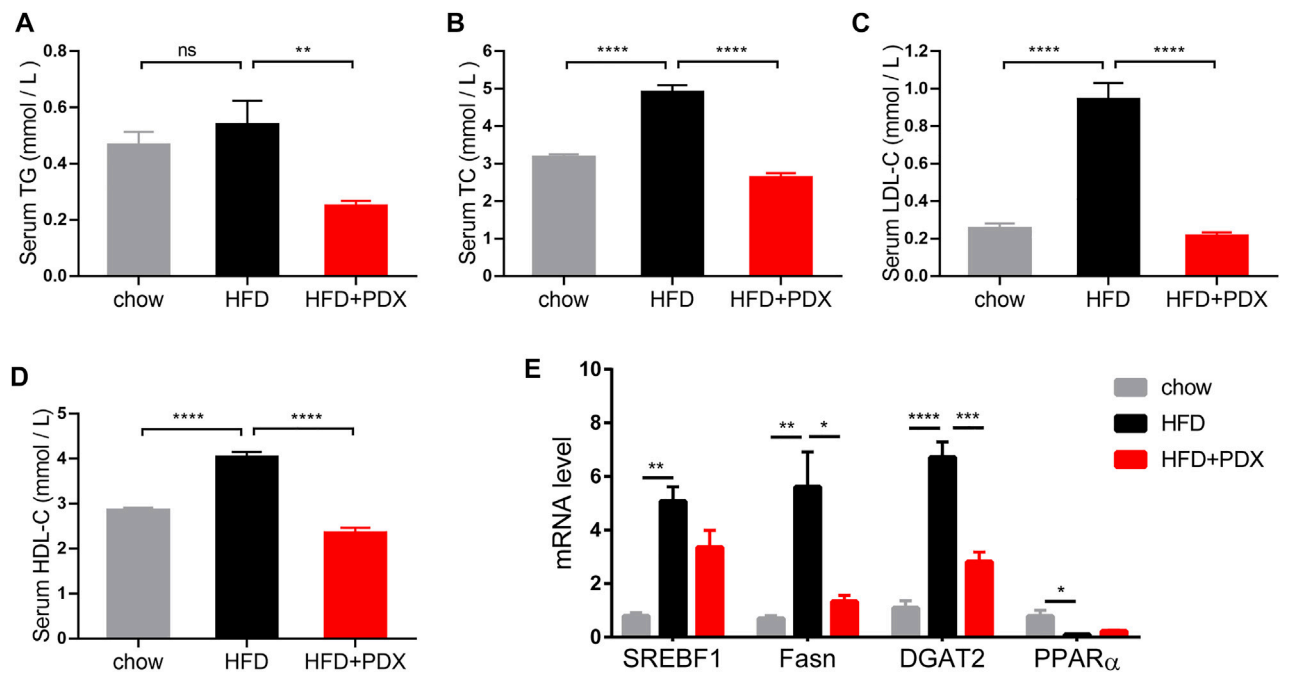

FIGURE 3 | PDX prevented dyslipidemia in HFD-fed mice (Part 1). **(A)** Serum TG. **(B)** Serum TC. **(C)** Serum LDL-C. **(D)** Serum HDL-C. **(E)** qPCR analysis of genes involved in lipid metabolism SREBF1, Fasn, DGAT2 and PPARα in epididymal adipose tissue. $n = 12$ (A–D) or $n = 4$ **(E)** per group. $^{*}p < 0.05$; $^{**}p < 0.01$; $^{***}p < 0.001$; $^{****}p < 0.0001$; ns, not statistically significant.

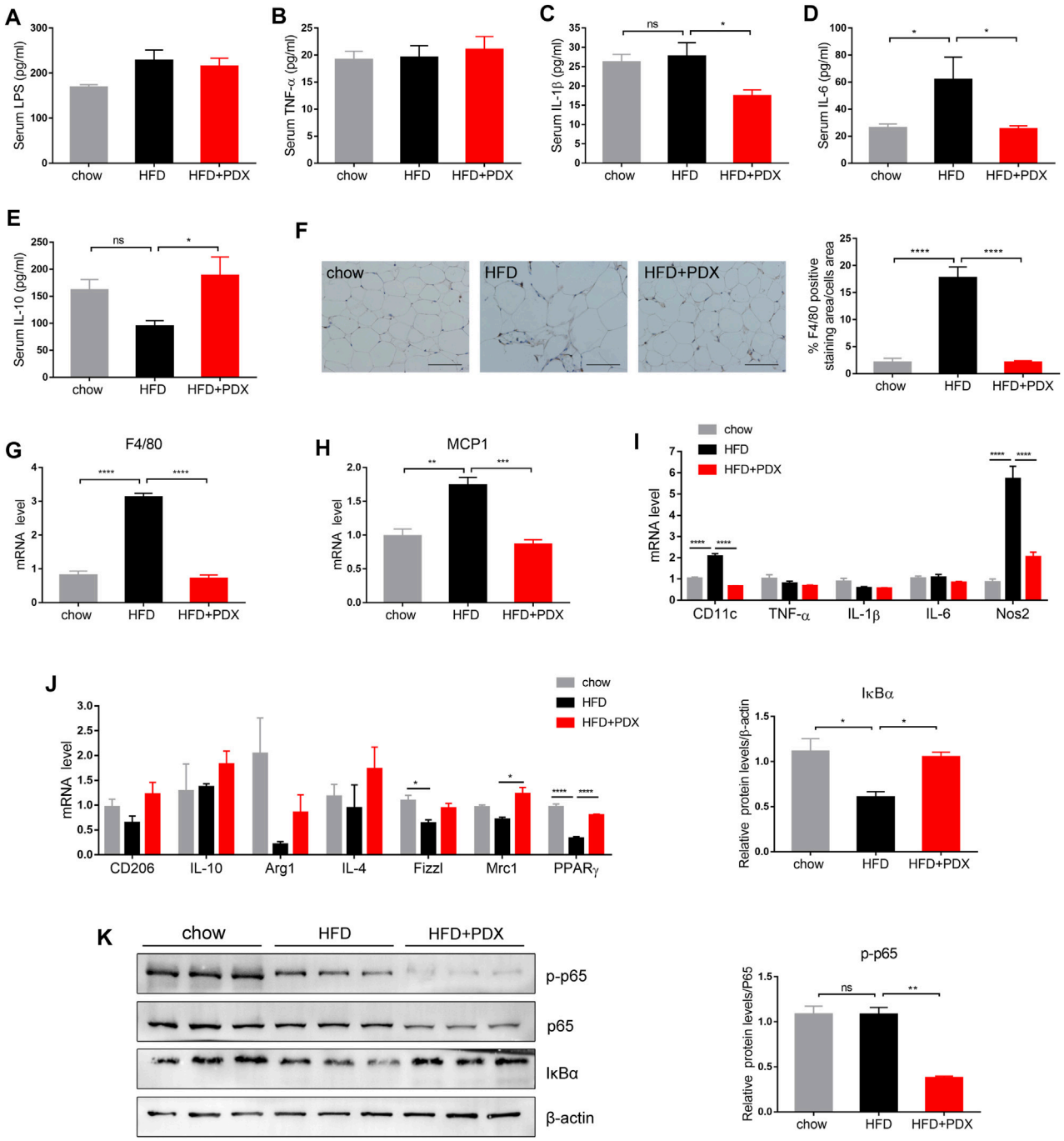

FIGURE 4 | PDX maintained a lower inflammation level and promoted M2 macrophage polarization in the adipose tissue of HFD-fed mice (Part 1). **(A)** Serum LPS. **(B)** Serum TNF-α **(B)**. **(C)** Serum IL-1β. **(D)** Serum IL-6. **(E)** Serum IL-10. **(F)** Representative images of immunohistochemical staining of epididymal adipose tissue against the specific macrophage maker F4/80 and the quantification of F4/80-positive staining area. Scale bar, 100 μm; magnification, x200. **(G)** qPCR analysis of the mRNA levels of F4/80 in epididymal adipose tissue. **(H)** qPCR analysis of the mRNA levels of MCP1 in epididymal adipose tissue. **(I)** qPCR analysis of the mRNA levels of M1 macrophage maker CD11c, TNF-α, IL-1β, IL-6 and Nos2 in epididymal adipose tissue. **(J)** qPCR analysis of the mRNA levels of M2 macrophage maker CD206, IL-10, Arg1, IL-4, Fizz1, Mrc1 and PPARγ in epididymal adipose tissue. **(K)** Western blot analysis of the proteins expression involved in NF-κB signaling pathway in epididymal adipose tissue. $n = 12$ **(A–F)**, $n = 4$ **(G–J)** or $n = 3$ **(K)** per group. $^{*}p < 0.05$; $^{**}p < 0.01$; $^{***}p < 0.001$; $^{****}p < 0.0001$; ns, not statistically significant.

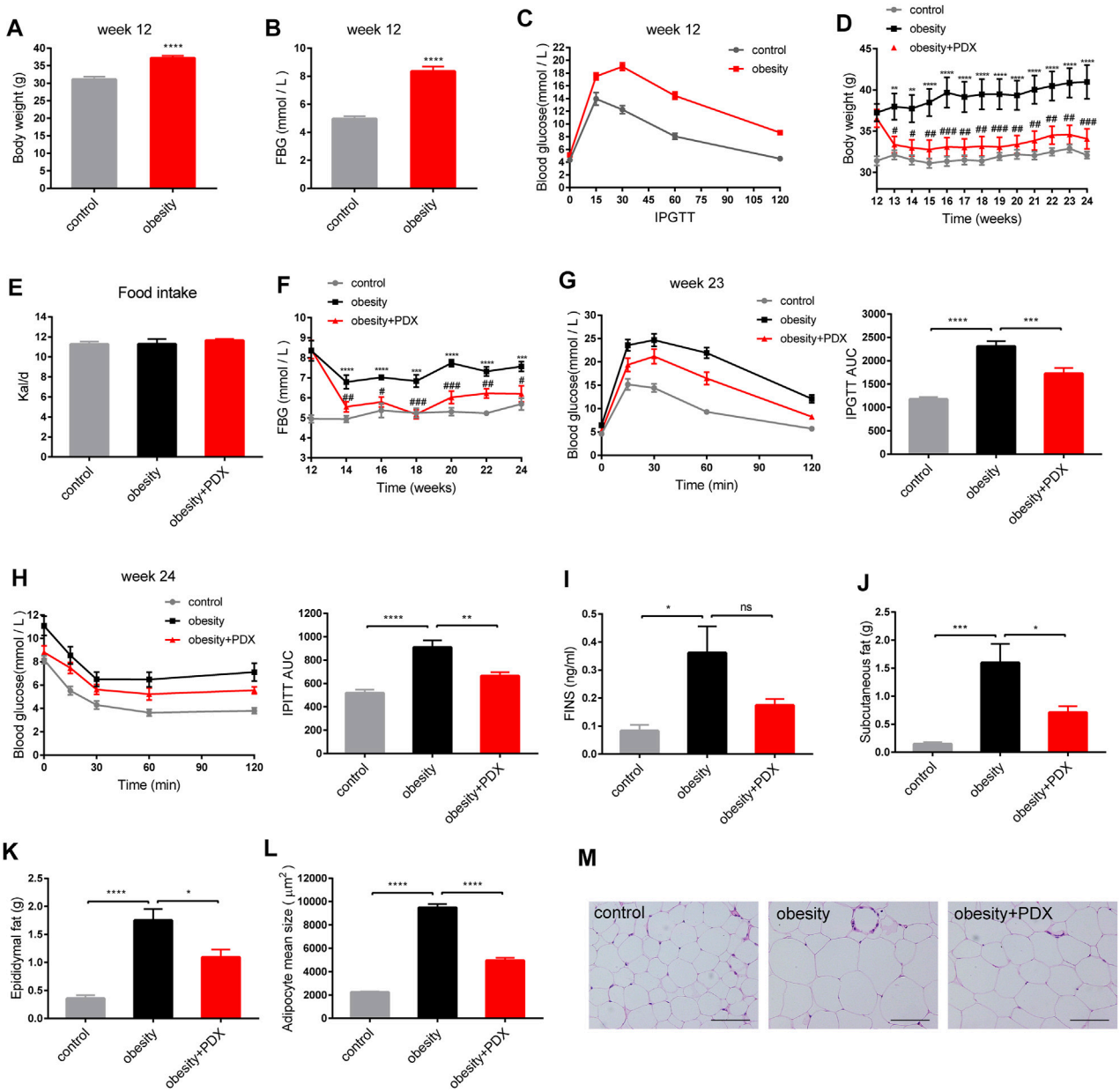

FIGURE 5 | PDX alleviated obesity-related traits in HFD-induced obese mice (Part 2). **(A–C)** C57BL/6 mice were fed a HFD for 12 weeks to establish an obesity model. **(A)** Body weight at week 12. **(B)** FBG at week 12. **(C)** IPGTT at week 12. **(D–M)** The HFD-induced obese mice were then treated with PDX for another 12 weeks. **(D)** Body weight. **(E)** Food intake measured as kilocalories per day. **(F)** FBG. **(G)** IPGTT and AUC measured during the IPGTT at week 23 (mM·min). **(H)** IPITT and AUC measured during the IPITT at week 24 (mM·min). **(I)** FINS. **(J)** Subcutaneous fat accumulation. **(K)** Epididymal fat accumulation. **(L)** Adipocyte mean size. **(M)** Representative images of H&E-stained epididymal adipose tissues. Scale bar, 100 μm; magnification, x200. $n = 10$ per group. $^{*}p < 0.05$; $^{**}p < 0.01$; $^{***}p < 0.001$; $^{****}p < 0.0001$; ns, not statistically significant.

with PDX or sterile saline for another 12 weeks. After 12 weeks of PDX treatment, the body weight and FBG of the obesity + PDX group were significantly reduced compared with those of the obesity group (**Figures 5D,F**), and there was no significant difference in food intake among the groups (**Figure 5E**). The IPGTT and IPITT results indicated that PDX treatment increased glucose tolerance and improved obesity-associated insulin resistance (**Figures 5G,H**). Moreover, FINS, subcutaneous fat accumulation, epididymal fat accumulation and adipocyte size were all significantly decreased in the obesity + PDX group compared with obesity group (**Figures 5I,K,L,M**).

As shown by the biochemical results, the serum TC, LDL-C and HDL-C levels in the obesity group were elevated compared with those in the control group, and PDX treatment reduced the

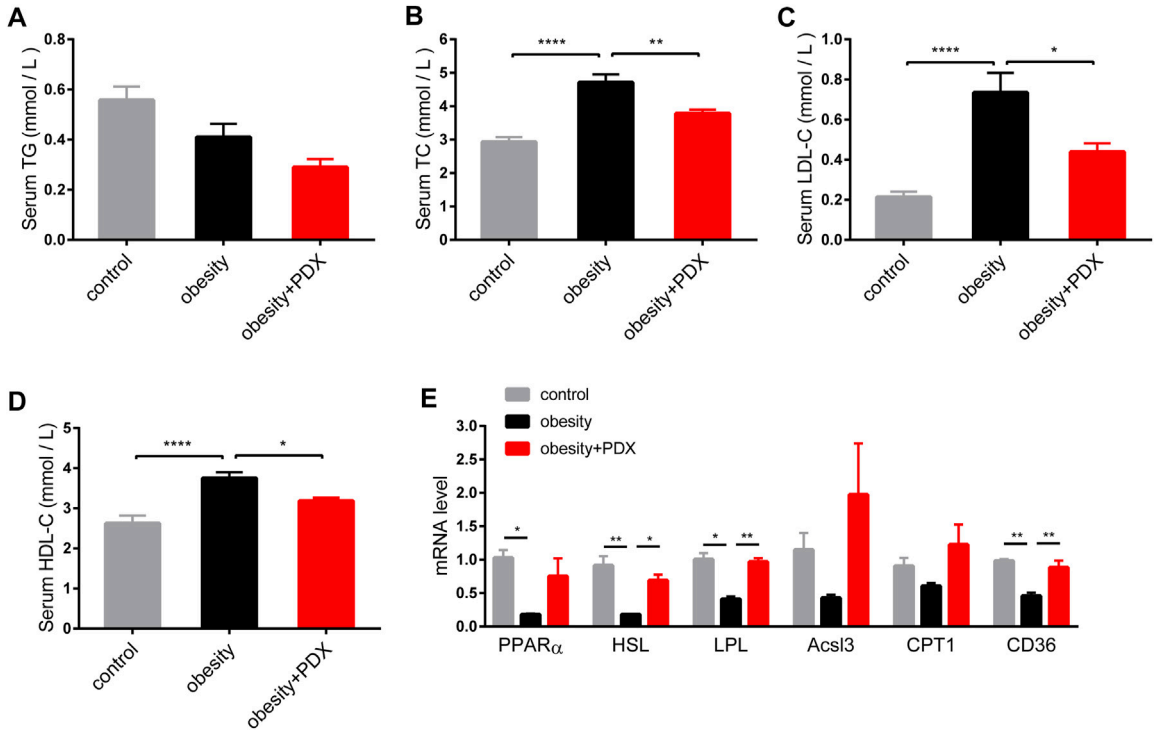

FIGURE 6 | PDX improved dyslipidemia in HFD-induced obese mice (Part 2). **(A)** Serum TG. **(B)** Serum TC. **(C)** Serum LDL-C. **(D)** Serum HDL-C. **(E)** qPCR analysis of genes involved in lipid metabolism PPARα, HSL, LPL, Acsl3, CPT1 and CD36 in epididymal adipose tissue. $n = 10$ **(A–D)** or $n = 4$ **(E)** per group. $^{*}p < 0.05$; $^{**}p < 0.01$; $^{***}p < 0.001$; $^{****}p < 0.0001$.

levels of these lipid profiles (**Figures 6B–D**). In addition, the mRNA levels of peroxisome proliferator-activated receptor α (PPARα), hormone-sensitive triglyceride lipase (HSL), lipoprotein lipase (LPL) and CD36 in epididymal adipose tissue were reduced significantly in obese mice compared with mice in the control group (**Figure 6E**). Notably, PDX treatment increased HSL, LPL and CD36 levels in the epididymal adipose tissue of obese mice (**Figure 6E**).

Obesity significantly increased the levels of serum LPS and IL-6, and PDX treatment reversed these levels of serum markers of inflammation (**Figures 7A,D**). There was no significant difference in serum TNF-α, IL-1β or IL-10 changes among the three groups (**Figures 7B,C,E**).

As shown by immunofluorescence staining, obesity largely increased the F4/80-positive staining area in epididymal adipose tissue, and PDX treatment significantly reduced macrophage infiltration (**Figure 7F**). Furthermore, F4/80 mRNA levels validated this result (**Figure 7G**). On the one hand, the CD11c mRNA level was significantly increased in epididymal adipose tissue of obesity group compared with the control group, and PDX treatment reversed the expression of CD11c (**Figure 7I**). On the other hand, the mRNA levels of CD206, IL-10, Fizz1, Mrc1 and PPARγ were reduced in obesity group, and PDX treatment significantly increased the levels of CD206, Fizz1 and PPARγ in epididymal adipose tissue (**Figure 7J**). Moreover, PDX treatment significantly increased the protein level of IκBα and reduced the level of p-p65 in the epididymal adipose tissue of obese mice (**Figure 7K**). The results indicated that PDX can inhibit NF-κB signaling in the epididymal adipose tissue of HFD-induced obese mice.

PDX Modulates the Gut Microbiota Structure in HFD-Induced Obese Mice (Part 2)

To explore the effect of PDX treatment on the gut microbiota in HFD-induced obese mice, we performed 16S rRNA sequencing of fecal samples. Compared with the control group, the obesity group had significantly fewer OTUs, and the PDX treatment group had slightly more OTUs (**Figure 8A**). However, the results revealed that there was no significant difference in the α diversity index (Chao1 index, Shannon index and Simpson index) between the obesity and obesity + PDX groups (**Figures 8B–D**). Principal coordinates analysis (PCoA) of the Bray-Curtis index for the gut microbiota showed that the control, obesity and obesity + PDX groups were clearly clustered into three separate groups (**Figure 8E**).

To further explore whether PDX treatment regulates gut microbiota structure in obese mice, the relative abundance of microbial taxa at different taxonomic levels was examined. At the phylum level, obesity reduced *Bacteroidetes* and increased *Firmicutes* abundance. However, *Bacteroidetes* and

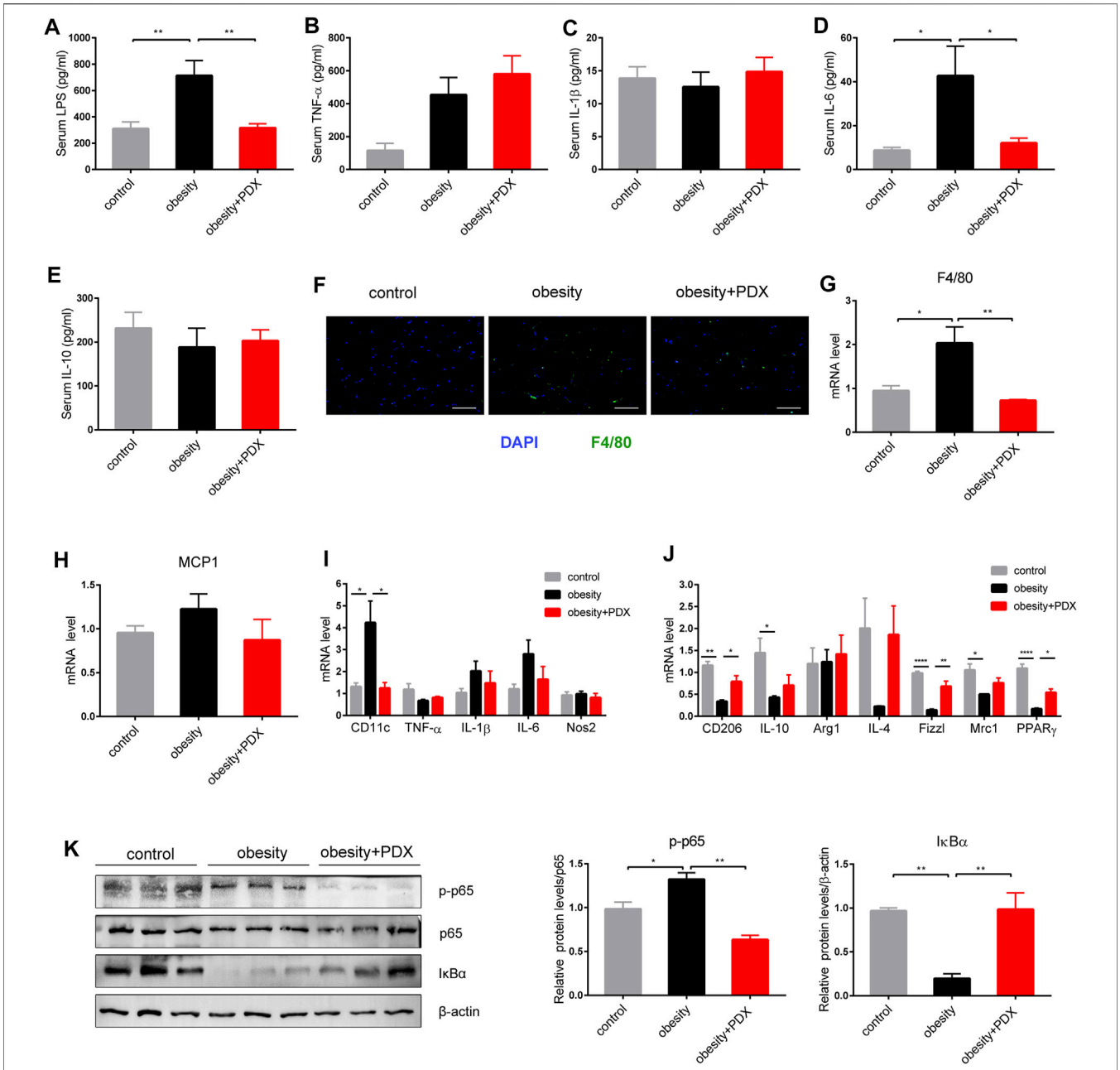

FIGURE 7 | PDX alleviated inflammation levels and promoted macrophage polarization toward M2 phenotype in the epididymal adipose tissue of HFD-induced obese mice (Part 2). **(A)** Serum LPS. **(B)** Serum TNF-α **(B)**. **(C)** Serum IL-1β. **(D)** Serum IL-6. **(E)** Serum IL-10. **(F)** Representative images of immunofluorescence stain of epididymal adipose tissue against the specific macrophage maker F4/80. Scale bar, 100 μm; magnification, x200. **(G)** qPCR analysis of the mRNA levels of F4/80 in epididymal adipose tissue. **(H)** qPCR analysis of the mRNA levels of MCP1 in epididymal adipose tissue. **(I)** qPCR analysis of the mRNA levels of M1 macrophage maker CD11c, TNF-α, IL-1β, IL-6 and Nos2 in epididymal adipose tissue. **(J)** qPCR analysis of the mRNA levels of M2 macrophage maker CD206, IL-10, Arg1, IL-4, Fizz1, Mrc1 and PPARγ in epididymal adipose tissue. **(K)** Western blot analysis of the proteins expression involved in NF-κB signaling pathway in epididymal adipose tissue. $n = 10$ **(A–F)**, $n = 4$ **(G–J)** or $n = 3$ **(K)** per group. $^{*}p < 0.05$; $^{**}p < 0.01$; $^{***}p < 0.001$; $^{****}p < 0.0001$.

Verrucomicrobia were increased, and *Firmicutes* was reduced significantly under PDX treatment (**Figures 9A,B**). Correspondingly, the gut microbiota of obesity + PDX group showed a lower *Firmicutes/Bacteroidetes* ratio than that of obesity group (**Figure 9B**). At the family level, mice in obesity + PDX group had a higher abundance of *Bacteroidaceae*, *Prevotellaceae*, *Burkholderiaceae* and *Tannerellaceae* and a lower abundance of *Lachnospiraceae* than the mice in obesity group (**Figures 9C,D**).

At the genus level, compared with the mice in the control group, obese mice had a higher abundance of *GCA-*

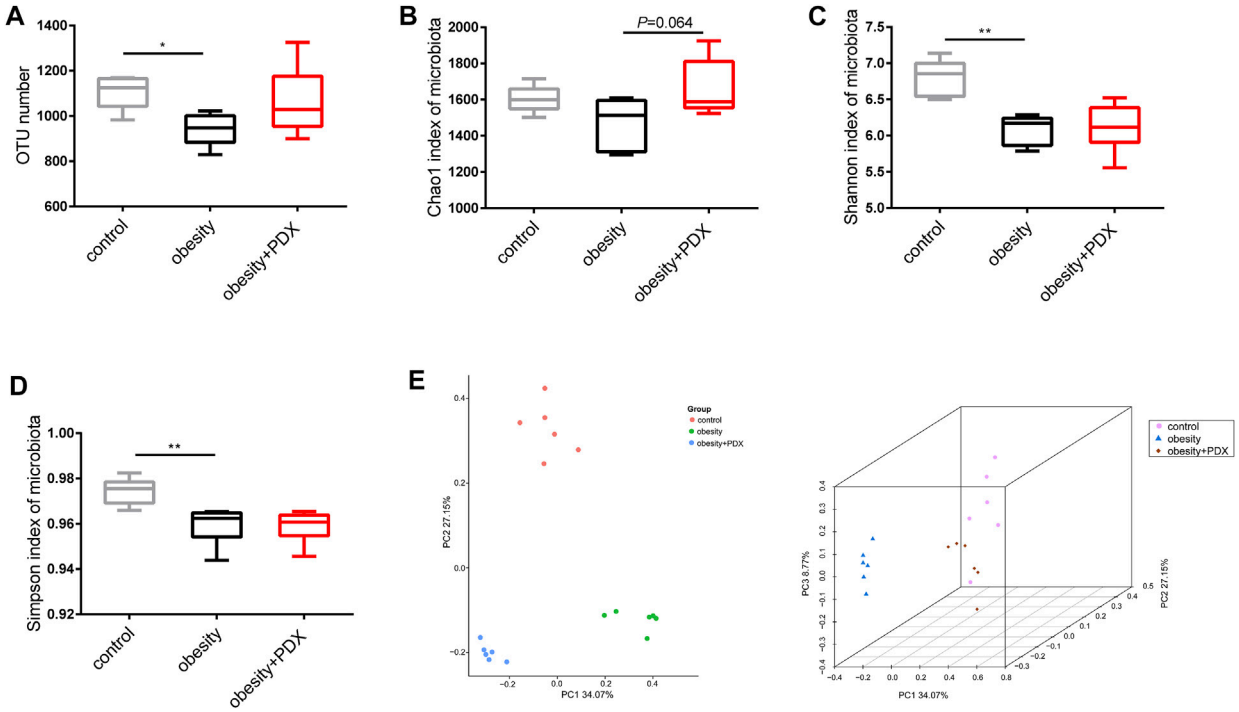

FIGURE 8 | Alpha and beta diversity analysis of gut microbiota in HFD-induced obese mice (Part 2). **(A)** OTU number. **(B)** Chao1 index of microbiota. **(C)** Shannon index of microbiota. **(D)** Simpson index of microbiota. **(E)** 2D and 3D PCoA plot (Bray-Curtis index) of microbial community structure in obese mice. OTU, operational taxonomic unit; PCoA, principal coordinate analysis. n = 6 per group. $^{*}p < 0.05$; $^{**}p < 0.01$.

900066575 and a lower abundance of *Ruminococcaceae_UCG-014* and *Muribaculum* (**Figures 10A,B**). However, mice in obesity + PDX group had a higher abundance of *Bacteroides*, *Alloprevotella*, *Ruminococcaceae_UCG-014*, *UBA 1819*, *Akkermansia*, *Parasutterella*, *Parabacteroides*, *Muribaculum* and *Ileibacterium* and a lower abundance of *GCA-900066575* than the mice in obesity group (**Figures 10A,B**). To identify the biomarker taxa that differentiate obese mice and PDX-treated obese mice, we performed LEfSe analysis and selected genera based on an LDA score >2. The cladogram revealed that *Bacteroidetes* members played an important role in the effects of PDX, generating beneficial effects (**Figure 10C**). Correspondingly, we observed an overrepresentation of *Bacteroides*, *Parabacteroides*, *Alloprevotella*, *Ileibacterium*, *Parasutterella*, *Ruminococcaceae_UCG-014*, *Muribaculum*, *Akkermansia*, *ASF356*, *Ruminiclostridium_5* and *UBA1819* in the PDX treatment group compared with the obesity group; therefore, these taxa can be considered biomarker taxa (**Figure 10D**). Moreover, *GCA-900066575* was overrepresented in the obesity group compared with the obesity + PDX group (**Figure 10D**). To further analyze the association between these genera and metabolic phenotypes, we performed Spearman correlation analysis comparing 9 bacterial genera with 9 metabolic parameters. The results showed that *GCA-900066575* was significantly positively correlated with subcutaneous fat, epididymal fat, body weight, FBG, serum TC, HDL-C, LDL-C and LPS (**Figure 10E**). However, *Bacteroides*, *Parabacteroides*, *Alloprevotella*, *Parasutterella*, *Ruminococcaceae_UCG-014*, *Muribaculum*, *Akkermansia* and *UBA1819* were negatively correlated with these parameters (**Figure 10E**).

DISCUSSION

In the present study, we demonstrated that PDX exerted beneficial effects on the prevention and treatment of obesity. PDX alleviated glucolipid metabolism disorders and adipose tissue inflammation in HFD-fed mice. Moreover, we found that PDX treatment significantly modulated the gut microbiota structure in obese mice. Previous studies have indicated that gut microbiota dysbiosis is one of the reasons for obesity and related disorders, and fecal microbial transplantation (FMT) is considered a potential source of novel therapeutics (Napolitano and Covasa, 2020; He et al., 2021; Voland et al., 2021). FMT from the obesity-associated human gut microbiota to mice can induce vascular dysfunction and glucose intolerance, and FMT from lean donors to patients with obesity can promote metabolic benefits (Mocanu et al., 2021; Russo et al., 2021). Recent studies over the past decade have revealed that many environmental factors, including diet, antibiotic exposure, energy intake and exercise, can dramatically influence the gut microbiota (Du et al., 2021; Giordan et al., 2021; Shi et al., 2021).

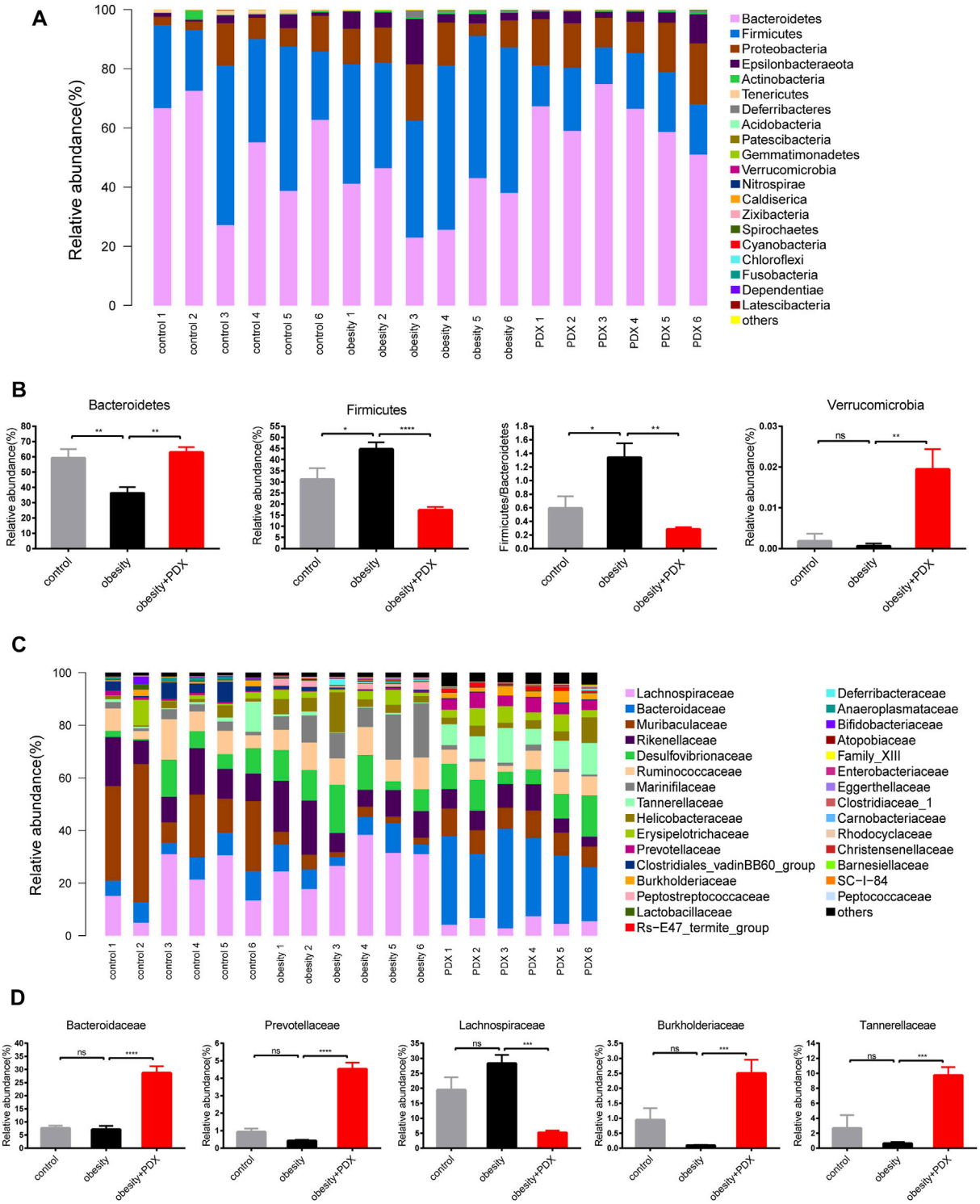

FIGURE 9 | PDX modulated the composition of gut microbiota at the phylum and family level in HFD-induced obese mice (Part 2). **(A)** Relative abundance of microbial taxa at the phylum level. **(B)** Relative abundance of *Bacteroidetes*, *Firmicutes*, *Verrucomicrobia* and *Firmicutes/Bacteroidetes* ratio. **(C)** Relative abundance of microbial taxa at the family level. Top 30 abundances are shown. **(D)** Relative abundance of *Bacteroidaceae, Prevotellaceae, Lachnospiraceae, Burkholderiaceae and Tannerellaceae*. $n = 6$ per group. $^{*}p < 0.05$; $^{**}p < 0.01$; $^{***}p < 0.001$; $^{****}p < 0.0001$; ns, not statistically significant.

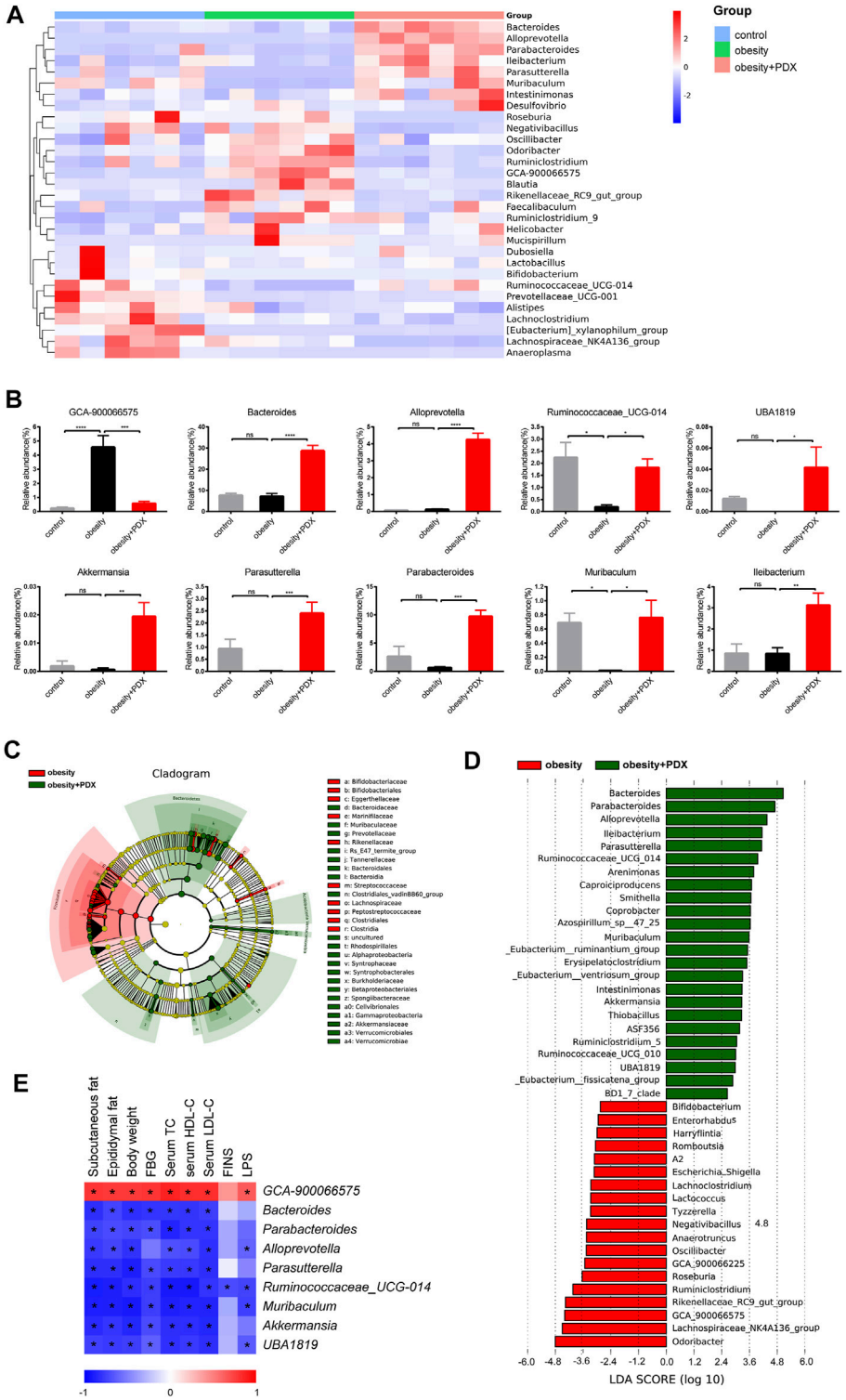

FIGURE 10 | PDX modulated the composition of gut microbiota at the genus level in HFD-induced obese mice (Part 2). **(A)** Heatmap analysis using taxonomic abundances at the genus level. Top 30 abundances are shown. **(B)** Relative abundance of *GCA-900066575, Bacteroides*, *Alloprevotella*, *Ruminococcaceae_UCG-014*, *UBA 1819*, *Akkermansia*, *Parasutterella*, *Parabacteroides*, *Muribaculum* and *Ileibacterium*. **(C)** Cladogram derived from LEfSe analysis, showing the relationship between taxon. **(D)** Linear discriminant analysis (LDA) scores derived from LEfSe analysis, showing biomarker taxa at the genus level (LDA score >2). **(E)** Heatmap analysis of the Spearman correlations between 9 genera and 9 metabolic parameters. $n = 6$ per group. $^{*}p < 0.05$; $^{**}p < 0.01$; $^{***}p < 0.001$; $^{****}p < 0.0001$; ns, not statistically significant.

Dietary fiber has been shown to improve obesity and is considered a potential therapy because it increases microbial fermentation of SCFAs (Schäfer et al., 2021; Thomson et al., 2021). A study indicated that PDX changes the gut microbiome, attenuates plasma TG and TC levels and regulates gene expression in the intestine of mice fed a Western diet for 14 days (Raza et al., 2017); however, we think the research period was somewhat short and not long enough to effectively improve metabolic disorders. Moreover, we performed a two-part study to certify the benefits of PDX on the prevention and treatment of obesity, which lasted for 12 or 24 weeks and focused on adipose tissue inflammation and gut microbiota modulation.

In our study, the PCoA results indicated that PDX treatment can modulate the gut microbiota in obese mice. PDX treatment increased the relative abundance of *Bacteroidetes* and *Verrucomicrobia* and decreased the relative abundance of *Firmicutes* and the *Firmicutes*/*Bacteroidetes* ratio in obese mice. On the one hand, the cladogram derived from LEfSe analysis revealed that *Bacteroidetes* members played an important role in the mediating the effects of PDX, generating beneficial effects; on the other hand, the genus LEfSe analysis indicated that *Bacteroides*, *Parabacteroides*, *Alloprevotella*, *Ileibacterium*, *Parasutterella*, *Ruminococcaceae_UCG-014*, *Muribaculum*, *Akkermansia*, *ASF356*, *Ruminiclostridium_5* and *UBA1819* were overrepresented in the obesity + PDX compared with the obesity group, and *GCA-900066575* was overrepresented in the obesity group. *Bacteroides* (family Bacteroidaceae), *Parabacteroides* (family Tannerellaceae), *Alloprevotella* (family Prevotellaceae) and *Muribaculum* (family Muribaculaceae) all belong to the phylum *Bacteroidetes*. *Bacteroidetes* members encode a proportionally higher number of carbohydrate-active enzymes (CAZymes such as glycoside hydrolases and polysaccharide lyases) than bacteria of other phyla, which enables the optimal use of dietary and host mucosal glycans (Lapébie et al., 2019). Similarly, a study indicated that curcumin alleviates HFD-induced hepatic steatosis and obesity via modulation of gut microbiota including *Akkermansia*, *Bacteroides* and *Parabacteroides* (Li et al., 2021) and these bacteria are all belong to SCFA-producing bacteria (Wu et al., 2021). *Akkermansia muciniphila* is widely considered a promising "next-generation beneficial microbe" for promoting beneficial effects on the metabolic disease, inflammatory bowel disease and tumour immunity, owing to various mechanisms including producing SCFAs, maintaining the integrity of gut barrier and reducing circulating LPS level (Yan et al., 2021; Yang et al., 2021; Zhang et al., 2021). Furthermore, *Parabacteroides goldsteinii* was reduced in HFD-fed mice, and oral treatment of the HFD-fed mice with live *Parabacteroides goldsteinii* reduced obesity (Wu et al., 2019). *Muribaculum* is reduced in mice with Crohn's disease (Dobranowski et al., 2019). Moreover, Spearman correlation analysis proved that *Bacteroides*, *Parabacteroides*, *Alloprevotella*, *Parasutterella*, *Ruminococcaceae_UCG-014*, *Muribaculum*, *Akkermansia* and *UBA1819* were negatively correlated with subcutaneous fat, epididymal fat, body weight, FBG, serum TC, HDL-C, LDL-C and LPS. *Ruminococcaceae_UCG-014* and *UBA1819* belong to the family *Ruminococcaceae*. Previous studies have shown that *Ruminococcaceae* can produce SCFAs and maintain a healthy gastrointestinal tract (McNabney and Henagan, 2017; Videvall et al., 2020). In addition, *Ruminococcaceae* is reduced in older people and aged monkeys (Biagi et al., 2016; Duan et al., 2019). Therefore, we conclude that PDX treatment can modulate the gut microbiota in obese mice and significantly increase several beneficial microbes, including *Bacteroides*, *Parabacteroides*, *Alloprevotella*, *Muribaculum*, *Akkermansia*, *Ruminococcaceae_UCG-014*, and *UBA 1819*.

HFD increased circulating LPS, a component of gram-negative bacterial cell walls, which is in agreement with previous studies (Reilly et al., 2021; You et al., 2021). HFD can alter gut microbiota and intestinal wall permeability, and then LPS is transported via lymph to the circulation by incorporation into chylomicrons (CMs) (Hersoug et al., 2016). LPS can recognize toll-like receptor 4 (TLR4) and then activate NF-κB signaling, which promotes the secretion of MCP1 and recruitment of proinflammatory macrophages (Catrysse and van Loo, 2017). Furthermore, obesity leads to release of pro-inflammatory mediators such as IL-1β, IL-6 and MCP-1, and then causes circulating monocytes recruitment and macrophages accumulation in adipose tissue (Russo et al., 2021). Our results showed that PDX treatment reduced serum LPS and IL6 levels and significantly inhibited NF-κB signaling in the epididymal adipose tissue of HFD-fed mice. Accordingly, macrophage infiltration was alleviated in epididymal adipose tissue. Macrophages are generally classified into the M1 (expressing high levels of CD11c, TNF-α, IL-1β, IL-6, and Nos2) and M2 (expressing high levels of CD206, CD163, IL-10, IL-4, Arg1, Fizz1, Mrc1, and PPARγ) phenotypes, which represent proinflammatory and anti-inflammatory macrophages, respectively (Shapouri-Moghaddam et al., 2018). M1 macrophages can promote glycolysis to produce lactate instead of metabolizing pyruvate to acetyl-CoA, and M2 macrophages favor beta-oxidation of fatty acids and oxidative phosphorylation to produce energy-rich molecules, which are beneficial to tissue repair and anti-inflammation (Russo et al., 2021). We found that HFD increased infiltration of M1 macrophages and reduced M2 macrophages. In addition, PDX reduced M1 macrophage infiltration and resulted in macrophage polarization toward the M2 phenotype in the epididymal adipose tissue of HFD-fed mice. Moreover, PDX treatment reduced serum lipid profiles including TC, LDL-C and HDL-C levels and improved glucose tolerance and insulin sensitivity. Interestingly, lipogenesis-related genes such as Fasn and DGAT2 were downregulated in Part 1 mice with PDX supplementation, and lipolysis-related genes such as HSL, LPL and CD36 were upregulated in Part 2 mice with PDX treatment. The presumed reason may be that mice in the Part 1 experiment were lean, whereas the mice in the Part 2 experiment became significantly obese with metabolic disorders when the PDX administration began. Therefore, we conclude that PDX significantly alleviates adipose tissue inflammation in HFD-fed mice, which may be mediated by modulating the structure of the gut microbiota.

The lack of direct proof of the causal relationship between the gut microbiota and adipose tissue inflammation and glucolipid metabolism is the major limitation of the study. Future studies, including antibiotic treatment, FMT studies

and oral treatment of live beneficial microbe, are needed, and we will continue our efforts to improve PDX studies and make clinical translation.

CONCLUSION

In conclusion, our results indicate that PDX plays an important role in the prevention and treatment of obesity. PDX can improve glucolipid metabolism and adipose tissue inflammation in HFD-fed mice, which may be mediated by modulating the structure of the gut microbiota. PDX treatment promotes the growth of beneficial microbes including *Bacteroides*, *Parabacteroides*, *Alloprevotella*, *Muribaculum*, *Akkermansia*, *Ruminococcaceae_UCG-014* and *UBA1819* that are associated with obesity improvement. Therefore, we conclude that PDX may become a promising nondrug therapy to prevent and treat obesity.

DATA AVAILABILITY STATEMENT

The raw data supporting the conclusion of this article will be made available by the authors, without undue reservation.

ETHICS STATEMENT

The animal study was reviewed and approved by the Ethics Committee of Xinhua Hospital affiliated to Shanghai Jiao Tong University School of Medicine.

AUTHOR CONTRIBUTIONS

QS, HG, QH and YN designed the project; QH, YN, QM and YL performed the experiments, QH and YY analyzed the data; QH and HG wrote the article; QS, HG, HR, HZ and XL reviewed and revised the article.

FUNDING

This work was supported by the National Natural Science Foundation of China (81970669), the Shanghai Sailing Program (18YF1415800), Hospital Funded Clinical Research, Xin Hua Hospital Affiliated to Shanghai Jiao Tong University School of Medicine (19XHCR21D), Chongming Science and Technology Commission (CKY 2020-18).

REFERENCES

Biagi, E., Franceschi, C., Rampelli, S., Severgnini, M., Ostan, R., Turroni, S., et al. (2016). Gut Microbiota and Extreme Longevity. *Curr. Biol.* 26, 1480–1485. doi:10.1016/j.cub.2016.04.016

Blüher, M. (2019). Obesity: Global Epidemiology and Pathogenesis. *Nat. Rev. Endocrinol.* 15, 288–298. doi:10.1038/s41574-019-0176-8

Canfora, E. E., Meex, R. C. R., Venema, K., and Blaak, E. E. (2019). Gut Microbial Metabolites in Obesity, NAFLD and T2DM. *Nat. Rev. Endocrinol.* 15, 261–273. doi:10.1038/s41574-019-0156-z

Catrysse, L., and van Loo, G. (2017). Inflammation and the Metabolic Syndrome: The Tissue-specific Functions of NF-Kb. *Trends Cel Biol* 27, 417–429. doi:10.1016/j.tcb.2017.01.006

Chassaing, B., Compher, C., Bonhomme, B., Liu, Q., Tian, Y., Walters, W., et al. (2021). Randomized Controlled-Feeding Study of Dietary Emulsifier Carboxymethylcellulose Reveals Detrimental Impacts on the Gut Microbiota and Metabolome. *Gastroenterology* 10 (21), S001603728–S001650858. doi:10.1053/j.gastro.2021.11.006

Costabile, A., Fava, F., Röytiö, H., Forssten, S. D., Olli, K., Klievink, J., et al. (2012). Impact of Polydextrose on the Faecal Microbiota: a Double-Blind, Crossover, Placebo-Controlled Feeding Study in Healthy Human Subjects. *Br. J. Nutr.* 108, 471–481. doi:10.1017/S0007114511005782

do Carmo, M. M., Walker, J. C., Novello, D., Caselato, V. M., Sgarbieri, V. C., Ouwehand, A. C., et al. (2016). Polydextrose: Physiological Function, and Effects on Health. *Nutrients* 8, 553–558. doi:10.3390/nu8090553

do Carmo, M. M. R., Sarmento, U. C., Cavalheiro, L. F., Fernandes, A., Filiú, W. F. O., Gielow, K. C. F., et al. (2018). Intake of Polydextrose Alters Hematology and the Profile of Short Chain Fatty Acids in Partially Gastrectomized Rats. *Nutrients* 10, 792. doi:10.3390/nu10060792

Dobranowski, P. A., Tang, C., Sauvé, J. P., Menzies, S. C., and Sly, L. M. (2019). Compositional Changes to the Ileal Microbiome Precede the Onset of Spontaneous Ileitis in SHIP Deficient Mice. *Gut microbes* 10, 578–598. doi:10.1080/19490976.2018.1560767

Du, Y., Gao, Y., Zeng, B., Fan, X., Yang, D., and Yang, M. (2021). Effects of Anti-aging Interventions on Intestinal Microbiota. *Gut Microbes* 13, 1994835. doi:10.1080/19490976.2021.1994835

Duan, J., Yin, B., Li, W., Chai, T., Liang, W., Huang, Y., et al. (2019). Age-related Changes in Microbial Composition and Function in Cynomolgus Macaques. *Aging (Albany NY)* 11, 12080–12096. doi:10.18632/aging.102541

Giordan, Q., Salleron, J., Vallance, C., Moriana, C., and Clement-Duchene, C. (2021). Impact of Antibiotics and Proton Pump Inhibitors on Efficacy and Tolerance of Anti-PD-1 Immune Checkpoint Inhibitors. *Front. Immunol.* 12, 716317. doi:10.3389/fimmu.2021.716317

Hamer, M., Gale, C. R., Kivimäki, M., and Batty, G. D. (2020). Overweight, Obesity, and Risk of Hospitalization for COVID-19: A Community-Based Cohort Study of Adults in the United Kingdom. *Proc. Natl. Acad. Sci. U S A.* 117, 21011–21013. doi:10.1073/pnas.2011086117

He, L. H., Yao, D. H., Wang, L. Y., Zhang, L., and Bai, X. L. (2021). Gut Microbiome-Mediated Alteration of Immunity, Inflammation, and Metabolism Involved in the Regulation of Non-alcoholic Fatty Liver Disease. *Front. Microbiol.* 12, 761836. doi:10.3389/fmicb.2021.761836

Hengst, C., Ptok, S., Roessler, A., Fechner, A., and Jahreis, G. (2009). Effects of Polydextrose Supplementation on Different Faecal Parameters in Healthy Volunteers. *Int. J. Food Sci. Nutr.* 60 (Suppl. 5), 96–105. doi:10.1080/09637480802526760

Hersoug, L. G., Møller, P., and Loft, S. (2016). Gut Microbiota-Derived Lipopolysaccharide Uptake and Trafficking to Adipose Tissue: Implications for Inflammation and Obesity. *Obes. Rev.* 17, 297–312. doi:10.1111/obr.12370

Koh, A., De Vadder, F., Kovatcheva-Datchary, P., and Bäckhed, F. (2016). From Dietary Fiber to Host Physiology: Short-Chain Fatty Acids as Key Bacterial Metabolites. *Cell* 165, 1332–1345. doi:10.1016/j.cell.2016.05.041

Kusminski, C. M., Bickel, P. E., and Scherer, P. E. (2016). Targeting Adipose Tissue in the Treatment of Obesity-Associated Diabetes. *Nat. Rev. Drug Discov.* 15, 639–660. doi:10.1038/nrd.2016.75

Lapébie, P., Lombard, V., Drula, E., Terrapon, N., and Henrissat, B. (2019). Bacteroidetes Use Thousands of Enzyme Combinations to Break Down Glycans. *Nat. Commun.* 10, 2043. doi:10.1038/s41467-019-10068-5

LeBlanc, E. S., Patnode, C. D., Webber, E. M., Redmond, N., Rushkin, M., and O'Connor, E. A. (2018). Behavioral and Pharmacotherapy Weight Loss Interventions to Prevent Obesity-Related Morbidity and Mortality in Adults: Updated Evidence Report and Systematic Review for the US Preventive Services Task Force. *JAMA* 320, 1172–1191. doi:10.1001/jama.2018.7777

Li, S., You, J., Wang, Z., Liu, Y., Wang, B., Du, M., et al. (2021). Curcumin Alleviates High-Fat Diet-Induced Hepatic Steatosis and Obesity in Association with

Modulation of Gut Microbiota in Mice. *Food Res. Int.* 143, 110270. doi:10.1016/j.foodres.2021.110270

Luoto, R., Ruuskanen, O., Waris, M., Kalliomäki, M., Salminen, S., and Isolauri, E. (2014). Prebiotic and Probiotic Supplementation Prevents Rhinovirus Infections in Preterm Infants: a Randomized, Placebo-Controlled Trial. *J. Allergy Clin. Immunol.* 133, 405–413. doi:10.1016/j.jaci.2013.08.020

Makki, K., Deehan, E. C., Walter, J., and Bäckhed, F. (2018). The Impact of Dietary Fiber on Gut Microbiota in Host Health and Disease. *Cell Host Microbe* 23, 705–715. doi:10.1016/j.chom.2018.05.012

Martel, J., Ojcius, D. M., Chang, C. J., Lin, C. S., Lu, C. C., Ko, Y. F., et al. (2017). Anti-obesogenic and Antidiabetic Effects of Plants and Mushrooms. *Nat. Rev. Endocrinol.* 13, 149–160. doi:10.1038/nrendo.2016.142

McNabney, S. M., and Henagan, T. M. (2017). Short Chain Fatty Acids in the Colon and Peripheral Tissues: A Focus on Butyrate, Colon Cancer, Obesity and Insulin Resistance. *Nutrients* 9, 1348. doi:10.3390/nu9121348

Mocanu, V., Zhang, Z., Deehan, E. C., Kao, D. H., Hotte, N., Karmali, S., et al. (2021). Fecal Microbial Transplantation and Fiber Supplementation in Patients with Severe Obesity and Metabolic Syndrome: a Randomized Double-Blind, Placebo-Controlled Phase 2 Trial. *Nat. Med.* 27, 1272–1279. doi:10.1038/s41591-021-01399-2

Napolitano, M., and Covasa, M. (2020). Microbiota Transplant in the Treatment of Obesity and Diabetes: Current and Future Perspectives. *Front. Microbiol.* 11, 590370. doi:10.3389/fmicb.2020.590370

Oikonomou, E. K., and Antoniades, C. (2019). The Role of Adipose Tissue in Cardiovascular Health and Disease. *Nat. Rev. Cardiol.* 16, 83–99. doi:10.1038/s41569-018-0097-6

Popkin, B. M., Du, S., Green, W. D., Beck, M. A., Algaith, T., Herbst, C. H., et al. (2020). Individuals with Obesity and COVID-19: A Global Perspective on the Epidemiology and Biological Relationships. *Obes. Rev.* 21, e13128. doi:10.1111/obr.13128

Ranucci, G., Buccigrossi, V., Borgia, E., Piacentini, D., Visentin, F., Cantarutti, L., et al. (2018). Galacto-Oligosaccharide/Polidextrose Enriched Formula Protects against Respiratory Infections in Infants at High Risk of Atopy: A Randomized Clinical Trial. *Nutrients* 10, 286. doi:10.3390/nu10030286

Raza, G. S., Putaala, H., Hibberd, A. A., Alhoniemi, E., Tiihonen, K., Mäkelä, K. A., et al. (2017). Polydextrose Changes the Gut Microbiome and Attenuates Fasting Triglyceride and Cholesterol Levels in Western Diet Fed Mice. *Sci. Rep.* 7, 5294. doi:10.1038/s41598-017-05259-3

Reilly, A. M., Yan, S., Huang, M., Abhyankar, S. D., Conley, J. M., Bone, R. N., et al. (2021). A High-Fat Diet Catalyzes Progression to Hyperglycemia in Mice with Selective Impairment of Insulin Action in Glut4-Expressing Tissues. *J. Biol. Chem.* 298, 101431. doi:10.1016/j.jbc.2021.101431

Reilly, S. M., and Saltiel, A. R. (2017). Adapting to Obesity with Adipose Tissue Inflammation. *Nat. Rev. Endocrinol.* 13, 633–643. doi:10.1038/nrendo.2017.90

Russo, S., Kwiatkowski, M., Govorukhina, N., Bischoff, R., and Melgert, B. N. (2021). Meta-Inflammation and Metabolic Reprogramming of Macrophages in Diabetes and Obesity: The Importance of Metabolites. *Front. Immunol.* 12, 746151. doi:10.3389/fimmu.2021.746151

Sanchis-Gomar, F., Lavie, C. J., Mehra, M. R., Henry, B. M., and Lippi, G. (2020). Obesity and Outcomes in COVID-19: When an Epidemic and Pandemic Collide. *Mayo Clin. Proc.* 95, 1445–1453. doi:10.1016/j.mayocp.2020.05.006

Schäfer, A. L., Eichhorst, A., Hentze, C., Kraemer, A. N., Amend, A., Sprenger, D. T. L., et al. (2021). Low Dietary Fiber Intake Links Development of Obesity and Lupus Pathogenesis. *Front. Immunol.* 12, 696810. doi:10.3389/fimmu.2021.696810

Shapouri-Moghaddam, A., Mohammadian, S., Vazini, H., Taghadosi, M., Esmaeili, S. A., Mardani, F., et al. (2018). Macrophage Plasticity, Polarization, and Function in Health and Disease. *J. Cel Physiol* 233, 6425–6440. doi:10.1002/jcp.26429

Shealy, N. G., Yoo, W., and Byndloss, M. X. (2021). Colonization Resistance: Metabolic Warfare as a Strategy against Pathogenic Enterobacteriaceae. *Curr. Opin. Microbiol.* 64, 82–90. doi:10.1016/j.mib.2021.09.014

Shi, H., Ge, X., Ma, X., Zheng, M., Cui, X., Pan, W., et al. (2021). A Fiber-Deprived Diet Causes Cognitive Impairment and Hippocampal Microglia-Mediated Synaptic Loss through the Gut Microbiota and Metabolites. *Microbiome* 9, 223. doi:10.1186/s40168-021-01172-0

Stefan, N., Birkenfeld, A. L., Schulze, M. B., and Ludwig, D. S. (2020). Obesity and Impaired Metabolic Health in Patients with COVID-19. *Nat. Rev. Endocrinol.* 16, 341–342. doi:10.1038/s41574-020-0364-6

Thomson, C., Garcia, A. L., and Edwards, C. A. (2021). Interactions between Dietary Fibre and the Gut Microbiota. *Proc. Nutr. Soc.* 80, 398–408. doi:10.1017/S0029665121002834

Tilg, H., Zmora, N., Adolph, T. E., and Elinav, E. (2020). The Intestinal Microbiota Fuelling Metabolic Inflammation. *Nat. Rev. Immunol.* 20, 40–54. doi:10.1038/s41577-019-0198-4

Videvall, E., Song, S. J., Bensch, H. M., Strandh, M., Engelbrecht, A., Serfontein, N., et al. (2020). Early-life Gut Dysbiosis Linked to Juvenile Mortality in Ostriches. *Microbiome* 8, 147. doi:10.1186/s40168-020-00925-7

Voland, L., Le Roy, T., Debédat, J., and Clément, K. (2021). Gut Microbiota and Vitamin Status in Persons with Obesity: A Key Interplay. *Obes. Rev.* 12, e13377. doi:10.1111/obr.13377

Ward, Z. J., Bleich, S. N., Cradock, A. L., Barrett, J. L., Giles, C. M., Flax, C., et al. (2019). Projected U.S. State-Level Prevalence of Adult Obesity and Severe Obesity. *N. Engl. J. Med.* 381, 2440–2450. doi:10.1056/NEJMsa1909301

Wilding, J. P. H., Mooney, V., and Pile, R. (2019). Should Obesity Be Recognised as a Disease. *BMJ* 366, l4258. doi:10.1136/bmj.l4258

Wu, T., Zhang, Y., Li, W., Zhao, Y., Long, H., Muhindo, E. M., et al. (2021). Lactobacillus Rhamnosus LRa05 Ameliorate Hyperglycemia through a Regulating Glucagon-Mediated Signaling Pathway and Gut Microbiota in Type 2 Diabetic Mice. *J. Agric. Food Chem.* 69, 8797–8806. doi:10.1021/acs.jafc.1c02925

Wu, T. R., Lin, C. S., Chang, C. J., Lin, T. L., Martel, J., Ko, Y. F., et al. (2019). Gut Commensal Parabacteroides Goldsteinii Plays a Predominant Role in the Anti-obesity Effects of Polysaccharides Isolated from Hirsutella Sinensis. *Gut* 68, 248–262. doi:10.1136/gutjnl-2017-315458

Xu, X.-Y., Zhao, C.-N., Li, B.-Y., Tang, G.-Y., Shang, A., Gan, R.-Y., et al. (2021). Effects and Mechanisms of tea on Obesity. *Crit. Rev. Food Sci. Nutr.* 27, 1–18. doi:10.1080/10408398.2021.1992748

Yan, J., Sheng, L., and Li, H. (2021). Akkermansia Muciniphila: Is it the Holy Grail for Ameliorating Metabolic Diseases. *Gut Microbes* 13, 1984104. doi:10.1080/19490976.202110.1080/19490976.2021.1984104

Yang, X., Guo, Y., Chen, C., Shao, B., Zhao, L., Zhou, Q., et al. (2021). Interaction between Intestinal Microbiota and Tumour Immunity in the Tumour Microenvironment. *Immunology* 164, 476–493. doi:10.1111/imm.13397

Ye, J., Zhao, Y., Chen, X., Zhou, H., Yang, Y., Zhang, X., et al. (2021). Pu-erh tea Ameliorates Obesity and Modulates Gut Microbiota in High Fat Diet Fed Mice. *Food Res. Int.* 144, 110360. doi:10.1016/j.foodres.2021.110360

You, D., Chul Jung, B., Villivalam, S. D., Lim, H.-W., and Kang, S. (2021). JMJD8 Is a Novel Molecular Nexus between Adipocyte-Intrinsic Inflammation and Insulin Resistance. *Diabetes* 22, db210596. doi:10.2337/db21-0596

Zhai, Z., Liu, J., Niu, K. M., Lin, C., Tu, Y., Liu, Y., et al. (2021). Integrated Metagenomics and Metabolomics to Reveal the Effects of Policosanol on Modulating the Gut Microbiota and Lipid Metabolism in Hyperlipidemic C57BL/6 Mice. *Front. Endocrinol. (Lausanne)* 12, 722055. doi:10.3389/fendo.2021.722055

Zhang, T., Ji, X., Lu, G., and Zhang, F. (2021). The Potential of Akkermansia Muciniphila in Inflammatory Bowel Disease. *Appl. Microbiol. Biotechnol.* 105, 5785–5794. doi:10.1007/s00253-021-11453-1

Zhao, L., Zhang, F., Ding, X., Wu, G., Lam, Y. Y., Wang, X., et al. (2018). Gut Bacteria Selectively Promoted by Dietary Fibers Alleviate Type 2 Diabetes. *Science* 359, 1151–1156. doi:10.1126/science.aao5774

Conflict of Interest: The authors declare that the research was conducted in the absence of any commercial or financial relationships that could be construed as a potential conflict of interest.

Publisher's Note: All claims expressed in this article are solely those of the authors and do not necessarily represent those of their affiliated organizations, or those of the publisher, the editors and the reviewers. Any product that may be evaluated in this article, or claim that may be made by its manufacturer, is not guaranteed or endorsed by the publisher.

Advantages of publishing in Frontiers

OPEN ACCESS
Articles are free to read for greatest visibility and readership

FAST PUBLICATION
Around 90 days from submission to decision

HIGH QUALITY PEER-REVIEW
Rigorous, collaborative, and constructive peer-review

TRANSPARENT PEER-REVIEW
Editors and reviewers acknowledged by name on published articles

Frontiers
Avenue du Tribunal-Fédéral 34
1005 Lausanne | Switzerland

Visit us: www.frontiersin.org
Contact us: frontiersin.org/about/contact

REPRODUCIBILITY OF RESEARCH
Support open data and methods to enhance research reproducibility

DIGITAL PUBLISHING
Articles designed for optimal readership across devices

FOLLOW US
@frontiersin

IMPACT METRICS
Advanced article metrics track visibility across digital media

EXTENSIVE PROMOTION
Marketing and promotion of impactful research

LOOP RESEARCH NETWORK
Our network increases your article's readership